WETLANDS AND WATER RESOURCES: ECOLOGICAL SOLUTIONS FOR THE ENVIRONMENT

EDITED BY: Guangzhi Sun, Xiaofei Yu, Yuanchun Zou and Guobin Fu
PUBLISHED IN: Frontiers in Earth Science and Frontiers in Environmental Science

frontiers Research Topics

ISSN 1664-8714
ISBN 978-2-83250-558-8
DOI 10.3389/978-2-83250-558-8

About Frontiers

Frontiers is more than just an open-access publisher of scholarly articles: it is a pioneering approach to the world of academia, radically improving the way scholarly research is managed. The grand vision of Frontiers is a world where all people have an equal opportunity to seek, share and generate knowledge. Frontiers provides immediate and permanent online open access to all its publications, but this alone is not enough to realize our grand goals.

Frontiers Journal Series

The Frontiers Journal Series is a multi-tier and interdisciplinary set of open-access, online journals, promising a paradigm shift from the current review, selection and dissemination processes in academic publishing. All Frontiers journals are driven by researchers for researchers; therefore, they constitute a service to the scholarly community. At the same time, the Frontiers Journal Series operates on a revolutionary invention, the tiered publishing system, initially addressing specific communities of scholars, and gradually climbing up to broader public understanding, thus serving the interests of the lay society, too.

Dedication to Quality

Each Frontiers article is a landmark of the highest quality, thanks to genuinely collaborative interactions between authors and review editors, who include some of the world's best academicians. Research must be certified by peers before entering a stream of knowledge that may eventually reach the public - and shape society; therefore, Frontiers only applies the most rigorous and unbiased reviews.
Frontiers revolutionizes research publishing by freely delivering the most outstanding research, evaluated with no bias from both the academic and social point of view. By applying the most advanced information technologies, Frontiers is catapulting scholarly publishing into a new generation.

What are Frontiers Research Topics?

Frontiers Research Topics are very popular trademarks of the Frontiers Journals Series: they are collections of at least ten articles, all centered on a particular subject. With their unique mix of varied contributions from Original Research to Review Articles, Frontiers Research Topics unify the most influential researchers, the latest key findings and historical advances in a hot research area! Find out more on how to host your own Frontiers Research Topic or contribute to one as an author by contacting the Frontiers Editorial Office: frontiersin.org/about/contact

WETLANDS AND WATER RESOURCES: ECOLOGICAL SOLUTIONS FOR THE ENVIRONMENT

Topic Editors:
Guangzhi Sun, Northeast Institute of Geography and Agroecology, Chinese Academy of Sciences (CAS), China
Xiaofei Yu, Northeast Normal University, China
Yuanchun Zou, Northeast Institute of Geography and Agroecology, Chinese Academy of Sciences, China
Guobin Fu, CSIRO Land and Water, Australia

Citation: Sun, G., Yu, X., Zou, Y., Fu, G., eds. (2023). Wetlands and Water Resources: Ecological Solutions for the Environment. Lausanne: Frontiers Media SA. doi: 10.3389/978-2-83250-558-8

Table of Contents

frontiers in Earth Science

ORIGINAL RESEARCH
published: 21 July 2021
doi: 10.3389/feart.2021.712134

Temperature Controls on the Erosion of Badland Slopes in the Nanxiong Basin, China

Zhi Chen[1,2]*, *Luobin Yan*[3]*, *Hua Peng*[1] *and Hong Shi*[4]

[1]School of Geography and Planning, Sun Yat-sen University, Guangzhou, China, [2]School of Geography and Planning, Nanning Normal University, Nanning, China, [3]School of Geographical Sciences, Southwest University, Chongqing, China, [4]School of Tourism and Historical Culture, Southwest Minzu University, Chengdu, China

Understanding the relationships between environmental variables and erosion rates in badlands is vital for forecasting sediment yields. While the controlling role of rainfall on badland erosion rates has long been recognized, here we assess the relative influences of temperature and precipitation on slope erosion rates in the Nanxiong Basin, Southeast China. The volume of weathered and transported fragments was measured within a bounded plot at ten-day intervals between May 1, 2016, and April 30, 2017, and temperature and precipitation were continuously recorded. Mann-Kendall τ correlation, Granger causality, impulse response, and variance decomposition analyses were performed. The results show that Granger causality relationships exist between the ten-day mean temperature (TMT) and ten-day mean erosion rates (TER) and between the ten-day total precipitation (TTP) amount and the TER. Moreover, our findings indicate that TMT and TTP explained 14.6 and 12.61% of the variability in slope erosion rates, respectively, which indicates that temperature had at least the same influence on slope erosion than precipitation. In addition, because 22.5% of the measured erosion occurred during periods when there were no erosive rain events, the importance of small dry slides for removing rock fragments from these humid slopes is emphasized.

Keywords: badlands, erosion rates, granger causality test, M-K tau test, nanxiong basin

OPEN ACCESS

Edited by:
Guobin Fu,
CSIRO Land and Water, Australia

Reviewed by:
Tao Gao,
Institute of Atmospheric Physics, (CAS), China
Liuqin Chen,
East China University of Technology, China

***Correspondence:**
Zhi Chen
chenzhi0111@nnnu.edu.cn
Luobin Yan
yanluobin@swu.edu.cn

Specialty section:
This article was submitted to Hydrosphere, a section of the journal Frontiers in Earth Science

Received: *19 May 2021*
Accepted: *06 July 2021*
Published: *21 July 2021*

Citation:
Chen Z, Yan L, Peng H and Shi H (2021) Temperature Controls on the Erosion of Badland Slopes in the Nanxiong Basin, China. Front. Earth Sci. 9:712134. doi: 10.3389/feart.2021.712134

INTRODUCTION

Badlands are commonly defined as 'intensely dissected natural landscapes where vegetation is sparse or absent and useless for agriculture (Bryan and Yair, 1982). Due to their high erosion rates, badlands are also viewed as degraded areas worldwide (Brandolini et al., 2017; Molina et al., 2009; Peng et al., 2015). Soft bedrock and a lack of vegetation both promote accelerated erosion in these landscapes that produce steep, highly dissected topography and the formation of gully networks and badlands (Fairbridge, 1968; Bocco, 1991). As a result, Badland areas have some of the highest erosion rates globally (Clarke and Rendell, 2010). Consequently, they are considered as 'ideal field laboratories' for studying landscape evolution, acting as miniature fluvial systems in which it is possible to directly observe hill slope-scale processes, interconnections, and resulting landforms (Bryan and Yair, 1982; Parsons and Abrahams, 1994; Campbell, 1997; Alexander et al., 2008; Dickie and Parsons, 2012; Yair et al., 2013).

Several factors and processes affect the development and dynamics of badlands, most notably lithology (Kasanin-Grubin and Bryan, 2007; Morenode las Heras and Gallart, 2016), climate (Bryan and Yair, 1982), and slope aspect (Nadal-Romero et al., 2007). Marked differences in badland slope morphology (Churchill, 1981) and species richness (Nadal-Romero et al., 2014) have been

recognized between aspects, and slope aspect can also be one of the most critical factors determining the intensity of physical weathering processes (Regüés et al., 2000). For a specific badland site, lithology and slope aspects are fixed over long temporal scales relative to climate. Thus, an important aspect of forecasting erosion rates in these landscapes is determining the influence of individual climatic factors.

The rate at which badland landforms develop is the subject of continued speculation (Clarke and Rendell, 2006). For example, erosion rates between 32 and 77 Mg ha yr^{-1} in non-vegetated badlands have been recorded in the Bardenas Reales, southeast Spain (Desir and Marin, 2009), compared with rates of between16 and 63 Mg ha yr^{-1} in vegetated badlands in the Penedès region of Spain (Martínezcasasnovas et al., 2010). In the Guadalajara badlands of Spain, erosion rates of up to 114 Mg ha yr^{-1} have been reported (Martín-Moreno et al., 2014).

Rainfall is an important driver of high erosion rates in badlands. For example, statistically significant relationships between sediment yield and the number of rainfall events have been reported (Cantón et al., 2001), which implies that wetting-drying cycles might have a more significant influence on weathering compared to the individual effects of heating and cooling cycles caused by temperature fluctuations (Cantón et al., 2001). Exceptions to this include badlands in Saudi Arabia, Kuwait, Qatar, and Yemen, where desert-like conditions prevail with substantial differences between day and night temperatures (Erguler and Shakoor, 2009). Erosion rates are assumed to be closely related to average annual precipitation (Bull and Kirkby, 2001), with the relationship between cumulative rainfall and cumulative erosion being particularly strong (Clarke and Rendell, 2006; Schumm, 1964). In addition, rain splash and creep caused by rainfall events can contribute to the detachment and transport of particles from slope face (Cantón et al., 2001). Thus, we hypothesized that in humid subtropical areas, erosion rates would be more strongly correlated with precipitation than temperature.

Although the role of temperature in the rapid weathering of badland materials has been studied (Yan et al., 2019), the impact of temperature on the erosion processes remains relatively understudied. Many existing studies on erosion rates in badlands have been undertaken on a yearly or decadal scale (Clarke and Rendell, 2006; Clarke and Rendell, 2010) and, as a result, the temperature is often averaged across an entire year. About methods, most previous studies have deployed erosion pins, which are considered an inaccurate means of monitoring short-term erosion rates and, therefore, have limited value in assessing the impacts of environmental variables. Thus, fine-scale erosion rate measurements are required to study the possible influences of temperature and predict future erosion rates to inform erosion-control measures (Cantón et al., 2001). Therefore, this study aimed to determine the relative contributions of temperature and rainfall to the erosion of badland slopes.

STUDY AREA

The Nanxiong Basin (24°33′–25°24′ N, 113°52′–114°45′ E), an ancient, Cretaceous faulted rift basin in the fold belt of the Nanling Mountains, is located in north Guangdong Province, southeast China. The basin has an elevation range of 48 to 1,421 m above sea level (Dogan and Aslan, 2017) and covers an area of 2,214 km^2 (**Figure 1**). The basin has a subtropical monsoon climate with long hot summers and short winters. According to the Nanxiong meteorological station (1956–2010), the mean annual temperature, precipitation, and potential evaporation rate are 19.6°C, 1,555.1 mm, and 1,678.7 mm, respectively (Yan et al., 2017). In addition, continuous successions of red fluvial-lacustrine clastics with a maximum thickness of more than 7 km are preserved in the basin (Ma et al., 2018).

Visually spectacular badland landscapes are well developed over a homogeneous and monotonous series of calcareous silty mudstones and siltstones in the Nanxiong Basin (**Figure 2**). These are incised into continental purple mudstones from the Nongshan Formation (En) in Dahangkeng Village, the Shanghu Formation (Esh) in Huangtian Village, and the Zhutian formation (Kzt) in Jiangtian Village. Most studies conducted in this area have focused on the nature of the purple soils rather than erosion of the badland landscapes themselves (Jiang et al., 2015).

MATERIALS AND METHODS

Erosion Monitoring

To control for slope aspect, we established two bounded plots (1.6 × 2 m) on two opposite slopes oriented in an E–W direction (**Figure 3**). Weathered fragments (detached material) that had been eroded and transported to the platforms at the foot of each slope were collected. The slopes were left untouched for 12 months. The upper part of each plot was open, and, in the lower part, the platform from which regolith was collected was bounded by a brick wall. Outlets to drain water in platforms were set in thewalls and were covered with a filter screen to trap regolith. At approximately ten-day intervals, regolith fragments were collected from the bases of the slopes, dried in an oven for 24 h at 100°C, and their dry weight was recorded. Given the fixed area of the bounded plots and experimental time interval, time-series erosion rate datasets could be easily calculated.

Given the problems associated with observations over just one season (Regüés et al., 1995), fragments were collected across an entire year, between May 1, 2016, and April 30, 2017. Given the low amounts of Ca_2CO_3 in the rocks forming this area (Yan et al., 2019), the potential loss of material from the dissolution of calcareous material was not considered. Moreover, given the low relief of these badlands (with a topographic range of approximately 20 m), topography was not considered. Unfortunately, one of the bounded plots was vandalized 3 months into the monitoring period, and, as such, results for one plot are discussed here.

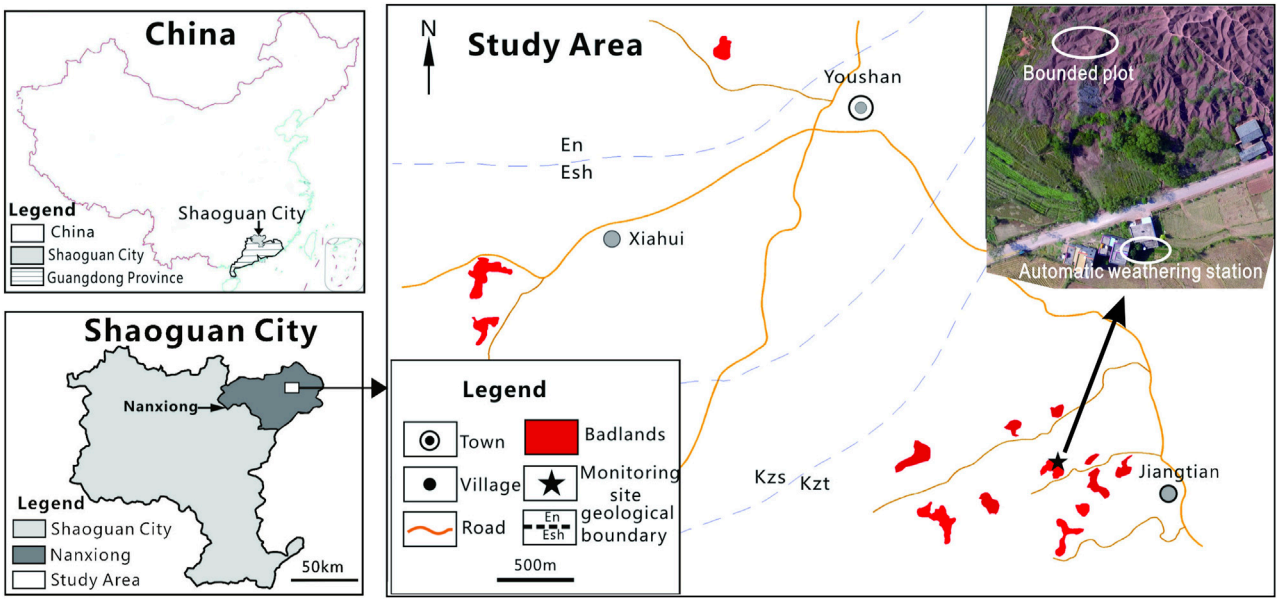

FIGURE 1 | Map of Nanxiong Basin in Guangdong Province and the Monitoring site.

FIGURE 2 | Badland landscape in Nanxiong Basin (Peng et al., 2015).

Rainfall and Temperature

An automatic weather station was installed 200 m away from the experimental plot, which was connected to an automatic data logger. Temperature and precipitation recordings were made at 10-min intervals over the 12 months of field monitoring.

Mann-Kendal τ Correlation Coefficient and Granger Causality

The Mann-Kendal (M-K) tau test is a nonparametric test that does not require data with a specified distribution. M-K τ correlation coefficients for the measured erosion rates and environmental variables (temperature and rainfall) were calculated using MATLAB software. The Granger causality test is a statistical test used to determine whether one time series is useful for forecasting another (Granger, 1969), which has been widely used to study the dynamic relationships between economic time-series (Granger, 1988). Here, Granger causality tests were performed using Eviews software (version 11), which can be used for general statistical analysis and econometric analyses, such as cross-section and panel data analysis, and time-series estimation and forecasting. All of the variables used in our analyses are presented in **Table 1**.

FIGURE 3 | The environment of the study site and the instruments for monitoring of erosion rates. We chose a site where the gully bottom is not steep to construct a cement platform to collect regolith depletion.

RESULTS

Erosion Rates and Erosional Modulus

The mean erosion rate for the whole year, which was calculated as the weight of fragments collected at the base of the experimental slope during the study year divided by the plot area, was 140 Mg ha^{-1} yr^{-1}. The highest erosion rate was logged during October 20th–30th, 2016, at 440 Mg ha^{-1} yr^{-1}. Conversely, the lowest erosion rates recorded were 2.92 Mg ha^{-1} yr^{-1}, 8.03 Mg ha^{-1} yr^{-1}, and 4.02 Mg ha^{-1} yr^{-1}, which occurred during January 1–11, January 11–20, and January 20–30, 2017, respectively (**Figure 4**).

August 2016 had the highest mean erosion rate at 313.58 Mg ha^{-1} yr^{-1} (calculated by dividing the sum erosion amount of each month and 12 months/year per area) (**Figure 3**). Conversely, the months with the lowest erosion rates were December, January, and February, at 4.76 Mg ha^{-1} yr^{-1}, 27.01 Mg ha^{-1} yr^{-1}, and 35.66 Mg ha^{-1} yr^{-1}.

Similar to most transport-limited slopes of badlands (Campbell and Honsaker, 1982), the badlands slope in Nanxiong Basin is covered with a thick layer of rock fragments, especially on the slope faces. As its slope is equal or close to the critical slope of fragments, even during periods without rain, weathered fragments were still found in the plot platform. For example, during September 13–21, 2016, and December 30, 2016, to January 11, 2017, there was a marked difference in erosion rates, at 195.64 Mg ha^{-1} yr^{-1} and 2.92 Mg ha^{-1} yr^{-1}.

Given that not all rainfall events cause erosion of the regolith, the term 'erosive rain' can be applied to those rainfall events to initiate transport. A threshold for such events of 12.7 mm of total rainfall has been suggested by Wischmeier and Smith, (1978), while Jiang and Li (1988) suggest a lower value of 10 mm that is more applicable to badlands considering the presence of dry regolith, which is more vulnerable to erosion. During the year-long study, no erosive rainfall events (>10 mm) were observed during several of the monitoring periods (**Table 2**). Without removing fragments caused by rain, the highest and lowest erosion rates were 195.64 Mg ha^{-1} yr^{-1} and 2.92 Mg ha^{-1} yr^{-1}, respectively, representing a difference of 65 times. The erosion occurring during these 'dry' periods accounted for 22.5% of the total erosion amount.

Statistical Analysis

The correlation coefficient between monthly and ten-day erosion rates and various environmental variables shown in **Table 1** was obtained by applying the M-K tau correlation. Strong correlations were observed between the environmental variables, including monthly mean temperature, monthly mean temperature of daily highest temperature, monthly mean temperature of daily lowest temperature, and monthly erosion rate. Most of the calculated correlations of the ten-day erosion rates with environmental variables were positive and statistically significant ($p \leq 0.01$) (**Table 1**). Based on these data, temperature appeared to significantly influence on erosion rates than rainfall during the study period.

Granger Causality Tests

Tried with different environmental variables, finally, ten-day mean temperature (TMT) and ten-day total precipitation (TTP) were selected to test the causality between variables. The results of

TABLE 1 | Nonlinear correlations for Monthly and Ten-day erosion rates and environmental variables.

Correlation coefficient	Monthly erosion rates	Correlation coefficient	Ten-day erosion rate
Monthly mean temperature	0.7878[a]	Ten-day mean temperature	0.4476[a]
Monthly total precipitation	0.3091	Ten-day total precipitation	0.4073[a]
Number of rainfall events	0.4545	Ten-day number of rainfall events	0.4871[a]
Total precipitation (only including rainfall events over 10 mm)	0.3273	Ten-day precipitation (only including each rainfall event over 10 mm)	0.4456[a]
Monthly mean temperature of daily highest temperature	0.8182[a]	Ten-day mean temperature of daily highest temperature	0.4839[a]
Monthly mean temperature of daily lowest temperature	0.8364[a]	Ten-day mean temperature of daily lowest temperature	0.5181[a]
Monthly highest temperature	0.3273	Ten-day highest temperature	0.4839[a]
Monthly mean temperature difference	0.1455	Ten-day mean temperature difference	0.0121

[a]*Statistically significant where* $p < 0.01$.

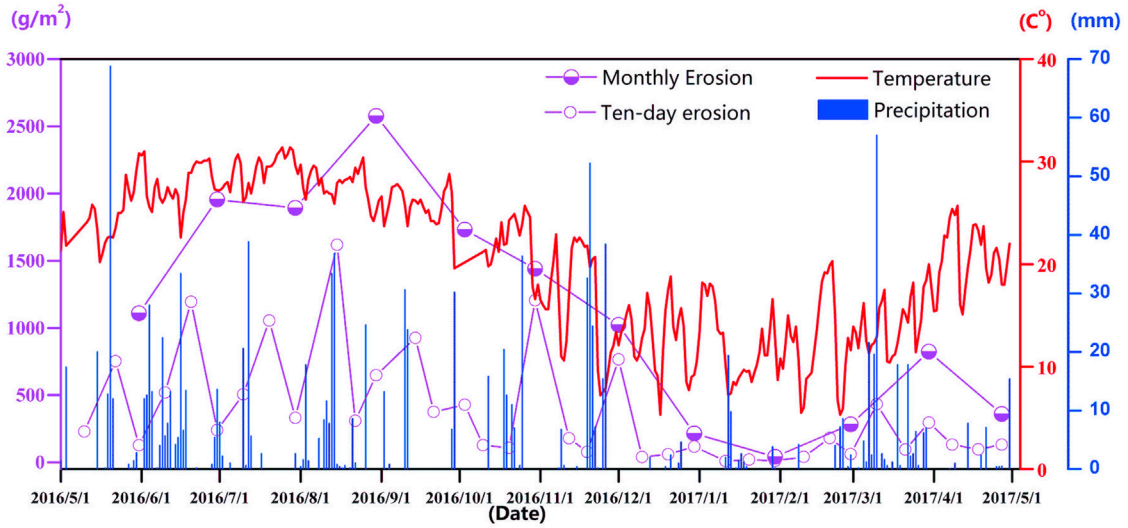

FIGURE 4 | Erosion amount and the environmental variables during the study period.

TABLE 2 | Erosion rates during study period.

Period	Mean temperature (°C)	Total precipitation (mm)	Erosive precipitation (mm)	Erosion rate (Mg ha^{-1} yr^{-1})
May 11, 2016–May 22, 2016	23.2	113.8	113	249.52
May 22, 2016–May 31, 2016	27.2	5.2	0	51.83
May 31, 2016–Jun 10, 2016	27.4	98	75	189.69
Jun 10, 2016–Jun 20, 2016	26.6	84	58	435.56
Jun 20, 2016–Jun 30, 2016	29.3	20	0	87.97
Jun 30, 2016–Jul 10, 2016	28.3	18	29.4	184.58
Jul 10, 2016–Jul 20, 2016	28.6	30	50	385.22
Jul 20, 2016–Jul 30, 2016	30.6	0	0	120.82
Jul 30, 2016–Aug 15, 2016	28.0	127.8	98	369.12
Aug 15, 2016–Aug 22, 2016	28.4	10	0	161.33
Aug 22, 2016–Aug 30, 2016	27.1	25.6	24.6	295.84
Aug 30, 2016–Sep 14, 2016	26.2	68.4	66	225.44
Sep 14, 2016–Sep 21, 2016	25.2	0	0	195.64
Sep 21, 2016–Oct 03, 2016	25.4	37	30	130.23
Oct 03, 2016–Oct 10, 2016	21.2	0	0	66.43
Oct 10, 2016–Oct 20, 2016	21.8	48.8	47	39.03
Oct 20, 2016–Oct 30, 2016	23	55	36	439.94
Oct 30, 2016–Nev 12, 2016	16.2	7.6	0	50.37
Nev 12, 2016–Nov 19, 2016	22.1	33	32.6	40.49
Nov 19, 2016–Dec 01, 2016	12.6	137.8	127	233.1
Dec 01, 2016–Dec 10, 2016	13.2	0	0	15.70
Dec 10, 2016–Dec 20, 2016	12.8	2.4	0	21.54
Dec 20, 2016–Dec 30, 2016	12.4	8	0	42.71
Dec 30, 2016–Jan 11, 2017	15	0	0	2.92
Jan 11, 2017–Jan 20, 2017	8.7	37	19	8.03
Jan 20, 2017–Jan 30, 2017	11.8	4	0	4.02
Jan 30, 2017–Feb 10, 2017	10.7	2.2	0	13.87
Feb 10, 2017–Feb 20, 2017	14.5	0	0	65.7
Feb 20, 2017–Feb 28, 2017	11	22.6	0	28.11
Feb 28, 2017–May 10, 2017	13	106.8	40	49.40
May 10, 2017–May 21, 2017	13.6	24.4	17.8	10.8
May 21, 2017–May 30, 2017	16	42.8	17.8	37.43
May 30, 2017–April 9, 2017	20.7	0.1	0	16.7
April 9, 2017–April 19, 2017	21.1	8.8	0	11.05
April 19, 2017–April 27, 2017	20.4	10.8	0	16.65
April 27, 2017–May 10, 2017	22.6	52	50	18.95
				4,315

TABLE 3 | Granger causality test results.

Dependent variable: TER (Ten-day erosion rate)			
Excluded	Chi-sq	df	Probability
TTP	4.978,858	1	0.0257
TMT	4.533,667	1	0.0332
All	7.262,643	2	0.0265

Note: df represents the degree of freedom; If probability is < 0.05, then a null hypothesis can be rejected, meaning that there is a causal relationship.

Granger causality tests are summarized in **Table 3**, which indicate variable causal links between erosion rates and TMT, erosion rates and TTP. Moreover, TTP and TMT were found to have positively contributed to increases in erosion rates (p = 0.05).

Impulse Response and Variance Decomposition

Impulse response analysis was deployed to analyze the dynamic relationship between erosion rate and environmental variables. As shown in **Figure 5**, providing a positive standard deviation shock is given to the residual of erosion rates, the rest of the variables react to this innovation. TTP response to erosion rates was found first to decrease, then fluctuate to become stationary in the long-term. The response of TMT to erosion rates fluctuated at first and then stabilized due to shocks stemming from TER. Since the impulse response tends towards stability, the Granger causality tests are reasonable.

The variance decomposition approach was adapted to compare the contribution of rainfall and temperature to erosion rates. From No. Seven periods, the impulse response tended towards stability. Thus, the result of the impulse response was deemed to be reliable. Moreover, to forecast precipitation and temperature impacts on erosion rates, a variance decomposition and impulse response analyses were performed (**Table 4**). According to thevariance decomposition analysis results presented in **Table 3**, 72.75% of the variation in erosion amounts could be attributed to innovative shocks within the variable itself. In comparison, the contribution made by TMT and TTP was 14.64 and 12.61%, respectively.

DISCUSSION

In some areas, frost action, snowmelt, and freeze-thaw processes are known to have important impacts on the weathering and erosion of badland surfaces (Regüés et al., 2000; Schumm, 1964; Regüés et al., 1995). In the Nanxiong Basin, with its subtropical climate, freezing occurs only a few times a year and it is not,

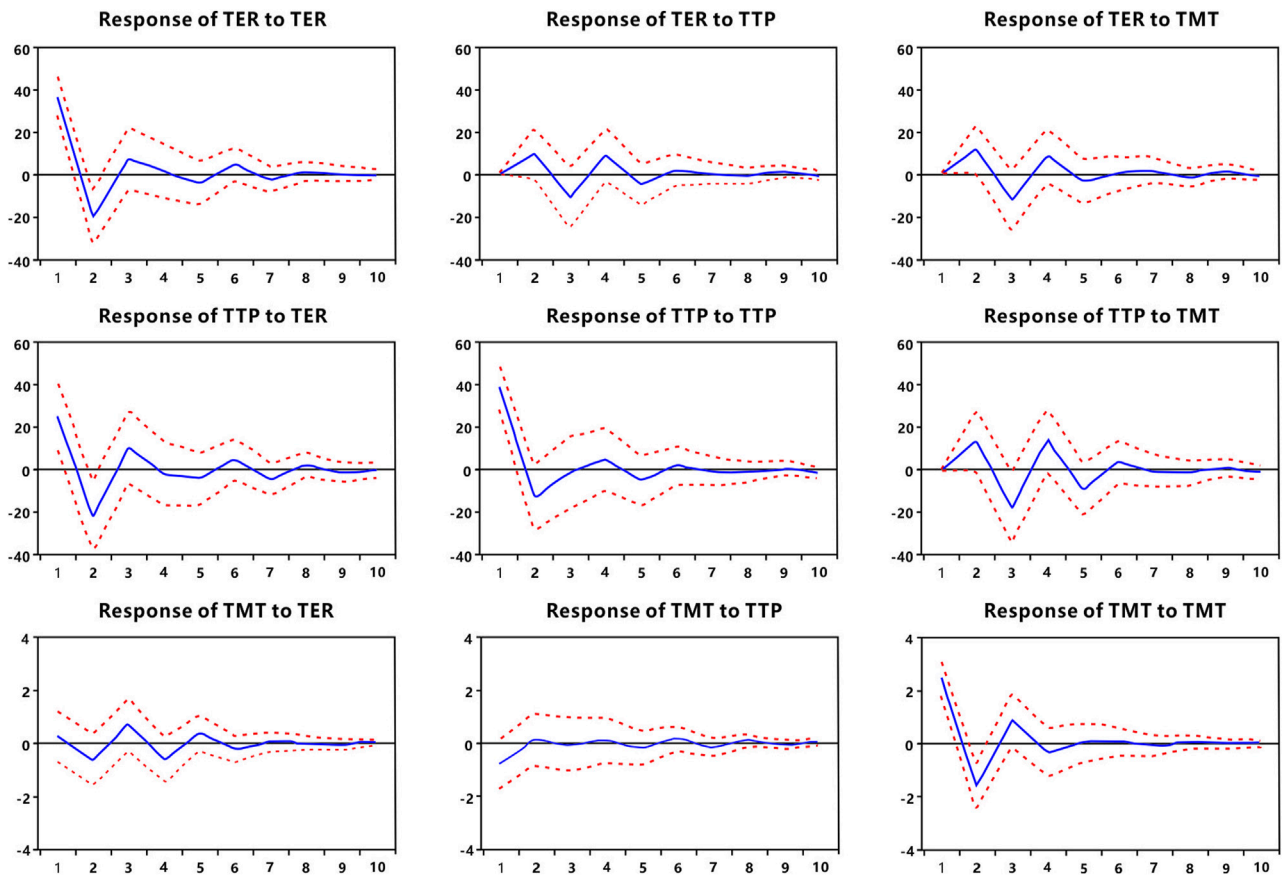

FIGURE 5 | Impulse responses of TER, TTP, and TMT.

TABLE 4 | Variance Decomposition of TER (Ten-day erosion rate).

Standard error	TER	TTP	TMT
36.69031	100.0000	0.000000	0.000000
44.66480	88.87317	4.484,976	6.641,857
48.21860	78.38479	9.334,726	12.28048
49.73430	73.73669	11.89211	14.37119
50.30136	72.83393	12.60055	14.56552
50.51167	72.94112	12.61316	14.44572
50.60956	72.95709	12.56648	14.47643
50.66356	72.85255	12.57843	14.56903
50.69095	72.77387	12.60292	14.62321
50.70251	72.75058	12.61334	14.63608

therefore, considered to be a significant geomorphic factor. Excluding freezing processes, badland erosion occurs in response to individual rain events *via* rain-splash, concentrated and unconcentrated surface flow, creep, mass movement, and piping (Bryan and Yair, 1982). Rain-splash and creep in particular shape the characteristic convexity of the upper slopes of badland landscapes (Parsons and Abrahams, 1994; Schumm, 1956; Carson and Kirkby, 1972). Surface runoff in the form of thin films is likely to be important for transporting material that has been detached and mobilized by splash and raindrop impact (Parsons and Abrahams, 1992; Abrahams et al., 1994). The effectiveness of creep and mudflow becomes apparent at high slope angles, where the thin weathered surface, once wetted, can begin to sag downslope under the influence of gravity (Clarke and Rendell, 2006). The impact of rain and mudflow was also notable at our study site, with mudflows appearing to transport most of the fragments from the slope face (**Figure 6**). A similar phenomenon is also recorded in Basilicata, Italy, where the effect of creep

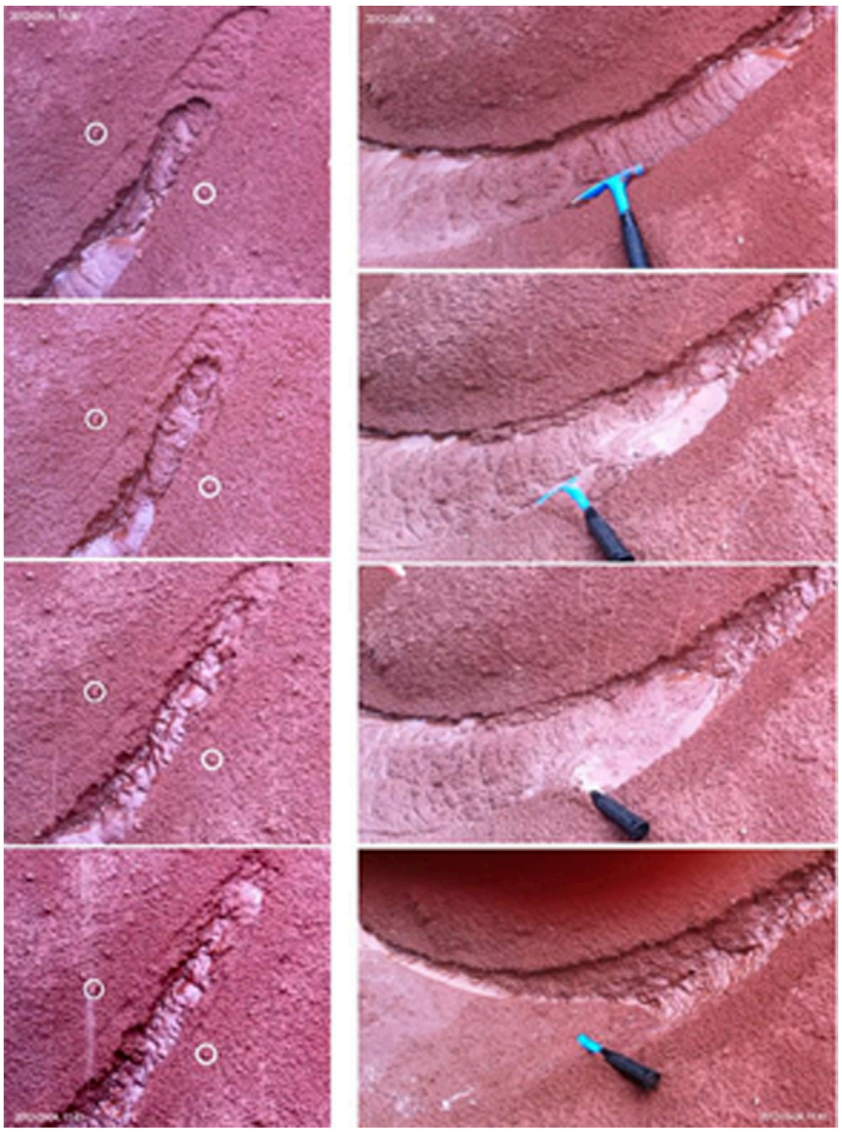

FIGURE 6 | Creep or mudflow occurs during continuous rain was observed during the monitoring period.

appears to be limited to a 10–40 mm thick weathered layer, where the sagging effect is visible on steep (>53°) Biancane slopes (Clarke and Rendell, 2006). Thus, we speculate that the mudflows explain how TTP is related to removal fragments in Badlands in Nanxiong Basin. Further research is now required to determine the precipitation threshold for mudflow initiation.

Gravity has been identified as the primary morphogenic process responsible for shaping slopes in badlands (Ciccacci et al., 2008). In Nanxiong, small slides of dry fragments under a small perturbation are another notable form of erosion. During the periods when no erosive rain events occurred, such small-scale slides resulted in the highest erosion rate of 195.64 Mg ha^{-1} yr^{-1}, which was almost 65 times higher than the lowest recorded erosion rate of 2.92 Mg ha^{-1} yr^{-1}. Parsons and Abrahams (1994) note that the maximum slope angles of badland surfaces are related to the angle of repose of dry weathered detritus. In the Nanxiong badlands, slope angle equals the angle of frictional resistance, thus promoting the transport of weathered fragments downslope. The initiation of small dry slides involves disturbing animals, such as birds and insects, and wind.

Badlands developed in sub-humid mountainous areas are subject to higher rates of denudation and more active dynamics compared to similar landscapes in arid or semiarid areas (Bull and Kirkby, 2001; Regüés and Gallart, 2004).

Previous studies demonstrated that wetting and drying cycles are more effective at causing the disintegration of clay-bearing rocks (Erguler and Shakoor, 2009; Yan, et al., 2019). However, in the field, precipitation amounts recorded between sampling periods did not significantly correlate with rock bulk density or surface mechanical resistance, indicating that regolith moisture does not depend solely on precipitation at this site but also related to temperature (Nadal-Romero et al., 2007). Thus, we speculate that the mean temperature contributes to increase the number of wetting and drying cycles. This might explain why, at our study site, mean temperature was found to contribute 14.6% of erosion rates, which was slightly higher than the contribution of total precipitation (12.6%).

It is apparent that mean temperature (including the mean lowest and highest temperatures) had a stronger relationship with erosion rates over monthly timescale than temperature difference. However, over a ten-day timescale, while the correlation was significant, the M-K tau coefficient was low. Remarkably, the mean temperature was found to have casual links with erosion rates rather than temperature differences. High temperatures were also found to be dominant in increasing erosion rates. Thus, it appears that the coefficient of the ten-day temperature difference and erosion rates resulted from a time-lag effect of temperature. Work is now needed using long-term datasets to quantify the nature of this time interval.

In this climate and lithology, mean temperature rather than temperature difference has more of an influence on the erosion rates of badland slopes. As for other dry badlands, weathering dynamics depend mainly on rainfall characteristics and water deficit (Sole´-Benet et al., 1997). For example, Gallart et al. (2002) reported that in the Vallcebre catchments of the Pyrenean ranges, the main controlling factor on badland development appears to be low temperatures rather than a lack of moisture. Indeed, at our subtropical study site, the temperature was found to have at least the same influence as precipitation on the erosion of badland slopes.

We applied the Granger causality method to examine the relationships between climate variables and erosion rates over short temporal scales. In this sense, the dataset we need for this test is not necessarily from two or more years, although we are aware that more extended datasets have preferable. Nevertheless, the impulse response has shown that the result of the impulse response is reliable. Thus we believe that studies with only one are fine.

CONCLUSION

Analysis based on M-K τ correlation tests suggests that temperature variables positively and significantly corelated with erosion rates in the Nanxiong badlands. Granger causality relationships were also derived for erosion rates and TMT and total TTP. The results of impulse response and variance decomposition analyses show that the relative contributions of TMT and TTP to erosion were 14.6 and 12.61% during the study period, respectively. This suggests that in this subtropical environment, high mean temperatures have at least the same influence on badland development as precipitation. This implies that mean temperature might be an important parameter for erosion forecasting.

During the year-long study, 22.5% of the total erosion amount occurred during periods when no erosive rain events occurred. During these periods, small slides of dry weathered fragments were important for the removal of material in this transport-limited humid badland landscape, while mudflow processes were important for transporting material during periods of continuous rain.

DATA AVAILABILITY STATEMENT

The original contributions presented in the study are included in the article/Supplementary Material, further inquiries can be directed to the corresponding authors.

AUTHOR CONTRIBUTIONS

CZ and YL: Investigation, Data curation, Writing Original draft, Reviewing and Editing. CZ and PH: Conceptualization, Methodology, Supervision, Project administration, Funding acquisition. SH: Software, Validation, Visualization.

FUNDING

This study was funded by the National Natural Science Foundation of China (Grant No. 41901005) and Fundamental Research Funds for the Central Universities (SWU 118202). The corresponding author gratefully acknowledges financial support from China Scholarship Council (Grant No. CSC201806995083).

REFERENCES

Abrahams, A. D., Howard, A. D., and Parsons, A. J. (1994). "Rock-Mantled Slopes," in *Geomorphology of Desert Envionments* (London: Chapman and Hall), 173–212. doi:10.1007/978-94-015-8254-4_8

Alexander, R. W., Calvo-Cases, A., Arnau-Rosalén, E., Mather, A. E., and Lázaro-Suau, R. (2008). Erosion and stabilisation sequences in relation to base level changes in the El Cautivo badlands, SE Spain. *Geomorphology* 100, 83–90. doi:10.1016/j.geomorph.2007.10.025

Bocco, G. (1991). Gully erosion: Processes and models. *Prog. Phys. Geogr. Earth Environ.* 15, 392–406. doi:10.1177/030913339101500403

Brandolini, P., Pepe, G., Capolongo, D., Cappadonia, C., Cevasco, A., Conoscenti, C., et al. (2017). Hillslope degradation in representative Italian areas: Just soil erosion risk or opportunity for development?. *Land Degrad. Dev.* 29, 3050–3068. doi:10.1002/ldr.2672

Bryan, R. B., and Yair, A. (1982). *Badland Geomorphology and Piping*. Norwich: Geobooks, 407.

Bull, N. J., and Kirkby, M. J. (2001). *Dryland Rivers: Processes and Management in Mediterranean Climates*. New Jersey, United States: Wiley.

Campbell, I. A. (1997). "Badlands and Badland Gullies," in *Arid Zone Geomorphology: Process, Form and Change in Drylands*. Editor D. S. G. Thomas (London: Belhaven), 159–183.

Campbell, I. A., and Honsaker, J. L. (1982). "Variability in Badlands Erosion; Problems of Scale and Threshold Identification," in *Space and Time in Geomorphology*. Editor C. E. Thorn (London: George Allen and Unwin.), 59–79.

Cantón, Y., Solé-Benet, A., Queralt, I., and Pini, R. (2001). Weathering of a gypsum-calcareous mudstone under semi-arid environment at Tabernas, SE Spain: laboratory and field-based experimental approaches. *Catena* 44, 111–132. doi:10.1016/s0341-8162(00)00153-3

Carson, M. A., and Kirkby, M. J. (1972). *Hillslope form and process*. UK: Cambridge University.

Churchill, R. R. (1981). Aspect-Related Differences in Badlands Slope Morphology. *Ann. Assoc. Am. Geogr.* 71, 374–388. doi:10.1080/13520806.1981.11759448

Ciccacci, S., Galiano, M., Roma, M. A., and Salvatore, M. C. (2008). Morphological analysis and erosion rate evaluation in badlands of Radicofani area (Southern Tuscany - Italy). *Catena* 74, 87–97. doi:10.1016/j.catena.2008.03.012

Clarke, M. L., and Rendell, H. M. (2010). Climate-driven decrease in erosion in extant Mediterranean badlands. *Earth Surf. Process. Landforms* 35, 1281–1288. doi:10.1002/esp.1967

Clarke, M. L., and Rendell, H. M. (2006). Process-form relationships in Southern Italian badlands: erosion rates and implications for landform evolution. *Earth Surf. Process. Landforms* 31, 15–29. doi:10.1002/esp.1226

Desir, G., and Marín, C. (2009). Caracterización de la erosión en áreas acarcavadas en la Fm. Tudela (Bardenas Reales, Navarra). *Cuadernos de Investigación Geográfica* 35, 195–213. doi:10.18172/cig.1218

Dickie, J. A., and Parsons, A. J. (2012). Eco-Geomorphological Processes within Grasslands, Shrublands and Badlands in the Semi-Arid Karoo, South Africa. *Land Degrad. Develop.* 23, 534–547. doi:10.1002/ldr.2170

Dogan, E., and Aslan, A. (2017). Exploring the relationship among CO 2 emissions, real GDP, energy consumption and tourism in the EU and candidate countries: Evidence from panel models robust to heterogeneity and cross-sectional dependence. *Renew. Sust. Energ. Rev.* 77, 239–245. doi:10.1016/j.rser.2017.03.111

Erguler, Z. A., and Shakoor, A. (2009). Relative contribution of various climatic processes in disintegration of clay-bearing rocks. *Eng. Geology.* 108, 36–42. doi:10.1016/j.enggeo.2009.06.002

Fairbridge, R. W. (1968). *The Encyclopedia of Geomorphology*. New York: Reinhold, 1295.

Gallart, F., Llorens, P., Latron, J., and Regüés, D. (2002). Hydrological processes and their seasonal controls in a small Mediterranean mountain catchment in the Pyrenees. *Hydrol. Earth Syst. Sci.* 6, 527–537. doi:10.5194/hess-6-527-2002

Granger, C. W. J. (1969). Investigating causal relations by econometric models and cross-spectral methods. *Econometrica* 37, 424–438. doi:10.2307/1912791

Granger, C. W. J. (1988). Some recent development in a concept of causality. *J. Econom.* 39, 199–211. doi:10.1016/0304-4076(88)90045-0

Jiang, J., Wang, J., and Wei, X. (2015). Study on the Purple Soil Water Properties in Nanxiong City. *Chin. Agric. Sci. Bull.* 31, 215–218.

Jiang, Z., and Li, X. (1988). Study on the Rainfall Erosivity and the Topographic Factor of Predicting Soil Loss Equation in the Loess Plateau. *Memoir Northwest. Inst. Soil Water Conservation Academia Sinica* 7, 40–45.

Kasanin-Grubin, M., and Bryan, R. (2007). Lithological properties and weathering response on badland hillslopes. *Catena* 70, 68–78. doi:10.1016/j.catena.2006.08.001

Ma, M., Liu, X., and Wang, W. (2018). Palaeoclimate evolution across the Cretaceous-Palaeogene boundary in the Nanxiong Basin (SE China) recorded by red strata and its correlation with marine records. *Clim. Past* 14, 287–302. doi:10.5194/cp-14-287-2018

Martín-Moreno, C., Fidalgo Hijano, C., Martín Duque, J. F., González Martín, J. A., Zapico Alonso, I., and Laronne, J. B. (2014). The Ribagorda sand gully (east-central Spain): Sediment yield and human-induced origin. *Geomorphology* 224, 122–138. The Ribagorda sand gully (east-central Spain): Sediment yield and human-induced origin. doi:10.1016/j.geomorph.2014.07.013

Martínezcasasnovas, J. A., Concepción Ramos, M., and Garcíahernández, D. (2010). Effects of land-use changes in vegetation cover and sidewall erosion in a gully head of the Penedès region (northeast Spain). *Earth Surf. Process. Landforms* 34, 1927–1937.

Molina, A., Govers, G., Cisneros, F., and Vanacker, V. (2009). Vegetation and topographic controls on sediment deposition and storage on gully beds in a degraded mountain area. *Earth Surf. Process. Landforms* 34, 755–767. doi:10.1002/esp.1747

Moreno-de las Heras, M., and Gallart, F. (2016). Lithology controls the regional distribution and morphological diversity of montane Mediterranean badlands in the upper Llobregat basin (eastern Pyrenees). *Geomorphology* 273, 107–115. doi:10.1016/j.geomorph.2016.08.004

Nadal-Romero, E., Petrlic, K., Verachtert, E., Bochet, E., and Poesen, J. (2014). Effects of slope angle and aspect on plant cover and species richness in a humid Mediterranean badland. *Earth Surf. Process. Landforms* 39, 1705–1716. doi:10.1002/esp.3549

Nadal-Romero, E., Regüés, D., Martí-Bono, C., and Serrano-Muela, P. (2007). Badland dynamics in the Central Pyrenees: Temporal and spatial patterns of weathering processes. *Earth Surf. Process. Landforms* 32, 888–904. doi:10.1002/esp.1458

Parsons, A. J., and Abrahams, A. D. (1994). *Geomorphology of Desert Environments*. Netherlands: Springer.

Parsons, A. J., and Abrahams, A. D. (1992). *Overland flow*. London: UCL Press, 307–334.

Peng, H., Yan, L. B., Chen, Z., Scott, S., and Luo, G. S. (2015). A preliminary study of desertification in red beds in the humid region of Southern China. *ACTA GEOGRAPHICA SINICA* 70, 1699–1707.

Regüés, D., and Gallart, F. (2004). Seasonal patterns of runoff and erosion responses to simulated rainfall in a badland area in Mediterranean mountain conditions (Vallcebre, southeastern Pyrenees). *Earth Surf. Process. Landforms* 29, 755–767. doi:10.1002/esp.1067

Regüés, D., Guàrdia, R., and Gallart, F. (2000). Geomorphic agents versus vegetation spreading as causes of badland occurrence in a Mediterranean subhumid mountainous area. *Catena* 40, 173–187. doi:10.1016/s0341-8162(99)00045-4

Regüés, D., Pardini, G., and Gallart, F. (1995). Regolith behaviour and physical weathering of clayey mudrock as dependent on seasonal weather conditions in a badland area at Vallcebre, Eastern Pyrenees. *Catena* 25, 199–212. doi:10.1016/0341-8162(95)00010-p

Schumm, S. A. (1964). Seasonal variations of erosion rates and processes on hillslopes in western Colorado. *Z. für Geomorphologie* 5, 215–238.

Schumm, S. A. (1956). The role of creep and rainwash on the retreat of badland slopes [South Dakota]. *Am. J. Sci.* 254, 693–706. doi:10.2475/ajs.254.11.693

Sole´-Benet, A., Calvo, A., and Cerda, A. (1997). Influences of micro-relief patterns and plant cover on runoff related processes in badlands from Tabernas (SE Spain). *Catena* 31, 23–38.

Wischmeier, W. H., and Smith, D. D. (1978). *USDA Agricultural Handbook*, 537.

Yair, A., Bryan, R. B., Lavee, H., Schwanghart, W., and Kuhn, N. J. (2013). The resilience of a badland area to climate change in an arid environment. *Catena* 106, 12–21. doi:10.1016/j.catena.2012.04.006

Yan, L., He, R., Kašanin-Grubin, M., Luo, G., Peng, H., and Qiu, J. (2017). The Dynamic Change of Vegetation Cover and Associated Driving Forces in Nanxiong Basin, China. *Sustainability* 9, 443. doi:10.3390/su9030443

Yan, L., Liu, P., Peng, H., Kašanin-Grubin, M., and Lin, K. (2019). Laboratory study of the effect of temperature difference on the disintegration of redbed softrock. *Phys. Geogr.*, 1–15.

Conflict of Interest: The authors declare that the research was conducted in the absence of any commercial or financial relationships that could be construed as a potential conflict of interest.

frontiers in Environmental Science

ORIGINAL RESEARCH
published: 30 July 2021
doi: 10.3389/fenvs.2021.736400

Groundwater Hydrograph Decomposition With the HydroSight Model

Feihe Kong[1,2], Jinxi Song[1,2], Russell S. Crosbie[3], Olga Barron[4], David Schafer[5] and Jon-Philippe Pigois[5]*

[1]Shaanxi Key Laboratory of Earth Surface System and Environmental Carrying Capacity, College of Urban and Environmental Sciences, Northwest University, Xi'an, China, [2]Institute of Qinling Mountains, Northwest University, Xi'an, China, [3]CSIRO Land and Water, Glen Osmond, SA, Australia, [4]CSIRO Land and Water, Wembley, WA, Australia, [5]Department of Water and Environmental Regulation, Victoria Park, WA, Australia

Groundwater, the most important water resource and the largest distributed store of fresh water in the world, supports sustainability of groundwater-dependent ecosystems and resilient and sustainable economy of the future. However, groundwater level decline in many parts of world has occurred as a result of a combination of climate change, land cover change and groundwater abstraction from aquifers. This study investigates the determination of the contributions of these factors to the groundwater level changes with the HydroSight model. The unconfined superficial aquifer in the Gnangara region in Western Australia was used as a case study. It was found that rainfall dominates long-term (1992–2014) groundwater level changes and the contribution rate of rainfall reduced because the rainfall decreased over time. The mean rainfall contribution rate is 77% for climate and land cover analysis and 90% for climate and pumping analysis. Secondly, the increasing groundwater pumping activities had a significant influence on groundwater level and its mean contribution rate on groundwater level decline is -23%. The land cover changes had limited influence on long-term groundwater level changes and the contribution rate is stable over time with a mean of 2%. Results also showed spatial heterogeneity: the groundwater level changes were mainly influenced by rainfall and groundwater pumping in the southern study region, and the groundwater level changes were influenced by the combination of rainfall, land cover and groundwater pumping in the northern study region. This research will assist in developing a quantitative understanding of the influences of different factors on groundwater level changes in any aquifer in the world.

Keywords: groundwater hydrograph decomposition, transfer function noise model, groundwater level decline, climate change, land cover change, groundwater abstraction, the Gnangara region

OPEN ACCESS

Edited by:
Yuanchun Zou,
Northeast Institute of Geography and Agroecology (CAS), China

Reviewed by:
Luan Zhaoqing,
Nanjing Forestry University, China
Ping Wang,
Institute of Geographic Sciences and Natural Resources Research (CAS), China

****Correspondence:***
Jinxi Song
jinxisong@nwu.edu.cn

Specialty section:
This article was submitted to Freshwater Science, a section of the journal Frontiers in Environmental Science

Received: *05 July 2021*
Accepted: *19 July 2021*
Published: *30 July 2021*

Citation:
Kong F, Song J, Crosbie RS, Barron O, Schafer D and Pigois J-P (2021) Groundwater Hydrograph Decomposition With the HydroSight Model. Front. Environ. Sci. 9:736400. doi: 10.3389/fenvs.2021.736400

INTRODUCTION

Groundwater is an important natural resource that supplies water to humans (Döll, 2009), especially as the primary source of drinking water for over two billion people (Famiglietti, 2014). In arid and semiarid regions, groundwater is also used for agricultural irrigation. At the global level, 50% of the domestic water supply, 40% of the industrial water supply and 20% of the irrigation water supply originate from groundwater (Zektser and Lorne, 2004). However, global groundwater depletion has been increasing since the 1960 (Wada et al., 2010). Many countries and regions now face serious

problems of excessive groundwater depletion, such as North Africa, North China, North America, the Middle East, South and Central Asia, and Australia (Konikow and Kendy, 2005). For example, groundwater depletion in the United States during 1900–2008 is estimated totals approximately 1,000 cubic kilometers (km^3) (Konikow, 2013). Groundwater depletion rate in North China based on GRACE was 2.2 ± 0.3 cm/yr from 2003 to 2010, which is equivalent to a volume of 8.3 ± 1.1 km^3/yr (Feng et al., 2013). Groundwater is often poorly monitored and managed (Famiglietti, 2014). This has led to notable social and economic impacts (Gleeson et al., 2012). As a result, more efforts and attention are required to better understand and manage groundwater resources.

Continuous groundwater level decline in unconfined and confined aquifers over a long period is an important depletion indicator (Zektser and Lorne, 2004). Groundwater level decline can not only impose negative influences on local economic and social development, but could also impose significant influences on natural streamflow and groundwater-dependent ecosystems (Wada et al., 2010; Fu et al., 2019). It has been widely recognized that groundwater level fluctuation is influenced not only by natural processes, such as precipitation, evaporation and river water stages (Zhou et al., 2020), but also by anthropogenic activities, such as groundwater abstraction (Shapoori et al., 2015a) and land use and land cover change (Yue et al., 2016; Cheng et al., 2017; Abiye et al., 2018). Therefore, it is necessary to detect these drivers and decompose groundwater hydrographs into individual drivers to support groundwater resource management and regional development.

A well-known method is time series analysis which has been widely adopted in groundwater hydrology to interpolate, simulate and predict groundwater levels and further quantify the effects of various drivers of groundwater level fluctuation (Peterson and Western, 2014; Peterson and Western, 2018; Obergfell et al., 2019). This method is relatively simple and requires few parameters, and the model is easily constructed and produces reliable results. The Hydrograph Analysis: Rainfall And Time Trends (HARTT) model proposed by Ferdowsian et al. (2001), Ferdowsian et al. (2002) and Ferdowsian and Pannell (2009) is a representative time series model for groundwater level modelling. Another time series approach model is the transfer function noise (TFN) model developed by von Asmuth et al. (2002) and von Asmuth et al. (2008). This model is based on predefined impulse response functions and simulates groundwater head observations by weighting input historical forcing data and estimating the noise component. TFN models, in contrast to the HARRT model, do not require groundwater level observation data obtained at regular time steps, and they do not assume a stationary climate (Peterson and Western, 2014). Therefore, the TFN model is readily applied in groundwater hydrograph modelling because groundwater observation data are not always acquired at regular time steps. This method has been applied in many studies, including the estimation of groundwater recharge (Obergfell et al., 2019) and aquifer hydraulic properties (Shapoori et al., 2015b) and even the decomposition of the observed groundwater head into different hydrological stresses (Peterson and Western, 2011; Shapoori et al., 2015c). In this study, the TFN model developed by Peterson and Western (2014) was adopted to separate the contributions of land cover change and groundwater pumping from that of rainfall variation to the observed groundwater level fluctuation.

The Gnangara groundwater system is one of the most important groundwater sources in Western Australia and is vital to the local drinking water supply, supplying over 40% of Perth's drinking water each year (Merz, 2009), as well as supporting nationally significant groundwater-dependent ecosystems, such as lakes, wetlands, woodlands and cave ecosystems (Western Australian Planning Commission, 2001). The Gnangara groundwater resources are a key factor to achieve sustainable social and economic growth in the region, and they provide approximately 60% of the potable water supply to the city of Perth (with a population 1.5 million people) (Elmahdi and McFarlane, 2009). However, the groundwater levels in this region have been found to decline in the unconfined (superficial aquifer with groundwater moves slowly) and confined aquifers (Leederville with a maximum thickness of more than 600 m and Yarragadee aquifers with a maximum thickness of more than 2000 m), over the last 40 years due to a combination of rainfall decline, groundwater abstraction for public and private water supply purposes (Iftekhar and Fogarty, 2017), evapotranspiration, and interception by pine plantations (Bekesi et al., 2009; Strobach, 2013). It has been widely accepted that the sustainability of the Gnangara groundwater resources and groundwater-dependent ecosystems is greatly threatened by the continued decline in groundwater levels (Xu, 2008). However, the relative contributions of these factors to the groundwater level decline remain uncertain. Therefore, quantitative estimation of the impact of the individual drivers on groundwater level dynamics is necessary for scientific and effective groundwater resource management in the Gnangara region.

The HydroSight program employed in this study is a highly flexible statistical toolbox developed by Peterson and Western (2014). It integrates multiple models, such as soil moisture and time series models, into one model provides an efficient means to build a wide range of groundwater time-series models and separate the impacts of different factors from climate on groundwater level without knowledge of programming knowledge (http://peterson-tim-j.github.io/HydroSight/). Based on this tool, this study focuses on long-term groundwater level change analysis in unconfined superficial aquifer to identify the controlling factors and quantitatively decompose groundwater hydrograph into different drivers, such as rainfall variability, land cover change (represented by the normalized difference vegetation index (NDVI)) and groundwater pumping (for public and private water supply purposes), in the Gnangara region. This study has implications for groundwater resource management and regional development.

Study Area

Site Location

The Gnangara region is a basin consisting of water-holding sands and gravels interspersed with clays in the coastal plain of the northern part of Perth, Western Australia (**Figure 1**). It covers an

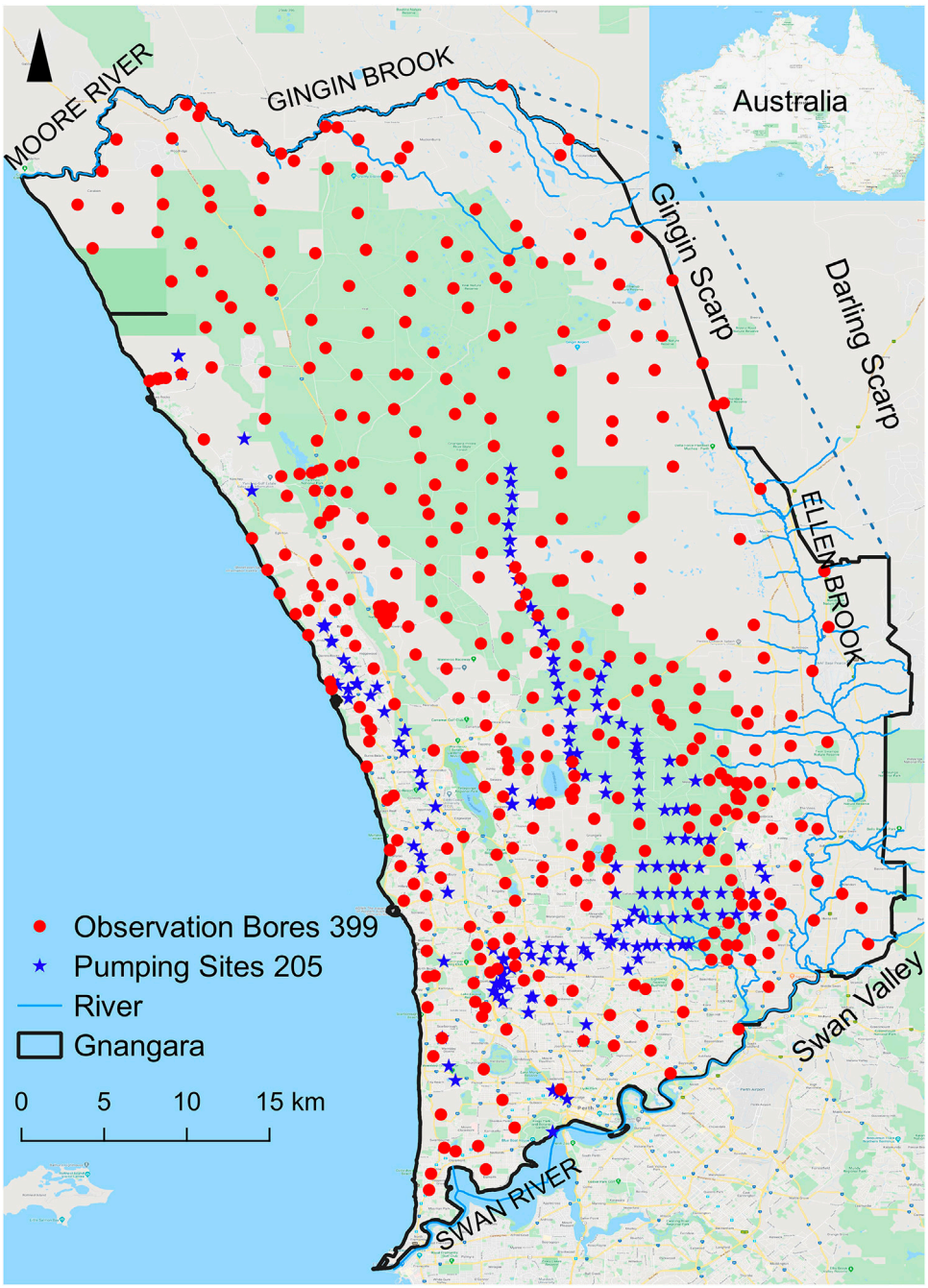

FIGURE 1 | Location of the observation and pumping sites in the Gnangara region, Western Australia.

area of 2,200 km^2 and is bounded by the Gingin Brook and Moore River to the north, the Swan River to the south, the Darling Scarp, Ellen Brook and Swan Valley to the east, and the Indian Ocean to the west (Davidson, 1995; Western Australian Planning Commission, 2001). This region experiences a Mediterranean climate with hot, dry summers and mild, wet winters. The long-term (1900–2017) mean annual rainfall is 758 mm and the mean annual potential evapotranspiration reaches 1,386 mm (calculated based on the daily rainfall and potential evapotranspiration which is extracted from the SILO Data Drill database, see the detail in 2.2.1). Approximately 80% of the rainfall and 23% of the potential evapotranspiration are concentrated from May to September (**Figure 2**). A dry climate period following 1968 was evaluated by cumulative deviation from the mean rainfall (CDFM) technique (**Figure 2**). Over the last 47 years (1970–2017), rainfall has declined by 13% below the long-term average (1900–2017), which has influenced the local ecosystem (Wilson et al., 2012).

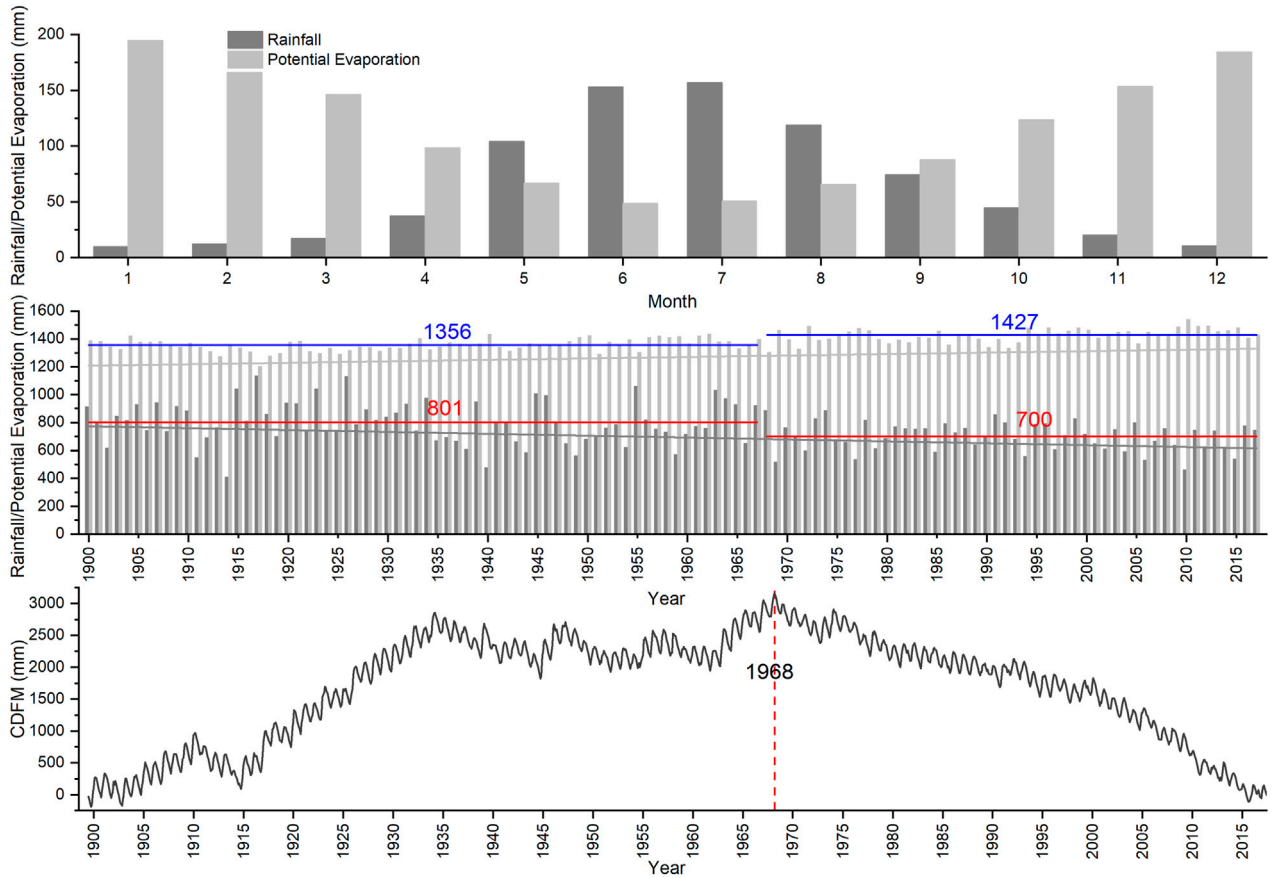

FIGURE 2 | Long-term averages of the monthly rainfall, annual rainfall and potential evapotranspiration, and dry climatic periods by cumulative deviation from mean rainfall (CDFM) in the Gnangara region.

The long-term mean annual rainfall was considered to determine the spatial distribution of rainfall in the Gnangara region via the empirical Bayesian kriging in ArcGIS 10.5 (**Figure 3A**). **Figure 3A** shows that the rainfall is high in the south and central part of the Gnangara region (up to 865 mm) and is low in north part of the Gnangara region (as low as 688 mm).

In the Gnangara groundwater system, plantation forestry is one of the major land use types (land use map in 1992 and 2018 extracted from Bureau of Rural Sciences (2006) and Australian Bureau of Agricultural and Resource Economics and Sciences (2018), **Supplementary Figure S1**). Approximately 17,000 ha of the area contains currently mature maritime pine (Pinus pinaster) plantations, located in the centre of the system (Forest Products Commission, 2009). Mature pines consume much water because the transpiration rate of pines is 23% higher than that of the native banksia woodland surrounding the pine plantation (Carbon et al., 1982; Tremayne, 2010). Urbanized areas mainly occur in the southwest and southeast of the system. Other land use types, such as pastures, are found along the eastern and northern margins of the system (Australian Bureau of Agricultural and Resource Economics and Sciences, 2018). The long-term mean annual NDVI at various sites was adopted to determine the spatial distribution of the NDVI in the Gnangara region via the empirical Bayesian kriging in ArcGIS 10.5 (**Figure 3B**) (with Root Mean Squared Error of 0.003). **Figure 3B** shows that high NDVI values largely occurred in the north and east of the Gnangara region, which are mainly covered with pine and banksia plantations and pastures. Low NDVI were mainly found in the south and middle west of the Gnangara region where urban areas are located.

The groundwater resources in the Gnangara region are mainly from winter rain. A high proportion of the precipitation infiltrates into the soil and recharges local groundwater due to the sandy soils with a high permeability occurring in the study area (Western Australian Planning Commission, 2001). The groundwater resources are usually abstracted for public water supply purposes, private water use, park and garden watering, industrial and commercial use, horticultural and agricultural irrigation, and domestic use. Approximately 42% of the extracted groundwater is used for the public water supply (Department of Water, 2009a).

The Gnangara groundwater system comprises four different hydrogeological aquifers and the 3D Aquifer Visualization of the Gnangara region can be found in http://www.bom.gov.au/water/groundwater/explorer/3d-aquifer-visual.shtml. The shallowest, unconfined superficial aquifer (its top surface is commonly termed the Gnangara Mound) which stretches across the coastal

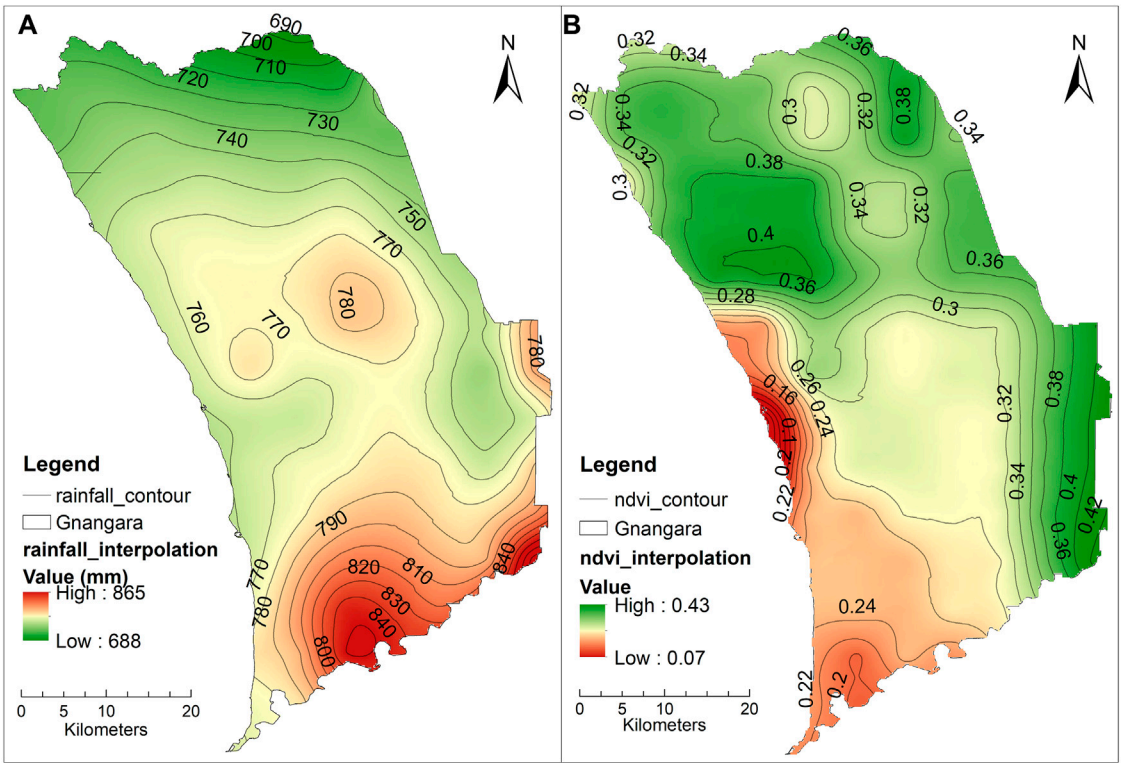

FIGURE 3 | Contour map of the rainfall **(A)** and NDVI **(B)** in the Gnangara region.

plain, with an average thickness of 45 m, a maximum thickness of 75 m and a depth to groundwater ranging from 3 to 20 m. From east to west, the sediments of the superficial aquifer generally vary from being predominantly clayey adjacent to the Darling Fault and Gingin Scarp, to a sandy succession in the central coastal plain area, and to sand and limestone within the coastal belt. The hydraulic properties of the superficial aquifer vary significantly depending on geology. The horizontal hydraulic conductivity increased from western and eastern margin to central with values of 0.1, 15, and 50 m/day in Guildford Clay, Bassendean Sand, Tamala limestone. The shallow, semi-confined Mirrabooka aquifer which is mainly occurs in the southern and eastern regions of the Gnangara region and varies in thickness to a maximum thickness of 160 m, and its horizontal hydraulic conductivity of this aquifer ranges from 4 to 10 m/day. The deep, partially confined Leederville aquifer below the superficial aquifer, extends beneath the entire coastal plain except in the north near the Swan Estuary and in the south-east corner, and is typically several hundred meters thick, consisting of discontinuous interbedded sandstones, siltstones and shales with horizontal hydraulic conductivity of the sandstone beds about 10 m/day and that of the siltstone and shale beds about 1×10^{-6} m/day. The Yarragadee aquifer is the deepest and major confined aquifer underlying the Perth Region and extending to the north and south within the Perth Basin. It is a multilayered aquifer often more than 2000 m thick, consisting of discontinuous interbedded sandstones, siltstones and shales with the average horizontal hydraulic conductivities range between 1×10^{-6} and 10 m/day., and it offers a vast storage and a robust supply of groundwater (Davidson and Yu, 2008; Department of Water, 2009a; Environmental Protection Authority, 2017). The Gnangara Mound developed because the vertical rainfall infiltration rate (about 1 m/day) exceeds the horizontal groundwater flow rate (ranges from 50 m/year to 1000 m/year) in the aquifer (Davidson, 1995; Davidson and Yu, 2008). Groundwater recharge of the superficial aquifer is highly variable and depends on the local rainfall, land use, and geological conditions (Davidson and Yu, 2008; Department of Water, 2009a). The superficial aquifer is predominantly recharged by rainfall in winter with some upward recharge, occurring from the underlying Leederville and Yarragadee aquifers (Department of Water, 2009a). Groundwater is naturally discharged into wetlands, rivers, springs and ocean, and groundwater undergoes vegetation transpiration and leaks into underlying aquifers during groundwater movement. Additional discharge is associated with groundwater abstraction (Davidson and Yu, 2008; Department of Water, 2009a).

Data Source

Climate Data

Climate data (1900–2017), including the daily precipitation and FAO56 potential evapotranspiration (FAO Penman-Monteith equation, Allen et al. (1998)), were extracted from the SILO Data Drill database created by the Queensland Government Department of Science, Information Technology and Innovation (DSITI). This dataset provides 0.05° gridded daily data and are constructed by

spatially interpolating the observational data with methods of a thin plate smoothing spline and ordinary kriging (Jeffrey et al., 2001) and can be accessed on the Internet at https://www.longpaddock.qld.gov.au/silo/. Minimum and maximum temperatures, solar radiation and vapor pressure prior to 1956 were interpolated by an anomaly interpolation technique (Zajaczkowski and Jeffrey, 2020). At each observation site, the acquired climate data exhibit a daily time-step and start at 20 years prior to the first observation date of the groundwater level.

Land Cover Data

The NDVI (Normalized Difference Vegetation Index) - high resolution gridded (0.05° * 0.05° grid) monthly NDVI dataset (1992–2017) used as the land cover change data in this study was obtained from the Australian Bureau of Meteorology website (http://www.bom.gov.au/metadata/catalogue/view/ANZCW0503900404.shtml). The satellite data originated from the Advanced Very High-Resolution Radiometer (AVHRR) instruments onboard the National Oceanic and Atmospheric Administration (NOAA) series of satellites operated by the US (http://noaasis.noaa.gov/NOAASIS/ml/avhrr.html). The NOAA-11, -14, -16 and -18 satellites were considered. The NDVI was used to examine the vegetation cover changes because the vegetation and non-vegetation area is easy to identify and historical land use information cannot be obtained. The NDVI value ranges from −1 to +1, where positive values indicate vegetation features and negative values indicate non-vegetation features (Gandhi et al., 2015).

Groundwater Monitoring Data

Groundwater monitoring data were retrieved from 325 observation bores in the unconfined superficial aquifer within the Gnangara region (**Figure 1**). The observation records are irregular and the data from 1992 to 2014 are used in this study. This dataset was provided by the Department of Water and Environmental Regulation, Government of Western Australia. The details of cite description can be downloaded for free from https://water.wa.gov.au/maps-and-data/monitoring/water-information-reporting.

Groundwater Abstraction

A groundwater abstraction dataset (2,324 pumping sites) collected from the different aquifers (mostly pertaining to from superficial aquifer) in the Gnangara region, from 1992–2014, was used in this study. These groundwater pumping data referred to the extraction for public and private water supply purposes. The groundwater abstraction data were obtained from the Department of Water and Environmental Regulation, Government of Western Australia.

METHODS

The Transfer Function Noise Model

The original TFN model was developed by von Asmuth et al. (2002) to simulate the groundwater level. This model includes three components: a deterministic component simulating the groundwater level due to the combined effect of all external factors, a residual series of the groundwater level and a constant component of the local drainage level. The Pearson type III distribution function was introduced by von Asmuth et al. (2002) to establish the precipitation and evapotranspiration impulse response functions. A revised version of the Pearson type III distribution function was adopted and five weaknesses in use for climatic stressors had been improved by Peterson and Western (2014). The first modification was to minimize the parameter covariance. The second modification was the calibration reproducibility was improved by undertaking a log 10 transformation of the parameters. The third modification was to reduce the impulse response function value at the start of the climate record. The fourth modification was to address the integration of the function from the first climate observation to negative infinity. The fifth modification was minimizing rounding errors in the numerical estimation of the integrals. Finally, **Eq. 1** details the linear TFN model comprising two components of precipitation and evaporation:

$$h_t = \int_{-\infty}^{t} P_\tau \theta(t-\tau)d\tau - \int_{-\infty}^{t} f_E E_\tau \theta(t-\tau)d\tau + n_t + d \quad (1)$$

where P_τ [LT^{-1}] and E_τ [LT^{-1}] are the daily precipitation and the daily potential evapotranspiration, respectively, and f_E [−] is a dimensionless parameter scaling the transfer function for application to the evapotranspiration signal. $\theta(t-\tau)$ is the impulse response function which was defined by von Asmuth and Bierkens (2005). n_t[L] is the residual series of groundwater level at time t, and is calculated by the observed groundwater head at time t subtracted from the modeled groundwater head at time t, d[L] is the constant component for local drainage level. To consider the groundwater level response to land cover change, von Asmuth et al. (2008) added a third integral to the time series model for the land cover change stressor, which involves a weighting the evapotranspiration integral by two parameters of the evaporation factor parameter f_L that depending on the soil and land cover and the historic fraction of vegetation clearing L_τ (**Eq. 2**):

$$h_t = \int_{-\infty}^{t} P_\tau \theta(t-\tau)d\tau - \int_{-\infty}^{t} f_E E_\tau \theta(t-\tau)d\tau - \int_{-\infty}^{t} f_L L_\tau E_\tau \theta(t-\tau)d\tau + n_t + d \quad (2)$$

However, the linear TFN model does not simulate the groundwater head well because of the nonlinearity between precipitation and groundwater head (Peterson and Western, 2014). Therefore, a vertically lumped soil moisture model (**Eq. 3**) was introduced into **Eq. 1**. The model is highly flexible and contains one to five parameters (KlemeŠ, 1986).

$$\frac{dS}{dt} = \mathrm{P}\left(1 - \frac{S}{\widehat{S_{cap}}}\right)^{\alpha} - \widehat{k_{sat}}\left(\frac{S}{\widehat{S_{cap}}}\right)^{\widehat{\beta}} - E_t\left(\frac{S}{\widehat{S_{cap}}}\right)^{\gamma} \quad (3)$$

where S [L] is the soil moisture at time t [T], $\widehat{S_{cap}}$ [L] is the antilog (log10)-transformed parameter related to the maximum soil moisture capacity S_{cap} [L], $\widehat{k_{sat}}$ [LT^{-1}] is the antilog (log10)-

transformed parameter related to the maximum vertical soil saturated conductivity k_{sat} [LT^{-1}], E_t [LT^{-1}] is the potential evapotranspiration rate at time t, α is a dimensionless parameter controlling the fraction of precipitation available for infiltration as the catchment wetness, $\widehat{\beta}$ is the antilog (log10) transformed dimensionless parameter controlling the free drainage as the catchment wetness, and γ is a dimensionless parameter controlling soil evapotranspiration.

In the process of transforming the precipitation and potential evapotranspiration time series data into the required TFN model input, the precipitation P_τ in **Eq. 1** can be replaced with the free drainage $\left(\frac{S}{\widehat{S_{cap}}}\right)^{\widehat{\beta}}$ or infiltration rate $\left(1-\frac{S}{\widehat{S_{cap}}}\right)^{\alpha}$, and the potential evapotranspiration E_t can be replaced with the soil evapotranspiration $\left(\frac{S}{\widehat{S_{cap}}}\right)^{\gamma}$ or groundwater potential evapotranspiration $E_t\left(1-\frac{S}{\widehat{S_{cap}}}\right)$. Two impulse response functions θ_P and θ_E for precipitation and evapotranspiration, respectively, were adopted in the time series model.

To consider for the groundwater level response to groundwater pumping, Shapoori et al. (2015a) and Shapoori et al. (2015c) added a third integral to the time series model (**Eq. 4**). Shapoori et al. (2015c) showed that models with and without groundwater evaporation produced similar results. Therefore, the second integral of groundwater evaporation was omitted in the models of this study.

$$h_t = \int_{-\infty}^{t}\left(\frac{S}{\widehat{S_{cap}}}\right)^{\widehat{\beta}}\theta_P(t-\tau)d\tau - \int_{-\infty}^{t}E_t\left(1-\frac{S}{\widehat{S_{cap}}}\right)\theta_E(t-\tau)d\tau - \int_{-\infty}^{t}Q_\tau\theta_{H\|F}(t-\tau)d\tau + n_t + d \tag{4}$$

where Q_τ [L^3T^{-1}] is the daily pumping rate. The response function $\theta_{H\|F}$ can either be the Hantush's equation for a leaky aquifer (Hantush, 1956; **Eq. 5**) or the Ferris and Knowles' well equation for a nonleaky aquifer (Ferris and Knowles, 1963; **Eq. 6**). The Ferris and Knowles' well equation without groundwater potential evapotranspiration was selected in this study due to the groundwater levels in most bores occurring deeper than 1 m according to tests conducted by Shapoori et al. (2015a):

$$\theta_H(t) = \frac{a}{t}exp\left(-\frac{b^2}{t}-c^2t\right) \tag{5}$$

$$\theta_F(t) = \frac{a}{t}exp\left(-\frac{b^2}{t}\right) \tag{6}$$

where a, b and c are parameters that only have a physical meaning if the basic Hantush assumptions are satisfied.

According to Peterson and Western (2014), there are 84 nonlinear TFN models based on 16 soil moisture models available within HydroSight. **Eqs 3**, **7** (Peterson and Western, 2014), **Eq. 8** (Peterson and Western, 2014), and **Eq. 9** (Siriwardena et al., 2011) are four model structures used in this study and is named as structure "cccc," "c1c1," "c0cc," "inf101." Structure cccc means all parameters are calibrated. Structure c1c1 means fixing $\alpha = \gamma = 1$. Structure c0cc means fixing $\alpha = 1$. Structure inf1c1 means fixing $\alpha = \gamma = 1$ *and* $\beta = 0$. Free drainage was chosen to transform the precipitation time series data into the required TFN model input. The Ferris and Knowles' well equation was selected as the response function.

$$\frac{dS}{dt} = P\left(1-\frac{S}{\widehat{S_{cap}}}\right) - \widehat{k_{sat}}\left(\frac{S}{\widehat{S_{cap}}}\right)^{\widehat{\beta}} - E_t\left(\frac{S}{\widehat{S_{cap}}}\right) \tag{7}$$

$$\frac{dS}{dt} = P - \widehat{k_{sat}}\left(\frac{S}{\widehat{S_{cap}}}\right)^{\widehat{\beta}} - E_t\left(\frac{S}{\widehat{S_{cap}}}\right) \tag{8}$$

$$\frac{dS}{dt} = P\left(1-\frac{S}{\widehat{S_{cap}}}\right) - E_t\left(\frac{S}{\widehat{S_{cap}}}\right) \tag{9}$$

Model Calibration and Evaluation

Following Shapoori et al. (2015a) and Shapoori et al. (2015c), the first 70% and last 30% of the observation records were designated as the calibration and evaluation periods, respectively. To identify individual parameter which produces the best possible fit to the hydrograph, the default calibration methods in the toolbox of Shuffled Complex Evolution with Principal Components Analysis - the University of California at Irvine (SP-UCI), developed by Chu et al. (2011), were used. SP-UCI is a global optimization algorithm based on the Shuffled Complex Evolution (SCE-UA) method (Duan et al., 1992) to address high-dimensional and complex problems.

Model Performance Assessment

The Akaike information criterion with correction (AICc) and Bayesian information criterion (BIC) (Burnham and Anderson, 2004) were used to account for the number of model parameters. The lower AICc and BIC indicates the better model. Moreover, the Nash-Sutcliffe efficiency (NSE) has been widely used to assess the goodness fit of a hydrograph (Ritter and Muñoz-Carpena, 2013; van der Spek and Bakker, 2017). Therefore, to assess the TFN model performance, the NSE (Nash and Sutcliffe, 1970) and unbiased NSE (Shapoori et al., 2015a) were adopted in the calibration and evaluation periods, respectively. NSE ranges from $-\infty$ to 1. The model is more accurate when the NSE value is closer to 1. At NSE = 1, the modelled data are a perfect match to the observed data (only if the measurements are free of errors). At NSE = 0, the modelled data are as accurate as the mean of the observed, and if NSE <0, the modelled data are less accurate than the mean observed data. Model performance can be evaluated as unsatisfactory if NSE ≤ 0.5, model performance can be evaluated as satisfactory if 0.50 < NSE≤0.65; model performance can be evaluated as good if

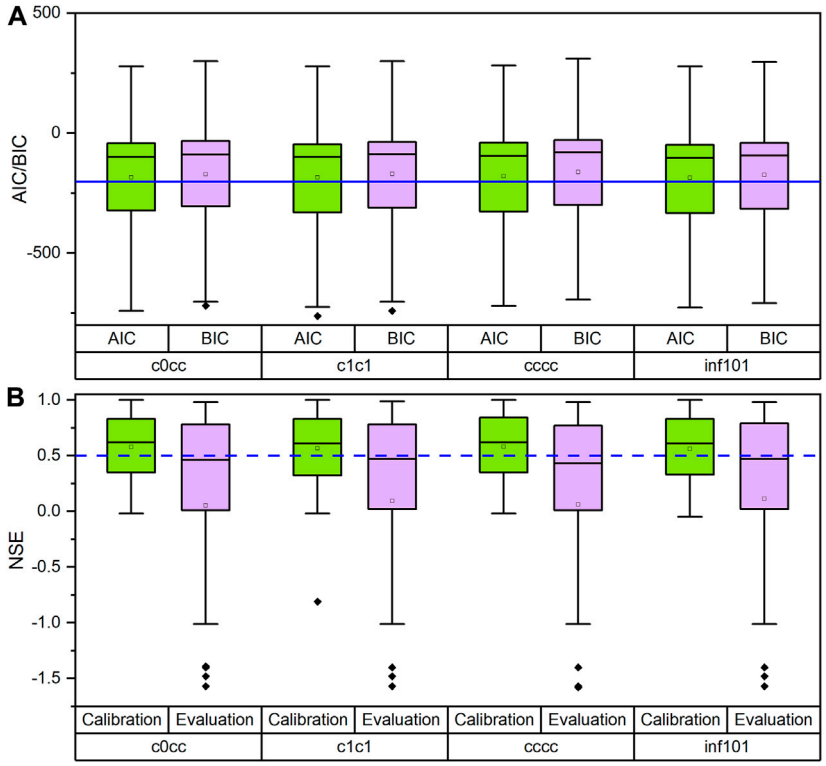

FIGURE 4 | Box plot of AICc, BIC **(A)** and NSE **(B)** results of the four soil model structures in the climate-only analysis. Note: Structure cccc means all parameters of k_{sat}, α, β, and γ are calibrated. Structure c1c1 means $\alpha = \gamma = 1$. Structure c0cc means $\alpha = 1$. Structure inf101 means $\alpha = \gamma = 1$ and $\beta = 0$.

0.65 < NSE≤0.75; model performance can be evaluated as very good if 0.75 < NSE≤0.1 (Moriasi et al., 2007; Moriasi et al., 2015).

Radius of Influence

Based on the current data on the study area, the Dupuit equation (Dupuit, 1863) was selected to calculate the radius of influence of pumping wells. In the confined aquifer, the Dupuit equation (**Eq. 10**) was used to calculate the radius of influence of pumping wells. In the unconfined aquifer, the Dupit equation (**Eq. 11**) (Dupuit, 1863) was used to calculate the radius of influence of pumping wells.

$$r = 10^{\frac{s_1 \log_{10} r_2 - s_2 \log_{10} r_1}{(s_1 - s_2)}} \quad (10)$$

$$r = 10^{\frac{s_1 (2H - s_1) \log_{10} r_2 - s_2 (2H - s_2) \log_{10} r_1}{(s_1 - s_2)(2H - s_1 - s_2)}} \quad (11)$$

where r [m] is the radius of influence of a pumping bore, s_1 and s_2 [m] are the drawdowns in the observation bores, r_1 and r_2 [m] are the distances between the observation and pumping bores, and H [m] is the thickness of the aquifer. In this study, the thickness of the unconfined aquifer was determined according to Smith and Pollock (2010).

RESULTS

Model Structure Comparison

To determine the most applicable model structure, four soil moisture model structures (structures cccc, c1c1, cocc and inf101) were tested in all bores for climate-only analysis. For AICc and BIC, there are not obvious differences between these four model structures, but structure cccc showed worse than other three model structures (**Figure 4A**). The climate-only analysis means the groundwater level is considered only influenced by rainfall. The NSE values of 325 bores using these four soil moisture models are listed in a box plot is shown in **Figure 4B**. During the calibration period, model structure inf101 performed the worst, with the lowest mean, median values of the NSE. The model structure cccc performed the best with the highest mean value of NSE in calibration but performed the worst with the lowest mean value of NSE. The model structure c0cc performed as good as model structure c1c1. Therefore, either model structure c1c1 with less parameters than c0cc was appropriate in this study. In this study, model structure c1c1 (**Eq. 7**) was chosen to model all the bores in the Gnangara region in all subsequent groundwater level analyses.

Model Performance

Climate Only

Sixty percent of the bores in climate-only (C) analysis during the calibration period produced an acceptable performance (NSE >0.5), of which 36% of the bores performed very good, 10% of the bores performed good and 14% of the bores performed satisfactorily. In addition, 40% of the bores performed unsatisfactorily. During the evaluation period, 48

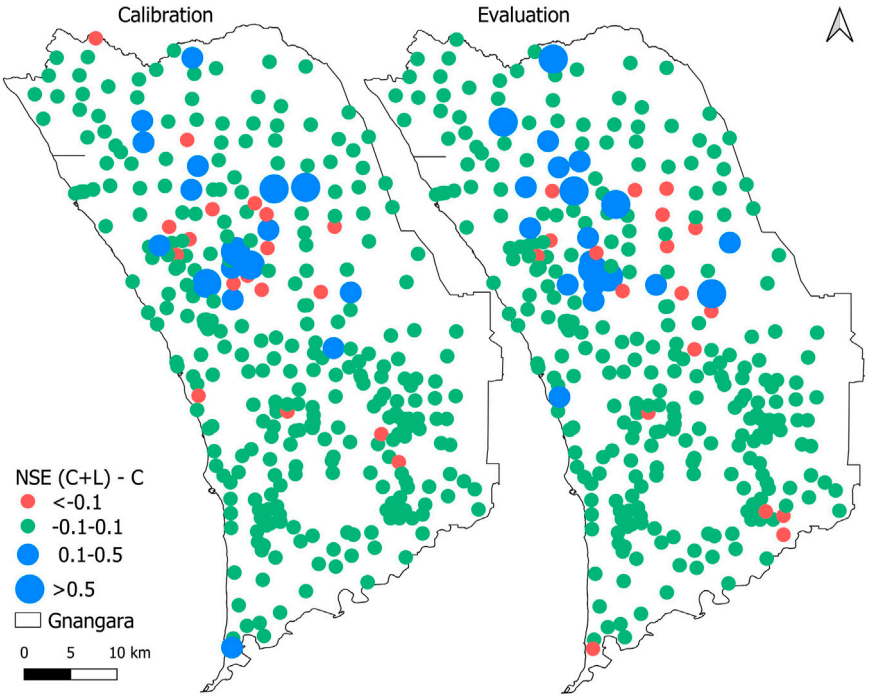

FIGURE 5 | Difference in NSE between the climate-only (C) analysis and the climate and land cover (C + L) analysis.

and 52% of total bores yielded an acceptable and unsatisfactory groundwater head modelling performance, respectively.

Spatially, bores producing an acceptable model performance in climate-only analysis predominantly occurred in the southeastern Gnangara, followed by the northern Gnangara, and an unsatisfactory performance was predominantly produced in central-western and northwestern Gnangara and the coastal area of the Gnangara region during the calibration period (**Supplementary Figure S2**). The spatial distribution of model performance during the evaluation period is similar with that during the calibration period. However, an unsatisfactory performance increased in south area of the Gnangara region (**Supplementary Figure S2**).

Climate and Land Cover

The model performance was improved during both the calibration and evaluation periods when the NDVI was added to the TFN model. The acceptable performance increased from 60 to 62%, especially the good and satisfactory performance level with an improvement of 2% during the calibration period. In addition, the unsatisfactory performance level was reduced by 2% during the calibration period. However, the acceptable performance level decreased from 48 to 47% during the evaluation period.

Among the 325 bores in the Gnangara region, an acceptable performance was largely attained in the south, southeast and north of the Gnangara region during the calibration and evaluation periods in the climate and land cover (C + L) analysis (**Supplementary Figure S2**). An unsatisfactory performance during the calibration and evaluation periods was predominantly distributed is mainly attained in the central-western and northwest of the Gnangara region (**Supplementary Figure S2**).

Figure 5 shows the spatial distribution and magnitude of the NSE improvement considering the land cover data were considered. The improvement was calculated by subtracting the NSE value of the climate-only analysis from the NSE value of the climate and land cover analysis. The model performance had decreased when the NSE change value was smaller than −0.1. The model performance remained stable when the NSE change value varied between −0.1 and 0.1. The model performance had improved when the NSE change value was larger than 0.1. During the calibration period, the NSE value at 17 bores had improved with the NSE change values ranging from 0.1 to 1.85 and 18 bores had been reduced by values ranging from −8.62 to −0.1. Most of the bores (290) remained stable, with NSE change values ranging from -0.1 to 0.1. During the evaluation period, the NSE value at 21 bores had improved with NSE change values ranging from 0.1 to 0.85, and at 19 bores, the performance had decreased with NSE change values ranging from -0.52 to −0.1. Most of the bores (285) remained stable, with NSE change values ranging from −0.1 to 0.1. In calibration and evaluation period, the NSE improved mainly at bores in northern Gnangara and the NSE declined mainly at bores in the northern parts of the Gnangara region.

Climate and Groundwater Pumping

According to the empirical Dupuit equation, the radius of influence of the pumping wells in the confined and unconfined aquifers ranged from 708 to 9,303 m, and 1,302 pumping sites were determined to influence 271 observation

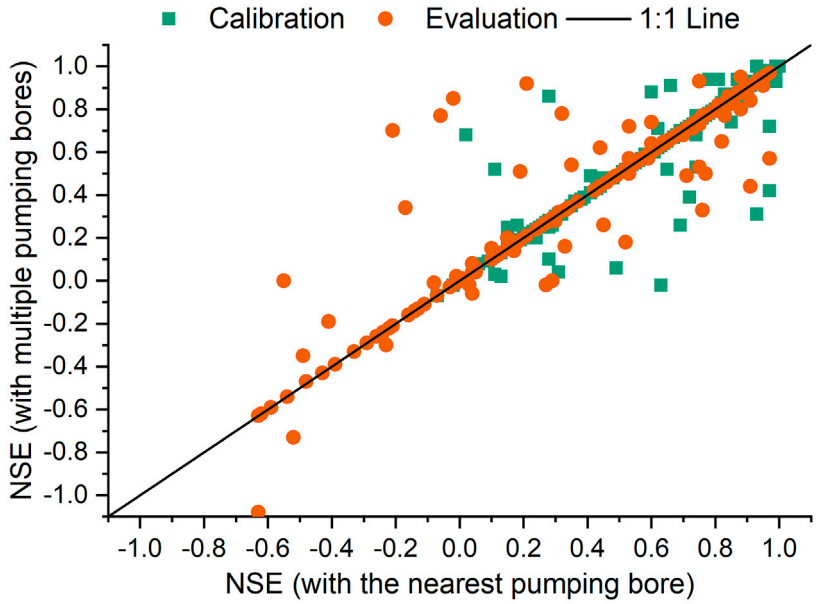

FIGURE 6 | Comparison NSE results between the climate and pumping analysis with the nearest pumping bore and multiple pumping bores.

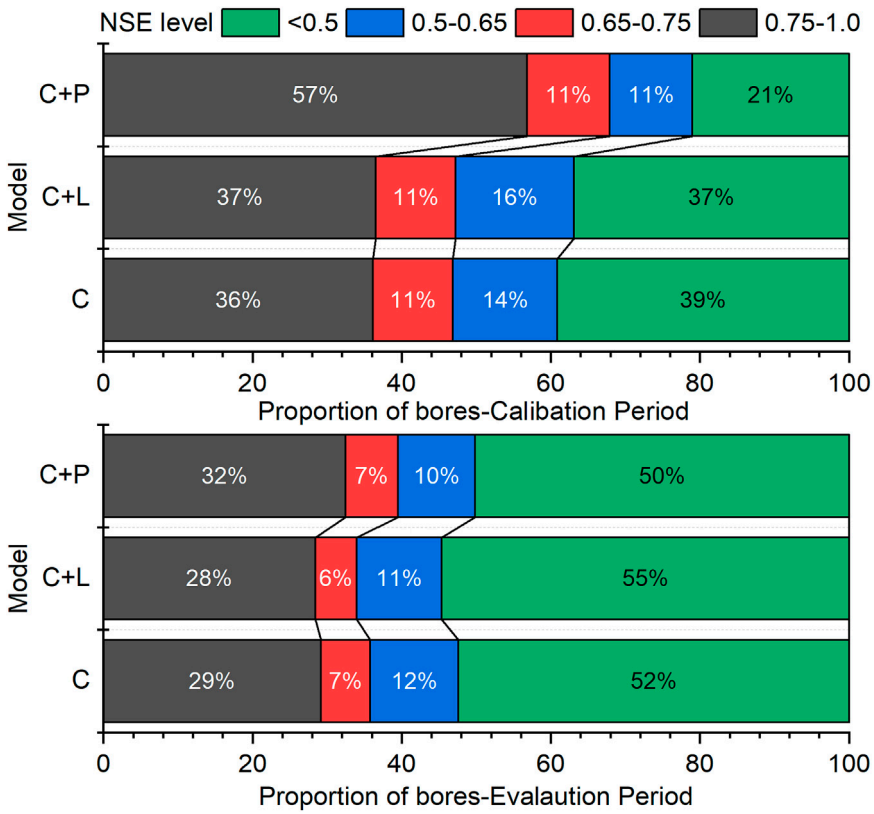

FIGURE 7 | Proportion of bores with different NSE levels of the climate-only (C) analysis, climate and land cover (C + L) analysis, and climate and pumping (C + P) analyses.

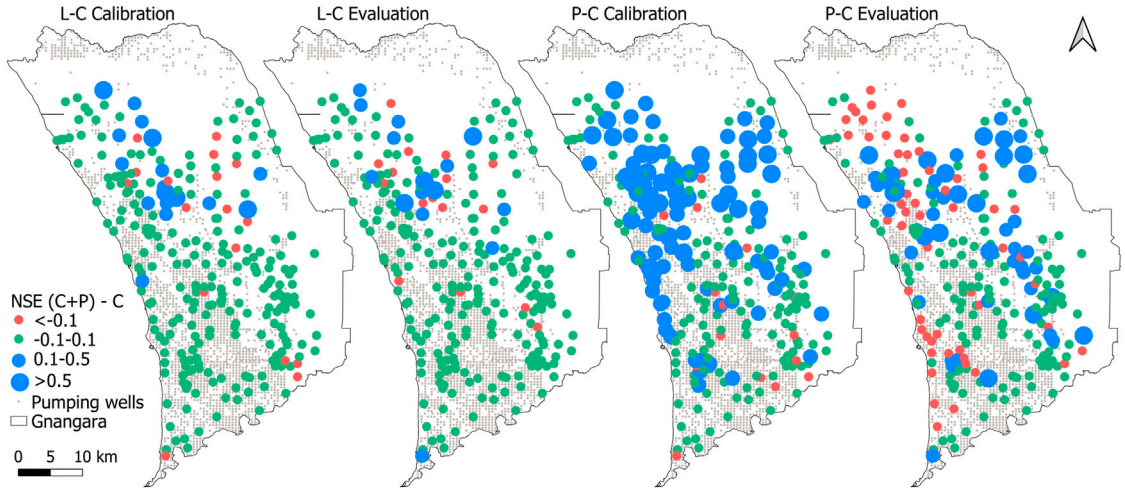

FIGURE 8 | Improvement in NSE of the climate and land cover, and the climate and pumping analyses.

sites. At these 271 observation sites, the groundwater pumping stressor was included to assess its contribution to the groundwater level changes. The corresponding modelling results of the C analysis and C + L analyses were separated and compared to climate and pumping analysis (C + P) results during the calibration and evaluation periods.

To validate the pumping well influence on the groundwater head, models with multiple bores and only the nearest bore were applied. The NSE of these two models are shown in **Figure 6**. During both the calibration and evaluation periods, the models containing one bore and multiple bores did not exhibit notable differences, but the model with one bore attained a slightly better performance than the model with multiple bores. Therefore, the model with one bore was applied in the climate and pumping stressor analysis.

During the calibration period, 60% of the bores produced an acceptable modelling performance, and 40% of the bores produced an unsatisfactory modelling performance in the C analysis (**Figure 7**). The acceptable model performance level had been improved by 3 and 19% in the C + L and C + P analyses, respectively. Especially for the very good performance rate had improved by 21% in the C + P analyses (**Figure 7**). Moreover, unsatisfactory model performance rate has been reduced by 2 and 18% for C + L and C + P analysis. During the evaluation period, the acceptable model performance rate increased slightly from 48% in the C analysis to 50% in the C + P analysis. In the C + L analyses, the acceptable model performance rate was even reduced by 3% (**Figure 7**). In general, the pumping analysis results were slightly better than the land cover analysis results during both the calibration and evaluation periods.

Among the 271 bores in the Gnangara region, an acceptable and unsatisfactory model performance predominantly occurred in the south and north (coastal region), respectively, of the study area in the C analysis (**Supplementary Figure S3**). In central and north area, the model performance level increased when the pumping stressor were considered (**Supplementary Figure S3**). The model performance level was improved at a few bores in north area for C + L analysis. During the evaluation period, the unsatisfactory performance level was much higher that during the calibration period, especially in the bores of central, coastal and north part (**Supplementary Figure S3**).

Figure 8 shows the spatial distribution and magnitude of the NSE improvement when the land cover and pumping data were considered. The improvement was calculated by subtracting the NSE value of the climate-only analysis from the NSE value obtained when the land cover and pumping data were included in the model, respectively. During the calibration period, most of the bores (140) remained stable, with NSE values ranging from −0.1 to 0.1. At 18 bores, the performance improved with NSE change values ranging from 0.1 to 0.85, and at 17 bores, the performance decreased with NSE change values ranging from −0.52 to −0.1 in the C + L analyses. During the evaluation period, 15 bores with an increased NSE value were found, with the NSE improvement ranging from 0.1 to 1.85, while 16 bores with a reduced NSE value were found with NSE reduction ranging from −0.1 to -8.62 during the calibration period. And 240 bores keep a stable NSE values. In the C + P analysis, the number of bores with an increased NSE in both the calibration (98, range: 0.1–0.98) and evaluation periods (59, range: 0.1–27.27) was larger than that in the C + L analysis. Moreover, the number of bores with an NSE reduction increased to 59 during the evaluation periods (range: 9.82~−0.1) compared to that during the calibration (15 bores) period. The bores with an NSE improvement in the C + L analysis were largely distributed in the upper part of the bores area during the calibration and evaluation periods (**Figure 8**). The bores with an NSE reduction and increase in the C + L analysis were mainly foundin north area of the Gnangara region. In the C + P analysis, the areas in the southwestern Gnangara with a high concentration of pumping wells, the model performance level did not exhibit a notable improvement. Areas with an NSE

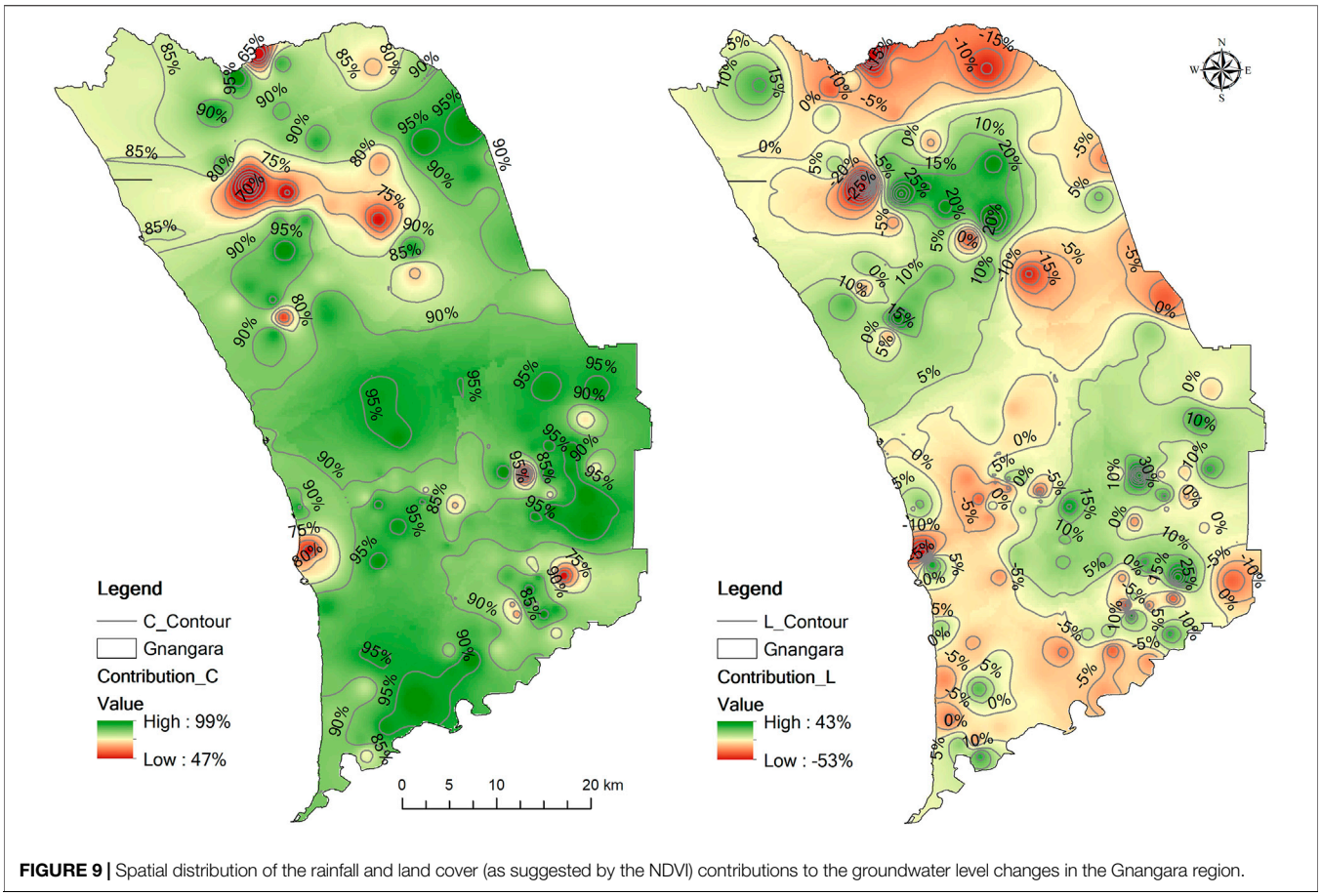

FIGURE 9 | Spatial distribution of the rainfall and land cover (as suggested by the NDVI) contributions to the groundwater level changes in the Gnangara region.

improvement primarily occurred in the north and central area of the Gnangara region.

Drivers' Contribution

Contribution in Space

To determine the spatial distribution of the contribution of each stressor to the groundwater level changes, the multiyear average rainfall, land cover, and pumping contribution rate of bores with NSE exceeding 0.5 (acceptable model performance) during both the calibration and evaluation periods were used to generate the spatial distribution of the contribution rate in the Gnangara region by the Inverse Distance Weighted method in ArcGIS 10.1 (**Figures 9**, **10**).

As shown in **Figure 9**, the multi-year mean contributions of rainfall and land cover to the groundwater level changes ranged from 44 to 99% and from -53 to 43%, respectively. A large rainfall contribution rate was mainly found in central and southern Gnangara region. In contrast to the rainfall recharge contribution, the land cover contribution can either be positive or negative. A positive land cover contribution (green area) was largely distributed in upper central and southeastern Gnangara region. In certain areas, such as the southwestern and central-western areas (light yellow area), the land cover contribution was very small. In the south-western, north margin, central-eastern parts (red areas) of Gnangara region, the contribution was negative.

As shown in **Figure 10**, the multi-year mean contributions of rainfall and pumping to the groundwater level changes ranged from 1 to 99% and from −1% to −99%, respectively. Large rainfall recharge contribution to the groundwater level changes mainly occurred in the southwestern and northwestern parts of the Gnangara region. In contrast to the rainfall recharge contribution, the pumping contribution to the groundwater level changes was negative. The bores most affected by pumping occurred in the north-eastern parts of the Gnangara region.

Contribution in Time

Over time, the multi-site mean contributions of climate change and land cover on groundwater level were 90 and 2% with ranges of 89–90% and 2.1–2.3%, respectively. The multi-site mean contributions of climate change and pumping were 77% and -23% with ranges of 68–99% and −1%~−32%, respectively. In the whole Gnangara region, the trend of the rainfall contribution slightly decreased from 1992 to 2014 (**Figure 11A**). The land cover contribution rate was stable from 1992 to 2014. The pumping contribution rate decreased from 1992 to 2014. However, the pumping contribution rate is negative, that means the pumping activities lowers the groundwater decline. Moreover, the trend of the contribution of factors on groundwater level were calculated. Seventy-four percent of the

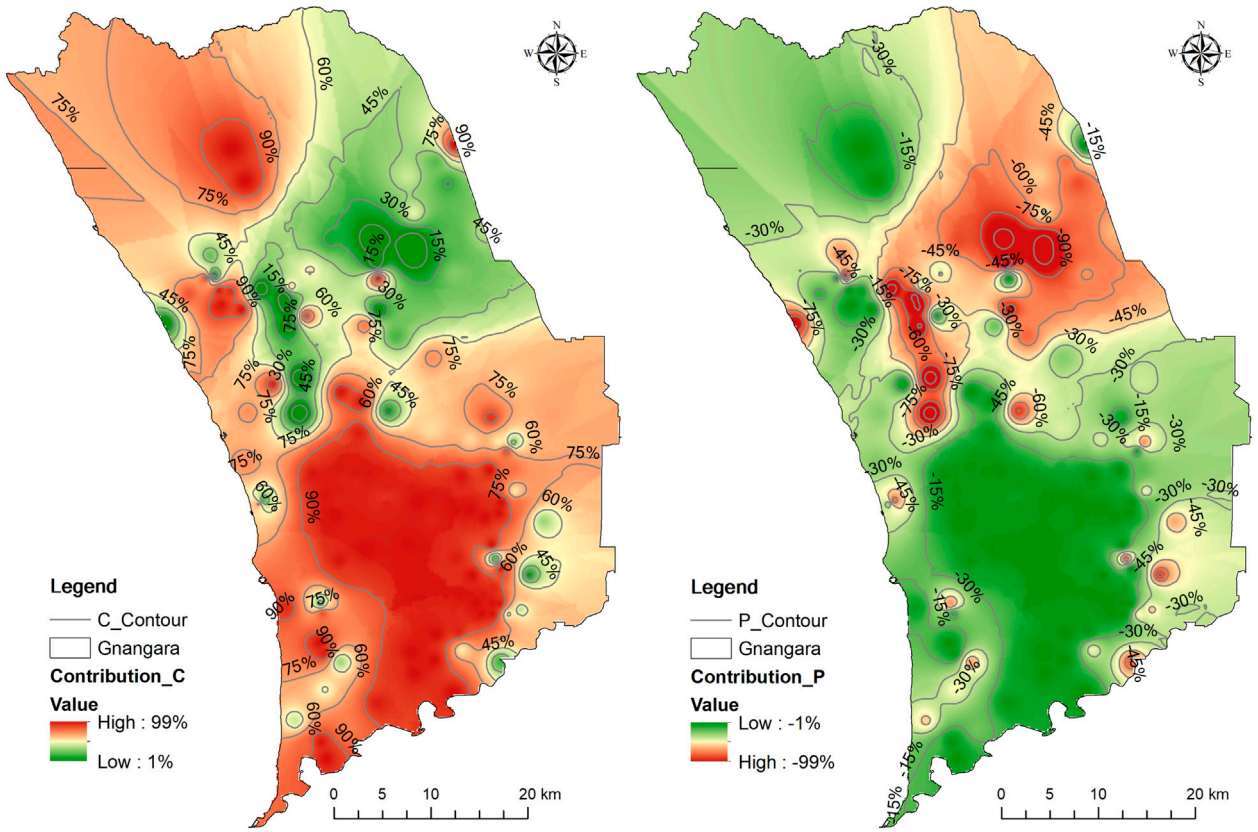

FIGURE 10 | Spatial distribution of the rainfall and pumping contributions to the groundwater level changes in the Gnangara region.

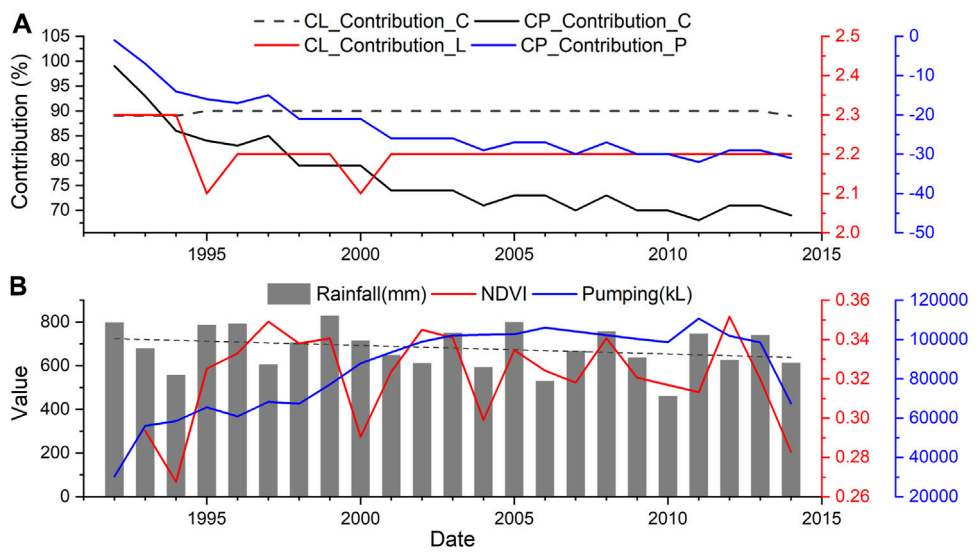

FIGURE 11 | Contribution rates in the climate-only (C), climate and land cover (C + L), and climate and pumping (C + P) analyses to the groundwater level changes **(A)**. Rainfall, NDVI and groundwater pumping in the Gnangara region **(B)**.

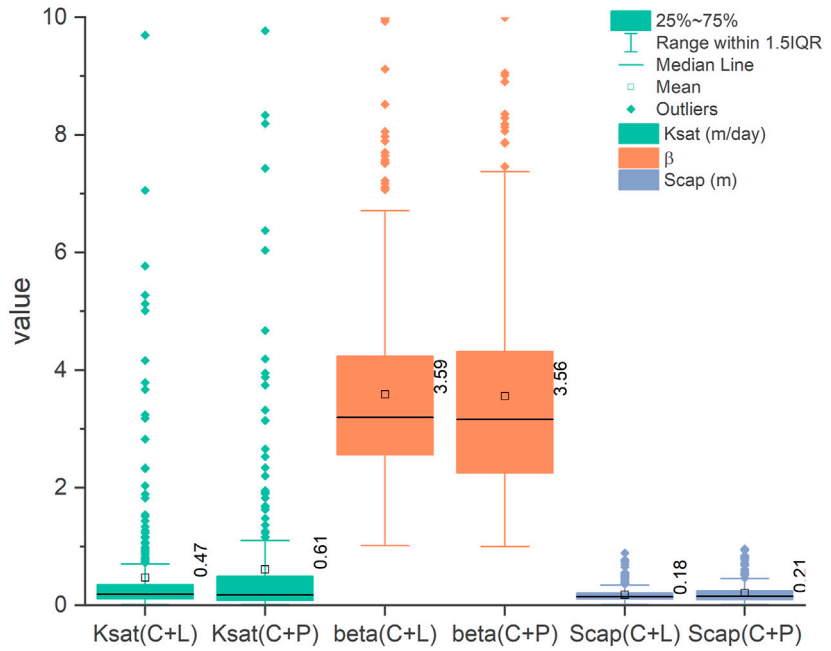

FIGURE 12 | Box plot of the calibrated parameters of the model.

rainfall contribution rate trend showed decline (<=−0.01) over time and 26% of the rainfall contribution rate trend showed stable (0) for C + L analysis. Eighteen percent of the land cover contribution rate trend showed decline over time, 70% of the land cover contribution rate trend showed stable, and 12% of the land cover contribution rate trend showed increase (≥0.01) for C + L analysis. Sixty percent of the rainfall contribution rate trend showed decline over time and 40% of the rainfall contribution rate trend showed stable for C + P analysis. Fifty-eight percent of the pumping contribution rate trend showed decline over time, 42% of the pumping contribution rate trend showed stable for C + P analysis.

Model Parameters

The variability of critical fitted parameters of the model was presented in a box plot (**Figure 12**) and the spatial distribution of the fitting parameters was presented in **Figure 13**. **Figure 12** showed that the Ksat, *β*, and Scap between C + L and C + P analysis is slight. Parameter of Ksat (maximum vertical conductivity) ranged from 0.01 to 10 m/day with mean of 0.47 and 0.61 m/day for C + L and C + P analysis, respectively. Parameter of β(power term for drainage rate) ranged from 1 to 10 with mean of 3.59 and 3.56 for C + L and C + P analysis, respectively. Parameter of Scap (soil moisture storage capacity) ranged from 0.01 to 1 m with mean of 0.18 and 0.21 m for C + L and C + P analysis, respectively. Spatially, **Figure 13** showed about 60% bores has the Ksat of 0.01–0.2 m/day for both C + L and C + P analysis. And larger Ksat (more than 2 m/day) was found in the northern Gnangara for C + L analysis and in both southern and northern Gnangara for C + P analysis. Parameter of β in spatial showed slight difference between C + L and C + P analysis and the larger β is mainly occurred in the north area of the Gnangara region. 84 and 76% bores has the Scap of 0.01–0.2 m. The bores with Scap larger than 0.4 m is dispersedly distributed in the study area.

DISCUSSION

Groundwater Hydrograph Decomposition Evaluation

The spatial distribution of the acceptable model performance level (in the southern Gnangara) in the climate-only analysis was consistent with the area with a high rainfall. Additionally, the areas with a large rainfall recharge contribution were largely found in the area with a high rainfall (**Figure 3**), while a small rainfall recharge contribution occurred in the area with a low rainfall. The rainfall always keeps higher contribution (47–99 and 1%–99%) than land cover (−53–43%) and groundwater pumping (−1% to −99%) contribution after the NDVI and groundwater pumping were included into the model, respectively. Generally, the area rainfall more than 770 mm have the contribution rate more than 75%. These results indicated that the spatial distribution of the rainfall recharge contribution to groundwater was consistent with the rainfall distribution based on a comparison of the rainfall recharge contribution graph (**Figures 9**, **10**) and rainfall graph were compared (**Figure 3**). Temporally, the rainfall contribution rate continually decreased and were higher than land cover and pumping contribution rate (**Figure 11A**), which is closely related to the rainfall reduction over time (**Figure 11B**). All of the above results indicate that the climate (precipitation) is the main factor influencing the

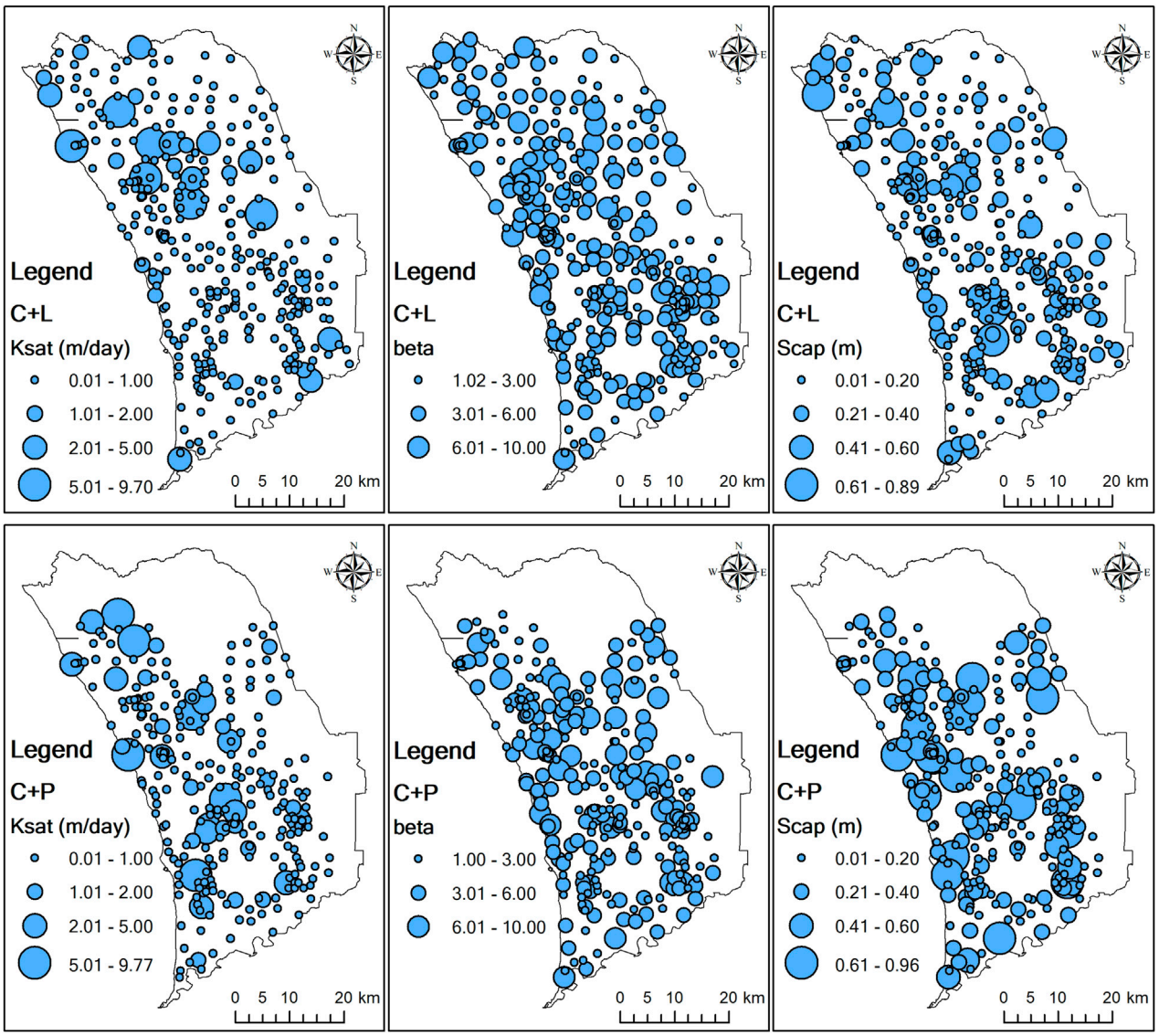

FIGURE 13 | Spatial distribution of the calibrated parameters of the model.

groundwater level in the Gnangara region (dominating the groundwater level changes). Yesertener (2005) and Gallardo (2013) also proposed that climate change is the primary factor influencing the groundwater level decline in the Gnangara region based on the cumulative deviation from main rainfall (CDFM) analysis method. This finding has been verified, and the contribution of climate change to the groundwater level changes in time and space have been quantified.

The model performance was improved at some bores in northern Gnangara when the land cover data were added to the model, indicating that the land cover change also exerts an impact on groundwater level changes. However, the land cover contribution on groundwater level was stable over time and the contribution rate kept at 2%. Although the land cover had changed in some area over time, the NDVI changes for the whole region is little (**Figure 11B**). This demonstrated that the land cover changes had influence on local long-term groundwater level changes, but the influence is limited and is stable over time. The locations of the sites with an improved model performance generally agreed with the vegetated area in the northern Gnangara region (suggested by high NDVI) (**Figure 3B**). In the central of the northern Gnangara region, the land cover contribution rate was higher and the NDVI was lower than surrounding areas, indicating a negative relationship between land cover changes and groundwater level changes. These indicated that the groundwater level in the northern Gnangara region was closely related to the local vegetation conditions. Although the land cover contribution rate is positive in central of the northern Gnangara region, the positive trend over time was decreasing because of the increased areas of conservation and

natural environments, especially the minimal use area (Bureau of Rural Sciences, 2006; Australian Bureau of Agricultural and Resource Economics and Sciences, 2018). In the margin of northern Gnangara region, the land cover changes lower the groundwater level due to the land use of grazing modified pastures reduced and the other minimal land use increased (Bureau of Rural Sciences, 2006; Australian Bureau of Agricultural and Resource Economics and Sciences, 2018). The plantation forests area reduced from 1992 to 2018 (Bureau of Rural Sciences, 2006; Australian Bureau of Agricultural and Resource Economics and Sciences, 2018). However, in the plantation forests area in land use map 2018, the land cover contribution rate is up to −53%. This is likely closely associated with the high density of pine plantations in these areas (Yesertener, 2007; Gallardo, 2013). In the southwestern area of the Gnangara region, urban use is the main land use, but the contribution is negative, that means other factors such as groundwater abstraction influenced the groundwater level.

The model performance was significantly improved after the pumping data were added to the model. In the south area of the study area, the model performance remained high. In the western part of the study area, which is the coastal region, the model performance remained unsatisfactory, although the land cover or pumping data were included. In the coastal areas, the climate, land cover and pumping exert limited impacts on the groundwater level changes, and other factors such as seawater intrusion, may impose major impact on the groundwater level changes. The limited changes in the groundwater level along the coast also occur due to the extremely high hydraulic conductivity of the Tamala limestone and proximity to the discharge zone (Costall et al., 2020). Other possibility of limited groundwater level changes may be from the boundary conditions (Morgan et al., 2012). As the C, C + L, and C + P analysis results indicated, the model performance was improved when the pumping data were considered, especially during the calibration period. However, the model performance was slightly improved when the land cover data were considered, and the performance at some sites was reduced. Moreover, the large pumping contribution (negative) to the groundwater level changes occurred in the northeast of the Gnangara region and did not always occur near the pumping sites, indicating that the distance between the bores and pumping wells and the density of the pumping wells are not critical elements in the determination of the pumping contribution to the groundwater level changes. In the southwestern Gnangara, the contribution rate mainly ranged between −15% and −40% (**Figure 10**). However, the groundwater pumping contribution continually increased over time due to the sustained groundwater abstraction (**Figure 11B**). It is obvious that groundwater pumping is highest in the 2011, and the pumping contribution on groundwater level is also highest with contribution value of −32% (**Figure 11B**). Results indicated that sustained groundwater pumping over time has a significant influence on groundwater level decline. Depletion of groundwater levels is a global phenomenon and is defined as long term water level declination caused by sustained groundwater pumping over time (Tularam and Krishna, 2009). More attention should be paid to manage the groundwater pumping activities to ensure the sustainable use of groundwater.

The fitted parameter of the maximum vertical conductivity of the model in this study has a value range 0.01–9.8 m/day and the maximum vertical conductivity of most of the bores is concentrated in range of 0.01–2 m/day. Salama et al. (2005) and Department of Water (2009b) calculated the hydraulic conductivity in the Gnangara, ranging from 0.56 to 6.38 m/day and from 0.01 to 5 m/day, respectively. The similar results indicated the results of fitted parameters of the maximum vertical conductivity is accepted and the results of the model are credible. Moreover, the fitted parameter of Ksat and Scap showed slight difference in C + L and C + P analysis, indicating that the maximum vertical conductivity and soil moisture storge capacity are important parameter of the model.

Uncertainties and Limitations

The approach adopted in this study is based on various assumptions and has limitations, which constrain the results of the groundwater hydrograph decomposition. It should be noted that this method assumes that the drivers (climate, land cover, and groundwater pumping) of the groundwater level changes are independent of each other, and the land cover and pumping were added into the model, respectively. However, the considered drivers interact with each other, which may complicate the evaluation results. Climate change (rainfall change) could lead to changes in vegetation, thus affecting groundwater recharge, and groundwater pumping may lead to groundwater level changes, thereby negatively impacting vegetation (Şen, 2015). Many factors influence groundwater level changes, but only three major drivers were considered to establish the model in this study. Other drivers such as bush fires, pine clearing, and groundwater evaporation, were not examined. And the surface water-groundwater interaction is also an important cause of groundwater level changes in many areas (Wang et al., 2014). Moreover, this model assumed that the aquifer is homogeneous, but the thickness, permeability and water-bearing structure of the aquifer affect the accuracy of the modelling results.

In this study, model was constructed for each individual observation bore of the Gnangara region. Then, for the whole Gnangara region, the groundwater level changes and its main factors can be assessed by interpolating the results of each bore. In the model construction, an optimal model structure fitted for the study area was used for each model to reduce the model running time and improve the model operation efficiency. In fact, one model structure cannot ensure the satisfactory model results of each site. Therefore, model performance in spatial is not always satisfactory. However, in the process of interpolation, only the satisfactory model performance was used to reduce the errors in spatial.

Other limitations arise from the dataset used. NDVI was selected as the representation of the land cover impact on the groundwater level changes. The NDVI may not be accurate enough to express all of the land cover situation. However, the vegetation and non-vegetation area is easy to identify and

historical land use information cannot be obtained. Furthermore, the groundwater level data at certain sites were fragmented or the number of observations was insufficient, but the established models allowed the simulation of irregular water level observations.

CONCLUSION

Understanding and interpreting changes in groundwater level is essential for long term management of both a groundwater resource and urban development. The present study quantitatively clarifies the impacts of three drivers, namely, climate change, land cover change and groundwater pumping (for public and private use) on the long-term groundwater level changes with HydroSight model. And the unconfined aquifer of Gnangara region in Western Australia was used as a case study.

Based on the three established independent models (climate-only analysis, climate and land cover analysis, and climate and pumping analysis models), climate always plays the most important role and positively contributes to the observed groundwater level changes. And groundwater decline in this region is mainly caused by the reduction in rainfall recharge over time. In the whole region, the contribution of the groundwater pumping to groundwater level decline is larger than that of land cover change. Temporally, from 1992 to 2014, the contribution of rainfall on the groundwater level of the Gnangara region decreased because the rainfall decreased over time. The mean pumping contribution rate is −23%, and the impact of groundwater pumping on the groundwater level decline continually increased from 1992 to 2014 because of the sustained groundwater pumping. The land cover changes had influence on long-term groundwater level changes, but the influence is limited and is stable over time with contribution rate of 2%. Spatially, in the southern Gnangara region, the groundwater level changes were mainly influenced by rainfall and pumping activities. In the northern Gnangara region, the groundwater level changes were influenced by the combination of rainfall, land cover and groundwater pumping.

The results of this study suggest that the improved groundwater hydrograph decomposition method is effective and can be easily applied in other regions due to its highly flexible. And this method improved the efficiency of data utilization, especially for the region which the groundwater head record is irregular. And the best-fit model for a certain study area can be obtained by trying different model structures. The findings of this study have important implications for research on the influence of various drivers on groundwater level changes and also provide notable guidance for local governments to rationally allocate and utilize groundwater resources. In areas where the groundwater level is mostly affected by groundwater pumping, other water resources should be utilized, such as rainfall runoff collected during the wet season for park irrigation, seawater desalinized, and surface water quality improved, while the groundwater abstraction reduction could ease the stress resulting from groundwater level decline.

DATA AVAILABILITY STATEMENT

The original contributions presented in the study are included in the article/**Supplementary Material**, further inquiries can be directed to the corresponding author.

AUTHOR CONTRIBUTIONS

FK contributed to the conceptualization, ideas, methodology, software programming, validation, original paper draft and visualization. JS supervised the project, helped results analysis, contributed to financial support. RSC, OB, DS and JPP contributed to study area definition, methods selection and results discussion. All authors contributed to manuscript revision, read, and approved the submitted version.

FUNDING

This study was jointly supported by the Key Research and Development Program of Shaanxi (Grant No. 2019ZDLSF05-02).

ACKNOWLEDGMENTS

The first author acknowledges the Chinese Scholarship Council for supporting his Ph.D. study at CSIRO Land and Water.

SUPPLEMENTARY MATERIAL

The Supplementary Material for this article can be found online at: https://www.frontiersin.org/articles/10.3389/fenvs.2021.736400/full#supplementary-material

REFERENCES

Abiye, T., Masindi, K., Mengistu, H., and Demlie, M. (2018). Understanding the Groundwater-Level Fluctuations for Better Management of Groundwater Resource: A Case in the Johannesburg Region. *Groundwater Sustainable* 7, 1–7. doi:10.1016/j.gsd.2018.02.004

Allen, R. G., Pereira, L. S., Raes, D., and Smith, M. (1998). Crop Evapotranspiration-Guidelines for Computing Crop Water Requirements-FAO Irrigation and Drainage Paper 56. *Fao. Rome* 300 (9), D05109.

Australian Bureau of Agricultural and Resource Economics and Sciences (2018). *Catchment Scale Land Use Mapping for Western Australia 2018*, Canberra, Australia: Department of Agriculture and Water Resources: Australian Bureau of Agricultural and Resource Economics and Sciences. [Dataset].

Bekesi, G., McGuire, M., and Moiler, D. (2009). Groundwater Allocation Using a Groundwater Level Response Management Method-Gnangara Groundwater System, Western Australia. *Water Resour. Manage.* 23 (9), 1665–1683. doi:10.1007/s11269-008-9346-5

Bureau of Rural Sciences (2006). *1992/93 Land Use of Australia, Version 3*, Canberra: Bureau of Rural Sciences. [Dataset]

Burnham, K. P., and Anderson, D. R. (2004). Multimodel Inference. *Sociol. Methods Res.* 33 (2), 261–304. doi:10.1177/0049124104268644

Carbon, B. A., Roberts, F. J., Farrington, P., and Beresford, J. D. (1982). Deep Drainage and Water Use of Forests and Pastures Grown on Deep Sands in a Mediterranean Environment. *J. Hydrol.* 55 (1), 53–63. doi:10.1016/0022-1694(82)90120-2

Cheng, L., Zhang, L., Chiew, F. H. S., Canadell, J. G., Zhao, F., Wang, Y.-P., et al. (2017). Quantifying the Impacts of Vegetation Changes on Catchment Storage-Discharge Dynamics Using Paired-Catchment Data. *Water Resour. Res.* 53 (7), 5963–5979. doi:10.1002/2017WR020600

Chu, W., Gao, X., and Sorooshian, S. (2011). A New Evolutionary Search Strategy for Global Optimization of High-Dimensional Problems. *Inf. Sci.* 181 (22), 4909–4927. doi:10.1016/j.ins.2011.06.024

Costall, A. R., Harris, B. D., Teo, B., Schaa, R., Wagner, F. M., and Pigois, J. P. (2020). Groundwater Throughflow and Seawater Intrusion in High Quality Coastal Aquifers. *Sci. Rep.* 10 (1), 9866. doi:10.1038/s41598-020-66516-6

Davidson, W. A., and Yu, X. (2008). "Perth Regional Aquifer Modelling System (PRAMS) Model Development: Hydrogeology and Groundwater Modelling," in *Hydrogeological Record Series HG 20* (Western Australia: Department of Water, Government of Western Australia).

Davidson, W. A. (1995). *Hydrogeology and Groundwater Resources of the Perth Region, Western Australia*. Perth, Western Australia: Geological Survey of WA.

Department of Water (2009a). "Gnangara Groundwater Areas Allocation Plan," in *Water Resource Allocation Planning Series* (Perth, Western Austrlia: Department of Water, Government of Western Australia).

Department of Water (2009b). "Perth Regional Aquifer Modelling System (PRAMS) Model Development_ Calibration of the Coupled Perth Regional Aquifer Model PRAMS 3.0," in *Hydrogeological Record Series HG 28* (Western Australia: Department of Water).

Döll, P. (2009). Vulnerability to the Impact of Climate Change on Renewable Groundwater Resources: a Global-Scale Assessment. *Environ. Res. Lett.* 4 (3), 035006. doi:10.1088/1748-9326/4/3/035006

Duan, Q., Sorooshian, S., and Gupta, V. (1992). Effective and Efficient Global Optimization for Conceptual Rainfall-Runoff Models. *Water Resour. Res.* 28 (4), 1015–1031. doi:10.1029/91wr02985

Dupuit, J. É. J. (1863). *Études théoriques et pratiques sur le mouvement des eaux dans les canaux découverts et à travers les terrains perméables: avec des considérations relatives au régime des grandes eaux, au débouché à leur donner, et à la marche des alluvions dans les rivières à fond mobile*. Paris, France: Dunod.

Elmahdi, A., and McFarlane, D. (2009). "A Decision Support System for a Groundwater System Case Study: Gnangara Sustainability Strategy Western Australia," in *18th World IMACS Congress and MODSIM09 International Congress on Modelling and Simulation*, 13–17 July 2009, Cairns, Australia: Modelling and Simulation Society of Australia and New Zealand and International Association for Mathematics and Computers in Simulation, 3803–3809.

Environmental Protection Authority (2017). *Environmental Management of Groundwater from the Gnangara Mound-Annual Compliance Report 2017*. Editor D.o. Water (Perth, Western Australia: Department of Water).

Famiglietti, J. S. (2014). The Global Groundwater Crisis. *Nat. Clim Change* 4 (11), 945–948. doi:10.1038/nclimate2425

Feng, W., Zhong, M., Lemoine, J.-M., Biancale, R., Hsu, H.-T., and Xia, J. (2013). Evaluation of Groundwater Depletion in North China Using the Gravity Recovery and Climate Experiment (GRACE) Data and Ground-Based Measurements. *Water Resour. Res.* 49 (4), 2110–2118. doi:10.1002/wrcr.20192

Ferdowsian, R., and Pannell, D. (2009). "Explaining Long-Term Trends in Groundwater Hydrographs," in *18th World IMACS/MODSIM Congress* (Cairns, Australia), 13–17.

Ferdowsian, R., Pannell, D. J., McCarron, C., Ryder, A., and Crossing, L. (2001). Explaining Groundwater Hydrographs: Separating Atypical Rainfall Events from Time Trends. *Soil Res.* 39 (4), 861–876. doi:10.1071/SR00037

Ferdowsian, R., Ryder, A., George, R., Bee, G., and Smart, R. (2002). Groundwater Level Reductions under lucerne Depend on the Landform and Groundwater Flow Systems (Local or Intermediate). *Soil Res.* 40 (3), 381–396. doi:10.1071/SR01014

Ferris, J., and Knowles, D. (1963). *The Slug-Injection Test for Estimating the Coefficient of Transmissibility of an Aquifer*, Washington, DC: US Gov.Print.Off. US geological survey water-supply paper.

Forest Products Commission (2009). *Gnangara Groundwater System Plantation Species Assessment : Final Report*. Perth, Western Australia: Forest Products Commission.

Fu, G., Crosbie, R. S., Barron, O., Charles, S. P., Dawes, W., Shi, X., et al. (2019). Attributing Variations of Temporal and Spatial Groundwater Recharge: A Statistical Analysis of Climatic and Non-climatic Factors. *J. Hydrol.* 568, 816–834. doi:10.1016/j.jhydrol.2018.11.022

Gallardo, A. H. (2013). Groundwater Levels under Climate Change in the Gnangara System, Western Australia. *J. Water Clim. Change* 4 (1), 52–62. doi:10.2166/wcc.2013.106

Gandhi, G. M., Parthiban, S., Thummalu, N., and Christy, A. (2015). Ndvi: Vegetation Change Detection Using Remote Sensing and Gis - A Case Study of Vellore District. *Proced. Comput. Sci.* 57, 1199–1210. doi:10.1016/j.procs.2015.07.415

Gleeson, T., Alley, W. M., Allen, D. M., Sophocleous, M. A., Zhou, Y., Taniguchi, M., et al. (2012). Towards Sustainable Groundwater Use: Setting Long-Term Goals, Backcasting, and Managing Adaptively. *Groundwater* 50 (1), 19–26. doi:10.1111/j.1745-6584.2011.00825.x

Hantush, M. S. (1956). Analysis of Data from Pumping Tests in Leaky Aquifers. *Trans. AGU* 37 (6), 702–714. doi:10.1029/tr037i006p00702

Iftekhar, M. S., and Fogarty, J. (2017). Impact of Water Allocation Strategies to Manage Groundwater Resources in Western Australia: Equity and Efficiency Considerations. *J. Hydrol.* 548, 145–156. doi:10.1016/j.jhydrol.2017.02.052

Jeffrey, S. J., Carter, J. O., Moodie, K. B., and Beswick, A. R. (2001). Using Spatial Interpolation to Construct a Comprehensive Archive of Australian Climate Data. *Environ. Model. Softw.* 16 (4), 309–330. doi:10.1016/S1364-8152(01)00008-1

KlemeŠ, V. (1986). Operational Testing of Hydrological Simulation Models. *Hydrological Sci. J.* 31 (1), 13–24. doi:10.1080/02626668609491024

Konikow, L. F., and Kendy, E. (2005). Groundwater Depletion: A Global Problem. *Hydrogeol J.* 13 (1), 317–320. doi:10.1007/s10040-004-0411-8

Konikow, L. F. (2013). *Groundwater Depletion in the United States (1900–2008): U.S. Geological Survey Scientific Investigations Report 2013–5079*, 63. Available at: http://pubs.usgs.gov/sir/2013/5079 Accessed July 25, 2021.

Merz, S. K. (2009). *Development of Local Area Groundwater Models - Gnangara Mound_Lake Bindiar Model Report*, Malvern, Australia: Department of Water, Western Australia.

Morgan, L. K., Werner, A. D., and Simmons, C. T. (2012). On the Interpretation of Coastal Aquifer Water Level Trends and Water Balances: A Precautionary Note. *J. Hydrol.* 470-471, 280–288. doi:10.1016/j.jhydrol.2012.09.001

Moriasi, D. N., Arnold, J. G., Liew, M. W. V., Bingner, R. L., Harmel, R. D., and Veith, T. L. (2007). Model Evaluation Guidelines for Systematic Quantification of Accuracy in Watershed Simulations. *Trans. ASABE* 50 (3), 885–900. doi:10.13031/2013.23153

Moriasi, D. N., Gitau, M. W., Pai, N., and Daggupati, P. (2015). Hydrologic and Water Quality Models: Performance Measures and Evaluation Criteria. *Trans. ASABE* 58 (6), 1763–1785. doi:10.13031/trans.58.10715

Nash, J. E., and Sutcliffe, J. V. (1970). River Flow Forecasting through Conceptual Models Part I - A Discussion of Principles. *J. Hydrol.* 10 (3), 282–290. doi:10.1016/0022-1694(70)90255-6

Obergfell, C., Bakker, M., and Maas, K. (2019). Identification and Explanation of a Change in the Groundwater Regime Using Time Series Analysis. *Groundwater* 57, 886–894. doi:10.1111/gwat.12891

Peterson, T., and Western, A. (2011). "Time-series Modelling of Groundwater Head and its De-composition to Historic Climate Periods," in Proceedings of the 34th World Congress of the International Association for Hydro-Environment Research and Engineering: 33rd Hydrology and Water Resources Symposium and 10th Conference on Hydraulics in Water Engineering, Brisbane, Australia, 6 June-1 July (Engineers Australia), 1677.

Peterson, T. J., and Western, A. W. (2014). Nonlinear Time-Series Modeling of Unconfined Groundwater Head. *Water Resour. Res.* 50 (10), 8330–8355. doi:10.1002/2013wr014800

Peterson, T. J., and Western, A. W. (2018). Statistical Interpolation of Groundwater Hydrographs. *Water Resour. Res.* 54(7), 4663–4680. doi:10.1029/2017WR021838

Ritter, A., and Muñoz-Carpena, R. (2013). Performance Evaluation of Hydrological Models: Statistical Significance for Reducing Subjectivity in Goodness-Of-Fit Assessments. *J. Hydrol.* 480, 33–45. doi:10.1016/j.jhydrol.2012.12.004

Salama, R. B., Silberstein, R., and Pollock, D. (2005). Soils Characteristics of the Bassendean and Spearwood Sands of the Gnangara Mound (Western Australia) and Their Controls on Recharge, Water Level Patterns and Solutes of the Superficial Aquifer. *Water Air Soil Pollut. Focus* 5 (1-2), 3–26. doi:10.1007/s11267-005-7396-8

Şen, Z. (2015). "Chapter Six - Climate Change, Droughts, and Water Resources," in *Applied Drought Modeling, Prediction, and Mitigation*. Editor Z. Şen (Boston: Elsevier), 321–391.

Shapoori, V., Peterson, T. J., Western, A. W., and Costelloe, J. F. (2015a). Decomposing Groundwater Head Variations into Meteorological and Pumping Components: a Synthetic Study. *Hydrogeol J.* 23 (7), 1431–1448. doi:10.1007/s10040-015-1269-7

Shapoori, V., Peterson, T. J., Western, A. W., and Costelloe, J. F. (2015b). Estimating Aquifer Properties Using Groundwater Hydrograph Modelling. *Hydrol. Process.* 29(26), 5424–5437. doi:10.1002/hyp.10583

Shapoori, V., Peterson, T. J., Western, A. W., and Costelloe, J. F. (2015c). Top-down Groundwater Hydrograph Time-Series Modeling for Climate-Pumping Decomposition. *Hydrogeol J.* 23 (4), 819–836. doi:10.1007/s10040-014-1223-0

Siriwardena, L., Peterson, T., and Western, A. (2011). "A State-wide Assessment of Optimal Groundwater Hydrograph Time Series Models," in *International Congress on Modeling and Simulation*, 19th International Congress on Modeling and Simulation, 12–16 December 2011. Perth, Australia, 2121–2127.

Smith, A., and Pollock, D. (2010). "Artificial Recharge Potential of the Perth Region Superficial Aquifer: Lake Preston to Moore River," in *CSIRO: Water for a Healthy Country Research Flagship*, Canberra, Australia.

Strobach, E. (2013). *Hydrogeophysical Investigation of Water Recharge into the Gnangara Mound*. Perth, Australia: Curtin University.

Tremayne, A. (2010). *Changes to Water Balance Due to Urbanisation*. Perth, Australia: University of Western Australia.

Tularam, A., and Krishna, M. (2009). *Long Term Consequences of Groundwater Pumping in Australia: A Review of Impacts Around the globe*, 4 (2), 151–166.

van der Spek, J. E., and Bakker, M. (2017). The Influence of the Length of the Calibration Period and Observation Frequency on Predictive Uncertainty in Time Series Modeling of Groundwater Dynamics. *Water Resour. Res.* 53 (3), 2294–2311. doi:10.1002/2016wr019704

von Asmuth, J. R., and Bierkens, M. F. P. (2005). Modeling Irregularly Spaced Residual Series as a Continuous Stochastic Process. *Water Resour. Res.* 41 (12), W12404. doi:10.1029/2004wr003726

von Asmuth, J. R., Bierkens, M. F. P., and Maas, K. (2002). Transfer Function-Noise Modeling in Continuous Time Using Predefined Impulse Response Functions. *Water Resour. Res.* 38 (12), 23-1–23-12. doi:10.1029/2001wr001136

von Asmuth, J. R., Maas, K., Bakker, M., and Petersen, J. (2008). Modeling Time Series of Ground Water Head Fluctuations Subjected to Multiple Stresses. *Groundwater* 46 (1), 30–40. doi:10.1111/j.1745-6584.2007.00382.x

Wada, Y., van Beek, L. P. H., van Kempen, C. M., Reckman, J. W. T. M., Vasak, S., and Bierkens, M. F. P. (2010). Global Depletion of Groundwater Resources. *Geophys. Res. Lett.* 37 (20), L20402–n. doi:10.1029/2010gl044571

Wang, P., Yu, J., Pozdniakov, S. P., Grinevsky, S. O., and Liu, C. (2014). Shallow Groundwater Dynamics and its Driving Forces in Extremely Arid Areas: a Case Study of the Lower Heihe River in Northwestern China. *Hydrol. Process.* 28 (3), 1539–1553. doi:10.1002/hyp.9682

Western Australian Planning Commission (2001). "Gnangara Land Use and Water Management Strategy Final Report," in *Ministry for the Environment (2005) Proposed National Standard for Human Drinking-Water Sources* Perth Australia: Western Australian Planning Commission.

Wilson, B. A., Valentine, L. E., Reaveley, A., Isaac, J., and Wolfe, K. M. (2012). Terrestrial Mammals of the Gnangara Groundwater System, Western Australia: History, Status, and the Possible Impacts of a Drying Climate. *Aust. Mammalogy* 34 (2), 202. doi:10.1071/am11040

Xu, C. (2008). Water Balance Analysis for the Gnangara Mound under Corporation Abstraction Scenarios of 105, 135 and 165 GL/A. *Leederville*. Western Australia, Australia: W.A.: Water Corporation.

Yesertener, C. (2005). Impacts of Climate, Land and Water Use on Declining Groundwater Levels in the Gnangara Groundwater Mound, Perth, Australia. *Australas. J. Water Resour.* 8 (2), 143–152. doi:10.1080/13241583.2005.11465251

Yesertener, C. (2007). "Assessment of the Declining Groundwater Levels in the Gnangara Groundwater mound," in *Hydrogeological Record Series, Report HG14*. (Perth, Western Australia: Department of Water, Government of Western Australia).

Yue, W., Wang, T., Franz, T. E., and Chen, X. (2016). Spatiotemporal Patterns of Water Table Fluctuations and Evapotranspiration Induced by Riparian Vegetation in a Semiarid Area. *Water Resour. Res.* 52 (3), 1948–1960. doi:10.1002/2015WR017546

Zajaczkowski, J., and Jeffrey, S. J. (2020). *Potential Evaporation and Evapotranspiration Data provided by SILO*, Department of Environment and Science, Queensland Government. [Dataset].

Zektser, I. S., and Lorne, E. (2004). "Groundwater Resources of the World: and Their Use," in *IhP Series on Groundwater* (Paris, France: Unesco). doi:10.1142/9789812702753_0061

Zhou, P., Wang, G., and Duan, R. (2020). Impacts of Long-Term Climate Change on the Groundwater Flow Dynamics in a Regional Groundwater System: Case Modeling Study in Alashan, China. *J. Hydrol.* 590, 125557. doi:10.1016/j.jhydrol.2020.125557

Conflict of Interest: The authors declare that the research was conducted in the absence of any commercial or financial relationships that could be construed as a potential conflict of interest.

frontiers in Environmental Science

ORIGINAL RESEARCH
published: 24 September 2021
doi: 10.3389/fenvs.2021.717458

Response of Sediment Microbial Communities to the Rural Wastewater in the Pond-Ditch Circulation System

Mengfei Yu[1†], *Yongtai Pan*[2†], *Lingli Yang*[3,4], *Wei Liu*[3,4], *Feng He*[3*] *and Lin Ma*[5,6*]

[1]*Hubei Provincial Key Laboratory for Protection and Application of Special Plants in Wuling Area, College of Life Sciences, South-Central University for Nationalities, Wuhan, China,* [2]*Research Center for Ecology and Environment of Qinghai-Tibetan Plateau, Tibet University, Lhasa, China,* [3]*State Key Laboratory of Freshwater Ecology and Biotechnology, Institute of Hydrobiology, Chinese Academy of Sciences, Wuhan, China,* [4]*College of Life Science, University of Chinese Academy of Sciences, Beijing, China,* [5]*CAS Key Laboratory of Aquatic Botany and Watershed Ecology, Wuhan Botanical Garden, Chinese Academy of Sciences, Wuhan, China,* [6]*Hubei Key Laboratory of Wetland Evolution and Ecological Restoration, Wuhan Botanical Garden, Chinese Academy of Sciences, Wuhan, China*

Microorganisms played important roles in nutrient removal in Pond-ditch circulation system (PDCS). However, dynamics of microbial community in the PDCS, and responses of rhizosphere and non-rhizosphere microbial community to rural wastewater remains unclear. In this paper, average operational taxonomic units numbers of sediment microbial varied from 10,254 to 17,112, and values in rhizosphere were higher than those of the non-rhizosphere ($p < 0.05$). *Bacillus*, *Clostridium sensu stricto 1*, and *Geobacter* were the predominant genera in PDCS sediment with relative abundances of 0.52–17.61%, 0.26–8.08%, and 0.20–4.58%, respectively. However, *Bacillus*, *Clostridium sensu stricto 1*, and *Geobacter* genera in rhizosphere were more abundant than those in non-rhizosphere at day 30. Chao 1 index ranged from 10,225 to 17,033 and showed significant positive correlations with all sediment properties ($p < 0.05$). Chao 1 and Shannon indices in rhizosphere were significant positively related to tartaric acid and total organic carbon, respectively; while significant correlation between Shannon and Simpson indices in non-rhizosphere and oxidation-reduction potential were detected ($p < 0.05$). Redundancy analysis suggested that lactic acids, proteins, and amino acids had strong positive effects on *Geobacter* and *Clostridiu sensu stricto 12* in the rhizosphere; while *Bacillus* and *Clostridium* in non-rhizosphere were significantly affected by sediment ammonia nitrogen and nitrate nitrogen. Environmental variables accounted for 66.9 and 60.3% of the total variation for the microbial community of non-rhizosphere and rhizosphere sediments, respectively. Our results highlight that root exudates and sediment available N alter predominant genera in the rhizosphere and non-rhizosphere, respectively, which is benefit for optimizing removal efficiency of PDCSs in large-scale applications.

Keywords: pond-ditch circulation system, rhizosphere bacteria, microbial community structure, diversity, redundancy analysis

OPEN ACCESS

Edited by:
Yuanchun Zou,
Northeast Institute of Geography and Agroecology (CAS), China

Reviewed by:
Jl An Sun,
Central and Southern China Minicipal Engineering Design and Research Institute Cor., Ltd., China
Weiqi Wang,
Fujian Normal University, China

****Correspondence:***
Lin Ma
malin@wbgcas.cn
Feng He
hefeng@ihb.ac.cn

[†]These authors have contributed equally to this work and share first authorship

Specialty section:
This article was submitted to Water and Wastewater Management, a section of the journal Frontiers in Environmental Science

Received: *31 May 2021*
Accepted: *20 July 2021*
Published: *24 September 2021*

Citation:
Yu M, Pan Y, Yang L, Liu W, He F and Ma L (2021) Response of Sediment Microbial Communities to the Rural Wastewater in the Pond-Ditch Circulation System. Front. Environ. Sci. 9:717458. doi: 10.3389/fenvs.2021.717458

INTRODUCTION

With the rapid development of economy and industrialization, the problem of water pollution in rural areas of China is getting worse. Large amounts of untreated domestic wastewater were discharged into the ponds, ditches, lakes, and rivers, which resulted in the deterioration of water environment and threatened the health of people (Bowes et al., 2015). In order to solve this problem, many types of wastewater treatment systems have been developed and widely used, such as constructed wetland system (Childers, 2020; Torrens et al., 2021), high-rate algal ponds (Evans et al., 2005), mineral-based small-scale active filter system (Gustafsson et al., 2008), sequencing batch reactor-biofilm system (Yin et al., 2015). Recently, our group have developed a new rural wastewater treatment system, pond-ditch circulation system (PDCS), which exhibits the advantages of high efficiency, cheap, and simple management and is an appropriate alternative for rural wastewater remediation (Ma et al., 2015a; Ma et al., 2015b).

In the PDCS, microorganisms played important roles in nitrogen (N) and phosphorus (P) removal. For example, approximately 79.5% of the total nitrogen removal was attributed to microbial process, especially nitrification and denitrification, which were mediated by a range of microbes, such as *amoA*, *arch-amoA*, *nirS,* and *nirK* genes (Ma et al., 2016). Meanwhile, anaerobic anammox bacteria have been widely used in nitrogen removal reactors due to their ability of converting ammonium into nitrogen gas under the anoxic conditions (Hu et al., 2010; Liu et al., 2020). The anaerobic anammox processes also performed a crucial role in nitrogen removal of the PDCS due to 41.3–50.3% contribution to nitrogen gas production (Ma et al., 2019). Similarly, some bacteria such as denitrifying phosphate-accumulating organisms can utilize nitrate (NO_3^--N) or nitrite (NO_2^--N) as the terminal electron receptor under the anoxic condition for the simultaneous removal of N and P (Li et al., 2019; Chen et al., 2021). Many studies reported that structures and diversities of microorganisms were affected by a number of abiotic and biotic factors, such as pH, temperature, oxygen concentration, carbon availability, hydraulic retention time, and plants (Khammar et al., 2005; Tomaszewski et al., 2017; Li et al., 2018; Liu et al., 2020).

Our previous studies have demonstrated that in the PDCS, aquatic plants participated in nutrient removal, were responsible for 10.1% N and 50% P reduction, respectively (Ma et al., 2016; Ma et al., 2019). Besides direct absorption, plants can also regulate the nutrient removal *via* root exudates such as sugars, polysaccharide, amino acids, and organic acids. These exudates can be used as the carbon and nitrogen sources, or stimulating signals by the rhizosphere microorganisms (Bais et al., 2006). This will in turn lead to the gathering of more microorganisms around the plant rhizosphere and result in "rhizosphere effect" (Egamberdieva et al., 2008). This "rhizosphere effect" is beneficial for the removal of nutrient in the rhizosphere microenvironment (Nie et al., 2015; Chen et al., 2016). and can exert significant impacts on the rhizosphere microorganisms (Li et al., 2016). Therefore, the compositions, diversities of both rhizosphere and non-rhizosphere sediment bacteria vary greatly. Although several studies have correlated environmental factors to the microbial communities in decentralized treatment approaches, how rhizosphere and non-rhizosphere sediment bacteria in the PDCS responds to abiotic environmental factors still remain unclear. Based on our previous studies, we assumed that biotic factors such as plants and microbial communities rather than abiotic environmental factors were the dominant factors for nutrient removal in the PDCSs.

In this study, we have built two small-scale PDCS systems to treat domestic wastewater in rural areas of Southern China. These systems continuously operated for 2 months. This study aimed to elucidate dynamic changes of microbial community structures and diversities between rhizosphere and non-rhizosphere sediments and their responses to the environmental factors. The main contents of this study are as follows: (1) the total efficiency of N and P removal in the PDCS; (2) bacterial clustering information in rhizosphere and non-rhizosphere microenvironments; (3) relative abundances and diversities of bacteria in rhizosphere and non-rhizosphere environments at phylum and genus levels; (4) spearman's correlation coefficient analysis between rhizosphere and non-rhizosphere microbial diversities, water quality, sediment properties, and root exudates; (5) redundancy analysis (RDA) of dominant bacterial species and environmental factors in the rhizosphere and non-rhizosphere of the PDCSs. Based on this research, we have elucidated the dynamic changes of microbial communities in the PDCSs and the relations between environmental variables and microbial communities. These findings will be helpful in the design and the optimization of nutrient removal in PDCSs and other nutrient removal systems in large-scale applications.

MATERIALS AND METHODS

Experimental Water and Sediments

The experimental sediments and water were collected and used as we previously described (Ma et al., 2015a). Briefly, four different types of water were collected from sites A, B, C, and D, respectively; two different types of sediments were sampled from sites A and C (**Figure 1A**). Initial total nitrogen concentrations in these four types of water were 3.28 mg L^{-1}, 24.22 mg L^{-1}, 4.16 mg L^{-1}, and 0.81 mg L^{-1}, respectively; While initial total phosphorus contents in the overlying water of sites A, B, C, and D were 0.26 mg L^{-1}, 2.0 mg L^{-1}, 0.4 mg L^{-1}, and 0.07 mg L^{-1}, respectively. The initial physic-chemical indices of water and sediments in pond 1, ditch, pond 2, and water distribution storage apparatuses were analyzed and presented in **Supplementary Tables S1, S2**.

Construction of the PDCS Systems

Two sets of rural wastewater treatment system, was designed and operated as we previously described elsewhere (Ma et al., 2021b). Briefly, the small-scale system consisted of six parts: a water distribution bucket, pond 1, ditch, pond 2, a water-storage tank, and a water pump (**Figure 1B**). The two ponds were laid with 10 cm sediments sampled from the sites A and C and planted with *Vallisneria natans L.*, respectively. Moreover, in the ditch, a 10 cm thick gravel layer was evenly spread and planted with *Iris*

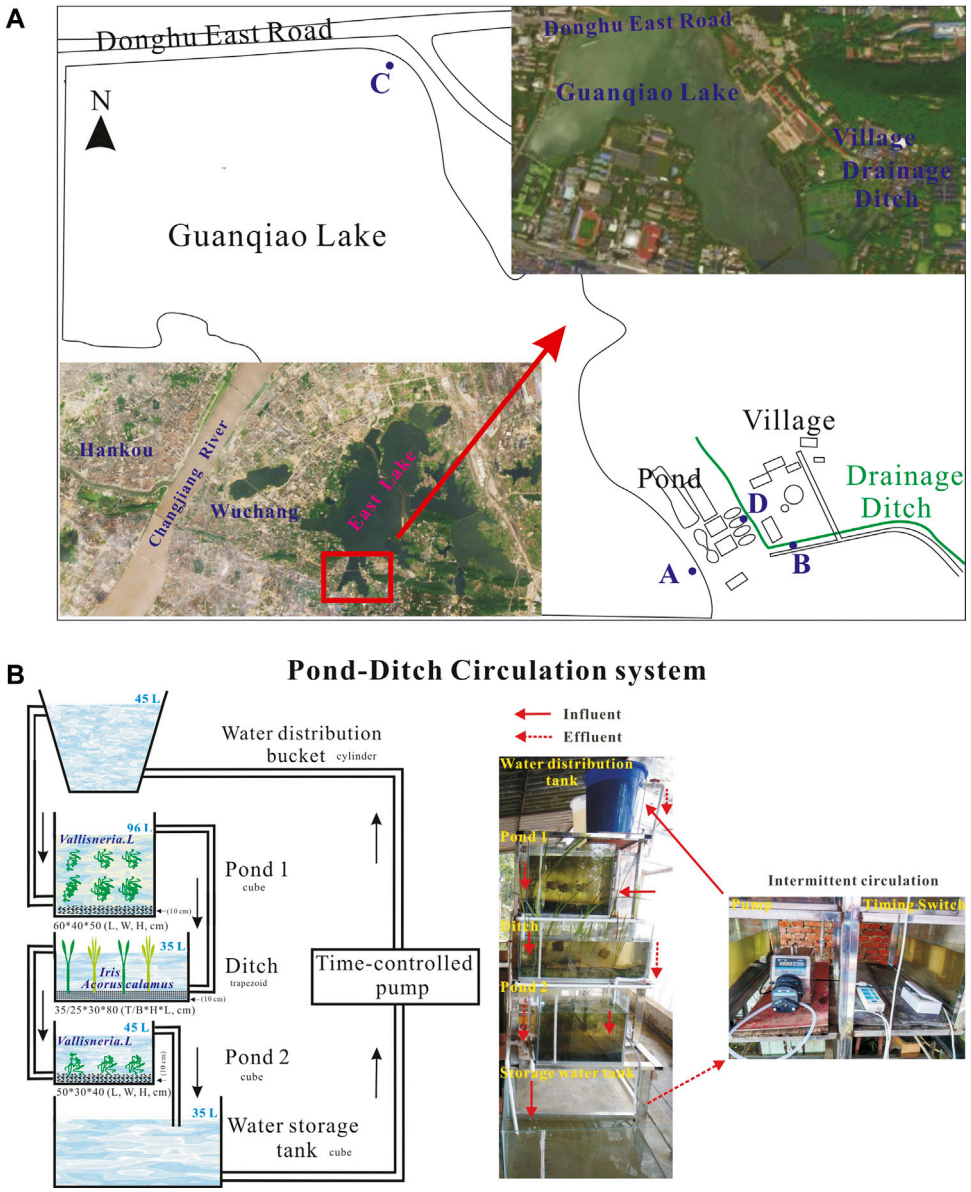

FIGURE 1 | Schematic diagram of the pond-ditch circulation system and sampling sites.

tectorum L. and *Acorus calamus L.* Then, these five microcosms were filled with 45 L, 96 L, 35 L, 45 L, and 35 L water sampled from sites D, A, B, C, and D, respectively. In the PDCS system, the running parameters was circulating every other 4 h with a water flow of 3.6 Lh^{-1}, thus resulting in 0.30 $m^3m^{-2}d^{-1}$, 0.43 $m^3m^{-2}d^{-1}$, and 0.37 $m^3m^{-2}d^{-1}$ hydraulic loading rates for pond 1, ditch, and pond 2, respectively. Meanwhile, in the static group, the velocity of water flow was zero.

Analysis of Water and Sediments

The system continuously ran for 60 days since the beginning of the operation. At days 1, 4, 7, 11, 15, 18, 22, 26, 30, 40, 50, and 60, 500 ml water samples were collected from pond 1, ditch, and pond 2 from the control (static) and PDCS systems, respectively. For these water samples, the 15 indices were analyzed as following: water salinity, dissolved oxygen (DO), pH, temperature (W-temp), oxidation-reduction potential (ORP), turbidity, total phosphorus (TP), total nitrogen (TN), inorganic nitrogen (IP), ammonia nitrogen (NH_4^+-N), nitrate nitrogen (NO_3^--N), nitrite nitrogen (NO_2^--N), total suspended solids (TSS) (State EPA of China, 2002), chemical oxygen demand (CODcr) and *Chl-a* (Holm-Hansen and Riemann, 1978).

Approximate 50 g rhizosphere and non-rhizosphere sediments in pond 1, ditch, and pond 2 of these two systems were also collected at days 15, 30, and 60, representing the early, middle, and late stages of the experiment, respectively (Zou et al., 2021). About 10 g of fresh sediment samples was used to measure water contents (WC) of each sediment sample gravimetrically.

The contents of organic matter were determined gravimetrically using approximate 5 g fresh sediment sample dried at 450°C for 3 h. The contents of total organic carbon (TOC) and sediment total nitrogen (STN) in air-dried and sieved sediment samples were determined using an elemental analyzer (Vario TOC cube, Hanau, Germany). The contents of NH_4^+-N, NO_3^--N, NO_2^--N in sediments were determined using an automatic nutrient analyzer (EasyChem plus, Systea, Italy). Sediment P fractions were measured using the SMT harmonized P extraction protocol, and the four main forms of P in sediment total phosphorus (STP), sediment inorganic phosphorus (SIP), NaOH-P, and HCl-P were analyzed as previously described (Ruban et al., 2001). The left sediments were mixed thoroughly and frozen in −20°C for future analysis. The dynamic changes of physic-chemical characteristics for the non-rhizosphere sediments for the PDCS systems were shown in **Supplementary Tables S3, S4**, respectively.

Analysis of Root Exudates

The contents of five types of root exudates proteins, polysaccharides, amino acids, lactic acids and tartaric acids were measured (Ma et al., 2021a). Briefly, 10 strains of *Vallisneria natas L.*, 1 strain of *Acorus calamus L.* and *Iris tectorum L.* were sampled from the ponds and ditches at days 15, 30, and 60, respectively. However, in the pond 1 of the static group, all *Vallisneria natans L.* died due to the deterioration of water quality in the early stage of the experiment. Therefore, root exudates for this microcosm were missed. After careful rinsing in the water, plant roots were immersed in 500 ml ultra-pure water for 24 h. The values of pH for these solutions were measured. Then, 400 ml culture solution was concentrated to 20 ml using a vacuum circumgyration evaporator. The contents of proteins and polysaccharides were analyzed using the coomassie brilliant blue method (Spector, 1978) and the anthrone-sulfuric acid chromatometry method (Grandy et al., 2000), respectively. The contents of amino acids were determined by an ICS 5000 + amino acid analyzer (model 120A, Thermo Fisher, United States). Meanwhile, the contents of tartaric acids in root exudates were measured using a DIONEX ICS-5000 + DP chromatograph (Thermo Fisher, United States). The initial and changes of proteins, polysaccharides, amino acids, lactic acids, tartaric acids, and pH of root exudates of aquatic plants were presented in **Supplementary Tables S5, S4**, respectively.

Construction of 16S rDNA Library

Bacterial DNA were extracted and used for 16S rDNA gene sequencing as previously described with some modifications (Poret-Peterson et al., 2019). Briefly, the total DNA of sediment samples was extracted using the PowerSoil DNA Isolation Kit according the manufacturer's instructions (MoBio, Carlsbad, CA, United States). Then, the concentrations and qualities of DNA samples were spectrophotometrically measured (Nanodrop 2000, NanoDrop Technology, Wilmington, DE, United States). The hypervariable V3-V4 regions of bacterial 16S rDNA were amplified using the specific bar-coded forward primer 5'-ACTCCTACGGGAGGC AGCAG-3' and reverse primer 518R, 5'-ATTACCGCGGCTGCT GG-3'. Polymerase chain reaction (PCR) amplification procedures were as follows: denaturation at 95°C for 3 min, denaturation at 95°C for 30 s, annealing at 55°C for 30 s, extension at 72°C for 30 s, 35 cycles. Following the pre-amplification, the qualified DNA samples were used in the next PCR amplification. Then, the amplified PCR products were purified and used to construct the 16S rDNA library.

Sequencing of 16S rDNA Gene and Data Analysis

Sequencing of PCR products were performed using the Illumina paired-end sequencing technology (Mega Genomics Corp. Beijing, China). Briefly, the raw data of bacterial 16S rDNA gene sequencing were demultiplexed, qualify-filtered by Trimmomatic using the specific filtering criteria of QIIME (Caporaso et al., 2010) and merged using the FLASH software. Chimeric sequences were determined and deleted using the UCHIME algorithm (Edgar et al., 2011). The operational taxonomic units (OTUs) were clustered with a threshold of 97% sequence similarity using UPARSE (version 7.1, http://drive5.com/uparse/), annotated and classified using the SILVA database. Sediment bacterial α-diversity was estimated *via* the observed chao1, Shannon, and Simpson indices.

Statistical Analysis

All data were presented as mean ± SEM. One-way ANOVA with Turkey's post hoc tests were performed to analyze the differences in water quality, sediment physic-chemical parameters, α-diversity and richness indices of sediment bacteria, root exudates in these two systems. Sediment bacterial community richness (presented as observed species and goods coverage) and α-diversity (presented as Chao 1, Simpson, and Shannon) in rhizosphere and non-rhizosphere microenvironments in these two systems were calculated in *R* version 3.5.2 using the vegan package (Zhou et al., 2020). Spearman's correlation coefficients were calculated to determine the associations among sediment microbial diversity, water quality, sediment properties, and root exudates. RDA was performed to determine the correlations between the top 10 sediments bacterial and abiotic environmental variables using the Canoco software (Version 5.0, Microcomputer, Ithaca, NY, United States). The RDA will be picked up and used as the appropriate ordination form when the longest gradient length of detrended correspondence analysis was <2. All statistical analyses were done in SPSS software (version 20.0, SPSS Inc., Chicago, United States). $p < 0.05$ was considered statistically significant.

RESULTS

Nutrient Removal Rates in PDCS Systems

The efficiencies of N and P removal in the two systems were demonstrated in **Figure 2**. In the PDCS, the concentrations of TN, NH_4^+-N, and NO_2^--N in the three microcosms pond 1, ditch, and pond 2 declined from day 4 and reached a plateau level at day 30. Contents of NO_3^--N in the PDCS remained at a low level before day 20, and then significantly increased, peaking at

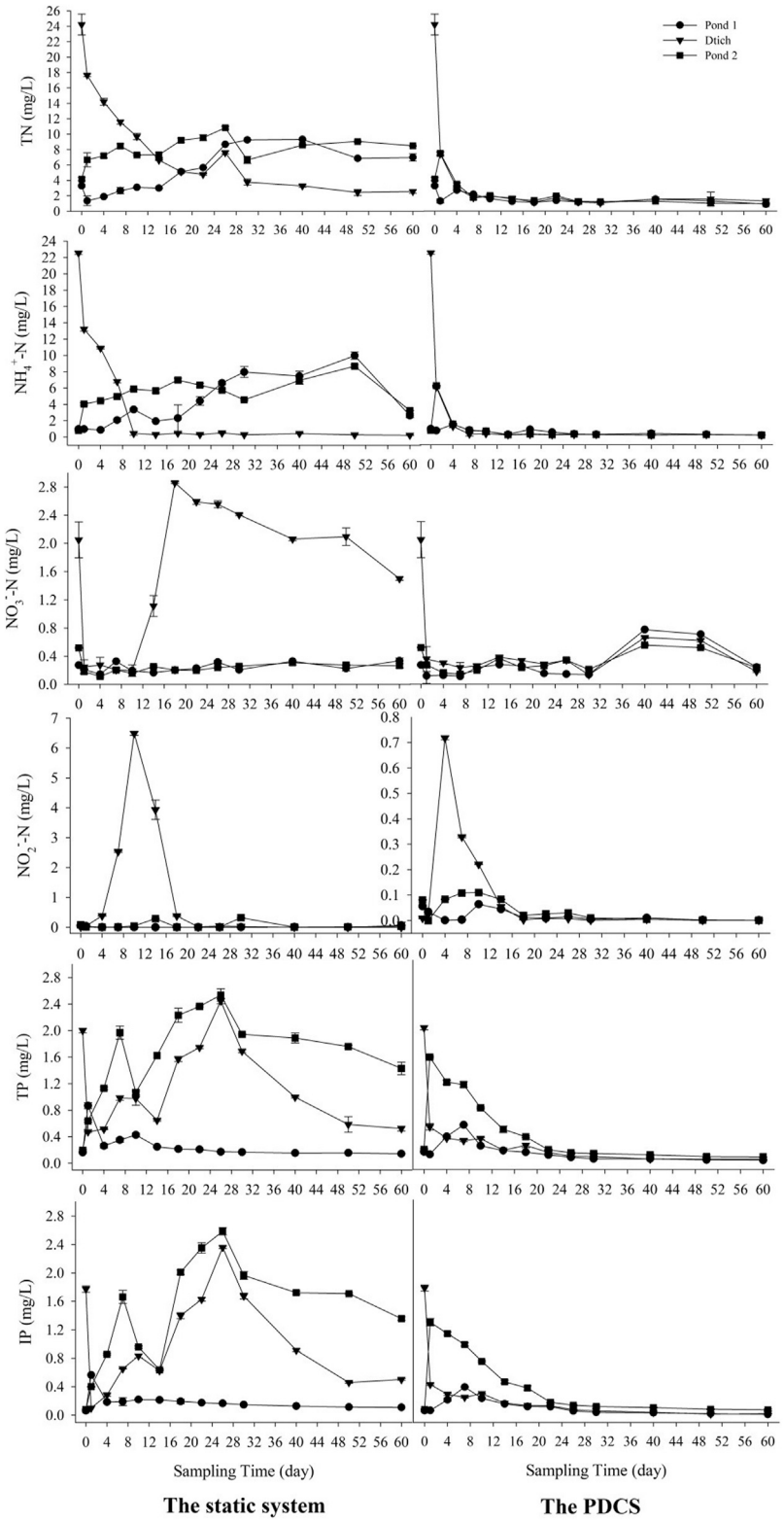

FIGURE 2 | Changes of TN, NH_4^+-N, NO_3^--N, NO_2^--N, TP, and IP in overlying water for two systems within 60 sampling days. In the circulation PDCS system, the water was circulated 3.6 L/h every other 4 h, while the control group was static.

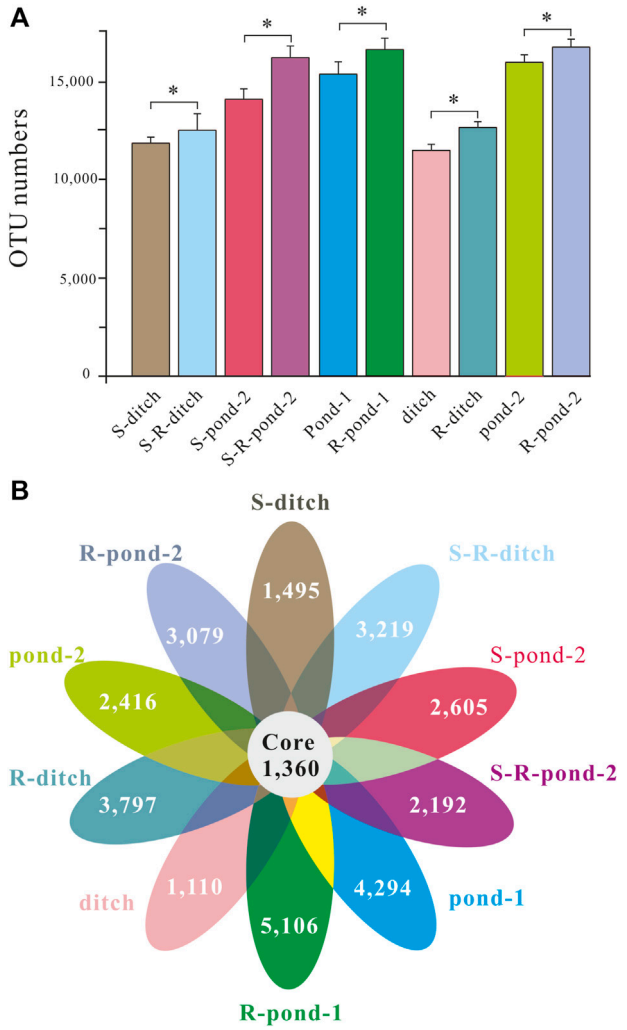

FIGURE 3 | OTU numbers and Venn diagram for two systems. **(A)** OTU numbers in the pond-1, R-pond-1, ditch, R-ditch, pond-2, R-pond-2 of the PDCS and S-ditch, S-R-ditch, S-pond-2, S-R-pond-2 of the control static group, respectively. Due to the death of plants in the pond-1 of the control static group died at the early stage, the data for the S-pond-1 and S-Rpond-1 were omitted. **(B)** Each circle represents a single microcosm of the PDCS systems. The numbers in the overlapping area of the circles represent the numbers of OTUs shared between the microcosms, while the numbers without overlaps represent the numbers of OTUs unique to these single microcosms.

day 40, and gradually declined to a low level. The final removal efficiencies for TN and NH_4^+-N in the PDCS system ranged from 72.7 ± 2.3 to 94.5 ± 1.5%, and 72.3 ± 2.6 to 99.1 ± 0.3%, respectively. For the P, in the PDCS, the concentrations of TP and IP in the three microcosm's pond 1, ditch, and pond 2 significantly declined from day 4 and reached a stable low level at day 30. The final removal efficiencies of TP in pond 1, ditch, and pond 2 in the PDCS system were 81.7 ± 2.3, 97.4 ± 1.1, and 77.8 ± 2.1%, respectively. Significant differences were detected in TN, NH_4^+-N, NO_3^--N, NO_2^--N, TP, and IP between these two systems ($p < 0.05$).

The values of the other six indices ORP, W-temp, pH, DO, turbidity, and salinity for water were presented in **Supplementary Figure S1**. The ORPs for the two systems increased from day 1 to day 15, and then decreased. The W-temp for these two systems fluctuated from 25.5 ± 0.3°C to 32.6 ± 0.2°C.The values of pH generally increased from 7.16 ± 0.13 from day 0 to 8.19 ± 0.15 at day 60. The values of DO also increased from 0.05 ± 0.01 to 5.4 ± 0.1 mg L^{-1}. For the turbidity, their values fluctuated two times and generally decreased. For the salinity, the change trend for the static system were increasing, the values in the PDCS remained at a stable level. Significant differences in pH, DO, salinity, and turbidity were observed between these two systems ($p < 0.05$).

OTU Analysis in Single Microcosms of the PDCS System

Both rhizosphere and non-rhizosphere sediments were sampled for analyzing the compositions of bacteria in two systems at days 15, 30, and 60, respectively. After quality control and filtering, twenty-four OTU numbers for eight microcosms were obtained (**Figure 3A**). Due to the death of plants in the pond 1 of the static system and the existence of two different types of plants in the ditches of the two systems, there were 452,989 ± 3,426 bacterial OTUs observed in the 36 rhizosphere/non-rhizosphere sediment samples. The OTU numbers in the S-ditch, S-pond 2, ditch, and pond 2 microcosms were all significantly lower than those of their corresponding rhizosphere counterparts, respectively ($p < 0.05$). Meanwhile, the OTU numbers in the microcosm of R-pond 1 was statistically insignificantly higher compared with that in the microcosm of pond 1 ($p < 0.05$). In order to show the unique and shared OTUs between the static and PDCS systems, a petal diagram was drawn based on the OTU analysis results (**Figure 3B**). The ten petals represented ten different microcosms in these two systems. There were 1,360 OTUs shared by the 10 microcosms. The numbers of unique OTUs in the S-ditch, ditch, and pond 2 microcosms were significantly lower than those of their corresponding counterparts ($p < 0.05$).

Heatmap of the Relative Abundances of Bacterial Communities

Relative abundances of top 35 bacteria at phylum and genus levels were statistically analyzed (**Figure 4**). The utmost dominant bacterial phyla in pond 2 of the two systems were Firmicutes, Deinococcus, and Armatimonadetes. The frequencies of these three bacterial phyla in the rhizosphere of pond 2 were more abundant in those of the non-rhizosphere. For the ditch of two systems, the dominant bacterial phyla were Bacteroidetes and Proteobacteria, their values in the rhizosphere were significantly higher than those of their corresponding non-rhizosphere groups. In addition, the frequencies of *Nitrospirae*, and *Acidobacteria* in the rhizosphere of pond 1 for two systems were significantly higher than those of their corresponding non-rhizosphere groups. At the genus level, *Geobacter* and *Pseudomanas* genera were in relatively higher abundances in the rhizosphere of pond 1 for the PDCS than those in the

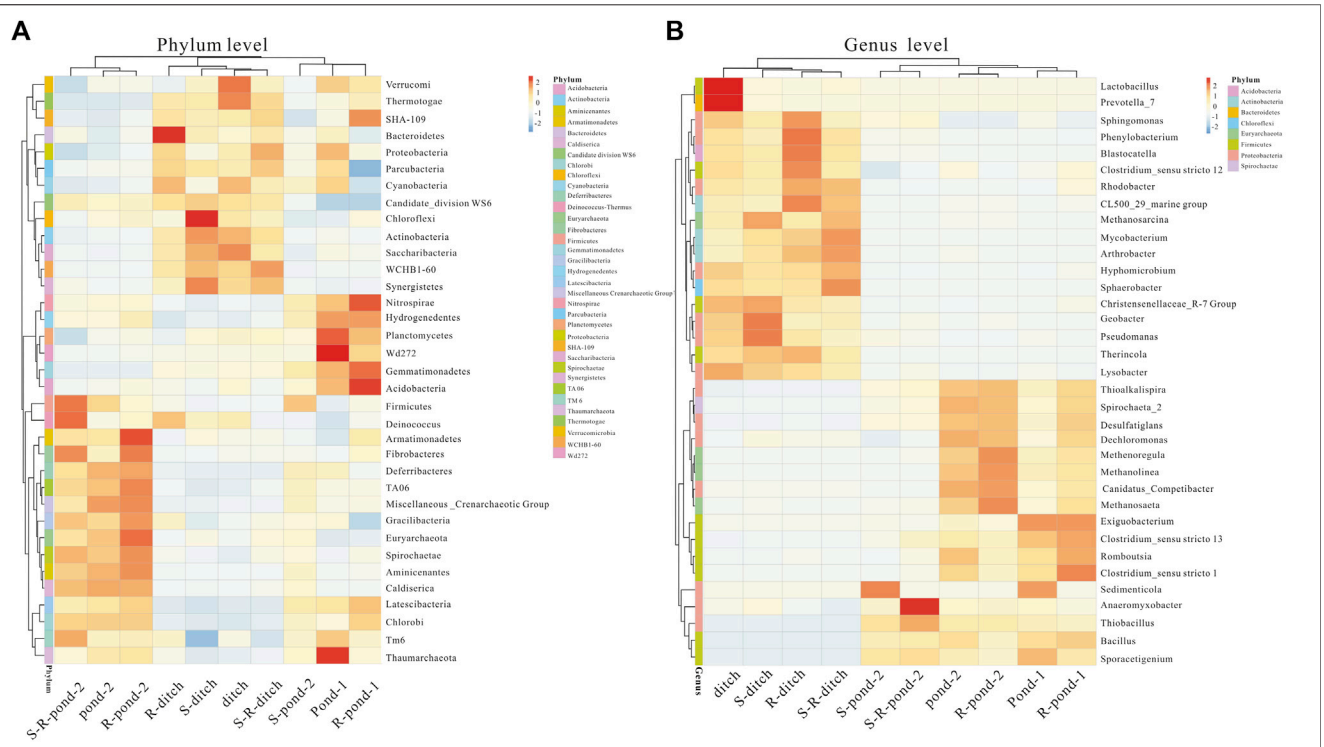

FIGURE 4 | Relative abundance heatmap of top 35 bacteria in rhizosphere and non-rhizosphere sediments in two systems at the phylum **(A)** and genus **(B)** levels.

non-rhizosphere. The frequencies of *Clostridium_sensu stricto 1*, *Romboutsia*, and *Clostridium_sensu stricto 13* genera in the rhizosphere of pond 1 for two systems were more abundant in those in non-rhizosphere. For the pond 2 of the PDCS, the dominant bacterial phyla were Methenoregula and Methanosaeta, their values in the rhizosphere were significantly higher than those of their corresponding non-rhizosphere groups.

Bacterial Community Structure Analysis of Rhizosphere/Non-Rhizosphere Sediment

Relative abundances of top 10 bacteria in rhizosphere and non-rhizosphere sediment samples at days 15, 30, and 60 at phylum and genus levels were analyzed and demonstrated in **Supplementary Figure S2** and **Figure 5**, respectively. At the phylum level, the most abundant bacteria in both rhizosphere and non-rhizosphere sediments of the PDCS were Proteobacteria, Firmicutes, Chloroflexi, Bacteroidetes, and Actinobacteria. Relative abundances for these five bacterial phyla in the rhizosphere of the PDCS ranged from 25.52 ± 2.68 to 53.44 ± 2.56%, 3.62 ± 0.37 to 45.2 ± 2.15%, 5.97 ± 0.67 to 15.06 ± 1.03%, 2.69 ± 0.28 to 9.01 ± 0.98%, and 1.92 ± 0.35 to 11.74 ± 0.51%, respectively. Meanwhile, relative abundances of these five bacterial phyla in the non-rhizosphere ranged from 20.76 ± 1.36 to 46.88 ± 1.57%, 2.12 ± 0.26 to 25.75 ± 1.18%, 6.63 ± 0.34 to 14.59 ± 0.43%, 2.32 ± 0.10 to 7.12 ± 0.23%, and 2.07 ± 0.16 to 14.26 ± 0.24%, respectively. Relative abundances of *Firmicutes* in two ponds of two systems increased from day 15 to day 30. At the middle of experiment (day 30), *Firmicutes* was found to be more enriched in the rhizosphere of ponds for two systems than those in the non-rhizosphere of two ponds. Meanwhile, the phylum Proteobacteria was more abundant in the rhizosphere of the ditch for two systems than those in the non-rhizosphere of the ditch at day 30.

At the genus level, the most abundant bacteria in both rhizosphere and non-rhizosphere sediments of the PDCS were *Bacillus*, *Geobacter*, and *Clostridium sensu stricto 1* genera. The relative abundances of these three bacterial genera in the rhizosphere of the PDCS ranged from 0.56 ± 0.02 to 19.52 ± 1.95%, 0.28 ± 0.03 to 8.50 ± 2.13%, and 0.13 ± 0.02 to 11.89 ± 0.36%, respectively. Meanwhile, the relative abundances of these three bacterial genera in the non-rhizosphere ranged from 0.12 ± 0.01 to 15.61 ± 0.68%, 0.20 ± 0.02 to 4.58 ± 0.32%, and 0.26 ± 0.01 to 8.08 ± 1.35%, respectively. Dominant genera in ditches of two systems were *Geobacter*. Relative abundances of ditches for two systems increased from day 15 to day 30, and then decreased (**Figure 5**). Meanwhile, the frequencies of *Geobacter* in genus *Proteobacteria* in the rhizosphere sediments of these two ditches at day 30 were significantly higher than those of their non-rhizosphere sediments ($p < 0.05$). Moreover, in the microcosms pond 1 and pond 2, the most dominant bacterial genera were *Bacillus* and *Clostridium sensus stricto 1*, and relative abundances of these two genera in

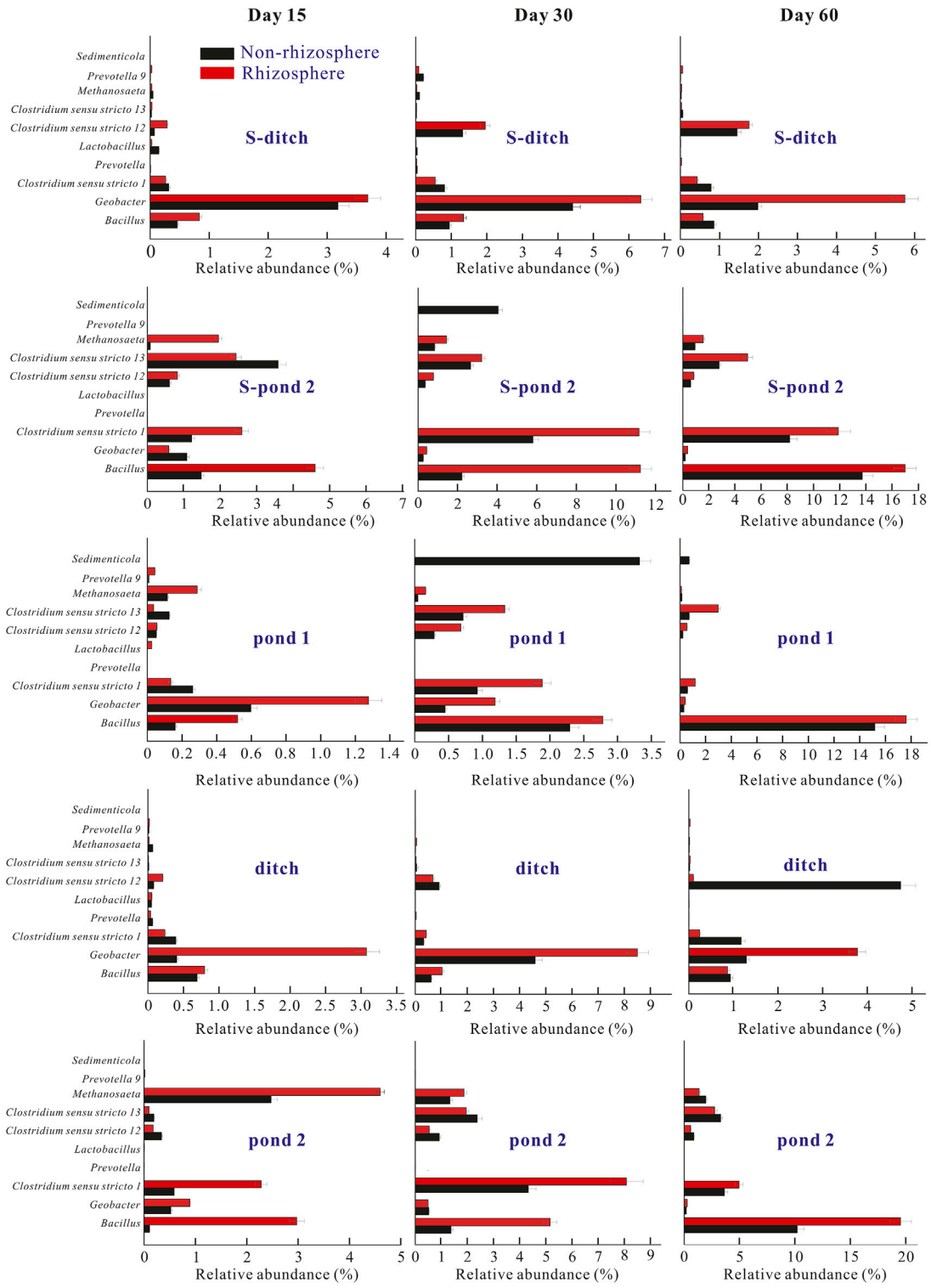

FIGURE 5 | Relative abundances of top 10 bacteria at the genus level in the two systems. The relative abundances of top 10 bacteria at the genus level at days 15, 30, and 60 were calculated. Abbreviations: In the static systems, S-ditch, S-R-ditch, S-pond-2, and S-R-pond-2 mean the sediments collected from the ditch, plant rhizosphere in the ditch, pond 2, plant rhizosphere in pond 2, respectively. The plants in the pond 1 of the static system died at the early stage of the experiment. In the PDCS, Pond-1, R-pond-1, ditch, R-ditch, pond-2, and R-pond-2 represented the sediments collected from the pond 1, plant rhizosphere of the pond 1, the ditch, plant rhizosphere in the ditch, pond 2, plant rhizosphere in the pond 2, respectively.

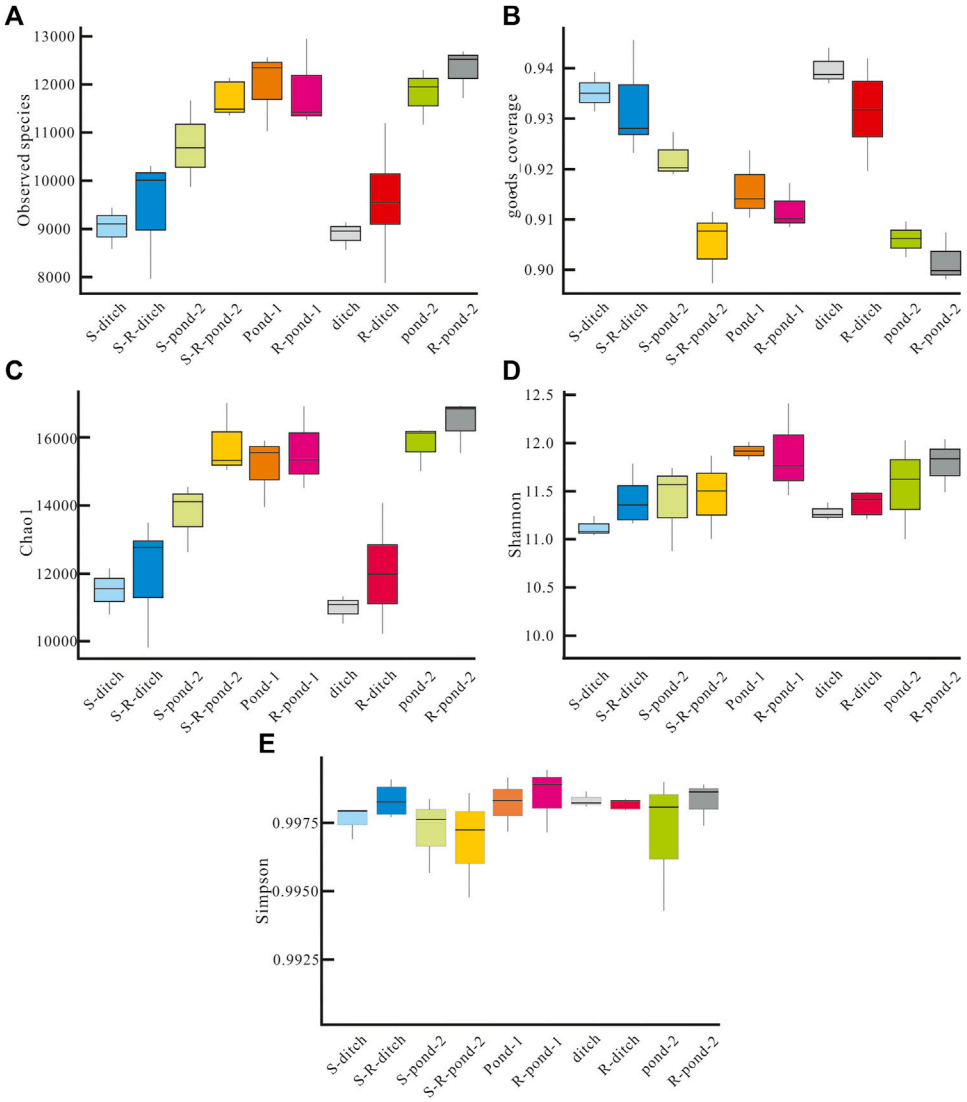

FIGURE 6 | Richness and diversity of rhizosphere and non-rhizosphere sediment bacteria in two systems. **(A)** Numbers of observed species, **(B)** the values of goods coverage, **(C)** the Chao1 index, **(D)** the Shannon index, and **(E)** the Simpson index of non-rhizosphere and rhizosphere sediment bacteria in different microcosms of two systems. S-ditch and S-R-ditch meant non-rhizosphere and rhizosphere ditch groups in the static system, respectively; Similarly, S-pond-2, and S-R-pond-2 meant non-rhizosphere and rhizosphere pond-2 groups in the static system, respectively. The same naming rules were applicable in pond-1, R-pond-1, ditch, R-ditch, pond-2, and R-pond-2 in the PDCS.

two ponds of the PDCS remarkably increased from day 15 to 30. The frequencies of *Bacillus* and *Clostridium sensus stricto 1* in the rhizosphere of ponds for the PDCS were higher than those in the non-rhizosphere (**Figure 5**).

Richness and α-Diversity Analysis of Rhizosphere and Non-Rhizosphere Sediment Bacteria

To further explore the effects of root exudates on bacterial community in the PDCS, the richness (presented as observed species, goods coverage) and α-diversity (presented as Chao1, Shannon and Simpson) of rhizosphere and non-rhizosphere sediment bacteria were performed. As shown in **Figure 6**, the values for the observed species in the rhizosphere and non-rhizosphere sediments in the PDCS ranged from 9,560 ± 1,235 to 12,500 ± 1,230 and 9,080 ± 1,254 to 12,100 ± 1,035, respectively. The numbers of observed species in the rhizosphere groups S-R-ditch, S-R-pond-2, R-ditch, and R-pond-2 were significantly higher than those of their corresponding non-rhizosphere groups S-ditch, S-pond-2, ditch, and pond-2, respectively. Meanwhile, the values for goods coverage in the rhizosphere and non-rhizosphere sediments in the PDCS ranged from 0.90 to 0.94 and 0.9 to 0.94, respectively. Moreover, Chao 1, Shannon, and Simpson indices in the PDCS ranged from 11,600 ± 1,396 to 16,400 ± 1,543, 11.3 ± 0.3 to 12.0 ± 0.3, and 0.9971 ± 0.0021 to 0.9979 ± 0.0003 in the rhizosphere

TABLE 1 | Spearman's correlation coefficients between sediment microbial diversity and water quality.

	Non-rhizosphere			Rhizosphere		
	Chao 1 index	**Shannon index**	**Simpson index**	**Chao 1 index**	**Shannon index**	**Simpson index**
TN (mg L^{-1})	−0.189	−0.185	−0.402	−0.066	−0.208	−0.253
NH_4^+-N (mg L^{-1})	0.102	0.067	−0.320	0.526[a]	0.240	−0.139
NO_3^--N (mg L^{-1})	−0.010	−0.169	−0.250	−0.226	−0.136	−0.053
NO_2^--N (mg L^{-1})	−0.018	−0.053	0.089	0.240	−0.025	−0.237
TP (mg L^{-1})	−0.232	−0.389	−0.179	0.016	−0.070	−0.123
IP (mg L^{-1})	−0.220	−0.412	−0.177	0.029	−0.064	−0.124
DO (mg L^{-1})	−0.081	0.052	0.464	−0.416	−0.149	0.234
Water pH	−0.045	0.070	−0.219	−0.313	−0.181	0.095
W-temp (°C)	0.088	−0.110	−0.479[a]	0.008	0.087	0.065
ORP (mV)	0.323	0.499[a]	0.562[a]	0.168	0.081	−0.091
Salinity (ppt)	0.216	0.241	0.471[a]	0.204	0.266	0.238
Turbidity (NTU)	0.355	0.113	−0.056	0.604[b]	0.549[b]	0.428

TN

[a]p< *0.05.*

[b]p< *0.01.*

TABLE 2 | Spearman's correlation coefficients between microbial diversity indices, sediment properties and root exudates.

	Non-rhizosphere			Rhizosphere		
	Chao 1 index	**Shannon index**	**Simpson index**	**Chao 1 index**	**Shannon index**	**Simpson index**
STN (g kg^{-1})	0.685[b]	0.264	−0.118	0.652[b]	0.292	−0.162
SNH_4^+-N (g kg^{-1})	0.787[b]	0.329	−0.303	0.699[b]	0.211	−0.279
SNO_3^--N (g kg^{-1})	0.682[b]	0.309	−0.049	0.623[b]	0.262	−0.129
STP (mg kg^{-1})	0.787[b]	0.280	−0.123	0.665[b]	0.345	−0.005
SIP (mg kg^{-1})	0.558[a]	−0.005	−0.276	0.439[a]	0.270	0.011
OM (g kg^{-1})	0.725[b]	0.291	−0.080	0.655[b]	0.192	−0.166
TOC (%)	0.641[b]	0.253	−0.222	0.790[b]	0.532[a]	0.114
Water content (%)	0.785[b]	0.330	−0.154	0.815[b]	0.414	−0.050
pH	—	—	—	−0.352	−0.155	0.136
Protein (mg L^{-1})	—	—	—	−0.042	0.044	−0.039
Polysaccharide (mg L^{-1})	—	—	—	0.261	0.227	0.188
Amino acid (nmol L^{-1})	—	—	—	−0.156	−0.334	−0.301
Lactic acid (mg L^{-1})	—	—	—	0.238	0.351	0.274
Tartaric acid (mg L^{-1})	—	—	—	0.460[a]	0.288	0.132

STN: sediment TN; SNH_4^+-N: sediment NH_4^+-N; SNO_3^--N: sediment NO_3^--N; OM: organic matter; STP: sediment TP; SIP: sediment IP.

[a]p< *0.05.*

[b]p< *0.01.*

sediments and ranged from 11,300 ± 286 to 15,900 ± 879, 11.1 ± 0.2 to 12.0 ± 0.2, and 0.9970 ± 0.0023 to 0.9977 ± 0.0002 in the non-rhizosphere sediment, respectively. Chao1 values in the five rhizosphere groups S-R-ditch, S-R-pond-2, R-pond-1, R-ditch, and R-pond-2 were all significantly higher than their corresponding non-rhizosphere groups S-ditch, S-pond-2, pond-1, ditch, and pond-2, respectively ($p < 0.05$). Similarly, the values of Shannon in the S-R-ditch, R-ditch and R-pond-2 groups were significantly higher than those of their corresponding non-rhizosphere groups S-ditch, ditch, and pond-2, respectively ($p < 0.05$). Moreover, Simpson values in the S-R-ditch, R-pond-1, and R-pond-2 were significantly higher than those of their corresponding non-rhizosphere groups S-ditch, pond-1, and pond-2, respectively ($p < 0.05$).

Spearman's correlation coefficients between microbial diversity indices and water quality were presented in **Table 1**. In the rhizosphere, Chao 1 index showed significant and positive correlations with NH_4^+-N and turbidity ($p < 0.05$). Meanwhile, turbidity was significantly positively correlated with the Shannon index ($p < 0.01$). In the non-rhizosphere, significant positive correlations between the ORP and the Shannon and Simpson indices were observed ($p < 0.05$); while Simpson index was significantly negatively correlated with W-temp, and was significantly positively associated with salinity ($p < 0.05$).

Spearman's correlation coefficients between microbial diversity indices, sediment properties, and root exudates were demonstrated in **Table 2**. In the rhizosphere, Chao 1 index showed significant correlation with sediment total nitrogen (STN), sediment ammonia nitrogen (SNH_4^+-N), sediment nitrate nitrogen (SNO_3^--N), STP, SIP, OM, TOC, WC, and tartaric acids respectively ($p < 0.01$). Meanwhile, TOC was

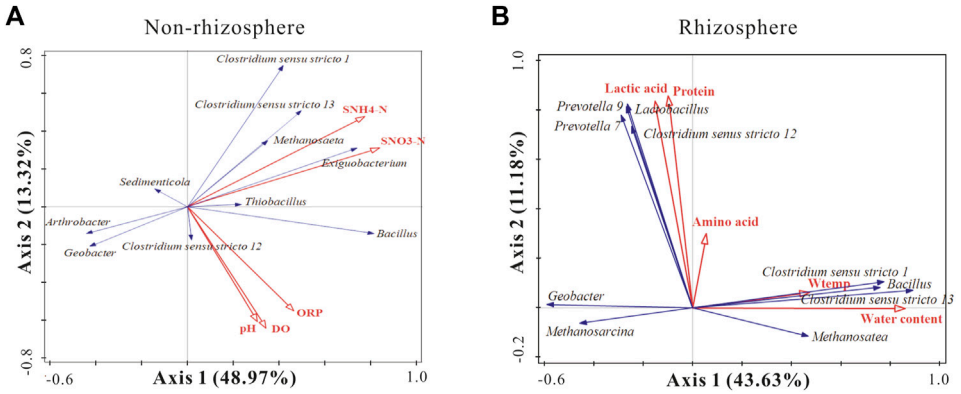

FIGURE 7 | RDA analysis of species composition of sediment bacterial taxa associated with significant environmental factors. The blue and red arrows indicate top 10 functional bacteria genus and significant environmental factors in the non-rhizosphere sediments **(A)** and the rhizosphere sediments **(B)**.

significantly positively related to Shannon index ($p < 0.05$). Similarly, in the non-rhizosphere sediments, Chao 1 index showed significant correlations with all measured sediment properties ($p < 0.05$).

Relationship Between Sediment Bacteria and Environmental Factors

As demonstrated in **Figure 7A**, the first two eigenvalues could explain 48.97 and 13.32% of the total variation at the genus level in the non-rhizosphere sediments, respectively. The environmental variables accounted for 66.9% of the total variation for the microbial community of non-rhizosphere sediments. In the non-rhizosphere sediment groups, SNH_4^+-N and SNO_3^--N exhibited significant positive effects on the dominant bacterial genera *Clostridium sensu stricto1*, *Clostridium sensu stricto 13*, and significant negative effects on *Arthrobacter* and *Geobacter*. Moreover, pH, DO, and ORP had strong positive effects on *Clostridium sensu stricto 12* and *Bacillus*.

As demonstrated in **Figure 7B**, the first two eigenvalues could explain 43.63 and 11.18% of the total variation at the genus level in the rhizosphere sediments, respectively. Environmental variables accounted for 60.3% of the total variation for the microbial community of rhizosphere sediments. In the rhizosphere, lactic acids, proteins, and amino acids showed significant positive effects on *Lactobacillus*, *Geobacter* and *Clostridiu sensu stricto 12*. Moreover, *Bacillus*, *Clostridium sensu stricto 1*, and *Clostridium sensu stricto 13* were significantly positively affected by W-temp and WC.

DISCUSSION

The Role of Bacteria in Nutrient Removal of the PDCS

In the present study, the averaged final TN and TP removal efficiencies of the PDCS at day 60 were mostly higher than that in IVCWs (51.6%) (Chang et al., 2015), in line with the mean value in algal pond combined with constructed wetlands (69.74%) (Zhao et al., 2016), yet lower than that in SFCWs (96.14%) (Li et al., 2020), suggesting the PDCS system was a valuable choice for rural wastewater remediation. Our previous study have demonstrated that microorganisms play important role in N and P removal in the PDCS (Ma et al., 2019). The removal of N was mainly contributed to simultaneous nitrification, anaerobic ammonium oxidation, and denitrification processes *via* the nitrogen-related bacteria (Zhao et al., 2019). In this paper, *Bacillus* was one of the three predominant genera in ponds and the ditch for the two systems, respectively. This finding was in line with the previous study reported that *Bacillus* was one of the six predominant bacterial genera for heterotrophic nitrification and aerobic denitrification in aquatic ecosystems (Qiao et al., 2020). Previous studies reported that *Bacillus*. sp. participated in aerobic denitrification in the PDCS, and *Clostridium* sp. was used for anaerobic ammonium-oxidizing in the sludge fermentation reactor (Yang et al., 2011; Ma et al., 2021b). A earlier study reported that rhizosphere bacteria played a pivotal role in regulating the P transformation and can utilize various P forms in wetland plants (Teng et al., 2018). *Geobacter* and *Bacillus*. sp. were known to act as polyphosphate-accumulating organisms, showing a strong capacity of poly-P accumulation and P storage (Schelfhout et al., 2015; Wang et al., 2019).

Comparison of Microbial Community Structure and Diversity Between Rhizosphere and Non-Rhizosphere Bacteria

The "rhizosphere effect" can lead to greatly variations in compositions and diversities of rhizosphere and non-rhizosphere sediment bacteria, where the impacts were influenced by seasons (Dewedar et al., 2009), soil types (Zhao et al., 2017), and plant species (Yin et al., 2018). The OTU numbers in the rhizosphere sediments of five microcosms were all higher than those of their counterparts in the non-rhizosphere, suggesting the presence of more

bacteria and more complex microbial communities in the rhizosphere sediments. Moreover, α-diversities of rhizosphere groups S-R-ditch, S-R-pond-2, R-pond-1, R-ditch, and R-pond-2 were all significantly higher than their corresponding counterparts ($p < 0.05$). These results indicated that compared with the non-rhizosphere, both the richnesses and diversities of microorganisms in the rhizosphere were enhanced due to the exudates from the plant roots (Stringlis et al., 2018). These effects will indirectly promote the roles of plants in nutrient removal in the PDCS. This was in line with the previous study in wetland plants which reported that "rhizosphere effects" affected the removal efficiency of nutrient *via* regulating the density and diversity of the rhizosphere microbes (Chen et al., 2016). Similarly, a recent study have reported that "rhizosphere effects" can result in the increase of relative abundances of some beneficial bacteria such as *Streptomycetaceae* and *Bacillaceae*, which exhibited significantly positive correlations with the uptake of N (Wu et al., 2021).

Both non-rhizosphere and rhizosphere groups shared five predominant bacterial genera, *Bacillus*, *Geobacter*, *Clostridium sensu stricto 1*, *Clostridium sensu stricto 12*, and *Clostridium sensu stricto 13*. These findings were consistent with the previous research in tidal marsh soil reported that relative abundances of *Geobacter*, *Bacillus*, *Clostridium* and *Shewanella* in the rhizosphere were higher than those in the bulk soil (Luo et al., 2018). However, at day 60, the relative abundance of *Geobacter* in the ditch of the PDCS was richer than those of two ponds; while frequencies of *Bacillus* and *Clostridium sensu stricto 1* in two ponds of the PDCS at day 60 were significantly higher than those in the ditch. This was mainly due to that differences in environmental factors such as soil types (Bakker et al., 2015) and plant species (Yin et al., 2018), resulting in varying root exudates composition and contents (Ma et al., 2021b), thereby affected the community structure of bacteria. Moreover, the frequencies of *Bacillus* and *Clostridium sensus stricto 1*, and *Geobacter* in the rhizosphere of ponds and the ditch for two systems at day 30 were higher than those in the non-rhizosphere (**Figure 5**). This was consistent with our results that protein and amino acids contents of *Vallisneria natans L.* in PDCS's two ponds increased from day 15 to 30 (**Supplementary Table S5**). This suggested that plants could adjust the secretion to cope with abiotic environmental stress (Edayilam et al., 2018). Relative higher proteins and amino acids values were conductive to increment of rhizosphere bacteria, which would be helpful in promoting the removal of nutrients (Bakker et al., 2015).

Responses of Rhizosphere and Non-Rhizosphere Bacteria to Abiotic Environmental Stress

Root exudates such as amino acids, organic acids, and sugars could provide carbon source for microbial growth and can drive sediment bacterial population richness and activities (Raaijmakers et al., 2009; Berendsen et al., 2012). Meanwhile, root exudates excreted by plants distributed in strong gradient manners from root surface into the soil. These root exudate gradients exert selective pressures, which affected the local microbial community structure such as their abundance and composition (Nunes da Rocha et al., 2009). Meanwhile, WC and W-temp played important roles in modulating the community structure of bacteria (Liddell et al., 2007; Gaumont-Guay et al., 2008). This was confirmed by our observations that Chao 1 indices of the rhizosphere and non-rhizosphere bacteria were both significantly correlated with water content (**Table 2**); while significant negative relationship between Simpson index and W-temp was only detected in the non-rhizosphere (**Table 1**). *Bacillus* and *Clostridium* sp. in the rhizosphere were significantly affected by water content and W-temp. Higher water content could enhance oxygen availability and diffusion rates in the sediment, which was benefit for *Bacillus* growth (Ma et al., 2021b). This was confirmed by our finding that the relative abundance of *Bacillus* was positively associated with DO in the non-rhizosphere (**Figure 7A**). In addition, Chao 1 index showed significant positive correlations with all measured sediment properties in the rhizosphere and non-rhizosphere (**Table 2**). Compared to the rhizosphere, *Bacillus* and *Clostridium* sp. in the non-rhizosphere were mainly affected by SNH_4^+-N and SNO_3^--N (**Figure 7A**). Nitrification and denitrification always occurred in adjacent area resulting in the NO_3^- formed by nitrification diffusing towards an anaerobic zone where it was the terminal electron receptor for the denitrification process (Lu et al., 2012).

CONCLUSION

The PDCS system exhibited great capabilities in reducing nutrients N and P from rural wastewater, with the removal efficiencies ranging from 72.7 to 97.4%. Microorganisms were largely responsible for N and P removal, however, the community structures and diversities of rhizosphere and non-rhizosphere sediment bacteria varied greatly. The average numbers of bacterial OTUs in the rhizosphere sediments were significantly higher than their corresponding counterparts ($p < 0.05$). In the PDCS, the different microcosms in both rhizosphere and non-rhizosphere sediments shared dominant bacterial genera, such as *Bacillus* and *Clostridium sensu stricto 1* for the ponds, and *Geobacter* for the ditch, respectively. Meanwhile, the contents of these three bacterial genera in the rhizosphere were higher than those of the non-rhizosphere at day 30. Moreover, Chao 1 index in both rhizosphere and non-rhizosphere was significantly positively correlated with all measured sediment properties, such as STN, STP, and OM. In the rhizosphere, Chao 1 index showed significant positive associations with NH_4^+-N, turbidity, tartaric acid, and Shannon index was significantly positively correlated with turbidity and TOC ($p < 0.05$). Similarly, in the non-rhizosphere, the Shannon and Simpson indices were associated with ORP ($p < 0.05$), respectively. RDA analysis demonstrated that exudates such as lactic acids, proteins, and amino acids exhibited strong positive effects on *Geobacter* and *Clostridiu sensu stricto 12* in the rhizosphere;

while *Bacillus* and *Clostridium* were significantly associated with SNH_4^+-N and SNO_3^--N in non-rhizosphere. Together, regulating root exudates and sediment available N will increase the richness and diversity of dominant microbial species in the rhizosphere and non-rhizosphere. These findings are beneficial for the optimization and design of PDCSs and other nutrient removal systems in large-scale wastewater treatment applications.

DATA AVAILABILITY STATEMENT

The data presented in the study are deposited in the National Genomics Data Center repository, accession number CRA004345.

AUTHOR CONTRIBUTIONS

MY, YP, LY, and WL performed the experiments. FH and LM designed the experiments and wrote the manuscript.

FUNDING

This work was supported by the National Natural Science Foundation of China (Grant numbers. 82070031, 51709255) and Hubei Provincial Key Laboratory of River Basin Water Resources and Eco-environmental Sciences, Changjiang River Scientific Research Institute open research program (Grant number. CKWV2019769/KY).

ACKNOWLEDGMENTS

The authors thank Weijun Tong (Institute of hydrobiology, Chinese Academy of Sciences) for his help in sampling.

SUPPLEMENTARY MATERIAL

The Supplementary Material for this article can be found online at: https://www.frontiersin.org/articles/10.3389/fenvs.2021.717458/full#supplementary-material

REFERENCES

Bais, H. P., Weir, T. L., Perry, L. G., Gilroy, S., and Vivanco, J. M. (2006). The Role of Root Exudates in Rhizosphere Interactions with Plants and Other Organisms. *Annu. Rev. Plant Biol.* 57 (1), 233–266. doi:10.1146/annurev.arplant.57.032905.105159

Bakker, M., Chaparro, J., Manter, D., and Vivanco, J. (2015). Impacts of Bulk Soil Microbial Community Structure on Rhizosphere Microbiomes of Zea mays. *Plant Soil* 392, 115–126. doi:10.1007/s11104-015-2446-0

Berendsen, R. L., Pieterse, C. M. J., and Bakker, P. A. H. M. (2012). The Rhizosphere Microbiome and Plant Health. *Trends Plant Sci.* 17 (8), 478–486. doi:10.1016/j.tplants.2012.04.001

Bowes, M. J., Jarvie, H. P., Halliday, S. J., Skeffington, R. A., Wade, A. J., Loewenthal, M., et al. (2015). Characterising Phosphorus and Nitrate Inputs to a Rural River Using High-Frequency Concentration-Flow Relationships. *Sci. Total Environ.* 511, 608–620. doi:10.1016/j.scitotenv.2014.12.086

Caporaso, J. G., Kuczynski, J., Stombaugh, J., Bittinger, K., Bushman, F. D., Costello, E. K., et al. (2010). QIIME Allows Analysis of High-Throughput Community Sequencing Data. *Nat. Methods* 7 (5), 335–336. doi:10.1038/nmeth.f.303

Chang, J. J., Wu, S. Q., Zhang, S. Y., Zhang, S. H., and Liang, W. (2015). Comparative Evaluation of Total Phosphorus Removal Performances for Treatment of Domestic and Secondary Wastewater Using Integrated Vertical-Flow Constructed Wetlands: Two Years' Experience. *Desalin Water Treat.* 56 (5), 1379–1388. doi:10.1080/19443994.2014.950343

Chen, H., Zhou, W., Zhu, S., Liu, F., Qin, L., Xu, C., et al. (2021). Biological Nitrogen and Phosphorus Removal by a Phosphorus-Accumulating Bacteria Acinetobacter Sp. Strain C-13 with the Ability of Heterotrophic Nitrification–Aerobic Denitrification. *Bioresour. Technol.* 322, 124507. doi:10.1016/j.biortech.2020.124507

Chen, Z.-J., Tian, Y.-H., Zhang, Y., Song, B.-R., Li, H.-C., and Chen, Z.-H. (2016). Effects of Root Organic Exudates on Rhizosphere Microbes and Nutrient Removal in the Constructed Wetlands. *Ecol. Eng.* 92, 243–250. doi:10.1016/j.ecoleng.2016.04.001

Childers, D. L. (2020). A Decade of Ecosystem-Scale Research at an Aridland Constructed Treatment Wetland. *Front. Env Sci-switz.* 8, 576936. doi:10.3389/fenvs.2020.576936

Dewedar, A., Bahgat, M., and Shabana, E. E. (2009). Seasonal Distribution and Activity of Nitrogen-Cycling Bacteria in Bardawil Lagoon, Egypt. *Int. J. Clin. Exp. Med.* 34 (2), 183–188. doi:10.2989/AJAS.2009.34.2.9.896

Edayilam, N., Montgomery, D., Ferguson, B., Maroli, A. S., Martinez, N., Powell, B. A., et al. (2018). Phosphorus Stress-Induced Changes in Plant Root Exudation Could Potentially Facilitate Uranium Mobilization from Stable Mineral Forms. *Environ. Sci. Technol.* 52 (14), 7652–7662. doi:10.1021/acs.est.7b05836

Edgar, R. C., Haas, B. J., Clemente, J. C., Quince, C., and Knight, R. (2011). UCHIME Improves Sensitivity and Speed of Chimera Detection. *Bioinformatics* 27 (16), 2194–2200. doi:10.1093/bioinformatics/btr381

Egamberdieva, D., Kamilova, F., Validov, S., Gafurova, L., Kucharova, Z., and Lugtenberg, B. (2008). High Incidence of Plant Growth-Stimulating Bacteria Associated with the Rhizosphere of Wheat Grown on Salinated Soil in Uzbekistan. *Environ. Microbiol.* 10 (1), 1–9. doi:10.1111/j.1462-2920.2007.01424.x

Evans, R. A., Cromar, N. J., and Fallowfield, H. J. (2005). Performance of a Pilot-Scale High Rate Algal Pond System Treating Abattoir Wastewater in Rural South Australia: Nitrification and Denitrification. *Water Sci. Technol.* 51 (12), 117–124. doi:10.1016/j.watres.2004.10.012

Gaumont-Guay, D., Black, T. A., Barr, A. G., Jassal, R. S., and Nesic, Z. (2008). Biophysical Controls on Rhizospheric and Heterotrophic Components of Soil Respiration in a Boreal Black spruce Stand. *Tree Physiol.* 28 (2), 161–171. doi:10.1093/treephys/28.2.161

Grandy, A. S., Erich, M. S., and Porter, G. A. (2000). Suitability of the Anthrone–Sulfuric Acid Reagent for Determining Water Soluble Carbohydrates in Soil Water Extracts. *Soil Biol. Biochem.* 32 (5), 725–727. doi:10.1016/S0038-0717(99)00203-5

Gustafsson, J. P., Renman, A., Renman, G., and Poll, K. (2008). Phosphate Removal by mineral-based Sorbents Used in Filters for Small-Scale Wastewater Treatment. *Water Res.* 42 (1-2), 189–197. doi:10.1016/j.watres.2007.06.058

Holm-Hansen, O., and Riemann, B. (1978). Chlorophyll a Determination: Improvements in Methodology. *Oikos* 30 (3), 438–447. doi:10.2307/3543338

Hu, B.-l., Zheng, P., Tang, C.-j., Chen, J.-w., van der Biezen, E., Zhang, L., et al. (2010). Identification and Quantification of Anammox Bacteria in Eight Nitrogen Removal Reactors. *Water Res.* 44 (17), 5014–5020. doi:10.1016/j.watres.2010.07.021

Khammar, N., Malhautier, L., Degrange, V., Lensi, R., Godon, J. J., and Fanlo, J. L. (2005). Link between Spatial Structure of Microbial Communities and Degradation of a Complex Mixture of Volatile Organic Compounds in

Peat Biofilters. *J. Appl. Microbiol.* 98 (2), 476–490. doi:10.1111/j.1365-2672.2004.02474.x

Li, H., Yang, X., Weng, B., Su, J., Nie, S. a., Gilbert, J. A., et al. (2016). The Phenological Stage of rice Growth Determines Anaerobic Ammonium Oxidation Activity in Rhizosphere Soil. *Soil Biol. Biochem.* 100, 59–65. doi:10.1016/j.soilbio.2016.05.015

Li, J., Li, J., Gao, R., Wang, M., Yang, L., Wang, X., et al. (2018). A Critical Review of One-Stage Anammox Processes for Treating Industrial Wastewater: Optimization Strategies Based on Key Functional Microorganisms. *Bioresour. Technol.* 265, 498–505. doi:10.1016/j.biortech.2018.07.013

Li, X., Li, Y., Lv, D., Li, Y., and Wu, J. (2020). Nitrogen and Phosphorus Removal Performance and Bacterial Communities in a Multi-Stage Surface Flow Constructed Wetland Treating Rural Domestic Sewage. *Sci. Total Environ.* 709, 136235. doi:10.1016/j.scitotenv.2019.136235

Li, Y., Zhao, S., Zhang, J., He, Y., Zhang, J., and Ge, R. (2019). Screening and Diversity Analysis of Aerobic Denitrifying Phosphate Accumulating Bacteria Cultivated from A2O Activated Sludge. *Processes* 7 (11), 827. doi:10.3390/pr7110827

Liddell, K., Krivtsov, V., Staines, H., Brendler, A., Garside, A., and Griffiths, B. (2007). A Study of Population Numbers and Ecological Interactions of Soil and forest Floor Microfauna. *Anim. Biol.* 57 (4), 467–484. doi:10.1163/157075607782232189

Liu, L., Ji, M., Wang, F., Wang, S., and Qin, G. (2020). Insight into the Influence of Microbial Aggregate Types on Nitrogen Removal Performance and Microbial Community in the Anammox Process - A Review and Meta-Analysis. *Sci. Total Environ.* 714, 136571. doi:10.1016/j.scitotenv.2020.136571

Lu, X., Yan, Y., Fan, J., and Wang, X. (2012). Gross Nitrification and Denitrification in Alpine Grassland Ecosystems on the Tibetan Plateau. *Arct Antarct Alp Res.* 44 (2), 188–196. doi:10.1657/1938-4246-44.2.188

Luo, M., Liu, Y., Huang, J., Xiao, L., Zhu, W., Duan, X., et al. (2018). Rhizosphere Processes Induce Changes in Dissimilatory Iron Reduction in a Tidal Marsh Soil: a Rhizobox Study. *Plant Soil* 433 (1), 83–100. doi:10.1007/s11104-018-3827-y

Ma, L., He, F., Huang, T., Zhou, Q., Zhang, Y., and Wu, Z. (2016). Nitrogen and Phosphorus Transformations and Balance in a Pond-Ditch Circulation System for Rural Polluted Water Treatment. *Ecol. Eng.* 94, 117–126. doi:10.1016/j.ecoleng.2016.05.051

Ma, L., He, F., Sun, J., Huang, T., Xu, D., Zhang, Y., et al. (2015a). Effects of Flow Speed and Circulation Interval on Water Quality and Zooplankton in a Pond–Ditch Circulation System. *Environ. Sci. Pollut. R.* 22 (13), 10166–10178. doi:10.1007/s11356-015-4195-2

Ma, L., He, F., Sun, J., Wang, L., Xu, D., and Wu, Z. (2015b). Remediation Effect of Pond–Ditch Circulation on Rural Wastewater in Southern China. *Ecol. Eng.* 77, 363–372. doi:10.1016/j.ecoleng.2014.11.036

Ma, L., Liu, W., Tan, Q., Zhou, Q., Wu, Z., and He, F. (2019). Quantitative Response of Nitrogen Dynamic Processes to Functional Gene Abundances in a Pond-Ditch Circulation System for Rural Wastewater Treatment. *Ecol. Eng.* 134, 101–111. doi:10.1016/j.ecoleng.2019.05.008

Ma, L., Yang, L., Liu, W., Zhang, Y., Zhou, Q., Wu, Z., et al. (2021a). Effects of Root Exudates on Rhizosphere Bacteria and Nutrient Removal in Pond-Ditch Circulation Systems (PDCSs) for Rural Wastewater Treatment. *Sci. Total Environ.* 785, 147282. doi:10.1016/j.scitotenv.2021.147282

Ma, L., Yang, L., Liu, W., Zhang, Y., Zhou, Q., Wu, Z., et al. (2021b). Environmental Factors and Microbial Communities Jointly Regulate Biological Dephosphorization Process in Pond-Ditch Circulation Systems (PDCSs) for Rural Wastewater Treatment. *Sci. Total Environ.* 758, 143629. doi:10.1016/j.scitotenv.2020.143629

Nie, S. a., Li, H., Yang, X., Zhang, Z., Weng, B., Huang, F., et al. (2015). Nitrogen Loss by Anaerobic Oxidation of Ammonium in rice Rhizosphere. *Isme J.* 9 (9), 2059–2067. doi:10.1038/ismej.2015.25

Nunes da Rocha, U., Van Overbeek, L., and Van Elsas, J. D. (2009). Exploration of Hitherto-Uncultured Bacteria from the Rhizosphere. *Fems Microbiol. Ecol.* 69 (3), 313–328. doi:10.1111/j.1574-6941.2009.00702.x

Poret-Peterson, A. T., Albu, S., McClean, A. E., and Kluepfel, D. A. (2019). Shifts in Soil Bacterial Communities as a Function of Carbon Source Used during Anaerobic Soil Disinfestation. *Front. Env Sci-switz.* 6, 160. doi:10.3389/fenvs.2018.00160

Qiao, Z., Sun, R., Wu, Y., Hu, S., Liu, X., Chan, J., et al. (2020). Characteristics and Metabolic Pathway of the Bacteria for Heterotrophic Nitrification and Aerobic Denitrification in Aquatic Ecosystems. *Environ. Res.* 191, 110069. doi:10.1016/j.envres.2020.110069

Raaijmakers, J. M., Paulitz, T. C., Steinberg, C., Alabouvette, C., and Moënne-Loccoz, Y. (2009). The Rhizosphere: a Playground and Battlefield for Soilborne Pathogens and Beneficial Microorganisms. *Plant Soil* 321 (1), 341–361. doi:10.1007/s11104-008-9568-6

Ruban, V., López-Sánchez, J. F., Pardo, P., Rauret, G., Muntau, H., and Quevauviller, P. (2001). Harmonized Protocol and Certified Reference Material for the Determination of Extractable Contents of Phosphorus in Freshwater Sediments – A Synthesis of Recent Works. *Fresen J. Anal. Chem.* 370 (2), 224–228. doi:10.1007/s002160100753

Schelfhout, S., De Schrijver, A., De Bolle, S., De Gelder, L., Demey, A., Du Pré, T., et al. (2015). Phosphorus Mining for Ecological Restoration on Former Agricultural Land. *Restor Ecol.* 23 (6), 842–851. doi:10.1111/rec.12264

Spector, T. (1978). Refinement of the Coomassie Blue Method of Protein Quantitation: A Simple and Linear Spectrophotometric Assay for ≤0.5 to 50 μg of Protein. *Anal. Biochem.* 86 (1), 142–146. doi:10.1016/0003-2697(78)90327-5

State EPA of China (2002). *Monitoring and Determination Methods for Water and Wastewater*. 4th ed. Beijing: China Environmental Science Press. (in Chinese).

Stringlis, I. A., Yu, K., Feussner, K., de Jonge, R., Van Bentum, S., Van Verk, M. C., et al. (2018). MYB72-dependent Coumarin Exudation Shapes Root Microbiome Assembly to Promote Plant Health. *P Natl. Acad. Sci. USA* 115 (22), E5213. doi:10.1073/pnas.1722335115

Teng, Z., Zhu, Y., Li, M., and Whelan, M. J. (2018). Microbial Community Composition and Activity Controls Phosphorus Transformation in Rhizosphere Soils of the Yeyahu Wetland in Beijing, China. *Sci. Total Environ.* 628-629, 1266–1277. doi:10.1016/j.scitotenv.2018.02.115

Tomaszewski, M., Cema, G., and Ziembińska-Buczyńska, A. (2017). Influence of Temperature and pH on the Anammox Process: A Review and Meta-Analysis. *Chemosphere* 182, 203–214. doi:10.1016/j.chemosphere.2017.05.003

Torrens, A., Folch, M., and Salgot, M. (2021). Design and Performance of an Innovative Hybrid Constructed Wetland for Sustainable Pig Slurry Treatment in Small Farms. *Front. Env Sci-switz.* 8 (304), 577186. doi:10.3389/fenvs.2020.577186

Wang, B., Guo, Y., Zhao, M., Li, B., and Peng, Y. (2019). Achieving Energy-Efficient Nitrogen Removal and Excess Sludge Reutilization by Partial Nitritation and Simultaneous Anammox Denitrification and Sludge Fermentation Process. *Chemosphere* 218, 705–714. doi:10.1016/j.chemosphere.2018.11.168

Wu, A.-L., Jiao, X.-Y., Wang, J.-S., Dong, E.-W., Guo, J., Wang, L.-G., et al. (2021). Sorghum Rhizosphere Effects Reduced Soil Bacterial Diversity by Recruiting Specific Bacterial Species under Low Nitrogen Stress. *Sci. Total Environ.* 770, 144742. doi:10.1016/j.scitotenv.2020.144742

Yang, X.-P., Wang, S.-M., Zhang, D.-W., and Zhou, L.-X. (2011). Isolation and Nitrogen Removal Characteristics of an Aerobic Heterotrophic Nitrifying–Denitrifying Bacterium, Bacillus Subtilis A1. *Bioresour. Technol.* 102 (2), 854–862. doi:10.1016/j.biortech.2010.09.007

Yin, J., Zhang, P., Li, F., Li, G., and Hai, B. (2015). Simultaneous Biological Nitrogen and Phosphorus Removal with a Sequencing Batch Reactor–Biofilm System. *Int. Biodeter Biodegr* 103, 221–226. doi:10.1016/j.ibiod.2015.02.019

Yin, X., Liu, G., Peng, L., Hua, Y., Wan, X., Zhou, W., et al. (2018). Microbial Community of Nitrogen Cycle-Related Genes in Aquatic Plant Rhizospheres of Lake Liangzi in winter. *J. Basic Microbiol.* 58 (11), 998–1006. doi:10.1002/jobm.201800220

Zhao, D., Wang, S., Huang, R., Zeng, J., Huang, F., and Yu, Z. (2017). Diversity and Composition of Bacterial Community in the Rhizosphere Sediments of Submerged Macrophytes Revealed by 454 Pyrosequencing. *Ann. Microbiol.* 67 (4), 313–319. doi:10.1007/s13213-017-1262-6

Zhao, Z., Song, X., Xiao, Y., Zhao, Y., Gong, Z., Lin, F., et al. (2016). Influences of Seasons, N/P Ratios and Chemical Compounds on Phosphorus Removal Performance in Algal Pond Combined with Constructed Wetlands. *Sci. Total Environ.* 573, 906–914. doi:10.1016/j.scitotenv.2016.08.148

Zhao, Z., Zhang, X., Wang, Z., Song, X., Cheng, M., Cheng, M., et al. (2019). Enhancing the Pollutant Removal Performance and Biological Mechanisms by Adding Ferrous Ions into Aquaculture Wastewater in Constructed Wetland. *Bioresour. Technol.* 293, 122003. doi:10.1016/j.biortech.2019.122003

Zhou, W., Jiang, X., Ouyang, J., Lu, B., Liu, W., and Liu, G. (2020). Environmental Factors, More Than Spatial Distance, Explain Community Structure of Soil Ammonia-Oxidizers in Wetlands on the Qinghai–Tibetan Plateau. *Microorganisms* 8 (6), 933. doi:10.3390/microorganisms8060933

Zou, L., Lu, Y., Dai, Y., Khan, M. I., Gustave, W., Nie, J., et al. (2021). Spatial Variation in Microbial Community in Response to as and Pb Contamination in Paddy Soils Near a Pb-Zn Mining Site. *Front. Env Sci-switz* 9 (138), 630668. doi:10.3389/fenvs.2021.630668

Conflict of Interest: The authors declare that the research was conducted in the absence of any commercial or financial relationships that could be construed as a potential conflict of interest.

Publisher's Note: All claims expressed in this article are solely those of the authors and do not necessarily represent those of their affiliated organizations, or those of the publisher, the editors and the reviewers. Any product that may be evaluated in this article, or claim that may be made by its manufacturer, is not guaranteed or endorsed by the publisher.

frontiers in Earth Science

ORIGINAL RESEARCH
published: 01 October 2021
doi: 10.3389/feart.2021.744224

Sustainable Development Evaluation and Its Obstacle Factors of the Weihe River Basin in Shaanxi Province, China

Yirui Wang[1,2], *Jinxi Song*[1,3]*, *Xuexian Zhang*[1,2] *and Haotian Sun*[3]

[1]State Key Laboratory of Soil Erosion and Dryland Farming on the Loess Plateau, Institute of Soil and Water Conservation, Chinese Academy of Sciences and Ministry of Water Resources, Yangling, China, [2]University of Chinese Academy of Sciences, Beijing, China, [3]Shaanxi Key Laboratory of Earth Surface System and Environmental Carrying Capacity, College of Urban and Environmental Sciences, Northwest University, Xi'an, China

The contradiction between economic growth, social development, and water environment deterioration represent significant challenges for river basin sustainable development. By constructing an indicator system of river basin sustainable development, the entropy method is adopted to conduct a quantitative evaluation of the cities sustainable development level for the Weihe River Basin in Shaanxi Province from 2009 to 2018, and the standard deviational ellipse is used to analyze the evolution of spatial distribution pattern of sustainable development in the study area. Furthermore, the obstacle degree model is applied to analyze the main obstacle factors restricting the improvement of river basin sustainable development. The results show that the sustainable development level of the Weihe River basin in Shaanxi Province improved slowly during the study period and significant regional differences among cities. This study provides a novel approach for future evaluation on sustainable development of the Weihe River basin and even the arid region in Northwest China, to achieve a win-win situation between economic and social development and ecological environment protection.

Keywords: sustainable development, the Weihe River basin, entropy method, standard deviational ellipse, obstacle model

OPEN ACCESS

Edited by:
Xiaofei Yu,
Northeast Normal University, China

Reviewed by:
Peng Li,
Xi'an University of Technology, China
Gary Feng,
National Laboratory for Agriculture and the Environment, Agricultural Research Service (USDA), United States

***Correspondence:**
Jinxi Song
jinxisong@nwu.edu.cn

Specialty section:
This article was submitted to Hydrosphere, a section of the journal Frontiers in Earth Science

Received: *20 July 2021*
Accepted: *23 August 2021*
Published: *01 October 2021*

Citation:
Wang Y, Song J, Zhang X and Sun H (2021) Sustainable Development Evaluation and Its Obstacle Factors of the Weihe River Basin in Shaanxi Province, China. Front. Earth Sci. 9:744224. doi: 10.3389/feart.2021.744224

INTRODUCTION

With 1% yearly growth of global water consumption (Wada et al. 2016), it is speculated that by 2050, more than 50% of the world's population will be chronically short of water (Roshan and Kumar, 2020). Water shortage will not only restrict social and economic development but also cause immeasurable damage to the ecological environment (Silva et al., 2019). Global water crisis is a barrier to sustainable development (Roshan and Kumar 2020); importance should be given to exploring the river basin sustainable development (RBSD).

Amid the unceasing appearance of global environment deterioration, resource depletion, population explosion, and other realistic problems, the concepts of sustainable development and the sustainable utilization of river basin have been recognized by many scholars. At present, the research on RBSD mainly focuses on the assessment of ecological health in the river basin Wu et al. (2020), Jamal et al. (2021); land use/cover changes and its environmental response in the river basin Shen and Ma (2020); optimization and management of water resources Chen et al. (2019), Ferreira et al. (2020); and ecological function zoning and ecological compensation of river basin (Melanie and John, 2018; Gao et al., 2019).

Much work has been done to RBSD during the past decades. A framework for quantitatively evaluating development sustainability was established with water-related eco-environmental carrying capacity as the core measure by Wang et al. (2014). Wang et al. (2019) used a pressure–state–response (PSR) model to quantify the sustainability of water resources in Beijing, China. D'Ambrosio et al. (2020) assessed the sustainability in water use at the basin scale through the water footprint. In recent years, evaluation methods such as system dynamics (Kotir et al. (2016), Pluchinotta et al. (2021), Song et al. (2018)) and sustainability index (Bui et al. (2019), Roobavannan et al. (2020)) have been widely used in the study of RBSD. However, with research concentrating on a single perspective, less attention was paid to the connection between the integrated socioeconomic development of the river basin and its water resources (Zhong et al., 2018). Besides, there is no unified and authoritative theoretical system for RBSD nor does it truly reflect the concept of sustainable development (Silva et al., 2020). Consideration is lacking in the coordinated development of society–economy–ecology to maximize the comprehensive benefits.

Some rivers in China suffer from problems such as the decline of sustainability and the deterioration of the natural environment caused by human activities (Fu et al., 2020). Among them, the problem of water shortage poses a threat to the sustainable development in arid and semiarid areas (Li J. et al., 2019). The Yellow River basin is a miniature of Asia and Africa's water resource deficit (Chen Y.-p. et al., 2020). As the largest tributary of the Yellow River basin, the Weihe River basin (WRB) is crucial to the sustainable development of the Yellow River basin. The ecological environment of WRB is seriously degraded Wang et al. (2019) and water resources have an obvious restrictive effect on regional development. The mechanism and difference in the midstream of the Yellow River basin can be clarified through the study of WRB, and it also offered a reference for the development of the upstream and downstream in the Yellow River basin.

The entropy weight method, standard deviational ellipse, and obstacle degree model are employed in this article. The entropy method is used to calculate the weight of each indicator, which can provide the basis for the comprehensive evaluation of multiple indicators. It avoids the deviation caused by human factors and makes the evaluation more objective. The method has been used for the evaluation of electric power development (Zhao et al. (2020)), carbon emission (Cui et al. (2021)), the sustainable development capability of agriculture Li Q. et al., (2019), and many other fields. The standard deviational ellipse method analyzes the directivity of spatial distribution well and reflects the concentration degree of each element in the spatial pattern. Standard deviational ellipse was used to examine the effects of land use policy on the spatiotemporal changes in the area of surface water by Xu et al. (2018). Zuo et al. (2021) revealed a dynamic evolution process of ecological civilization construction. Du et al. (2019) investigated the relationship between economic growth and carbon emissions from the construction industry. The obstacle degree model is a mathematical statistical model to calculate the impact factor, and it is widely used in many aspects of comprehensive evaluation of ecological resources and environment such as cultivated land resources security Huang et al. (2021), water resource security (Zhang et al., 2019), etc.

In this article, an indicator system of RBSD is established to analyze the temporal and spatial variation of sustainable development with the case study of WRB in Shaanxi Province. Next, the obstacle degree model is introduced to investigate the main impediments that affect RBSD, with countermeasures put forward accordingly. The project has a theoretical value for implementing scientific development view and enriching sustainable development theory. As for realistic significance, WRB in the northwest arid region of China is selected as a specific case, providing operational and referable suggestions for remodeling the development and evolution process of different rivers.

MATERIAL AND METHODS

Study Area

Weihe River basin (34°–37°N, 104°–110°E; **Figure 1**), originating from Niaoshu Mountain in Gansu Province, flows into the Yellow River basin in Shaanxi Province. It lies in the north of Qinling Mountain, south of Liupanshan Mountain, the east of Loess hilly and gully region, and the west of Guanzhong Plain. Located in the warm temperate zone, WRB in Shaanxi Province has a subhumid continental climate, with an annual mean temperature of 7.8–13.5°C and an annual precipitation of 500–800 mm (Zhao et al., 2016). The main stream of WRB in Shaanxi Province, a length of 502.40 km, covers a drainage area of 67,108 km^2, accounting for 50% of the total drainage area of the Yellow River basin in Shaanxi Province. The average annual runoff of the whole river is 1.04 × 1010 m^3, of which the runoff in Shaanxi Province is 6.27 × 109 m^3, with the flooding period (July to September) accounting for about 60% (Deng et al., 2020).

The Weihe River is the mother river of Shaanxi, related to the rise and fall of economic and social development in Shaanxi Province. The core of Guanzhong–Tianshui economic region, WRB, plays an important role in the western development strategy of China. By the end of 2018, the population of the study area grew to 2.45×10^7 people and GDP 9.87×10^{14} yuan (Shaanxi Provincial Bureau of Statistics, 2019). The total water resources quantity in the study area, 7.25 × 109 m^3, only accounted for 1.95% of that in Shaanxi Province. Only covering one-third of the land area of Shaanxi Province, WRB in Shaanxi Province discharged over three-fourths of the wastewater in Shaanxi Province. The water supply and water consumption of WRB in Shaanxi Province compose more than half of Shaanxi Province, 57.50% and 59.37%, respectively (Shaanxi Province Department of Water Resources, 2018). This study involves five cities on the main stream of WRB in Shaanxi Province, including Xi'an, Tongchuan, Baoji, Xianyang, and Weinan.

In recent years, remarkable changes have taken place in WRB with the intensification of human activities and the rapid development of the regional economy and society. However, multiple issues have attracted public concern, such as insufficient water resources, aggravated water pollution,

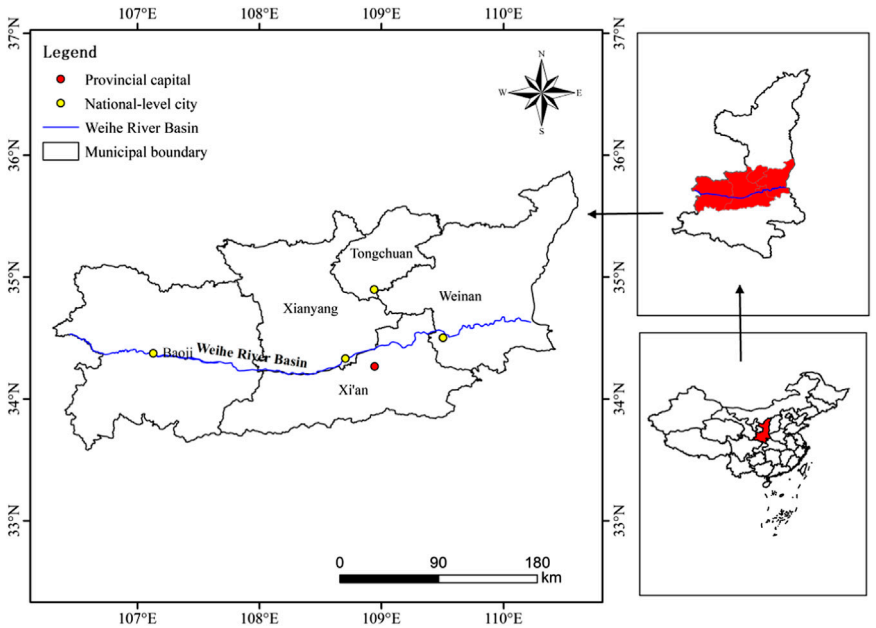

FIGURE 1 | The location of study area in China.

overexploitation of groundwater, and incomplete containment of soil and water loss. Therefore, the study on sustainable development of WRB in Shaanxi Province is of great significance for promoting green development of the economy and society in Shaanxi province.

Construction of Indicator System

The indicator system was based on the United Nations Sustainable Development Goals (SDGs) and China's National Plan on Implementation of the 2030 Agenda for Sustainable Development. To clarify the status of RBSD, this article regarded water resources as the core, the basin as a research space, and the complex system composed of human and nature in the basin as a research object. According to the construction principle of indicator system and covering the main environmental and socioeconomic issues contained in the concept of sustainable development with Chinese characteristics, the evaluation indicator is divided into a hierarchical system consisting of target layer (A), system layer (B), subsystem layer (C), and indicator layer (D).

The indicators were chosen for systematicness, completeness, representativeness, and accessibility. In terms of the actual situation, the water resource characteristics, and the evaluation content of WRB, 31 indicators were selected to construct the indicator system of RBSD (**Table 1**).

Calculation of Weight and the Level of Sustainable Development

To eliminate the magnitude difference among the data, the deviation standardization formula is adopted for each indicator, so that the results are all within the range of (0,1).

Positive Indicator

$$Y_{ij} = \frac{x_{ij} - \min(x_i)}{\max(x_i) - \min(x_i)}. \quad (1)$$

Negative Indicator

$$Y_{ij} = \frac{\max(x_i) - x_{ij}}{\max(x_i) - \min(x_i)}. \quad (2)$$

Here, x_{ij} and Y_{ij} are the original and normalized values of the ith indicator in the year j, respectively.

In information theory, entropy is a measure of uncertainty. According to the characteristics of entropy, the discrete degree of indicator layer can be measured by calculating the entropy value. The larger the discrete degree of indicator, the greater the influence of indicator on a comprehensive evaluation. The entropy method is used to quantify the information of each indicator with the Shannon entropy (Shannon, 1948). Information entropy is employed to calculate the weight of each indicator layer to achieve an objective quality evaluation.

Assuming that there are m evaluation objects and n evaluation indicators, a matrix A with n rows and m columns can be established:

$$A = \left(x_{ij}\right)_{n\times m}. \quad (3)$$

The proportion Z_{ij} of the ith indicator in the year j is given as follows:

$$Z_{ij} = \frac{Y_{ij}}{\sum_{i=1}^{m} Y_{ij}}. \quad (4)$$

The entropy k_i of the ith indicator is as follows:

TABLE 1 | The evaluation indicator system of river basin sustainable development.

Target layer (A)	System layer (B)	Subsystem layer (C)	Indicator layer (D)	Weight
Sustainable development	Economic development (B_1)	Economic level (C_1)	Gross domestic product (D_1)	0.0544
			Financial revenue (D_2)	0.0885
			Fixed assets investment (D_3)	0.0439
			Per capita GDP (D_4)	0.0266
		Economic structure (C_2)	Proportion of secondary industry in GDP (D_5)	0.0193
			Proportion of tertiary industry in GDP (D_6)	0.0474
		Economic efficiency (C_3)	The growth rate of total retail sales of consumer goods (D_7)	0.0085
			GDP growth rate (D_8)	0.0243
			The imbalance rate of fiscal revenue and expenditure (D_9)	0.0164
	Social development (B_2)	Population scale and quality (C_4)	Population quantity (D_{10})	0.0307
			Natural growth rate of population (D_{11})	0.0299
			Number of college students per 10,000 persons (D_{12})	0.1153
		Living standard of residents (C_5)	Per Capita Disposable Income of Rural Households (D_{13})	0.0216
			Average salary of urban workers (D_{14})	0.0227
			Coverage rate of population with access to tap water (D_{15})	0.0150
			Urban living area per capita (D_{16})	0.0571
		Quality of social development (C_6)	Proportion of education and technology expenditure in local financial expenditure (D_{17})	0.0231
			Number of medical beds per 10,000 persons (D_{18})	0.0171
			Urban unemployment rate (D_{19})	0.0097
			Green coverage rate of built-up area (D_{20})	0.0154
	Ecological development (B_3)	Water resource condition (C_7)	Amount of water resources per capita (D_{21})	0.0774
			Annual precipitation (D_{22})	0.0202
			Irrigated area (D_{23})	0.0263
			Water production coefficient (D_{24})	0.0263
		Water environmental quality (C_8)	Discharge amount of industrial wastewater (D_{25})	0.0121
			Urban sewage treatment rate (D_{26})	0.0087
			Ammonia nitrogen discharge (D_{27})	0.0143
			Chemical oxygen demand discharge (D_{28})	0.0106
		Ecological control (C_9)	Treatment capacity of facilities for wastewater treatment (D_{29})	0.0276
			Investment in water conservancy construction as percentage of GDP (D_{30})	0.0617
			The growth rate of soil erosion control (D_{31})	0.0281

$$k_i = -\frac{1}{\ln m}\sum_{i=1}^{m}\left(z_{ij}\ln z_{ij}\right). \quad (5)$$

The redundancy g_i of the information entropy of the ith indicator is as follows:

$$g_i = 1 - k_i. \quad (6)$$

The weight w_i of each indicator is calculated as follows:

$$w_i = \frac{g_i}{\sum_{i=1}^{n} g_i}. \quad (7)$$

The comprehensive evaluation of RBSD is calculated as follows:

$$RBSD = \sum_{i=1}^{n} Y_{ij} W_i. \quad (8)$$

Obstacle Degree Model

In the process of sustainable development evaluation, it is not only necessary to measure the level of RBSD but also to understand the critical factors that affect RBSD. Therefore, the obstacle degree model (Chen Y. et al. (2020), Fan and Fang (2020)) is introduced to analyze the obstacle factors of RBSD so as to carry out the pathological diagnosis in a practical application. The formula is as follows:

$$P_{ij} = 1 - x_{ij}, \quad (9)$$

$$Q_{ij} = \frac{P_{ij} W_j}{\sum_{j=1}^{n} P_{ij} W_j}, \quad (10)$$

where Q_{ij} represents the obstacle degree of the ith indicator in the year j, and P_{ij} is the deviation degree of indicator i in year j.

Data

In view of accessible and limited data, this article chose 2009 to 2018 as the research period and five cities of WRB in Shaanxi Province were selected as samples to establish a comprehensive indicator system for the sustainable development of WRB in Shaanxi Province. Data were collected from the China Urban Statistical Yearbooks (2010–2019), Shaanxi Statistical Yearbooks (2010–2019), and Shaanxi Water Resources Bulletins (2009–2018). In addition, missing data were obtained by the interpolation method.

RESULTS

Temporal Analysis

The evaluation levels of sustainable development of WRB in Shaanxi Province rose from 1.29 in 2009 to 1.87 in 2018 with an upward overall trend and a subtle fluctuation (**Figure 2** and

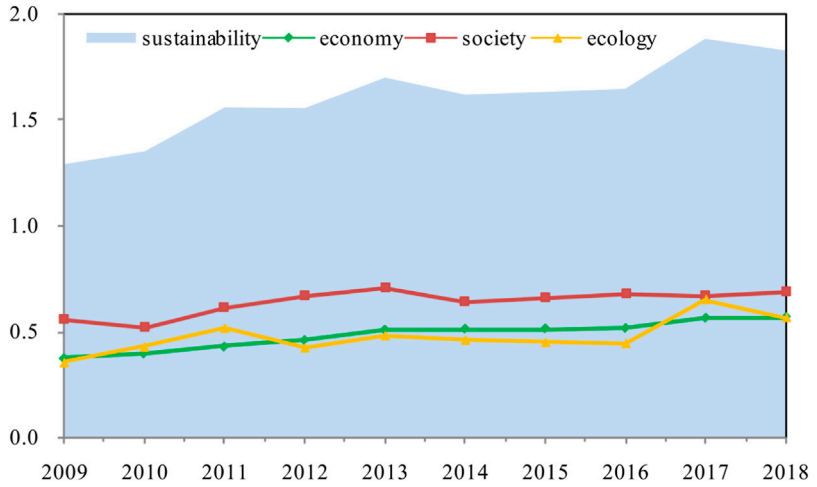

FIGURE 2 | The comprehensive evaluation value for river basin sustainable development.

TABLE 2 | The assessment results on river basin sustainable development.

Region	Item	2009	2010	2011	2012	2013	2014	2015	2016	2017	2018
Xi'an	A	0.42	0.42	0.48	0.49	0.55	0.57	0.59	0.62	0.64	0.65
	B_1	0.14	0.15	0.17	0.18	0.21	0.23	0.23	0.23	0.26	0.27
	B_2	0.21	0.19	0.21	0.23	0.26	0.25	0.27	0.28	0.27	0.27
	B_3	0.08	0.08	0.10	0.08	0.09	0.09	0.10	0.10	0.11	0.11
Tongchuan	A	0.20	0.23	0.26	0.25	0.26	0.25	0.23	0.22	0.24	0.23
	B_1	0.06	0.05	0.06	0.06	0.07	0.06	0.05	0.05	0.05	0.05
	B_2	0.09	0.10	0.11	0.12	0.13	0.12	0.11	0.10	0.09	0.10
	B_3	0.05	0.08	0.09	0.06	0.07	0.07	0.07	0.06	0.09	0.08
Baoji	A	0.26	0.25	0.32	0.31	0.32	0.28	0.28	0.27	0.32	0.37
	B_1	0.06	0.06	0.07	0.08	0.08	0.08	0.08	0.08	0.09	0.09
	B_2	0.09	0.08	0.11	0.11	0.12	0.10	0.10	0.09	0.09	0.11
	B_3	0.10	0.11	0.14	0.12	0.13	0.11	0.10	0.09	0.13	0.17
Xianyang	A	0.20	0.22	0.25	0.26	0.30	0.25	0.26	0.28	0.32	0.27
	B_1	0.06	0.06	0.07	0.07	0.09	0.08	0.08	0.08	0.09	0.08
	B_2	0.09	0.08	0.10	0.11	0.11	0.09	0.11	0.12	0.11	0.11
	B_3	0.05	0.07	0.09	0.07	0.09	0.08	0.08	0.08	0.13	0.09
Weinan	A	0.21	0.23	0.24	0.24	0.26	0.26	0.25	0.26	0.36	0.29
	B_1	0.06	0.06	0.06	0.07	0.07	0.07	0.07	0.06	0.07	0.07
	B_2	0.08	0.07	0.08	0.08	0.08	0.08	0.08	0.09	0.10	0.10
	B_3	0.08	0.09	0.10	0.09	0.11	0.11	0.11	0.11	0.19	0.12
Total region	A	1.29	1.35	1.55	1.55	1.69	1.61	1.63	1.64	1.88	1.82
	B_1	0.37	0.40	0.43	0.46	0.51	0.51	0.51	0.52	0.56	0.57
	B_2	0.55	0.52	0.61	0.66	0.70	0.64	0.66	0.68	0.66	0.69
	B_3	0.36	0.43	0.52	0.43	0.48	0.46	0.45	0.45	0.65	0.57

Table 2). The inflection points were detected between 2013 and 2017, and the values remained around 1.6 from 2014 to 2016.

At the regional scale, the levels of sustainable development in different regions (**Table 2** and **Figure 3A**). The level of sustainable development in Xi'an was much higher than that of the other four cities (Tongchuan, Baoji, Xianyang, and Weinan) from 2009 to 2018. It indicated that the levels of sustainable development of these four cities had different levels of hysteresis, and different regions showed diversified development. The value of Tongchuan was the lowest, hovering between 0.20 and 0.26. The levels of sustainable development in four cities except Tongchuan had seen a yearly increase.

The economic development system (B_1) and the social development system (B_2) were on a similar development track compared with the sustainable development system (A) (**Figures 3B,C**). In comparison, the value of the ecological development system (B_3) was far lower than that of the economic development system (B_1) and social development system (B_2) (**Figure 3D**), indicating the lag of ecological development behind local

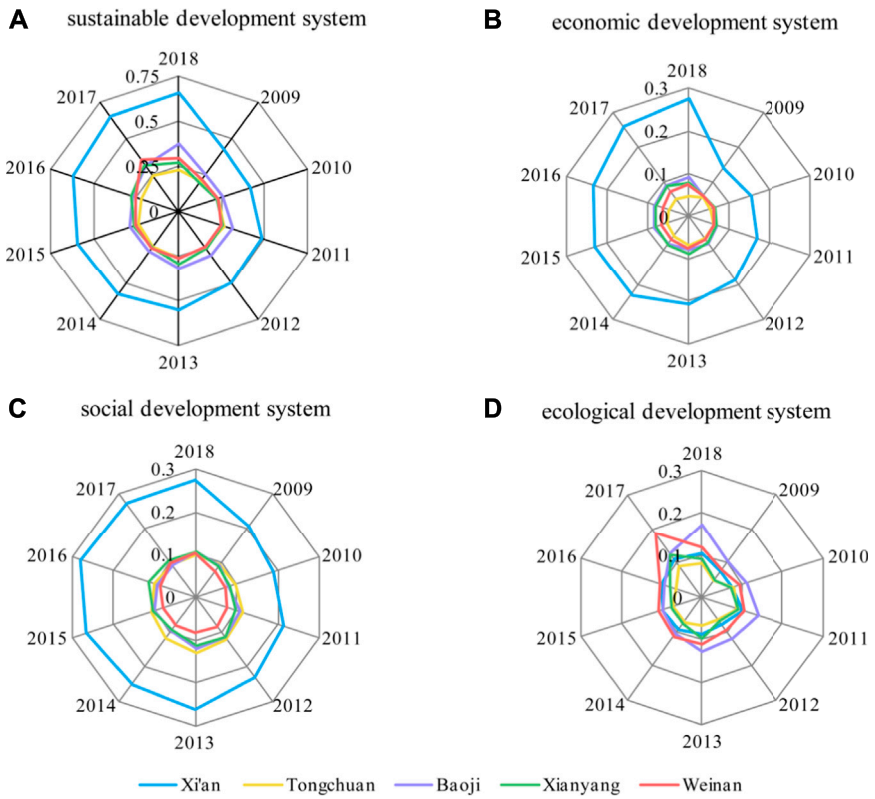

FIGURE 3 | The evaluation value of river basin sustainable development by score-radar maps **(A)** sustainable development, **(B)** economic development, **(C)** social development, and **(D)** ecological development.

economic and social development. In the economic development system (B_1) and the social development system (B_2), the values of the four cities (Tongchuan, Baoji, Xianyang, and Weinan) were relatively centralized, with only the value of Xi'an being far ahead than that of the rest (**Figure 3A**). In the ecological development system (B_3), the increased values of Weinan in 2017 and Baoji in 2018 were 0.19 and 0.17, respectively, while the values of the other three cities (Xi'an, Tongchuan, and Xianyang) were relatively stable over the past decade. The level of sustainable development in the ecological system was the lowest, illustrating that the ecological development lagged behind economic and social development in WRB in Shaanxi Province and sustainable development was unbalanced.

Spatial Analysis

Through the change of the spatial distribution for the sustainable development of WRB in Shaanxi Province (**Figure 4**) and calculation of the relative parameters of standard deviational ellipse (**Table 3**) from 2009 to 2018, the evolution of spatial pattern was analyzed from four aspects of spatial distribution (center, shape, range, and direction) to account for the dynamic changes of spatial difference.

The spatial distribution centers of sustainable development of WRB in Shaanxi Province were adjacent to Xi'an and Xianyang in 2009–2018. Overall, the spatial distribution center shifted to the north, showing that the accelerated growth speed of cities in the northern part of the axis, and the enhanced influence on the overall distribution pattern of the study area. The rotation angle of the standard deviational ellipse of spatial distribution dropped with a small counterclockwise rotation, suggesting that the study area in the northeastern cities were growing faster than the southwestern cities.

From the perspective of a spatial distribution shape, the long axis of the ellipse increased first and then shortened. Such a trend indicated that the spatial distribution shape changed from dispersion to polarization and then to dispersion. The changes in the short axis were the opposite. On the whole, the spatial distribution ellipse showed an obvious flattening trend; that is, the long axis grew and the short axis shrank. Afterward, the flattening trend gradually weakened and the directivity abated.

Obstacle Factor

The obstacle degree of 31 indicators ranked by the obstacle degree model (**Table 4** and **Figure 5**). The biggest obstacle degree was the number of college students per 10,000 (D_{12}). Prior to 2013, the financial revenue (D_2) and the amount of water resource per capita (D_{21}) were ranked second and third, respectively. The rankings were reversed from 2013 to 2017, indicating that the influence of economic obstacles on sustainable development of WRB in Shaanxi Province was gradually weakened with the increase of financial revenue. The fourth obstacle indicator was the investment in water conservancy as a percentage of

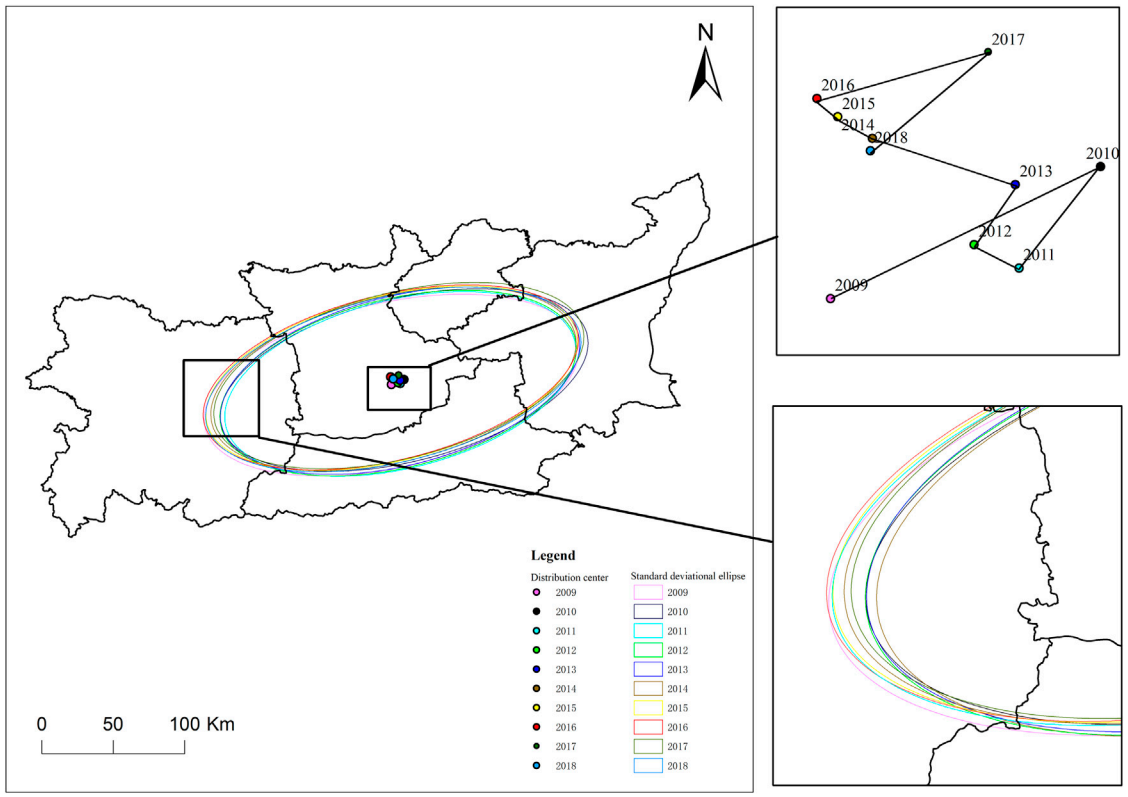

FIGURE 4 | The evolution of a spatial distribution pattern on the river basin sustainable development. D_1–D_{31} represent the obstacle degree of the corresponding indicator.

TABLE 3 | The parameters of standard deviational ellipse of the river basin sustainable development.

Year	Deviation along X/km	Deviation along Y/km	Rotation/(°)	Shape-area/(km)^2
2009	68.98	135.67	73.01	29,398.81
2010	68.11	134.03	71.51	28,676.29
2011	70.30	127.72	71.20	28,206.24
2012	70.41	129.73	71.25	28,693.96
2013	70.40	131.13	70.66	29,000.05
2014	69.19	132.91	71.58	28,888.93
2015	68.97	135.31	71.60	29,313.00
2016	68.86	136.71	71.53	29,572.08
2017	68.95	135.21	70.72	29,285.12
2018	68.99	136.60	71.78	29,604.14

GDP (D_{30}), while the fifth obstacle factors alternated between the gross domestic product (D_1) and urban living area per capita (D_{16}).

DISCUSSION

Extended Implication

The ecological development of WRB in Shaanxi Province fell so far behind economic and social development on the whole during 2009–2018, despite the striking advancement of ecological development that had been made at the later stage of the study. The improvement of ecological development cannot be separated from the management behavior of the government. China attaches great importance to RBSD in the face of environmental degradation and water shortage. In 2014, President Xi Jinping called for a water control policy of "giving priority to saving water, balancing space, systematic treatment, and exerting force all-sided." From 2016 to 2017, the Shaanxi provincial government issued a series of policies such as the Overall Plan for the Construction of Weihe Ecological Zone in Shaanxi Province and the Implement Plan

TABLE 4 | Dominant obstacle indicators and the order of obstacle degree on the river basin sustainable development.

Year	1	2	3	4	5
2009	D_{12} (12.73%)	D_2 (11.08%)	D_{21} (9.67%)	D_{30} (7.89%)	D_1 (6.52%)
2010	D_{12} (12.47%)	D_2 (10.94%)	D_{21} (9.45%)	D_{30} (7.85%)	D_1 (6.43%)
2011	D_{12} (13.44%)	D_2 (11.14%)	D_{21} (9.53%)	D_{30} (8.19%)	D_1 (6.55%)
2012	D_{12} (13.22%)	D_2 (10.69%)	D_{21} (10.25%)	D_{30} (8.18%)	D_1 (6.34%)
2013	D_{12} (13.63%)	D_{21} (10.78%)	D_2 (10.62%)	D_{30} (8.39%)	D_1 (6.37%)
2014	D_{12} (13.28%)	D_{21} (10.58%)	D_2 (10.01%)	D_{30} (8.49%)	D_1 (6.02%)
2015	D_{12} (12.96%)	D_{21} (10.71%)	D_2 (9.74%)	D_{30} (8.40%)	D_{16} (5.95%)
2016	D_{12} (13.07%)	D_{21} (10.97%)	D_2 (9.90%)	D_{30} (8.59%)	D_{16} (6.41%)
2017	D_{12} (14.53%)	D_{21} (11.44%)	D_2 (10.55%)	D_{30} (6.87%)	D_1 (6.81%)
2018	D_{12} (14.32%)	D_2 (10.17%)	D_{21} (9.36%)	D_{30} (8.89%)	D_{16} (6.53%)

The table only listed the top five factors of obstacle degree.

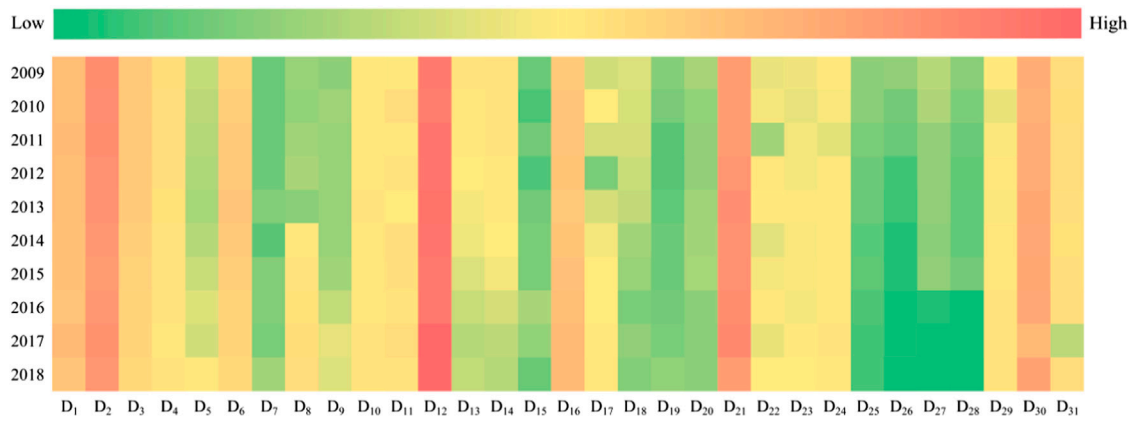

FIGURE 5 | The obstacle degree of 31 indicators.

Comprehensively of River Administrator in Shaanxi Province. Subsequently, a major national strategy of "Ecological conservation and high-quality development of the Yellow River basin" was proposed in 2019. WRB is a typical region with water shortage and underdeveloped economy, and water resources pose an obvious constraint on the sustainable development of WRB in Shaanxi Province. The water resources shortage and ecological environment pollution hamper the sustainable development of the economy and society. Conversely, the long-term development model has only focused on the aspects of economy and society, exerting great pressure on the ecological environment. Thus, solving the contradiction between economic and social development and environmental protection should be considered pivotal to the sustainable development of WRB in Shaanxi Province. The government departments must attach importance to the basin ecological management and water resources conservation for the sake of ensuring sustainable development of WRB in Shaanxi Province.

Among the five cities, Xi'an was identified as the region with the highest level of sustainable development during the study period, while Tongchuan was the lowest. Xi'an has developed into the only megacity in northwest China by virtue of its sound economic-social development foundation and the status as the central city of Shaanxi Province. Xi'an is in a high-speed state of sustainable development; its core leading role constantly enhanced, exerting a siphon effect. Meanwhile, Tongchuan, as a resource–based city in its early development stage, is facing the pressure of resource exhaustion, limited natural conditions, and prominent environmental problems, impeding its sustainable development. The results revealed evident polarization among regions as well as unsynchronized sustainable development. The study area belongs to an important exploitation area of Guanzhong Plain urban agglomeration, having formed a superior economic base in the long-term development. The western development provided favorable conditions for resource-rich regions, which is the main reason for the internal differences in sustainable development among regions. Besides, the implementation of the Belt and Road Initiative has greatly promoted regional coordination and sustainable development.

The results of obstacle degree unexpectedly discovered that the amount of water resource per capita (D_{21}) and the investment in water conservancy as a percentage to GDP (D_{30}) in the ecological development system (B_3) were vital factors hindering sustainable development of WRB in Shaanxi Province. The ecological environment, especially water resources, acts as a primary in the river basin sustainable development. Water conservancy

construction is regarded as the basic support and important guarantee for promoting economic growth, social progress, and ecological control. In recent years, investment in water conservancy construction and water conservancy projects have seen a continuous increase, especially the construction of the Water Diversion from Hanjiang River to Weihe River basin project (172 major national water conservancy projects of China in 2015 and 10 major water ecological projects of Shaanxi Province in 2017), bringing obvious ecological–economic benefits.

Limitation and Improvement

Indicator Optimization

Including environmental, social, and economic factors, sustainability indicators have been considered as a potential assessment method (Rama et al., 2020). GDP (D_1), an important comprehensive statistical indicator in the economic accounting system, is often used to measure the economic status of a country. Its limitation is that it does not involve the ecological environment. Under a rapid social and economic development, GDP cannot fully represent the relationship between human activities and ecological environment, nor can it uncover resource consumption and environmental loss incurred by the economic development. To overcome the above shortcomings, the current system of national economic accounting was reformed based on the sustainable development, with the indicator green GDP (sustainable income) introduced. Green GDP is the calculation of environmental resource elements in a comprehensive environmental–economic accounting system, namely, environmental resource cost and protection services fees are deducted from GDP. Green GDP implicates a harmonious sustainable development model between economic growth and ecological environment, which is conducive to evaluating the effect of economic growth. However, the existing literature is insufficient to answer the question of what is the difference between GDP and green GDP in China (Wu and Han, 2020). Although a traditional indicator (GDP) was used in this article, it does not mean that green GDP is meaningless. In the follow-up work, it can be considered to reasonably adopt the indicator of green GDP in the indicator system of sustainable development and explore the change for RBSD.

Ammonia nitrogen discharge (D_{27}) and chemical oxygen demand discharge (D_{28}) are the indicators of water environmental quality (C_8) in the ecological development system (B_3); they represent an eutrophication degree and an organic pollutant content in river basin, respectively. According to the Shaanxi Water Resources Bulletin in 2018, the major pollutants exceeding the standard in WRB in Shaanxi Province were ammonia nitrogen, chemical oxygen demand, and total phosphorus. However, the indicator of total phosphorus is not involved in our indicator system due to the lack of data; therefore, it is unclear whether this indicator will lead to the variation on sustainable development of WRB in Shaanxi Province. In addition, the publicly obtained data by the government may need further adjustment according to the actual measured values in the field.

WRB is characterized by severe soil erosion owing to overexploitation, especially in the mining area, highway, railway, and other engineering construction sections. Severe soil and water loss not only threatens the downstream of WRB, but also aggravates the deterioration of the ecological environment. Therefore, given the actual development situation of WRB, the suitable indicators were selected when constructing the indicator system for the sustainable development of WRB in Shaanxi Province. Particularly, the growth rate of soil erosion control (D_{31}) was added to the indicator system. Such an indicator has not been extensively used in sustainable development research but is conducive to the planning and decision-making of basin management. Because the factors affecting RBSD are diversified, whether the indicators in the established indicator system for our study are applicable to other regions remains to be further explored.

Basin Management

Studies in China focusing on water resource management have emphasized the effective utilization of water resources while neglecting the protection of water quality (Cai et al., 2017; Zhou et al., 2015). Few studies have focused on the sustainable development of basin management, especially in arid areas of northwest China.

According to China's current water law, basin management is combined with the administrative division management. The inevitable consequence is a segmented state, a kind of transition from water resources management to administrative management. Division management hinders overall planning, unified supervision, and rational allocation. Under the restriction of market economy and traditional thoughts, the local government is driven by their respective economic interests, which conflicts with the unified basin management, especially in the exploitation, utilization, and protection of natural resources.

In the practice of RBSD, developed countries such as Australia, the United States, and Germany give importance to the sustainable development, and the coordination of population, resource, and environment, highlighting the long-term management and basin integrity, while taking into account the comprehensive utilization of water resources and engineering measures. Social, ecological, and environmental factors should be reflected in the planning, with the river basin managed as a unit, not as an administrative division. Kotir et al. (2016) investigated the interaction between the population, the water resource, and the agricultural development of the Volta River basin in West Africa, and it could enhance sustainable management within the basin. Wei et al. (2017) describe the evolution of the societal value of water resources in Australia over a period of 169 years and then provide management practices focused on the sustainable water resource use. The theory of RBSD had benefited the development and management practices of river basin ecosystems, such as the Amazon River (Ioris, 2020), the Mississippi River Piazza and La Peyre (2011), the Tennessee River Secchi and Mcdonald (2019), and the Rhine River Jeannot et al. (2018), offering a reference for RBSD in China.

A New Perspective on Sustainability Assessment

The framework of the planetary boundary in 2009 was considered as one of the most symbolic achievements in the field of quantification of international resource and environmental carrying capacity in recent years (Rockström et al., 2009; Running, 2012). The concept first defined the maximum safety threshold of the earth's ecosystem in a series of environmental problems, such as climate change, water resources consumption, land use, nitrogen and phosphorus cycle, and loss of biodiversity. It is used to judge environmental sustainability as a whole (Steffen et al., 2015). Environmental sustainability can comprehensively reflect the complex effects of human activities on the earth's ecosystem and provide a policy basis for key fields of environmental governance.

Studies of planetary boundaries have concentrated on global, national, and regional scales (Dao et al., 2018; Huang et al., 2020). Water resource consumption is a compound environmental problem; its influence scope is mainly a river basin. Combining with the planetary boundary framework, the safe interval of water resources utilization and RBSD can be discussed, providing the development space and early warning threshold for regional sustainable development.

CONCLUSION

This article constructed an indicator system of sustainable development. The entropy method and standard deviational ellipse were used to evaluate temporal and spatial variations for sustainable development of WRB in Shaanxi Province. The obstacle degree model was used to calculate and rank the factors that hindered its sustainable development. First, from the perspective of temporal analysis, the overall rise of sustainable development of WRB in Shaanxi Province is accompanied by regional differences. Economic development is synchronous with the social development, while the ecological development is relatively backward. Second, from the perspective of a spatial pattern evolution, the center of distribution moves north and rotates counterclockwise, the shape variation being dispersion-polarization-dispersion. Lastly, the main obstacle factors affecting the sustainable development of WRB in Shaanxi Province during 2009–2018 include the number of college students per 10,000 (D_{12}), local government revenue (D_2), amount of water resource per capita (D_{21}), investment in water conservancy as a percentage to GDP (D_{30}), gross domestic product (D_1), and urban living area per capita (D_{16}).

DATA AVAILABILITY STATEMENT

The raw data supporting the conclusions of this article will be made available by the authors, without undue reservation.

AUTHOR CONTRIBUTIONS

YW: conceptualization, methodology, data curation, investigation, writing-original draft, and writing-review and editing. JS: conceptualization, supervision, validation, project administration, and funding acquisition. XZ: writing-review and editing and validation. HS: writing-review and editing and Validation.

FUNDING

This study was supported by the Special Funds of the National Natural Science Foundation of China (Grant No.42041004), The Key Research and Development Program of Shaanxi (Grant 2019ZDLSF05-02) and the Hundred Talents Project of the Chinese Academy of Sciences (Grant A315021406).

REFERENCES

Brown, M. G., and Quinn, J. E. (2018). Zoning Does Not Improve the Availability of Ecosystem Services in Urban Watersheds. A Case Study from Upstate South Carolina, USA. *Ecosystem Serv.* 34, 254–265. doi:10.1016/j.ecoser.2018.04.009

Bui, N. T., Kawamura, A., Bui, D. D., Amaguchi, H., Bui, D. D., Truong, N. T., et al. (2019). Groundwater Sustainability Assessment Framework: A Demonstration of Environmental Sustainability index for Hanoi, Vietnam. *J. Environ. Manage.* 241, 479–487. doi:10.1016/j.jenvman.2019.02.117

Cai, J., Varis, O., and Yin, H. (2017). China's Water Resources Vulnerability: A Spatio-Temporal Analysis during 2003-2013. *J. Clean. Prod.* 142 (4), 2901–2910. doi:10.1016/j.jclepro.2016.10.180

Chen, J., Mei, Y., and Xiao, W. (2019). Establishment of the Ecological Relationships and Properties of the Lhasa River Basin Water Resources System, China. *Sustainable Cities Soc.* 47, 101477. doi:10.1016/j.scs.2019.101477

Chen, Y.-p., Fu, B.-j., Zhao, Y., Wang, K.-b., Zhao, M. M., Ma, J.-f., et al. (2020a). Sustainable Development in the Yellow River Basin: Issues and Strategies. *J. Clean. Prod.* 263, 121223. doi:10.1016/j.jclepro.2020.121223

Chen, Y., Zhu, M., Lu, J., Zhou, Q., and Ma, W. (2020b). Evaluation of Ecological City and Analysis of Obstacle Factors under the Background of High-Quality Development: Taking Cities in the Yellow River Basin as Examples. *Ecol. Indicators* 118, 106771. doi:10.1016/j.ecolind.2020.106771

Cui, X., Zhao, T., and Wang, J. (2021). Allocation of Carbon Emission Quotas in China's Provincial Power Sector Based on Entropy Method and ZSG-DEA. *J. Clean. Prod.* 284, 124683. doi:10.1016/j.jclepro.2020.124683

D'Ambrosio, E., Gentile, F., and De Girolamo, A. M. (2020). Assessing the Sustainability in Water Use at the basin Scale through Water Footprint Indicators. *J. Clean. Prod.* 244, 118847. doi:10.1016/j.jclepro.2019.118847

Dao, H., Peduzzi, P., and Friot, D. (2018). National Environmental Limits and Footprints Based on the Planetary Boundaries Framework: The Case of Switzerland. *Glob. Environ. Change* 52, 49–57. doi:10.1016/j.gloenvcha.2018.06.005

Deng, W., Song, J., Sun, H., Cheng, D., Zhang, X., Liu, J., et al. (2020). Isolating of Climate and Land Surface Contribution to basin Runoff Variability: A Case Study from the Weihe River Basin, China. *Ecol. Eng.* 153, 105904. doi:10.1016/j.ecoleng.2020.105904

Du, Q., Zhou, J., Pan, T., and Wu, M. (2019). Relationship of Carbon Emissions and Economic Growth in China's Construction Industry. *J. Clean. Prod.* 220, 99–109. doi:10.1016/j.jclepro.2019.02.123

Fan, Y. P., and Fang, C. L. (2020). Evolution Process and Obstacle Factors of Ecological Security in Western China, a Case Study of Qinghai Province. *Ecol. Indic.* 117, 106659. doi:10.1016/j.ecolind.2020.106659

Ferreira, S. C. G., De Lima, A. M. M., and Corrêa, J. A. M. (2020). Indicators of Hydrological Sustainability, Governance and Water Resource Regulation in the Moju River basin (PA) - Eastern Amazonia. *J. Environ. Manage.* 263, 110354. doi:10.1016/j.jenvman.2020.110354

Fu, J., Zang, C., and Zhang, J. (2020). Economic and Resource and Environmental Carrying Capacity Trade-Off Analysis in the Haihe River basin in China. *J. Clean. Prod.* 270, 122271. doi:10.1016/j.jclepro.2020.122271

Gao, X., Shen, J., He, W., Sun, F., Zhang, Z., Guo, W., et al. (2019). An Evolutionary Game Analysis of Governments' Decision-Making Behaviors and Factors Influencing Watershed Ecological Compensation in China. *J. Environ. Manage.* 251, 109592. doi:10.1016/j.jenvman.2019.109592

Huang, L., Feng, Y., Zhang, B., and Hu, W. (2021). Spatio-temporal Characteristics and Obstacle Factors of Cultivated Land Resources Security. *Sustainability* 13, 8498. doi:10.3390/su13158498

Huang, L. H., Hu, A. H., and Kuo, C.-H. (2020). Planetary Boundary Downscaling for Absolute Environmental Sustainability Assessment - Case Study of Taiwan. *Ecol. Indicators* 114, 106339. doi:10.1016/j.ecolind.2020.106339

Ioris, A. A. R. (2020). Socioecological Economics of Water Development in the Brazilian Amazon: Elements for a Critical Reflection. *Ecol. Econ.* 173, 106654. doi:10.1016/j.ecolecon.2020.106654

Jeannot, B., Weill, S., Eschbach, D., Schmitt, L., and Delay, F. (2018). A Low-Dimensional Integrated Subsurface Hydrological Model Coupled with 2-D Overland Flow: Application to a Restored Fluvial Hydrosystem (Upper Rhine River - France). *J. Hydrol.* 563, 495–509. doi:10.1016/j.jhydrol.2018.06.028

Kotir, J. H., Smith, C., Brown, G., Marshall, N., and Johnstone, R. (2016). A System Dynamics Simulation Model for Sustainable Water Resources Management and Agricultural Development in the Volta River Basin, Ghana. *Sci. Total Environ.* 573, 444–457. doi:10.1016/j.scitotenv.2016.08.081

Li, J., Zhang, D., and Su, B. (2019a). The Impact of Social Awareness and Lifestyles on Household Carbon Emissions in China. *Ecol. Econ.* 160, 145–155. doi:10.1016/j.ecolecon.2019.02.020

Li, Q., Wang, W., Jiang, X., Lu, D., Zhang, Y., and Li, J. (2019b). Optimizing the Reuse of Reclaimed Water in Arid Urban Regions: A Case Study in Urumqi, Northwest China. *Sustainable Cities Soc.* 51, 101702. doi:10.1016/j.scs.2019.101702

Mosaffaie, J., Salehpour Jam, A., Tabatabaei, M. R., and Kousari, M. R. (2021). Trend Assessment of the Watershed Health Based on DPSIR Framework. *Land Use Policy* 100, 104911. doi:10.1016/j.landusepol.2020.104911

Piazza, B. P., and La Peyre, M. K. (2011). Nekton Community Response to a Large-Scale Mississippi River Discharge: Examining Spatial and Temporal Response to River Management. *Estuarine, Coastal Shelf Sci.* 91 (3), 379–387. doi:10.1016/j.ecss.2010.11.001

Pluchinotta, I., Pagano, A., Vilcan, T., Ahilan, S., Kapetas, L., Maskrey, S., et al. (2021). A Participatory System Dynamics Model to Investigate Sustainable Urban Water Management in Ebbsfleet Garden City. *Sustainable Cities Soc.* 67, 102709. doi:10.1016/j.scs.2021.102709

Rama, M., González-García, S., Andrade, E., Moreira, M. T., and Feijoo, G. (2020). Assessing the Sustainability Dimension at Local Scale: Case Study of Spanish Cities. *Ecol. Indicators* 117, 106687. doi:10.1016/j.ecolind.2020.106687

Rockström, J., Steffen, W., Noone, K., Persson, A., Chapin, F. S., Lambin, E. F., et al. (2009). A Safe Operating Space for Humanity. *Nature* 461 (7263), 472–475. doi:10.1038/461472a

Roobavannan, M., Kandasamy, J., Pande, S., Vigneswaran, S., and Sivapalan, M. (2020). Sustainability of Agricultural basin Development under Uncertain Future Climate and Economic Conditions: A Socio-Hydrological Analysis. *Ecol. Econ.* 174, 106665. doi:10.1016/j.ecolecon.2020.106665

Roshan, A., and Kumar, M. (2020). Water End-Use Estimation Can Support the Urban Water Crisis Management: A Critical Review. *J. Environ. Manage.* 268, 110663. doi:10.1016/j.jenvman.2020.110663

Running, S. W. (2012). A Measurable Planetary Boundary for the Biosphere. *Science* 337 (6101), 1458–1459. doi:10.1126/science.1227620

Secchi, S., and Mcdonald, M. (2019). The State of Water Quality Strategies in the Mississippi River Basin: Is Cooperative Federalism Working? *Sci. Total Environ.* 677, 241–249. doi:10.1016/j.scitotenv.2019.04.381

Shaanxi Province Department of Water Resources (2018). Shaanxi Water Resources Bulletin 2018. [2020-5-22]. Available at: http://slt.shaanxi.gov.cn/gb-zxfw-news-3-dfnj-93956. (in Chinese).

Shaanxi Provincial Bureau of Statistics (2019). *Shaanxi Statistical Yearbook 2019*. Beijing: China Statistics Press. (in Chinese).

Shannon, C. E. (1948). A Mathematical Theory of Communication. *Bell Syst. Tech. J.* 27 (3), 379–423. doi:10.1002/j.1538-7305.1948.tb01338.x

Shen, Q., and Ma, Y. (2020). Did Water Diversion Projects lead to Sustainable Ecological Restoration in Arid Endorheic Basins? Lessons from Long-Term Changes of Multiple Ecosystem Indicators in the Lower Heihe River Basin. *Sci. Total Environ.* 701, 134785. doi:10.1016/j.scitotenv.2019.134785

Silva, J. d., Fernandes, V., Limont, M., Dziedzic, M., Andreoli, C. V., and Rauen, W. B. (2020). Water Sustainability Assessment from the Perspective of Sustainable Development Capitals: Conceptual Model and index Based on Literature Review. *J. Environ. Manage.* 254, 109750. doi:10.1016/j.jenvman.2019.109750

Silva, L. C. C. d., Filho, D. O., Silva, I. R., Pinto, A. C. V. e., and Vaz, P. N. (2019). Water Sustainability Potential in a university Building - Case Study. *Sustainable Cities Soc.* 47, 101489. doi:10.1016/j.scs.2019.101489

Song, J., Tang, B., Zhang, J., Dou, X., Liu, Q., and Shen, W. (2018). System Dynamics Simulation for Optimal Stream Flow Regulations under Consideration of Coordinated Development of Ecology and Socio-Economy in the Weihe River Basin, China. *Ecol. Eng.* 124, 51–68. doi:10.1016/j.ecoleng.2018.09.024

Srinivas, R., Singh, A. P., Dhadse, K., Garg, C., and Deshmukh, A. (2018). Sustainable Management of a River basin by Integrating an Improved Fuzzy Based Hybridized SWOT Model and Geo-Statistical Weighted Thematic Overlay Analysis. *J. Hydrol.* 563, 92–105. doi:10.1016/j.jhydrol.2018.05.059

Steffen, W., Richardson, K., Rockström, J., Cornell, S. E., Fetzer, I., Bennett, E. M., et al. (2015). Planetary Boundaries: Guiding Human Development on a Changing Planet. *Science* 347 (6223), 1259855. doi:10.1126/science.1259855

Wada, Y., Flörke, M., Hanasaki, N., Eisner, S., Fischer, G., Tramberend, S., et al. (2016). Modeling Global Water Use for the 21st century: the Water Futures and Solutions (WFaS) Initiative and its Approaches. *Geosci. Model. Dev.* 9, 175–222. doi:10.5194/gmd-9-175-2016

Wang, Q., Li, S., and Li, R. (2019a). Evaluating Water Resource Sustainability in Beijing, China: Combining PSR Model and Matter-Element Extension Method. *J. Clean. Prod.* 206, 171–179. doi:10.1016/j.jclepro.2018.09.057

Wang, X., Su, P., Lin, Q., Song, J., Sun, H., Cheng, D., et al. (2019b). Distribution, Assessment and Coupling Relationship of Heavy Metals and Macroinvertebrates in Sediments of the Weihe River Basin. *Sustainable Cities Soc.* 50, 101665. doi:10.1016/j.scs.2019.101665

Wang, Z.-g., Luo, Y.-z., Zhang, M.-h., and Xia, J. (2014). Quantitative Evaluation of Sustainable Development and Eco-Environmental Carrying Capacity in Water-Deficient Regions: A Case Study in the Haihe River Basin, China. *J. Integr. Agric.* 13 (1), 195–206. doi:10.1016/S2095-3119(13)60423-2

Wei, J., Wei, Y., and Western, A. (2017). Evolution of the Societal Value of Water Resources for Economic Development versus Environmental Sustainability in Australia from 1843 to 2011. *Glob. Environ. Change* 42, 82–92. doi:10.1016/j.gloenvcha.2016.12.005

Wu, J., Mao, R., Li, M., Xia, J., Song, J., Cheng, D., et al. (2020). Assessment of Aquatic Ecological Health Based on Determination of Biological Community Variability of Fish and Macroinvertebrates in the Weihe River Basin, China. *J. Environ. Manage.* 267, 110651. doi:10.1016/j.jenvman.2020.110651

Wu, S., and Han, H. (2020). Sectoral Changing Patterns of China's green GDP Considering Climate Change: An Investigation Based on the Economic Input-Output Life Cycle Assessment Model. *J. Clean. Prod.* 251, 119764. doi:10.1016/j.jclepro.2019.119764

Xu, F., Li, H., and Bao, H. (2018). Performance Comparisons of Land Institution and Land Regulation Systems on Water Area Decrease. *Habitat Int.* 77, 12–20. doi:10.1016/j.habitatint.2017.12.009

Zhang, K., Shen, J., He, R., Fan, B., and Han, H. (2019). Dynamic Analysis of the Coupling Coordination Relationship between Urbanization and Water Resource Security and its Obstacle Factor. *Ijerph* 16, 4765. doi:10.3390/ijerph16234765

Zhao, A., Zhu, X., Liu, X., Pan, Y., and Zuo, D. (2016). Impacts of Land Use Change and Climate Variability on green and Blue Water Resources in the Weihe River Basin of Northwest China. *Catena* 137, 318–327. doi:10.1016/j.catena.2015.09.018

Zhao, D., Li, C., Wang, Q., and Yuan, J. (2020). Comprehensive Evaluation of National Electric Power Development Based on Cloud Model and Entropy Method and TOPSIS: A Case Study in 11 Countries. *J. Clean. Prod.* 277, 123190. doi:10.1016/j.jclepro.2020.123190

Zhong, S. Z., Yuan, J., Kong, H. N., Liu, B., Tian, X., Chen, W., et al. (2018). Emergy-based Sustainability Evaluation of Erhai Lake Basin in China. *J. Clean. Prod.* 178, 142–153. doi:10.1016/j.jclepro.2018.01.019

Zhou, Y., Guo, S., Xu, C.-Y., Liu, D., Chen, L., and Wang, D. (2015). Integrated Optimal Allocation Model for Complex Adaptive System of Water Resources Management (II): Case Study. *J. Hydrol.* 531, 977–991. doi:10.1016/j.jhydrol.2015.10.043

Zuo, Z., Guo, H., Cheng, J., and Li, Y. (2021). How to Achieve New Progress in Ecological Civilization Construction? - Based on Cloud Model and Coupling Coordination Degree Model. *Ecol. Indicators* 127, 107789. doi:10.1016/j.ecolind.2021.107789

Conflict of Interest: The authors declare that the research was conducted in the absence of any commercial or financial relationships that could be construed as a potential conflict of interest.

Publisher's Note: All claims expressed in this article are solely those of the authors and do not necessarily represent those of their affiliated organizations, or those of the publisher, the editors, and the reviewers. Any product that may be evaluated in this article, or claim that may be made by its manufacturer, is not guaranteed or endorsed by the publisher.

frontiers in Environmental Science

ORIGINAL RESEARCH
published: 02 November 2021
doi: 10.3389/fenvs.2021.713831

A Bayesian Decision Model for Optimum Investment and Design of Low-Impact Development in Urban Stormwater Infrastructure and Management

Mo Wang[1], Yu Zhang[1], Dongqing Zhang[2], Yingsheng Zheng[1]*, Shiqi Zhou[3] and Soon K. Tan[4]*

[1]College of Architecture and Urban Planning, Guangzhou University, Guangzhou, China, [2]Guangdong Provincial Key Laboratory of Petrochemical Pollution Processes and Control, School of Environmental Science and Engineering, Guangdong University of Petrochemical Technology, Guangzhou, China, [3]College of Design and Innovation, Tongji University, Shanghai, China, [4]School of Civil and Environmental Engineering, Nanyang Technological University, Shanghai, Singapore

OPEN ACCESS

Edited by:
Guobin Fu,
CSIRO Land and Water, Australia

Reviewed by:
Vhahangwele Masindi,
Council for Scientific and Industrial Research (CSIR), South Africa
Rajesh Singh,
Central University of Gujarat, India

***Correspondence:**
Dongqing Zhang
dqzhang3377@outlook.com
Yingsheng Zheng
zhengyingsheng@gzhu.edu.cn

Specialty section:
This article was submitted to Water and Wastewater Management, a section of the journal Frontiers in Environmental Science

Received: *24 May 2021*
Accepted: *28 September 2021*
Published: *02 November 2021*

Citation:
Wang M, Zhang Y, Zhang D, Zheng Y, Zhou S and Tan SK (2021) A Bayesian Decision Model for Optimum Investment and Design of Low-Impact Development in Urban Stormwater Infrastructure and Management. Front. Environ. Sci. 9:713831. doi: 10.3389/fenvs.2021.713831

Uncertainties concerning low-impact development (LID) practices over its service life are challenges in the adoption of LID. One strategy to deal with uncertainty is to provide an adaptive framework which could be used to support decision-makers in the latter decision on investments and designs dynamically. The authors propose a Bayesian-based decision-making framework and procedure for investing in LID practices as part of an urban stormwater management strategy. In this framework, the investment could be made at various stages of the service life of the LID, and performed with deliberate decision to invest more or suspend the investment, pending the needs and observed performance, resources available, anticipated climate changes, technological advancement, and users' needs and expectations. Variance learning (VL) and mean-variance learning (MVL) models were included in this decision tool to support handling of uncertainty and adjusting investment plans to maximize the returns while minimizing the undesirable outcomes. The authors found that a risk-neutral investor tends to harbor greater expectations while bearing a higher level of risks than risk-averse investor in the VL model. Constructed wetlands which have a higher prior mean performance are more favorable during the initial stage of LID practices. Risk-averse decision-makers, however, could choose porous pavement with stable performance in the VL model and leverage on potential technological advancement in the MVL model.

Keywords: climate change, stormwater management, Bayesian, life span, low-impact development, porous pavement, constructed wetland

INTRODUCTION

Low-impact development (LID) practices such as incorporation of constructed wetland (CW) and porous pavement (PP) in stormwater management are decentralized elements that could be used to manage storm runoff through retention and infiltration at source (Ahiablame and Shakya, 2016). As an important adaptation strategy, LID is growing in popularity due to its anticipated social, esthetic, and environmental benefits, as well as its flexibility and compatibility to blend in with architecture

and landscape, particularly in a high-density urban area (Ahiablame et al., 2012; Yuan et al., 2018). Decision-making tools for selecting, sizing, and design of LID at various plot scales such as a single project development site, urban sub-catchment, or at a regional level have been developed (Bakhshipour et al., 2019; Wang et al., 2020). However, the robustness associated with the LID devices has not been addressed (Pyke et al., 2011; Bahrami et al., 2019). Bracmort et al. (2006) stated that although a "design life of LID" had been established, the effective duration and performance of a LID during its design life span remained uncertain. Naturally, LID efficiency would vary over time (Koch et al., 2014; Chen et al., 2016). Like all stormwater ancillaries, the efficiency of LID devices is likely to decrease over time due to progressive degradation and deterioration of the structural elements, clogging of pervious surfaces, and sedimentation. Periodic maintenance would no doubt restore the performance of LID to some degree.

Many reported studies have focused on certain aspects of hydrologic performance of LID based on field or experimental investigations (Montalto et al., 2007; Emerson et al., 2010; Thompson et al., 2016; Hou et al., 2019). Some hydrological or hydraulic modeling studies have focused on the potential variations in long-term performances of LID but these studies assumed that LID functions perfectly after installation (Liu et al., 2015; Wang et al., 2021). There are only a handful of studies that had developed techniques to address long-term efficiency of LID and incorporated this consideration into the models to simulate the actual performance (Bracmort et al., 2006). Liu et al. (2018) presented a life-time modeling framework for assessing the efficiency of LID technologies and long-term performances of CWs and grass buffer strips in removing total phosphorus. Wang et al. (2021) illustrated that the hydrological robustness of a wetland system would decrease significantly over its service life cycle once long-term performance for LID practices is considered.

Selecting an appropriate LID solution is becoming more complicated and more challenging due to high uncertainty of climate change in recent years (Larsen et al., 2016) on top of the uncertainty associated with long-term performance of LID. Obviously, the combined effects and uncertainties of climate change and its long-term efficiency would further complicate decisions to invest on LID practices. Several researchers suggested that a realistic modeling method should consider both the internal uncertainties of LID's dynamic hydrological performance and external uncertainties such as climate change (Pyke et al., 2011; Yazdanfar and Sharma, 2015). There are still knowledge gaps and potential opportunities for further development of models and tools which could be used to support decision-making of LID.

An investment on LID often involves a long-term planning horizon, hinging on management objectives, available resources, risk appetite, and potential benefits of LID. The challenge is how to structure the information on the cost-benefits of LID and include a variety of structural uncertainties and climate scenarios. A multi-scenario analysis with adaptive options including a decision-tree analysis, real options analysis (Woodward et al., 2014; Sturm et al., 2017), dynamic adaptive policy pathways, and multi-stage stochastic programming (MSP) has been considered. In this approach, adaptation strategies can be modified dynamically and progressively based on updated information (Shi et al., 2019). A Bayesian analysis is widely used in the multi-scenario analysis with adaptive options. The Bayesian approach begins with an assumed initial distribution of certain variables, which is then refined progressively until an optimum state is obtained (Kelly and Kolstad, 1999). Other reported studies that include these are by Liu et al. (2017) and Tang et al. (2018) on regional flood risk; Jacobi et al. (2013) on water quality improvement; Hung and Hobbs (2019) on green infrastructures; and Webster et al. (2017) on climate mitigation technologies.

The objective of this study is to develop a reliable Bayesian-based and coupled optimization model which addresses uncertainty and risk associated with long-term efficiency of LID and potential climate change.

MATERIALS AND METHODS

The proposed methodology for optimized design and investment of LID based on Bayesian learning and anticipated long-term efficiency over its design life span is described herein. The procedure includes several steps as represented schematically in **Figure 1**. Two urban sub-catchments in Guangzhou are used as the test catchments in this study.

There are five main blocks in the work flow process: 1) preparation of input data and focusing on the hydrological characteristics of a test catchment; 2) select an appropriate hydrological model; the model is used for hydrologic simulation of stormwater runoff through the test catchments; 3) a Bayesian learning model which is used to assess the performance of LID practices under different investment strategies and various degrees of LID implementation; 4) a coupled optimization model which is used for developing the optimum investment strategy (optimum LID implementation); and 5) final decision module, in which the outcome of the above processes is used to determine the extent of the LID and its configuration such that the objective could be achieved optimally and with optimum investment.

Long-Term Efficiency of Low-Impact Development

Test Catchment and Climate Scenarios

Guangzhou, a high-density city in China, has the most severe urban flooding risk among the 136 large coastal cities in the world (Hallegatte et al., 2013). The rainfall distribution is non-uniform throughout the year due to the impacts of subtropical monsoon climate. Using selected multi-global climate models (GCMs) and the corresponding representative concentration pathways (RCPs) scenarios in Guangzhou, occurrences of extreme storms are expected to rise dramatically over the next 30 years (Zhang et al., 2017).

Two test catchments selected for this study were located at 23°04′ N; 113°12′ E, and they were residential sub-catchments S01

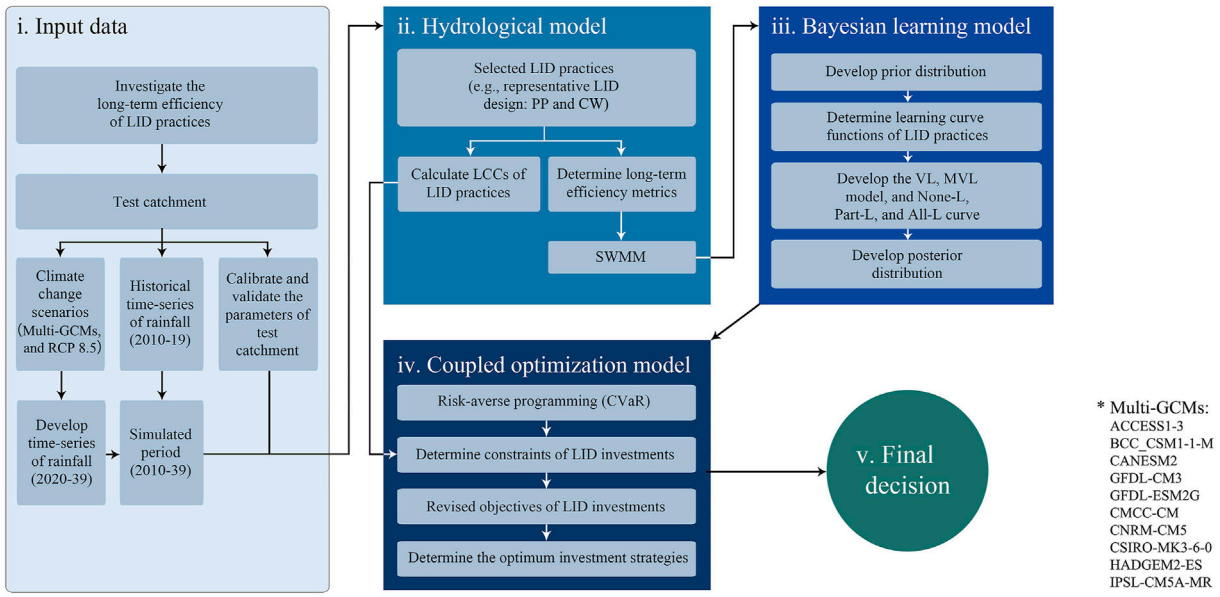

FIGURE 1 | Flowchart of the methodology for the coupled Bayesian optimization model of LID investments. Note: PP, permeable pavement; CW, constructed wetland; LCC, life cycle cost; SWMM, Storm Water Management Model; VL, variance learning; MVL, mean-variance learning; None-L, none learning; Part-L, part learning; All-L, all learning; CVaR, conditional value at risk.

TABLE 1 | Characteristic parameters of sub-catchment S01 and S02.

Parameter	Unit	S01	S02
Area	ha	2.000	1.500
Characteristic slope	%	0.019	0.184
Proportion of impermeable area	%	50.000	92.000
Manning's n for impervious areas	—	0.025	0.024
Manning's n for pervious areas	—	0.150	0.150
Depression storage of impervious	mm	0.100	0.206
Depression storage of pervious	mm	10.000	10.000
Max infiltration rate	mm/h	103.810	103.810
Min infiltration rate	mm/h	11.440	11.440
Decay constant	d	2.750	2.750

Note: source of parameters selected from Zhu et al. (2019).

TABLE 2 | Parameters of the permeable pavement (PP) and constructed wetland (CW) in SWMM.

Layers	Parameters	PP	CW
Surface layer	Berm height (mm)	—	300
	Vegetation volume fraction (m^3/m^3)	—	0.05
	Surface roughness (Manning's n)	0.012	0.1
	Surface slope (percent)	0.5	0.5
Soil layer	Thickness (mm)	—	900
	Porosity (m^3/m^3)	—	0.5
	Field capacity (volume fraction) (m^3/m^3)	—	0.15
	Wilting point (volume fraction) (m^3/m^3)	—	0.08
	Conductivity (mm/hr)	—	50
	Conductivity slope	—	10
	Suction head (mm)	—	80
Pavement	Thickness (mm)	100	—
	Void ration (voids/solids) (m^3/m^3)	0.15	—
	Impervious surface fraction	0	—
	Permeability (mm/hr)	500	—
	Clogging factor	0	—
Storage layer	Thickness (mm)	300	300
	Void ration (voids/solids) (m^3/m^3)	0.4	0.67
	Seepage rate to native soil (mm/hr)	13	13
	Clogging factor	0	0
Underdrain layer	Flow coefficient	2.5	2.5
	Flow exponent	0.5	0.5
	Offset height (mm)	100	150

Note: sources from Rossman and Huber (2016).

and S02 (**Supplementary Figure S1**). The land surface area of S01 and S02 included a different proportion of impermeable areas. The hydrologic parameters of both sub-catchments, as shown in **Table 1**, had been established and calibrated using ten rainfall events and validated using another 25 events over the period of 2013–15. The Kling–Gupta efficiency and Nash–Sutcliffe efficiency were above 0.7 and 0.6, respectively (Zhu et al., 2019).

Historical rainfall data (2010–19) were collected from the rainfall station at the Baiyun International Airport, Guangzhou. In order to extract independent rainfall events from continuous time series, the inter-event time definition method with a duration of 12 h was adopted (Joo et al., 2014). "Future" rainfall data were established based on observed data and projections based on multi-GCMs (**Figure 1**) as well as RCPs introduced by IPCC in its Fifth Assessment Report (O'Neill et al., 2014). The median ensemble model of multi-GCMs was adopted to project rainfall events over the projected period. RCP 8.5, a high emission scenario reflecting the increasing greenhouse gas emissions leading to radiative forcing of 8.5 W/m^2 in 2,100, was selected as the climate change scenario (Lee et al., 2014). The projected period of

TABLE 3 | Construction costs of constructed wetland (n m^2) and permeable pavement (n m^2) used in this study.

Construction work	PP	BC	Unit price ($)	PP	BC
Plant (m^2)	—	n	20	—	20 n
Asphalt pavement (m^3)	0.1 n	—	150	15 n	—
Soil (m^3)	—	0.9 n	30	—	27 n
Gravel (m^3)	0.3 n	0.3 n	50	15 n	15 n
Pipe (m)	$n^{0.5}$	$n^{0.5}$	15	15 $n^{0.5}$	15 $n^{0.5}$
Geotextile (m^2)	n	n	1	n	n
Excavation (m^3)	0.4 n	1.2 n	4	1.6 n	4.8 n
Disposal (m^3)	0.4 n	0.9 n	5	2 n	4.5 n

Note: The data are mainly from a local inquiry internet platform for engineering materials [www.gldjc.com (accessed May 28, 2019)].

2020–39 was adopted. In so doing a 30-year planning horizon and LID's life span (assumed to be 30 years) (Vineyard et al., 2015) was established, with the first 10 years (2010–19) of observed rainfall time series and 20 years (2020–39) of projected rainfall time series.

Hydrologic Model and LID Practices

The Storm Water Management Model (SWMM), a dynamic hydrologic model, was used to simulate the hydrological processes for a single and continuous rainfall event on an urban catchment. The result was used in the planning and design of various LID technologies (Kong et al., 2017). The underlying surface of catchment was treated as a non-linear reservoir (Palla and Gnecco, 2015). The Horton model for infiltration and dynamic wave routing was selected for rainfall loss and confluence routing (Rossman and Huber, 2016).

Although both PP and CW have been widely used in LID practices for reducing peak flow and pollution loads at source, their construction structures, materials, costs, and maintenance as well as applicabilities are quite different (Wang et al., 2019). In this study, PP and CW were adopted as representative LID elements, and the corresponding structural parameters are listed in **Table 2**. The surface area and width of the PP and CW were used to describe the extent of LID conceptually.

Annual runoff volume reduction was set as the main parameter in the optimization (maximized cost-saving) of investment. The construction costs of LID practices are included in **Table 3**. The annualized maintenance costs were defined as a certain fraction of the capital costs, that is, 4.0% for PP and 8.0% for CW (Houle et al., 2013; Wang et al., 2020). The life cycle cost (LCC) of LID was a long-term cost over the service life time, and they were adopted as the investment budget. LCCs of PP and CW were calculated using the capital and maintenance costs over a service life time of 30 years (Rossman and Huber, 2016). Construction of PP and CWs was set to be ready at the beginning of year 1, while the maintenance costs were incurred at some point in time between years 1–30 (Wang et al., 2020). A present value (PV) accounting was performed by compiling all LCC and discounted to the 2018 United States dollar ($) value. The LCC of PP and CWs were calculated as:

$$LCC = C_{\text{capital}} + PV_{O\&M}, \tag{1}$$

$$PV_{O\&M} = \sum_{n=1}^{30} O\&M \frac{1}{(1+i)^n}, \tag{2}$$

where C_{capital} is the capital cost of LID, $PV_{O\&M}$ is the present value of the maintenance costs, n is the number of year in service, and i is the discount rate reflecting the depreciation in value over time (Reis and Shortridge, 2020). A discount rate of 2% was adopted in this study (Dong, 2018).

Long-Term Efficiency Metrics

Following the long-term performance modeling framework for LID developed by Liu et al. (2018), the effective performance of PP was assumed to degrade linearly over time and is shown in **Figure 2A** (Emerson et al., 2010; Haile et al., 2016). The decrease in PP effectiveness was mainly attributable to physical degradation such as clogging of the pores and sediment accumulation over the surface. **Figure 2B** shows the potential change in the mean CW effectiveness normally distributed during a typical year following the annual vegetative growth and decay cycle.

The composite efficiency of PP and CW is shown in **Figure 2C**. It is derived by superimposing the cyclic trend of the CW on the linearly decreasing trend of the PP. The relationship of LSE_{mean_PP} is as follow:

$$LSE_{mean\_PP} = -a \times x + b, \tag{3}$$

where a is the slope (assumed to have a default value of 0.020 ± 0.005) (Liu et al., 2018), and b is the intercept set to 1, since the initial efficiency of PP was set to 100%.

The mean efficiency for CW (LSE_{mean_BC}) was reflected as a series of normal distribution with attenuated magnitude (**Figure 2C**), which emulated the natural characteristics of decreasing efficiency from year-to-year. The (LSE_{mean_BC}) was assumed normally distributed (Forbes et al., 2011) as:

$$LSE_{mean\_BC} = pdf\_norm(x|\sigma,\mu) = \frac{1}{\sigma\sqrt{2\pi}} e^{\frac{-(x-\mu)^2}{2\sigma^2}}, \tag{4}$$

where σ is the standard deviation (assumed to have a default value of 1.0 and a range of 0.5–5.0) (Liu et al., 2018); μ is the mean of x (assumed to be 0); and x has a value between −6 and +6 (the range of 12 months).

For the first year of CW's service life, the highest mean efficiency ($LSE_{highest\_BC}$) was set to 100%. To reflect the downward trend of CW's performance, $LSE_{highest\_BC}$ was assumed to decay with a reduction factor, LSE_{nh} year-on-year:

$$LSE_{highest\_BC} = 100\% \times (1 - LSE_{nh})^{N-1}, \tag{5}$$

where N is the number of years of the design life span, and LSE_{nh} reflects the progressive reduction of potential maximum efficiency year-on-year, and is assumed to have a default value of 2.0 ± 1.0%.

For the annual rainfall–runoff reduction, it was necessary to establish the statistics for the total runoff generated in the events for the y^{th} year as follow:

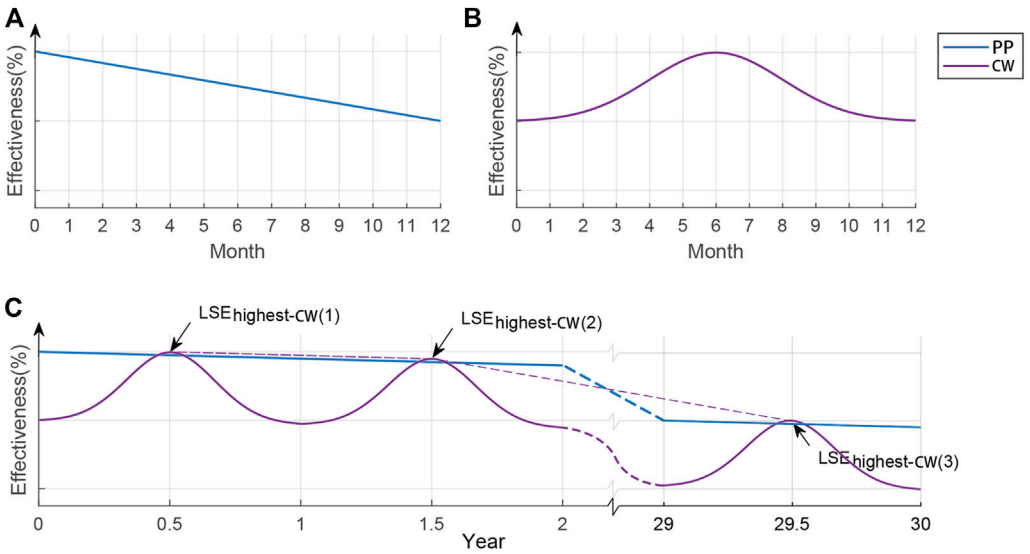

FIGURE 2 | (A) Potential mean PP effectiveness during each year, **(B)** potential mean CW effectiveness during each year, and **(C)** example of composite mean PP and CW effectiveness over the design life span.

$$R_{ov}(y) = V_y - \sum_{k=1}^{n} V(k,y) \times LSE_{mean}, \quad (6)$$

where $R_{ov}(y)$ is the reduction runoff volume of LID practices in year y (from 2010–39), V_y is the yth year annual runoff volume generated for non-LID catchment, n is the number of rain events in year y, and LSE_{mean} is the mean efficiency of LID practices.

Bayesian Learning Programming

A Bayesian-based multi-stage decision model (with "prior" and "posterior" predictive distribution) was adopted to model the implementation process of the LID. The model analyzes various schemes of implementation, while considering opportunities and risks progressively. Certain schemes might change course at some future stages, depending on the level of achievement attained at that time. A two-stage decision model was incorporated in the LID scheme (investment decision) in this study. The main constraints were certain pseudo-random events and acceptable risk-averse levels.

"Prior" Distributions

According to the terminology of Bayesian inference theory, the distribution on the hydrological performances of LID practices at the initial stage, called the "prior" distribution, was assumed to be normally distributed (μ, σ^2, where μ and σ^2 were the mean and variance of performances, respectively) based on the simulated ensemble of LID function units.

$$P_{ave}(u,s) = \frac{1}{Y} \times \frac{\sum_{y=1}^{Y} R_{ov}(u,s)}{LCC(u,s)}, \forall u \in \{\mathrm{PP}, \mathrm{BC}\}, \forall s \in \mathrm{S}, \quad (7)$$

where $P_{ave}(u,s)$ represents LID function objectives, Y is 30 years of the simulated period, $u \in \{\mathrm{PP}, \mathrm{BC}\}$ represented the investments in PP or CW, $s \in \mathrm{S}$ represents the LID investment scenario s in S scenarios, and $R_{ov}(u,s)$ and $LCC(u,s)$ are the storm runoff volume reduction and life cycle costs for u LID type in scenario s, respectively. The LID function objective contains a single parameter, that is, storm runoff reduction. $P_{ave}(u,s)$ was therefore adopted as an index for average annual runoff volume reduction and reflected as reduced investment amount per $ per year in scenario s.

Learning Curve Function

A learning curve was assumed to be a function of the transformed relationship of investment on LID practices based on potential information gains from Bayesian Inference (Hung and Hobbs, 2019). These information gains were used to update the knowledge/beliefs regarding "posterior" distribution of the hydrological performance of LID practices in the second stage (Ferioli et al., 2009). A variance learning (VL) model and a mean-variance learning (MVL) model were proposed for various learning curve functions. The VL model was defined as a learning process which could only reduce the uncertainty of LID's performance, whereas the MVL model assumed that the learning process could reduce uncertainty and improve the expected performance through technological advancement or cost reduction. Thus, the MVL model might be viewed as an extension of the VL model. The VL curve for variance reduction was expressed in the form of a two-step function (**Figure 3A**) representing one of the three possible learning pathways (None-L, Part-L, and All-L) that would take place. None-L was defined as one that the posterior distribution was identical to its prior; Part-L was defined as one that the posterior distribution variances were less than the prior distributions but not zero, and All-L was defined as one that the posterior distribution variance was set to zero. The learning curve function for reducing uncertainty of u LID solution in scenario s at Stage II (denoted *Uncertainty*

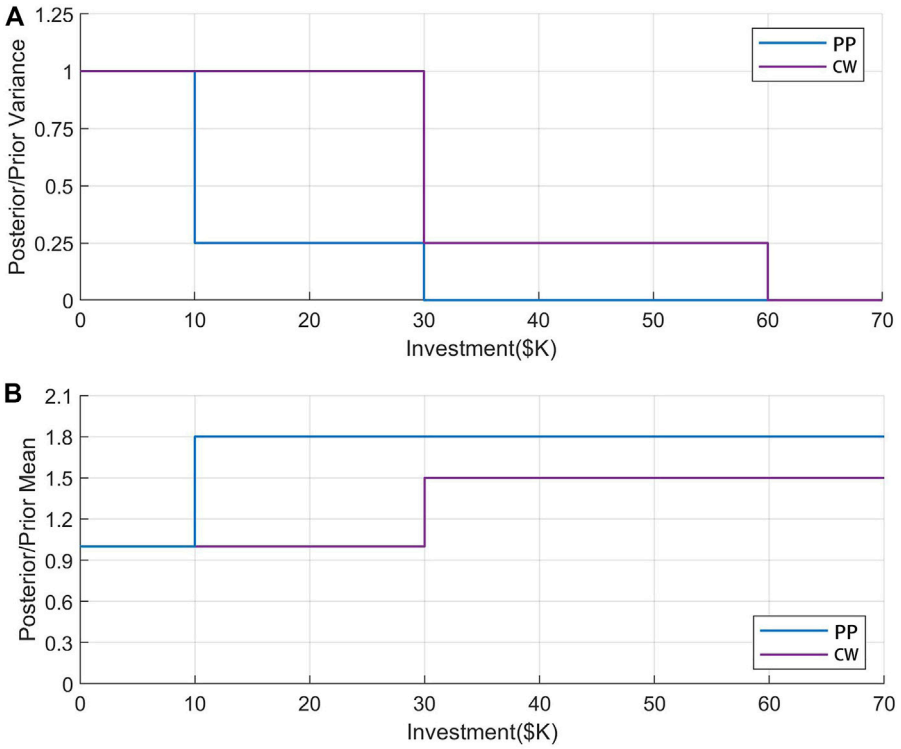

FIGURE 3 | (A) Variance learning curve functions used in the VL and the MVL models and **(B)** learning curve functions for the expected value improvement in the MVL model.

$(x_{2\_s,\ u})$) for both VL and MVL models was defined as follows.

$$Uncertainty\left(x_{II,u,s}\right) = \beta\sigma^2 \begin{cases} \beta = 1, if\ Th^{\text{Part-L}} > x_{II,u,s} & (None - L\ takes\ place) \\ 0 < \beta < 1,\ if\ Th^{\text{Part-L}} \le x_{II,u,s} < Th^{\text{All-L}} & (Part - L\ takes\ place) \\ \beta = 0, , if\ Th^{\text{All-L}} \le x_{II,u,s} & (All - L\ takes\ place) \end{cases}, \tag{8}$$

where β is a scaling constant that is used to adjust the variance. The parameters $Th^{\text{Part-L}}$ and $Th^{\text{All-L}}$ are the threshold values for investments needed for Part-L and All-L cases, respectively.

In the MVL model, the learning curve function for mean improvement in scenario s of u LID type at Stage II (denoted by $Mean\ (x_{II,\ u,\ s})$) is assumed to have a single level only, and has a threshold value equaled to $Th^{\text{Part-L}}$ (**Figure 3B**), as shown as below.

$$Mean\left(x_{II,u,s}\right)\begin{cases} \gamma\mu, \gamma > 1, if\ Th^{\text{Part-L}} \le x_{II,u,s} \\ \mu, if\ x_{II,u,s} < Th^{\text{Part-L}} \end{cases}, \tag{9}$$

where γ is the scaling constant that could be used to adjust the posterior mean. The abscissa, investment ($), was indicated the extent/magnitude of LID.

Bayesian Optimization Formulation

The objective of the optimization process was to improve the relationship between LCC and the expected reductions in runoff volume based on the decision to invest on LID at various stages of development, and pending the resources, progressive learning, and risk constraints. Between expenditures and risk, tradeoffs were evaluated by adjusting the investment budget and risk appetite. Minimizing the risk of reduced efficiency was considered as one of the main considerations of investment on LID (Yamout et al., 2007). Conditional Value at Risk (CVaR), which reflects the average level of "portfolio excess loss," is adopted as a reliable and valid index of the potential risk (Bakhtiari et al., 2019). This index was used as the index of "poor outcomes." The optimization process portrayed risk-averse preferences by adopting CVaR constraints. If the constraint was binding, the decision was likely to be an investment that would elevate the expected performance under the worst risk conditions. The higher value of CVaR was desirable for maximum storm runoff volume reduction.

The VL model for investment optimization was calculated as follow:

$$s_{opt} = arg\max_{s\in S}\left[fP_{ave}\left(u,s\right)\right] = \text{Maximize}\ f_s\left(x_I, x_{II}\right), \tag{10}$$

$$f_s\left(x_I, x_{II}\right) = \frac{1}{Y} \times \left\{ C_{I,u,s}x_{I,u,s} + \frac{T_{II}}{T}\left[\frac{1}{S}\sum_{s=1}^{S}\left(C_{II\_n,u,s}x_{II\_n,u,s} + C_{II\_a,u,s}x_{II\_a,\ u,\ s} + C_{II\_p,\ u,s}x_{II\_p,u,s}\right)\right]\right\}, \tag{11}$$

subject to

$$\begin{cases} -x_{I,u} + TH_u^{\text{Part}} L_{Part,u} \le 0 \\ -x_{I,u} + TH_u^{\text{All}} L_{All,u} \le 0 \\ L_{None,u} + L_{Part,u} + L_{All,u} = 1 \end{cases}, \forall u \in \{\text{PP, BC}\}, \quad (12)$$

$$\begin{cases} z_s \ge \tau - f_s(x_I, x_{II}), \forall s \in S \\ \tau - \dfrac{1}{(1-\alpha)S} \displaystyle\sum_{s=1}^{S} z_s \end{cases}, \quad (13)$$

where **Eqs 12**, **13** are learning and risk constraints, respectively; x is a decision variable; x_I, and x_{II} are stage I, and II, respectively; $x_{II\_n,u,s}$, $x_{II\_p,u,s}$ and $x_{II\_a,u,s}$ are the investment vector at stage II for the None-L, Part-L, and All-L case in scenario s, respectively; $C_{I,u,s}$ is the reduction capacity of the storm runoff volume at stage I in scenario s; $C_{II\_n,u,s}$, $C_{II\_a,u,s}$, and $C_{II\_p,u,s}$ are the expected posterior mean of storm runoff volume reduction for the None-L, All-L, and Part-L cases at stage II in scenario s, respectively; $L_{None,u}$, $L_{Part,u}$ and $L_{All,u}$ are binary vector indicating whether (=1) or not (=0) None-L, Part-L, and All-L would occur for each of the u LID types; τ is an auxiliary variable used to calculate CVaR; and z_s is the stormwater reduction below τ in scenario s. In addition, it assumed equal likely of each scenario s.

The MVL model reflects technological improvement that would lead to added increase of the mean of the "posteriors" in comparison with the VL model. Therefore, the objective **Eq. 10** may be revised as follow:

$$\text{Maximize } f_s(x_I, x_{II}) = \frac{1}{Y} \times \left\{ C_{I,u,s} x_{I,u,s} + \frac{T_{II}}{T} \left[\frac{1}{S} \sum_{s=1}^{S} \left(C_{II\_n,u,s} x_{II\_n,u,s} + C_{II\_a,u,s}^{MVL} x_{II\_a,u,s} + C_{II\_p,u,s}^{MVL} x_{II\_p,u,s} \right) \right] \right\}, \quad (14)$$

where $C_{II\_a,u,s}^{MVL}$ and $C_{II\_p,u,s}^{MVL}$ are "posterior" mean of the storm runoff volume reduction rate for the All-L and Part-L cases in scenario s at stage II in the MVL model, respectively.

Discussion on the Assumptions Made

The constraints imposed on investment included the overall budget, learning relationships, and risk appetite. A budget per hectare of $100K was suggested for LID implemented at the test sub-catchment. Thus, the budgets for S01 and S02 were set to $200K and $150K, respectively. A two-stage investment process was developed to optimize the LID planning process. Stage I began at the start of the project, and Stage II would begin at year 4 in the 30-year planning horizon. Once installed, the LID would continue to generate storm runoff volume reduction until the end of the planning period.

The learning curves assumed in the VL model are displayed in **Figure 3A**. There, *Uncertainty* ($x_{II,u,s}$) = 1 indicated that the investment was below the threshold and would trigger learning; *Uncertainty* ($x_{II,u,s}$) = 0.25 meant that the investment would result in Part-L and the variance was reduced to a quarter of the original value. Here, Part-L thresholds corresponded to setting $10K and $30K for PP and CW, respectively. *Uncertainty* ($x_{II,u,s}$) = 0 meant that full information in All-L was obtained in Stage II so that the variance was reduced to zero. All-L thresholds corresponded to setting $30K and $60K for PP and CW, respectively. In the MVL model, the thresholds for 80 and 50% meant that improvements were assumed at setting $10K and $30K for PP and CW, respectively, and were the same as the Part-L thresholds in the VL model (**Figure 3B**). Besides, a lower bound value was placed on $\text{CVaR}_{0.05}$ as a minimal acceptable storm runoff volume reduction.

RESULTS

"Prior" Distributions of the Performance of a Low-Impact Development

Statistically, the average annual rainfall from 2010 to 2019 was 2,253 mm. The climate ensemble of RCP 8.5 showed a small increase (0.9%) for the projected period (2020–39) of 2,272 mm for the median ensemble model. Although the median was close to that of the observed climate, the projected changes in monthly precipitation were still highly uncertain, especially in the

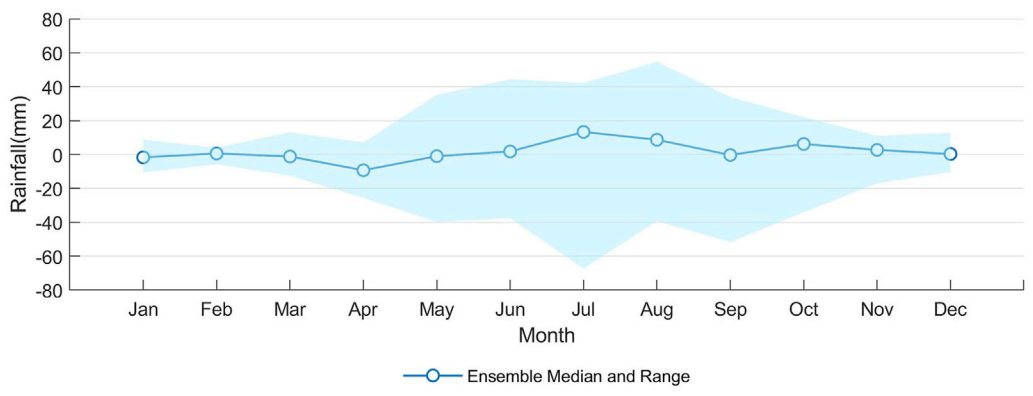

FIGURE 4 | Projected changes in monthly precipitation compared to historical average data in Guangzhou during the simulated period for RCP 8.5. Note: source of information published by the Climate Change Knowledge Portal of the World Bank Group (https://climateknowledgeportal.worldbank.org [accessed 23 Jan 2020]).

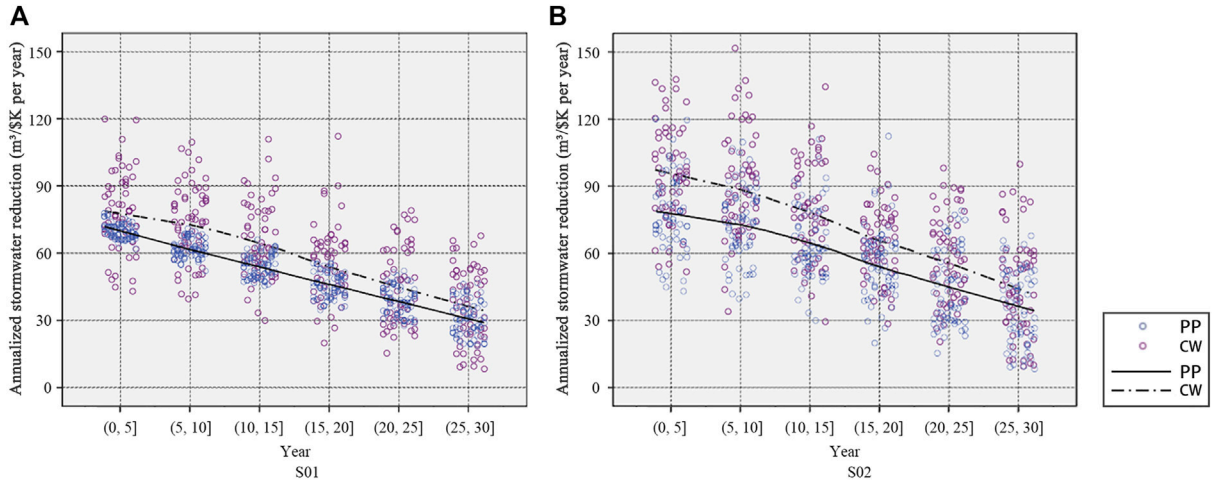

FIGURE 5 | Annualized stormwater reduction of LIDs in **(A)** S01 and **(B)** S02 based on the long-term effectiveness analysis in a simulated period.

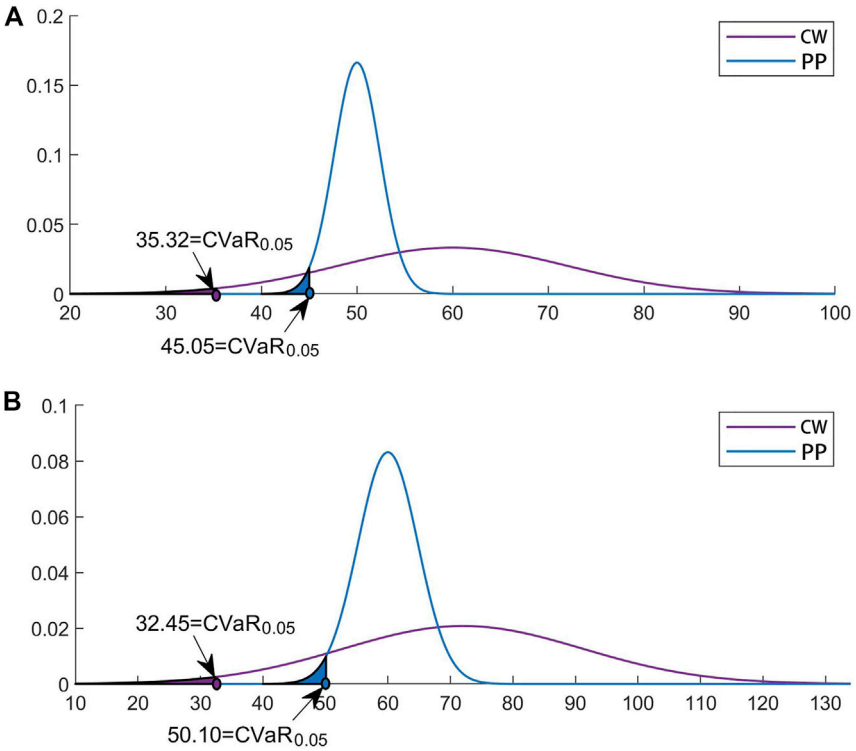

FIGURE 6 | Prior distribution of LIDs with normal distribution in **(A)** S01 and **(B)** S02.

monsoon. (**Figure 4**). The projected change in monthly precipitation in July (μ is 9.4 mm; σ^2 is 1,008.4 mm) is the most obvious, and its variance is nearly 110 times that in February. **Figure 4** shows that Guangzhou could be subject to more severe urban flooding and drought due to significantly increased precipitation during the rainy season but decreasing rainfall during the dry season. Other studies focusing on climate change impacts reported similar findings (Huang et al., 2018). Deng et al. (2018) reported that seasonal storms and drought might occur more frequently with greater intensity in most areas of Guangzhou.

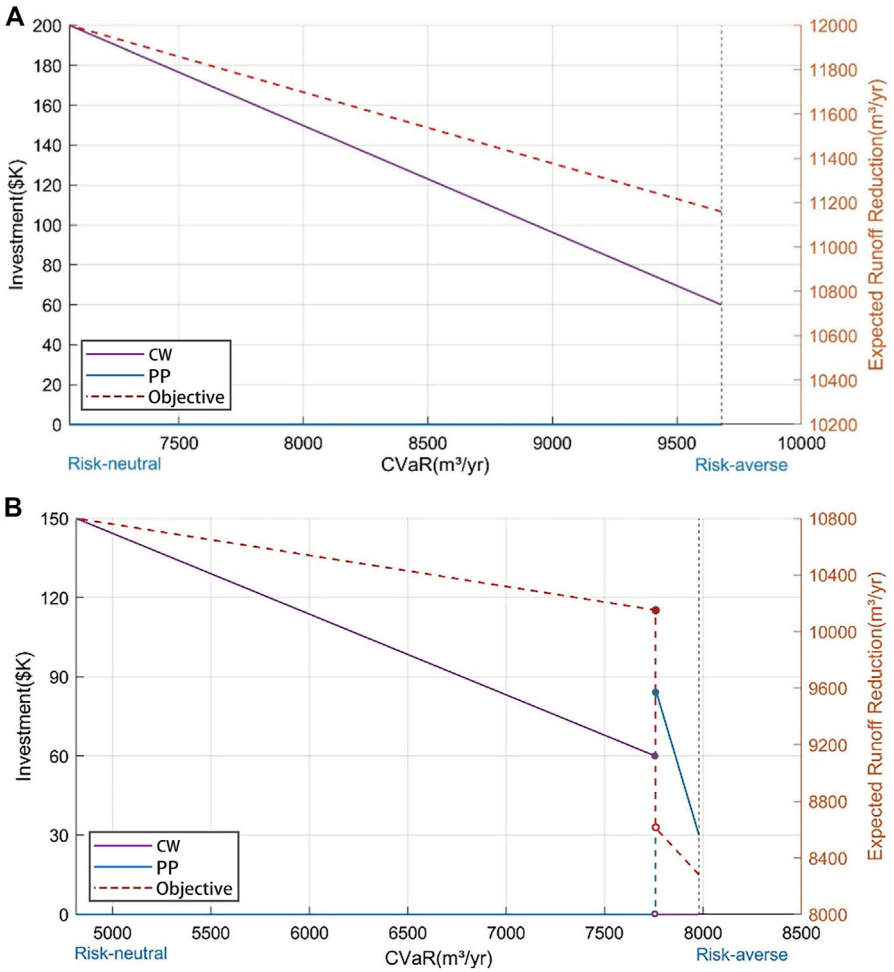

FIGURE 7 | Investment strategies at Stage I **(left axis)** and the objective function values **(right axis)** from the VL model for CVaR0.05 in **(A)** S01 and **(B)** S02.

Figure 5 illustrates the annualized storm runoff volume reduction, averaged over the 30-year time horizon. The performances of PP and CW showed a significant downward trend attributable to decreasing efficiency based on the long-term performance curves of LIDs. It was noted that the performance curves were calculated according to the average performance as recorded in the long-term time series for both LIDs. Therefore, extreme scenarios would not be reflected within the scenario of a particularly stable long-term performance or rapid degradation. At the end of service life, long-term effectiveness of PP would remain between 25.0 and 55.0% and appeared normally distributed. However, in its last year of service life, the highest efficiencies of CW would range from 10.0 to 70.0% with greater fluctuation.

More frequent heavy rainfall events following climate change would have exceeded the LID's drainage capacity and reduce the hydrological efficiency of LID. The performance of CW was found to be superior than that of PP in S01 and S02 during the same period. Also, the efficiency of storm runoff volume reduction through LID in S01 was relatively lower than that in S02. This result was attributed to the lower impervious rate in S01, which led to lower rainfall losses and hence lower runoff volume reduction.

By calculating the "prior" distribution of LIDs based on long-term effectiveness, the performances of both LIDs appeared normally distributed. $CVaR_{0.05}$ was used to calculate the risk values of "prior" probability for LIDs under long-term performance (**Figure 6**). As a result, investment on CW was found to be more cost-efficient than that for PP, but the uncertainty with the performance of CW was higher. Also, CW showed lower CVaR values, reflecting its potentially higher risk. These findings were found to be consistent with those reported by others (Liu et al., 2018). It was noted that the unit performance of LID in S02 was better than that in S01 but it also showed a significant level of uncertainty.

Variance Learning Model

Though the same unit budget (a budget of $100K per hectare {assumed}) was invested in LID, the performance and risk thresholds corresponding to different test catchments were different (**Figure 7**). The VL model was examined for $CVaR_{0.05}$ with values ranging from 7,060 m^3/yr to 9,678 m^3/yr

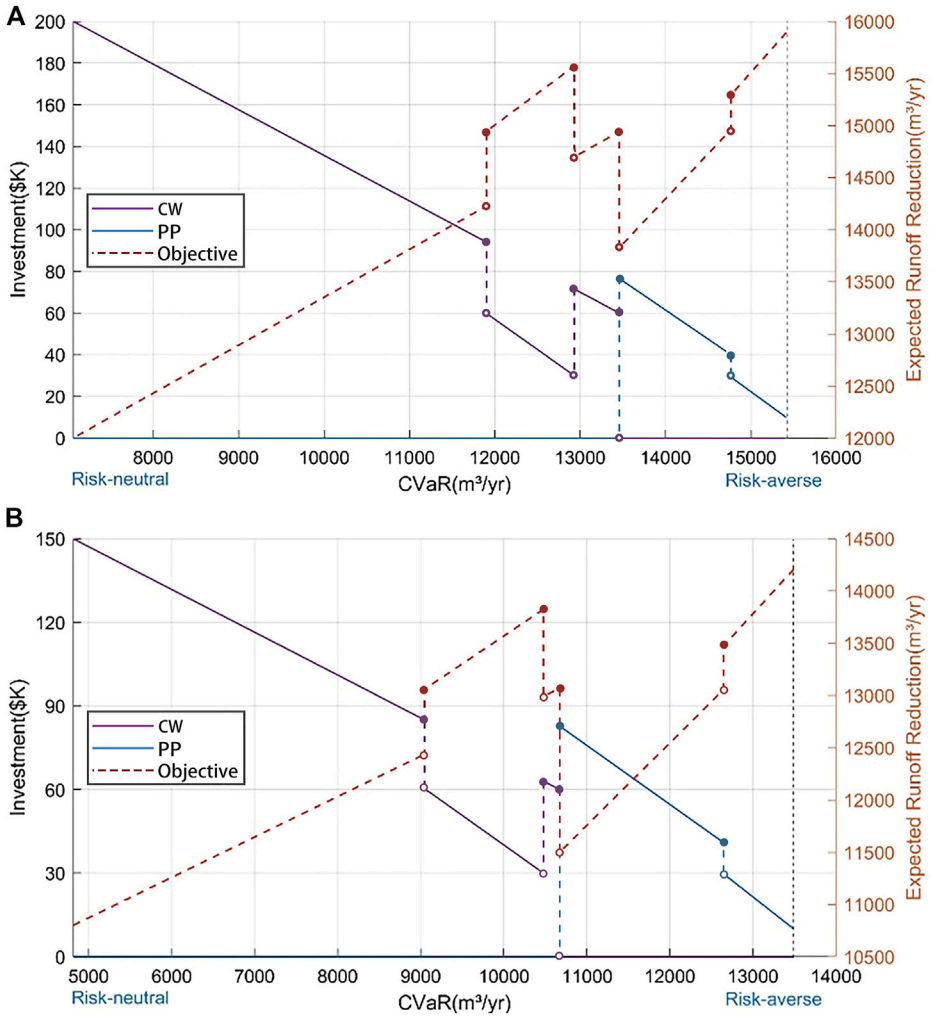

FIGURE 8 | Investment strategies at Stage I **(left axis)**, and the objective function values **(right axis)** from the MVL model for CVaR0.05 in **(A)** S01 and **(B)** S02.

in S01 and 4,815 m^3/yr to 7,980 m^3/yr in S02. S01, at a CVaR of 7,060 m^3/yr, which was the alternative that maximizes the expected storm runoff volume reduction, achieved a value of 12,000 m/yr. High value of CVaR had higher stability at the expense of lower expected hydrological performance. CVaR could increase to as much as 9,678 m^3/yr, with an increase of 37.1%. However, the corresponding expected storm runoff volume reduction was reduced by about 7.0% from 12,000 to 11,160 m^3/yr. Thus, it appeared that the risk capacity determined the expected reduction of runoff. Meanwhile, CVaR showed a 65.7% increase from 4,815 m^3/yr to 7,980 m^3/yr, while the expected storm runoff volume reduction fell about 23.3% from 10,800 m^3/yr to 8,280 m^3/yr in S02.

Not surprisingly, the optimal strategy was one in which all allotted budgets were invested in CW at Stage I for a risk-neutral decision-maker since CW had proven track of good performance with a higher "prior" mean, even if PP were to degrade more slowly than CW, and CW only portrayed a marginally higher effectiveness than PP at around the middle of each year from **Figure 2**. It is worth noting that the average annual runoff control over the service life time was adopted as the performance level in this study. Limited hydrological management ability of CW in the later period was ignored, since CW degrades faster than PP over time.

There was no strong incentive to invest in PP or take advantage of learning on the VL model since "to wait" means that there would be no derived benefit during the initial 3 years, which then led to lower surface runoff reduction over the 30-year period. However, were him showed a risk-averse attitude, the manager might act to save some amount of budget for the next stage or mix his investment with more LID alternatives, or to wait to obtain better estimates of LID performance. For instance, when 7,060 m^3/yr < CVaR ≤ 9,678 m^3/yr, the model suggested making investments in CW and also saving some amount of budget for Stage II.

In the case of S02, the optimal solutions were more complex. With 4,815 m^3/yr < CVaR ≤ 7,758 m^3/yr, the model suggested making investments in CW, while saving some amount of budget to leverage on "All-L" in CW. However, with 7,758 m^3/yr < CVaR ≤ 7,980 m^3/yr, the model suggested investing in PP to the tune of $85.5K to $30K for "All-L″ at Stage I and saving the

balance to invest at Stage II in order to further reduce the risk. It was noted that CVaR showed a 2.9% increase from investing in CW to PP. However, the expected storm runoff volume reduction decreased dramatically by about 18.4% from 10,152 to 8,280 m^3/yr. Note that PP was not recommended for the risk-neutral decision-makers since its efficacy is limited, but it was added for the conservative or risk-averse one due to its obvious stability of hydrological performance.

Mean-Variance Learning Model

The MVL model added other sets of learning functions to the VL model, for which the expected performances of PP and CW could be improved. As a result, the MVL model depicted a lower incentive to make investment at Stage I to increase the expected volume reduction, as compared to the VL model. A recommended initial decision is to make a partial or delayed investment first, and then decide when more information becomes available. The losses at Stage I may increase, but better long-term outcomes could be achieved by reducing the loss of structural performance and potential technological change for LID, since it avoids irreversible investment at the initial stage and retains the option of future expansion (Gersonius et al., 2013). Meanwhile, the expectation is one with the highest return when the investment strategy is extremely risk averse. This means that aggressive and high-risk investment strategies at the initial stage do not necessarily lead to high expectations when considering the uncertainty of technological development.

Figure 8 illustrates the expected storm runoff volume reduction as a function of $CVaR_{0.05}$. The objective values in MVL models were higher than the results in VL models due to anticipated technological improvements with a decrease in capital costs or an increase in hydrological efficiency for a "new" LID device. Moreover, with an increased CVaR value, the expected runoff volume reduction showed an upward trend of fluctuation, which was the opposite of the VL model. For instance, in S01, CVaR could be significantly increased from 7,060 m^3/yr to 15,415 m^3/yr, and the corresponding expected storm runoff volume reduction increased by about 32.4%, from 12,000 to 15,890 m^3/yr. This was the result of investing a limited amount of budget at Stage I to activate technological improvements, resulting in the reductions of posterior variance and an expected increase in LID. With the assumed technological improvement, the CVaR value could be as high as 15,415 m^3/yr and 13,490 m^3/yr in S01 and S02, respectively. In the VL model, the CVaR had a cup of 10,000 m^3/yr in both sub-catchments, whereas the maximum expected storm runoff volume reduction in the MVL model increased by about 32.4 and 40.0% for S01 and S02, respectively, when compared with the VL model. It was also noted that, in S01, and with CVaR set to 13,480 m^3/yr or higher, the MVL also suggested investment of more than $10K in PP in Stage I to obtain "Part-L" for improving the efficiency of LID. Here, PP was not invested in the VL model as PP had a higher potential to enhance its performance with a relatively lower uncertainty in Stage II.

CONCLUSION

A coupled long-term efficiency analysis of LID and a Bayesian learning model has been proposed. The model has the ability to minimize urban flooding risk and maximize expected storm runoff volume reduction through optimal investment in LID. As a dynamic decision-making tool, the model could be implemented in stages with deliberate decision to invest more or suspend investment on the LID elements at various times, pending the observed performance (progressive updates of performance) of the LID, resources available, environmental changes, technological advancement, and users' needs and expectations. Each and every stage of the development is to be designed and built after a Bayesian update of the probabilistic performance function for each LID option. The goal of this Bayesian update is to support the engineers and administrators on the improvement of the design and investment, respectively, by having to minimize uncertainty and to maximize returns leveraging on potential technological advancements and reducing cost. The proposed framework and procedure can also be applied to the planning and investment planning in other fields that involve some degree of uncertainty. Despite the successful illustration of the framework reported herein, the authors emphasize that simulation of long-term LID efficiencies and the modification/validation of learning curves based on the Bayesian method can be further enhanced. A rapid and efficient method for calibration and verification for the data-driven Bayesian model needs to be further investigated.

DATA AVAILABILITY STATEMENT

The raw data supporting the conclusions of this article will be made available by the authors, without undue reservation.

AUTHOR CONTRIBUTIONS

MW: conceptualization, methodology, writing—original draft preparation, and supervision; YuZ: software, data curation, and visualization; DZ: methodology, validation, and supervision; YiZ: formal analysis, investigation, and data curation; SZ: software, data curation, and visualization; ST: methodology, validation, and supervision.

FUNDING

This work was supported by the National Natural Science Foundation of China (grant number 51808137) and the Natural Science Foundation of Guangdong Province (grant number 2019A1515010873).

SUPPLEMENTARY MATERIAL

The Supplementary Material for this article can be found online at: https://www.frontiersin.org/articles/10.3389/fenvs.2021.713831/full#supplementary-material

REFERENCES

Ahiablame, L. M., Engel, B. A., and Chaubey, I. (2012). Effectiveness of Low Impact Development Practices: Literature Review and Suggestions for Future Research. *Water Air Soil Pollut.* 223 (7), 4253–4273. doi:10.1007/s11270-012-1189-2

Ahiablame, L., and Shakya, R. (2016). Modeling Flood Reduction Effects of Low Impact Development at a Watershed Scale. *J. Environ. Manage.* 171, 81–91. doi:10.1016/j.jenvman.2016.01.036

Bahrami, M., Bozorg-Haddad, O., and Loáiciga, H. A. (2019). Optimizing Stormwater Low-Impact Development Strategies in an Urban Watershed Considering Sensitivity and Uncertainty. *Environ. Monit. Assess.* 191 (6), 340. doi:10.1007/s10661-019-7488-y

Bakhshipour, A. E., Dittmer, U., Haghighi, A., and Nowak, W. (2019). Hybrid green-blue-gray Decentralized Urban Drainage Systems Design, a Simulation-Optimization Framework. *J. Environ. Manage.* 249, 109364. doi:10.1016/j.jenvman.2019.109364

Bakhtiari, P. H., Nikoo, M. R., Izady, A., and Talebbeydokhti, N. (2019). A Coupled Agent-Based Risk-Based Optimization Model for Integrated Urban Water Management. *Sustain. Cities Soc.* 53, 101922. doi:10.1016/j.scs.2019.101922

Bracmort, K. S., Arabi, M., Frankenberger, J., Engel, B. A., and Arnold, J. G. (2006). Modeling long-term water quality impact of structural BMPs. *T. ASABE.* 49 (2), 367–374. doi:10.13031/2013.20411

Chen, H., Grieneisen, M. L., and Zhang, M. (2016). Predicting Pesticide Removal Efficacy of Vegetated Filter Strips: A Meta-Regression Analysis. *Sci. Total Environ.* 548-549, 122–130. doi:10.1016/j.scitotenv.2016.01.041

Deng, S., Chen, T., Yang, N., Qu, L., Li, M., and Chen, D. (2018). Spatial and Temporal Distribution of Rainfall and Drought Characteristics across the Pearl River basin. *Sci. Total Environ.* 619-620, 28–41. doi:10.1016/j.scitotenv.2017.10.339

Dong, Y. (2018). Performance Assessment and Design of Ultra-high Performance concrete (UHPC) Structures Incorporating Life-Cycle Cost and Environmental Impacts. *Construction Building Mater.* 167, 414–425. doi:10.1016/j.conbuildmat.2018.02.037

Emerson, C. H., Wadzuk, B. M., and Traver, R. G. (2010). Hydraulic Evolution and Total Suspended Solids Capture of an Infiltration Trench. *Hydrol. Process.* 24 (8), 1008–1014. doi:10.1002/hyp.7539

Ferioli, F., Schoots, K., and van der Zwaan, B. C. C. (2009). Use and Limitations of Learning Curves for Energy Technology Policy: A Component-Learning Hypothesis. *Energy Policy* 37 (7), 2525–2535. doi:10.1016/j.enpol.2008.10.043

Forbes, C., Evans, M., Hastings, N., and Peacock, B. (2011). *Statistical Distributions*. John Wiley & Sons.

Gersonius, B., Ashley, R., Pathirana, A., and Zevenbergen, C. (2013). Climate Change Uncertainty: Building Flexibility into Water and Flood Risk Infrastructure. *Climatic Change* 116 (2), 411–423. doi:10.1007/s10584-012-0494-5

Haile, T. M., Hobiger, G., Kammerer, G., Allabashi, R., Schaerfinger, B., and Fuerhacker, M. (2016). Hydraulic Performance and Pollutant Concentration Profile in a Stormwater Runoff Filtration Systems. *Water Air Soil Pollut.* 227 (1), 34. doi:10.1007/s11270-015-2736-4

Hallegatte, S., Green, C., Nicholls, R. J., and Corfee-Morlot, J. (2013). Future Flood Losses in Major Coastal Cities. *Nat. Clim Change* 3 (9), 802–806. doi:10.1038/nclimate1979

Hou, J., Han, H., Qi, W., Guo, K., Li, Z., and Hinkelmann, R. (2019). Experimental Investigation for Impacts of Rain Storms and Terrain Slopes on Low Impact Development Effect in an Idealized Urban Catchment. *J. Hydrol.* 579, 124176. doi:10.1016/j.jhydrol.2019.124176

Houle, J. J., Roseen, R. M., Ballestero, T. P., Puls, T. A., and Sherrard, J. (2013). Comparison of Maintenance Cost, Labor Demands, and System Performance for LID and Conventional Stormwater Management. *J. Environ. Eng.* 139 (7), 932–938. doi:10.1061/(asce)ee.1943-7870.0000698

Huang, H., Chen, X., Zhu, Z., Xie, Y., Liu, L., Wang, X., et al. (2018). The Changing Pattern of Urban Flooding in Guangzhou, China. *Sci. Total Environ.* 622-623, 394–401. doi:10.1016/j.scitotenv.2017.11.358

Hung, F., and Hobbs, B. F. (2019). How Can Learning-By-Doing Improve Decisions in Stormwater Management? A Bayesian-Based Optimization Model for Planning Urban green Infrastructure Investments. *Environ. Model. Softw.* 113, 59–72. doi:10.1016/j.envsoft.2018.12.005

Jacobi, S. K., Hobbs, B. F., and Wilcock, P. R. (2013). Bayesian Optimization Framework for Cost-Effective Control and Research of non-point-source Sediment. *J. Water Resour. Plann. Manage.* 139 (5), 534–543. doi:10.1061/(asce)wr.1943-5452.0000282

Joo, J., Lee, J., Kim, J. H., Jun, H., and Jo, D. (2014). Inter-event Time Definition Setting Procedure for Urban Drainage Systems. *Water* 6 (1), 45–58. doi:10.3390/w6010045

Kelly, D. L., and Kolstad, C. D. (1999). Bayesian Learning, Growth, and Pollution. *J. Econ. Dyn. Control.* 23 (4), 491–518. doi:10.1016/s0165-1889(98)00034-7

Koch, B. J., Febria, C. M., Gevrey, M., Wainger, L. A., and Palmer, M. A. (2014). Nitrogen Removal by Stormwater Management Structures: A Data Synthesis. *J. Am. Water Resour. Assoc.* 50 (6), 1594–1607. doi:10.1111/jawr.12223

Kong, F., Ban, Y., Yin, H., James, P., and Dronova, I. (2017). Modeling Stormwater Management at the City District Level in Response to Changes in Land Use and Low Impact Development. *Environ. Model. Softw.* 95, 132–142. doi:10.1016/j.envsoft.2017.06.021

Larsen, T. A., Hoffmann, S., Lüthi, C., Truffer, B., and Maurer, M. (2016). Emerging Solutions to the Water Challenges of an Urbanizing World. *Science* 352 (6288), 928–933. doi:10.1126/science.aad8641

Lee, J. W., Hong, S. Y., Chang, E. C., Suh, M. S., and Kang, H. S. (2014). Assessment of Future Climate Change over East Asia Due to the RCP Scenarios Downscaled by GRIMs-RMP. *Clim. Dynam.* 42 (3-4), 733–747. doi:10.1007/s00382-013-1841-6

Liu, R., Chen, Y., Wu, J., Gao, L., Barrett, D., Xu, T., et al. (2017). Integrating Entropy-Based Naïve Bayes and GIS for Spatial Evaluation of Flood Hazard. *Risk Anal.* 37 (4), 756–773. doi:10.1111/risa.12698

Liu, Y., Ahiablame, L. M., Bralts, V. F., and Engel, B. A. (2015). Enhancing a Rainfall-Runoff Model to Assess the Impacts of BMPs and LID Practices on Storm Runoff. *J. Environ. Manage.* 147, 12–23. doi:10.1016/j.jenvman.2014.09.005

Liu, Y., Engel, B. A., Flanagan, D. C., Gitau, M. W., McMillan, S. K., Chaubey, I., et al. (2018). Modeling Framework for Representing Long-Term Effectiveness of Best Management Practices in Addressing Hydrology and Water Quality Problems: Framework Development and Demonstration Using a Bayesian Method. *J. Hydrol.* 560, 530–545. doi:10.1016/j.jhydrol.2018.03.053

Montalto, F., Behr, C., Alfredo, K., Wolf, M., Arye, M., and Walsh, M. (2007). Rapid Assessment of the Cost-Effectiveness of Low Impact Development for CSO Control. *Landscape Urban Plann.* 82 (3), 117–131. doi:10.1016/j.landurbplan.2007.02.004

O'Neill, B. C., Kriegler, E., Riahi, K., Ebi, K. L., Hallegatte, S., Carter, T. R., et al. (2014). A New Scenario Framework for Climate Change Research: the Concept of Shared Socioeconomic Pathways. *Climatic Change* 122 (3), 387–400.

Palla, A., and Gnecco, I. (2015). Hydrologic Modeling of Low Impact Development Systems at the Urban Catchment Scale. *J. Hydrol.* 528, 361–368. doi:10.1016/j.jhydrol.2015.06.050

Pyke, C., Warren, M. P., Johnson, T., LaGro, J., Scharfenberg, J., Groth, P., et al. (2011). Assessment of Low Impact Development for Managing Stormwater with Changing Precipitation Due to Climate Change. *Landscape Urban Plann.* 103 (2), 166–173. doi:10.1016/j.landurbplan.2011.07.006

Reis, J., and Shortridge, J. (2020). Impact of Uncertainty Parameter Distribution on Robust Decision Making Outcomes for Climate Change Adaptation under Deep Uncertainty. *Risk Anal.* 40, 494–511. doi:10.1111/risa.13405

Rossman, L. A., and Huber, W. (2016). *Storm Water Management Model Reference Manual Volume I–Hydrology*. Cincinnati, OH, USA: US Environmental Protection Agency.

Shi, R., Hobbs, B. F., and Jiang, H. (2019). When Can Decision Analysis Improve Climate Adaptation Planning? Two Procedures to Match Analysis Approaches with Adaptation Problems. *Climatic Change* 157, 611–630. doi:10.1007/s10584-019-02579-3

Sturm, M., Goldstein, M. A., Huntington, H., and Douglas, T. A. (2017). Using an Option Pricing Approach to Evaluate Strategic Decisions in a Rapidly Changing Climate: Black–Scholes and Climate Change. *Clim. Chang.* 140 (3-4), 437–449. doi:10.1007/s10584-016-1860-5

Tang, X., Shu, Y., Lian, Y., Zhao, Y., and Fu, Y. (2018). A Spatial Assessment of Urban Waterlogging Risk Based on a Weighted Naïve Bayes Classifier. *Sci. Total Environ.* 630, 264–274. doi:10.1016/j.scitotenv.2018.02.172

Thompson, J., Sattar, A. M. A., Gharabaghi, B., and Warner, R. C. (2016). Event-based Total Suspended Sediment Particle Size Distribution Model. *J. Hydrol.* 536, 236–246. doi:10.1016/j.jhydrol.2016.02.056

Vineyard, D., Ingwersen, W. W., Hawkins, T. R., Xue, X., Demeke, B., and Shuster, W. (2015). Comparing green and Grey Infrastructure Using Life Cycle Cost and Environmental Impact: a Rain Garden Case Study in Cincinnati, OH. *J. Am. Water Resour. Assoc.* 51 (5), 1342–1360. doi:10.1111/1752-1688.12320

Wang, M., Zhang, D., Cheng, Y., and Tan, S. K. (2019). Assessing Performance of Porous Pavements and Bioretention Cells for Stormwater Management in Response to Probable Climatic Changes. *J. Environ. Manage.* 243, 157–167. doi:10.1016/j.jenvman.2019.05.012

Wang, M., Zhang, D., Wang, Z., Zhou, S., and Tan, S. K. (2021). Long-term Performance of Bioretention Systems in Storm Runoff Management under Climate Change and Life-Cycle Condition. *Sustain. Cities Soc.*, 102598. doi:10.1016/j.scs.2020.102598

Wang, Z., Zhou, S., Wang, M., and Zhang, D. (2020). Cost-benefit Analysis of Low-Impact Development at Hectare Scale for Urban Stormwater Source Control in Response to Anticipated Climatic Change. *J. Environ. Manage.* 264, 110483. doi:10.1016/j.jenvman.2020.110483

Webster, M., Fisher-Vanden, K., Popp, D., and Santen, N. (2017). Should We Give up after Solyndra? Optimal Technology R&D Portfolios under Uncertainty. *J. Assoc. Environ. Resource Economists* 4 (S1), S123–S151. doi:10.1086/691995

Woodward, M., Kapelan, Z., and Gouldby, B. (2014). Adaptive Flood Risk Management under Climate Change Uncertainty Using Real Options and Optimization. *Risk Anal.* 34 (1), 75–92. doi:10.1111/risa.12088

Yamout, G. M., Hatfield, K., and Romeijn, H. E. (2007). Comparison of New Conditional Value-At-Risk-Based Management Models for Optimal Allocation of Uncertain Water Supplies. *Water Resour. Res.* 43 (7). doi:10.1029/2006wr005210

Yazdanfar, Z., and Sharma, A. (2015). Urban Drainage System Planning and Design - Challenges with Climate Change and Urbanization: a Review. *Water Sci. Technol.* 72 (2), 165–179. doi:10.2166/wst.2015.207

Yuan, Z., Liang, C., and Li, D. (2018). Urban Stormwater Management Based on an Analysis of Climate Change: A Case Study of the Hebei and Guangdong Provinces. *Landscape Urban Plann.* 177, 217–226. doi:10.1016/j.landurbplan.2018.04.003

Zhang, H., Wu, C., Chen, W., and Huang, G. (2017). Assessing the Impact of Climate Change on the Waterlogging Risk in Coastal Cities: A Case Study of Guangzhou, South China. *J. Hydrometeorol.* 18 (6), 1549–1562. doi:10.1175/jhm-d-16-0157.1

Zhu, Z., Chen, Z., Chen, X., and Yu, G. (2019). An Assessment of the Hydrologic Effectiveness of Low Impact Development (LID) Practices for Managing Runoff with Different Objectives. *J. Environ. Manage.* 231, 504–514. doi:10.1016/j.jenvman.2018.10.046

Conflict of Interest: The authors declare that the research was conducted in the absence of any commercial or financial relationships that could be construed as a potential conflict of interest.

Publisher's Note: All claims expressed in this article are solely those of the authors and do not necessarily represent those of their affiliated organizations, or those of the publisher, the editors, and the reviewers. Any product that may be evaluated in this article, or claim that may be made by its manufacturer, is not guaranteed or endorsed by the publisher.

frontiers in Earth Science

ORIGINAL RESEARCH
published: 10 December 2021
doi: 10.3389/feart.2021.782287

Quantitative Assessment of the Contributions of Climate Change and Human Activities to Vegetation Variation in the Qinling Mountains

Dandong Cheng[1,2], *Guizeng Qi*[1,2]*, *Jinxi Song*[1,2], *Yixuan Zhang*[1,2], *Hongying Bai*[1,2] *and Xiangyu Gao*[2]

[1]*Shaanxi Key Laboratory of Earth Surface System and Environmental Carrying Capacity, College of Urban and Environmental Sciences, Northwest University, Xi'an, China,* [2]*Institute of Qinling Mountains, Northwest University, Xi'an, China*

Quantitative assessment of the contributions of climate change and human activities to vegetation change is important for ecosystem planning and management. To reveal spatial differences in the driving mechanisms of vegetation change in the Qinling Mountains, the changing patterns of the normalized difference vegetation index (NDVI) in the Qinling Mountains during 2000–2019 were investigated through trend analysis and multiple regression residuals analysis. The relative contributions of climate change and human activities on vegetation NDVI change were also quantified. The NDVI shows a significant increasing trend (0.23/10a) from 2000 to 2019 in the Qinling Mountains. The percentage of areas with increasing and decreasing trends in NDVI is 87.96% and 12.04% of the study area, respectively. The vegetation change in the Qinling Mountains is caused by a combination of climate change and human activities. The Tongguan Shiquan line is a clear dividing line in the spatial distribution of drivers of vegetation change. Regarding the vegetation improvement, the contribution of climate change and human activities to NDVI increase is 51.75% and 48.25%, respectively. In the degraded vegetation area, the contributions of climate change and human activities to the decrease in NDVI were 22.11% and 77.89%, respectively. Thus, vegetation degradation is mainly caused by human activities. The implementation of policies, such as returning farmland to forest and grass, has an important role in vegetation protection. It is suggested that further attention should be paid to the role of human activities in vegetation degradation when formulating corresponding vegetation protection measures and policies.

Keywords: normalized difference vegetation index (NDVI), quantitative analysis, climate change, human activities, the Qinling Mountains

OPEN ACCESS

Edited by:
Guangzhi Sun,
Northeast Institute of Geography and Agroecology (CAS), China

Reviewed by:
Weili Duan,
Xinjiang Institute of Ecology and Geography (CAS), China
Pengfei Li,
Xi'an University of Science and Technology, China
Changfeng Sun,
Institute of Earth Environment (CAS), China

***Correspondence:**
Guizeng Qi
guizeng_qi@163.com

Specialty section:
This article was submitted to Hydrosphere, a section of the journal Frontiers in Earth Science

Received: *24 September 2021*
Accepted: *10 November 2021*
Published: *10 December 2021*

Citation:
Cheng D, Qi G, Song J, Zhang Y, Bai H and Gao X (2021) Quantitative Assessment of the Contributions of Climate Change and Human Activities to Vegetation Variation in the Qinling Mountains. Front. Earth Sci. 9:782287. doi: 10.3389/feart.2021.782287

1 INTRODUCTION

The continuous intensification of global climate change and human activities has been impacting the stability of the global terrestrial ecosystem (Duan et al., 2020). As the main component of the terrestrial ecosystem, vegetation plays an irreplaceable role in the mutual adjustment of atmosphere–soil–water, global carbon balance adjustment, and the maintenance of global climate stability (Cheng et al., 2017; Zhang et al., 2021). Vegetation is one of the most sensitive indicators in response to global change (Landuyt et al., 2019), and exploring vegetation change trends

and driving mechanisms has become a focus of global change research, which is of great significance to assess the carbon sequestration capacity of vegetation and the evolution mechanism of terrestrial ecosystems.

Previous studies have pointed out that climate change is one of the main driving forces of vegetation variation (Piao et al., 2015; Ge et al., 2021). With temperature closely associated with the beginning and end of vegetation photosynthesis (Braswell et al., 1997), the continuous increase in temperature prolongs the vegetation growing periods (Ji et al., 2020), which in return promotes vegetation growth, especially in high-latitude areas and mountain areas (Nemani et al., 2003; Xu et al., 2017; Myers-Smith et al., 2020). However, the temperature increase aggravates the occurrence of drought, inhibiting vegetation growth in middle-to-low latitude regions, and arid and semi-arid regions (Ichii et al., 2002; Zeng et al., 2020; Huang et al., 2021). Precipitation is another important factor affecting vegetation variation (Piao et al., 2015; Shi et al., 2021). In arid and semi-arid regions, insufficient precipitation is the main factor that restricts vegetation growth (Vicente-Serrano et al., 2013). However, in humid areas, the increase in precipitation lowers the temperature and radiation, thereby, inhibiting vegetation growth (Nemani et al., 2003). Besides climate change, the impact of human activities on vegetation growth cannot be ignored. Human activities, such as urban expansion, agricultural production, and returning farmland to forests and grasses, are important factors affecting the spatial pattern of vegetation and its growth (Yan et al., 2019; Huang et al., 2020; Qin et al., 2021; Shi et al., 2021). Meanwhile, since the industrial revolution, the rapid increase in CO_2 and other greenhouse gas emissions caused by human activities has promoted the photosynthesis of vegetation (Leakey et al., 2009), resulting in the fertilization effect of CO_2, promoting the growth of global vegetation (Zhu et al., 2016). Both climate change and human activities impact vegetation variation, which may intensify the spatial difference of vegetation change. Therefore, quantifying the impact of driving factors on vegetation change is essential to ecosystem management and vegetation response to global changes.

In the past, the study of spatial vegetation changes often involves remote sensing data (Duan et al., 2021). Among them, the Normalized Difference Vegetation Index (NDVI), a commonly used vegetation index, is closely related to vegetation primary productivity and leaf area index and is also a good indicator of vegetation cover and growth status (Ichii et al., 2002; Mao et al., 2012; Kai et al., 2020; Shi et al., 2021). The quantitative assessment method of the impact of climate change and human activities on vegetation variation mainly involves mathematical statistical methods, including correlation analysis, principal component analysis, and least-squares method (Wold et al., 1987; Qin et al., 2021). However, uncertainties exist in the processes and factors of the impact on vegetation change (Cai et al., 2016). A single-scale analysis of influencing factors may obscure the actual impact of driving factors, whereas the multiple regression residuals analysis method is able to overcome the drawbacks of the single-scale analysis, with a good application in the quantitative evaluation of multiple driving factors (Ovakoglou et al., 2018; Song et al., 2018; Kai et al., 2020; Qin et al., 2021).

The Qinling Mountains, located at the boundary between the temperate monsoon climate and the subtropical monsoon climate, is an important north–south geographic boundary in China, which has particular significance for the local natural geographic environment due to the obvious differences in climate and vegetation zones between the north and south of the Qinling Mountains (Qi et al., 2021). Previous studies revealed qualitatively the vegetation cover changes in the Qinling Mountains due to climate change and human activities (Wang and Bai, 2017; Deng et al., 2018b; Liu et al., 2018; Li et al., 2019; Kai et al., 2020; Qin et al., 2021). However, spatial differences in the effects of climate change and human activities in the Qinling Mountains have not been clearly revealed, so it is necessary to analyze the drivers of vegetation change in the Qinling Mountains in detail in the spatial differences analysis, which is essential for understanding the spatial variability of vegetation ecosystem change and its response mechanism research (Deng et al., 2018b).

Based on MODIS NDVI remote sensing data from 2000 to 2019 in the Qinling Mountains and data from 32 meteorological stations, this paper employs trend analysis and multiple regression residual analysis to evaluate the driving mechanism of vegetation changes in the Qinling Mountains and quantitatively evaluate the driving factors. The study provides a scientific basis for the construction of ecological civilization in the Qinling Mountains and the response of the ecosystem to climate fluctuations.

2 MATERIALS AND METHODS

2.1 Study area

The Qinling Mountains is a huge east–west mountain range in central China, between 32°40′N~34°35′N and 105°30′E~111°3′E, with an elevation of 195–3,767.2°m and a total area of 61,900 km^2 (Qi et al., 2021). There are significant climatic differences between the northern and southern slopes of the Qinling Mountains (NSQM and SSQM) (Qi et al., 2021), the NSQM under a warm temperate semihumid climate, while the SSQM a humid northern subtropical climate. The Qinling Mountains is also the geographical boundary between the north and south of China and a sensitive area for climate change, which is generally consistent with the 0°C isotherm in January, the 800-mm annual equivalent precipitation line, and the 2,000-h sunshine hour line (Bai et al., 2012). The Qinling Mountains is the dividing line between five key elements: geography, climate, biology, water system, and soil (Deng et al., 2018a; Deng et al., 2019; Hu et al., 2020; Wang et al., 2020).

2.2 Data Sources

The meteorological data are the monthly average temperature and monthly precipitation of 32 meteorological stations in the Qinling Mountains during 2000–2019, provided by the National Earth System Science Data Sharing Infrastructure (www.geodata.cn) and the Shaanxi Meteorological Bureau. The spatial distribution of meteorological stations is shown in **Figure 1**. This paper uses the ANUSPLIN method to interpolate the temperature and precipitation (Hutchinson and Xu, 2013). Compared with other spatial interpolation methods, the

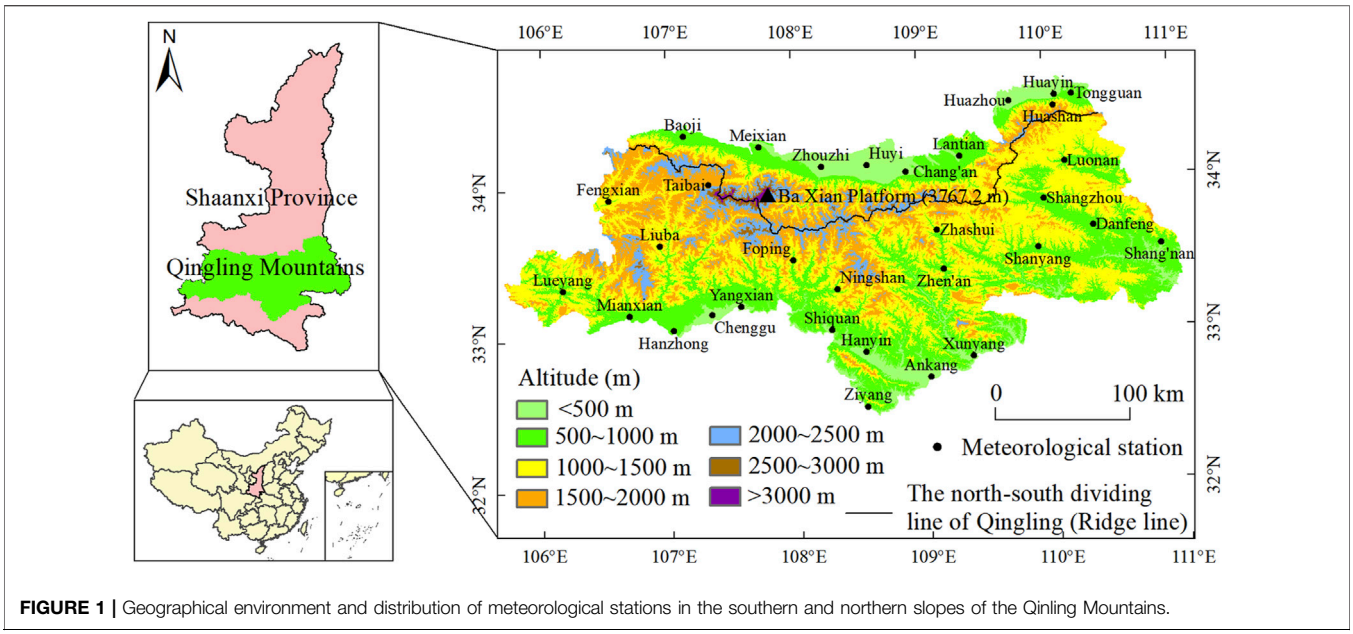

FIGURE 1 | Geographical environment and distribution of meteorological stations in the southern and northern slopes of the Qinling Mountains.

ANUSPLIN method induces less error in interpolation accuracy in a complex mountain environment (Xu et al., 2017; Qi et al., 2019; Qi et al., 2021). The DEM (spatial resolution: 250 m) is obtained via the National Geomatics Centre of China.

This paper uses the NDVI index of the growing season to measure the vegetation status. According to the climate and vegetation growth in the Qinling Mountains, the vegetation-growing season is from March to October (Deng et al., 2019). NDVI data were obtained from the MOD13Q1 dataset of NASA (https://ladsweb.modaps.eosdis.nasa.gov/search/order/1/MOD13Q1–6), with a spatial resolution of 250 m × 250 m, and a time resolution of 16 days.

The MODIS Reprojection Tool (MRT) is used for image splicing, projection, and format conversion, and maximum value composite (MVC) is used to eliminate the influence of cloud, atmosphere, and Sun altitude to synthesize monthly NDVI data, which can effectively reflect the vegetation coverage of the area.

Method

2.3.1 Change Trend Analysis

The trends in this study were calculated using linear least-squares regression. The calculation formula is as follows:

$$slope = \frac{n\sum_{i=1}^{n} ix_i - \sum_{i=1}^{n} i\sum_{i=1}^{n} x_i}{n\sum_{i=1}^{n} i^2 - \left(\sum_{i=1}^{n} i\right)^2} \quad (1)$$

where n is the time series, x_i denotes the value of the x at time i; slope>0 or slope<0 indicates an upward or downward trend for x; $slope > 0$ indicates the increase in x, and $slope < 0$ indicates otherwise.

Partial correlation analysis is a geostatistical method based on correlation analysis (Sun et al., 2020). When two variables are related to the third variable, the influence of one of the variables will be excluded, with only the degree of correlation between the other two variables considered, which has proven effective in eliminating other influencing factors:

$$R_{xy\cdot z} = \frac{R_{xy} - R_{xz}R_{yz}}{\sqrt{\left(1 - R_{xz}^2\right)\left(1 - R_{yz}^2\right)}} \quad (2)$$

where $R_{xy\cdot z}$ represents the partial correlation coefficient between variable x and variable y after excluding variable z, R_{xy} represents the partial correlation coefficient between variable x and variable y, and R_{xz} and R_{yz} represent the same meaning as R_{xy}.

The change trend and the partial correlation significance test are all determined by the t-test, and the results are divided into four levels: extremely significant ($p \le 0.01$), significant ($0.01 < p \le 0.05$), weakly significant ($0.05 < p \le 0.1$), and insignificant ($p > 0.1$).

2.3.2 Multiple Regression Residual Analysis

Multiple regression residual analysis is employed to study the impact of climate change and human activities on vegetation NDVI changes and their relative contributions. The details of the method are as follows (Evans and Geerken 2004; Wessels et al., 2007):

① The binary regression model was constructed based on the growing season NDVI and the spatial temperature and precipitation time series datasets, in which temperature and precipitation were independent variables, and NDVI in the growing season was the dependent variable.
② According to the constructed model of step ①, the predicted NDVI is obtained ($NDVI_{CC}$, which represents the impact of climate change on vegetation change).
③ According to the difference between the remotely sensed NDVI observation value ($NDVI_{obs}$) and the predicted value of NDVI ($NDVI_{CC}$) in the growing season of the Qinling Mountains, the NDVI residual ($NDVI_{HA}$) is

TABLE 1 | Classification of the impacts of climate change and human activities on vegetation restoration (10^{-3} a^{-1}).

slope (NDVI)[a]	Influence level
<−2.0	Severe inhibition
−2.0~−1.0	Moderate inhibition
−1.0~−0.2	Mild inhibition
−0.2–0.2	No effect
0.2~−1.0	Mild promotion
1.0–2.0	Moderate promotion
>2.0	Severe promotion

calculated, which represents the influence of human activities on vegetation change.

The calculation formula is as follows:

$$NDVI_{CC} = a \times Tem + b \times \mathrm{Pre} + c \quad (3)$$

$$NDVI_{HA} = NDVI_{obs} - NDVI_{CC} \quad (4)$$

where $NDVI_{CC}$ and $NDVI_{obs}$ refer to the predicted value of NDVI based on the regression model, and the observed value of NDVI based on remote sensing image (dimensionless), respectively; a, b and c are model parameters; and Tem (°C) and Pre (mm) refer to the growing season average temperature and cumulative precipitation, respectively.

2.3.3 Determination of Driving Factors for Vegetation normalized difference vegetation index change

The slopes of $NDVI_{obs}$, $NDVI_{CC}$, and $NDVI_{HA}$ during the growing season were calculated. The positive slopes represent, respectively, the increase in NDVI, the promotion of NDVI by climate change, and by human activities, while the negative slopes represent, respectively, the decline of NDVI, the inhibition of NDVI increase by climate change, and by human activities.

According to the impact of climate change and human activities on vegetation, $slope(NDVI_{obs})$, $slope(NDVI_{CC})$, and $slope(NDVI_{HA})$ are classified into seven levels to better determine the impact of the driving factors (**Table 1**) (Kai et al., 2020). Meanwhile, the relative contribution rates of the driving factors to vegetation changes are calculated according to the contribution of different driving factors and the trend of vegetation change (**Table 2**) (Sun et al., 2020).

3 RESULTS

3.1 Temporal and Spatial Change Trends of Vegetation normalized difference vegetation index

The NDVI of the Qinling Mountains in the growing season during 2000–2019 showed a significant increase, with the rate of increase being 0.23/10a ($p < 0.01$) (**Figure 2**). Specifically, the rate of increase was 0.013/10a ($p < 0.05$) on the NSQM, and 0.026/10a ($p < 0.01$) on the SSQM. The NDVI during the growing season fluctuated between 0.64 and 0.70 on the NSQM, and between 0.69 and 0.76 on the SSQM. The NDVI on the SSQM is significantly higher than that on the NSQM. In the past 20 years, the vegetation coverage on the SSQM is not only higher than the NSQM but also displayed better signs of continuous improvement. This may be related to the expansion of the urban agglomeration on the NSQM.

The change trend of NDVI during the growing season showed spatial heterogeneity in the Qinling Mountains during 2000–2019 (**Figure 3**). The area with increasing and decreasing trends of NDVI accounted for 87.96% and 12.04%. Among them, the areas with increasing and decreasing trends of NDVI accounted for 75.18% and 24.82% of the NSQM, and 91.30% and 8.70% of the NSQM, respectively.

The area with a significant increase in NDVI accounts for 59.21% of the Qinling Mountains (**Figure 3B**), which was mainly distributed in the eastern region (i.e., Zhen'an, Zhashui, Shanyang, etc.); the area with a significant decrease in NDVI only accounted for 4.00% of the study area, which is mainly located in Huyi, Chang'an, and Huazhou in the NSQM, and Hanzhong, Ankang, and Chenggu in the SSQM. Meanwhile, the areas with insignificant NDVI change are mainly distributed in the central region of the Qinling Mountains.

3.2 Analysis of the Driving Forces of Vegetation Change

With the continuous intensification of human activities, to reveal the internal mechanism of vegetation change, we must not only consider the impact of climate change but also account for the contribution of human activities. The area where climate change contributed to the increase in NDVI accounted for 84.04% of the

TABLE 2 | Identification criterion and contribution calculation of the drivers of NDVI change.

slope ($NDVI_{obs}$)[a]	Driving factors	slope ($NDVI_{CC}$)[b]	slope ($NDVI_{HA}$)[c]	Contribution proportion of CC (%)	Contribution proportion of CC (%)
>0	CC and HA	>0	>0	$\frac{slope(NDVI_{CC})}{slope(NDVI_{obs})}$	$\frac{slope(NDVI_{HA})}{slope(NDVI_{obs})}$
	CC	>0	<0	100	0
	HA	<0	>0	0	100
<0	CC and HA	<0	<0	$\frac{slope(NDVI_{CC})}{slope(NDVI_{obs})}$	$\frac{slope(NDVI_{HA})}{slope(NDVI_{obs})}$
	CC	<0	>0	100	0
	HA	>0	<0	0	100

$slope(NDVI_{obs})$ refers to the slope of NDVI observations based on remote sensing data; $slope(NDVI_{CC})$ refers to the slope of NDVI predicted values based on binary regression, indicating that climate change affects NDVI; $slope(NDVI_{HA})$ refers to the NDVI residual tendency rate, which represents the slope of NDVI under the influence of human activities. CC, climate change; HA, human activities.

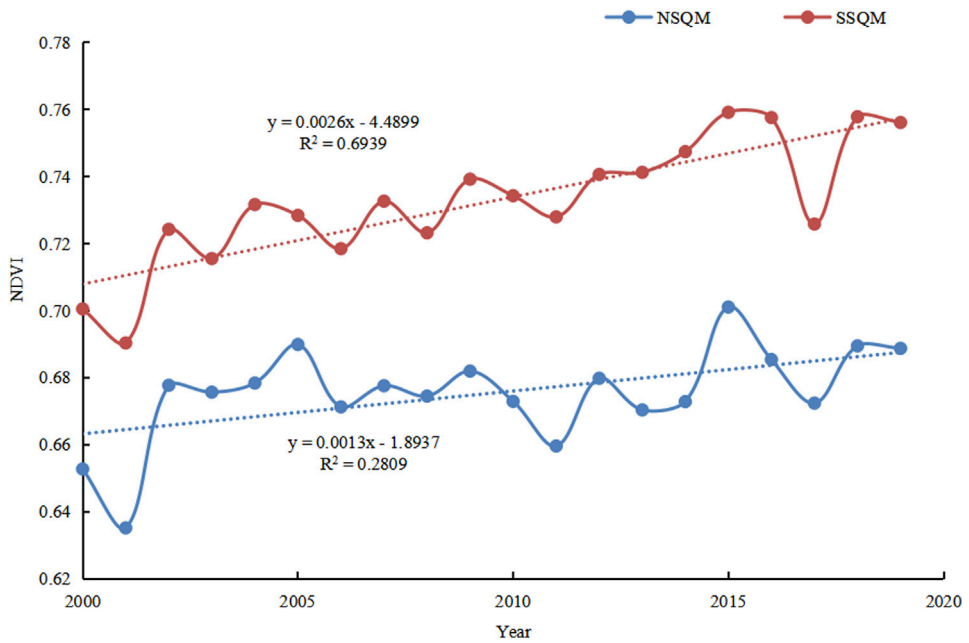

FIGURE 2 | Interannual variation of growing season normalized difference vegetation index (NDVI) in the northern and southern slopes of the Qinling Mountains (NSQM and SSQM) during 2000–2019.

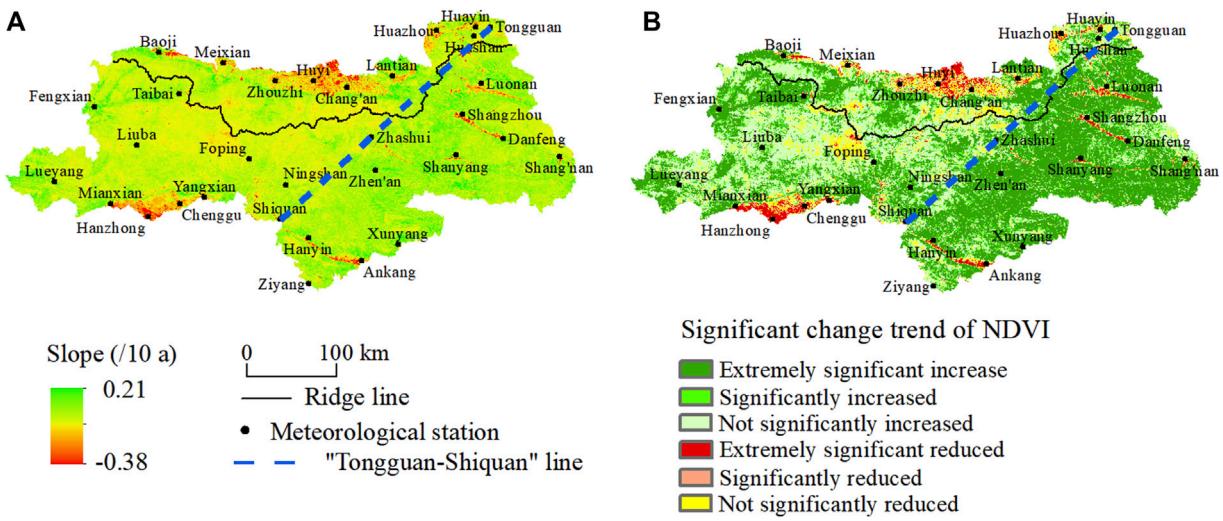

FIGURE 3 | Spatial distribution of trend and the significance for NDVI in the NSQM and SSQM during 2000–2019.

Qinling Mountains, of which the severe and moderately promoted areas accounted for 56.97% of the Qinling Mountains, distributed in the eastern region and the area around the Qinling Mountains. The impact of climate change on the increase of NDVI showed that the lightly promoted area accounted for 27.07% of the Qinling Mountains, which is mainly distributed in the central areas of the Qinling Mountains. The inhibited impact of climate change on the increase in NDVI accounted for 7.54% of the Qinling Mountains, of which the area of moderate and severe inhibition is only 2.17% of the Qinling Mountains. It shows that climate change in the past 20 years is beneficial to vegetation growth in most areas of the Qinling Mountains.

The impact of human activities on the increase in NDVI is that the promoted area accounts for 73.63% of the Qinling Mountains, of which the severely and moderately promoted areas accounted for 52.77% of the Qinling Mountains, mainly distributed in the eastern part of the Qinling Mountains (**Figure 4B**). It may be

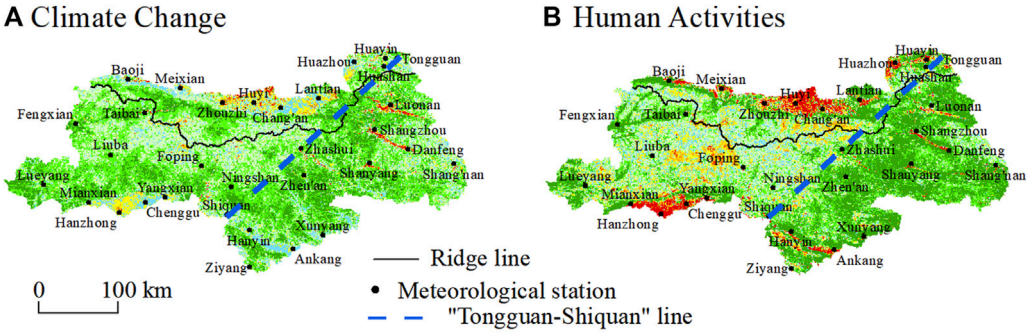

The impacts of climate change or human activities	Proportion						
	Severely inhibition	Moderately inhibition	Mildly inhibition	Not effect	Mildly promotion	Moderately promotion	Severely promotion
Climate change	0.80%	1.37%	5.37%	8.42%	27.07%	38.44%	18.53%
Human activities	4.46%	3.81%	9.38%	8.73%	20.85%	21.67%	31.10%

FIGURE 4 | Spatial distribution of the impacts of climate change and human activities on vegetation restoration in the Qinling Mountains during 2000–2019.

related to the Natural Forest Protection Project and the Grain for Green Project. The area where the influence of human activities on the increase in NDVI is inhibited accounts for 17.65% of the Qinling Mountains, mainly located at low elevations (i.e., Huyi, Chang'an, Huazhou, and Hanzhong, Chenggu, Ankang), which are urban areas that have seen expansion. The moderately promoted area of the impact on NDVI increase of climate change accounts for a relatively high proportion, while the severely promoted area of human activity impact on NDVI increase is relatively high; the proportion of areas where human activities have inhibited the rise of NDVI is far greater than climate change. It indicates that human activities have a more direct and rapid impact on vegetation than climate change. A dividing line along Tongguan–Shiquan exists for the spatial distribution of climate change and human activity impact on NDVI in the Qinling Mountains. The impact of human activities on vegetation is more obvious east of the "Tongguan–Shiquan" divide.

The NDVI change is caused by climate change and human activities, accounting for 80.17% of the Qinling Mountains, among which 73.45% were found to increase and 6.72% decreased (**Figure 5**). The region of NDVI change caused by climate change alone accounted for 11.26% of the Qinling Mountains, mainly distributed in the central region (i.e., Liuba, Foping, Taibai, etc.); the region of NDVI change caused by human activities alone accounted for 8.57% of the Qinling Mountains. Regarding the NSQM and SSQM, the proportion of the NSQM where the NDVI decreases due to the combined influence of climate and human factors is much higher than that of the SSQM, but the area with increased NDVI is smaller than the SSQM.

3.3 Spatial Distribution of Driving Factors of Vegetation Change in Qinling Mountains

The NDVI change is caused by climate change and human activities, accounting for 80.17% of the Qinling Mountains, among which 73.45% were found to increase, and 6.72% decreased (**Figure 5**). The region of NDVI change caused by climate change alone accounted for 11.26% of the Qinling Mountains, mainly distributed in the central region (i.e., Liuba, Foping, Taibai, etc.); the region of NDVI change caused by human activities alone accounted for 8.57% of the Qinling Mountains. Regarding the NSQM and SSQM, the proportion of the NSQM where the NDVI decreases due to the combined influence of climate and human factors is much higher than that of the SSQM, but the area with increased NDVI is smaller than the SSQM.

3.4 Contribution of Climate Change and Human Activities to Vegetation Improvement or Degradation

Regarding vegetation improvement area (**Figure 6A** and **Figure 6B**), the contribution of climate change to vegetation improvement was higher than that of human activities in the Qinling Mountains (51.75% vs. 48.25%), including the NSQM (53.42% vs. 46.58%) and the SSQM (51.41% vs. 48.59%).

Regarding climate change, the largest area was characterized with 40%–60% contribution to vegetation improvement (**Figure 6A**). The regions where the climate change contribution rates are more than 80% were distributed in the central region of the Qinling Mountains. Regarding human activities, the largest area was found with 40%–60% contribution to vegetation improvement (**Figure 6B**). The highest rates of human activity contribution (over 80%) were distributed in the eastern part of the Qinling Mountains.

Regarding vegetation degradation area (**Figures 6C**, **D**), the contribution proportion of human activities to vegetation degradation was larger than that of climate change in the Qinling Mountains (77.89% vs. 22.11%), including the NSQM (81.78% vs. 18.22%) and the SSQM (75.02% vs. 24.98%).

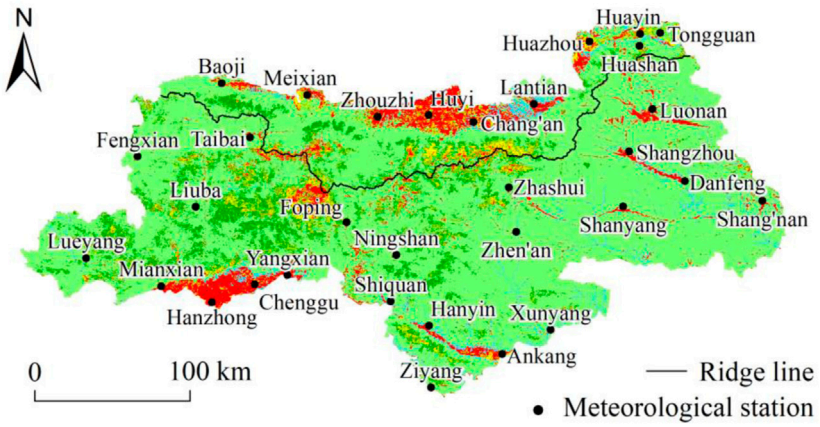

The driving forces	NDVI slope > 0			NDVI slope < 0		
	CC and HA	CC	HA	CC and HA	CC	HA
Proportions of QM	73.45%	10.44%	4.07%	6.72%	0.82%	4.50%
Proportions of NSQM	58.90%	10.93%	5.35%	14.76%	1.08%	8.98%
Proportions of SSQM	77.25%	10.32%	3.73%	4.62%	0.74%	3.34%

FIGURE 5 | Drivers of vegetation cover change in the Qinling Mountains during 2000–2019.

As for climate change, the region with a contribution rate of 0%–20% was the largest, while for human activities, the regions with a contribution rate of more than 80% are the largest. The vegetation degradation is mainly caused by human activities, while the contribution of climate change is small.

3.5 Spatial Distribution of Dominant Factors in Vegetation normalized difference vegetation index Changes

In this study, the classification criteria for the leading factors of vegetation change are as follows: When the contribution rate of climate change is more than human activities, it is defined as "climate dominated." On the contrary, it is defined as "human dominated."

The percentage of climate-dominated vegetation improvement is smaller than that of human dominated (48.42% vs. 51.58%) (**Figure7**), while the percentage of climate-dominated vegetation degradation is smaller than that of human dominated (17.56% vs. 82.44%). The above shows that the impact of climate change on vegetation change is smaller than that of human activities in the Qinling Mountains.

4 DISCUSSION

The vegetation changes in the Qinling Mountains are caused by the combined effects of climate change and human activities. On the one hand, it may be due to the continuous increase in temperature and precipitation, which promotes the growth of vegetation (Deng et al., 2018a; Qi et al., 2021), and the deposition of atmospheric carbon dioxide and nitrogen also enhances the growth of vegetation (Leakey et al., 2009). On the other hand, the implementation of vegetation restoration projects is conducive to vegetation restoration (i.e., the Grain for Green project), increasing vegetation coverage, and improving the management level of vegetation ecosystems.

The vegetation in the central region of Qinling Mountains was affected by climate change to a lesser extent, while in the surrounding region, it was affected by climate change to a greater extent (**Figure 4A**). This may be due to the high vegetation coverage in the central Qinling Mountains with little room for vegetation improvement. The vegetation of these regions is mildly promoted. Vegetation changes are not only affected by climate change but also human activities (Liu et al., 2018) (Qin et al., 2021). Population density, policy orientation, and topographical conditions will all affect the impact of human activities on vegetation changes (Li et al., 2017; Zheng et al., 2019). In areas with large slopes and complex terrain, the impact of human activities on vegetation changes is weakened. In this study, the eastern region with low altitude and low slope was found to have a high contribution rate of human activities to vegetation improvement, which is particularly obvious in the east of the "Tongguan–Shiquan line" (**Figure 4B**, **Figure 6B**).

In the degraded vegetation areas of the Qinling Mountains, human activities contributed 77.89% to the vegetation change (**Figure 6D**). It has been pointed out that land cover changes in Chang'an, Huyi, Lantian, and Huazhou in the Qinling Mountains are mainly the conversion of forest land and grassland to construction land (Guo et al., 2018), which may be the reason for the high contribution rate of human activities to the decrease of NDVI.

The central part of Foping also exhibits high human activity contribution with the NDVI declining significantly, which was related to the conversion of forested grassland to construction land during the construction of scenic areas (Guo et al., 2018).

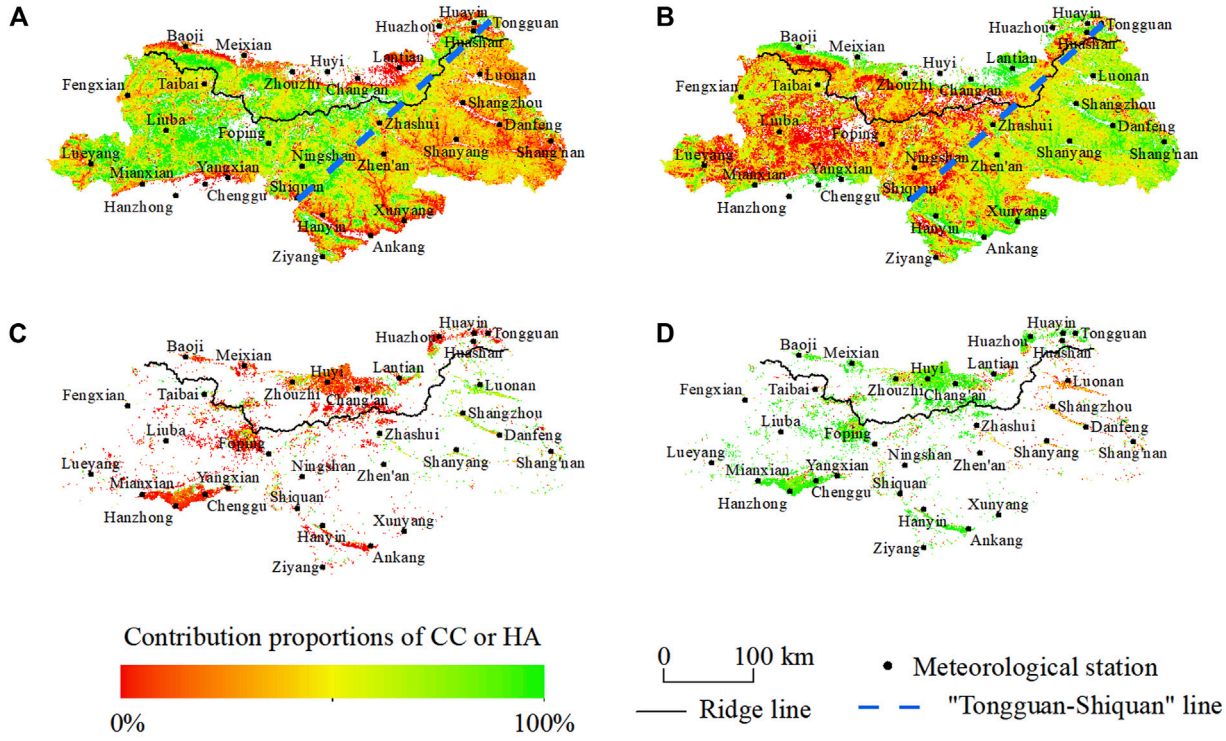

The contribution of driving forces		Pixel proportion (%) Vegetation improvement 0~20%	20~40%	40~60%	60~80%	>80%	Pixel proportion (%) Vegetation degradation 0~20%	20~40%	40~60%	60~80%	>80%
CC	QM	8.91	21.81	33.65	16.04	19.58	45.05	19.75	13.20	7.54	14.46
	NSQM	12.64	15.08	26.97	19.88	25.43	51.67	25.34	9.68	4.32	8.99
	SSQM	8.14	23.21	35.05	15.24	18.37	39.94	15.44	15.92	10.03	18.68
HA	QM	7.72	17.36	36.42	23.61	14.89	2.45	5.06	8.86	13.25	70.39
	NSQM	10.62	21.61	29.31	16.39	22.07	1.44	2.88	6.46	16.91	72.30
	SSQM	7.12	16.48	37.90	25.10	13.41	3.24	6.75	10.72	10.40	68.89

FIGURE 6 | Spatial distributions of the contribution proportions of **(A)** climate change and **(B)** human activities to vegetation improvement, **(C)** climate change, and **(D)** human activities to vegetation degradation in the Qinling Mountains (CC, climate change; HA, human activities in the figure).

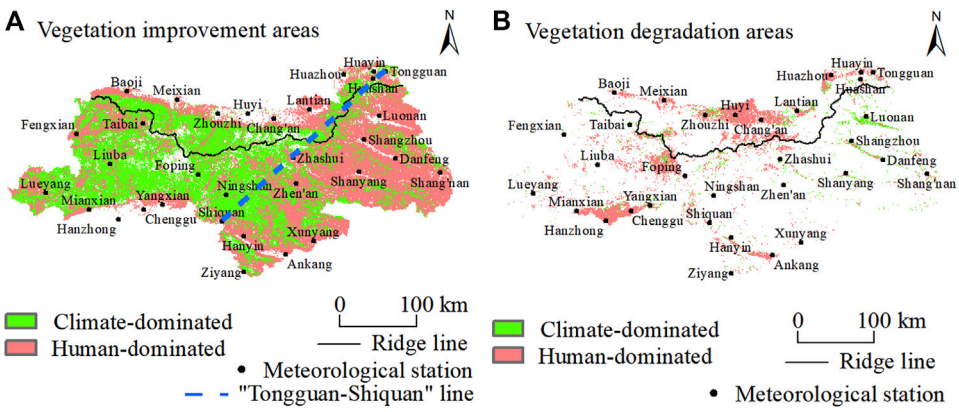

FIGURE 7 | Spatial distributions of the climate and human dominated in the Qinling Mountains. **(A)** Vegetation improvement areas and **(B)** vegetation degradation areas.

Human activities in the eastern part of the Qinling Mountains leads to an increase in vegetation NDVI (**Figure 6**), which was due to the implementation of artificial ecological projects, which has significantly improved the vegetation. Previous studies have pointed out that the vegetation coverage in the eastern part of the Qinling Mountains has increased significantly (Wang et al., 2016; Li et al., 2019), which was similar to the results of this study. The improvement of vegetation in this area is the main contribution of human activities. Therefore, the implementation of ecological engineering projects plays a significant role in the improvement of vegetation coverage.

Regarding the vegetation ecosystem change, there may be some normal ecological succession during the evolution of vegetation ecosystem leading to vegetation change, which needs to be improved by adding more detailed vegetation distribution data later. In the study, severe vegetation degradation was identified in the low-elevation areas in the Qinling Mountains, with the main factor of degradation being human activities. However, whether this area was converted to construction land or cultivated land after degradation deserves further exploration. Moreover, the deviation of NDVI data quality may lead to some errors in the results, which may cause certain errors in the research. Although this study has certain shortcomings, the research and analysis in this article are still a good attempt to quantitatively assess the influence factors of vegetation change.

5 CONCLUSION

This paper investigated the spatial and temporal variability characteristics of NDVI and quantitatively assessed the relative contribution of the drivers of NDVI change in the Qinling Mountains. The results show that the NDVI value in the Qinling Mountains exhibited a significant increasing trend at a rate of 0.23/10a during 2000–2019. The combined impact of climate change and human activities were the main driving force for the change and spatial difference of vegetation NDVI in the Qinling Mountains. The "Tongguan–Shiquan line" is not only the dividing line for the intensity of vegetation change but also separates the climatic- and human-dominated type. In terms of the vegetation improvement area, the contribution of climate change to the NDVI increase is greater than that of human activities (51.75% vs. 48.25%). In terms of vegetation degradation area, the area of climate change as the leading factor accounted for 17.56%, and the area with human activities as the dominant factor accounted for 82.44%. It is more important to establish stricter measures for human activities.

DATA AVAILABILITY STATEMENT

The original contributions presented in the study are included in the article/supplementary material, further inquiries can be directed to the corresponding author.

AUTHOR CONTRIBUTIONS

DC: Data Analysis, writing-original draft. GQ: Writing-review and editing. JS: Project administration. YZ: Formal analysis. HB: Conceptialization. XG: Investigation, Validation.

FUNDING

This study was jointly supported by the Special Funds of the National Natural Science Foundation of China (Grant No. 42041004), Key Research and Development Program of Shaanxi Province, China(Grant No. 2019ZDLSF05-02), Shaanxi Province Water Conservancy Science and Technology Project(Grant No.2021slkj-13).

REFERENCES

Bai, H., Ma, X., Gao, X., and Hou, X. (2012). Variations in January Temperature and 0°C Isothermal Curve in Qinling Mountains Based on DEM. *Acta Geographica Sinica* 67 (11), 1443–1450. (in Chinese). doi:10.11821/xb201211001

Braswell, B. H., Schimel, D. S., Linder, E., and Moore, B. (1997). The Response of Global Terrestrial Ecosystems to Interannual Temperature Variability. *Science* 278 (5339), 870–873. doi:10.1126/science.278.5339.870

Cai, Y., Yue, W., Xu, L., Yang, Z., and Rong, Q. (2016). Sustainable Urban Water Resources Management Considering Life-Cycle Environmental Impacts of Water Utilization under Uncertainty. *Resour. Conservation Recycling* 108, 21–40. doi:10.1016/j.resconrec.2016.01.008

Cheng, L., Zhang, L., Wang, Y.-P., Canadell, J. G., Chiew, F. H. S., Beringer, J., et al. (2017). Recent Increases in Terrestrial Carbon Uptake at Little Cost to the Water Cycle. *Nat. Commun.* 8 (1), 110. doi:10.1038/s41467-017-00114-5

Deng, C., Bai, H., Gao, S., Huang, X., Meng, Q., Zhao, T., et al. (2018a). Comprehensive Effect of Climatic Factors on Plant Phenology in Qinling Mountains Region during 1964-2015. *Acta Geographica Sinica* 73 (05), 917–931. (in Chinese). doi:10.1016/j.ecolind.2021.108211

Deng, C., Bai, H., Gao, S., Liu, R., Ma, X., Huang, X., et al. (2018b). Spatial-temporal Variation of the Vegetation Coverage in Qinling Mountains and its Dual Response to Climate Change and Human Activities. *J. Nat. Sci.* 33 (03), 425–438. (in Chinese). doi:10.11849/zrzyxb.20170139

Deng, C., Bai, H., Gao, S., Zhao, T., and Ma, X. (2019). Differences and Variations in the Elevation-dependent Climatic Growing Season of the Northern and Southern Slopes of the Qinling Mountains of China from 1985 to 2015. *Theor. Appl. Climatol* 137 (1), 1159–1169. doi:10.1007/s00704-018-2654-7

Duan, W., Maskey, S., Chaffe, P. L. B., Luo, P., He, B., Wu, Y., et al. (20212021). Recent Advancement in Remote Sensing Technology for Hydrology Analysis and Water Resources Management. *Remote Sensing* 13 (6), 1097. doi:10.3390/rs13061097

Duan, W., Zou, S., Chen, Y., Nover, D., Fang, G., and Wang, Y. (2020). Sustainable Water Management for Cross-Border Resources: The Balkhash Lake Basin of Central Asia, 1931-2015. *J. Clean. Prod.* 263, 121614. doi:10.1016/j.jclepro.2020.121614

Evans, J., and Geerken, R. (2004). Discrimination between Climate and Human-Induced Dryland Degradation. *J. Arid Environments* 57 (4), 535–554. doi:10.1016/S0140-1963(03)00121-6

Ge, W., Deng, L., Wang, F., and Han, J. (2021). Quantifying the Contributions of Human Activities and Climate Change to Vegetation Net Primary Productivity Dynamics in China from 2001 to 2016. *Sci. Total Environ.* 773, 145648. doi:10.1016/j.scitotenv.2021.145648

Hu, Y., Yao, Y., and Kou, Z. (2020). Exploring on the Climate Regionalization of Qinling-Daba Mountains Based on Geodetector-SVM Model. *Plos one* 15 (11), e0241047. doi:10.1371/journal.pone.0241047

Huang, S., Zheng, X., Ma, L., Wang, H., Huang, Q., Leng, G., et al. (2020). Quantitative Contribution of Climate Change and Human Activities to

Vegetation Cover Variations Based on GA-SVM Model. *J. Hydrol.* 584, 124687. doi:10.1016/j.jhydrol.2020.124687

Huang, W., Duan, W., and Chen, Y. (2021). Rapidly Declining Surface and Terrestrial Water Resources in Central Asia Driven by Socio-Economic and Climatic Changes. *Sci. Total Environ.* 784, 147193. doi:10.1016/j.scitotenv.2021.147193

Hutchinson, M. F., and Xu, T. (2013). *Anusplin Version 4.4 User Guide*. Available at: http://fennerschool.anu.edu.au/files/anusplin44.pdf.

Ichii, K., Kawabata, A., and Yamaguchi, Y. (2002). Global Correlation Analysis for NDVI and Climatic Variables and NDVI Trends: 1982-1990. *Int. J. Remote Sensing* 23 (18), 3873–3878. doi:10.1080/01431160110119416

Ji, S., Ren, S., Li, Y., Dong, J., Wang, L., Quan, Q., et al. (2021). Diverse Responses of spring Phenology to Preseason Drought and Warming under Different Biomes in the North China Plain. *Sci. Total Environ.* 766, 144437. doi:10.1016/j.scitotenv.2020.144437

Kai, J., Fei, W., Han, J. Q., Shi, S. Y., and Ding, W. B. (2020). Contribution of Climatic Change and Human Activities to Vegetation NDVI Change over China during. 1982-2015. *Acta Geographica Sinica* 75 (5), 961–974. (in Chinese). doi:10.11821/dlxb202005006

Landuyt, D., De Lombaerde, E., Perring, M. P., Hertzog, L. R., Ampoorter, E., Maes, S. L., et al. (2019). The Functional Role of Temperate forest Understorey Vegetation in a Changing World. *Glob. Change Biol.* 25 (11), 3625–3641. doi:10.1111/gcb.14756

Leakey, A. D. B., Ainsworth, E. A., Bernacchi, C. J., Rogers, A., Long, S. P., and Ort, D. R. (2009). Elevated CO2 Effects on Plant Carbon, Nitrogen, and Water Relations: Six Important Lessons from FACE. *J. Exp. Bot.* 60 (10), 2859–2876. doi:10.1093/jxb/erp096

Li, G., Sun, S., Han, J., Yan, J., Liu, W., Wei, Y., et al. (2019). Impacts of Chinese Grain for Green Program and Climate Change on Vegetation in the Loess Plateau during 1982-2015. *Sci. Total Environ.* 660, 177–187. doi:10.1016/j.scitotenv.2019.01.028

Li, J., Peng, S., and Li, Z. (2017). Detecting and Attributing Vegetation Changes on China's Loess Plateau. *Agric. For. Meteorology* 247, 260–270. doi:10.1016/j.agrformet.2017.08.005

Liu, Z., Liu, Y., and Li, Y. (2018). Anthropogenic Contributions Dominate Trends of Vegetation Cover Change over the Farming-Pastoral Ecotone of Northern China. *Ecol. Indicators* 95, 370–378. doi:10.1016/j.ecolind.2018.07.063

Mao, D., Wang, Z., Luo, L., and Ren, C. (2012). Integrating AVHRR and MODIS Data to Monitor NDVI Changes and Their Relationships with Climatic Parameters in Northeast China. *Int. J. Appl. Earth Observation Geoinformation* 18, 528–536. doi:10.1016/j.jag.2011.10.007

Myers-Smith, I. H., Kerby, J. T., Phoenix, G. K., Bjerke, J. W., Epstein, H. E., Assmann, J. J., et al. (2020). Complexity Revealed in the Greening of the Arctic. *Nat. Clim. Chang.* 10 (2), 106–117. doi:10.1038/s41558-019-0688-1

Nemani, R. R., Keeling, C. D., Hashimoto, H., Jolly, W. M., Piper, S. C., Tucker, C. J., et al. (2003). Climate-Driven Increases in Global Terrestrial Net Primary Production from 1982 to 1999. *Science* 300 (5625), 1560–1563. doi:10.1126/science.1082750

Ovakoglou, G., Alexandridis, T. K., Clevers, J. G. P. W., Cherif, I., Kasampalis, D. A., Navrozidis, I., et al. "Spatial Enhancement of Modis Leaf Area Index Using Regression Analysis with Landsat Vegetation Index," in IGARSS 2018 - 2018 IEEE International Geoscience and Remote Sensing Symposium, July 2018Valencia, Spain, 8232–8235. doi:10.1109/IGARSS.2018.8519387

Piao, S., Yin, G., Tan, J., Cheng, L., Huang, M., Li, Y., et al. (2015). Detection and Attribution of Vegetation Greening Trend in China over the Last 30 Years. *Glob. Change Biol.* 21 (4), 1601–1609. doi:10.1111/gcb.12795

Qi, G., Bai, H., Meng, Q., Zhao, T., and Guo, S. (2019). Climate Change in the Qinling Mountains in Spring during 1959-2018. *Arid Zone Res.* 36 (5), 1079–1091. (in Chinese). doi:10.13866/j.azr.2019.05.04

Qi, G., Bai, H., Zhao, T., Meng, Q., and Zhang, S. (2021). Sensitivity and Areal Differentiation of Vegetation Responses to Hydrothermal Dynamics on the Southern and Northern Slopes of the Qinling Mountains in Shaanxi Province. *Acta Geographica Sinica* 76 (1), 44–56. (in Chinese). doi:10.11821/dlxb202101004

Qin, X., Liu, W., Mao, R., Song, J., Chen, Y., Ma, C., et al. (2021). Quantitative Assessment of Driving Factors Affecting Human Appropriation of Net Primary Production (HANPP) in the Qilian Mountains, China. *Ecol. Indicators* 121, 106997. doi:10.1016/j.ecolind.2020.106997

Shaozhuang, G., Hongying, B., Qing, M., Ting, Z., Xiaoyue, Y., and Guizeng, Q. (2020). Landscape Pattern Changes of woodland and Grassland and its Driving Forces in Qinling Mountains. *Acta Eco Sin* 40 (1), 130–140. (in Chinese). doi:10.5846/stxb201811072418

Shi, S., Yu, J., Wang, F., Wang, P., Zhang, Y., and Jin, K. (2021). Quantitative Contributions of Climate Change and Human Activities to Vegetation Changes over Multiple Time Scales on the Loess Plateau. *Sci. Total Environ.* 755, 142419. doi:10.1016/j.scitotenv.2020.142419

Song, J., Tang, B., Zhang, J., Dou, X., Liu, Q., and Shen, W. (2018). System Dynamics Simulation for Optimal Stream Flow Regulations under Consideration of Coordinated Development of Ecology and Socio-Economy in the Weihe River Basin, China. *Ecol. Eng.* 124, 51–68. doi:10.1016/j.ecoleng.2018.09.024

Sun, W., Song, X., Mu, X., Gao, P., Wang, F., and Zhao, G. (2015). Spatiotemporal Vegetation Cover Variations Associated with Climate Change and Ecological Restoration in the Loess Plateau. *Agric. For. Meteorology* 209-210 (1), 87–99. doi:10.1016/j.agrformet.2015.05.002

Sun, Y.-L., Shan, M., Pei, X.-R., Zhang, X.-K., and Yang, Y.-L. (2020). Assessment of the Impacts of Climate Change and Human Activities on Vegetation Cover Change in the Haihe River basin, China. *Phys. Chem. Earth, Parts A/B/C* 115, 102834. doi:10.1016/j.pce.2019.102834

Vicente-Serrano, S. M., Gouveia, C., Camarero, J. J., Begueria, S., Trigo, R., Lopez-Moreno, J. I., et al. (2013). Response of Vegetation to Drought Time-Scales across Global Land Biomes. *Proc. Natl. Acad. Sci.* 110 (1), 52–57. doi:10.1073/pnas.1207068110

Wang, B., Xu, G., Li, P., Li, Z., Zhang, Y., Cheng, Y., et al. (2020). Vegetation Dynamics and Their Relationships with Climatic Factors in the Qinling Mountains of China. *Ecol. Indicators* 108, 105719. doi:10.1016/j.ecolind.2019.105719

Wang, S., Fu, B., Piao, S., Lü, Y., Ciais, P., Feng, X., et al. (2016). Reduced Sediment Transport in the Yellow River Due to Anthropogenic Changes. *Nat. Geosci* 9 (1), 38–41. doi:10.1038/ngeo2602

Wessels, K. J., Prince, S. D., Malherbe, J., Small, J., Frost, P. E., and VanZyl, D. (2007). Can Human-Induced Land Degradation Be Distinguished from the Effects of Rainfall Variability? A Case Study in South Africa. *J. Arid Environments* 68 (2), 271–297. doi:10.1016/j.jaridenv.2006.05.015

Wold, S., Esbensen, K., and Geladi, P. (1987). Principal Component Analysis. *Chemometr Intell. Lab.* 2 (1), 37–52. doi:10.1016/0169-7439(87)80084-9

Xu, H.-J., Wang, X.-P., and Yang, T.-B. (2017). Trend Shifts in Satellite-Derived Vegetation Growth in Central Eurasia, 1982-2013. *Sci. Total Environ.* 579, 1658–1674. doi:10.1016/j.scitotenv.2016.11.182

Yan, Y., Liu, X., Wen, Y., and Ou, J. (2019). Quantitative Analysis of the Contributions of Climatic and Human Factors to Grassland Productivity in Northern China. *Ecol. Indicators* 103, 542–553. doi:10.1016/j.ecolind.2019.04.020

Zeng, Z., Li, Y., Wu, W., Zhou, Y., Wang, X., Huang, H., et al. (2020). Spatio-Temporal Variation of Drought within the Vegetation Growing Season in North Hemisphere (1982-2015). *Water* 12 (8), 2146. doi:10.3390/w12082146

Zhang, X., Song, J., Wang, Y., Deng, W., and Liu, Y. (2021). Effects of Land Use on Slope Runoff and Soil Loss in the Loess Plateau of China: A Meta-Analysis. *Sci. Total Environ.* 755, 142418. doi:10.1016/j.scitotenv.2020.142418

Zheng, K., Wei, J.-Z., Pei, J.-Y., Cheng, H., Zhang, X.-L., Huang, F.-Q., et al. (2019). Impacts of Climate Change and Human Activities on Grassland Vegetation Variation in the Chinese Loess Plateau. *Sci. Total Environ.* 660, 236–244. doi:10.1016/j.scitotenv.2019.01.022

Zhu, Z., Piao, S., Myneni, R. B., Huang, M., Zeng, Z., Canadell, J. G., et al. (2016). Greening of the Earth and its Drivers. *Nat. Clim Change* 6 (8), 791–795. doi:10.1038/nclimate3004

Conflict of Interest: The authors declare that the research was conducted in the absence of any commercial or financial relationships that could be construed as a potential conflict of interest.

Publisher's Note: All claims expressed in this article are solely those of the authors and do not necessarily represent those of their affiliated organizations, or those of the publisher, the editors and the reviewers. Any product that may be evaluated in this article, or claim that may be made by its manufacturer, is not guaranteed or endorsed by the publisher.

frontiers in Environmental Science

ORIGINAL RESEARCH
published: 15 December 2021
doi: 10.3389/fenvs.2021.805513

Assessing the Impact of Optimization Measures on Sustainable Water Resource Management in the Guanzhong Area, China

Bin Tang, Ruichen Mao, Jinxi Song, Haotian Sun, Feihe Kong, Dandong Cheng and Xiangyu Gao*

Shaanxi Key Laboratory of Earth Surface System and Environmental Carrying Capacity, College of Urban and Environmental Sciences, Northwest University, Xi'an, China

Limited water resources and rapid socioeconomic development pose new challenges to watershed water resource management. By integrating the perspectives of stakeholders and decision-makers, this study aims to identify cases and approaches to achieve sustainable water resources management. It improves and expands the experience of previous project research. The comparative evaluation provides an analytical basis to verify the importance of stakeholder participation in water policy interactions. The results show that if an effective demand management policy is not implemented, the Guanzhong area will not meet water demand in the future. Through the combination of water-saving policies, water transfer projects and other measures, the available water resources will continue into the future. Optimizing management measures, improving the ecological environment, and encouraging stakeholder participation will help change this situation, although supply-side limitations and future uncertainties likely cause unsustainable water. Therefore, decision-makers should pay attention to the application potential of water-saving and other measures to reduce dependence on external water sources. In addition, the three sustainable development decision-making principles identified in this paper can promote the fairness and stability of water policy.

Keywords: impact assessment, optimization measures, sustainable water resource management, scenarios analysis, the Guanzhong area

OPEN ACCESS

Edited by:
Yuanchun Zou,
Northeast Institute of Geography and Agroecology (CAS), China

Reviewed by:
Jialiang Cai,
Aalto University, Finland
Zunaira Asif,
Concordia University, Canada

****Correspondence:***
Jinxi Song
jinxisong@nwu.edu.cn

Specialty section:
This article was submitted to Water and Wastewater Management, a section of the journal Frontiers in Environmental Science

Received: *30 October 2021*
Accepted: *29 November 2021*
Published: *15 December 2021*

Citation:
Tang B, Mao R, Song J, Sun H, Kong F, Cheng D and Gao X (2021) Assessing the Impact of Optimization Measures on Sustainable Water Resource Management in the Guanzhong Area, China. Front. Environ. Sci. 9:805513. doi: 10.3389/fenvs.2021.805513

INTRODUCTION

Water resources are the core element of sustainable development. In the past few decades, people have increasingly recognized the importance of water resources and their services to socioeconomic development and eco-environmental protection (Bakker, 2012; Gleeson et al., 2012; UNEP, 2012). However, due to the uneven distribution of global water resources, rapid population growth and social water scarcity, watershed-scale water resource management is becoming increasingly challenging, especially in developing countries with water scarcity (Vörösmarty et al., 2000; Mirauda and Ostoich, 2011; Liu et al., 2013; Kotir et al., 2016). It is necessary to formulate adaptive water resource management policies to achieve social, economic and environmental sustainability (UNDP, 2015; Naghdi et al., 2021). Decision-makers are caught between the two options: strengthening the development of external water resources and optimizing the management of internal water resources, although both come with deficiencies. External resources may lead to

water dependence and water conflict (Poff et al., 2003), while internal management is prone to blind policies and measures leading to an unsustainable occurrence. Therefore, researchers emphasize the use of new tools and technologies to improve water resource management, avoiding conflicts caused by water scarcities (Babel et al., 2005; Xu et al., 2013). Any behavior related to water resources may have an impact on related processes in the water system. The complex relationships and feedback among different systems present obstacles to understanding sustainable water resource management and evaluating water policies (Simonovic, 2009; Sterman, 2012; Mohamed et al., 2020). Unless the ecological environment and human uses of water are more clearly considered, the unsustainability of water will continue to worsen.

We conceptualize sustainable water resource management as a dynamic interaction between social economy and ecosystems in response to human driving factors. Deemed a suitable tool to study complex human-environmental systems, the system dynamics explains complex phenomena and processes by simulating system behavior and its changes over time (Sterman, 2000; Simonovic, 2009). Sustainable water resource management involves water resource planning and decision-making by using feedback views and models, integrating all aspects of the water system (Liu et al., 2015; Sahin et al., 2015; Behboudian et al., 2021). System dynamics uses the characteristics of feedback to find the root of the problem from the perspective of system structure, which is conducive to strengthening the understanding of the objective world and testing the effects of various policy measures (Simonovic, 2009; Sivapalan, 2015).

The system dynamics model (SDM) is a mature modeling tool that includes different advanced modeling platforms. This model is based on the developer's concentrated thinking on the system and can be adjusted according to the level and experience of different users, thereby promoting the consensus of stakeholders. Moreover, the SD model can simulate a variety of scenarios to evaluate the impact of decisions and measures and identify effective adaptation strategies. Hence, the SDM provides an understanding of the long-term dynamic behavior of complex systems and the response of intervention measures, combining climate, resources, social, economic and environmental factors and decision-making measures in an integrated manner (Zare et al., 2019). At present, some system simulation models of different watersheds around the world have been developed based on SDM methods (Dawadi and Ahmad, 2013; Gohari et al., 2013; Sun et al., 2017; Bakhshianlamouki et al., 2020; Naderi et al., 2021). The diversity of their applications is helpful to research in the field of sustainable development.

The Chinese government proposed a major national strategy in 2019, the ecological protection and high-quality development of the Yellow River Basin. The Yellow River Basin is an important ecological barrier and economic zone in China and is of great significance to China's social economic development and ecological security. As the largest tributary of the Yellow River, Weihe River Basin water resource management will directly affect the implementation of the national strategy. However, the limited water resources hinder the development of the socio economic and ecological environment in the basin. To tackle this issue, the Weihe River Basin management department is expanding the available water resources in the region through reservoir construction and water transfer projects. This management program of seeking external water sources is considered an effective solution to water scarcities. However, if the impact of related factors is not considered, providing more water will be counterproductive (Song et al., 2018). The comprehensive solution to the water scarcity problem is the goal of policy optimization, which is to control the behavior of the system through multiple strategic options and improve the reliability of water resources in the basin. Thus, a new evaluation framework is established based on the previous research of our project team (Song et al., 2018). The model was originally developed for water scarcity. This study will review and expand developed models and understanding to solve the challenges of sustainable water resource management related to the socio-economic and ecological environment.

Assessment of Water Management: A New Case Example

This paper improves the system dynamics model recently developed by the project team, and re-evaluates the socio-economic and ecological environmental dimensions of sustainable water resource management from a new perspective. Compared to the previous study, the structure of some subsystems has been optimized, the impact of ecosystem services on rebalancing between systems has been identified, and the importance and participation of stakeholders have been considered in the system.

The project team, decision-makers, and stakeholders emphasized that the decision-making on the sustainability of water resources must be strengthened under effective overall guidance. To optimize the result, the opinions of stakeholders affected by the watershed should be taken into account and applied to decision support at the system level (Zilio et al., 2019). In this sense, our research expects to help local communities develop their solutions and provide them to decision-makers.

Site Description

The Weihe River originates from Niaoshu Mountain in southwestern Weiyuan County, Dingxi City, Gansu Province, passes through the three provinces of Gansu, Ningxia and Shaanxi, and flows into the Yellow River in Tongguan County, Shaanxi Province. As the largest primary tributary in the Yellow River Basin, the Weihe River has a total length of 818 km and a drainage area of approximately 1.34×10^5 km^2. The Guanzhong area, an area of approximately 55,000 km^2, is an important political, economic and cultural core area of Shaanxi Province, with the total economic volume accounting for 70% of Shaanxi Province (**Figure 1**). The Weihe River is known as the mother river in the Guanzhong area, supporting production and domestic water demands (Dou et al., 2018).

The Guanzhong area contains a wide range of water supply projects and construction plans. The management department of the Weihe River has proposed building a rich regional water supply network based on a natural water system supplemented by artificial water transmission channels in recent years. Meanwhile, supporting reservoirs have been built or are under construction, such as the Dongzhuang Reservoir, Doumen Reservoir and

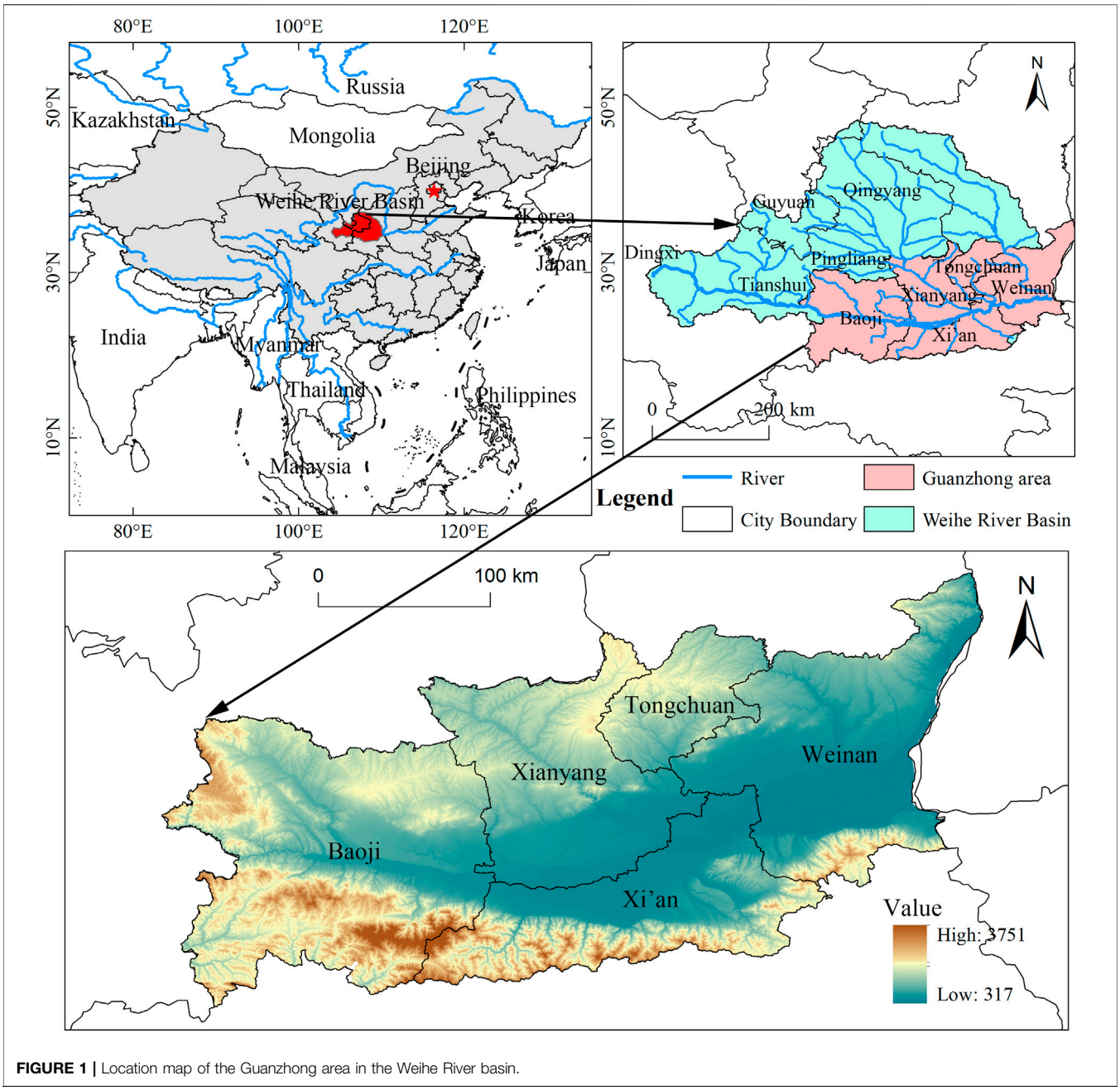

FIGURE 1 | Location map of the Guanzhong area in the Weihe River basin.

Tingkou Reservoir. Managers hope to achieve the goal of water security in the Weihe River Basin by improving the water supply capacity and water utilization efficiency of the Guanzhong area. The time-consuming construction of water conservancy projects may present difficulty to the assessment.

Data Sources

Multiple data sources were involved in the model parameterization. There are seven types of data required by the model (including population, economy, household life, land and food, water supply and demand, wastewater recycling, and the ecological environment). These data have been provided by the project team and re-collection. Data sources include the statistical yearbook of Shaanxi Province (SXBS (Shaanxi Bureau of Statistics), SXITNBSC (Shaanxi Investigation Team of National Bureau of Statistics of China), 2002–2020), the Water Resources Bulletin, Shaanxi Water Conservancy Statistical Yearbook and some literature. Key parameters, values and data source information are provided in **Table 1**.

METHODOLOGY

System Dynamics Model

The development of SDM was considered to be a valuable thinking and learning process. A model based on the system

TABLE 1 | Details of some important parameter values and date sources used in the Guanzhong area.

Variable	Initial values used (unit)	Source
Stock variable		
Total population	21.6432 (10^6 persons)	Statistical yearbook
The primary industry AV	16.304 (10^9 yuan)	Statistical yearbook
The secondary industry AV	59.810 (10^9 yuan)	Statistical yearbook
The tertiary industry AV	59.736 (10^9 yuan)	Statistical yearbook
Per capita disposable income of urban households	4,336 (yuan)	Statistical yearbook
Per capita net income of rural households	1,628 (yuan)	Statistical yearbook
Total cultivated field area	1,609.86 (10^3 ha)	Statistical yearbook
Grain yield	6.8038 (10^6 t)	Statistical yearbook
Urban green area	11,409 (ha)	Statistical yearbook and Urban master planning
Constant		
Per capita food consumption	395 (kg/persons)	The compendium of food planning
Agriculture water consumption coefficient	0.65(-)	Wei et al. (2012)
Urban domestics water consumption coefficient	0.55(-)	Wei et al. (2012)
Wastewater plant treatment rate	0.65(%)	Wei et al. (2012)
Interbasin water transfer	1.205 (10^9 m^3)	Water resources planning
Rainwater use	0.011 (10^9 m^3)	Cui (2009); Statistical yearbook
Karst water	0.13 (10^9 m^3)	Huang (2007)
Annual mean selfproduced water	7.3561 (10^9 m^3)	Wei et al. (2012)
Multi-annual mean inflow	3.5759 (10^9 m^3)	Wei et al. (2012)
Multi-annual minimum outflow	0.4839 (10^9 m^3)	Wei et al. (2012)
Basic instream flow	1.6 (10^9 m^3)	Tang, (2018)
Instream flow for pollution dilution	2.93 (10^9 m^3)	Tang, (2018)
Instream flow for sediment transport	6.089 (10^9 m^3)	Tang, (2018)

framework can reveal the cause of the problem, provide predictive results, and choose a solution. Such a view is widely recognized in system dynamics and review literature (Zare et al., 2019). SDM is a method that can provide comprehensive results by outputting system results via focusing on the relationship between and within each system element through a comprehensive and dynamic perspective, which is important for specific aspects of the modeling process.

Model Improvement

For a detailed introduction of the sub-system, please refer to the previous research of the project team (Song et al., 2018). Here we focus on the improvement of the model, which is mainly divided into the following two aspects:

Ecological Environment Subsystem

We have broadened the selectivity of the ecological environment subsystem. In this paper, we extend the key role of water resources in the socio-economic and ecological environment. Ecosystem integrity is the principle in the pursuit of sustainable water resource management. The sustainability of water depends on the provision of ecosystem services. This interdependence indicates that water policy should prioritize ecosystems and their services. Sustainable water resource management emphasizes the gradual reduction of water vulnerability, so the corresponding policy formulation must be internalized by all stakeholders, instead of solely relying on the management department.

People are increasingly aware of the importance of protecting environmental flows (Scott et al., 2021). However, the demand for environmental flow is not linear. Decision-makers need to use environmental flow as a dynamic parameter for different purposes, rather than a fixed value. The redesigned subsystem can define appropriate environmental flows based on the opinions of policy stakeholders, such as designing environmental flows with different ecological functions or adding time functions to simulate cascading changes in time series. We used three different environmental flow configurations to simulate the different attitudes of stakeholders towards ecological water use in this study.

Land and Food Resource Subsystem

We have optimized the structure of the original model subsystem and to promote the link between land use and grain yield more accurately. Water resources are the basis of food security. Land and food systems depend on the provision of water resources system services. Water resources policies should consider the irrigation of crops in local communities to provide people with sufficient water to sustain food production. Therefore, we re-expanded this complex relationship between land and food and optimized the structure of the original model. We have added two new stock variables total sown area (TSA) and Sown Area of grain crops (SAGC). TSA and SAGC refer to the total sown area of various crops and grain in crops throughout the year, respectively. The improved subsystem will simulate the process of system feedback through four stock variables. The specific operation methods include: 1) Establish Multiple-crop index (MCI) parameters between total cultivated field area (TCA) and total sown area (TSA), MCI represents the ratio of TSA to TCA; 2) Establish the ratio of total sown area and sown area of grain crops (GCSI) parameters between TSA and sown area of grain crops (SAGC), GCSI represents the ratio of SAGC to TSA; 3) Establish per unit area of grain production (PUA) parameters between Grain

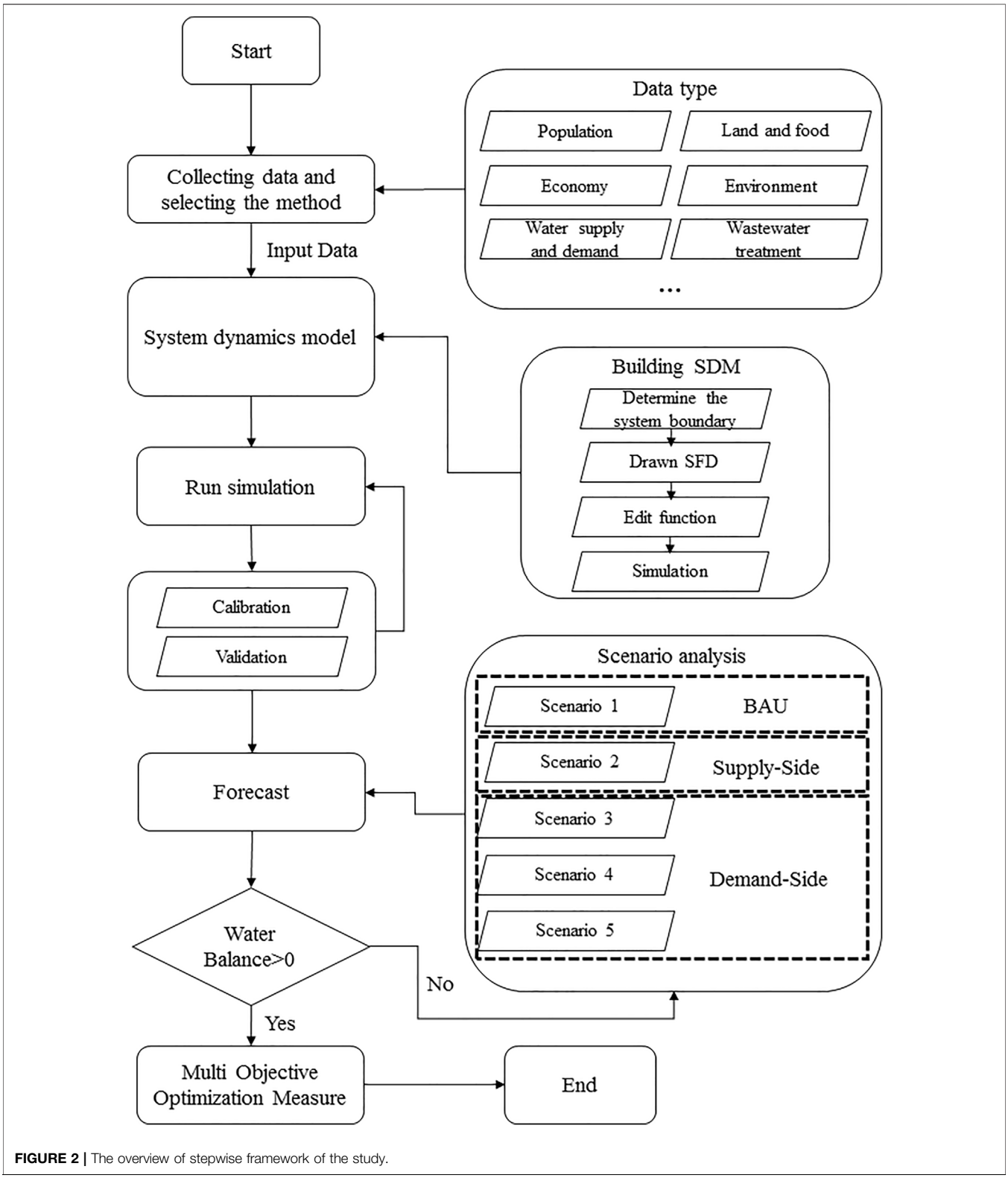

FIGURE 2 | The overview of stepwise framework of the study.

yield (GY) and SAGC, and PUA parameters represent the ratio of SAGC to GY. Generally speaking, unless there are significant changes in technology and policies, these control parameters will remain within a fixed range. The improved model structure can examine the prediction results of grain yield through the above land use control parameters, thereby improving the assessment of food security in the subsystem.

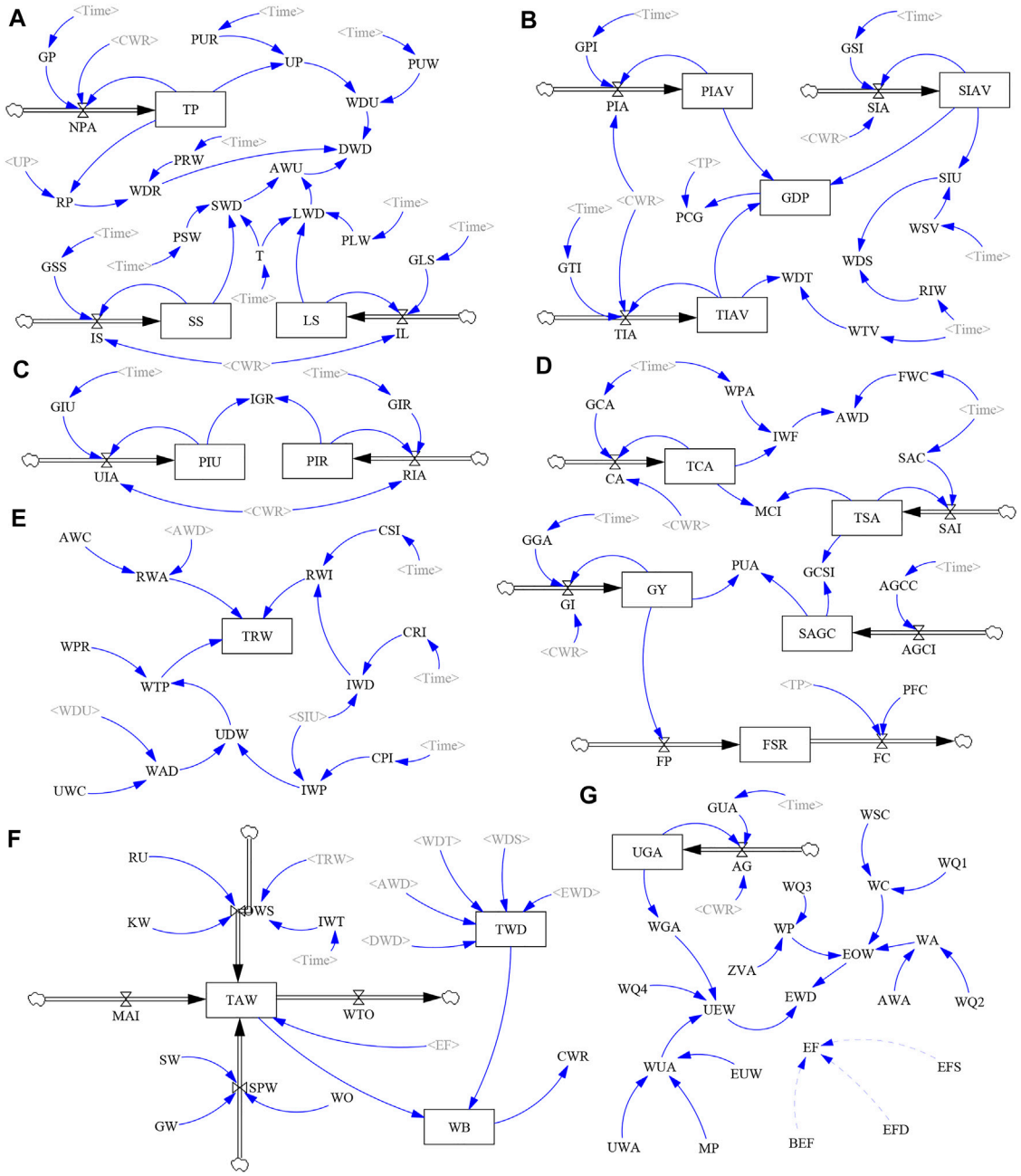

FIGURE 3 | A system dynamic stock-flow diagram of the improve system, including subsystems of **(A)** population, **(B)** economy, **(C)** the livelihoods of people, **(D)** land and food resource, **(E)** recycled water, **(F)** water supply and demand, **(G)** ecological environment.

Model Setting

A framework of the flow chart of this research is shown in **Figure 2**. The boundaries of the improved model were limited to the Guanzhong area. The model consists of seven interrelated subsystems, including 123 variables. The new stock-flow diagram (SFD) of the improved model indicates the direction and change of feedback between different systems (**Figure 3**). System simulation was achieved using the professional system dynamics software package Vensim PLE (www.vensim.com). The model simulation time is from 2001 to 2060, and the time step is 1 year. The input data related to the model were collected in 2001–2019 and used for the model calibration and verification.

Model Testing

Compared with the black box model driven by pure data, SDM pays more attention to the rationality of system structure (Sterman, 2000). This point of view runs through the entire process of developer modeling, such as determining system goals,

TABLE 2 | Descriptions of the four scenarios.

Policy scenario	Scenario classification	Description
Scenario 1	Business as usual	The watershed characteristics remain unchanged. Policy, technology and growth rate remain at the current level.
Scenario 2	Water transfer project	Supply-side management. Water policy favors investment in water conservancy facilities, such as interbasin water transfer and reservoir construction.
Scenario 3	Low-level development	Demand-side management. The low-level development scenario mainly simulates slower growth and technological development. The water policy tends to simply reduce water demand.
Scenario 4	Middle-level development	This scenario represents the medium level of demand-side management. This scenario is to observe the changes after model adjustment and avoid going from one extreme to another.
Scenario 5	High-level development	Demand-side management. The high-level development scenario mainly simulates the socioeconomic growth and technological improvement. The water policy reduces water demand by saving water.

drawing causal loop diagrams and constructing stock-flow diagrams. To this end, a series of tests were performed, including testing of the system structure, overall consistency and model error. To achieve the relevant goals of system research, a test of the system structure and overall consistency was carried out to determine whether the model fit the actual system. The model error was used to study the accuracy of the model output. The data simulated by the model were compared with the historical data to ensure consistency.

In this study, the test tools in the Vensim PLE software package, the coefficient of determination (R^2), discrepancy coefficient (U_0), the absolute relative error (ARE) and the mean absolute relative error (MARE) test combinations were used to verify the model. The system structure test will be completed by the software package tool. The coefficient of determination (**Eq. 1**), the discrepancy coefficient (**Eq. 2**), the absolute relative error (**Eq. 3**) and the mean absolute relative error (**Eq. 4**) were employed to test the performance of the model. Furthermore, the views of some experts and stakeholders were collected to verify of SD model.

$$R^2 = \left(\frac{\mathrm{Cov}\left(Y_{sim} - Y_{obs}\right)}{\sigma Y_{sim} - \sigma Y_{obs}}\right)^2 \tag{1}$$

$$U_0 = \frac{\sqrt{\sum \left(Y_{sim} - Y_{obs}\right)^2}}{\sqrt{\sum Y_{sim}^2 + \sum Y_{obs}^2}} \tag{2}$$

$$\mathrm{ARE} = \left|\frac{\left(Y_{sim} - Y_{obs}\right)}{Y_{obs}}\right| \tag{3}$$

$$\mathrm{MARE} = \frac{1}{n}\sum_{t=1}^{n}\left|\frac{\left(Y_{sim} - Y_{obs}\right)}{Y_{obs}}\right| \tag{4}$$

where Y_{sim} and Y_{obs} are the simulated and observed data point for the tested parameter, respectively; Cov (Y_{sim}, Y_{obs}) is the covariance of the simulated and observed data; and σY_{sim} and σY_{obs} are the standard deviations of simulated and observed sets of values.

Scenario Analysis

Scenario analysis can be used to assess future uncertainties and help develop water resource management strategies (Carter et al., 2007). Combined with the existing planning research of government departments and expert opinions, the management policies are identified as five scenarios. These five scenarios reflect the impact of different measures and stakeholders on the system. First, we propose a business as usual (BAU) scenario. The other four scenarios control system behavior through the supply-side, demand-side management and stakeholder attitudes. The description and parameter settings of each scenario are displayed in **Tables 2**, **3**. The parameter settings of the water resource utilization efficiency are summarized in **Table 4**.

RESULTS

Model Calibration and Validation

The structure and unity of the system were confirmed before running the model. To conduct model calibration and validation, we divide the simulation results and the historical data series during the period of 2001–2019 into two parts. One part from 2001–2014 is used for model calibration, and the rest was used for model validation. These tests will contribute to improving the reliability and confidence of the SD model. **Figure 4** shows the test results of the relevant variables. Among the tested system parameters, the coefficients of determination (R^2) values of TP and UGA are relatively low, at 0.89 and 0.87, respectively. The urban expansion and new talent introduction policies in the Guanzhong area may be the cause of this deviation. The maximum and the minimum values of the model difference discrepancy coefficient (U_0) are 0.0009 and 0.002, respectively. Meanwhile, the mean absolute relative error (MARE) of the model during calibration and verification are 0.016 and 0.033, respectively. The results of the model showed that the simulated values were in good agreement with the observed values.

Simulation Results

Business As Usual Scenario

In the BAU scenario, the system show similar development results for the three different environmental flow configurations. With the continuous growth of water demand caused by social and economic development, the available water resources in the Guanzhong area will be depleted. **Figure 5** shows the simulation results of the water resource balance, indicating that the water resources of the Weihe River Basin under the three configurations are unsustainable. The water resources that meet the allocation of sediment transport will face water scarcity in 2043. It is predicted that the water scarcity in the Guanzhong area

TABLE 3 | Description of the parameter settings in five scenarios.

Policy scenario	Description of parameters
Scenario 1	Business as usual (BAU)
Scenario 2	Interbasin water transfer is increased by 128%; All other parameter values are held at their base case values.
Scenario 3	Growth rate of Population is increased by 2‰; Growth rate of primary industry AV is increased by 0.8%; Growth rate of secondary industry AV is increased by 5%; Growth rate of tertiary industry AV is increased by 5%; Population urbanization rate is increased to 70%; Growth rate of the cultivated area is increased by -0.3%; Growth rate of the grain yield is increased by 0.1%, respectively; All other parameter values are held at their base case values.
Scenario 4	The growth rate is between Scenario 3 and Scenario 5.
Scenario 5	Growth rate of Population is increased by 6‰; Growth rate of primary industry AV is increased by 3%; Growth rate of secondary industry AV is increased by 12%; Growth rate of tertiary industry AV is increased by 15%; Population urbanization rate is increased to 90%; Growth rate of the cultivated area is increased by 0.5%; Growth rate of the grain yield is increased by 1.5%, respectively; All other parameter values are held at their base case values.

TABLE 4 | Assumptions of the water resource utilization efficiency in different scenarios.

Variables	BAU	Scenario 3	Scenario 4	Scenario 5
Water demand per capita urban population per day (L)	140	160	120	100
Water demand per capita rural population per day (L)	80	70	90	100
Water use per unit of secondary industrial AV ($m^3 10^{-4}$yuan)	6	10	4	2
Water use per unit of tertiary industry AV ($m^3 10^{-4}$yuan)	0.7	1	0.6	0.3
Water use per cultivated area ($m^3 mu^{-1}$)	120	140	110	100
Rate of industrial water repeating use (%)	85	75	95	99
Wastewater plant treatment rate (%)	0.65	0.55	0.85	0.95
Per capita large livestock water use per day (L)	60	50	65	70
Per capita small livestock water use per day (L)	50	45	55	60

will reach 1.4×10^9 m^3 in 2060. The simulation results in **Table 5** show that the total population decreased by 0.2731×10^6 people and is affected by restrictions on the growth of water resources. GDP decreased from 63,883.2 $\times$ 10^9 yuan to 45,108.5 $\times$ 10^9 yuan, and PCG also showed a downward trend. With the reduction in the disposable income of households, the gap index has slightly expanded. In terms of land and grain, the reduction in cultivated land accelerated from $1{,}354.25 \times 10^3$ ha reduced to $1{,}340.56 \times 10^3$ ha. The grain output per unit area remained relatively stable, while the grain output decreased relatively. The current food self-sufficiency rate in the Guanzhong area fluctuates between 0.8 and 0.9. The simulation results showed that the future food self-sufficiency rate in the Guanzhong area fluctuates between 0.7 and 0.8, further increasing the food security risk. **Table 5** shows the simulation results of some stock variables in the BAU scenario.

Scenario Analyses

Figures 6, **7** show the change trend of the selected variables of the four scenarios due to different supply-side and demand-side management policies and measures in the simulation range (2020–2060).

Scenario 2 produced similar results as Scenario 1. Under the condition that the system meets the environmental requirements of the sediment transportation configuration, water scarcity is expected in 2054 in the later stage of simulation. Compared with Scenario 1, the water transfer project alleviated water scarcity and reduced the risk to water resources in the Guanzhong area. The increase of 1×10^9 m^3 of water resources in the second phase of the Han-to-Weihe River Diversion Project delayed the occurrence of water scarcity by 12 years. Although the improvement of available water resources impacted the balance of water resources, it did not benefit the water savings, because the water demand will not be reduced. The pressure on water resources brought about by social and economic development cannot be eliminated. However, the simulation results show that the supply-side solution provides promising results for solving water scarcity.

The simulation results of scenario 3 show that sacrificing the speed of socio-economic development cannot have a positive impact on watershed water resources. Water-saving measures are a key policy lever for reducing water consumption in river basins. Although reducing the speed of social and economic development can lower the demand for water resources in the early stage, the decline of technology and policy will further aggravate the shortage of water resources. The simulation results in **Figure 6** show that the unsustainability of water resources increases under the low development mode. The system predicts water scarcity in 2048, reaching 1.69×10^9 m^3 in 2060, with the upward trend of industrial water use will becoming steep. The implementation of this policy of demand-side management requires a re-examination of the adverse effects of development and technological regression on the future management of the Guanzhong region.

The system can meet the water demand of each department during the whole simulation period without water scarcity in scenario 4. Although the speed of social-economic development increased, the sustainability of water resources was significantly

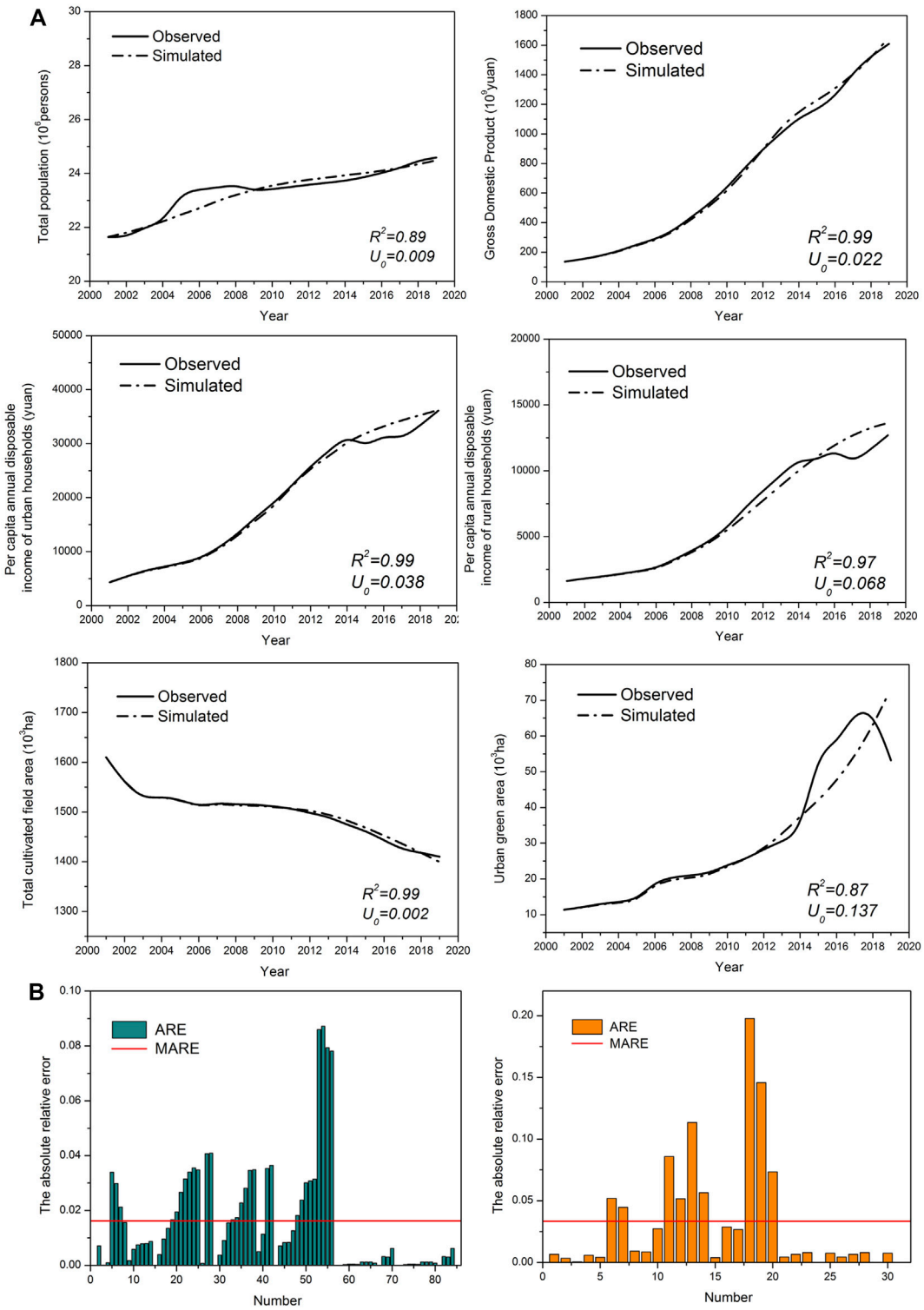

FIGURE 4 | Results of calibration and validation, **(A)** the coefficient of determination (R^2) and discrepancy coefficient (U_0) between simulated results and observed data, **(B)** calibration and validation results using Absolute Relative Error (ARE) and Mean ARE (MARE).

enhanced due to the improvement of water-saving technologies. Agricultural water use began to show a slight downward trend. Industrial water use is controlled. Tertiary industry water use tended to be flat in the later period. Compared with scenario 3, this scenario seems to provide a satisfactory solution to achieve sustainable water resource management.

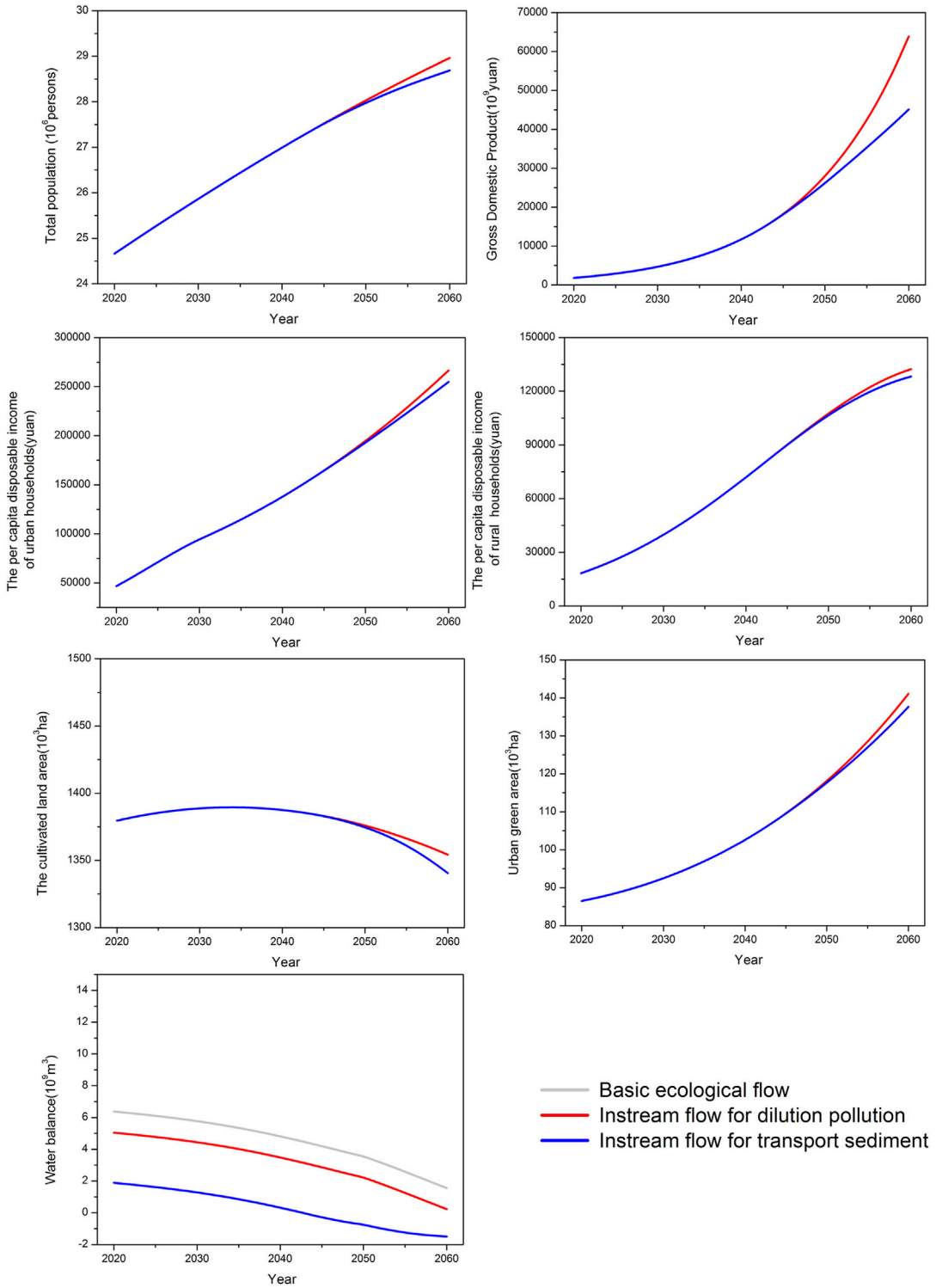

FIGURE 5 | The simulation results of BAU scenarios under three EF allocations (BEF, EFD, EFS).

The results of Scenario 5 emphasize the key role of water-saving technologies in the sustainable use of water resources and social and economic development. Compared with the previous scenario, the growth rate of the socio-economic sector parameter and water-saving plan in this scenario improved. However, in addition to the steady growth of agricultural water, domestic water, and ecological water, the demand for industrial water and tertiary industry water exhibited a downward trend. Regarding

TABLE 5 | Simulated values of the social economic variables in the BAU scenarios.

Subsystem	Variable	BEF and EFD			EFS		
		2020	2040	2060	2020	2040	2060
Population	TP	2,466.2	2,699.25	2,896.06	2,466.2	2,699.25	2,868.75
Economy	GDP	18,164.9	117,105	638,832	18,164.9	117,105	451,085
	PCG	73,655.4	433,841	2,205,870	73,655.4	433,841	1,572,410
people's livelihood	PIU	46,764.5	137,853	266,447	46,764.5	137,853	254,818
	PIR	18,274.5	71,966.8	132,362	18,274.5	71,966.8	127,526
	IGR	2.5	1.9	2.0	2.5	1.9	2.0
Land and food resources	TCA	1,379.56	1,387.51	1,354.25	1,379.56	1,387.51	1,340.56
	GY	709.637	837.819	922.704	709.637	837.819	906.581
	FSR	0.728	0.786	0.806	0.728	0.786	0.800

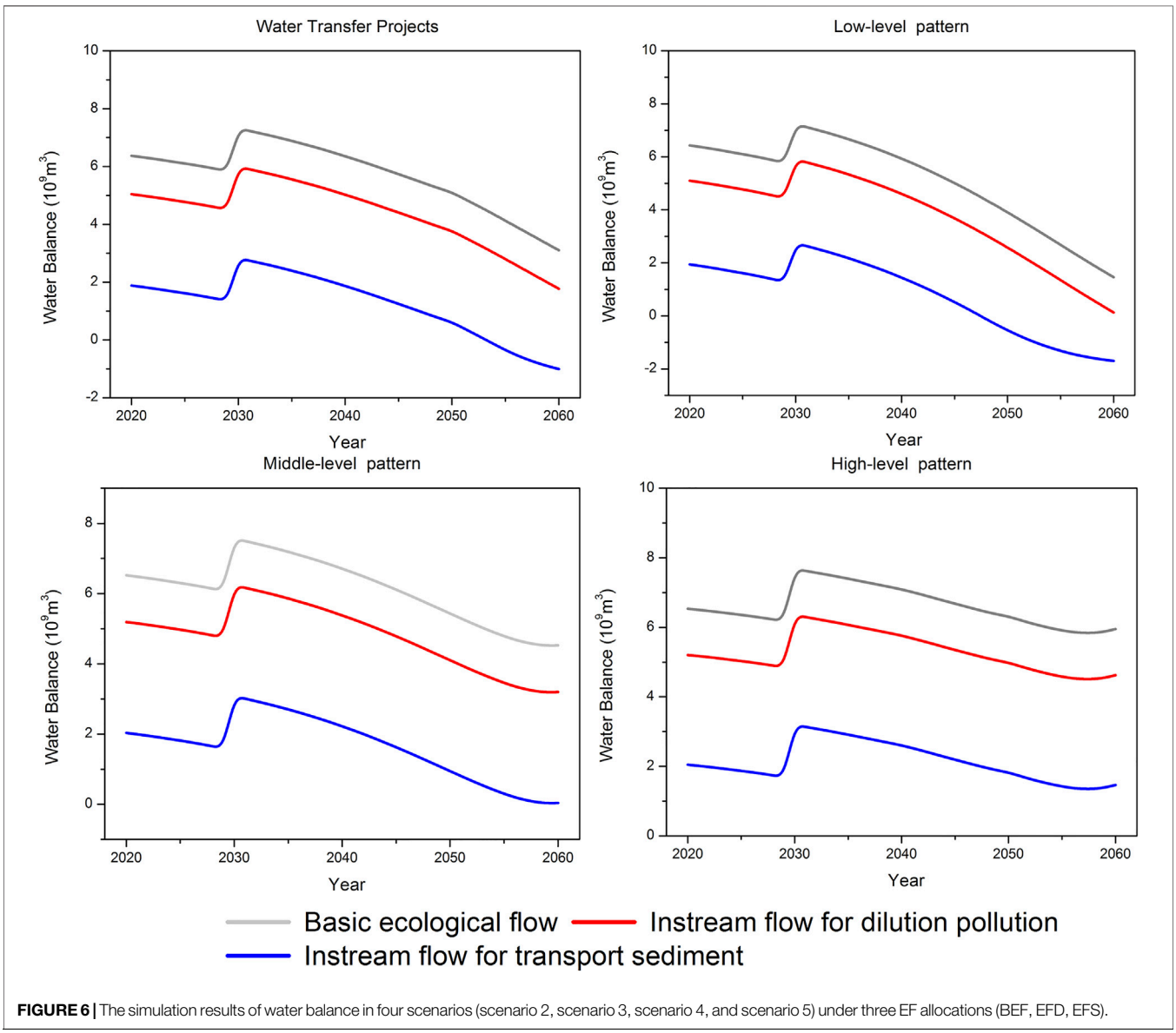

FIGURE 6 | The simulation results of water balance in four scenarios (scenario 2, scenario 3, scenario 4, and scenario 5) under three EF allocations (BEF, EFD, EFS).

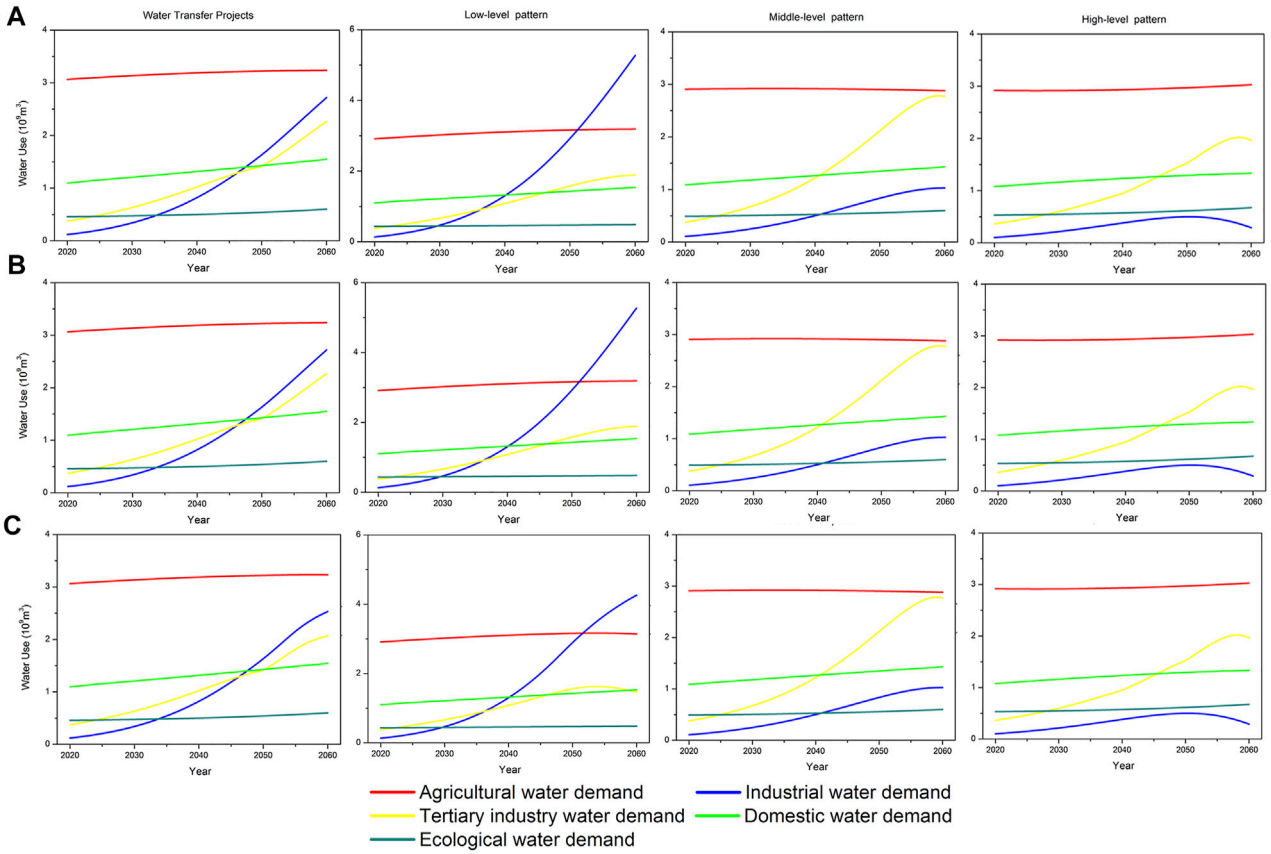

FIGURE 7 | The behavior of water use variables under three EF allocations, **(A)** base ecological flow, **(B)** instream flow for dilution pollution, **(C)** instream flow for transport sediment.

the water resource balance, this scenario yielded increased water resource reliability and reduced vulnerability, indicating that improving demand-side management (improving water resource utilization efficiency) as a water policy can fully meet the rapid social and economic development in the future.

Sustainability Evaluation

The results of the model analysis show that the attitudes of stakeholders will different water distribution and management. The three types of environmental flows represent different stakeholders' perceptions of the importance of ecological water use in water distribution. This will directly affect water resource planning and the formulation of management policies. At this point, achieving sustainable management of water resources requires continuous trade-offs between uses and users. The vulnerability of water resources can be reduced under the dual management of the supply-demand side, and the sustainable development of the social economy and the ecological environment can be realized in the Guanzhong area.

In addition, this scenario-based analysis show that the management department can provide sufficient available water resources through the water transfer project on the supply side. However, this development model is unsustainable in the long run due to the problem of water limiting growth. Relying on demand-side management and other measures to provide reliable and sufficient water resources to meet development needs will be a new challenge for watershed water resource management. This is the fundamental problem of the governance of water-deficient areas, and the area's development exceeds the limit of available water resources (Bahaddin et al., 2018).

This study has similar results with previous studies in some respects. For example, the two-research emphasized that improving water use efficiency is a driving factor of sustainable water management. However, the focus of this study is to explore the impact of supply-side and demand-side management on community water management and policy-making, especially in water scarcity areas. Simultaneously, we have emphasizes that stakeholder participation is of great significance to sustainable water resources management. The following discussion will focus on these contents.

DISCUSSION

Restricted Development

Although the results of the model show that the development of the supply side and the improvement of demand-side management can achieve the sustainability of water resources

in the Guanzhong area. However, the implementation of water policies may be limited by human and climate driving factors and cause water scarcity, such as extreme arid climates and unequal water competition. The new water management policy in the Guanzhong area is still in the process of planning and construction, which undoubtedly enhances the uncertainty of sustainable water resource management in the future.

The scenario analysis showed that water scarcity limits not only social and economic growth but also affects other aspects of the system. First, Water scarcities will widen the income gap between urban and rural residents, affecting the well-being of residents. A decline in income will impact the level of consumption, which affects the expenditure on water resources. Income and expenditure determine the attitude of stakeholders: when income does not exceed expenditure expectations, no one has shown interest in improving water management; but due to the negative impact of water pressure, the water-saving awareness of stakeholders will be improved. Some studies have shown that water price increases will directly affect water consumption (Li et al., 2018). Managers can control water prices to promote water savings and reduce wastewater discharge. Second, the improved model shows that there are food security risks in the Guanzhong area. This is a different answer from previous research. It may be necessary to purchase sufficient food from outside regions if no measures are taken in the future. Water scarcity may exacerbate the imbalance between food supply and demand. The changes in grain production impact land use and could even affect the ecosystem (Yang F. et al., 2021). Therefore, ensuring adequate water resources is the key to the future social and economic development of the Guanzhong area.

Policy Implications

In Scenario 2, the water transfer project increased the available water resources in the Guanzhong area. The construction of water conservancy projects is expensive and time-consuming, and their impact on the ecological environment and biodiversity is difficult to evaluate (Abell et al., 2008; Jiang et al., 2020). However, such projects as an effective management tool are currently being implemented in the Guanzhong area, positively impacting local development. Although relying on external water resources enhances the water resources carrying capacity of the Guanzhong area, the water transfer projects may be forced to stop in case of a water crisis in the water transfer basin, thus affecting the downstream water-receiving area. Management strategies tend to be biased towards supply-side development in the case of water scarcity, but people are increasingly aware of the potential of demand-side management and other solutions. The system simulation results show that focusing on demand-side management is more effective than water supply-side management.

All scenario analyses show that the sustainable utilization of water resources in the Guanzhong area must rely on improving water resource utilization efficiency, which is an important policy decision point. Scenario 5 is the best solution for demand-side management, including increasing the agricultural water consumption coefficient and wastewater plant treatment rate and reducing the water use per unit of industry AV, water use per cultivated area and per capita water use per day. As mentioned in other studies, the effectiveness of water-saving technologies as a solution to problems is controversial (Bian et al., 2014; Yang S. et al., 2021). The implementation of this measure often requires sufficient technical, financial and policy support, especially the increase in public awareness and participation. If the reduction of water demand through development speed was carried out without considering water efficiency, such a measure may harm social and economic development, as shown in scenario 3. Thus, the best policy for sustainable water resource management is to improve demand-side management to reduce water consumption in various departments.

Environmental Water Indication

People are increasingly aware of the importance of environmental flows in watershed management (Wei et al., 2020). If we want to maintain the ecological functions of the river, it is necessary to ensure sufficient water for the environment. However, our experience shows that water use is not suitable for all purposes. Satisfying ecosystem functions is likely to affect drinking water or other human uses. Sometimes, decision-makers will introduce demand standards into supply-side-oriented management, thereby formulating a failed water policy.

Sustainable water management policies mean that decision-makers need to weigh the balance between water production, recreation, landscape, and biological protection. Decision-makers should consider future policy changes and stability to reduce conflicts of interest in water distribution. The improved model structure no longer sets the environmental flow as a fixed maximum value. The design should consider the different needs of stakeholders and provide more results through "selection" to improve the management of water resources. We selected three different configurations of environmental flow in this study. These represent the attitudes of different stakeholders, respectively. The results show that, if no measures were taken, the water resources in the Guanzhong area would not meet the ecological needs of sediment transportation in the future. However, some studies suggest that with the improvement of soil and water conservation and the ecological environment, the river sediment content of the Yellow River Basin has seen a yearly decrease (Sun et al., 2020; Zhao et al., 2021). Ecological water will be released into social and economic development in the future, which may require decision-makers to weigh the distribution of water in the system and the potential risks.

Other Measures

The managers have developed several other solutions to supplement the sustainable water resources management strategy in the Guanzhong area. These include the diversification of water resources, the change of the model that completely relies on the surface water and groundwater in the region, and the water management department actively expanding the use of recycled water and rainwater to meet water demand. An irrigation network will be constructed to

TABLE 6 | The supply structure of water resources in the Guanzhong area (Unit: 10^9 m^3).

Year	Surface water	Groundwater	Waste water reuse	Rain use
2010	2.223	2.646	0.033	0.007
2011	2.521	2.507	0.032	0.008
2012	2.561	2.647	0.039	0.009
2013	2.579	2.627	0.090	0.008
2014	2.670	2.619	0.119	0.006
2015	2.711	2.619	0.173	0.007
2016	2.642	2.602	0.192	0.007
2017	2.829	2.533	0.209	0.009
2018	2.900	2.453	0.247	0.009
2019	2.858	2.383	0.273	0.009

connect the local water conservancy facilities (reservoirs and dams). Promote the gathering of industrial parks for companies by recycled water use. Finally, innovative building regulations require land developers for new projects to comply with green building standards to obtain development permits.

At present, the Guanzhong area is improving the utilization rate of recycled water and rainwater through industrial upgrading and sponge city construction. Meanwhile, the river ecosystem protection plan is incorporated into the water policy management to ensure ecological safety. However, the management strategies announced by the water department seem to be slightly overlapping and hollow and it is difficult for some stakeholders to find specific approaches. **Table 6** shows the supply of water resources in the Guanzhong area in the past 10 years. The Guanzhong area still relies on traditional water resources, and there is still a lot of room for the development of other water sources. Moreover, the water body is over-exploited or polluted and may threaten stakeholders in remote supply. It is difficult to find inter-regional water rights trading and compensation mechanisms in public information.

A variety of policies and measures may promote the solution of the water problem, including adjustment of tax structure, rainwater collection, and greywater reuse by urban households, policy incentives (incentives or subsidies) to reduce water demand, and encourage stakeholders to participate in planning.

Uncertainties of Climate Change

A critical uncertainty factor in our research is that the supply and demand of water resources caused by climate change are not considered. Studies have evaluated the impact of climate change and human activities on hydrological processes and water resources activities in different regions (Ahn and Merwade, 2014; Ran and Tao, 2017; Wang et al., 2020). Most of these studies focus on changes in water availability (Grouillet et al., 2015; Omer et al., 2020). Climate change, including extreme events such as droughts and floods, may affect ecosystem services and water resources utilization throughout the basin (Brendel et al., 2017). Therefore, close connections exist among climatic conditions, water users, and distribution methods. However, the impact of human activities on water resources has exceeded climate change, especially when people are aware of adopting various measures to deal with the adverse effects of climate conditions. For instance, the supply-side plan is based on the construction of water conservancy projects to integrate flood and water supply management. Decision-makers need to consider effective management policies to meet the challenges of future climate.

Comparative Assessment

The previous research of the project team was based on the perspective of decision-makers, integrating all aspects of the water system to solve the problem of water shortage. In this study, we integrate model developers, stakeholders, and decision-makers into the same perspective, and employ improved model structures to simulate the impact of supply-side and demand-side management on water resources management strategies. The case study in the Guanzhong area summarizes the three principles of sustainable water resources management. These have been verified in our research and lead to our conclusions.

First of all, sustainable water resources management depends on the carrying capacity of water resources, the level of regional development and the common understanding of stakeholders. The case of the Guanzhong region shows that economically developed regions can determine ecological environmental protection and regulate demand through enhanced supply-side and demand-side dual management. In other words, Water policy can avoid unsustainable water management by combining supply-demand side measures. However, supply-side development may not be affordable in underdeveloped and disadvantaged regions. Decision-makers must weigh fairness between regions and systems. How stakeholders view and reach a common understanding is crucial to determining the results of water policies. Therefore, we recognize that demand-side management is more important than supply-side development in water-scarce areas. Reducing water demand can replace new water resources development plans and avoid falling into supply-oriented management. This is a point neglected in previous studies.

Second, improving ecosystem services is the basic goal of the sustainable development of water resources, which is closely related to the socio-economic system. Stakeholders may cause differences in demand management results for different purposes. The improved model structure shows that the ecological environment and social economy may be rebalanced at the expense of part of the ecological function. Specifically, high-quality water, availability, and fair access are the core values of sustainable water resources management. However, sustainable water resources management should be phased. The dynamic balance between systems requires water policy to pay more attention to fairness, stability and reduce conflicts of interest.

Third, no water policy can completely avoid the unsustainability of water resources due to extreme weather disasters and poor governance policies. Decision-makers should consider the stakeholders' opinions in the decision-making process, which may reduce the human influence. The participation of stakeholders in water resources management has been reflected in the formulation of national-level strategies. However, this approach is still difficult to achieve in small and medium-sized river basins. This is mainly related to the division

of administrative boundaries, the complexity of the governance structure, and the difficulty for decision-makers to refer to the opinions of users in the design process. Stakeholder leadership has emerged in water management at local and regional levels and this could translate into policy impact in the future (Scott et al., 2021). In addition, the open platform owned by SDM provides the possibility for stakeholder participation. Common values and more new ideas are considered, planned, and executed will help improve the efficiency of sustainable management strategies. This was verified in this study.

CONCLUSION

Water resources management should consider the participation of stakeholders and integrate all major components and problems into an overall system for research with decision-makers Otherwise, some policies and measures formulated cannot solve the current problems and even worsen after spending limited resources and time. Based on new perspectives and improved models, we compare and analyze the impact on sustainable water resource management through supply-side and demand-side management and other policy measures. The research aims to establish a new framework to evaluate the best policies and measures for sustainable development, not just research on water scarcity. This paper expands the three decision-making principles that we believe are related to sustainable development: 1) Follow a systematic and comprehensive approach to ensure sustainable development. Decision-makers need to weigh the differences between systems and regions to promote consensus among stakeholders; 2) Sustainable water resources management is phased, providing scientific water policies to achieve fairness, stability and reducing conflicts of interest; and 3) The uncertainty of future changes should be considered, the participation of stakeholders should be encouraged and promoted the efficiency of sustainable water management strategies. Beyond the principles set out above, consider the impact of the following policies on system behavior in the long run, which will lead to sustainable water management:

- Water transfer projects reduce the vulnerability of water resources, but water transfer measures between river basins are unsustainable in the long run.
- Demand-side management (improving water resource utilization efficiency) and other methods (irrigation systems, wastewater treatment, rainwater and reclaimed water reuse, etc.) are more important than supply-side development (as new water resources), especially in economically disadvantaged areas. Reducing water use in various sectors can replace new water resources development plans.
- The improvement of the eco-environment will help release water resource and further promote social economic development.
- The participation of stakeholders is essential to determine the results of water policies, which will help decision-makers weigh water allocation and policy risks and minimize the impact of human factors.

To improve the model in future research work, the recommendations are as follows. First, we hope that more stakeholders will participate, which can promote the optimization of the system structure and improve the performance of the model. Second, the analysis of scenarios may not be comprehensive and factors such as extreme arid climate have not been considered. More scenarios can help improve the quality of water policy management.

DATA AVAILABILITY STATEMENT

The original contributions presented in the study are included in the article/**Supplementary Material**, further inquiries can be directed to the corresponding author.

AUTHOR CONTRIBUTIONS

BT contributed to the conceptualization, ideas, methodology, model improvement, validation, original paper draft and visualization. RM, HS, FK, and DC contributed to results discussion and edit the paper. JS supervised the project, helped results analysis, contributed to financial support. XG contributed to study area definition and data re-collection. All authors contributed to manuscript revision, read, and approved the submitted version.

FUNDING

This study was supported by the Special Funds of the National Natural Science Foundation of China (Grant No. 42041004), Program for Key Science and Technology Innovation Team in Shaanxi Province (Grant No. 2014KCT-27) and the Shaanxi Province Water Conservancy Science and Technology Project (No. 2021slkj-13).

SUPPLEMENTARY MATERIAL

The Supplementary Material for this article can be found online at: https://www.frontiersin.org/articles/10.3389/fenvs.2021.805513/full#supplementary-material

REFERENCES

Abell, R., Thieme, M. L., Revenga, C., Bryer, M., Kottelat, M., Bogutskaya, N., et al. (2008). Freshwater Ecoregions of the World: A New Map of Biogeographic Units for Freshwater Biodiversity Conservation. *BioScience* 58 (5), 403–414. doi:10.1641/b580507

Ahn, K.-H., and Merwade, V. (2014). Quantifying the Relative Impact of Climate and Human Activities on Streamflow. *J. Hydrol.* 515, 257–266. doi:10.1016/j.jhydrol.2014.04.062

Babel, M. S., Gupta, A. D., and Nayak, D. K. (2005). A Model for Optimal Allocation of Water to Competing Demands. *Water Resour. Manage.* 19 (6), 693–712. doi:10.1007/s11269-005-3282-4

Bahaddin, B., Mirchi, A., Watkins, D., Jr., Ahmad, S., Eliot, R., and Madani, K. (2018). "System Archetypes in Water Resource Management," in World Environmental and Water Resources Congress 2018: Watershed Management, Irrigation and Drainage, and Water Resources Planning and Management (Reston, VA: American Society of Civil Engineers Reston), 130–140. doi:10.1061/9780784481400.012

Bakhshianlamouki, E., Masia, S., Karimi, P., van der Zaag, P., and Sušnik, J. (2020). A System Dynamics Model to Quantify the Impacts of Restoration Measures on the Water-Energy-Food Nexus in the Urmia lake Basin, Iran. *Sci. Total Environ.* 708, 134874. doi:10.1016/j.scitotenv.2019.134874

Bakker, K. (2012). Water Security: Research Challenges and Opportunities. *Science* 337 (6097), 914–915. doi:10.1126/science.1226337

Behboudian, M., Kerachian, R., Motlaghzadeh, K., and Ashrafi, S. (2021). Evaluating Water Resources Management Scenarios Considering the Hierarchical Structure of Decision-Makers and Ecosystem Services-Based Criteria. *Sci. Total Environ.* 751, 141759. doi:10.1016/j.scitotenv.2020.141759

Bian, Y., Yan, S., and Xu, H. (2014). Efficiency Evaluation for Regional Urban Water Use and Wastewater Decontamination Systems in China: A DEA Approach. *Resour. Conservation Recycling* 83, 15–23. doi:10.1016/j.resconrec.2013.11.010

Carter, T. R., Jones, R. N., Lu, X., Bhadwal, S., Conde, C., Mearns, L. O., et al. (2007). "New Assessment Methods and the Characterisation of Future Conditions," in *Climate Change 2007: Impacts, Adaptation and Vulnerability. Contribution of Working Group II to the Fourth Assessment Report of the Intergovernmental Panel on Climate Change*. Editors M. L. Parry, O. F. Canziani, J. P. Palutikof, P. J. van der Linden, and C. E. Hanson (Cambridge, United Kingdom: Cambridge University Press), 133–171.

Cui, Z. L. (2009). *Study on the Water Resources Allocation for the Weihe River in Shaanxi Province*. Yangling, China: Northwest A&F University. (in Chinese).

Dawadi, S., and Ahmad, S. (2013). Evaluating the Impact of Demand-Side Management on Water Resources under Changing Climatic Conditions and Increasing Population. *J. Environ. Manag.* 114, 261–275. doi:10.1016/j.jenvman.2012.10.015

Dou, X., Song, J., Wang, L., Tang, B., Xu, S., Kong, F., et al. (2018). Flood Risk Assessment and Mapping Based on a Modified Multi-Parameter Flood hazard index Model in the Guanzhong Urban Area, China. *Stoch Environ. Res. Risk Assess.* 32 (4), 1131–1146. doi:10.1007/s00477-017-1429-5

Gleeson, T., Wada, Y., Bierkens, M. F. P., and van Beek, L. P. H. (2012). Water Balance of Global Aquifers Revealed by Groundwater Footprint. *Nature* 488 (7410), 197–200. doi:10.1038/nature11295

Gohari, A., Eslamian, S., Mirchi, A., Abedi-Koupaei, J., Massah Bavani, A., and Madani, K. (2013). Water Transfer as a Solution to Water Shortage: A Fix that Can Backfire. *J. Hydrol.* 491, 23–39. doi:10.1016/j.jhydrol.2013.03.021

Grouillet, B., Fabre, J., Ruelland, D., and Dezetter, A. (2015). Historical Reconstruction and 2050 Projections of Water Demand under Anthropogenic and Climate Changes in Two Contrasted Mediterranean Catchments. *J. Hydrol.* 522, 684–696. doi:10.1016/j.jhydrol.2015.01.029

Huang, X. G. (2007). *Shaanxi Province Water Resources Natural Gift Characteristic and its Development Make Use of Strategic Research*. Xi'an, China: Chang'an University. (in Chinese).

Jiang, H., Simonovic, S. P., Yu, Z., and Wang, W. (2020). A System Dynamics Simulation Approach for Environmentally Friendly Operation of a Reservoir System. *J. Hydrol.* 587, 124971. doi:10.1016/j.jhydrol.2020.124971

Kotir, J. H., Smith, C., Brown, G., Marshall, N., and Johnstone, R. (2016). A System Dynamics Simulation Model for Sustainable Water Resources Management and Agricultural Development in the Volta River Basin, Ghana. *Sci. Total Environ.* 573, 444–457. doi:10.1016/j.scitotenv.2016.08.081

Li, Z., Li, C., Wang, X., Peng, C., Cai, Y., and Huang, W. (2018). A Hybrid System Dynamics and Optimization Approach for Supporting Sustainable Water Resources Planning in Zhengzhou City, China. *J. Hydrol.* 556, 50–60. doi:10.1016/j.jhydrol.2017.11.007

Liu, H., Benoit, G., Liu, T., Liu, Y., and Guo, H. (2015). An Integrated System Dynamics Model Developed for Managing lake Water Quality at the Watershed Scale. *J. Environ. Manag.* 155, 11–23. doi:10.1016/j.jenvman.2015.02.046

Liu, S., Crossman, N. D., Nolan, M., and Ghirmay, H. (2013). Bringing Ecosystem Services into Integrated Water Resources Management. *J. Environ. Manag.* 129, 92–102. doi:10.1016/j.jenvman.2013.06.047

Mirauda, D., and Ostoich, M. (2011). Surface Water Vulnerability Assessment Applying the Integrity Model as a Decision Support System for Quality Improvement. *Environ. Impact Assess. Rev.* 31 (3), 161–171. doi:10.1016/j.eiar.2010.07.003

Mohamed, M. M., El-Shorbagy, W., Kizhisseri, M. I., Chowdhury, R., and McDonald, A. (2020). Evaluation of Policy Scenarios for Water Resources Planning and Management in an Arid Region. *J. Hydrol. Reg. Stud.* 32, 100758. doi:10.1016/j.ejrh.2020.100758

Naderi, M. M., Mirchi, A., Bavani, A. R. M., Goharian, E., and Madani, K. (2021). System Dynamics Simulation of Regional Water Supply and Demand Using a Food-Energy-Water Nexus Approach: Application to Qazvin Plain, Iran. *J. Environ. Manag.* 280, 111843. doi:10.1016/j.jenvman.2020.111843

Naghdi, S., Bozorg-Haddad, O., Khorsandi, M., and Chu, X. (2021). Multi-objective Optimization for Allocation of Surface Water and Groundwater Resources. *Sci. Total Environ.* 776, 146026. doi:10.1016/j.scitotenv.2021.146026

Omer, A., Elagib, N. A., Zhuguo, M., Saleem, F., and Mohammed, A. (2020). Water Scarcity in the Yellow River Basin under Future Climate Change and Human Activities. *Sci. Total Environ.* 749, 141446. doi:10.1016/j.scitotenv.2020.141446

Poff, N. L., Allan, J. D., Palmer, M. A., Hart, D. D., Richter, B. D., Arthington, A. H., et al. (2003). River Flows and Water Wars: Emerging Science for Environmental Decision Making. *Front. Ecol. Environ.* 1 (6), 298–306. doi:10.1890/1540-9295(2003)001[0298:rfawwe]2.0.co;2

Ran, Z., and Tao, F. (2017). Contributions of Climate Change and Human Activities to Runoff Change in Seven Typical Catchments across China. *Sci. Total Environ.* 605-606 (dec.15), 219–229. doi:10.1016/j.scitotenv.2017.06.210

Sahin, O., Stewart, R. A., and Porter, M. G. (2015). Water Security through Scarcity Pricing and Reverse Osmosis: a System Dynamics Approach. *J. Clean. Prod.* 88, 160–171. doi:10.1016/j.jclepro.2014.05.009

Scott, C. A., Zilio, M. I., Harmon, T., Zuniga-Teran, A., Díaz-Caravantes, R., Hoyos, N., et al. (2021). Do ecosystem Insecurity and Social Vulnerability lead to Failure of Water Security. *Environ. Develop.* 38, 100606. doi:10.1016/j.envdev.2020.100606

Simonovic, S. P. (2009). *Managing Water Resources: Methods and Tools for a Systems Approach*. London;Paris: UNESCO.

Sivapalan, M. (2015). Debates-Perspectives on Socio-Hydrology: Changing Water Systems and the "tyranny of Small Problems"-Socio-Hydrology. *Water Resour. Res.* 51 (6), 4795–4805. doi:10.1002/2015WR017080

Soledad Brendel, A., Yael Bohn, V., and Piccolo, M. C. (2017). Variabilidad de la precipitación y su relación con los rendimientos agrícolas en una región semiárida de la llanura pampeana (Argentina). *Estud. Geogr.* 78 (282), 7–29. doi:10.3989/estgeogr.201701

Song, J., Tang, B., Zhang, J., Dou, X., Liu, Q., and Shen, W. (2018). System Dynamics Simulation for Optimal Stream Flow Regulations under Consideration of Coordinated Development of Ecology and Socio-Economy in the Weihe River Basin, China. *Ecol. Eng.* 124, 51–68. doi:10.1016/j.ecoleng.2018.09.024

Sterman, D. J. (2000). *Business Dynamics: Systems Thinking and Modelling for a Complex World*. United States of America: The McGraw-Hill Companies.

Sterman, J. D. (2012). "Sustaining Sustainability: Creating a Systems Science in a Fragmented Academy and Polarized World," in *Sustainability Science: The Emerging Paradigm and the Urban Environment*. Editors M. P. Weinstein and R. E. Turner (New York, NY: Springer New York), 21–58. doi:10.1007/978-1-4614-3188-6_2

Sun, P., Wu, Y., Gao, J., Yao, Y., Zhao, F., Lei, X., et al. (2020). Shifts of Sediment Transport Regime Caused by Ecological Restoration in the Middle Yellow River Basin. *Sci. Total Environ.* 698, 134261. doi:10.1016/j.scitotenv.2019.134261

Sun, Y., Liu, N., Shang, J., and Zhang, J. (2017). Sustainable Utilization of Water Resources in China: A System Dynamics Model. *J. Clean. Prod.* 142, 613–625. doi:10.1016/j.jclepro.2016.07.110

SXBS (Shaanxi Bureau of Statistics), SXITNBSC (Shaanxi Investigation Team of National Bureau of Statistics of China) (2002–2020). *Shaanxi Statistical Yearbook*. Beijing: China Statistics Press. (in Chinese).

Tang, B. (2018). *Rational Allocation of Economic Water and Ecological Water for River Health in the Weihe River*. Xi'an, China: Northwest University. (in Chinese).

UNDP (2015). Goal 6: Clean Water and Sanitation. [WWW Document]. UNDP. https://www.undp.org/content/undp/en/home/sustainable-development-goals/goal-6-clean-water-and-sanitation.html (Accessed April 16, 2020).

UNEP (2012). *Status Report on the Application of Integrated Approaches to Water Resources Management*.

Vörösmarty, C. J., Green, P., Salisbury, J., and Lammers, R. B. (2000). Global Water Resources: Vulnerability from Climate Change and Population Growth. *Science* 289 (5477), 284–288. doi:10.1126/science.289.5477.284

Wang, W., Zhang, Y., and Tang, Q. (2020). Impact Assessment of Climate Change and Human Activities on Streamflow Signatures in the Yellow River Basin Using the Budyko Hypothesis and Derived Differential Equation. *J. Hydrol.* 591 (7401), 125460. doi:10.1016/j.jhydrol.2020.125460

Wei, S., Yang, H., Song, J., Abbaspour, K. C., and Xu, Z. (2012). System Dynamics Simulation Model for Assessing Socio-Economic Impacts of Different Levels of Environmental Flow Allocation in the Weihe River Basin, China. *Eur. J. Oper. Res.* 221 (1), 248–262. doi:10.1016/j.ejor.2012.03.014

Wei, S., Zhao, J., and Tong, X. (2020). Impacts of Socio-Economic Status and Environmental Attitudes of Locals on E-Flow Allocation in Weihe River Basin, China. *HydroResearch* 3, 158–165. doi:10.1016/j.hydres.2020.11.004

Xu, J., Tu, Y., and Zeng, Z. (2013). Bilevel Optimization of Regional Water Resources Allocation Problem under Fuzzy Random Environment. *J. Water Resour. Plann. Manage.* 139 (3), 246–264. doi:10.1061/(ASCE)WR.1943-5452.0000248

Yang, F., Wang, D., Zhao, L., and Wei, F. (2021). Efficiency Evaluation for Regional Industrial Water Use and Wastewater Treatment Systems in China: A Dynamic Interactive Network Slacks-Based Measure Model. *J. Environ. Manage.* 279 (6), 111721. doi:10.1016/j.jenvman.2020.111721

Yang, S., Bai, Y., Alatalo, J. M., Wang, H., Jiang, B., Liu, G., et al. (2021). Spatio-temporal Changes in Water-Related Ecosystem Services Provision and Trade-Offs with Food Production. *J. Clean. Prod.* 286, 125316. doi:10.1016/j.jclepro.2020.125316

Zare, F., Elsawah, S., Bagheri, A., Nabavi, E., and Jakeman, A. J. (2019). Improved Integrated Water Resource Modelling by Combining DPSIR and System Dynamics Conceptual Modelling Techniques. *J. Environ. Manag.* 246, 27–41. doi:10.1016/j.jenvman.2019.05.033

Zhao, Y., Hu, C., Zhang, X., Lv, X., Yin, X., and Wang, Z. (2021). Response of Sediment Discharge to Soil Erosion Control in the Middle Reaches of the Yellow River. *Catena* 203, 105330. doi:10.1016/j.catena.2021.105330

Zilio, M. I., Seitz, C., Scordo, F., Gil, V., Zapperi, P., Costilla, P., et al. (2019). Is Collaborative Management Always Possible? the Case of Sauce Grande River Basin, Argentina. *Int. J. River Basin Manage.* 17 (2), 251–261. doi:10.1080/15715124.2018.1546727

Conflict of Interest: The authors declare that the research was conducted in the absence of any commercial or financial relationships that could be construed as a potential conflict of interest.

Publisher's Note: All claims expressed in this article are solely those of the authors and do not necessarily represent those of their affiliated organizations, or those of the publisher, the editors and the reviewers. Any product that may be evaluated in this article, or claim that may be made by its manufacturer, is not guaranteed or endorsed by the publisher.

frontiers in Earth Science

ORIGINAL RESEARCH
published: 18 January 2022
doi: 10.3389/feart.2021.805276

Daily Variations in pCO_2 and fCO_2 in a Subtropical Urbanizing Lake

Rongjie Yang[1], Yingying Chen[1], Jie Du[2], Xiangjun Pei[3], Jinghua Li[1], Zan Zou[1] and Huixing Song[1]**

[1]College of Landscape Architecture, Sichuan Agricultural University, Chengdu, China, [2]Jiuzhaigou National Nature Reserve Administration, A'ba Tibetan and Qiang Autonomous Prefecture, A'ba, China, [3]Institute of Ecological and Environment, Chengdu University of Technology, Chengdu, China

The transfer of CO_2 from lakes to the atmosphere is a component of the global carbon equilibrium, while the quantification of the CO_2 partial pressure (pCO_2) is critical for exploring the contribution of freshwater CO_2 emissions in the regional/global carbon budget. To investigate the daily variability of pCO_2 and CO_2 fluxes (fCO_2), we conducted *in situ* biweekly pCO_2 detection at 7:00, 10:00, 14:00, and 17:00 China Standard Time (CST) from Jan. to Sept. 2020 in the subtropical urbanizing Qinglonghu Lake in Chengdu, Sichuan, China. The pCO_2 during the daytime varied greatly from 8.3 to 1,061.3 μatm, with an average of 137.7 μatm, while the average pCO_2 (n = 11) clearly gradually decreased from 7:00 CST (204.9 ± 295.7 μatm) to 17:00 CST (93.5 ± 105.5 μatm). Similarly, the average fCO_2 values were −19.3 (±27.5), −24.8 (±20.7), −29.2 (±9.1) and −30.4 (±10.7) mmol m^2 h^{-1} at 7:00–17:00 CST, respectively. Further, we observed a negative correlation between pCO_2 and water temperature and dissolved oxygen, but a positive correlation between pCO_2 and total organic carbon and chlorophyll *a*. By a systematic overview of previously published data, we also discussed the differences and uncertainties in pCO_2 and fCO_2 estimates at regional and global scales. We therefore speculate that uncertainties may exist in the contributions of CO_2 balance on lake surface in regional/global carbon budgets due to this daily pCO_2 variation.

Keywords: CO_2 evasion, CO_2 fluxes, environmental factors, middle-eutropher, pCO_2, subtropical urbanizing lake

OPEN ACCESS

Edited by:
Xiaofei Yu,
Northeast Normal University, China

Reviewed by:
Bernhard Wehrli,
ETH Zürich, Switzerland
Andrea Pain,
University of Maryland Center for Environmental Science (UMCES), United States

****Correspondence:***
Xiangjun Pei
Peixj0119@tom.com
Huixing Song
Songhuixing@sicau.edu.cn

Specialty section:
This article was submitted to Hydrosphere, a section of the journal Frontiers in Earth Science

Received: *30 October 2021*
Accepted: *20 December 2021*
Published: *18 January 2022*

Citation:
Yang R, Chen Y, Du J, Pei X, Li J, Zou Z and Song H (2022) Daily Variations in pCO_2 and fCO_2 in a Subtropical Urbanizing Lake. Front. Earth Sci. 9:805276. doi: 10.3389/feart.2021.805276

INTRODUCTION

Since the Industrial Revolution, human activities, such as the consumption of fossil fuels and the exacerbation of land development (e.g., uncontrolled deforestation and rapid urbanization), have increased atmospheric carbon (C) by approximately 40% (Xu et al., 2019; Li Q. et al., 2020; Wang et al., 2021). From 2007 to 2016, approximately 10.7 ± 1.2 Gg C yr^{-1} of anthropogenic carbon was released into the atmosphere globally, of which 4.7 ± 0.1 Gg C yr^{-1} remains in the atmosphere (Le Quéré et al., 2018; Chen and Hu, 2019; León-Palmero et al., 2020). The absorption of carbon dioxide (CO_2) by the ocean (ca. 2.4 ± 0.5 Gg C yr^{-1}) has caused ocean acidification (an increase of ca. 30% acidity) or surface-water pH decline (ca. 0.1 units), resulting in a decline of marine biodiversity and ecosystem functions (Dickinson et al., 2012; Chen et al., 2017; Chen and Hu, 2019). Furthermore, CO_2 emitted into the atmosphere from aquatic ecosystems, including inland freshwater ecosystems, such as urban lakes, can greatly contribute to climate change, as verified by previous works (IPCC, 2014; Wen et al., 2017). Correspondingly, the global carbon balance and hydrological processes are rapidly becoming urgent issues in studies of anthropogenic impacts.

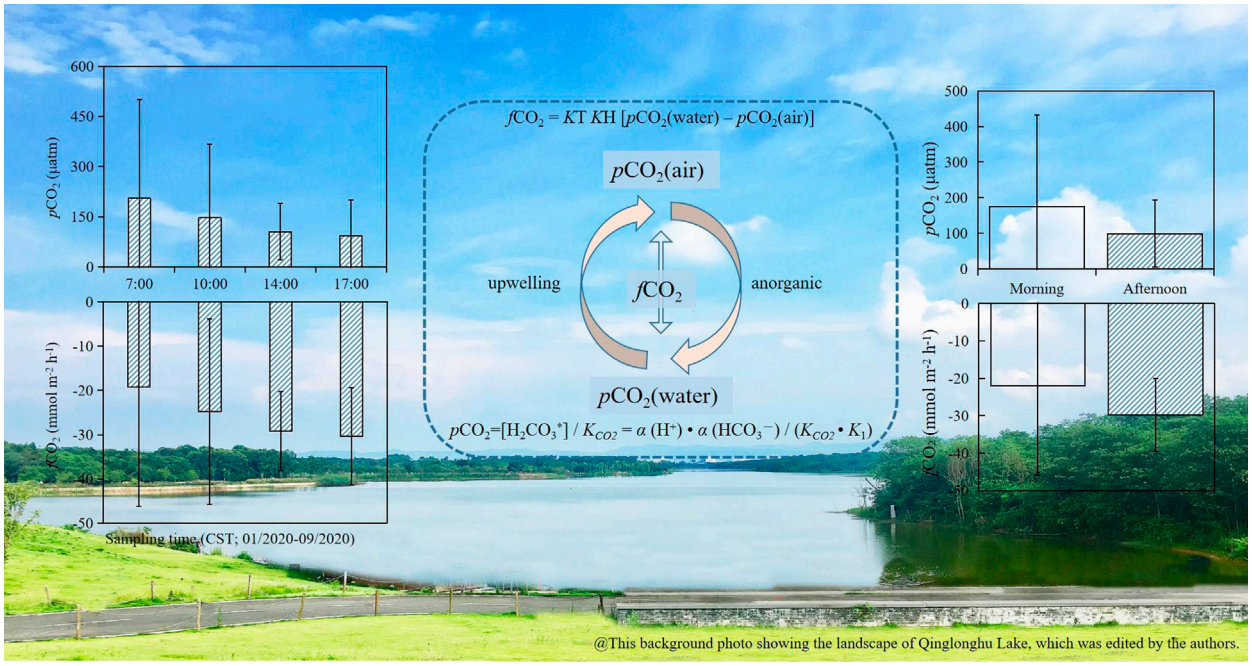

GRAPHICAL ABSTRACT |

Inland waters are a small but crucial part of the global carbon cycle (Peter et al., 2014; Yang et al., 2019); the net carbon flux of aquatic ecosystems per unit area is greater than that of surrounding terrestrial ecosystems (Karim et al., 2011). Many publications have reported that 90% of inland lakes worldwide are supersaturated with CO_2 compared to the atmosphere and are therefore considered sources of atmospheric CO_2 (Cole et al., 1994; Karim et al., 2011). As a result, CO_2 outgassing from inland lakes represents a significant contribution to the global carbon equilibrium (Marce et al., 2015). Based on previous evaluations, CO_2 emissions from global inland lakes to the atmosphere are more than 1.4 Pg C yr^{-1} (Li et al., 2012; Keller et al., 2020), of which 60% are from freshwater lakes and 40% are from saline lakes (Cole et al., 1994; Tranvik et al., 2009; Raymond et al., 2013). Furthermore, the level of dissolved CO_2 in inland lakes is higher than the typical level (i.e., 380–420 μatm; Sabine et al., 2004; Abril et al., 2014; Li Q. et al., 2020, Li S. et al., 2020) of atmospheric CO_2, suggesting that freshwater has the potential to degas aqueous CO_2 into the atmosphere (Li et al., 2012). Therefore, CO_2 emissions from inland lakes to the atmosphere are an important part of the global and regional carbon budget.

The surface-water CO_2 partial pressure (hereafter pCO_2) is one of the key parameters quantified in research works to better understand the changes in carbon cycling globally. In general, surface-water pCO_2 is mainly controlled by four interrelated phenomena: thermodynamic effects, physical mixing, biological activities, and water-atmosphere CO_2 inter-exchange (Yang et al., 2019; Wang et al., 2021). Aquatic environmental variables, such as surface acidity (Pardue et al., 1988), trophic states (Tonetta et al., 2014), chlorophyll level (Xu et al., 2019; Yang et al., 2019), and water temperature (Marotta et al., 2009; Kosten et al., 2010), and other parameters, such as dissolved oxygen (DO), wind speed and solar radiation (Marce et al., 2015; Chen et al., 2017), are closely related to these four phenomena and might cause fluctuations in the spatial-temporal variability of pCO_2 and CO_2 evasion. Regarding inland freshwater systems, numerous studies have been conducted to investigate pCO_2 and CO_2 evasion in large rivers (with widths greater than 100 m), such as the Amazon (Richey et al., 2002; Abril et al., 2014), Mississippi (Crawford et al., 2016), Yangtze (Li et al., 2012; Liu et al., 2017) and Yellow Rivers (Ran et al., 2015). The results have revealed that the concentrations of CO_2 in these rivers are higher than those in the overlying atmosphere (i.e., that these rivers exhibit CO_2 supersaturation), suggesting that these rivers are the "source" of CO_2 in the atmosphere (Yoon et al., 2017; Li S. et al., 2020). Unlike the conditional conversion between the "source" and "sink" roles of marine ecosystems (Sabine et al., 2004; Yan et al., 2018), most inland lakes/reservoirs function as net "sources" of CO_2 because they are heterotrophic systems, similar to rivers (Cole et al., 1994; Richey et al., 2002; Gu et al., 2011), while some small productive lakes as carbon "sinks" (Maier et al., 2021 and related refs.). Currently, the temporal variability of CO_2 in lakes/streams is taken into account in many studies, which find similar relationships between photosynthesis and remineralization in response to variations in solar insolation (Alin and Johnson, 2007; Callbeck et al., 2010; Marotta et al., 2010; Tonetta et al., 2014). However, lots of the field data collected for CO_2 evasion estimation have low temporal resolution, such as weekly to quarterly, and therefore ignore the diurnal variation in pCO_2 and thus the CO_2 flux.

FIGURE 1 | Geographical location of Qinglonghu Lake in the city of Chengdu, Sichuan, Southwest China. *Ws* represents the location of water sample collection and on-site dynamic monitoring. The above is a modified graph based on the Google® Maps (https://www.google.cn/maps).

In addition, aquatic pCO_2 is markedly affected by photosynthesis (P) and respiration (R), which are driven by temperature and radiation in different geographic regions (Marotta et al., 2010; Tonetta et al., 2014; Xu et al., 2019). For example, the average CO_2 flux in the headwater catchment area of the Alaska Highlands, in Arctic tundra, is 5.1 μmol C m^2 s^{-1} (Crawford et al., 2013), while the average CO_2 emissions in the two reservoirs in Spain (Guadalcacín and Bornos), in the Mediterranean climate, are between 5.6 and 34.7 μmol C m^2 s^{-1} (Morales-Pineda et al., 2014). Accordingly, the influences of diel pCO_2 changes on the estimation of CO_2 degassing and uncertainties in these estimates remain unclear, although the estimation of CO_2 emissions on a regional/global scale has been strengthened through many studies. Thus, to reduce the uncertainty of CO_2 evasion estimation, we need to consider the changes in air-water pCO_2 and CO_2 flux (i.e., fCO_2) over the span of a day, thereby limiting these factors that cause data scatters and variances.

There is still a knowledge gap regarding the daily change in pCO_2 and fCO_2, while previous studies mainly focused on weekly to quarterly data. Based on the aforementioned background, an *in situ* investigation of the daily changes in pCO_2 and fCO_2 in a subtropical urbanized lake (named Qinglonghu Lake) was conducted in Chengdu, Southwest China. Specifically, the objectives of our study are to 1) monitor fortnightly the water-air pCO_2 and related environmental parameters during the daytime from Jan. to Sept. 2020; 2) evaluate fCO_2 by employing the measured pCO_2 and discuss the uncertainties in CO_2 evasion estimation; and 3) explore the roles of environmental factors and the in-lake CO_2 exchange behaviours. The findings will significantly improve our understanding of the mechanisms of daily pCO_2 variations and increase the accuracy of CO_2 evasion estimations in freshwater environments.

METHODS

Site Description

This study was conducted at Qinglonghu Lake (longitude 104°11′14″ E, latitude 30°38′26″ N) in Chengdu, Southwest China (**Figure 1**). The lake is located in the Round-the-city Ecological Zone of Chengdu, which is the largest urban wetland in the city and is used for the construction of a lake-forest system. The lake has an open water surface of approximately 82 ha, a circumference of 12 km, and a depth ranging from 0.5 to 6.0 m (Li and Cai, 2019). The lake was irrigated from the Dongfeng Canal in April 2008 and officially opened in Jan. 2016.

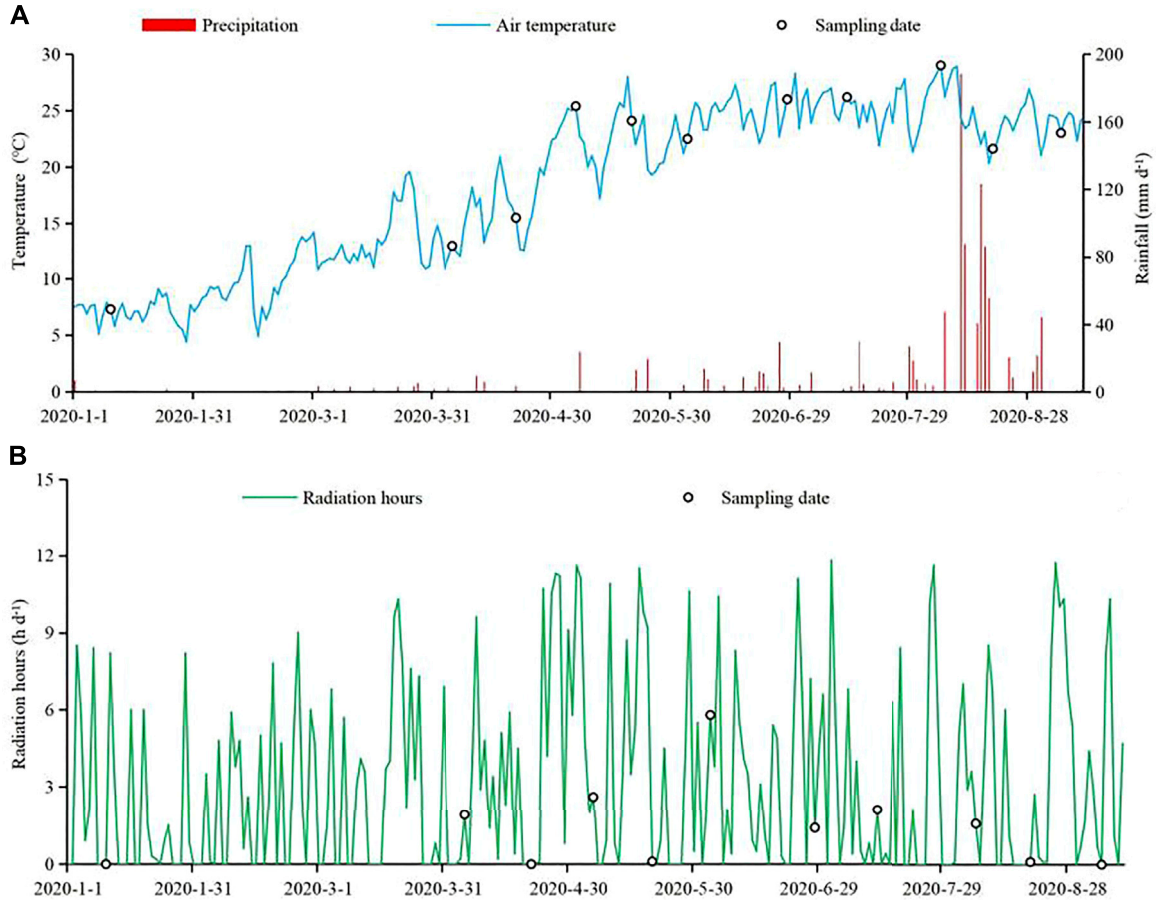

FIGURE 2 | Daily air temperature and precipitation (**(A)**; mm d^{-1}) and radiation (**(B)**; h d^{-1}) during the study period in Qinglonghu Lake. The hollow circles represent the dates of sampling and monitoring of water samples. The data in the above figures have been authorized by the National Meterological Data Center of China (https://data,cma,cn/) via the authors' emails.

The study region has a humid subtropical climate with a long frost-free period and abundant rainfall; the average annual air temperature is 16.5°C, with the lowest air temperature in January (4.6°C) and the highest air temperature in July or August (~37.5°C). During the 9-months investigation period, the average daily air temperature around the lake was −5 to 30°C, with the highest air temperature in August and the lowest air temperature in January (**Figure 2A**). Moreover, the annual average rainfall is approximately 900 mm. Less precipitation occurs in spring, but more precipitation occurs in summer (e.g., ~200 mm in Aug. 2020), which can easily cause floods. The annual average number of solar radiation hours is approximately 1,032, and the number of radiation hours from April to August was higher than that from January to March during the study period (**Figure 2B**).

Field Measurements

In this study, we conducted biweekly field trips from Jan. to Sept. 2020 to measure pCO_2 and related water quality parameters. Based on previous full-scale investigations, an open site near the lake outflow was selected for water sample collection and parameter monitoring (**Figure 1**). During each trip, *in situ* measurements were taken at 7:00, 10:00, 14:00, and 17:00 China Standard Time (CST) at approximately 2 m from the lake shore, which was based on previous studies such as Perkins et al. (2015), Xu et al. (2019), and Yang et al. (2019). All measurements were carried out at the same location. To minimize the influences of rainfall/runoff and avoid the potential bias in measurements, all trips were made on sunny days to avoid weather conditions such as rainfall, winds and runoff by adjusting the timing. All on-site detected parameters (including pH, water temperature (t_{water}), transparency (TPC), turbidity (FNU), electrical conductivity (EC), total dissolved solids (TDS), DO, bicarbonate (HCO_3^-; BCB) and carbonate (CO_3^{2-}; CB) were measured at a depth of 30–50 cm below the water surface, and recordings were taken after the instrument reading had remained stable for 3–5 min.

Among the detected parameters, TPC was measured using a black-and-white disc with a diameter of 200 mm, while FNU was monitored using a TSS portable turbidity meter (HACH, TSS Portable, Danaher, United States). The other parameters, including pH, EC, TDS, and t_{water} were measured by a Hanna

multiparameter pen-type detector (Hanna-HI9829, Hanna Instruments Co., Ltd., Italy). The DO and DO saturation (DO %) were monitored using a Hanna-HI98186 portable high-precision DO meter.

Unlike oceanography, there is currently no consistent definition of an appropriate method for measuring or calculating pCO_2 in freshwater. There are direct and indirect methods for measuring pCO_2 using acidimetric titrations. An indirect method that greatly simplifies the alkalinity determination procedure by titrating to pH 4.5 and has been widely used, especially for freshwater with pH > 7 and low organic carbon, i.e., pCO_2 is calculated via pH/alkalinity in particular (Telmer and Veizer, 1999; Butman and Raymond, 2011; Wang et al., 2011). Moreover, currently direct measurements of water pCO_2 remain scarce in freshwater, and most published pCO_2 data are calculated from temperature, pH and total alkalinity using the above indirect method (e.g., Li et al., 2013; Abril et al., 2015; Varol and Li, 2017; Xiao et al., 2020; Ni et al., 2021). As we know, the alkalinity and pH are critical for pCO_2 calculations, in particular, a pH difference of 0.005 unit could affect pCO_2 calculations (Li et al., 2013). Therefore, we carefully scrutinized the values as follows: 1) the pH probes were carefully calibrated, 2) the *in situ* pH values were recorded when the pH stabilized in 0.01 units for 3–5 min, and 3) three replicates for individual samples were determined for alkalinity and the mean values were taken. Our investigation found that our studied freshwater lake has the pH from circumneutral to basic (~8.8) and the alkalinity exceeding 1,000 μmol L^{-1} (Abril et al., 2015), suggesting that the calculation of pCO_2 from pH, alkalinity and temperature is effective reliability. Following the previous classic **Eq. 1**, therefore, pCO_2 was calculated by detecting the pH, bicarbonate, ion concentrations and Henry's law constant (K_h) of water (Telmer and Veizer, 1999).

$$CO_2 + OH^- + H^+ \Leftrightarrow H_2CO_3^* \Leftrightarrow H^+ + HCO_{3^-} \Leftrightarrow 2H^+ + CO_3^{2-} \quad (1)$$

Thus, we collected 100 ml of water samples into a 250 ml Erlenmeyer flask and then added 4 drops of phenolphthalein indicator. We also employed an HCl standard solution to titrate the solution until it became just faded or colourless and then recorded the amount of standard solution (defined as P) after it turned red. If the solution was colourless after adding the phenolphthalein indicator, it was considered unnecessary to titrate the HCl standard solution again. Subsequently, we continuously added 3 drops of standard methyl orange indicator into the Erlenmeyer flask, standardized the flask with the HCl standard solution until it turned from orange-yellow to orange-red, and then recorded the amount of standard solution (defined as M). Accordingly, the total consumption of HCl standard solution (defined as T) in the water sample was calculated as follows **Eq. 2**:

$$T = M + P \quad (2)$$

According to the different values of P (i.e., $P = T$, $p > 1/2T$, $P = 1/2T$, $p < 1/2T$, $P = 0$), the following calculation **Eqs. 3**, **4** of CB and BCB were employed:

$$CB = [2 \times P \times C_{HA} \times 30.005]/V \times 1000 \quad (3)$$

$$BCB = [(M - P) \times C_{HA} \times 61.017]/V \times 1000 \quad (4)$$

where C_{HA} represents the concentration of HCl standard solution (mol L^{-1}) and V represents the water sample volume (ml). In this study, C_{HA} was 0.025 mol L^{-1}, while V was 100 ml. In addition, (30.005) indicates the mass of CO_3^{2-} in grams (g) equivalent to 1.00 ml of HCl standard solution (C_{HA} = 1.00 mol L^{-1}), while (61.017) indicates that of HCO_3^- in grams (g).

After completing the on-site data collection, we collected water samples using a homemade polyethylene grab sampler at 7:00, 10:00, 14:00 and 17:00 CST on each trip for laboratory analysis. Briefly, 500 ml water samples were collected, and 0.5 ml $MgCO_3$ suspension (1%) was added for the determination of water chlorophyll *a* (Chl*a*). The lake water (20 ml) was filtered with a microporous membrane (50 mm × 0.45 μm; Jiangsu Green-Union Scientific Instrument Co., Ltd., Jiangsu, China) and then stored in polyethylene bottles to determine total carbon (TC) and inorganic carbon (IC). In addition, we collected 50 ml water samples and filtered them with a microporous membrane for anion (i.e., fluoride/F^-, chloride/Cl^-, sulfate/SO_4^{2-}, and nitrate/NO_3^-) detection. All samples were stored in acid-washed high-density polyethylene bottles that were capped tightly and placed in cooling vessels with enough ice during transportation.

Laboratory Analyses

The Chl*a* in water samples was detected using the acetone method following a previous protocol (The National Environmental Protection Agency, 2002). Briefly, a quantitative volume of water sample was poured onto the suction filter with a fibre membrane for complete suction filtration. The filter membrane with phytoplankton was then removed, dried at a low temperature in a refrigerator for 8 h, and fully ground with $MgCO_3$ powder and 2 ml of 90% acetone to extract Chl*a*. The extraction solution was then centrifuged at 3,500 × *g* for 10 min. The supernatant was ground with 2 ml of acetone, centrifuged again for 10 min, and then transferred/diluted to 10 ml with acetone. Finally, the treated supernatant was detected by using an UV1901PCS ultraviolet spectrophotometer (Youke Instruments, Shanghai, China) at 750, 663, 645, and 630 nm, with 90% acetone as a blank. The Chl*a* concentration (mg m^{-3}) was calculated following formula **Eq. 5**:

$$Ch1a = \{[11.64 \times (D_{663} - D_{750}) - 2.16 \times (D_{645} - D_{750}) + 0.10 \times (D_{630} - D_{750})] \times V_1\}/V \times CL \quad (5)$$

where V is the volume of the water sample (L), D is the absorbance, V_1 is the constant volume of the extraction solution, and CL is the optical path of the cuvettes (cm).

Four anions were determined by ion chromatography following the National Environmental Protection Standards of China (HJ 84-2016). Briefly, the water samples were filtered through a 0.45 μm microporous membrane to determine the standard curves (F^-, R^2 = 0.9996; Cl^-, R_2 = 0.9991; NO_3^-, R^2 = 0.9998; SO_4^{2-}, R^2 = 0.9999). The concentrations (mg L^{-1}) of the four anions were then detected using IC-2800 ion chromatography (Beijing Dongxi Analytical Instrument Co., Ltd., Beijing, China).

To analyze trophic states, the other parameters such as NT (nitrate; **Supplementary Methods S1**), TP (total phosphorus; **Supplementary Methods S2**), TDN (total dissolved nitrogen; **Supplementary Methods S3**) and eutrophication evaluation [*TLI* (∑); **Supplementary Methods S4**] also were evaluated.

TC and IC were analyzed using a Total Organic Carbon Analyser (TOC-L CPH Basic System; Shimadzu Co., Kyoto, Japan). Briefly, 0–50 ml of organic carbon (i.e., potassium hydrogen phthalate), inorganic carbon (i.e., sodium carbonate/bicarbonate) and KNO_3 standard solution were added to 50 ml colorimetric tubes and then diluted. The standard curves (IC: R^2 = 1.0000; TC: R^2 = 1.0000; see **Supplementary Figure S1**) were measured by using the TOC-L CPH analyser. Before detection, these samples were bubbled with nitrogen to remove inorganic carbon (CO_2) (Kortelainen, 1993; Bisutti et al., 2004). Moreover, a filter was used when the tested water samples contained insoluble particles, and the pore size of the filter membrane was ≤60 μm. During the detection, to ensure that no-air (CO_2) entered, the sampling tubes were submerged below the liquid surface, and the nozzle of the tube was placed at about 1/3 of the height of the solution near the bottom of the container. The calculations of TC and IC (mg L^{-1}) were based on the peak height of the absorption peak, which subtracts the correction value of the peak height from the blank test absorption peak. Accordingly, the total organic carbon (TOC) concentration (mg L^{-1}) was estimated using **Eq. 6**

$$\mathrm{TOC} = \mathrm{TC} - \mathrm{IC} \tag{6}$$

pCO_2 and CO_2 Flux Calculation

Detection of pCO_2

Previous studies have confirmed that dissolved inorganic carbon in water is composed of HCO_3^-, CO_3^{2-}, H_2CO_3, and dissolved CO_2. When the aqueous solution is in equilibrium, the concentration of each component is related to the pH, temperature and ionic strength of the water (ref. Cole and Caraco, 1998; Telmer and Veizer, 1999; Yao et al., 2007; Abril et al., 2015). Accordingly, in our work, based on the pH, HCO_3^-, CO_3^{2-}, K_h and ions in water, the water-air pCO_2 was calculated employing the CB equilibrium model (see **Supplementary Methods S5** in detail). Based on the Henry's Law, pCO_2 (μatm) is calculated by the following **Eq. 7**:

$$pCO_2 = \left[H_2CO_3^*\right]/K_{CO2} = \alpha(H^+)\cdot\alpha\left(HCO_3^*\right)/\left(K_{CO2}\cdot K_1\right) \tag{7}$$

where α (H^+) and α (HCO_3^-) represent the ion activities of [H^+] and [HCO_3^-], respectively (**Eqs. 8**, **9**), while *I* represents the ionic strength **Eq. 10**.

$$\alpha(H^+) = 10^{-[\mathrm{pH}]} \tag{8}$$

$$\alpha\left(HCO_3^-\right) = \left[HCO_3^-\right]\times 10^{-0.5\sqrt{I}} \tag{9}$$

$$I = 0.5\left(\left[K^+\right] + 4\left[Ca^{2+}\right] + \left[Na^+\right] + 4\left[Mg^{2+}\right] + \left[Cl^-\right] + 4\left[SO_4^{2-}\right] + \left[NO^{3-}\right] + \left[HCO_3^-\right]\right) \tag{10}$$

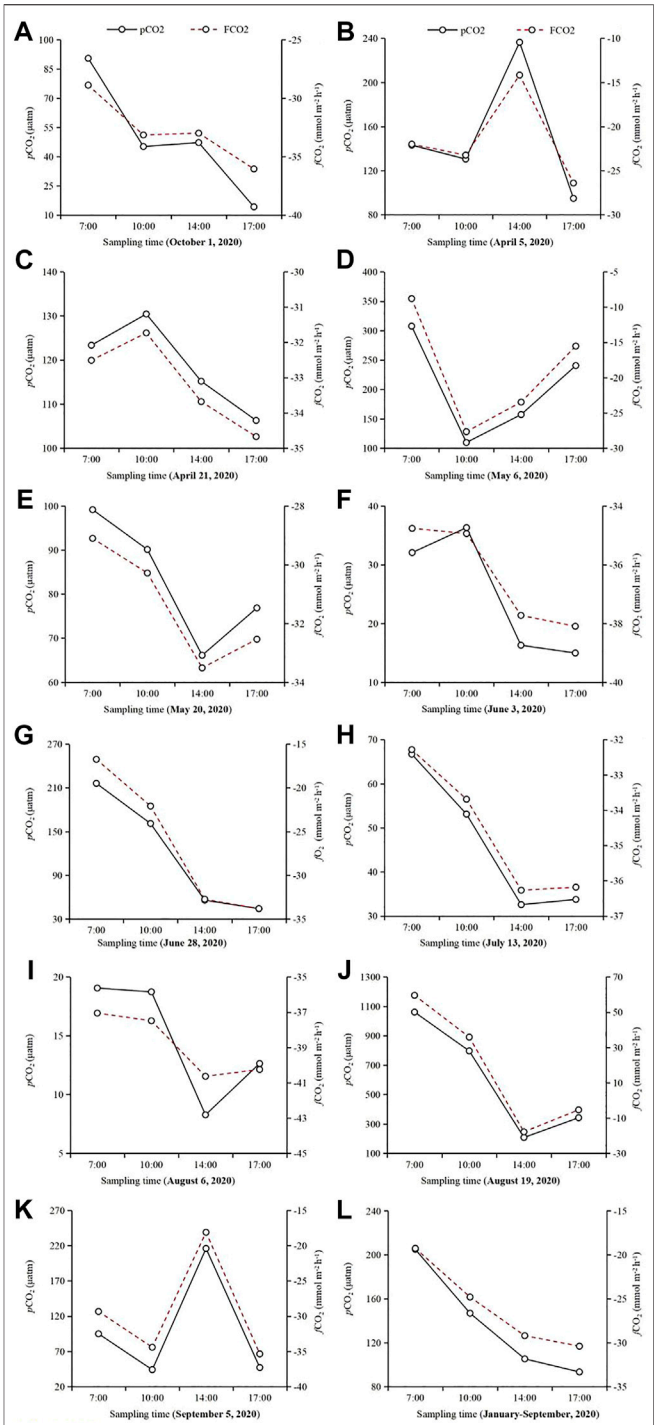

FIGURE 3 | Hourly measurements of water pCO_2 and estimation of fCO_2 in Qinglonghu Lake. **(A–K)**: The dots represents the pCO_2 (solid line) and fCO_2 (dotted lines) at each sampling time (n = 1). **(L)**: The dots represent the average pCO_2 (solid line) and fCO_2 (dotted line) of all measurements (n = 11) at each sampling time during the study.

Calculation of fCO_2

CO_2 diffusion at the water-air interface is affected by factors such as the difference in pCO_2 between the atmosphere and water, temperature, salinity, and wind speed. Therefore, the calculation of water-air fCO_2 in our study was based on the stagnant-layer model as follows **Eq. 11** (ref. Cai and Wang,

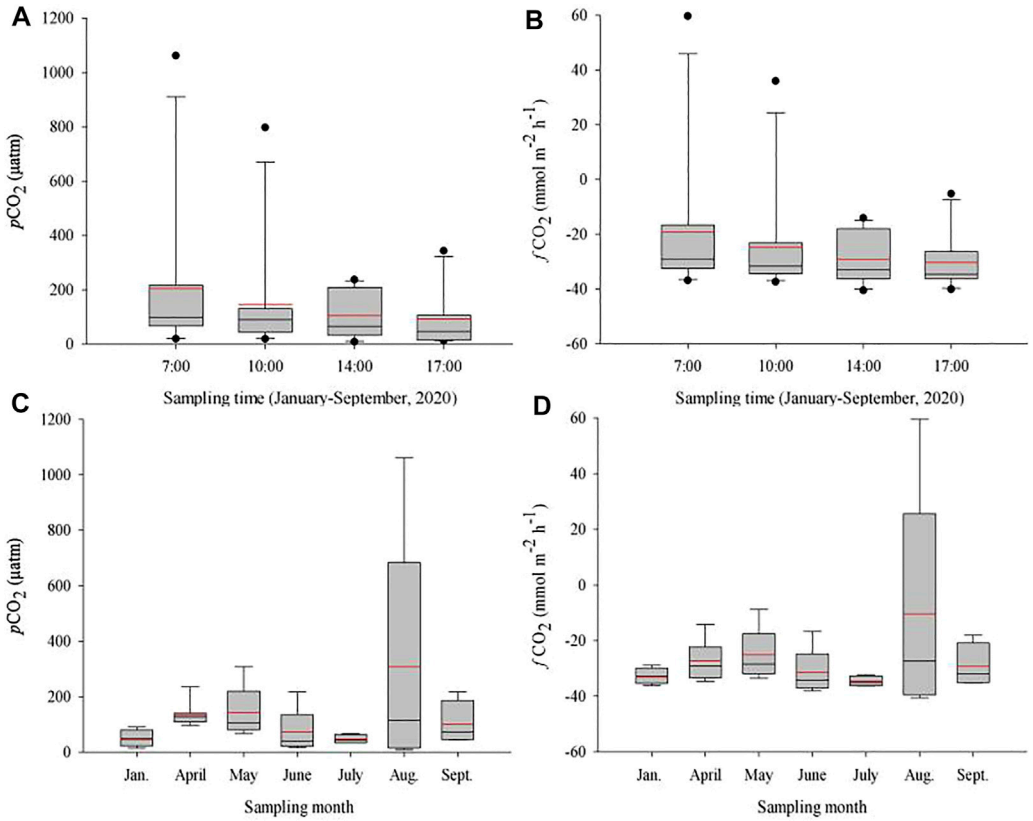

FIGURE 4 | Hourly and monthly changes in water pCO_2 **(A,C)** and fCO_2 **(B,D)** at different sampling times Jan. to Sept. 2020 in Qinglonghu Lake. The black line, red line, lower edge, upper edge, bars, dots in or outside the boxes refer to median and mean values, 25th and 75th, 5th and 95th, and <5th and >95th percentiles of all data, respectively. Figures A and B were drawn based on the data of all measures values (n = 11) at each sampling time during the study period, while Figures C and D were drawn based on the data of all measurements (n = 4, 8) in each sapmling month.

1998; Bade and Cole, 2006; see **Supplementary Methods S6** in detail):

$$fCO_2 = K_T K_H \left[pCO_{2(water)} - pCO_{2(air)} \right] \quad (11)$$

where fCO_2 indicates the flux of CO_2 at the water-air interface (mmol m^2 h^{-1}), K_H indicates the solubility of CO_2 at a certain temperature (mol L^{-1} atm^{-1}; ref. Weiss, 1970), K_T represents the gas exchange rate of CO_2 (cm h^{-1}; ref. Katul and Liu, 2017). Moreover, K_T was converted from the standardized Schmidt number of 600 (K_{600}) according to the following **Eq. 12** (Jahne et al., 1987):

$$K_T = K_{600} \times \left(\frac{600}{Sc_{CO2}} \right)^n \quad (12)$$

where n is the Schmidt number exponent that depends on the surface state of the water. n is 0.50 when the wind speed exceeds 3.7 m s^{-1} and 0.75 when the wind speed is lower than 3.7 m s^{-1} (Guérin et al., 2007). Based on the findings of Cole and Caraco (1998), the Schmidt number is taken as 0.67 under normal circumstances. [Sc_{CO_2}] represents the Schmidt number of CO_2 at a given temperature (t) (Wanninkhof, 1992). The following **Eq. 13** was used to obtain the value of K_{600} (Vachon and Prairie, 2013):

$$K_{600} = 2.07 + 0.215 U_{10^{1.7}} \quad (13)$$

where U_{10} is the wind speed normalized to a height of 10 m above the water surface at the sampling time (m s^{-1}; ref. Cole and Caraco, 1998). The data were compiled from the database of the National Meteorological Science Data Center of China (http://data.cma.cn/, Chengdu, Sichuan). This observation station is located in Longquanyi, Chengdu, which is close to the studied lake (less than 5 km away). The data were authorized by the application and were selected based on the average maximum value of 10 min of measurement on the sampling day.

Data Analysis

In this study, all statistical analyses were performed by IBM-SPSS Statistics software (IBM Corp., Armonk, New York, United States) from the contribution software platform provided (http://ms.sicau.edu.cn/soft/detail/52) for Tukey's tests at the significance level of 0.05. The figures constructed in the present study, including **Figures 4**, **6**, were generated using

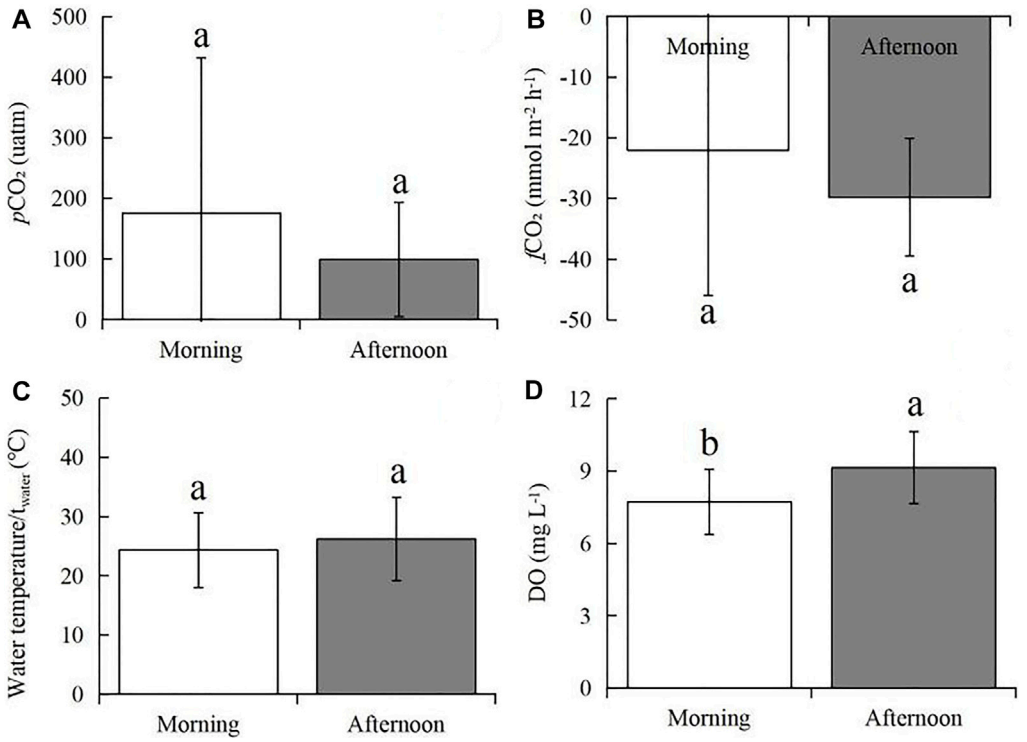

FIGURE 5 | Differences in average pCO_2 **(A)**, fCO_2 **(B)**, t_{water} **(C)**, and DO **(D)** between the morning hours (7:00–10:00 CST) and the afternoon hours (4:00–17:00 CST). The rectangular bars represent the average values of all measurements at two tome points, while the error bars represents the standard deviations (SDs) among a total of 24 testing results. Different lowercase letters indicate that the mean values are significantly different between morning and afternoon hours at $p < 0.005$ according to Turkey' tests.

TABLE 1 | Hourly changes in water quality parameters in Qinglonghu Lake.

Time/CST	t_{water}/°C	pH/NU	EC/μs cm^{-1}	TDS/mg L^{-1}	TPC/cm	FNU/NTU	DO/mg L^{-1}	Chl*a*/mg m^{-3}
7:00	23.67 ± 6.34a	8.77 ± 0.46a	254.91 ± 28.15a	127.36 ± 14.15a	54.68 ± 9.31a	15.86 ± 19.55a	7.32 ± 1.22b	28.64 ± 11.52a
10:00	24.99 ± 6.56a	8.84 ± 0.39a	253.09 ± 26.7a	125.55 ± 12.60a	55.55 ± 10.62a	11.19 ± 2.25a	8.11 ± 1.40ab	30.31 ± 14.01a
14:00	26.22 ± 6.99a	8.89 ± 0.42a	249.27 ± 27.46a	124.45 ± 13.79a	54.00 ± 10.21a	10.98 ± 2.64a	8.79 ± 1.30ab	27.48 ± 13.83a
17:00	26.20 ± 7.39a	8.98 ± 0.46a	251.45 ± 34.19a	124.00 ± 14.29a	52.91 ± 10.49a	11.44 ± 2.82a	9.48 ± 1.64a	31.80 ± 14.79a

*Different lowercase letters indicate that the means are significantly different among different sampling times (*p *< 0.05). Moreover, the values at each sampling time are the means of all measurements during the study (*n *= 11). t_{water}, water temperature; EC, electrical conductivity; TDS, total dissolved solids; TPC, transparency; FNU, turbidity; DO, dissolved oxygen; and Chl*a*, chlorophyll a.*

SigmaPlot 14.0 (Systat Software Inc., San Jose, California, United States).

RESULTS AND DISCUSSION

The Sink-Source Behaviours of CO_2 in the Mesoeutrophic Urbanizing Lake

As urbanization has accelerated in recent years, anthropogenic waste emissions have increased sharply, which has inevitably caused the deterioration of water quality in urbanizing lakes, the changes in hydrological processes, and the destruction of the water-nutrient-carbon cycle (Li S. et al., 2020). Therefore, studying the carbon dynamics of lakes and their CO_2 exchange behaviour is of great significance for understanding the carbon emissions of urbanizing lakes in developing countries.

In the present study, our field investigations showed that on all most of the sampling days from Jan. to Sept. 2020 except April 5 (with the highest pCO_2 at 14:00 CST; **Figure 3B**), May 6 (with the lowest pCO_2 at 10:00 CST; **Figure 3C**) and Sept. 5 (with the highest pCO_2 at 14:00 CST; **Figure 3K**), the concentrations of pCO_2 significantly decreased from early morning (at 7:00 CST) to late afternoon (at 17:00 CST). Among the daily pCO_2, the lowest values occurred between 14:00 and 17:00 CST, and the highest occurred between 7:00 and 10:00 CST (**Figures 3A–L**, **4**). Furthermore, the average pCO_2 (n = 11) showed a clear and gradually decreasing trend from 7:00 CST to 17:00 CST, with

average decreases rate of 39.0% from 7:00 (240.9 ± 295.7 μatm) to 10:00 CST (146.9 ± 220.5 μatm), 28.3% from 10:00 to 14:00 CST (105.4 ± 85.3 μatm), and 11.3% from 14:00 to 17:00 CST (93.5 ± 105.5 μatm) (**Figure 4A**). These findings revealed that this studied lake could be a sink of CO_2 throughout the season from January to September (except for August 19), while a sink-source phenomenon was discovered in Capitol/University Lake in central Louisiana, United States (Xu et al., 2019; Yang et al., 2019).

Interestingly, the pCO_2 on the sampling dates other than August 19 was below 400 μatm (**Figure 3**), although the pCO_2 values in the mornings were higher than those in the afternoons (**Figure 5**), which may be due mainly to the large amount of atmospheric precipitation (i.e., 80–200; **Table 1**) compared to that in our previous study (0–85 mm of rainfall; Yang et al., 2019). Studies showed that precipitation affects aquatic pCO_2, mainly due to its impact on soil respiration and carbon transport (Hope et al., 2004; Li et al., 2017). After short-term atmospheric precipitation, the biodegradation and decomposition of the labile fractions toward the top soil layers via runoff (Ran et al., 2015) are also important sources of dissolved CO_2. However, for the lake area during the dry season, long-term and high-intensity floods offset the contribution of soil CO_2 erosion input (Luo et al., 2019), thereby significantly diluting the control of lake pCO_2 and CO_2 exchange. Further, many previous studies have confirmed that precipitation stimulates complex chemical reactions at the water-air interface. The principle of these processes can be explained by the classic carbonate equilibrium equation as follows **Eq. 14**:

$$CO_2 + H_2O \leftrightarrow H_2CO_3 \leftrightarrow H^+ + HCO_3^- \leftrightarrow 2H^+ + CO_3^{2-} \quad (14)$$

When rainwater with a pH value lower than the lake water falls on the lake surface, the amount of free ion H^+ greatly increases, causing the balance of carbonates existing in the water to be disturbed and moving to the left. Therefore, in the case of excessive H^+, especially acid rain in urban areas, an extra amount of CO_2 will be produced in the surface water. Furthermore, atmospheric precipitation represents a certain chemical pressure, which depends on the quasi-stable daily rhythm of CO_2 consumption and emission by aquatic organisms. Once the CO_2 content in the surface water is excessive for a short period of time, the biota cannot respond quickly to this change, causing most of the gas to be discharged into the atmosphere. These findings have been confirmed by previous studies on the influence of atmospheric precipitation on the changes in CO_2 content at the water-air interface of the Lake Baikal in southern Eastern Siberia, Russia (Domysheva et al., 2007), University Lake in Baton Rouge, Louisiana, United States (Xu et al., 2019) and other lakes (Hastie et al., 2018 and related refs.). Accordingly, in our study, precipitation on the lake surface facilitated CO_2 exchange and can be regarded as an additional source. Besides, because the sampling site is relatively open, the overall wind speed is relatively high; this wind accelerates the exchange of water-soluble gases with the atmosphere, decreasing the pCO_2 at the water-air interface. In agreement with this study, previous publications have reported that the regression between pCO_2 and wind speed was the largest with a no-time-lag negative correlation (Morales-Pineda et al., 2014), suggesting that the acceleration of CO_2 gas-water exchange, as the main process, promoted the decrease in pCO_2 (Podgrajsek et al., 2015; Shao et al., 2015). Therefore, combining the daily CO_2 dynamic information from atmospheric precipitation and wind-speed improves the accuracy of CO_2 estimation.

TABLE 2 | Comprehensive nutritional status index *TLI (∑)* of Qinglonghu Lake.

Parameters	Means	*TLI (j)*	W_j	$W_j \times TLI\ (j)$	*TLI (∑)*
Chl*a* (mg m^{-3})	29.56	61.78	0.3261	20.14	63.15
TP (mg L–1)	0.85	54.27	0.2301	12.49	
TN (mg L^{-1})	3.26	74.55	0.2192	16.34	
TPC (m)	0.54	63.13	0.2246	14.18	

Chla, chlorophyll a; TP, total phosphorus; TN, total nitrogen; TPC, transparency. TLI (∑) *is the comprehensive nutritional status index,* W_j *is the relative weight of the nutritional status index of the* j*-th parameter, and* TLI (j) *is the nutritional status index representing the* j*-th parameter. The means are the average of all the measured indexes (*n = 44*) in this lake during the study period. In this study, NT and TDN were converted to TN (see Supplementary Fig. S2).*

In our study, the daily average pCO_2 for the whole period (i.e., Jan. to Sept. 2020) was 108.2 ± 100.8 μatm; at the monthly level, the highest daily average pCO_2 was August (308.5 ± 407.4 μatm), while the lowest was July (23.3 ± 16.4 μatm) (**Figure 4C**). Correspondingly, the levels of daily average fCO_2 decreased from 7:00 to 17:00 CST (from −19.3 ± 27.5 to −30.4 ± 10.7 mmol m^2 h^{-1}) (**Figures 3**, **4**), while the daily average fCO_2 ranged from −10.4 (±38.5) mmol m^2 h^{-1} in Aug. 2020 to −27.3 (±7.2) mmol m^2 h^{-1} in April 2020, with an average fCO_2 of −27.3 (±10.7) mmol m^2 h^{-1} (**Figures 4B,D**). These lower values indicate that the biological productivity at 1.0 m depth far surpassed CO_2 dissolution into the water. Similarly, a previous work regarding lake CO_2 evasion in central Louisiana, United States, showed that lake water can serve alternately as a seasonal source-sink of CO_2 (Xu and Xu, 2015). However, the global size distribution of lakes and ponds is a key source of uncertainty in calculating gas exchange and its contribution. Holgerson and Raymond (2016) analyzed the CO_2 concentration of 427 lakes/ponds with a surface area ranging from 2.5 m^2 to 674 km^2. The results showed that very small ponds accounted for 8.6% of the global lakes/pond area, but accounted for 15.1% of CO^2 emissions, and decreased with the increasing in the area of these lakes, which may be due to shallow water, high sediment and edge-to-water volume ratios, and frequent mixing (Kankaala et al., 2013; Holgerson, 2015). Therefore, whether the seasonal source-sink of lakes contribute to the global carbon budget depends on the flux (grams of CO_2 per unit area) and the relative contribution of such lake systems to the global lake area, which needs further investigation against our studied lake.

Many previous studies have confirmed that the two main biogeochemical processes influencing pCO_2 changes in freshwater systems are photosynthesis (P) and respiration (R) (Alin and Johnson, 2007). In this study, according to the variability of daily pCO_2 and fCO_2 (**Figures 3**, **4**), the CO_2

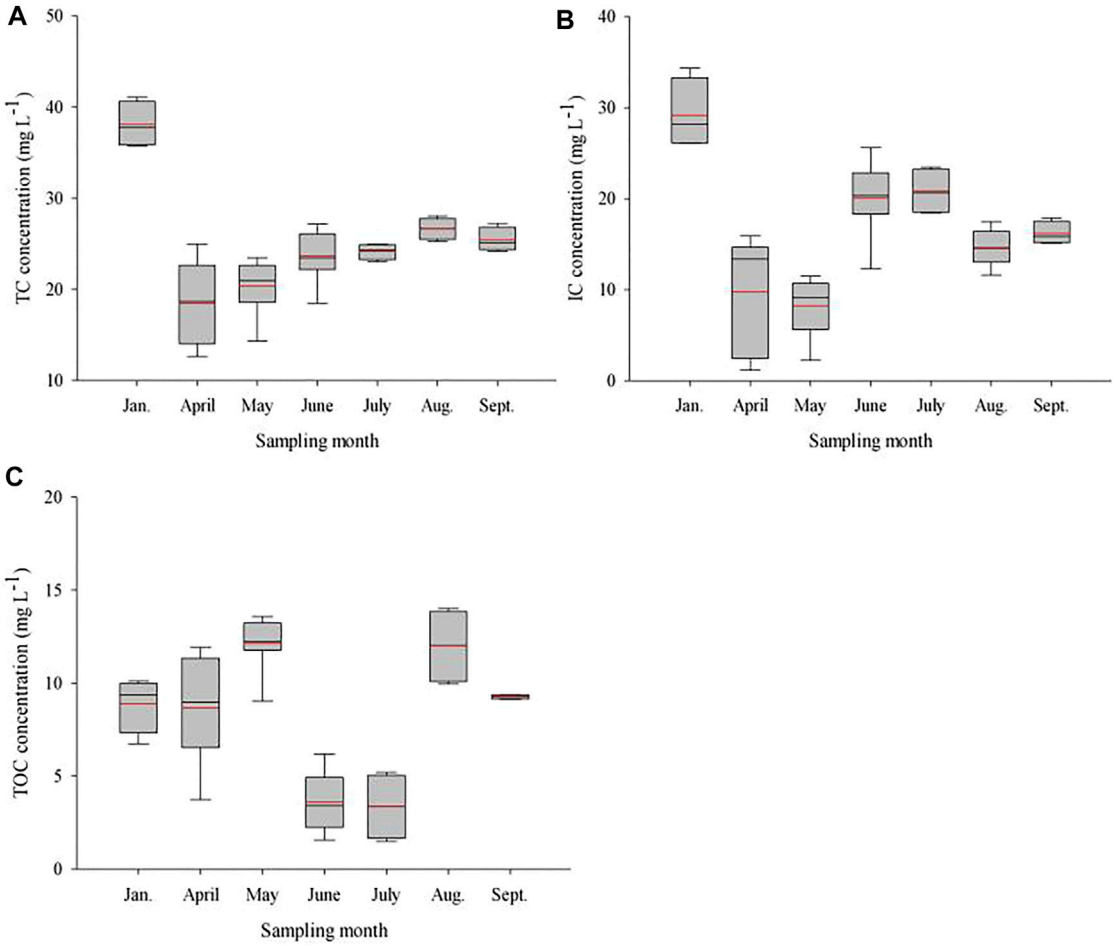

FIGURE 6 | Monthly changes in water TC, IC, and TOC in Qinglonghu Lake. The symbol of the box diagrams is similar to **Figure 4**. The above figires were made based on the data of all measurements (n = 4, 8) in each sampling month.

dynamics in the mesoeutrophic urbanizing lake were mainly driven by P during the daytime and impacted by the balance of P and R (Tranvik et al., 2009; Karim et al., 2011). Similar findings have been reported in our previous works (Xu et al., 2019; Yang et al., 2019) and in other studies of aquatic systems (Peng et al., 2012; Tonetta et al., 2014; Wang et al., 2021). In general, the P and R processes follow a circadian rhythm; that is, C fixation is limited to the day, but R occurs through the whole 24 h cycle (Schelske, 2006). Furthermore, strong negative correlations between DO and both pCO_2 and fCO_2 occurred during the daytime (i.e., −0.482** for pCO_2/DO and −0.502** for fCO_2/DO) in this study (**Table 2**, **Supplementary Table S1**), suggesting the pCO_2 on the water surface mainly caused mainly by R is higher than the atmospheric CO_2 when P is less than R (i.e., P:R < 1.0). In other words, this process is heterotrophic. In contrast, pCO_2 in autotrophic ecosystems is lower than CO_2 in the atmosphere (Gu et al., 2011). When P:R > 1.0, the lake may be supersaturated with CO_2. Previous studies showed that the inorganic carbon loading is the main factor influencing dissolved CO_2 concentration in lakes/reservoirs in the United States (Mcdonald et al., 2013). Further, water temperature could cause the concentrations of dissolved gases to rise, and the daily trends of pCO_2 and DO can become similar because both gases become more difficult to dissolve at higher temperatures. However, in the present work, pCO_2 and DO exhibited opposite responses to water temperature changes (**Table 2**, **Supplementary Table S1**; **Figures 5A,D**), indicating that the main force influencing dissolved gas concentration is the balance between P and R (Xu et al., 2019).

Studies have shown that lakes in temperate regions could be considered heterotrophic when the concentration of dissolved organic carbon is higher than 6.0 mg C L^{-1} (Carignan et al., 2000). It is generally believed that due to heterogeneous loading of organic matter, pCO_2 increases as the organic carbon in lake water increases (Sobek et al., 2005; Xu et al., 2019). In this study, a similar positive correlation between TOC and pCO_2 was detected at all water sampling points (**Supplementary Table S1**), indicating that 7:00 CST may be the transition point between P and R. Moreover, a significantly positive

TABLE 3 | Daily correlation between pCO_2 and fCO_2 and time in Qinglonghu Lake (n = 4).

R-squared	pCO_2 ($y_1 = b_0\, e^{b1\, x}$)			fCO_2 ($y_2 = b_0'x + b_1'$)		
	b_0	b_1	R^2	b_0'	b_1'	R^2
01/10/2020	271.3	−3.79	0.815	−14.7	−25.4	0.835
04/05/2020	171.3	−0.36	0.030	−1.6	−20.6	0.003
04/21/2020	145.5	−0.41	0.725	−6.1	−30.1	0.743
05/06/2020	210.0	−0.21	0.007	−10.5	−13.6	0.052
05/20/2020	121.5	−0.78	0.646	−9.8	−26.5	0.784
06/03/2020	70.70	−2.24	0.812	−9.2	−31.8	0.903
06/28/2020	770.8	−4.16	0.957	−44.1	−4.30	0.948
07/13/2020	110.0	−1.81	0.898	−10.2	−29.5	0.912
08/06/2020	29.80	−1.53	0.502	−9.2	−34.2	0.836
08/19/2020	2782	−3.45	0.708	−178.8	107	0.830
09/05/2020	86.50	−0.14	0.001	1.1	−29.8	0.001

Fitting parameters and regression coefficients (r^2) for daily exponential correlations between pCO_2 (y_1; μatm) and time (x; h) and daily linear correlations between CO_2 fluxes (y_2; mmol m^2 h^{-1}) and time (x; h).

relationship between TOC and Chl*a* (p <0.05) was observed, indicating the TOC in this productive lake mainly sources from autochthonous production (**Figure 6A–C**, **Supplementary Figure S5**). In accordance with the results of Gu et al. (2011), the aforementioned result indicated that this phenomenon may be related to the consumption and decomposition of chlorophyll-containing materials overnight and the daytime production of aquatic organisms, which further supports the conclusion that major biological processes are controlling factors.

Main Environmental Variables Contributing to the Dynamics of CO_2

A previous investigation by Sobek et al. (2003) confirmed that TOC and pCO_2 are co-variable in boreal lakes, which is interpreted as in-lake R of mainly terrestrial derived from TOC or DOC. However, in addition to the formation of aquatic R of pCO_2 in the lake sediments, pCO_2 supersaturation on the water surface may be the result of terrestrial R, by inputting groundwater with supersaturated pCO_2 from soil R (Worrall et al., 2005; Stets et al., 2009). In this study, the CO_2 dynamics during the daytime caused by pCO_2 changes were mainly P and were driven by the availability of sunlight and nutrients, while R was regulated by water temperature and organic loading (Yvon-Durocher et al., 2010; Yang et al., 2019; Wang et al., 2021). However, current discussions on whether lakes are oversaturated have put forward to various hypotheses. For example, Weyhenmeyer (2008) et al. proposed that if the aquatic R of TOC is the main factor for predicting pCO_2 supersaturation along aquatic conduits, the observed increase in dissolved organic carbon (DOC) in many old/new rivers of northern latitudes may lead to an increase in CO_2 outflow. The other scholars speculated that if a large part of aquatic pCO_2 can be related to terrestrial R transferring to aquatic conduits through groundwater input, the conclusion that TOC is the main causal predictor of CO_2 supersaturation in boreal lakes will need to be reconsidered (Algesten et al., 2004; Sobek et al., 2005). Comprehensively, Humborg et al. (2010) has verified, in the Swedish watershed, CO_2 supersaturation along aquatic conduits is limited by terrestrial/aquatic R and weathering. Therefore, the mechanisms causing over- or under-saturation in freshwater lakes are complicated, which needs to be studied from multiple carriers and perspectives.

Previous works showed that productive systems are more likely to be CO_2 sinks (Marotta et al., 2010; Yang et al., 2019), while a higher nutrient could promote the biological activity of aquatic P and then leading to more CO_2 absorption (Cole and Caraco, 2001). Based on the detection of Chl*a*, TP, TN and TPC, the nutritional status index [i.e., TLI (∑)] of this urbanizing lake was 63.15 (**Table 2**, **Supplementary Figure S2**), suggesting that a variable relationships between pCO_2 and N/P was found (**Supplementary Table S2**, **Supplementary Methods S4**; Li et al., 2018), which thus was defined as a middle-eutropher lake. The average DO and TP of this lake (including four anions; **Supplementary Figure S6**, **Supplementary Table S3**) were recorded as 8.43 (**Supplementary Figure S3**) and <0.01 mg L^{-1} (**Supplementary Figure S2**), respectively, and therefore being classified as class I abiding by the national standard (GB 3838-2002). For lakes with different nutrients, the diel CO_2 changes are different. For example, the dynamic changes in CO_2 in a typical tropical productive lake were highly dependent on biological metabolism during the diurnal cycle (Reis and Barbosa, 2014), while no significant diel changes in fCO_2 were found in oligotrophic lakes (Morin et al., 2018). In addition, diurnal changes in CO_2 and related parameters in lakes with different nutrients change seasonally (e.g., **Supplementary Figure S2–S4**). In this study, the daily variations in pCO_2 on April 5 and Sept. 5 2020, were opposite each other (**Figure 3**). Similarly, during the peak period of Chl*a*, the diurnal changes in August and September were obvious, whereas no obvious temporal changes occurred in the other months (Shao et al., 2015).

Besides, changes in lake CO_2 are also closely related to temperature and pH. In this study, a weak negative correlation between water temperature and daily pCO_2 was observed (**Table 2**), indicating an increase in gas solubility and a decrease in CO_2 absorption at low temperatures. The diurnal changes in pCO_2 affected by water temperature were therefore usually smaller (R^2 = −0.030 for pCO_2; R^2 = −0.043 for fCO_2; **Table 3**, **Supplementary Table S3**) than the biologically induced changes (Nimick et al., 2011; Morales-Pineda et al., 2014). Moreover, the lake water temperature during the daytime was almost constant in this study (**Figure 5C**); further, the average daily t_{water} was negatively correlated with daily pCO_2 (**Table 3**), indicating that daily t_{water} influenced on the CO_2 level in the late afternoon. Therefore, we speculate that there may be a temperature threshold in subtrophic water. When the t_{water} exceeds this threshold, pCO_2 might be extremely low in the late afternoon due to active P. Accordingly, there is a relationship between CO_2 and pH in lakes, as shown in this study (R^2 = −0.823** for pCO_2, R^2 = −0.825** for fCO_2; **Supplementary Table S1**), suggesting that the critical threshold for the pH value shifts from the CO_2 absorption

capacity to the emission source (Wilson-McNeal et al., 2020)). In river systems, the river represents a CO_2 sink when the pH value exceeds 8.59 but acts as a CO_2 source when the pH value is less than 8.59 (Li et al., 2020a, Li et al., 2020b). Therefore, we speculate that the increases in EC and nutrient levels in the lake system are closely related to urban development, and that anthropogenic emissions may lower the pH value (see **Supplementary Table S1**), leading to an increase in aqueous pCO_2 (Richey et al., 2002; Ran et al., 2015; Liu et al., 2017).

Uncertainties in CO_2 Evasion Evaluation Owing to Daily pCO_2 Fluctuations

Owing to the variations of pCO_2, the interaction of CO_2 source-sink within a day is driven by many factors, especially daylight and thus the biological processes in the lake (Cole and Caraco, 1998; Maberly et al., 2013; León-Palmero et al., 2020). Findings of our study indicated, due to daily fluctuations, considerable uncertainties in the current estimations of CO_2 evasion from regional and global lake systems. On the one hand, most current estimates of annual CO_2 evasion from freshwater lakes are mainly calculated using data collected from measurements with poor temporal coverage (i.e., weekly or monthly) (Cole et al., 2007) or low-frequency time series (Peter et al., 2014). For daily change, as in our study, the time frame (from 7:00 to 17:00 CST) for observing a decrease in pCO_2 is actually short, the variable level therefore may cause an underestimation or overestimation for the daily CO_2 based on one-time measurement. On the other hand, the observations were made at 3 h intervals from morning to afternoon (**Figures 3, 4**), with no measurements conducted during the nighttime. The CO_2 evasion during the nighttime could be stronger than that during the daytime, which may be due to darkness favors R over P (Xu et al., 2019), or to physical changes in the water column (Wang et al., 2021). For instance, Reis and Barbosa (2014) observed a tropical productive lake in Brazil for two consecutive days showing, the average pCO_2 (565 matm from 21:00 to 5:00 BRT) during the nighttime was higher than that during the daytime (436.1 matm from 9:00 to 17:00 BRT). In agreement, based on direct measurements in the Ross Barnett reservoir, fCO_2 during the nighttime (0.39 μmol m^{-2} s^{-1}) was ca. 70% greater than that during the daytime (0.23 μmol m^{-2} s^{-1} from 08:00 to 20:00 CST) over the 1-year study period (Liu et al., 2016). In addition, Gu et al. (2011) presented an investigation of limnological data collected from 1987 to 2006, suggesting the average pCO_2 (i.e., 224 μatm) at nighttime was slightly higher than that during the daytime but undersaturation with reference to atmospheric pCO_2. A study conducted in Lake Lochaber in eastern Nova Scotia, Canada, showed that 65–95% of total CO_2 emissions in a day actually occur at night, which is 21:00 to 7:00 Atlantic Daylight Time (Spafford and Risk, 2018).

The uncertainties among studies in CO_2 estimates may also be partly due to differences in geographic region (Schelske, 2006). In a study of carbon dynamics in two Mediterranean reservoirs in southern Spain, by relying on different models, Morales-Pineda et al. (2014) found that the average CO_2 emissions ranged from 8.0 to 12.5 mmol C m^{-2} d^{-1} in Guadalcacín but ranged from 33.0 to 50.0 mmol C m^{-2} d^{-1} in Bornos. Further, on a daily scale, variability in pCO_2 was closely related to the diurnal cycle of metabolic activity, with a minimum pCO_2 value between 15:00 and 18:00 Central European Time and a maximum value between 22:00 and 06:00 CET. Reis and Barbosa (2014) also observed a significant difference in CO_2 flux between daytime and nighttime in Lake Carioca, Brazil. Interestingly, CO_2 outgassing was lower at 1:00 Brasilia Time than at other times of day, with a maximum of 2.4 mmol C m^{-2} d^{-1} and an average of 0.9 mmol C m^{-2} d^{-1}. Watras et al. (2015) focused on two small seepage lakes in northern Wisconsin, suggesting that the diel cycle is controlled by biological activities, which mediate the production and destruction of organic matter based on daily CO_2 dynamics (0.32 mg C m^{-2} d^{-1}). From October 2011 to September 2013, a strong diurnal change in fCO_2 from −0.45 to 0.98 g C m^{-2} d^{-1} in western Lake Erie in North America was found by Shao et al. (2015). However, no clear diurnal variation was observed in a small boreal lake (i.e., Lake Kuivajärvi) in Finland, although the average diel fCO_2 was 0.7 μmol C m^{-2} s^{-1} (Mammarella et al., 2015), while the clear diurnal cycles of fCO_2 in three lakes with different characteristics in southwestern Sweden (Natchimuthu et al., 2017).

Furthermore, previous studies have also proved that C derived from terrestrial systems could cause CO_2 oversaturation in lakes, where DOC serve as a direct substrate for CO_2 production or as a proxy for inorganic C loading (Roehm et al., 2009; Humborg et al., 2010). In this regard, the relationship between pCO_2 and DOC could be a key feature for explaining the regional differences in lake pCO_2 regulation (Lapierre and del Giorgio, 2012). A strong positive correlation in pCO_2-DOC indicates that *in-situ* oxidation of terrestrial organic C plays a leading role in the excessive CO_2 production in lakes, or the significant contribution of DOC related driving factors to pCO_2 effects (Larsen et al., 2011). On the contrary, a weak/negative correlation would indicate either a strong contribution from other drivers that are not related to DOC, or drivers that are related to DOC but have an opposite effect on pCO_2, respectively. Lapierre and del Giorgio (2012) found that the proxy for lake metabolic balance and terrestrial C exports accounted for a large part of these patterns in the lake pCO_2-DOC relationship, indicating that the key driver of the difference in pCO_2-DOC is the integration of the average regional TP: DOC ratio and altitude. Based on the findings from these and our studies, we argue that great uncertainties may exist in current regional and global estimations of CO_2 evasion from lake systems.

CONCLUSION

In the current work, we systematically investigated the daily fluctuations in pCO_2 and related parameters at 3 h intervals from morning to afternoon from Jan. to Sept., 2020 in a subtropical urbanizing lake. Several interesting findings have resulted from the work. From early mornings to late afternoons, strongly decreasing pCO_2 and fCO_2 trends were observed except on 2 days on which unusual rainfall/wind

occurred. The daily pCO_2 was highest at 7:00 CST (1,061.3 μatm on August 19) and lowest at 17:00 CST (12.6 μatm on August 6), while the average pCO_2 was highest at 7:00 CST (204.9 ± 295.7 μatm) and lowest at 17:00 CST (93.5 ± 105.5 μatm). As a result, the highest daily fCO_2 occurred in the morning hours (−19.3 ± 27.5 and −24.8 ± 20.7 mmol m^{-2} h^{-1} at 7:00 and 10:00 CST, respectively) and in the afternoon hours (−29.2 ± 9.1 and −30.4 ± 10.7 mmol m^{-2} h^{-1} at 14:00 and 17:00 CST, respectively). These findings revealed that the daily CO_2 exchange in the studied subtropical urbanizing lake reflects the dynamics of ecosystem metabolism and remineralization reactions. Accordingly, we speculate that nighttime pCO_2/fCO_2 may be much higher than daytime pCO_2/fCO_2, which would indicate that the entire lake is undersaturated and a carbon sink during daylight hours. In addition, there was a strong negative correlation between pCO_2 and each of pH, t_{water}, and DO but a positive correlation between pCO_2 and each of TOC and Chl*a*, suggesting that uncertainties in the estimation of fCO_2 at regional/global scales owing to some factors such as geographical region and temporal coverage. Future work needs to constrain these critical factors and overall uncertainty and determine the levels of accuracy needed to enable robust CO_2 estimations at different scales.

DATA AVAILABILITY STATEMENT

The original contributions presented in the study are included in the article/**Supplementary Material**, further inquiries can be directed to the corresponding authors.

AUTHOR CONTRIBUTIONS

RY: Conceptualization, Methodology, Software, Formal analysis, Investigation, Data Curation, Writing-Original Draft, Visualization. YC: Software, Formal analysis, Investigation. JD: Project administration, Funding acquisition. XP: Conceptualization, Writing-Review and Editing, Funding acquisition. JL: Investigation. ZZ: Investigation. HS: Conceptualization, Methodology, Resources, Data Curation, Writing-Review and Editing, Supervision, Project administration, Funding acquisition.

FUNDING

This work was partially supported by the Specialized Fund for the Post-Disaster Reconstruction and Heritage Protection in Sichuan (grant No., 5132202019000128), the Technology Innovation R & D Project in Chengdu (grant No., 2019-YFYF-00040-SN), the Landscape and Recreation Research Center Project in Sichuan (grant No., JGYQ2019025), the Science and Technology Innovation Seedling Project in Sichuan (grant No., 2020118) and the Innovation and Entrepreneurship Training Program for College Students at Sichuan Agricultural University and in Sichuan Province (grant Nos., 202010626104, S202010626104).

ACKNOWLEDGMENTS

The authors acknowledge the Sichuan Keshengxin Environmental Technology Co., Ltd., College of Environmental Sciences and Institute of Landscape Architecture at Sichuan Agricultural University in Chengdu, China, for assisting in the detection of partial water samples for this study. Sincere thanks also go to Drs. Li Li and Shiliang Liu; Mses. Jia Wei, Yuling Qiu, Kezhu Lu, Qianrui Liu, and Xiaoyang Ke; Messrs. Di Li, Ting Lei, Xingyu Zhu, Jianglin Yu, Lijuan Yang, and Hongyu Wu; and other research assistants for their outstanding laboratory and field assistance. The authors also thank Drs. Y. Jun Xu and Zhen Xu from Louisiana State University in Baton Rouge, United States, for their previous trial-design guidance; the Qinglonghu Lake Management Center for providing permission and transportation for the field trials; American Journal Experts (https://www.aje.com/#) for their language editing services for our draft manuscript; and the editors and two reviewers for their helpful comments and suggestions.

SUPPLEMENTARY MATERIAL

The Supplementary Material for this article can be found online at: https://www.frontiersin.org/articles/10.3389/feart.2021.805276/full#supplementary-material

REFERENCES

Abril, G., Bouillon, S., Darchambeau, F., Teodoru, C. R., Marwick, T. R., Tamooh, F., et al. (2015). Technical Note: Large Overestimation of pCO_2Calculated from pH and Alkalinity in Acidic, Organic-Rich Freshwaters. *Biogeosciences* 12, 67–78. doi:10.5194/bg-12-67-2015

Abril, G., Martinez, J.-M., Artigas, L. F., Moreira-Turcq, P., Benedetti, M. F., Vidal, L., et al. (2014). Amazon River Carbon Dioxide Outgassing Fuelled by Wetlands. *Nature* 505, 395–398. doi:10.1038/nature12797

Algesten, G., Sobek, S., Bergström, A.-K., Ågren, A., Tranvik, L. J., and Jansson, M. (2004). Role of Lakes for Organic Carbon Cycling in the Boreal Zone. *Glob. Change Biol* 10, 141–147. doi:10.1111/j.1365-2486.2003.00721.x

Alin, S. R., and Johnson, T. C. (2007). Carbon Cycling in Large Lakes of the World: A Synthesis of Production, Burial, and lake-atmosphere Exchange Estimates. *Glob. Biogeochem. Cycles* 21, a–n. doi:10.1029/2006GB002881

Bade, D. L., and Cole, J. J. (2006). Impact of Chemically Enhanced Diffusion on Dissolved Inorganic Carbon Stable Isotopes in a Fertilized lake. *J. Geophys. Res.* 111. doi:10.1029/2004JC002684

Bisutti, I., Hilke, I., and Raessler, M. (2004). Determination of Total Organic Carbon–An Overview of Current Methods. *Trend. Anal. Chem.* 23, 10–11. doi:10.1016/j.trac.2004.09.003

Butman, D., and Raymond, P. A. (2011). Significant Efflux of Carbon Dioxide from Streams and Rivers in the United States. *Nat. Geosci* 4, 839–842. doi:10.1038/ngeo1294

Cai, W.-J., and Wang, Y. (1998). The Chemistry, Fluxes, and Sources of Carbon Dioxide in the Estuarine Waters of the Satilla and Altamaha Rivers, Georgia. *Limnol. Oceanogr.* 43, 657–668. doi:10.4319/lo.1998.43.4.0657

Callbeck, C. M., Ehrenfels, B., Baumann, K. B. L., Wehrli, B., and Schubert, C. J. (2021). Anoxic Chlorophyll Maximum Enhances Local Organic Matter Remineralization and Nitrogen Loss in Lake Tanganyika. *Nat. Commun.* 12, 830. doi:10.1038/s41467-021-21115-5

Carignan, R., Planas, D., and Vis, C. (2000). Planktonic Production and Respiration in Oligotrophic Shield Lakes. *Limnol. Oceanogr.* 45, 189–199. doi:10.4319/lo.2000.45.1.0189

Chen, S., Hu, C., Cai, W.-J., and Yang, B. (2017). Estimating Surface pCO_2 in the Northern Gulf of Mexico: Which Remote Sensing Model to Use. *Continental Shelf Res.* 151, 94–110. doi:10.1016/j.csr.2017.10.013

Chen, S., and Hu, C. (2019). Environmental Controls of Surface Water pCO_2 in Different Coastal Environments: Observations from marine Buoys. *Continental Shelf Res.* 183, 73–86. doi:10.1016/j.csr.2019.06.007

Cole, J. J., and Caraco, N. F. (1998). Atmospheric Exchange of Carbon Dioxide in a Low-Wind Oligotrophic lake Measured by the Addition of SF6. *Limnol. Oceanogr.* 43, 647–656. doi:10.4319/lo.1998.43.4.0647

Cole, J. J., Caraco, N. F., Kling, G. W., and Kratz, T. K. (1994). Carbon Dioxide Supersaturation in the Surface Waters of Lakes. *Science* 265, 1568–1570. doi:10.1126/science.265.5178.1568

Cole, J. J., Cole, J. J., Caraco, N. F., and Caraco, N. F. (2001). Carbon in Catchments: Connecting Terrestrial Carbon Losses with Aquatic Metabolism. *Mar. Freshw. Res.* 52, 101–110. doi:10.1071/mf00084

Cole, J. J., Prairie, Y. T., Caraco, N. F., McDowell, W. H., Tranvik, L. J., Striegl, R. G., et al. (2007). Plumbing the Global Carbon Cycle: Integrating Inland Waters into the Terrestrial Carbon Budget. *Ecosystems* 10, 172–185. doi:10.1007/s10021-006-9013-8

Crawford, J. T., Loken, L. C., Stanley, E. H., Stets, E. G., Dornblaser, M. M., and Striegl, R. G. (2016). Basin Scale Controls on CO_2 and CH_4emissions from the Upper Mississippi River. *Geophys. Res. Lett.* 43, 1973–1979. doi:10.1002/2015gl067599

Crawford, J. T., Striegl, R. G., Wickland, K. P., Dornblaser, M. M., and Stanley, E. H. (2013). Emissions of Carbon Dioxide and Methane from a Headwater Stream Network of interior Alaska. *J. Geophys. Res. Biogeosci.* 118, 482–494. doi:10.1002/jgrg.20034

Dickinson, G. H., Ivanina, A. V., Matoo, O. B., Pörtner, H. O., Lannig, G., Bock, C., et al. (2012). Interactive Effects of Salinity and Elevated CO_2 Levels on Juvenile Eastern Oysters, *Crassostrea virginica*. *J. Exp. Biol.* 215, 29–43. doi:10.1242/jeb.061481

Domysheva, V. M., Panchenko, M. V., Pestunov, D. A., and Sakirko, M. V. (2007). Influence of Atmospheric Precipitation on the CO_2 Exchange with the Water Surface of Lake Baikal. *Dokl. Earth Sci.* 415, 740–743. doi:10.1134/s1028334x07050182

Gu, B., Schelske, C. L., and Coveney, M. F. (2011). Low Carbon Dioxide Partial Pressure in a Productive Subtropical lake. *Aquat. Sci.* 73, 317–330. doi:10.1007/s00027-010-0179-y

Guérin, F., Abril, G., Serça, D., Delon, C., Richard, S., Delmas, R., et al. (2007). Gas Transfer Velocities of CO_2 and CH_4 in a Tropical Reservoir and its River Downstream. *J. Mar. Sys.* 66, 161–172.

Hastie, A., Lauerwald, R., Weyhenmeyer, G., Sobek, S., Verpoorter, C., and Regnier, P. (2018). CO_2 Evasion from Boreal Lakes: Revised Estimate, Drivers of Spatial Variability, and Future Projections. *Glob. Change Biol.* 24, 711–728. doi:10.1111/gcb.13902

Holgerson, M. A. (2015). Drivers of Carbon Dioxide and Methane Supersaturation in Small, Temporary Ponds. *Biogeochemistry* 124, 305–318. doi:10.1007/s10533-015-0099-y

Holgerson, M. A., and Raymond, P. A. (2016). Large Contribution to Inland Water CO_2 and CH_4 Emissions from Very Small Ponds. *Nat. Geosci* 9, 222–226. doi:10.1038/ngeo2654

Hope, D., Palmer, S. M., Billett, M. F., and Dawson, J. J. C. (2004). Variations in Dissolved CO_2 and CH_4 in a First-Order Stream and Catchment: an Investigation of Soil-Stream Linkages. *Hydrol. Process.* 18, 3255–3275. doi:10.1002/hyp.5657

Humborg, C., Mörth, C.-M., Sundbom, M., Borg, H., Blenckner, T., Giesler, R., et al. (2010). CO_2 Supersaturation along the Aquatic Conduit in Swedish Watersheds as Constrained by Terrestrial Respiration, Aquatic Respiration and Weathering. *Glob. Change Biol* 16, 1966–1978. doi:10.1111/j.1365-2486.2009.02092.x

IPCC (Intergovernmental Panel on Climate Change) (2014). "Climate Change 2014: Synthesis Report," in *Contribution of Working Groups I, II and III to the Fifth Assessment Report of the Intergovernmental Panel on Climate Change*. Editors R. K. Pachauri and L. A. Meyer, 1–151.

Jähne, B., Heinz, G., and Dietrich, W. (1987). Measurement of the Diffusion Coefficients of Sparingly Soluble Gases in Water. *J. Geophys. Res.* 92, 10767–10776. doi:10.1029/jc092ic10p10767

Kankaala, P., Huotari, J., Tulonen, T., and Ojala, A. (2013). Lake-size Dependent Physical Forcing Drives Carbon Dioxide and Methane Effluxes from Lakes in a Boreal Landscape. *Limnol. Oceanogr.* 58, 1915–1930. doi:10.4319/lo.2013.58.6.1915

Karim, A., Dubois, K., and Veizer, J. (2011). Carbon and Oxygen Dynamics in the Laurentian Great Lakes: Implications for the CO_2 Flux from Terrestrial Aquatic Systems to the Atmosphere. *Chem. Geology.* 281, 133–141. doi:10.1016/j.chemgeo.2010.12.006

Katul, G., and Liu, H. (2017). Multiple Mechanisms Generate a Universal Scaling with Dissipation for the Air-water Gas Transfer Velocity. *Geophys. Res. Lett.* 44, 1892–1898. doi:10.1002/2016gl072256

Keller, P. S., Catalán, N., von Schiller, D., Grossart, H.-P., Koschorreck, M., Obrador, B., et al. (2020). Global CO_2 Emissions from Dry Inland Waters Share Common Drivers across Ecosystems. *Nat. Commun.* 11, 2126. doi:10.1038/s41467-020-15929-y

Kortelainen, P. (1993). Content of Total Organic Carbon in Finnish Lakes and its Relationship to Catchment Characteristics. *Can. J. Fish. Aquat. Sci.* 50, 1477–1483. doi:10.1139/f93-168

Kosten, S., Roland, F., Da Motta Marques, D. M. L., Van Nes, E. H., Mazzeo, N., Sternberg, L. d. S. L., et al. (2010). Climate-dependent CO_2 emissions from Lakes. *Glob. Biogeochem. Cycles* 24, a–n. doi:10.1029/2009GB003618

Lapierre, J.-F., and del Giorgio, P. A. (2012). Geographical and Environmental Drivers of Regional Differences in the lake pCO_2 versus DOC Relationship across Northern Landscapes. *J. Geophys. Res.* 117, a–n. doi:10.1029/2012JG001945

Larsen, S., Andersen, T., and Hessen, D. O. (2011). The pCO_2 in Boreal Lakes: Organic Carbon as a Universal Predictor. *Glob. Biogeochem. Cycles* 25, a–n. doi:10.1029/2010GB003864

Le Quéré, C., Andrew, R. M., Friedlingstein, P., Sitch, S., Pongratz, J., Manning, A. C., et al. (2018). Global Carbon Budget 2017. *Earth Syst. Sci. Data* 10, 405–448. doi:10.5194/essd-10-405-2018

León-Palmero, E., Morales-Baquero, R., and Reche, I. (2020). Greenhouse Gas Fluxes from Reservoirs Determined by Watershed Lithology, Morphometry, and Anthropogenic Pressure. *Environ. Res. Lett.* 15, 044012. doi:10.1088/1748-9326/ab7467

Li, Q., Guo, X., Zhai, W., Xu, Y., and Dai, M. (2020a). Partial Pressure of CO_2 and Air-Sea CO_2 Fluxes in the South China Sea: Synthesis of an 18-year Dataset. *Prog. Oceanography* 182, 102272. doi:10.1016/j.pocean.2020.102272

Li, S., Lu, X. X., and Bush, R. T. (2013). CO_2 Partial Pressure and CO_2 Emission in the Lower Mekong River. *J. Hydrol.* 504, 40–56. doi:10.1016/j.jhydrol.2013.09.024

Li, S., Lu, X. X., He, M., Zhou, Y., Li, L., and Ziegler, A. D. (2012). Daily CO_2 Partial Pressure and CO_2 Outgassing in the Upper Yangtze River basin: A Case Study of the Longchuan River, China. *J. Hydrol.* 466-467, 141–150. doi:10.1016/j.jhydrol.2012.08.011

Li, S., Luo, J., Wu, D., and Jun Xu, Y. (2020b). Carbon and Nutrients as Indictors of Daily Fluctuations of pCO_2 and CO_2 Flux in a River Draining a Rapidly Urbanizing Area. *Ecol. Indicators* 109, 105821. doi:10.1016/j.ecolind.2019.105821

Li, S., Ni, M., Mao, R., and Bush, R. T. (2018). Riverine CO_2 Supersaturation and Outgassing in a Subtropical Monsoonal Mountainous Area (Three Gorges Reservoir Region) of China. *J. Hydrol.* 558, 460–469. doi:10.1016/j.jhydrol.2018.01.057

Li, W., and Cai, Y. M. (2019). Integration of Nature, Ecology, and Humanities: the Phase I Project of Qinglonghu Wetland in Shiling, Chengdu. *Sichuan Archit* 39, 53–59. doi:10.3969/j.issn.1007-8983.2019.06.020

Li, Y., Yang, X., Han, P., Xue, L., and Zhang, L. (2017). Controlling Mechanisms of Surface Partial Pressure of CO_2 in Jiaozhou Bay during Summer and the Influence of Heavy Rain. *J. Mar. Syst.* 173, 49–59. doi:10.1016/j.jmarsys.2017.04.006

Liu, H., Zhang, Q., Katul, G. G., Cole, J. J., Chapin, F. S., III, and MacIntyre, S. (2016). Large CO_2 Effluxes at Night and during Synoptic Weather Events Significantly Contribute to CO $_2$ Emissions from a Reservoir. *Environ. Res. Lett.* 11, 064001. doi:10.1088/1748-9326/11/6/064001

Liu, S., Lu, X. X., Xia, X., Yang, X., and Ran, L. (2017). Hydrological and Geomorphological Control on CO_2 Outgassing from Low-Gradient Large Rivers: An Example of the Yangtze River System. *J. Hydrol.* 550, 26–41. doi:10.1016/j.jhydrol.2017.04.044

Luo, J., Li, S., Ni, M., and Zhang, J. (2019). Large Spatiotemporal Shifts of CO_2 Partial Pressure and CO_2 Degassing in a Monsoonal Headwater Stream. *J. Hydrol.* 579, 124135. doi:10.1016/j.jhydrol.2019.124135

Maberly, S. C., Barker, P. A., Stott, A. W., and De Ville, M. M. (2013). Catchment Productivity Controls CO_2 Emissions from Lakes. *Nat. Clim. Change* 3, 391–394. doi:10.1038/nclimate1748

Maier, M.-S., Teodoru, C. R., and Wehrli, B. (2021). Spatio-temporal Variations in Lateral and Atmospheric Carbon Fluxes from the Danube Delta. *Biogeosciences* 18, 1417–1437. doi:10.5194/bg-18-1417-2021

Mammarella, I., Nordbo, A., Rannik, Ü., Haapanala, S., Levula, J., Laakso, H., et al. (2015). Carbon Dioxide and Energy Fluxes over a Small Boreal lake in Southern Finland. *J. Geophys. Res. Biogeosci.* 120, 1296–1314. doi:10.1002/2014jg002873

Marcé, R., Obrador, B., Morguí, J.-A., Lluís Riera, J., López, P., and Armengol, J. (2015). Carbonate Weathering as a Driver of CO_2 Supersaturation in Lakes. *Nat. Geosci* 8, 107–111. doi:10.1038/ngeo2341

Marotta, H., Duarte, C. M., Meirelles-Pereira, F., Bento, L., Esteves, F. A., and Enrich-Prast, A. (2010). Long-Term CO_2 Variability in Two Shallow Tropical Lakes Experiencing Episodic Eutrophication and Acidification Events. *Ecosystems* 13, 382–392. doi:10.1007/s10021-010-9325-6

Marotta, H., Duarte, C. M., Sobek, S., and Enrich-Prast, A. (2009). Large CO_2 disequilibria in Tropical Lakes. *Glob. Biogeochem. Cycles* 23, a–n. doi:10.1029/2008GB003434

Mcdonald, C. P., Stets, E. G., Striegl, R. G., and Butman, D. (2013). Inorganic Carbon Loading as a Primary Driver of Dissolved Carbon Dioxide Concentrations in the Lakes and Reservoirs of the Contiguous United States. *Glob. Biogeochem. Cycles* 27, 285–295. doi:10.1002/gbc.20032

Morales-Pineda, M., Cózar, A., Laiz, I., Úbeda, B., and Gálvez, J. Á. (2014). Daily, Biweekly, and Seasonal Temporal Scales of pCO_2 variability in Two Stratified Mediterranean Reservoirs. *J. Geophys. Res. Biogeosci.* 119, 509–520. doi:10.1002/2013jg002317

Morin, T. H., Rey-Sánchez, A. C., Vogel, C. S., Matheny, A. M., Kenny, W. T., and Bohrer, G. (2018). Carbon Dioxide Emissions from an Oligotrophic Temperate lake: An Eddy Covariance Approach. *Ecol. Eng.* 114, 25–33. doi:10.1016/j.ecoleng.2017.05.005

Natchimuthu, S., Sundgren, I., Gålfalk, M., Klemedtsson, L., and Bastviken, D. (2017). Spatiotemporal Variability of lake pCO_2 and CO_2 Fluxes in a Hemiboreal Catchment. *J. Geophys. Res. Biogeosci.* 122, 30–49. doi:10.1002/2016jg003449

Ni, M., Ge, Q., Li, S., Wang, Z., and Wu, Y. (2021). Trophic State index Linked to Partial Pressure of Aquatic Carbon Dioxide in a Typical Karst Plateau lake. *Ecol. Indicators* 120, 106912. doi:10.1016/j.ecolind.2020.106912

Nimick, D. A., Gammons, C. H., and Parker, S. R. (2011). Diel Biogeochemical Processes and Their Effect on the Aqueous Chemistry of Streams: a Review. *Chem. Geology.* 283, 3–17. doi:10.1016/j.chemgeo.2010.08.017

Pardue, J. H., Delaune, R. D., and Patrick, W. H., Jr (1988). Effect of Sediment pH and Oxidation-Reduction Potential on PCB Mineralization. *Water Air Soil Pollut.* 37, 439–447. doi:10.1007/bf00192953

Peng, X., Wang, B., Liu, C., Liu, X., and Wang, F. (2012). Diurnal Variations of pCO_2 in Relation to Environmental Factors in the cascade Reservoirs along the Wujiang River, China. *Chin. J. Geochem.* 31, 41–47. doi:10.1007/s11631-012-0547-5

Peter, H., Singer, G. A., Preiler, C., Chifflard, P., Steniczka, G., and Battin, T. J. (2014). Scales and Drivers of temporal pCO_2 dynamics in an Alpine Stream. *J. Geophys. Res. Biogeosci.* 119, 1078–1091. doi:10.1002/2013jg002552

Podgrajsek, E., Sahlée, E., and Rutgersson, A. (2015). Diel Cycle of lake-air CO_2flux from a Shallow lake and the Impact of Waterside Convection on the Transfer Velocity. *J. Geophys. Res. Biogeosci.* 120, 29–38. doi:10.1002/2014jg002781

Ran, L., Lu, X. X., Yang, H., Li, L., Yu, R., Sun, H., et al. (2015). CO_2outgassing from the Yellow River Network and its Implications for Riverine Carbon Cycle. *J. Geophys. Res. Biogeosci.* 120, 1334–1347. doi:10.1002/2015jg002982

Raymond, P. A., Hartmann, J., Lauerwald, R., Sobek, S., McDonald, C., Hoover, M., et al. (2013). Global Carbon Dioxide Emissions from Inland Waters. *Nature* 503, 355–359. doi:10.1038/nature12760

Reis, P. C., and Barbosa, F. A. (2014). Diurnal Sampling Reveals Significant Variation in CO_2 Emission from a Tropical Productive lake. *Braz. J. Biol.* 74, S113–S119. doi:10.1590/1519-6984.01713

Richey, J. E., Melack, J. M., Aufdenkampe, A. K., Ballester, V. M., and Hess, L. L. (2002). Outgassing from Amazonian Rivers and Wetlands as a Large Tropical Source of Atmospheric CO_2. *Nature* 416, 617–620. doi:10.1038/416617a

Roehm, C. L., Prairie, Y. T., and del Giorgio, P. A. (2009). The pCO_2 dynamics in Lakes in the Boreal Region of Northern Québec, Canada. *Glob. Biogeochem. Cycles* 23, a–n. doi:10.1029/2008GB003297

Sabine, C. L., Feely, R. A., Gruber, N., Key, R. M., Lee, K., Bullister, J. L., et al. (2004). The Oceanic Sink for Anthropogenic CO_2. *Science* 305, 367–371. doi:10.1126/science.1097403

Schelske, C. L. (2006). Comment on the Origin of the "fluid Mud Layer" in Lake Apopka, Florida. *Limnol. Oceanogr.* 51, 2472–2480. doi:10.4319/lo.2006.51.5.2472

Shao, C., Chen, J., Stepien, C. A., Chu, H., Ouyang, Z., Bridgeman, T. B., et al. (2015). Diurnal to Annual Changes in Latent, Sensible Heat, and CO_2 Fluxes over a Laurentian Great Lake: A Case Study in Western Lake Erie. *J. Geophys. Res. Biogeosci.* 120, 1587–1604. doi:10.1002/2015jg003025

Sobek, S., Algesten, G., Bergström, A.-K., Jansson, M., and Tranvik, L. J. (2003). The Catchment and Climate Regulation of pCO_2 in Boreal Lakes. *Glob. Change Biol* 9, 630–641. doi:10.1046/j.1365-2486.2003.00619.x

Sobek, S., Tranvik, L. J., and Cole, J. J. (2005). Temperature independence of Carbon Dioxide Supersaturation in Global Lakes. *Glob. Biogeochem. Cycles* 19, a–n. doi:10.1029/2004GB002264

Spafford, L., and Risk, D. (2018). Spatiotemporal Variability in Lake-Atmosphere Net CO_2 Exchange in the Littoral Zone of an Oligotrophic Lake. *J. Geophys. Res. Biogeosci.* 123, 1260–1276. doi:10.1002/2017jg004115

Stets, E. G., Striegl, R. G., Aiken, G. R., Rosenberry, D. O., and Winter, T. C. (2009). Hydrologic Support of Carbon Dioxide Flux Revealed by Whole-lake Carbon Budgets. *J. Geophys. Res.* 114, G01008. doi:10.1029/2008JG000783

Telmer, K., and Veizer, J. (1999). Carbon Fluxes, pCO_2 and Substrate Weathering in a Large Northern River basin, Canada: Carbon Isotope Perspectives. *Chem. Geology.* 159, 61–86. doi:10.1016/s0009-2541(99)00034-0

The National Environmental Protection Agency (NEPA), The Editorial Board of Water and Wastewater Monitoring/Analysis Methods (EB) (2002). *The Monitoring and Analysis Methods of Water and Wastewater*. Fourth Edition. Beijing: China Environmental Science Press.

Tonetta, D., Fontes, M. L. S., and Petrucio, M. M. (2014). Determining the High Variability of pCO_2 and pO_2 in the Littoral Zone of a Subtropical Coastal lake. *Acta Limnol. Bras.* 26, 288–295. doi:10.1590/s2179-975x2014000300008

Tranvik, L. J., Downing, J. A., Cotner, J. B., Loiselle, S. A., Striegl, R. G., Ballatore, T. J., et al. (2009). Lakes and Reservoirs as Regulators of Carbon Cycling and Climate. *Limnol. Oceanogr.* 54, 2298–2314. doi:10.4319/lo.2009.54.6_part_2.2298

Vachon, D., and Prairie, Y. T. (2013). The Ecosystem Size and Shape Dependence of Gas Transfer Velocity versus Wind Speed Relationships in Lakes. *Can. J. Fish. Aquat. Sci.* 70, 1757–1764. doi:10.1139/cjfas-2013-0241

Varol, M., and Li, S. (2017). Biotic and Abiotic Controls on CO_2 Partial Pressure and CO_2 Emission in the Tigris River, Turkey. *Chem. Geology.* 449, 182–193. doi:10.1016/j.chemgeo.2016.12.003

Wang, F., Wang, B., Liu, C.-Q., Wang, Y., Guan, J., Liu, X., et al. (2011). Carbon Dioxide Emission from Surface Water in cascade Reservoirs-River System on the Maotiao River, Southwest of China. *Atmos. Environ.* 45, 3827–3834. doi:10.1016/j.atmosenv.2011.04.014

Wang, Y., Qi, D., Wu, Y., Gao, Z., Sun, H., Lin, H., et al. (2021). Biological and Physical Controls of pCO_2 and Air-Sea CO_2 Fluxes in the Austral Summer of 2015 in Prydz Bay, East Antarctica. *Mar. Chem.* 228, 103897. doi:10.1016/j.marchem.2020.103897

Wanninkhof, R. (1992). Relationship between Wind Speed and Gas Exchange over the Ocean. *J. Geophys. Res.* 97, 7373–7382. doi:10.1029/92jc00188

Watras, C. J., Morrison, K. A., Crawford, J. T., McDonald, C. P., Oliver, S. K., and Hanson, P. C. (2015). Diel Cycles in the Fluorescence of Dissolved Organic Matter in Dystrophic Wisconsin Seepage Lakes: Implications for Carbon Turnover. *Limnol. Oceanogr.* 60, 482–496. doi:10.1002/lno.10026

Weiss, R. F. (1970). The Solubility of Nitrogen, Oxygen and Argon in Water and Seawater. *Deep Sea Res. Oceanographic Abstr.* 17, 721–735. doi:10.1016/0011-7471(70)90037-9

Wen, Z., Song, K., Shang, Y., Fang, C., Li, L., Lv, L., et al. (2017). Carbon Dioxide Emissions from Lakes and Reservoirs of China: A Regional Estimate Based on

the Calculated pCO_2. *Atmos. Environ.* 170, 71–81. doi:10.1016/j.atmosenv.2017.09.032

Weyhenmeyer, G. A. (2008). Water Chemical Changes along a Latitudinal Gradient in Relation to Climate and Atmospheric Deposition. *Climatic Change* 88, 199–208. doi:10.1007/s10584-007-9331-7

Wilson-McNeal, A., Hird, C., Hobbs, C., Nielson, C., Smith, K. E., Wilson, R. W., et al. (2020). Fluctuating Seawater pCO_2/pH Induces Opposing Interactions with Copper Toxicity for Two Intertidal Invertebrates. *Sci. Total Environ.* 748, 141370. doi:10.1016/j.scitotenv.2020.141370

Worrall, F., Burt, T., and Adamson, J. (2005). Fluxes of Dissolved Carbon Dioxide and Inorganic Carbon from an upland Peat Catchment: Implications for Soil Respiration. *Biogeochemistry* 73, 515–539. doi:10.1007/s10533-004-1717-2

Xiao, Q., Duan, H., Qi, T., Hu, Z., Liu, S., Zhang, M., et al. (2020). Environmental Investments Decreased Partial Pressure of CO_2 in a Small Eutrophic Urban lake: Evidence from Long-Term Measurements. *Environ. Pollut.* 263, 114433. doi:10.1016/j.envpol.2020.114433

Xu, Y. J., Xu, Z., and Yang, R. (2019). Rapid Daily Change in Surface Water pCO_2 and CO_2 Evasion: A Case Study in a Subtropical Eutrophic lake in Southern USA. *J. Hydrol.* 570, 486–494. doi:10.1016/j.jhydrol.2019.01.016

Xu, Z., and Xu, Y. J. (2015). Determination of Trophic State Changes with Diel Dissolved Oxygen: a Case Study in a Shallow lake. *Water Environ. Res.* 87, 1970–1979. doi:10.2175/106143015x14362865226716

Yan, H., Yu, K., Shi, Q., Lin, Z., Zhao, M., Tao, S., et al. (2018). Air-sea CO_2 Fluxes and Spatial Distribution of Seawater pCO_2 in Yongle Atoll, Northern-central South China Sea. *Continental Shelf Res.* 165, 71–77. doi:10.1016/j.csr.2018.06.008

Yang, R., Xu, Z., Liu, S., and Xu, Y. J. (2019). Daily pCO_2 and CO_2 Flux Variations in a Subtropical Mesotrophic Shallow lake. *Water Res.* 153, 29–38. doi:10.1016/j.watres.2019.01.012

Yao, G., Gao, Q., Wang, Z., Huang, X., He, T., Zhang, Y., et al. (2007). Dynamics of CO_2 Partial Pressure and CO_2 Outgassing in the Lower Reaches of the Xijiang River, a Subtropical Monsoon River in China. *Sci. Total Environ.* 376, 255–266. doi:10.1016/j.scitotenv.2007.01.080

Yoon, T. K., Jin, H., Begum, M. S., Kang, N., and Park, J.-H. (2017). CO_2 Outgassing from an Urbanized River System Fueled by Wastewater Treatment Plant Effluents. *Environ. Sci. Technol.* 51, 10459–10467. doi:10.1021/acs.est.7b02344

Yvon-Durocher, G., Jones, J. I., Trimmer, M., Woodward, G., and Montoya, J. M. (2010). Warming Alters the Metabolic Balance of Ecosystems. *Phil. Trans. R. Soc. B* 365, 2117–2126. doi:10.1098/rstb.2010.0038

Conflict of Interest: The authors declare that the research was conducted in the absence of any commercial or financial relationships that could be construed as a potential conflict of interest.

Publisher's Note: All claims expressed in this article are solely those of the authors and do not necessarily represent those of their affiliated organizations, or those of the publisher, the editors, and the reviewers. Any product that may be evaluated in this article, or claim that may be made by its manufacturer, is not guaranteed or endorsed by the publisher.

frontiers in Environmental Science

ORIGINAL RESEARCH
published: 24 January 2022
doi: 10.3389/fenvs.2021.829376

Numerical Investigation of the Effects of Aquatic Vegetation on Wind-Induced Wave and Current Characteristics in Shallow Lakes

Chenhui Wu[1,2], *Shiqiang Wu*[1]*, *Xiufeng Wu*[1]*, *Jiangyu Dai*[1]*, *Ang Gao*[1] and *Fan Yang*[1]

[1]State Key Laboratory of Hydrology-Water Resources and Hydraulic Engineering, Nanjing Hydraulic Research Institute, Nanjing, China, [2]College of Water Conservancy and Hydropower Engineering, Hohai University, Nanjing, China

Aquatic vegetation is one of the important parts of the shallow lake ecosystem, which has an important impact on the characteristics of wind-driven wave and current. In this article, we embed the vegetation module into the flow model TELEMAC-3D and the wave model TOMAWAC, respectively, and construct the coupling model of flow–wave–vegetation in the open source model Open TELEMAC-MASCARET. Through the verification of two sets of experimental data, it has been proven that the model can well reproduce the influence of vegetation on current and wave. Then, the model is applied to the wind-driven wave and current simulation of a typical shallow lake, Taihu Lake. The results show that the model can accurately reproduce the characteristics of wind-driven wave and current. Aquatic vegetation significantly changes the velocity, wave height, and local three-dimensional circulation flow in the vegetation patches. At the same time, the existence of aquatic vegetation reduces the material exchange rate between the vegetation area and the outside world, which has a significant impact on the material transport characteristics of the lake. Sensitivity analysis shows that the influence of aquatic vegetation should not be ignored in the simulation of wind-induced wave current and material transport in shallow lakes.

Keywords: aquatic vegetation, flow–wave–vegetation coupling model, shallow lake, wind-induced wave and current, Open TELEMAC-MASCARET

OPEN ACCESS

Edited by:
Yuanchun Zou,
Northeast Institute of Geography and Agroecology (CAS), China

Reviewed by:
Ronghua Ma,
Nanjing Institute of Geography and Limnology (CAS), China
Abdul Jalil,
Wuxi University, China

***Correspondence:**
Shiqiang Wu
sqwu@nhri.cn
Xiufeng Wu
xfwu@nhri.cn
Jiangyu Dai
jydai@nhri.cn

Specialty section:
This article was submitted to Freshwater Science, a section of the journal Frontiers in Environmental Science

Received: *05 December 2021*
Accepted: *30 December 2021*
Published: *24 January 2022*

Citation:
Wu C, Wu S, Wu X, Dai J, Gao A and Yang F (2022) Numerical Investigation of the Effects of Aquatic Vegetation on Wind-Induced Wave and Current Characteristics in Shallow Lakes. Front. Environ. Sci. 9:829376. doi: 10.3389/fenvs.2021.829376

1 INTRODUCTION

Shallow lakes are one of the most important parts of the Earth's natural resources, which have the functions of improving ecological environment, protecting phytoplankton, and maintaining biodiversity (Temmerman et al., 2013). However, with the continuous improvement of urbanization and climate change, shallow lakes are facing the problems of eutrophication and ecosystem degradation (Lürling et al., 2016). The health of the lake ecosystem is greatly affected by its own characteristics of wave and current. Wind is the main driving force of lake water movement, together with the geometric structure, topography, and aquatic vegetation patches of the lake; it determines the circulation structure of the lake (Li et al., 2016; Yang et al., 2019). Aquatic vegetation is one of the key components of the shallow lake ecosystem, mainly in the form of vegetation patches in the lake, which provides food resources for primary producers and plays a key role in the transportation and circulation of lake water (Gaylord et al., 2003). At the same time, patches of vegetation often change the direction of water flow and affect the circulation structure of lake water,

which is of great ecological significance (Barbier et al., 2008; Lu and Dai, 2017). In order to evaluate the resilience of the shallow lake ecosystem, we need to understand the interaction mechanism among vegetation, wind-induced wave, and current, and the material transport characteristics (Pang et al., 2015).

In light of the significant importance of vegetation ecology, a great deal of research has been done on the interaction between lake dynamics and aquatic vegetation in shallow lakes. The methods in previous studies include field-based observation (Resende et al., 2019), laboratory experiment (Dan and Hua, 2014; Banerjee et al., 2015), and physically based hydrodynamic modeling (Werner et al., 2005; Kim et al., 2015; Zhang et al., 2019a). Generally speaking, the remoteness and complexity in the majority of vegetation patches have limited the field observation study on the interaction between hydrodynamics and aquatic vegetation (Karim et al., 2015). The vegetation effects from the laboratory experiment did not consider the complexity of the real environment, so it cannot be extended to the more general situations in shallow lakes (Nepf, 2011). With the development of computer technology, numerical simulation has gradually become an important tool to improve the aquatic ecosystem of shallow lakes. How to accurately simulate the resistance of vegetation is the focus of numerical simulation research. The common method is to increase the Manning coefficient of vegetation patch location, which has been widely used in a two-dimensional depth-averaged model (Morin et al., 2000), but this method cannot explain the complex three-dimensional vertical structure of water flow within and over submerged vegetation (Sheng et al., 2012). In view of the three-dimensional flow, the RANS equations are solved with a vegetation drag term in the momentum equations and the corresponding vegetation-induced turbulence production terms in the turbulence closure equation (standard k-ε turbulence model, GLS model, and LES method, and other methods) (Jin et al., 2007; Chi-wai and Afis, 2019); this methodology has been verified by a large number of flume data with varying vegetation submergence ratios, densities, and velocities areas (Kombiadou et al., 2014). Scholars have used the numerical simulation method to simulate the influence of vegetation on the wind-induced current in the shallow lakes, but these studies are based on the two-dimensional hydrodynamic model (Xu et al., 2018) and use the method of increasing local Manning coefficient to simulate the vegetation resistance (Li et al., 2020), so it is unable to describe the submerged vegetation effect and the three-dimensional characteristics of shallow lake flow field. In recent years, several open-source three-dimensional models which allow custom editing to study the complex interactions between vegetation and water flow have been developed, such as FVCOM (Morales–Marín et al., 2017), SCHISM (Zhang et al., 2019b), and ROMS (Beudin et al., 2017). These models use the method of adding body resistance into momentum equations to simulate the resistance of vegetation and are widely used to study the attenuation of vegetation on coastal storm surge (Zhang et al., 2019a). However, these models have not been applied to study the complex interaction among aquatic vegetation, wind-induced wave, and current characteristics in shallow lakes. Given these backgrounds, it is necessary to improve the understanding of the role of floodplain vegetation, and fill information gaps regarding the vegetation effects on the wind-induced wave and current characteristics in the shallow lakes.

This article aimed to establish a model to study the effects of aquatic vegetation on wind-induced wave and current characteristics in shallow lakes by establishing an appropriate vegetation resistance module and coupling it with an open-source numerical model. We first describe in detail the establishment process of the flow–wave–vegetation coupling model in **Section 2**, and then 2 sets of laboratory data are applied to verify the reliability of the coupling model in **Section 3**. In **Section 4**, the model is applied to a typical shallow lake, Taihu Lake, and the influence of vegetation on the wind-induced wave and current characteristics in the lake are studied. Finally, a brief conclusion is drawn in **Section 5**.

2 METHODS

Open TELEMAC-MASCARET is a set of open-source models for solving free surface flows, including the three-dimensional flow model TELEMAC-3D and the wave model TOMAWAC. In this article, the vegetation module was established based on FORTRAN (Add body resistance to the momentum equation. Add the vegetation turbulence term to the standard k-ε turbulence model. Add the dissipative term of vegetation to the wave spectrum energy balance equation); the module was coupled with TELEMAC-3D and TOMAWAC through the model coupling toolbox (MCT). Finally, the flow–wave–vegetation coupling model was constructed.

2.1 Flow Model

TELEMAC-3D (Hervouet, 2007) is a set of calculation module for simulating three-dimensional non-hydrostatic free surface flow, which is solved by the unstructured grid and finite element method. Its governing equation can be described by the RANS equation:.

$$\frac{\partial \overline{u_i}}{\partial x_i} = 0, \tag{2.1}$$

$$\frac{\partial \overline{u_i}}{\partial t} + \overline{u_j}\frac{\partial \overline{u_i}}{\partial x_j} = -\frac{1}{\rho}\frac{\partial \bar{P}}{\partial x_i} + g_i + \frac{\partial}{\partial x_j}\left[\nu\left(\frac{\partial \overline{u_i}}{\partial x_j} + \frac{\partial \overline{u_j}}{\partial x_i}\right) - \overline{u_i' u_j'}\right] + F_w - F_v + F_s. \tag{2.2}$$

Based on the non-hydrostatic assumption, the total pressure can be written as the sum of hydrostatic pressure and hydrodynamic pressure.

$$\bar{P} = P_{atm} + \rho g\left(Z_s - z\right) + \overline{P_{dyn}}, \tag{2.3}$$

where $\overline{u_i}$ ($\overline{u_1} = \bar{u}, \overline{u_2} = \bar{v}, \overline{u_3} = \bar{w}$) is the time average velocity in three directions; t is the time; $\bar{P}$ is the time average pressure; ρ is the density of water; ν is the dynamic viscosity; g_i is the acceleration of gravity in direction i; F_w is the wind stress

term; F_v is the resistance term of aquatic vegetation; F_s is the wave radiation stress term, and Mellor radiation stress formula was used for calculation; P_{atm} is the atmospheric pressure; Z_s is the water surface elevation; and $\overline{P_{dyn}}$ is the time averaged hydrodynamic pressure.

The wind stress term can be written as follows:

$$F_w = \frac{\rho air}{\rho} C_d W \vec{W}, \tag{2.4}$$

where ρair is the air density near the water surface, W is the wind speed, and C_d is the drag coefficient of wind stress, which is calculated by the formula proposed by Large and Pond (Large and Pond, 1981).

The resistance term of aquatic vegetation considering the porous media effect can be written as (Sonnenwald et al., 2019)

$$F_v = 0.5 \frac{D_v N_v C_{dv}}{1-\varphi} \overline{u_i} \sqrt{\overline{u_i u_j}} H(z - h_v), \tag{2.5}$$

where D_v is the diameter of vegetation, N_v is the number of plants per square meter, C_{dv} is the resistance coefficient of vegetation, φ is the density of vegetation and $\varphi = \pi N_v {D_v}^2/4$, z is the z coordinate of the node, h_v is the height of vegetation, and $H(x)$ is the Heaviside function.

$$H(z - h_v) = \begin{cases} 0, z > h_v \\ 1, z \le h_v \end{cases}. \tag{2.6}$$

In this study, the standard k-ε turbulence model was used to close **Eqs. 2.1, 2.2**, and the transport equation of turbulent kinetic energy k and turbulent dissipation rate ε can be written as (King et al., 2012)

$$\frac{\partial k}{\partial t} + \overline{u_j} \frac{\partial k}{\partial x_j} = \frac{\partial}{\partial x_j} \left[\left(\nu + \frac{\nu_t}{\sigma_k} \right) \frac{\partial k}{\partial x_j} \right] + T + P - G - \varepsilon, \tag{2.7}$$

$$\frac{\partial \varepsilon}{\partial t} + \overline{u_j} \frac{\partial \varepsilon}{\partial x_j} = \frac{\partial}{\partial x_j} \left[\left(\nu + \frac{\nu_t}{\sigma_\varepsilon} \right) \frac{\partial \varepsilon}{\partial x_j} \right] + C_{1\varepsilon} \frac{\varepsilon}{k} [P + (1 - C_{3\varepsilon}) G] - C_{2\varepsilon} \frac{\varepsilon^2}{k} + T\tau^{-1}, \tag{2.8}$$

where P is the turbulence production term, G is the term of gravity source, T is the source term of k equation, $T\tau^{-1}$ is the source term of ε equation, and ν_t is turbulent dynamic viscosity.

$$\nu_t = C_\mu \frac{k^2}{\varepsilon}, \tag{2.9}$$

$$T = F_v \vec{v}, \tag{2.10}$$

$$\tau = \min \left(\frac{1}{C_{2\varepsilon}^*} \frac{k}{\varepsilon}, \frac{1}{C_{2\varepsilon}^* \sqrt{C_\mu}} \sqrt[3]{\frac{L^2}{T}} \right), \tag{2.11}$$

$$L = C_l \sqrt{\frac{1-\varphi}{N_v}}, \tag{2.12}$$

where $C_\mu = 0.09$; C_l is a coefficient that scales the vegetation patch geometry to the mean turbulence length scale, with a value of 0.8 based on the study of Uittenbogaard (Vossen and Uittenbogaard, 2004); and σ_k and σ_ε are Prantdl numbers, where $C_{1\varepsilon} = 1.44$, $C_{2\varepsilon} = 1.92$, $\sigma_k = 1.0$, and $\sigma_\varepsilon = 1.3$.

2.2 Wave Model

TOMAWAC is the third generation of the spectral wave model. By accurately solving the non-linear wave energy transfer, it can solve the spectral energy balance equation without being limited by the shape of the wave spectrum. In the Cartesian coordinate system, the energy balance equation of spectrum can be written as follows:

$$\frac{\partial N}{\partial t} + \frac{\partial N\dot{x}}{\partial x} + \frac{\partial N\dot{y}}{\partial y} + \frac{\partial \dot{k}x}{\partial kx} + \frac{\partial \dot{k}y}{\partial ky} = Q(kx, ky, x, y, t), \tag{2.13}$$

where n is the wave action density, $k = (kx,ky) = (ksin\theta, ksin\theta)$ is the wave number vector, θ represents the direction of wave propagation, and Q represents the source term including wind, vegetation, and terrain effects.

Based on the Rayleigh probability density function and replacing the wave height (H) with the root mean square wave height (Hrms), the influence of vegetation on waves can be written as the following equation (Bacchi et al., 2014):

$$Q_v = \frac{1}{\sigma 2\sqrt{\pi}} \rho C_{dv} B_v N_v \left(\frac{kg}{2\sigma} \right)^3 \frac{\sinh(k\alpha h) + 3\sinh(k\alpha h)}{3k\cosh^3(kh)} H_{rms}, \tag{2.14}$$

where σ is the wave frequency and α is the ratio of vegetation height to local water depth.

3 MODEL VERIFICATION

In this section, we will use the flow–wave–vegetation coupling model constructed in the previous section to reproduce the two groups of model tests (Løvås, 2000; Neumeier, 2007), and compare the numerical simulation results with the model test results to illustrate the accuracy of the coupling model.

3.1 Open Channel Flow with Submerged Vegetation

Neumeier studied the three-dimensional flow field and turbulence characteristics at the tip of Spartina through a large number of flume experiments. Here, we take experiment BB to verify the accuracy of the coupling model. The computational domain size and model parameters of the numerical simulation are consistent with Neumeier's model test as far as possible. The experimental tank is 5 m long, 0.3 m wide, and 0.46 m high. Vegetation is laid from 2 m away from the inlet of the tank to the end of the tank.

The flow velocity at the inlet of the flume is 0.066 m/s, the water depth is 0.32 m, the average height of vegetation is 0.153 m, the average diameter is 0.0035 m, the vegetation density is 1,200 stem/m^2, and the vegetation resistance coefficient is calculated by the formula proposed in the study by Kothyari et al. (2009). The calculation area is divided into unstructured

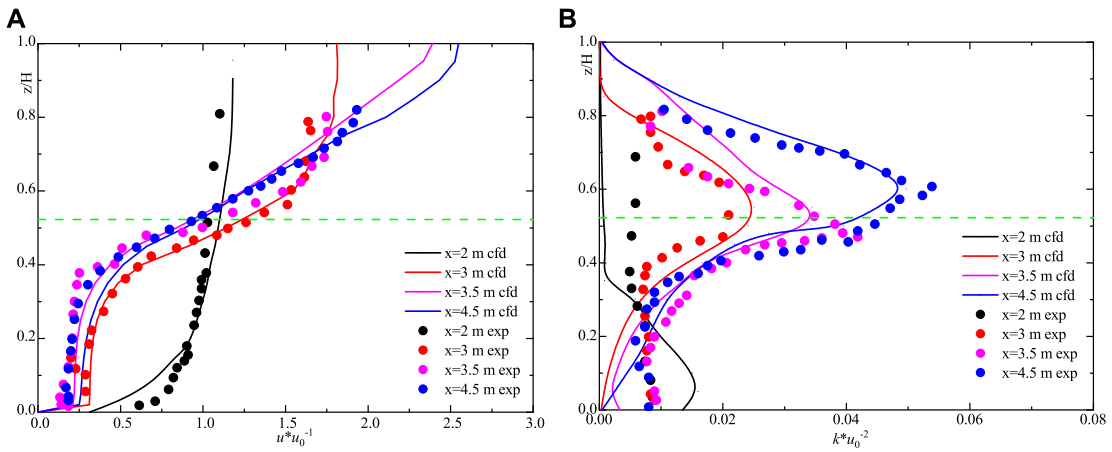

FIGURE 1 | Comparison of numerical simulation and model test: **(A)** dimensionless velocity and **(B)** dimensionless turbulent kinetic energy.

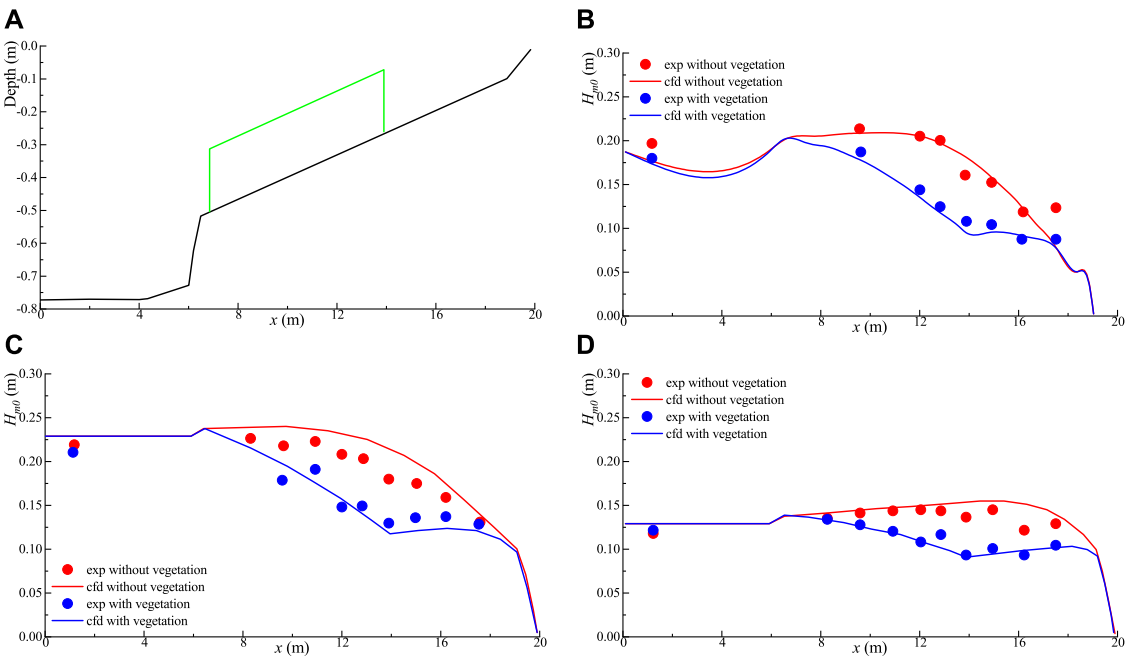

FIGURE 2 | Comparison between numerical simulation and model test on the influence of vegetation patches on breaking wave height: **(A)** Bathymetry; **(B)** Case1; **(C)** Case2; and **(D)** Case3.

grids with 12,224 elements and 26,653 nodes, and 20 layers of grids are distributed unevenly along the vertical direction. In order to meet the requirements of the turbulence model for the boundary layer, the boundary layer is locally dandified. The calculation step is set to 0.2 s.

The comparison of numerical simulation and model test is shown in **Figure 1**. The position z, stream-wise velocity u, and turbulent kinetic energy k are dimensionless by water depth H, inlet velocity u_0, and the square of inlet velocity $u02$, respectively. The results of numerical simulation in the vegetation layer are in good agreement with those of the model, while those above the canopy are in poor agreement. The location and magnitude of the maximum turbulent kinetic energy are well simulated by the model, and the numerical simulation results of some locations are quite different from those of the physical model. This is due to the fact that different vegetation types and positions have different resistance coefficients along the vertical direction, and the whole resistance of vegetation patches is replaced by a resistance coefficient in the model calculation, which leads to errors. In general, the model can capture the effect of vegetation on flow.

TABLE 1 | Parameters of the incident wave in test condition.

Case	Incident wave height, H_{m0} (m)	Period of incident wave, T_{m0} (s)	Water depth, h (m)
1	0.180	3.5	0.69
2	0.220	2.5	0.77
3	0.125	3.5	0.77

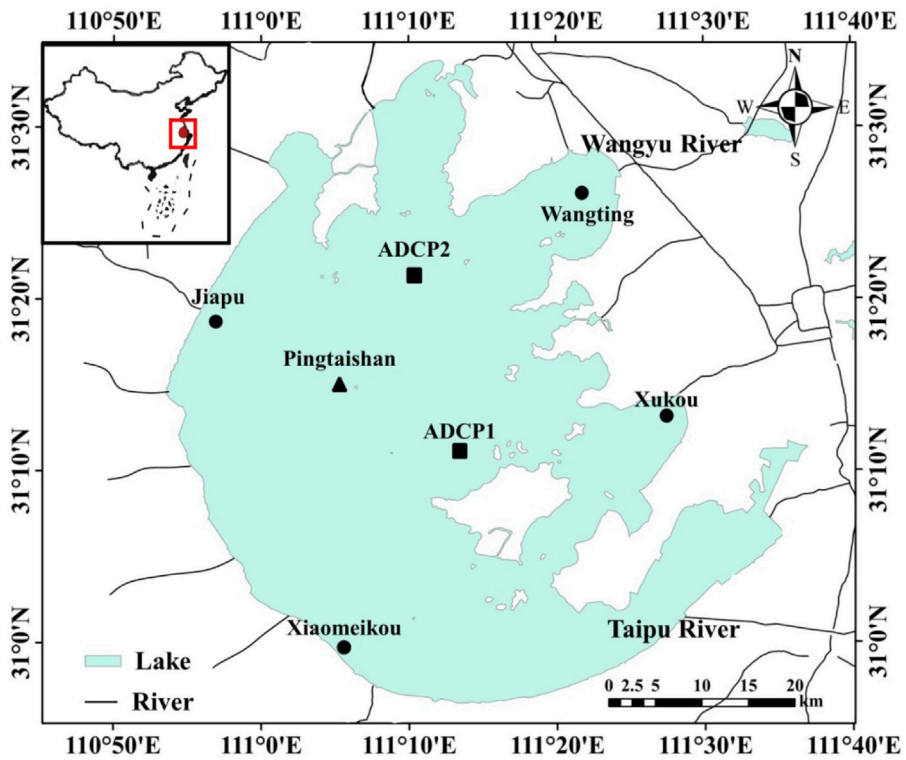

FIGURE 3 | Geographical location of the study area, surrounding rivers, and monitoring points (where circular points are water-level verification points; square points are speed verification points; triangle points are wave height verification points).

3.2 Wave Through Emergent Vegetation

Based on wave flume, Lovas studied the effects of vegetation on wave propagation with different incident breaking wave parameters in shallow water. The experimental wave flume is 40 m long and 0.6 m wide. The artificial seaweed is placed on the slope of 1:30, and the vegetation patch is 7.26 m long. The model terrain is shown in **Figure 2A**. The height and diameter of artificial seaweed are 0.2 and 0.025 m respectively, and the vegetation density is 1,200 stem/m^2. In this calculation, three conditions including four different incident wave heights, two incident wave periods, and two water depths are selected to verify the simulation accuracy of the model for broken wave propagation and the vegetation dissipation process. The parameters of incident wave in the test conditions are shown in **Table 1**. The JONSWAP spectrum was used in the model, and the vegetation resistance coefficient was calculated by the formula proposed in the study by Kothyari et al. (2009). An unstructured grid is used in the calculation domain, and the calculation step is set to 0.2 s.

The comparison of numerical simulation and model test on the influence of vegetation patches on breaking wave height is shown in **Figure 2** above. The red data represent condition without vegetation, and the blue data represent condition with vegetation. It can be seen that in the process of wave propagation on the slope, the wave height decreases gradually. The wave energy dissipation provided by vegetation and topography contributes to the wave height attenuation, and the attenuation effect of vegetation on the wave is obvious. The results of numerical simulation are consistent with the experimental data under the three conditions, and the two sets of data are in good agreement, which indicates that the model can effectively simulate the propagation process of waves in vegetation patches.

4 MODEL APPLICATION

4.1 Study Area and Model Set up

Taihu Lake is located in the lower reaches of the Yangtze River Delta in Southeast China. It is the third largest freshwater lake in China, and its geographical location is shown in **Figure 3**. As a typical large shallow lake, the total area of Taihu Lake Basin is 36,900 m^2, the total area of Lake area is 2427.8 m^2, the average water depth is 1.9 m, and the maximum water depth is no more than 3 m. The Taihu Lake Basin has a subtropical monsoon climate, with an average annual rainfall of 1,200 mm, mainly in the monsoon season from May to September. Due to global warming and environmental pollution in recent years, algae blooms often occur in Taihu Lake, which has a devastating impact on the ecosystem (Jalil et al., 2019).

The lake is connected to more than 150 rivers, many of which are seasonal. Because Taihu Lake is located in an area with strong human activities, a large number of water conservancy projects have made the inflow and outflow of the Lake strongly interfered by human activities. The main driving force of flow and wave field is wind. The dominant wind direction is southeast in summer and northwest in winter.

In recent years, the distribution and density of vegetation patches in Taihu Lake have changed with time, which affects the hydrodynamic characteristics, sediment, wave characteristics, and the stability of the lake ecosystem. The main vegetation types in Taihu Lake can be divided into submerged vegetation, emergent vegetation, and floating vegetation. Among them, submerged vegetation is dominated by *Vallisneria natans* and *Ceratophyllum demersum* L., emergent vegetation is dominated by *Phragmites australis* and *Zizania latifolia*, and floating vegetation is dominated by *Potamogeton microdentatus*. We used *Vallisneria natans* and *Phragmites australis* as the dominant of submerged vegetation and emergent vegetation, respectively, considering the influence of floating vegetation on the flow field of shallow lake is relatively small compared with the other two kinds of vegetation (Xu et al., 2018). In this study, only the effects of submerged vegetation and emergent vegetation on the characteristics of wind-driven current and wave are considered.

An unstructured grid is used in the computational domain. The horizontal grid consists of 1,25,433 cells and 59,386 nodes, and the size of the grid is between 30 and 150 m. The vertical grid is arranged in 30 layers according to the sigma coordinate, and the local refinement is carried out at the bottom and free surface. The average maximum depth slope of the grid is less than 0.33 to avoid the pressure gradient error caused by sigma transformation. The global calculation step is set to 1 s to satisfy the CFL stability condition. The model uses cold start and MURD (multidimensional upwind residual distribution scheme) scheme to deal with the convection and diffusion of variables.

The dataset of vegetation characteristics (regional distribution and density of vegetation) in the Taihu Lake region in 2016 was used in the numerical simulation, and the data were from the National Mathematical Center of Earth System Science of China (http://lake.geodata.cn/index.html); based on the Landsat remote sensing data in 2016, the image data of aquatic vegetation was obtained through band combination and image change technology, and the decision tree was constructed on the basis of the image data. Finally, the classification and density estimation results of aquatic vegetation were obtained. The regional distribution of vegetation in the Taihu Lake area is shown in **Figure 4**.

The input parameters of the vegetation model include the identification vector of each vegetation distribution area, resistance coefficient of vegetation, average height, and average width. The product of average height and average width is used to characterize the effective resistance area per unit volume of vegetation. Based on field investigation and the related literature (Wang et al., 2016), the density of submerged vegetation and emergent vegetation was set as 100 stem/m^2 and 150 stem/m^2, respectively, the average height of individual plant was set as 0.5 and 1.5 m, respectively, and the average width of individual plant was set as 0.007 and 0.015 m, respectively. The resistance coefficients of submerged vegetation and emergent vegetation are calculated through Hua's research (Hua et al., 2013).

4.2 Model Verification

The data of 2016 were used to verify the numerical model. The average daily discharge of more than 150 tributaries connected with Taihu Lake in 2016 was generalized to 15 discharge boundaries as the driving force of the inflow and outflow of the lake (Liu et al., 2018); the daily rainfall evaporation data of VM1 station, hourly wind speed, and wind direction of WH1 station are collected as the atmospheric driving force of the model. **Figure 5** shows the wind field data used to drive the model. For the treatment of bottom friction, the equivalent roughness is adopted, and 0.022 m is used for the whole bottom of the lake area. The background horizontal turbulence viscosity is set as 10^{-4} m^2/s, and the vertical turbulence viscosity is set as 10^{-6} m^2/s.

In terms of model validation, hourly water level data of three stations from WL1 to WL3 during May 1 to December 1 were used to verify the water level results of hydrodynamic simulation. The surface velocity of VM1 and VM2 every 3 h from June 25 to 30 was used to verify the results. Daily wave height data from WH1 station from 29 May to 28 July were used to verify the results of wind wave simulation.

Figure 6 shows the simulated and observed data of the water level, velocity, and wave height of six stations, and the reliability of the calculated results is verified by RMSE and SS (Murphy, 1992). Even though the three water level monitoring points are located in different locations of the lake, the fluctuation of the water level shows a similar trend. This is because the water level of the lake is mainly regulated by tributary flow, rainfall, and evaporation. The wind speed has relatively little influence on the fluctuation of the water level. The velocity of VM1 and VM2, and the wave height of WH1 showed a similar trend to the wind speed, indicating that the flow field and wave field in Taihu Lake were mainly regulated by wind speed and direction, respectively. On the whole, the amplitude and phase of the water level, velocity, and wave obtained by simulation and observation are in good agreement.

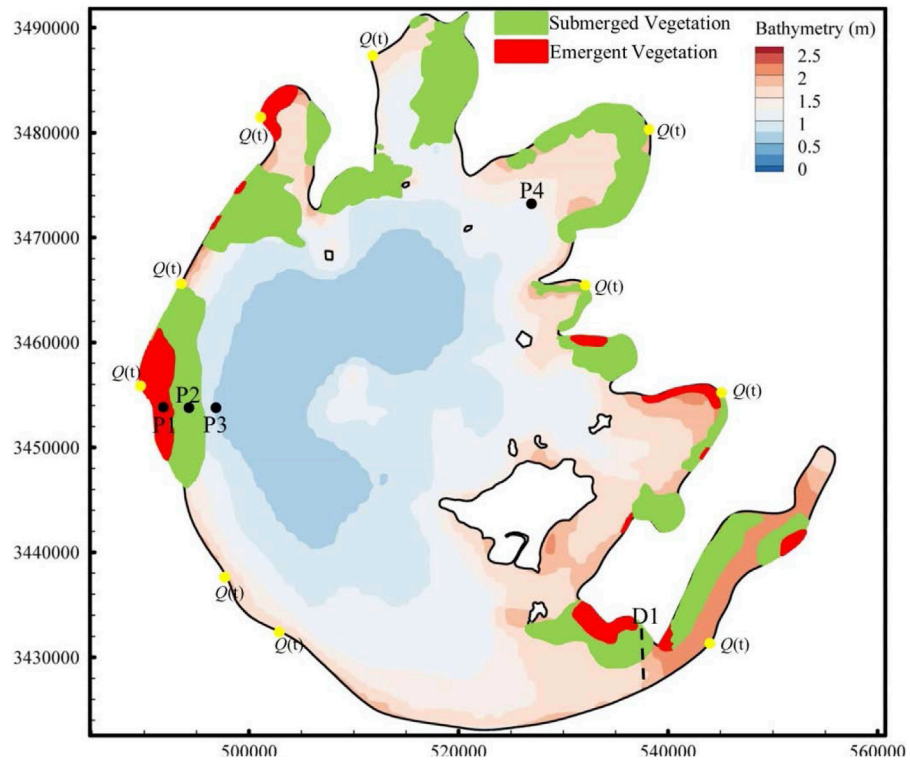

FIGURE 4 | Regional distribution of vegetation in the Taihu Lake area. P1–P4 are the observation points, and D1 is the observation section of numerical simulation.

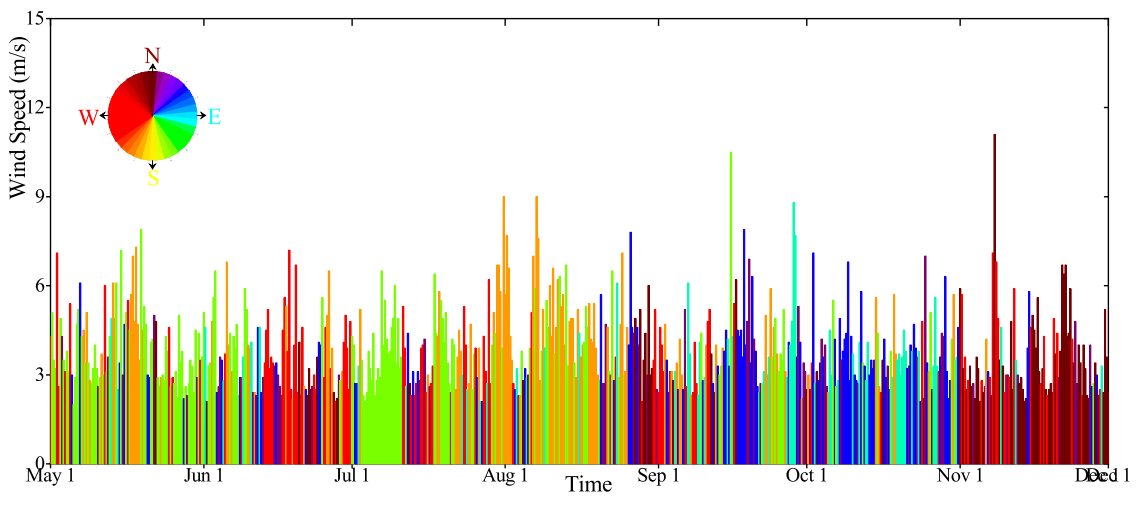

FIGURE 5 | Wind speed and direction during calculation time.

4.3 The Effect of Vegetation on the Wind-Induced Current

Observed wind (see **Figure 5**) shows it could blow persistently at one prevailing direction for a couple of days until it changes direction, while the wind speed changes daily. Under the influence of stable wind direction, complex topography, and boundary of Taihu Lake, a variety of relatively stable circulation gyres will be formed in the lake after vertical averaging.

Figure 7 shows the depth-averaged flow field without the consideration of vegetation, and the velocity of the lake varies greatly in different regions. In the three northern bays, the

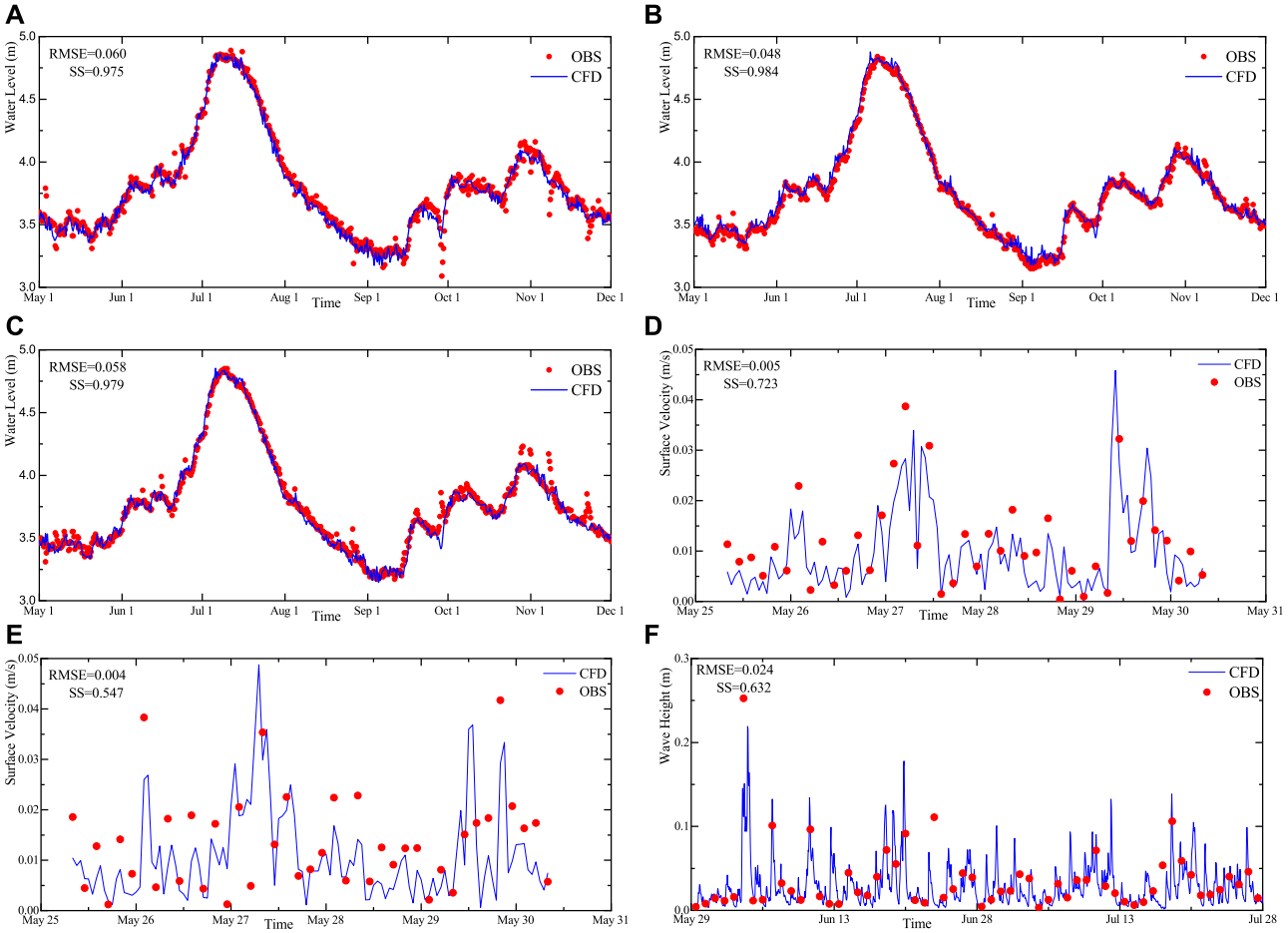

FIGURE 6 | Comparison between numerical simulation results and observed data. **(A)** WL1, **(B)** WL2, **(C)** WL3, **(D)** VM1, **(E)** VM2, and **(F)** WH1.

structures of circulation gyres are similar where two small circulation gyres with opposite directions are formed. The direction of circulations near the entrances of the three bays is clockwise in July when the southeast wind is dominant and counterclockwise in November when the northwest wind is dominant. A slender circulation gyre has been formed along the west coast of the lake, and the average circulation direction is clockwise in July and counterclockwise in November. Several small-scale gyres with different sizes and directions appeared in the central region of the lake under the influence of the high velocity area in the southwest region and the topography of Xishan Island. By comparing the average circulation patterns of Taihu Lake in July and November, it can be seen that the circulation characteristics are similar but the circulation direction is opposite under the influence of different directions of dominant wind (Li et al., 2011).

Figure 8 shows the depth-averaged flow field with the consideration of vegetation. Due to the blockage effect of vegetation, the flow velocity decreases significantly in the lake area with vegetation, and increases to a certain extent in the vicinity of vegetation patches due to the agglomeration of kinetic energy (Tse et al., 2016). The vegetation patches distributed at the entrance of Zhushan Bay and the central part of Meiliang Bay reduces the local current velocity and the water exchange capacity with the central area. Due to the existence of large areas of submerged vegetation and emergent vegetation, the current velocity decreases near the southwest bank of Taihu Lake, thus changing the structure of slender circulation in this region. At the entrance of Dongtaihu Bay, the flow velocity at the vegetation patches on the north side decreased sharply. Due to the narrow bay, the kinetic energy was tightly surrounded by the vegetation patches and the north side, so the flow velocity in this area increased significantly compared with that without considering the vegetation. In summary, it is found that the circulation characteristic of the lake in the two cases is similar, regardless of whether the influence of vegetation is considered, but the circulation structure of the vegetation patch and its vicinity will change significantly.

Figure 9 shows the temporal variation of the velocity difference among the three monitoring points. Among them, P1 is located in the emergent vegetation patch near the west bank of the lake, P2 is located in the submerged vegetation patch, and P3 is located in the non-vegetation area, affected by the

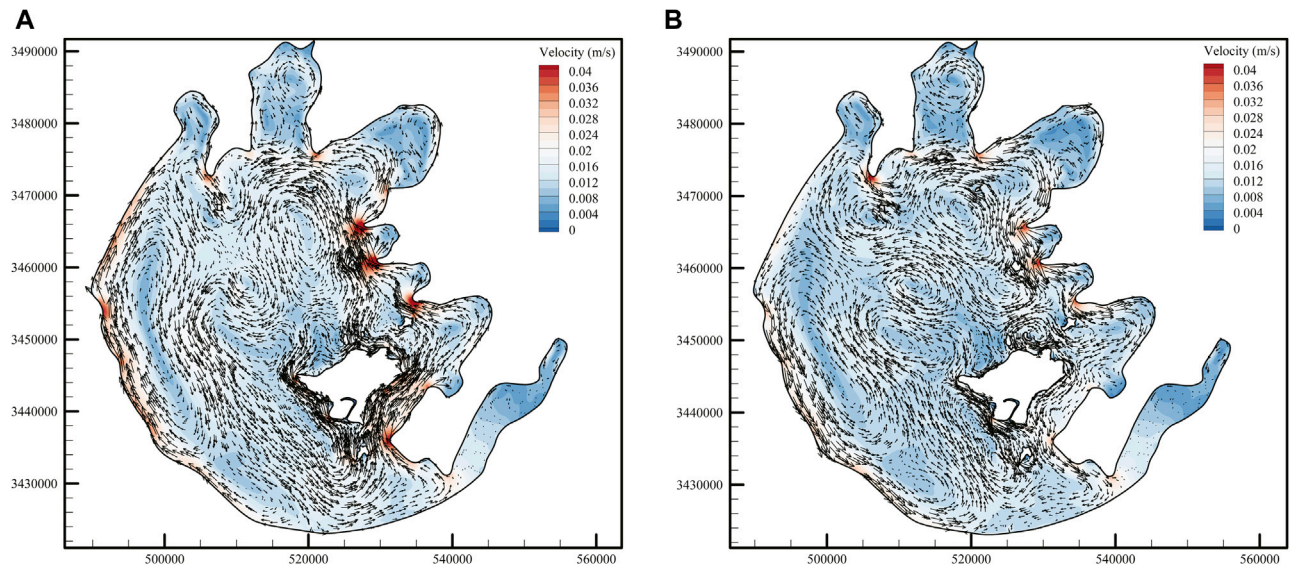

FIGURE 7 | Monthly mean depth-averaged flow field without the consideration of vegetation: **(A)** July and **(B)** November.

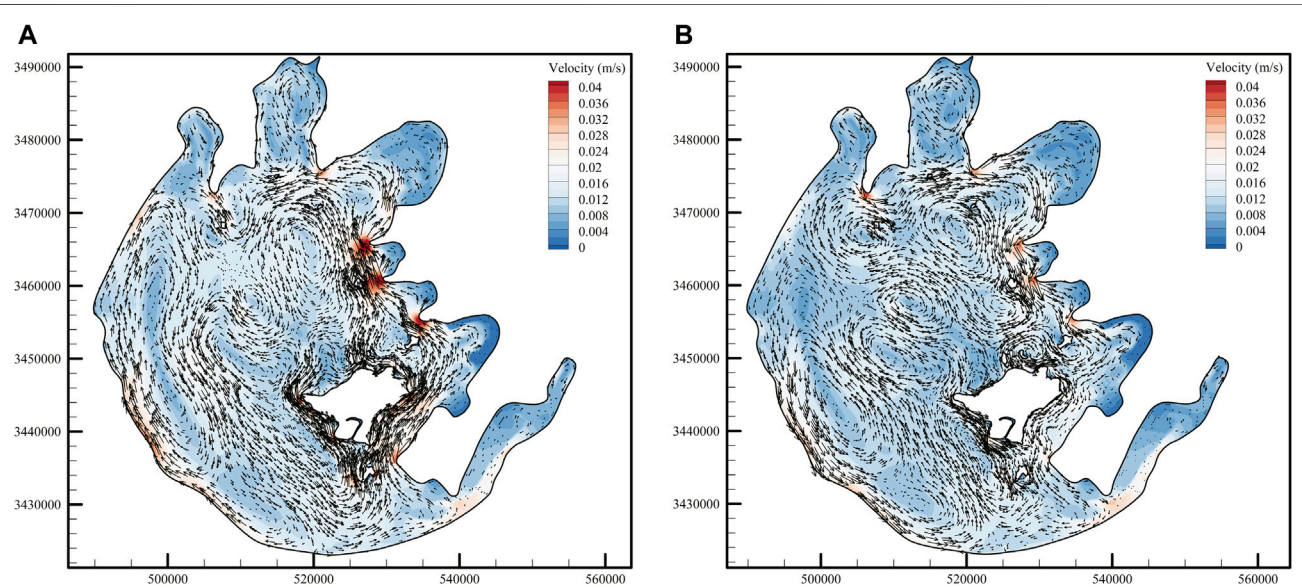

FIGURE 8 | Monthly mean depth-averaged flow field with the consideration of vegetation: **(A)** July and **(B)** November.

topography of Taihu Lake and local wind field; the area where the three points are located is prone to elongated circulation gyre near the west shore (see **Figure 7**). The velocity difference of P1 is greater than that of P2, indicating that the blocking effect of emergent vegetation is stronger than that of submerged vegetation. The velocity difference of P3 is mostly less than 0, which is due to the redistribution of kinetic energy caused by the influence of vegetation obstruction near the west coast. As a result, the flow velocity in this region with vegetation is greater than that without vegetation. Meanwhile, when the velocity difference of P1 is large, the velocity difference of P2 and P3 is also large.

Figure 10 shows the vertical flow field of the cross section shown by the dotted line in the figure. The submerged vegetation is distributed on the north side of the entrance of Dongtaihu Bay (see the green dotted line in **Figure 4B**). In the absence of vegetation, due to the shear action of wind stress, the flow velocity on the free surface is higher than that at the bottom. Meanwhile, influenced by the circulation and the compensation flow at the bottom, the section forms a

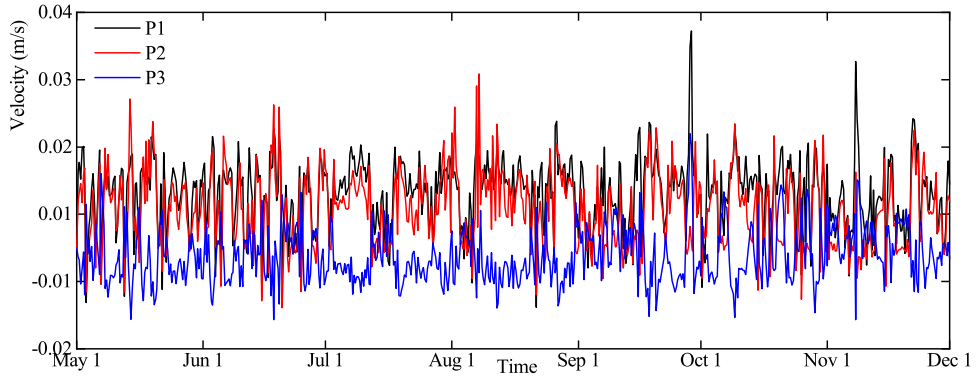

FIGURE 9 | Time variation of velocity difference at monitoring points; positive values in the figure indicate that the flow velocity under the condition of without vegetation is higher than that under the condition of with vegetation.

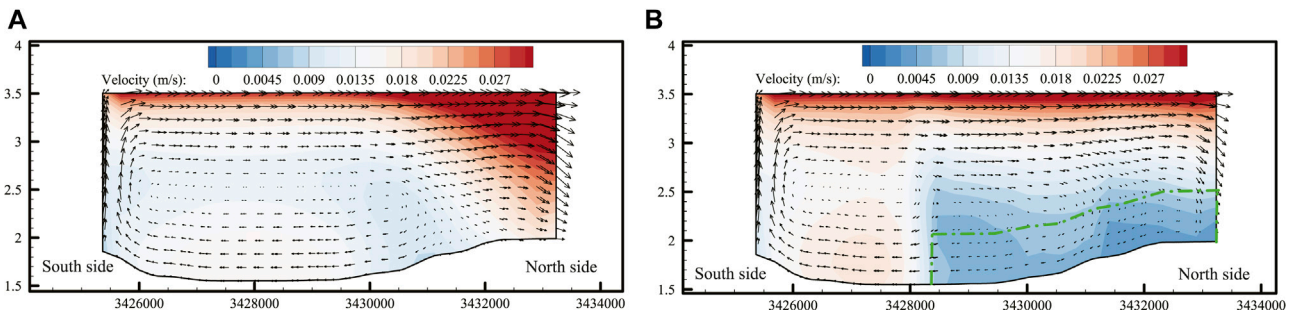

FIGURE 10 | Vertical velocity distribution of the section of Dongtaihu Bay in July; green dots in the figure represent vegetation patches. **(A)** Without vegetation and **(B)** with vegetation.

clockwise secondary flow, and the average velocity on the north side of the section is higher than that on the south side. When considering the influence of vegetation, the flow velocity of vegetation patch decreases due to the blocking effect of vegetation. The average velocity on the north side of the section decreased, while the velocity on the south side of the section increased significantly due to the redistribution of kinetic energy, which was much higher than that without considering the influence of vegetation. The presence of local vegetation patches changed the secondary flow characteristics of the section. Episodic shear flow over the top of the vegetation has a capacity to redistribute constituents and organisms positioned deeply within the vegetation, remote from open water (Abdul et al., 2017a).

4.4 The Effect of Vegetation on the Wind-Induced Wave

Figure 11 shows the average wave height distribution of the lake in July with and without the consideration of vegetation, and the simulation results of other monthly averages are similar to the figure, so they will not be repeated. As shown in **Figure 11A**, the high wave height mainly occurs in the areas with large wind blowing fetch and deep water depth. Comparing the distribution of wave height and the topography of Taihu Lake, it can be seen that the area with the maximum water depth is very similar to the area with the maximum wave height. **Figure 11B** shows the wave height distribution with the consideration of vegetation. It can be seen that there is no obvious change in the wave height of submerged vegetation patches. Under the influence of blocking effect of emergent vegetation, the wave height on the west bank and the north bank of the entrance of Dongtaihu Bay decreased significantly; this is because the resistance coefficient, vegetation height, and the width of submerged vegetation are much lower than those of emergent vegetation, making the ability of submerged vegetation to reduce wind-induced wave worse than that of emergent vegetation. The simulation results show that emergent vegetation has the potential to provide coastline protection by reducing wave height.

Figure 12 shows the time sequence changes of wave height difference at monitoring points P1 and P2. It can be seen from the figure that the wave height difference at the emergent vegetation patch is much higher than that at the submerged vegetation patch (Parvathy et al., 2017). According to **Figure 5**, when the wind direction is southeast and lasts for a long time, the wind blowing fetch and wave height of P1 and P2 points

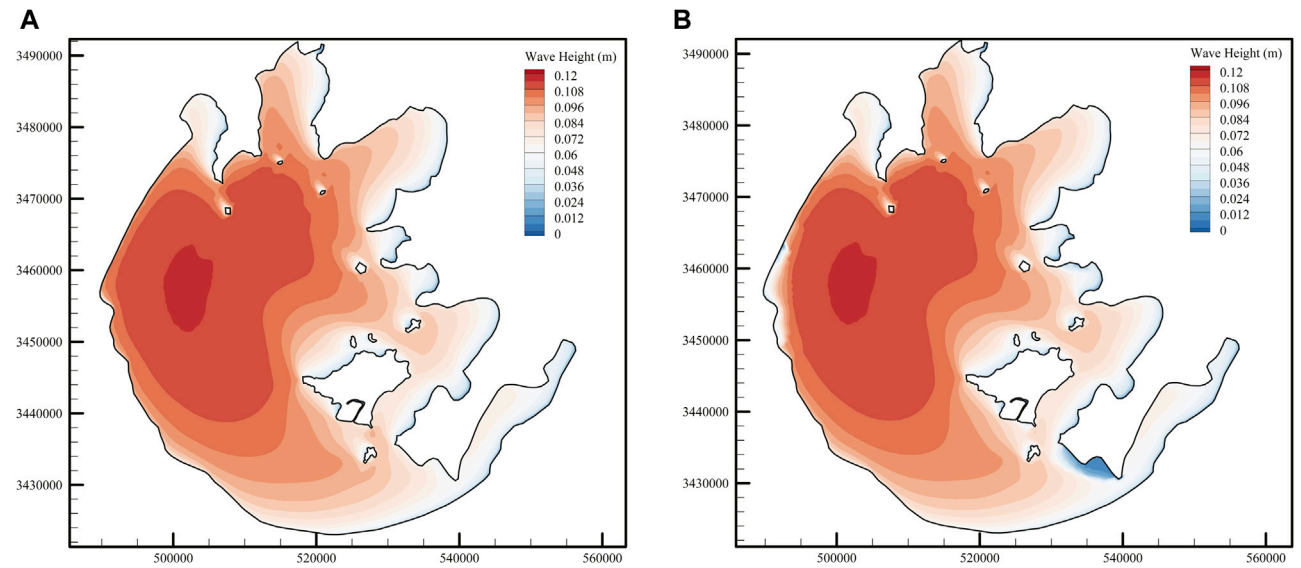

FIGURE 11 | Average wave height distribution of Taihu Lake with and without vegetation in July. **(A)** Without vegetation and **(B)** with vegetation.

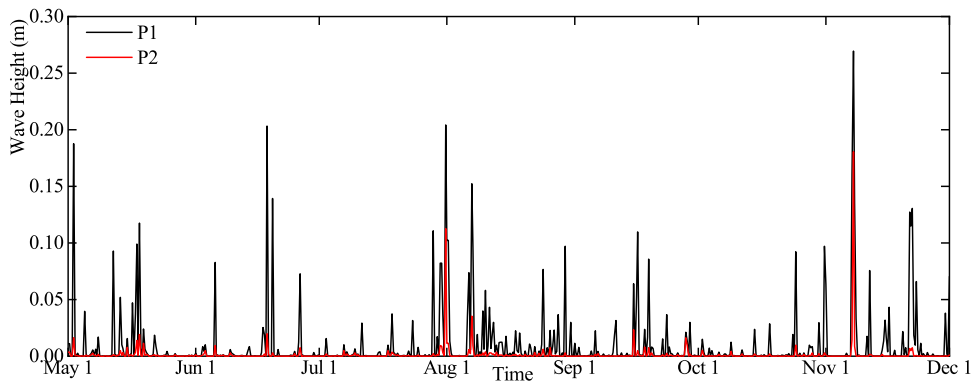

FIGURE 12 | Time variation of wave height difference at monitoring points; positive values in the figure indicate that the wave height under the condition of without vegetation is higher than that under the condition of with vegetation.

are larger, and the larger the incident wave height is, the more obvious the wave height attenuation of vegetation water area is. Therefore, it is feasible to protect the lake bank embankment project by arranging appropriate emergent vegetation patches on the west bank of the lake to reduce the high wind-induced wave caused by typhoons in summer.

4.5 The Effects of Vegetation on Material Transport Characteristics

In order to study the influence of vegetation on the material transport characteristics of Taihu Lake, the tracer was continuously released at the inlet of Wangyu River at the amount of 1 kg/s, and the initial tracer concentration in the calculation domain was set to 0. Here, in this study, depth-averaged tracer concentration is presented. **Figure 13** shows the concentration distribution of the tracer in the lake at different times without the consideration of vegetation; after leaving Gonghu Bay, the tracer entered the central area of the lake and was mixed into these bays due to the influence of small-scale circulation gyres. As the dominant wind direction in July was opposite to that in November, the high tracer concentration area in Taihu Lake was located in the northwest region under the dominance of southeast wind in July, while the high tracer concentration area under the dominance of northwest wind in November was located in the southeast region. Combined with the monthly mean flow field in Taihu Lake shown in **Figure 7**, it has been found that the transport characteristics of tracer in Taihu Lake are mainly controlled by different circulation structures under the influence of different wind directions.

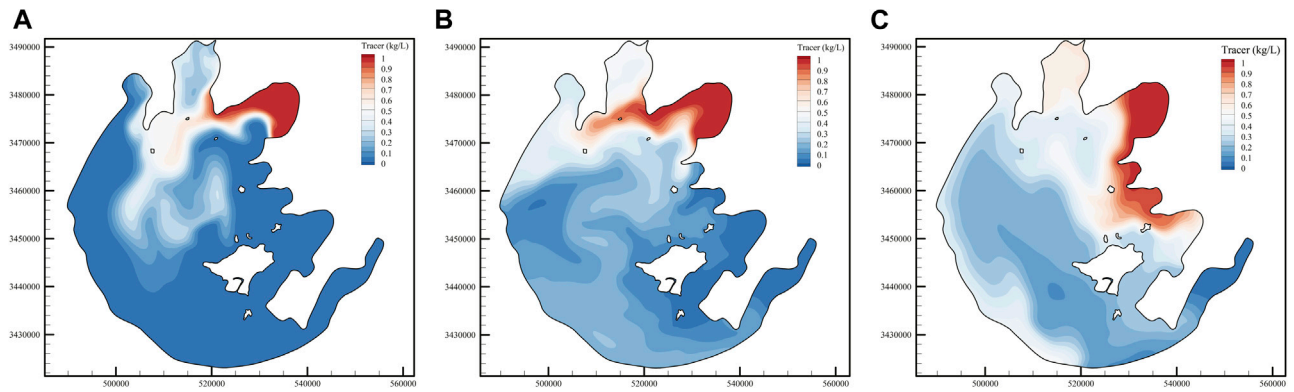

FIGURE 13 | Time series of tracer concentration images without the consideration of vegetation: **(A)** Jul, 31st, **(B)** Sept, 30th, and **(C)** Nov, 30th.

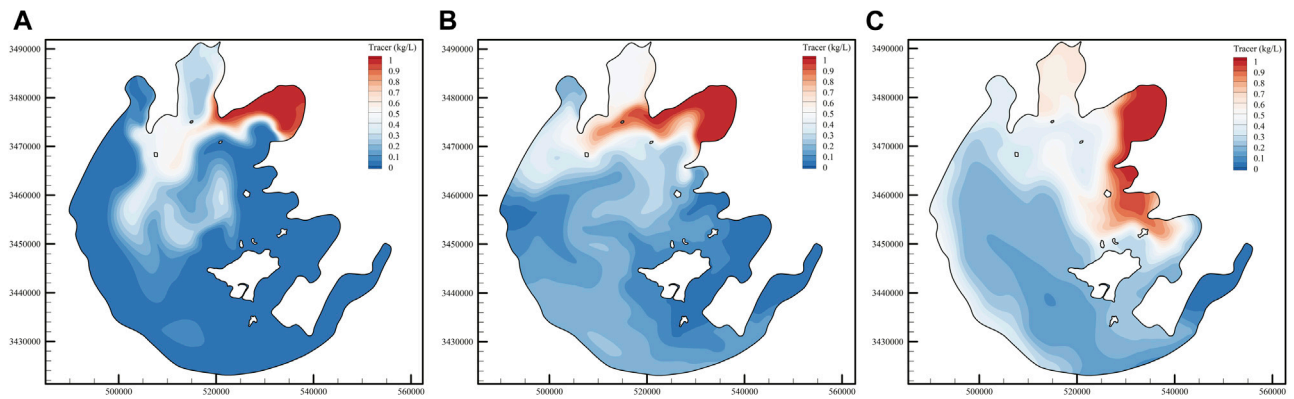

FIGURE 14 | Time series of tracer concentration images with the consideration of vegetation: **(A)** Jul, 31st, **(B)** Sept, 30th, and **(C)** Nov, 30th.

Figure 14 shows the concentration distribution of the tracer in the lake at different times with the consideration of vegetation. Combined with **Figures 13**, **15**, it can be seen that vegetation can "delay" the transport of the tracer. For example, without the consideration of vegetation, tracers have been spread throughout the whole Gonghu Bay on 30 July, and covered most of the Zhushan Bay. With the consideration of vegetation, the concentration of the tracer in the southern part of Gonghu Bay and the northern part of Zhushan Bay decrease significantly. No significant difference is found in the concentration of tracer in the two regions, whether vegetation is considered or not on 30 September. These conditions also occur on the west bank of the lake on 30 September and in the Xukou Bay area on 30 November. The area with large concentration difference of tracer gradually evolves from the three northern bays to the southwest region of Taihu Lake, which is related to the mainstream movement direction of the tracer. The maximum difference of tracer concentration at different times can reach 0.29 kg/s, and the tracer area under the condition of considering vegetation is smaller than that without considering vegetation. The main reason for the difference in tracer concentration is due to the blocking effect of vegetation, which reduces the local velocity and changes the circulation structure, thus affecting the convection and diffusion of the tracer. In summary, the presence of vegetation reduces the exchange rate between vegetation patches and the outside world, and has an important effect on the material transport characteristics of the lake.

4.6 Sensitivity Analysis

In the vegetation resistance term, density, height, and diameter of vegetation largely determine the resistance per unit area. In different seasons, the density, height, and diameter of each vegetation patch in the lake are different, but most of the models use constant values that do not change with time and space, which is bound to have a great impact on the results.

In order to study the effects of different vegetation parameter values on the characteristics of wind-induced wave and current in Taihu Lake, sensitivity analysis was conducted for vegetation density in this section. The reference density (150 stem/m^2 for emergent vegetation and 100 stem/m^2 for submerged vegetation) was n = 1.0 and n = 0 for the absence of vegetation. **Figure 16**

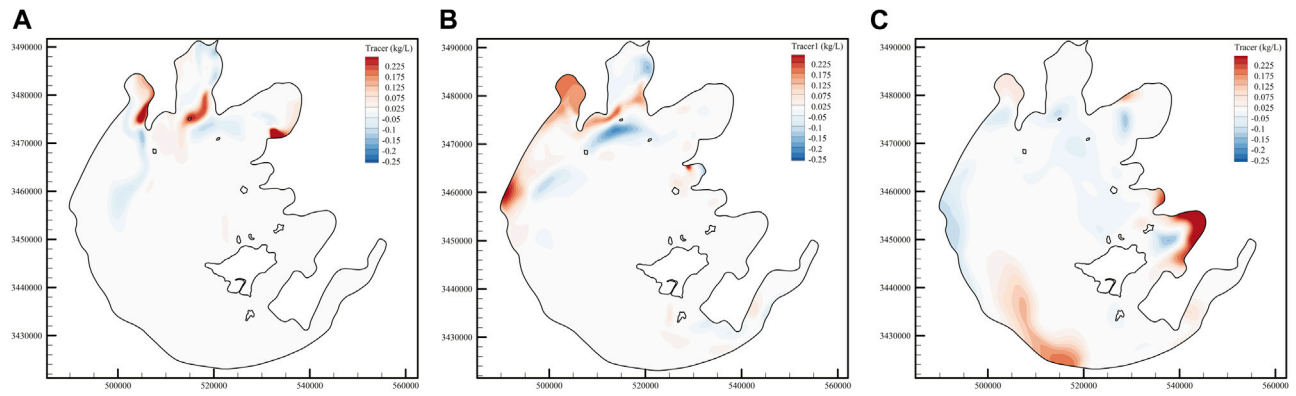

FIGURE 15 | Spatial influence of vegetation on tracer concentration; positive values in the figure indicate that the tracer concentration under the condition of without vegetation is higher than that under the condition of with vegetation. **(A)** Jul, 31st, **(B)** Sept, 30th, and **(C)** Nov, 30th.

shows the influence of different vegetation densities on the results. With the gradual increase of vegetation density, the velocity of P1 gradually decreases. Meanwhile, due to the redistribution of kinetic energy, the velocity of P3 increases, and the trend of decreasing or rising velocity flattens out with the increase of vegetation density. Similar effects also appear in the simulation of wave height. The wave height at P1 and P2 decreases with the increase of vegetation density, and the decreasing trend of velocity gradually flattens out. Meanwhile, the decreasing gradient of wave height at P1 is much lower than that of P1, indicating that the capacity of emergent vegetation to reduce wind-induced wave is greater than that of submerged vegetation. As can be seen from **Figure 16C**, the concentration of the tracer at P1 point showed a trend of gradual increase and then decrease over time without the consideration of vegetation. In the case of considering the influence of vegetation, the change of tracer concentration at P1 is similar to that without considering vegetation, but the inflection point (the point where tracer concentration changes from an upward trend to a downward trend) appears later, and the maximum tracer concentration decreases. With the gradual increase of vegetation density, the inflection point appeared later, and the maximum concentration of tracer gradually decreased. Even if the overall vegetation density is reduced to 25% of the reference density (37.5 stem/m^2 for emergent vegetation and 25 stem/m^2 for submerged vegetation), the results of the wind-induced wave and current characteristics of shallow lakes with the consideration of vegetation are significantly different from those without the consideration of vegetation. Therefore, the influence of vegetation should not be ignored in the numerical simulation of lake dynamics.

5 DISCUSSION

As a typical eutrophic lake, the algae bloom usually exists in Taihu Lake, which is closely related to the characteristics of wind-induced wave and current (Abdul et al., 2017b). The nutrients would be transported due to strong wind-induced current. At the same time, wind waves are also conducive to the re-suspension of the sediment and to promote the release of nutrients from the sediment. The model application in **Section 4** shows the applicability of the flow–wave–vegetation coupling model in the numerical simulation of shallow lakes with vegetation patches. The results show that the presence of vegetation patches significantly changes the characteristics of the wind-induced wave, current, and material transport in shallow lakes. This shows that the layout of submerged and emergent vegetation patches in appropriate areas can change the lake hydrodynamic structure in local areas where algae bloom usually occurs, so as to reduce the probability of algae bloom. These results provide meaningful information for the study of long-term vegetation evolution in shallow lakes.

However, the flow–wave–vegetation coupling model established above has some limitations and uncertainties. Different from the similar and evenly distributed vegetation in the laboratory, the vegetation parameters in the natural environment are often uncertain, and the vegetation types, growth degree, density, project area, and drag coefficient in different regions are often different (Li et al., 2020). At present, methods such as NDVI estimation (Adamala et al., 2016) and field sampling have been widely used to retrieve vegetation parameters in shallow lakes. But the error of observation and the different choice of the calculation model will lead to the different results of vegetation parameters under different schemes (Lamchin et al., 2020). As shown in the sensitivity analysis in **Section 4.6**, there are obvious differences in the wind-induced wave, current, and material transport characteristics with different vegetation densities (Smith et al., 2016), but these vegetation parameters are often roughly summarized in mathematical models (Weiming and Marsooli, 2012); for example, the vegetation density in the whole vegetation patch is set to the same value (although the vegetation density in different areas of the same vegetation patch is different); this leads to the distortion of the calculation results. In the future, it is necessary to refine the resistance module of vegetation, so as to

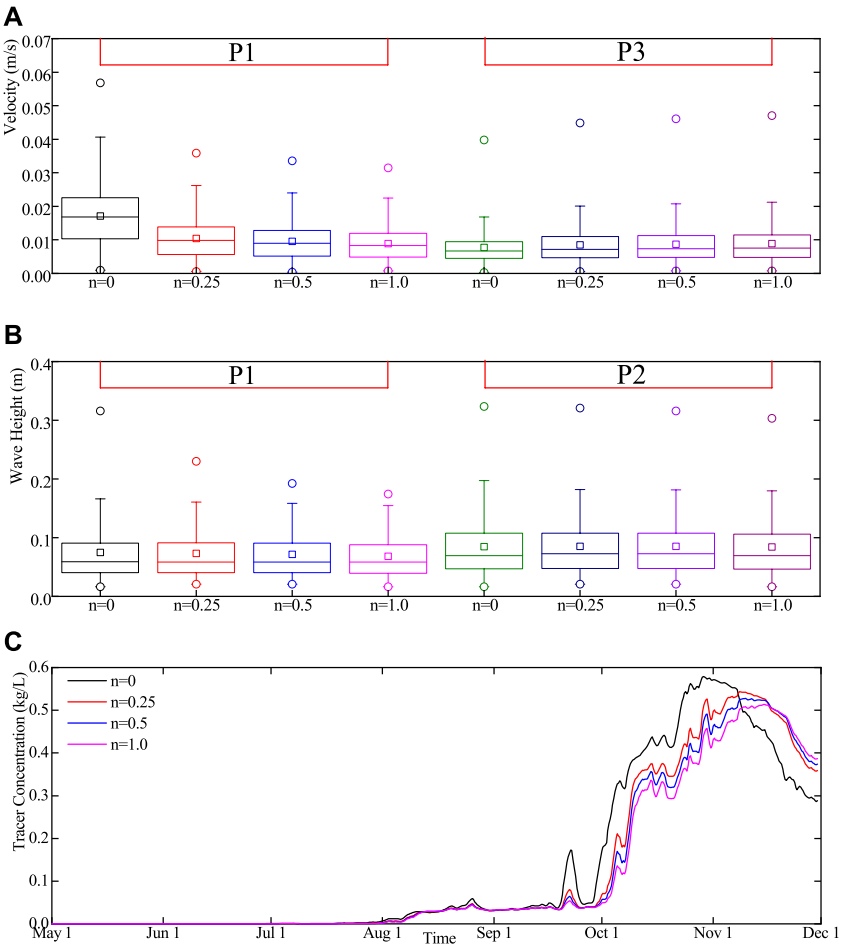

FIGURE 16 | Sensitivity analysis of the influence of vegetation density on the results: **(A)** sensitivity analysis of velocity at P1 and P3, **(B)** sensitivity analysis of wave height at P1 and P2, and **(C)** sensitivity analysis of tracer concentration at P1.

make the calculation results of the model closer to the real situation.

Meanwhile, the application of the flow–wave–vegetation coupling model also touches the challenge of simulating the long-term and large-scale vegetation growth and attenuation process. The distribution and parameters of vegetation patches will change periodically with different seasons, but the coupling model does not take into account the response of vegetation to nutrients, light intensity, and suspended sediment concentration, so it cannot simulate the process of vegetation growth and attenuation (Cerco and Moore, 2001). The AED model (http://aed.see.uwa.edu.au/research/models/AED/) is coupled with the Open TELEMAC-MASCARET model; the model takes into account the carbon, nitrogen, and phosphorus cycles, as well as the effects of other related factors such as dissolved oxygen, light, and suspended sediment, and can simulate the biochemical process and ecological function among phytoplankton, zooplankton, and environment. We can refer to the Cai (2018) method in the future, by splitting vegetation parameters into leaves, roots, and stems, and parameterizing their relationships with variables such as water quality, light intensity, and suspended sediment concentration; coupling the response among vegetation, hydrodynamic force and wave, and the response between vegetation parameters and ecological action, a complete ecological model was established to consider the impact of vegetation on wind-induced wave and current. The fully coupled model can be used to simulate the algae bloom and ecological processes in shallow lakes. The vegetation module based on the Open TELEMAC-MASCARET in this article can provide some reference for such research.

6 CONCLUSION

Based on the Open TELEMAC-MASCARET model, we implanted the vegetation module into the 3d flow model TELEMAC-3D and the wave model TOMAWAC, respectively, and built the flow–wave–vegetation coupling model. Through two sets of laboratory data verification, it has been proven that the model can well capture the complex three-dimensional flow structure and turbulent characteristics near vegetation patches, and accurately predict the attenuation

characteristics of waves in the waters with vegetation patches. The model was then applied to the simulation of wind-induced wave and current in Taihu Lake, a typical shallow lake. By comparing the calculated results with the measured data, it has been shown that the model can accurately reproduce the long-term wind-induced wave and current characteristics of shallow lakes. It is found that vegetation has a significant effect on the velocity of the vegetation patch and its adjacent area, and also changes the three-dimensional circulation structure, so as to redistribute constituents and organisms positioned deeply within the vegetation, remote from open water. The resistance of emergent vegetation is higher than that of submerged vegetation, and the attenuation ability of wave is also stronger than that of submerged vegetation. The presence of vegetation reduces the exchange rate between vegetation patches and the outside area, and has an important effect on the material transport characteristics of the lake. The change of velocity and wave height gradually flattens out with the increase of vegetation density, and the sensitivity analysis results show that the influence of vegetation should not be ignored in the numerical simulation of hydrodynamic lake. This model helps to better understand the impact of aquatic vegetation on the natural environment and provides a useful tool for decision-making on the potential ecological benefits of aquatic vegetation.

DATA AVAILABILITY STATEMENT

The raw data supporting the conclusion of this article will be made available by the authors, without undue reservation.

AUTHOR CONTRIBUTIONS

All authors listed have made a substantial, direct and intellectual contribution to the work and approved it for publication.

FUNDING

This work was jointly funded by the National Key R&D Program of China (2018YFC0407200) and the Special Research Fund of the Nanjing Hydraulic Research Institute (Y120010).

REFERENCES

Abdul, J., Yiping, L., Wei, D., Jianwei, W., Xiaomeng, G., Wencai, W., et al. (2017). Wind-Induced Flow Velocity Effects on Nutrient Concentrations at Eastern Bay of Lake Taihu, China. *Environ. Sci. Pollut. Res.* 24, 17900–17911. doi:10.1007/s11356-017-9374-x

Abdul, J., Yiping, L., Du, W., Wencai, W., Jianwei, W., Xiaomeng, G., et al. (2017). The Role of Wind Field Induced Flow Velocities in Destratification and Hypoxia Reduction at Meiling Bay of Large Shallow Lake Taihu, China. *Environ. Pollut.* 232, 591–602. doi:10.1016/j.envpol.2017.09.095

Adamala, S., Rajwade, Y. A., and Reddy, Y. V. K. (2016). Estimation of Wheat Crop Evapotranspiration Using NDVI Vegetation index. *J. Appl. Nat. Sci.* 8 (1), 159–166. doi:10.31018/jans.v8i1.767

Bacchi, V., Gagnaire, E., Durand, N., and Benoit, M. (2014). "Wave Energy Dissipation by Vegetation in TOMAWAC," in XXIst Telemac-Mascaret User Conference, Grenoble, France, 15–17 October, 2014.

Banerjee, T., Muste, M., and Katul, G. (2015). Flume Experiments on Wind Induced Flow in Static Water Bodies in the Presence of Protruding Vegetation. *Adv. Water Resour.* 76, 11–28. doi:10.1016/j.advwatres.2014.11.010

Barbier, E. B., Koch, E. W., Silliman, B. R., Hacker, S. D., Wolanski, E., Primavera, J., et al. (2008). Coastal Ecosystem-Based Management with Nonlinear Ecological Functions and Values. *Science* 319 (5861), 321–323. doi:10.1126/science.1150349

Beudin, A., Kalra, T., Ganju, N., and Warner, J. C. (2017). Development of a Coupled Wave-Flow-Vegetation Interaction Model. *Comput. Geosciences* 100, 76–86. doi:10.1016/j.cageo.2016.12.010

Cai, X. (2018). *Impact of Submerged Aquatic Vegetation on Water Quality in Cache Slough Complex, Sacramento-San Joaquin Delta- A Numerical Modeling Study*. Sacramento, CA: The College of William and Mary in Virginia.

Cerco, C. F., and Moore, K. (2001). System-Wide Submerged Aquatic Vegetation Model for Chesapeake Bay. *Estuaries* 24 (4), 522–534. doi:10.2307/1353254

Chi-wai, L., and Afis, O. B. (2019). Hybrid Modeling of Flows Over Submerged Prismatic Vegetation with Different Areal Densities. *Eng. Appl. Comput. Fluid Mech.* 13 (1), 493–505. doi:10.1080/19942060.2019.1610501

Dan, W., and Hua, Z. (2014). The Effect of Vegetation on Sediment Resuspension and Phosphorus Release under Hydrodynamic Disturbance in Shallow Lakes. *Ecol. Eng.* 69, 55–62. doi:10.1016/j.ecoleng.2014.03.059

Gaylord, B., Denny, M. W., and Koehl, M. A. R. (2003). Modulation of Wave Forces on Kelp Canopies by Alongshore Currents. *Limnol. Oceanogr.* 48 (2), 860–871. doi:10.4319/lo.2003.48.2.0860

Hervouet, J.-M. (2007). *Hydrodynamics of Free Surface Flows: Modelling with the Finite Element Method*. West Sussex, UK: Wiley, 360.

Hua, Z., Wu, D., Kang, B., and Li, Q. (2013). Flow Resistance and Velocity Structure in Shallow Lakes with Flexible Vegetation under Surface Shear Action. *J. Hydraul. Eng.* 139, 612–620. doi:10.1061/(asce)hy.1943-7900.0000712

Jalil, A., Li, Y., Zhang, K., Gao, X., Wang, W., Khan, H. O. S., et al. (2019). Wind-Induced Hydrodynamic Changes Impact on Sediment Resuspension for Large, Shallow Lake Taihu, China. *Int. J. Sediment Res.* 34 (3), 205–215. doi:10.1016/j.ijsrc.2018.11.003

Jin, K.-R., Ji, Z.-G., and James, R. T. (2007). Three-Dimensional Water Quality and SAV Modeling of a Large Shallow Lake. *J. Great Lakes Res.* 33 (1), 28–45. doi:10.3394/0380-1330(2007)33[28:twqasm]2.0.co;2

Karim, F., Dutta, D., Marvanek, S., Petheram, C., Ticehurst, C., Lerat, J., et al. (2015). Assessing the Impacts of Climate Change and Dams on Floodplain Inundation and Wetland Connectivity in the Wet-Dry Tropics of Northern Australia. *J. Hydrol.* 522, 80–94. doi:10.1016/j.jhydrol.2014.12.005

Kim, H. S., Nabi, M., Kimura, I., and Shimizu, Y. (2015). Computational Modeling of Flow and Morphodynamics through Rigid-Emergent Vegetation. *Adv. Water Resour.* 84, 64–86. doi:10.1016/j.advwatres.2015.07.020

King, A. T., Tinoco, R. O., and Cowen, E. A. (2012). A K-ε Turbulence Model Based on the Scales of Vertical Shear and Stem Wakes Valid for Emergent and Submerged Vegetated Flows. *J. Fluid Mech.* 701, 1–39. doi:10.1017/jfm.2012.113

Kombiadou, K., Ganthy, F., Verney, R., Plus, M., and Sottolichio, A. (2014). Modelling the Effects of Zostera Noltei Meadows on Sediment Dynamics: Application to the Arcachon Lagoon. *Ocean Dyn.* 64 (10), 1–18. doi:10.1007/s10236-014-0754-1

Kothyari, U. C., Hashimoto, H., and Hayashi, K. (2009). Effect of Tall Vegetation on Sediment Transport by Channel Flows. *J. Hydraulic Res.* 47 (6), 700–710. doi:10.3826/jhr.2009.3317

Lamchin, M., Wang, W., Lim, C.-H., Ochir, A., Ukrainski, P., Gebru, B., et al. (2020). Understanding Global Spatio-Temporal Trends and the Relationship between Vegetation Greenness and Climate Factors by Land Cover during 1982-2014. *Glob. Ecol. Conservation* 24, e01299. doi:10.1016/j.gecco.2020.e01299

Large, W. G., and Pond, S. (1981). Open Ocean Momentum Flux Measurements in Moderate to Strong Winds. *J. Phys. Oceanography* 11 (3), 336–342. doi:10.1175/1520-0485(1981)011<0324:oomfmi>2.0.co;2

Li, Y., Acharya, K., and Yu, Z. (2011). Modeling Impacts of Yangtze River Water Transfer on Water Ages in Lake Taihu, China. *Ecol. Eng.* 37 (2), 325–334. doi:10.1016/j.ecoleng.2010.11.024

Li, Y., Teng, Y.-C., Kelly, D. M., and Zhang, K. (2016). A Numerical Study of the Impact of hurricane-induced Storm Surge on the Herbert Hoover Dike at Lake Okeechobee, Florida. *Ocean Dyn.* 66 (12), 1699–1714. doi:10.1007/s10236-016-1001-8

Li, Y., Zhang, Q., Tan, Z., and Yao, J. (2020). On the Hydrodynamic Behavior of Floodplain Vegetation in a Flood-Pulse-Influenced River-lake System (Poyang Lake, China). *J. Hydrol.* 585, 124852. doi:10.1016/j.jhydrol.2020.124852

Liu, S., Ye, Q., Wu, S., and Stive, M. (2018). Horizontal Circulation Patterns in a Large Shallow Lake: Taihu Lake, China. *Water* 10, 1–27. doi:10.3390/w10060792

Løvås, S. M. (2000). *Hydro-physical Conditions in Kelp Forests and the Effect on Wave Dumping and Dune Erosion: A Case Study on Laminaria Hyperborea*. Norway: University of Trondheim.

Lu, J., and Dai, H. C. (2017). Three Dimensional Numerical Modeling of Flows and Scalar Transport in a Vegetated Channel. *J. Hydro-Environment Res.* 16, 27–33. doi:10.1016/j.jher.2017.05.001

Lürling, M., Mackay, E., Reitzel, K., and Spears, B. M. (2016). Editorial - A Critical Perspective on Geo-Engineering for Eutrophication Management in Lakes. *Water Res.* 97, 1–10. doi:10.1016/j.watres.2016.03.035

Morales-Marín, L. A., French, J. R., and Burningham, H. (2017). Implementation of a 3D Ocean Model to Understand upland lake Wind-Driven Circulation. *Environ. Fluid Mech.* 17, 1255–1278. doi:10.1007/s10652-017-9548-6

Morin, J., Leclerc, M., Secretan, Y., and Boudreau, P. (2000). Integrated Two-Dimensional Macrophytes-Hydrodynamic Modeling. *J. Hydraulic Res.* 38 (3), 163–172. doi:10.1080/00221680009498334

Murphy, A. H. (1992). Climatology, Persistence, and Their Linear Combination as Standards of Reference in Skill Scores. *Wea. Forecast.* 7 (4), 692–698. doi:10.1175/1520-0434(1992)007<0692:cpatlc>2.0.co;2

Nepf, H. M. (2011). Flow and Transport in Regions with Aquatic Vegetation. *Annu. Rev. Fluid Mech.* 44 (1), 123–142. doi:10.1146/annurev-fluid-120710-101048

Neumeier, U. (2007). Velocity and Turbulence Variations at the Edge of Saltmarshes. *Continental Shelf Res.* 27, 1046–1059. doi:10.1016/j.csr.2005.07.009

Pang, C.-C., Wang, F., Wu, S.-Q., and Lai, X.-J. (2015). Impact of Submerged Herbaceous Vegetation on Wind-Induced Current in Shallow Water. *Ecol. Eng.* 81 (8), 387–394. doi:10.1016/j.ecoleng.2015.04.021

Parvathy, K. G., Umesh, P. A., and Bhaskaran, P. K. (2017). Inter-seasonal Variability of Wind-Waves and Their Attenuation Characteristics by Mangroves in a Reversing Wind System. *Int. J. Climatology* 37 (c4), 5089–5106. doi:10.1002/joc.5147

Resende, A. F. d., Schöngart, J., Streher, A. S., Ferreira-Ferreira, J., Piedade, M. T. F., and Silva, T. S. F. (2019). Massive Tree Mortality from Flood Pulse Disturbances in Amazonian Floodplain Forests: The Collateral Effects of Hydropower Production. *Sci. Total Environ.* 659, 587–598. doi:10.1016/j.scitotenv.2018.12.208

Sheng, Y. P., Lapetina, A., and Ma, G. (2012). The Reduction of Storm Surge by Vegetation Canopies: Three-Dimensional Simulations. *Geophys. Res. Lett.* 39 (20), 1–5. doi:10.1029/2012gl053577

Smith, J. M., Bryant, M. A., and Wamsley, T. V. (2016). Wetland Buffers: Numerical Modeling of Wave Dissipation by Vegetation. *Earth Surf. Process. Landforms* 41 (6), 847–854. doi:10.1002/esp.3904

Sonnenwald, F., Guymer, I., and Stovin, V. (2019). A CFD-Based Mixing Model for Vegetated Flows. *Water Resour. Res.* 55 (3), 2322–2347. doi:10.1029/2018wr023628

Temmerman, S., Meire, P., Bouma, T. J., Herman, P. M. J., Ysebaert, T., and De Vriend, H. J. (2013). Ecosystem-Based Coastal Defence in the Face of Global Change. *Nature* 504 (7478), 79–83. doi:10.1038/nature12859

Tse, I. C., Poindexter, C. M., and Variano, E. A. (2016). Wind-Driven Water Motions in Wetlands with Emergent Vegetation. *Water Resour. Res.* 52, 2571–2581. doi:10.1002/2015wr017277

Vossen, B. V., and Uittenbogaard, R. (2004). "Subgrid-Scale Model for quasi-2D Turbulence in Shallow Water," in *Shallow Flows*. London, UK: Taylor & Francis Group. doi:10.1201/9780203027325.ch72

Wang, C., Fan, X.-l., Wang, P.-f., Hou, J., and Qian, J. (2016). Flow Characteristics of the Wind-Driven Current with Submerged and Emergent Flexible Vegetations in Shallow Lakes. *J. Hydrodyn* 28 (5), 746–756. doi:10.1016/s1001-6058(16)60677-7

Weiming, W., and Marsooli, R. (2012). A Depth-Averaged 2D Shallow Water Model for Breaking and Non-Breaking Long Waves Affected by Rigid Vegetation. *J. Hydraulic Res.* 50 (6), 558–575. doi:10.1080/00221686.2012.734534

Werner, M. G. F., Hunter, N. M., and Bates, P. D. (2005). Identifiability of Distributed Floodplain Roughness Values in Flood Extent Estimation. *J. Hydrol.* 314, 139–157. doi:10.1016/j.jhydrol.2005.03.012

Xu, T.-P., Zhang, M.-L., Jiang, H.-Z., Tang, J., Zhang, H.-X., and Qiao, H.-T. (2018). Numerical Investigation of the Effects of Aquatic Plants on Wind-Induced Currents in Taihu Lake in China. *J. Hydrodyn* 31, 778–787. doi:10.1007/s42241-018-0091-9

Yang, P., Fong, D. A., Lo, E. Y. M., and Monismith, S. G. (2019). Circulation Patterns in a Shallow Tropical Reservoir: Observations and Modeling. *J. Hydro-environment Res.* 27, 75–86. doi:10.1016/j.jher.2019.09.002

Zhang, J., Fan, X., Liang, D., and Liu, H. (2019). Numerical Investigation of Nonlinear Wave Passing through Finite Circular Array of Slender Cylinders. *Eng. Appl. Comput. Fluid Mech.* 13, 102–116. doi:10.1080/19942060.2018.1557561

Zhang, Y., Gerdts, N., Ateljevich, E., and Nam, K. (2019). Simulating Vegetation Effects on Flows in 3D Using an Unstructured Grid Model: Model Development and Validation. *Ocean Dyn.* 70 (2), 1–18. doi:10.1007/s10236-019-01333-8

Conflict of Interest: The authors declare that the research was conducted in the absence of any commercial or financial relationships that could be construed as a potential conflict of interest.

Publisher's Note: All claims expressed in this article are solely those of the authors and do not necessarily represent those of their affiliated organizations, or those of the publisher, the editors and the reviewers. Any product that may be evaluated in this article, or claim that may be made by its manufacturer, is not guaranteed or endorsed by the publisher.

frontiers in Earth Science

ORIGINAL RESEARCH
published: 24 January 2022
doi: 10.3389/feart.2021.813287

Time-Lag Effect: River Algal Blooms on Multiple Driving Factors

Chengjian Liu[1,2]*, *Yan Chen*[1,2,3], *Lei Zou*[4], *Bingfen Cheng*[1,2] and *Tonghui Huang*[1,2]

[1]State Key Laboratory of Environmental Criteria and Risk Assessment, Chinese Research Academy of Environmental Sciences, Beijing, China, [2]State Environmental Protection Key Laboratory of Estuarine and Coastal Research, Chinese Research Academy of Environmental Sciences, Beijing, China, [3]Chongqing Institute of Green and Intelligent Technology, Chinese Academy of Sciences, Chongqing, China, [4]Key Laboratory of Water Cycle and Related Land Surface Processes, Institute of Geographic Sciences and Natural Resources Research, Chinese Academy of Sciences, Beijing, China

Compared to the eutrophication of lakes and reservoirs, the mechanism of river algal blooms in a flowing water body are more complicated, and often lead to serious consequence in catchment scale. Due to the simultaneous impact of a variety of environmental pressures, the water ecosystem integrity state often shows a response characteristic of accumulation, complexity and time lag, therefore it is difficult to use conventional hydrodynamic and water quality models to scientifically characterize and analyze. The lower Hanjiang River (HR) is an important influence area of the middle route of the South-to-North Water Diversion Project (SNWDP) in China, continuous river blooms issue has become a major national concern. In this study, a time-lag analysis approach was developed to identify the causes of algal blooms formation and the time-lag response law in the lower HR, including principal component analysis (PCA), grey relation analysis (GRA), and Almon Distributed Lag Model. Results found that, the hydrological regime (ΔH) contributes the most to the river bloom, especially due to the flow hindrance of the Yangtze River (YR) and the water project upstream. It is also found that the algal bloom outbreak in the lower HR is not an immediate response to the driving factors. It has a time lag of about 1 period (10 days) in the response with antecedent driving factors. Finally, we discussed the influence and its responding mechanism of ΔH on the growth of phytoplankton. The research can provide early warning for the prevention and control of algal blooms in the large river system.

Keywords: river algal blooms, time-lag effect, drive factors, river ecosystem, Hanjiang River

OPEN ACCESS

Edited by:
Guobin Fu,
CSIRO Land and Water, Australia

Reviewed by:
Jun Xia,
Wuhan University, China
Li He,
Tianjin University, China

***Correspondence:**
Chengjian Liu
chengjianliu@stumail.nwu.edu.cn

Specialty section:
This article was submitted to Hydrosphere, a section of the journal Frontiers in Earth Science

Received: *11 November 2021*
Accepted: *06 December 2021*
Published: *24 January 2022*

Citation:
Liu C, Chen Y, Zou L, Cheng B and Huang T (2022) Time-Lag Effect: River Algal Blooms on Multiple Driving Factors. Front. Earth Sci. 9:813287. doi: 10.3389/feart.2021.813287

1INTRODUCTION

Algal blooms as an extreme form of water eutrophication (Whitehead et al., 2015), usually occur in relatively static water bodies such as lakes and reservoirs (Cheng et al., 2019). However, the anthropogenic regulation of rivers (i.e., dam construction, flood protection, and water extraction) can greatly change the hydrological conditions in the rivers, causing severe environmental loss of river connectivity (Zhou et al., 2013; Maavara et al., 2015). Therefore, algal blooms have become one of the serious environmental issue at catchment scale that are greatly disturbed by human activities (Jeong et al., 2007; Mitrovic et al., 2007). Algal blooms prevent sunlight from penetrating the water surface, causing the death of aquatic life (Bhat et al., 2006). On the other hand, many phytoplankton species can produce potent toxins that can cause direct or indirect harm to various lives through the food chain and food web (Hallegraef, 1993). The causal

analysis and driving mechanism of algal blooms in large hydrological-regulated rivers have become a major concern, as the algal blooms in these rivers not only lead to deteriorating water quality and aquatic ecosystems but also restrict socioeconomic developments and threaten public health with a greater sphere of influence.

Because of the nonlinearity and time-lag of aquatic ecological process, river blooms are not only caused by a single driving factor but also resulting of a combination of multiple driving factors under antecedent environmental conditions (Xia et al., 2020). There is a general perspective that river blooms are mainly caused by sufficient nutrients, suitable climatic conditions, and slow hydrological conditions (Mitrovic et al., 2007; Jung et al., 2009; Jung et al., 2011; Yang et al., 2011; Liu et al., 2016; Ji et al., 2017). In the most algal bloom rivers, nutrients often meet the basic conditions for algae growth, so they are not the main limiting factor for algal blooms (Mischke et al., 2011; Yang et al., 2012; Oliver et al., 2014). However, increased nutrient loads could lead to harmful algal blooms increase (Zhou et al., 2001; Wang, 2006; Li et al., 2014). With higher water temperature and longer water retention time at low flow rates, which can promote the growth of algae in the Hunter River, Australia (Mitrovic et al., 2007). Even though physical and chemical conditions are conducive to the growth of algae, the hydrodynamic conditions also determine the occurrence of algal blooms in the tributaries of the Three Gorges Reservoir, China (Ji et al., 2017; Chuo et al., 2019). Experimental studies have shown that hydrodynamic conditions (i.e., fluctuations and agitation of water flow) usually have a significant impact on the migration, diffusion, growth, and accumulation of algae (Chung et al., 2008; Lucas et al., 2009; Whitehead et al., 2015). Fluctuations in hydrological conditions can change the migration and transformation of nutrients, the transmission of solar radiation, and the migration of algae (McKiver and Neufeld, 2009; Istvánovics and Honti, 2012). In addition, the gentle hydrological situation will reduce the turbidity of the water body, which help the growth and reproduction of algae (Wang, 1974). All of the above studies show that the hydrologic regime is an important driving factor for river-type algal blooms (Mitrovic et al., 2007; Cheng et al., 2019; Xia et al., 2020). However, few studies have explored the time-lag response of algal blooms to driving factors.

Time-lag response refers to a response relationship with a certain time lag between the dependent variable and the independent variable. The majority of research on river algal blooms focuses on phytoplankton and driving the short-term "snapshot effect" between factors (Jeong et al., 2007). However, the time-lag effect not only has an important explanatory effect on the field observation results of microalgae communities under natural conditions but also has an important effect on the simulation, prediction, and early warning of water bloom outbreaks (Harris, 1983). Studies have shown that there is a lag of at least 2 years between the population dynamics of *Microcystis aeruginosa* and *Stephanodiscus hantzschii* and hydrological environment (i.e., the quantity of dam storage and discharge) in the lower Nakdong River, South Korea (Jeong et al., 2007). Other studies on the Nakdong River have also proved this conclusion. In a normal year, the response period of the Chl*a* concentration in the Nam River dam to rainfall is 1 month later than that of other dams, while in a wet year, the lag response period is 2 months (Kim et al., 2009). In fact, in previous studies of algal blooms in the HR, scholars proposed the importance of the time-lag effect (Yang et al., 2012; Xia et al., 2020). According to the study of algal blooms in HR, some scholars have pointed out the importance of the time-lag effect. Yang et al. (2011) proposed that the time lag effect is a frontier issue in the study of river-type algal blooms. Furthermore, through the gradient boosting machine (GBM), it is proved that the use of the environmental factors (especially the hydrological situation) in the first 10 days can better predict the algal blooms of the HR, China (Xia et al., 2020). The above research shows that different rivers and water bodies have different time lags. However, few studies have quantitatively revealed the length of the lag response time of algal blooms to various driving factors. It is necessary to carry out a quantitative analysis of the time-lag effect between river algal blooms and its multiple driving factors, in order to reveal the mechanism of river water ecological degradation.

Plenty of algal blooms occurred in the lower HR, and it is essential to analyze them from multiple angles. Therefore, this study aims to reveal the response mechanism of river algal blooms based on the analysis of interactions of those influencing factors, by quantitatively determining the time-lag response of algal bloom to multiple driving factors. We conduct following studies including 1) determining the key driving factors regulating the algal blooms in the lower HR. 2) evaluating the time-lag effect of influencing factors by analyzing data collected from field surveys with principal component analysis (PCA), Almon Distributed Lag Model and curve fitting. PCA was carried out to classify the environmental factors. Almon Distributed Lag Model was applied to establish the optimal lag time of every variable. Curve fitting was applied to quantitatively describe the impact of hydrological regimes on algal blooms. Finally, we expect to propose a method for predicting river water ecological degradation in advance.

2 MATERIALS AND METHODS

Study Area

The HR is the largest tributary of the YR of China (**Figure 1**). It flows from the northwest to the southeast and joins the YR in Wuhan City (Li et al., 2009). The annual discharge from the HR to the YR is 33.2 billion m^3 (Xin et al., 2020). The average annual temperature is 16°C. The average annual precipitation amounts to 700–1,000 mm, with >80% occurring between May to September (Chen et al., 2007). Danjiangkou Reservoir, as the water source for the middle route of the South-to-North Water Diversion Project, is located in the middle reaches of the HR (Xia et al., 2016). Flowing through the most economically-developed region in Hubei Province, the middle and lower reaches of the HR are the most important source of drinking water for coastal cities (Xia et al., 2012; Cheng et al., 2019). However, the wastewater influent to the HR with nutrients and organic matters has increased in the

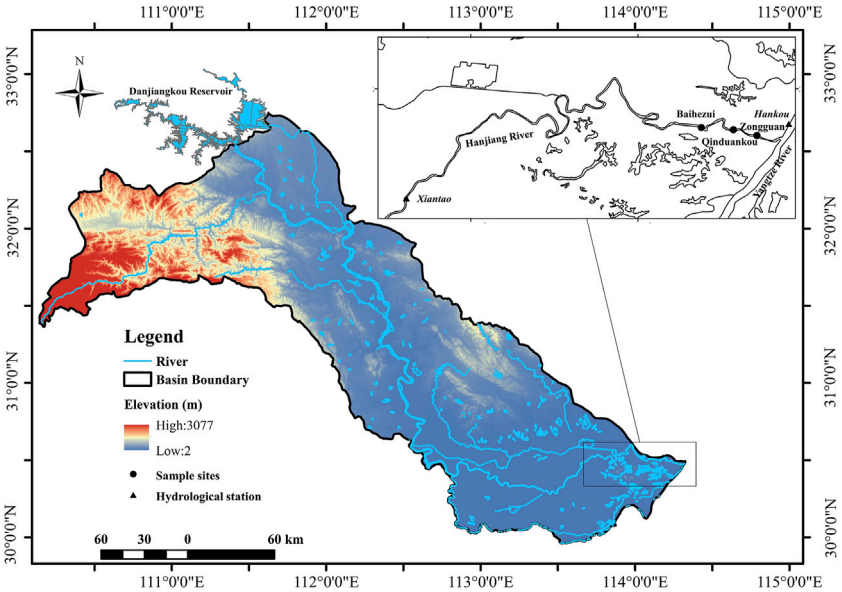

FIGURE 1 | Overview of the study area and sample sites. Water levels were measured at the Xiantao Station for the HR and at the Hankou Station for the YR. Water quality and Chl*a* were measured at three sample sites: Baihezui (BHZ), Qinduandou (QDK), and Zongguan (ZG).

past 30–40 years as a consequence of rapid urbanization, economic growth, and intensification of agricultural productivity (Xie et al., 2004). In addition, the opening of the middle route of the SNWDP has also changed the hydrologic situation of the lower reaches of the HR (Cao et al., 2020). The middle and lower reaches of the HR have been plagued by algal blooms. There have been lots of algal blooms in this area since 1992 (Li et al., 2020). The driving factors for the algal blooms in the lower reaches of the HR are complex. It is not only related to the water environmental factors of the HR but also to the hydrological situation in the estuary confluence area (backwater area) (Xia et al., 2020) (**Figure 1**). As the impact of algal blooms on the lower reaches of the HR becomes more and more serious, it has become one of the urgent problems to be solved (Xie et al., 2006; Li, 2007).

Data Collection and Processing

Unlike lakes or other rivers, the causes of algal blooms in the lower HR are extremely complex. Because the lower HR is located in the area affected by the middle route of the SNWDP and also in the hydrological change area where the HR merges into the YR. In this study, we used the algal blooms data (Chlorophyll-a concentration, Chl*a*) at Baihezui (BHZ), Qinduankou (QDK), and Zongguan (ZG) sample sites located in the lower HR every 10 days from February to April in 2004–2014. We collected the hydrological data of the Xiantao (XT) and Hankou (HK) hydrologic stations during the same period from the YR Water Conservancy Commission Hydrological Bureau. The hydrological data include daily flow (QH), flow velocities (vH), and water level (WLH) in the Xiantao Station; daily flow (QY), flow velocities (vY), and water level (WLY) in the Hankou Station. Furthermore, we calculated the water level difference (ΔH) between the two hydrological stations. In addition, 10 days water quality data (i.e., water temperature (WT), total nitrogen concentration (TN), and total phosphorus concentration (TP)) at the BHZ, QDK, and ZG stations were provided by the YR Basin Ecological and Environmental Supervision Authority. 1 L of water sample was filtered *in situ* and taken back to the laboratory for the analysis of nutrients, including TP and TN, using ammonium molybdate spectrophotometric method and alkaline potassium digestion UV spectrophotometric method. WT was determined using a HACH Hydrolab MI-parameter Meter. The above datasets were used for analysis.

Methods

2.1.1PCA

PCA (Zhou et al., 2017) is often used to classify the dominant environmental factors and define the effects of the hidden variables (major components) on the biomass of phytoplankton in the study area. The standardized environmental factor data, including hydrological data and water quality data, were used for PCA.

$$\begin{aligned} z_1 &= a_{11}x_1 + a_{12}x_2 + a_{13}x_3 + \cdots + a_{1n}x_n \\ z_2 &= a_{21}x_1 + a_{22}x_2 + a_{23}x_3 + \cdots + a_{2n}x_n \\ z_3 &= a_{31}x_1 + a_{32}x_2 + a_{33}x_3 + \cdots + a_{3n}x_n \\ &\vdots \\ z_m &= a_{m1}x_1 + a_{m2}x_2 + a_{m3}x_3 + \cdots + a_{mn}x_n \end{aligned} \quad (1)$$

where z_m (m = 1,2,3,...) are principal components; x_n (n = 1,2,3,...) are original variables; and a_{11} to a_{mn} are weight

coefficients. If principal components exist plurally, these principal components are independent of one another. We used the Kaiser-Meyer-Olkin measure of sampling adequacy and Bartlett's spherical value at the significance level of 0.05 to test for statistical significance. Only the components whose accumulative contribution rate reached 80 percent were taken into account (Lee et al., 2009; Yin et al., 2012). The data can be normalized through SPSS 22.0 software.

2.1.2 Almon Distributed Lag Model

Almon Distributed Lag Model (Almon, 1965) was used to analyze the time-lag effect of algal blooms on each driving factor quantitatively.

The Almon Lag Model as

$$Y_t = \alpha + \beta_0 X_t + \beta_1 X_{t-1} + \beta_2 X_{t-2} + \cdots + \beta_k X_{t-k} + u_t \quad (2)$$

where Y_t is a dependent variable, $X_t, X_{t-1}, \cdots, X_{t-k}$ are linearly combined independent variables (i.e., a sequence of influencing factor values in a current 10 day period, a previous 10 day period, and a k_{th} previous 10 day period; in this embodiment, a time interval of the data is 10 days), u_t is a random interference term, $\alpha, \beta_0, \beta_1, \cdots, \beta_k$ are model coefficients, and k is a lag time.

To eliminate the multicollinearity between variables in different lag periods, the polynomial distributed lag method is used:

$$\beta_i = a_0 + a_1 q + a_1 q^2 + \cdots + a_m q^m \quad (3)$$

where, m is the order number of a polynomial, and generally, $m < k$.

By substituting **Eq. 3** into **Eq. 2**, we get:

$$\begin{aligned} Y_t &= a + \sum_{q=0}^{k} (a_0 + a_1 q + a_1 q^2 + \cdots + a_m q^m) X_{t-q} + u_t \\ &= a + a_0 Z_{0t} + a_1 Z_{1t} + a_2 Z_{2t} + \cdots + a_m Z_{mt} + u_t \end{aligned} \quad (4)$$

It is transformed into the regression of Y on a reconstructed variable Z.

By using **Eq. 4**, estimated values $\hat{a}, \hat{a}_0, \hat{a}_1, \cdots$ and $\hat{a}_m$ of $a, a_0, a_1, \cdots$ and a_m are obtained through linear regression. Then the estimated values $\hat{\beta}_0, \hat{\beta}_1, \hat{\beta}_2$ and $\hat{\beta}_k$ of β are calculated through **Eq. 5** and substituted into **Eq. 2**, to obtain a sequence of estimated values of Y (that is, Chl*a*) for a maximum lag time k at the current moment.

$$\begin{aligned} \hat{\beta}_0 &= \hat{a}_0 \\ \hat{\beta}_1 &= \hat{a}_0 + \hat{a}_1 + \hat{a}_2 + \cdots + \hat{a}_m \\ \hat{\beta}_2 &= \hat{a}_0 + 2\hat{a}_1 + 4\hat{a}_2 + \cdots + 2^m \hat{a}_m \\ \hat{\beta}_3 &= \hat{a}_0 + 3\hat{a}_1 + 9\hat{a}_2 + \cdots + 3^m \hat{a}_m \\ &\cdots\cdots \\ \hat{\beta}_k &= \hat{a}_0 + k\hat{a}_1 + k^2 \hat{a}_2 + \cdots + k^m \hat{a}_m \end{aligned} \quad (5)$$

The correlation coefficient between the estimated Y_t and the measured Y_t was used to determine an optimal lag time. If the correlation coefficient no longer increases with the increase of k, a value of k at this time is considered to be the optimal lag time (Liu, 2019; Özbay and Toker, 2021).

3 RESULTS

Characterization of Chl*a* and Driving Factors

A variety of driving factors were used to determine the driving effect on algal blooms. According to their availability, we divide them into algal bloom characterization data, water quality data, and hydrological data. The statistics of the different driving factors, including the mean, minimum (min), maximum (max), standard deviation (SD), and coefficient of variation (CV), are listed in **Table 1**. The maximum of Chl*a* during the three sites is 67.8 μg/L (ZG). The variability of Chl*a* at ZG is also the largest (0.20–67.8 μg/L). Statistics of TP are similar at three sites including BHZ (mean 0.12 mg/L; min 0.05 mg/L; max 0.35 mg/L; SD 0.04; CV 0.35), QDK (mean 0.12 mg/L; min 0.05 mg/L; max 0.35 mg/L; SD 0.04; CV 0.34), and ZG (mean 0.12 mg/L; min 0.04 mg/L; max 0.30 mg/L; SD 0.04; CV 0.36). The situations of TN and WT are similar to that of TP. The differences among the three sites are not significant. Regarding hydrological data, the flow and velocity of the HR are less than those of the YR. Moreover, the ΔH is in a state of volatility.

According to the level of Chl*a*, the biomass in the three sections were in a state of flux. The average value of Chl*a* was high in other years except for the years 2005 and 2007 (**Figures 2A–C**). For TP and TN, a similar trend was exhibited. TN was in a state of rising volatility from 2004 to 2014, but TP had relatively large fluctuations during the year, relative to TN (**Figures 2D–I**). In addition, the WT showed a unique trend, and the change had a certain periodicity, about 6–7 years (**Figures 2J–L**).

We used the hydrological data of hydrological situation in Xiantao (located in HR) and Hankou (located in YR) to represent the hydrological conditions of the HR and the YR, respectively. The results are shown in **Figure 3**. We can see that the hydrological situation of the YR had changed significantly, compared to that of the HR. The two low values of QY appeared in 2006 and 2011 and the WLY was also at a low peak. As shown in **Figure 3B**, ΔH had been showing a downward trend since 2011 and the direct causes are the increase of WLY and the decrease of WLH **Figure 4**.

RESULT OF PRINCIPAL COMPONENT ANALYSIS

The normalized data met the analysis requirements of PCA. The results of PCA at three sites (BHZ, QDK, and ZG) are as follows (**Figure 4**). At the BHZ sample site, three principal components have been selected and their total contribution rate reached 81.1%. The first two components together represented 70.5% of the total variation. The first principal component explained 47.4% of the total variation and the second principal component explained 23.1% of the total variation. Moreover, the third principal component explained 10.6% of the total variation. The Radar chart of the score for each variable at the BHZ site indicated that WT, QH, vH, QY, vY, WLH, and WLY had high capacities in the first principal component, while ΔH had high capacity in the second principal component. In addition, TP and

TABLE 1 | Mean, range (min, max), standard deviation (SD), and coefficient of variation (CV) of chlorophyll-a and the associated environmental factors during 2004–2014.

Categories	Variables	Mean	Min	Max	SD	CV
BHZ	Chl*a* (μg/L)	6.12	0.30	63.00	8.91	1.46
	TP (mg/L)	0.12	0.05	0.35	0.04	0.35
	TN (mg/L)	1.88	0.40	4.28	0.31	0.16
	WT (°C)	17.1	3.0	32.1	7.14	0.42
QDK	Chl*a* (μg/L)	5.78	0.20	46	7.96	1.37
	TP (mg/L)	0.12	0.05	0.35	0.04	0.34
	TN (mg/L)	1.90	0.96	3.13	0.25	0.13
	WT (°C)	17.1	3.0	32.0	7.17	0.42
ZG	Chl*a* (μg/L)	6.08	0.20	67.80	8.96	1.47
	TP (mg/L)	0.12	0.04	0.30	0.04	0.36
	TN (mg/L)	1.89	0.67	3.72	0.28	0.15
	WT (°C)	17.2	3.0	31.0	7.18	0.42
hydrological data	QH (m^3/d)	1,223.75	331.60	7,224.00	1,137.40	0.93
	vH (m/s)	0.90	0.59	2.02	0.24	0.27
	QY (m^3/d)	18,387.76	7,660	51,200	9,475.91	0.52
	vY (m/s)	1.07	0.7	1.65	0.20	0.19
	WLY (m)	17.80	13.51	25.61	3.06	0.17
	WLH (m)	25.56	22.57	34.15	2.04	0.08
	ΔH (m)	7.76	0.51	13.51	2.38	0.31

TN were dominant in the third principal component. More specific PCA results are shown in **Supplementary Appendix A**.

The results of PCA at the QDK and ZG sites are similar to that at the BHZ site. It is worth noting that the second principal component only contains the variable ΔH, which contributes 23.1, 23.3, and 23.3% of interpretation at the BHZ, QDK, and ZG sites respectively. Therefore, the ΔH is considered as an important factor influencing the algal blooming in the lower HR.

The above analysis shows that there is not much difference between each variable among the three sites, so we will average the variable values of the three sites. GRA was used to determine the correlation between each environmental driving factor and Chl*a* during 2004–2014. ΔH achieves the highest degree of relevance, which is 0.8960. WT, TN, TP are then in turn. The results are shown in **Supplementary Appendix B**.

Result of Almon Distributed Lag Model

Furthermore, we analyzed the annual change trends of Chl*a* and ΔH during the four consecutive years of algal blooms from 2008 to 2011. The results are shown in **Supplementary Appendix C**. During the algal blooming period, the ΔH between Xiantao and Hankou was always at a low level. The relatively gentle hydrological regime was suitable for the growth of phytoplankton. We also found that the ΔH was already at a low level during the pre-order time when the Chl*a* appeared high. Therefore, the growth of phytoplankton was not an "instantaneous" response to hydrological driving factors but a response lagged a certain amount of time. The response time of the algal blooms in 2008–2011 has a relatively significant lag effect, which means that the change of the water level usually occurs before the algal bloom occurs.

To analyze the time-lag response of algal blooms to various driving factors, we identified four main variables based on the previous analysis, including ΔH, WT, TP, and TN. Furthermore, the Almon Distributed Lag Model was used to determine the effect of algal bloom on various driving factors. The length of the lag time of the driving factors and the average value of the variable are continued to be used. The analysis results are as follows (**Figures 5**, **6**). For the driving factor ΔH, when we used the data from the same period as Chl*a*, the correlation coefficient (*r*) of the measured and simulated values of Chl*a* was 0.240 ($p > 0.05$). When we used the ΔH data of the current period and the 1 period ahead (10 days) at the same time, it was 0.297 ($p < 0.05$). Furthermore, when we used the ΔH data of the current period, 1 period ahead (10 days), and two periods ahead (20 days), the result became 0.298 ($p < 0.05$). In addition, the results for the driving factor WT are 0.040 ($p > 0.05$), 0.285 ($p < 0.05$), and 0.288 ($p < 0.05$). For the driving factor TN, the results are 0.071 ($p > 0.05$), 0.209 ($p > 0.05$), and 0.210 ($p > 0.05$). Regarding the driving factor TP, the results are 0.475 ($p < 0.05$), 0.493 ($p < 0.01$), and 0.492 ($p < 0.01$).

Furthermore, from **Figure 6** we can infer that when the lag time was set to two periods ahead (20 days), the *r* did not continue to increase or the increase was very small. For the increased range in *r*, WT achieved the largest value of 0.248 and TP had the smallest value of 0.017. Therefore, we set 1 period ahead (10 days) as the optimal time-lag length, which is the most significant impact on the algal blooms in the lower HR are the driving factors in the current period and the 1 period ahead (10 days).

4 DISCUSSION

Driving Factors Algal Blooms in the Lower Hanjiang River

Based on the results of PCA and GRA, the roles of the different environmental factors were evaluated during the river-type algal blooms. TP and TN exhibited no significant effects on Chl*a*

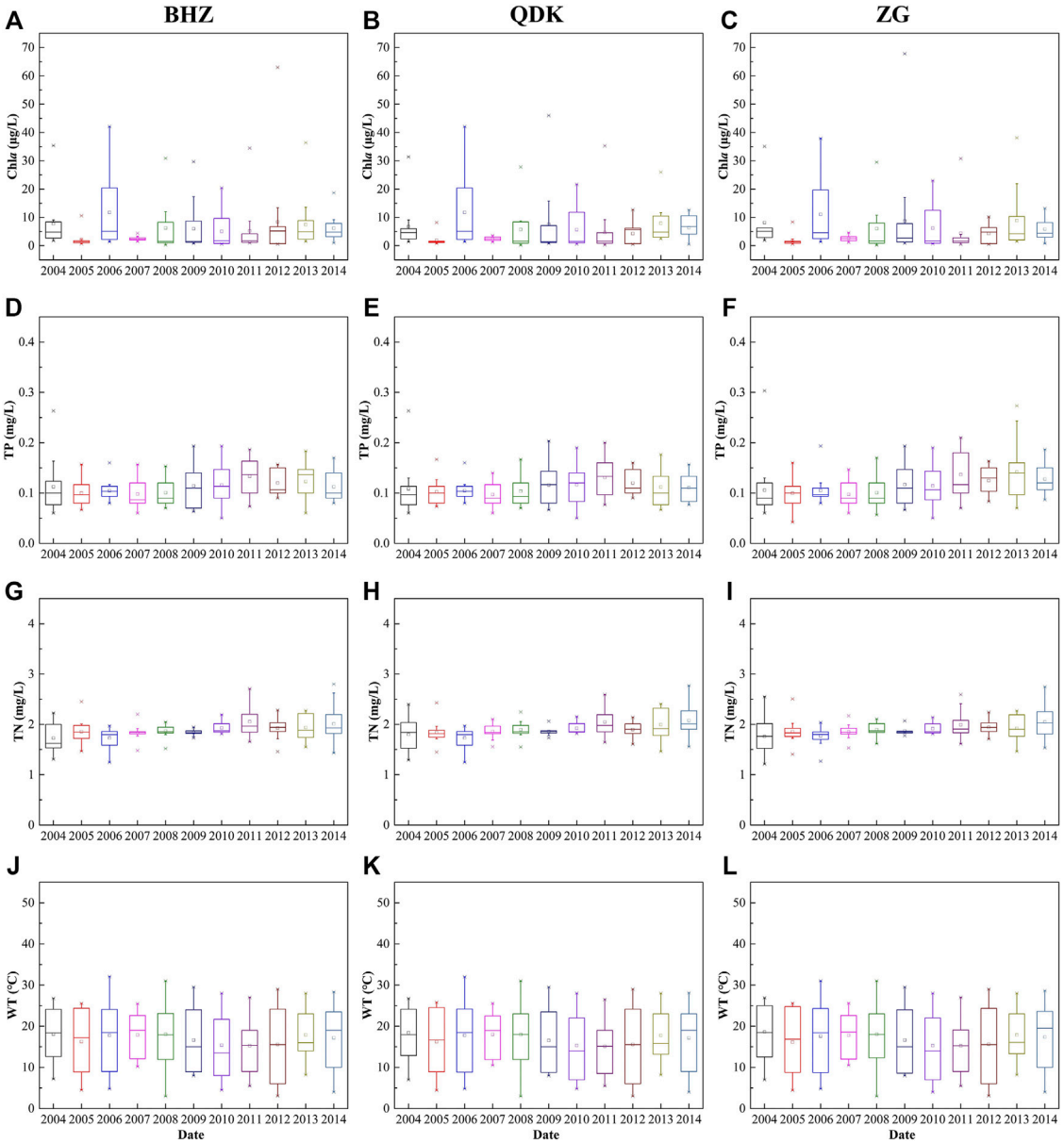

FIGURE 2 | Chl*a* and water quality in the lower HR.

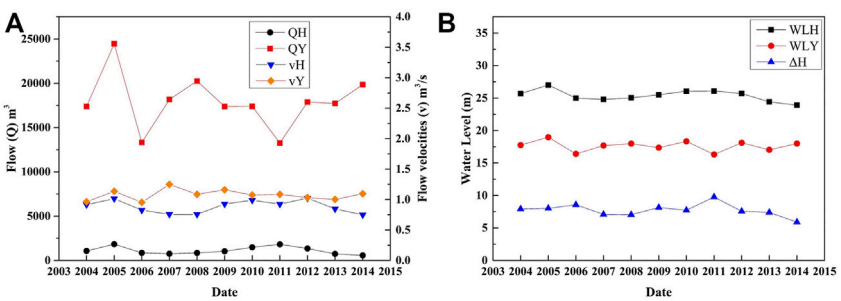

FIGURE 3 | Hydrological regime in the lower HR.

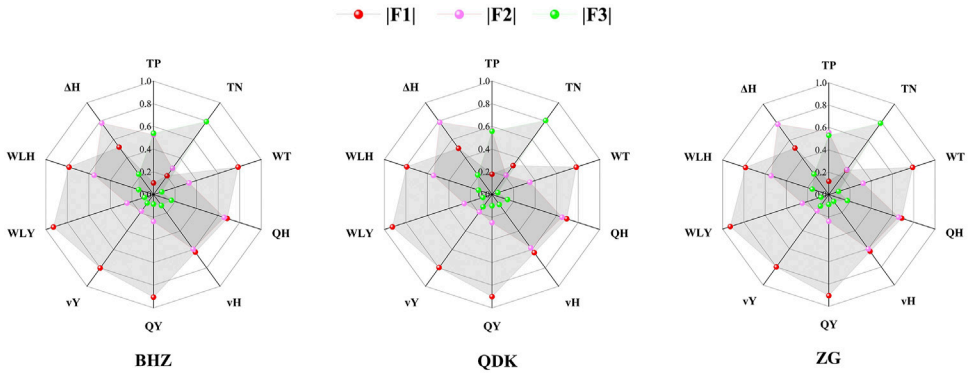

FIGURE 4 | Absolute value of principal component score for each variable at the three sample sites.

during the diatom algal blooms. Although they are critical for the growth of diatoms, their concentrations were high enough to support the diatom bloom (Zhang et al., 2008). Previous studies have confirmed that nutrients are not a necessary limiting factor for most river algal bloom events, but nutrients are a prerequisite for the occurrence of algal blooms (Mitrovic et al., 2007; Yang et al., 2017). Our results show that the GRA scores of the concentration of Chl*a* and the concentrations of TP and TN are ranked behind those of the ΔH and WT. Similar to our research, Zeng et al. (2006) believed that there is no significant positive correlation between the concentration of phytoplankton and Chl*a* and the content of nutrients in the Three Gorges reservoir area. Besides, during the outbreak of algal blooms in the lower HR, the concentrations of TN and TP have far met the needs of phytoplankton growth, and there is a continuous supply without restriction. Moreover, water temperature is essential for the growth of phytoplankton (Carey et al., 2012). Does low temperature constrain the growth rates of heterotrophic protists become a question, and Rose and Caron (2007) gave a negative answer. Any aquatic organism has its optimal growth temperature range and the suitable water temperatures for the growths of blue algae, green algae, and blue-green algae are approximately 30–35°C, 20–25°C, and 15–20°C, respectively (Cheng et al., 2019). However, diatom algae as the dominant species in the spring algal blooms of HR, have an optimal growth temperature range of 5–15°C (Ha et al., 2002; Kim et al., 2007). Some experimental results in the laboratory showed that the growth rate of *S.hantzschii* decreased when the temperature exceeded 20°C (Jung et al., 2011). Therefore, the temperature recovery period in late winter and early spring is a window period for the growth of diatoms and also a period when water blooms are prone to outbreaks in the lower reaches of the HR.

Our analysis also show that, ΔH is closely related to the algal blooms in the lower HR as a variable that comprehensively expresses the hydrological situation of the HR and the YR. Many researchers have also proposed that the hydrological regime is the most important driving factor for the outbreak of river algal blooms (Yang et al., 2011; Kim et al., 2019; Xia et al., 2019; Xia et al., 2020). A lower water level difference indicates a smaller flow rate. It decreases the loss of phytoplankton caused by flow flushing and provides phytoplankton more retention time to enlarge their biovolumes (Fisher, 1996). In addition, sometimes gentle hydrological conditions can lead to thermal stratification in some regulated rivers, which promotes the growth of diatoms (Bormans and Webster, 1998). The lack of underwater sunlight will reduce the biomass of underwater phytoplankton in turbulent rivers (Reynolds and Descy, 1996). The lower flow rate will reduce the disturbance of the water body, which reduces the turbidity and increases the transparency. Therefore, ΔH was found to provide new insights for the prevention and control of river algal blooms.

Time-Lag Response of Algal Bloom Outbreaks to Multiple Driving Factors

Time-lag response widely exists in the biological world due to the complexity of aquatic ecological processes. Dependent on the algal species and the magnitude of the nutrient pulse, the cell division has different states (Collos, 1986). For different phytoplanktons, their growth can be divided into two different strategies. One is that the body of certain phytoplanktons does not accumulate nutrients. The growth of these phytoplanktons and the absorption of nutrients are closely integrated. Therefore, these phytoplanktons have a rapid stress growth response to the stimulation of nutrients. In contrast, other kinds of phytoplanktons have the ability to accumulate a large amount of nutrients in the body and carry out complex transformation and absorption processes. The time lags in cell division are usually more than 24 h (Collos, 1986). Our studies show that the length of the time lag in response of the algal blooms to the driving factors is 1 period (10 days) in HR. It is consistent with previous studies. For example, Xia et al. (2020) have proposed river algal blooms are well predicted by antecedent environmental conditions, especially hydrological factors.

However, it is hard to quantify the time-lag effect of algal bloom outbreaks to various driving factors. Although we were not able to conduct a more detailed analysis since the time interval of our data is 10 days, results are similar to the conclusions of many

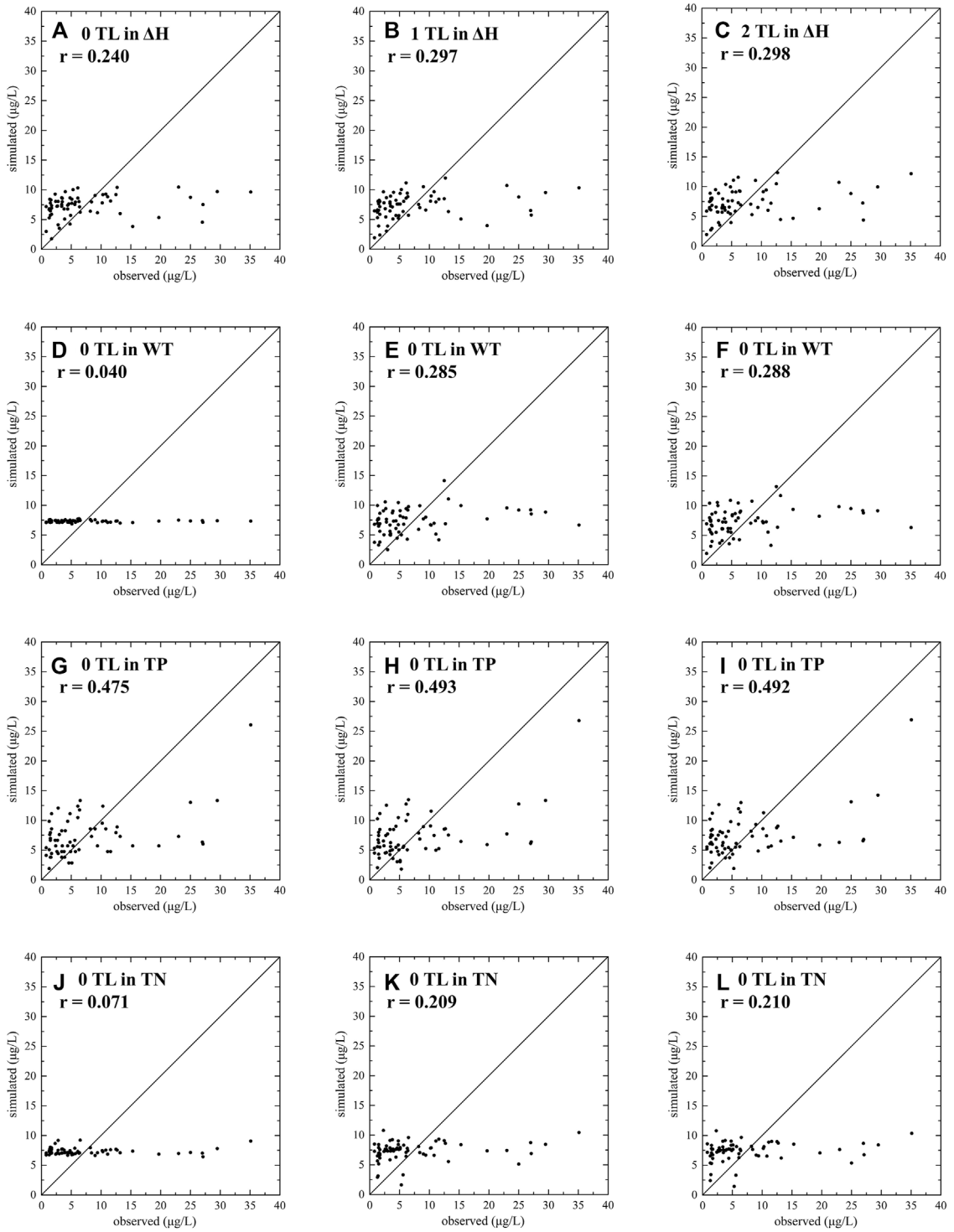

FIGURE 5 | Results of Almon Distributed Lag Model. TL, Time-lag length.

other studies. Based on the artificial neural network model, it was indicate that the time lag in response to environmental variables is often between 7 and 14 days (Lee et al., 2003). Moreover, some studies show that the length of time lag between the algal bloom outbreak and the driving factors is 2–4 days in lakes (Recknagel et al., 2013). In addition, the length of time lag is related to the distance between the driving element monitoring point and the algal bloom monitoring point, which includes the time involved

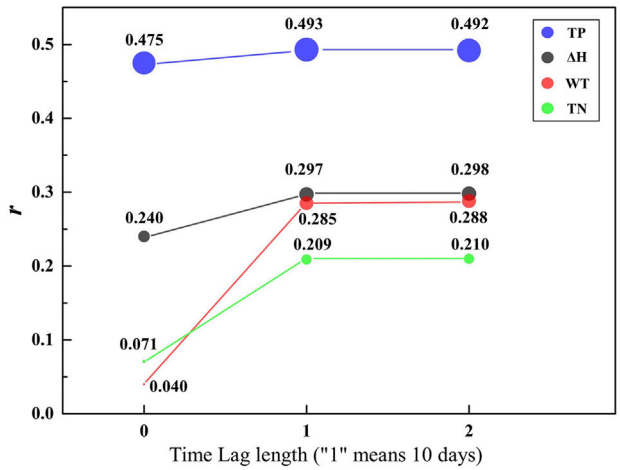

FIGURE 6 | The change of *r* under different time-lag lengths and different driving factors.

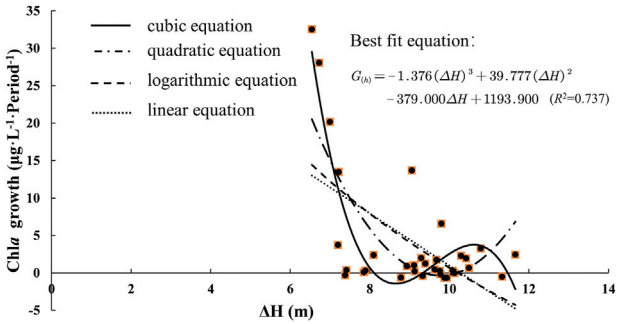

FIGURE 7 | Nonlinear fitting between Chl*a* growth and ΔH at the lower HR.

in environmental variable migration and exercise (Jeong et al., 2007). Our research area is located at the confluence of estuaries where the HR merges into the YR, it is also the sensitive impact area of mega water project. Therefore, the intrusion of the YR water also affects the driving factors in the study area, and it makes the causes of blooms are more complex. By utilizing the time-lag response of algal bloom outbreaks to the driving factors, hydrological regulations that are feasible and efficient to implement can be developed to reduce the potential risk of river algal blooms (Mitrovic et al., 2007; Xin et al., 2020). As demonstrated above, hydrological data are easy to observe and effective for early warning of algal bloom outbreaks. Based on the hydrological sensitivity of algal blooms, we can adjust the interactive hydrological situation of the YR and HR to alleviate algal blooms.

Effects of Hydrological Regime on Algal Blooms

We have also found that the ΔH affects the ecological processes and flow patterns of the river channel in several ways. When ΔH becomes smaller, the YR's supporting effect on the HR is obvious and its inflow become hindered. This promotes the formation of a stable hydrological environment similar to a lake reservoir in the estuary confluence area. It provides a site and environmental stimulation for the growth and reproduction of phytoplankton. From **Figure 3**, we can see that the water level fluctuation of the YR is more intense than that of the HR. The change of the water level of the YR contributes the most to the change of ΔH. We infer that the water level change was highly affected by the impoundment of the Danjiangkou Reservoir upstream, which also decreases the ΔH. The drop of ΔH forms a backwater area in the estuary area (Qu et al., 2014), which lengthens the residence time of the water body and slows down the changes in hydrological situation (Yin et al., 2012). The nutrients, such as nitrogen and phosphorus, in the YR are significantly overloaded (Li et al., 2007; Liu et al., 2018). The backflow of the YR causes nutrients to enter the Han River, which promotes the growth of phytoplankton and increases the probability of algal blooms.

This study shows that there is a significant correlation between Chl*a* and ΔH, and the ΔH contributed most to the algal blooms (Appendix B). Therefore, it can be concluded that the hydrological condition of the YR has greatly contributed to the occurrence of algal blooms in the lower HR. To further analyze the relationship between phytoplankton growth ($G_{(h)}$) and ΔH, we assume a specific environment. At this time, the water quality and climate conditions are kept in a relatively stable state. Furthermore, we performed a curve fitting analysis on the phytoplankton change rate and the two-periods ΔH data. The results (**Figure 7**) show that a cubic equation can fit the correlation best, compared to a quadratic equation, logarithmic equation, and linear equation. The fitting equation is as follows.

$$G_{(h)} = -1.376(\Delta H)^3 + 39.777(\Delta H)^2 - 379.000\Delta H + 1193.900 \quad (R^2 = 0.737) \tag{6}$$

Some experiments have been conducted to analyze the mechanism underlying the correlation between hydrological regimes and algal blooms by estimating the suitable hydrological conditions (Zheng et al., 2009; Yin et al., 2012). Our results imply that the growth rate of Chl*a* first decreases with the increase of water level then increases. After that, it keeps decreasing. This fluctuation is related to the growth habit of diatoms. As the ΔH increases, phytoplankton is washed away to reduce (Yang et al., 2012). Diatoms are suitable for growth in water bodies with a certain flow rate (Zheng et al., 2009). At the same time, the proper flow rate also reduces the settlement of phytoplankton (Xia et al., 2019). During the treatment of algae blooms in the lower reaches of the HR in 2018, the discharge flow rate of Danjiangkou Reservoir was increased to 800 m^3/s but the elimination of algal blooms did not achieve the expected effect. When the discharge flow increased to 1,300 m^3/s, the algal bloom

outbreak was further curbed (Li et al., 2020). Therefore, we can make early decisions and warnings for the prevention and control of algal blooms in the lower HR by discovering the key driving role of ΔH based on the time-lag effect of the algal bloom outbreak.

5 CONCLUSION

In this study, we used a variety of statistical analysis methods and the Almon Time Lag Model to investigate the algal blooms during a decade (2003–2014) in the lower HR, which is the largest tributary of the YR of China. It is found that all hydrological conditions, nutrients, and water temperature contributed to the outbreak of river algal blooms. In particular, hydrological conditions contributed the most to the outbreak of algal blooms in the rivers. Hydrological conditions contained only the principal component of a variable ΔH, contributing more than 23% of the explanatory power. Moreover, the gray correlation between Chl*a* and ΔH was the highest, which was 0.896. In addition, there was a time lag of about 1 period (10 days) in response to the main driving factors of algal bloom outbreaks. These findings provide new discovery for the simulation and early warning of algal blooms, as well as provide time to take emergency measures for the upcoming algal bloom in advance. Therefore, the water level relationship between the YR and the HR should be harmonized to destroy the hydrological regime that is conducive to the growth of phytoplankton. Traditionally, the elimination of algal blooms in the lower HR mainly relied on the flushing of upstream water, which sometimes resulted in the waste of many high-quality freshwater resources. This study is limited by the scale of the data interval and the analysis of the length of the time lag can be further improved. With the rapid expansion of human activities and the intensification of climate change, many rivers will suffer from algae blooms in the future. Therefore, our research provides a baseline for the prevention and control of algae blooms in other rivers.

DATA AVAILABILITY STATEMENT

The original contributions presented in the study are included in the article/**Supplementary Material**, further inquiries can be directed to the corresponding author.

AUTHOR CONTRIBUTIONS

CL and YC contributed to the conceptualization, ideas, methodology, original paper draft and visualization. LZ, BC and TH contributed to study area definition, methods selection and results discussion. All authors contributed to article revision, read, and approved the submitted version.

FUNDING

This work was supported by National Key R&D Program of China (grant No. 2021YFC3201003), The National Natural Science Foundation of China (grant No. 51879252), The Fundamental Research Funds for the Central Public-interest Scientific Institution (grant No. 2021KSKY-04), The Special Fund for Basic Scientific Research of Central Public Research Institutes (2020YSKY-003).This work is supported and funded by the Chinese Research Academy of Environmental Sciences.

SUPPLEMENTARY MATERIAL

The Supplementary Material for this article can be found online at: https://www.frontiersin.org/articles/10.3389/feart.2021.813287/full#supplementary-material

REFERENCES

Almon, S. (1965). The Distributed Lag between Capital Appropriations and Expenditures. *Econometrica* 33, 178–196. doi:10.2307/1911894

Bhat, S. R., Devi, P., D'Souza, L., Verlecar, X. N., and Naik, C. G. (2006). *Harmful Algal Blooms*. India: TERI Press.

Bormans, M., and Webster, I. T. (1998). Dynamics of Temperature Stratification in lowland Rivers. *J. Hydraulic Eng.* 124, 1059–1063. doi:10.1061/(asce)0733-9429(1998)124:10(1059)

Cao, S., Xia, R., Zhang, Y., Li, Z., Ren, Y., and Ta, L. (2020). Characteristics and Response of Ecological Environment in Downstream of Hanjiang River before and after Running of Middle Route of South-To-North Water Diversion Project. *Res. Environ. Sci.* 33, 1431–1439. doi:10.13198/j.issn.1001-6929.2019.07.30

Carey, C. C., Ibelings, B. W., Hoffmann, E. P., Hamilton, D. P., and Brookes, J. D. (2012). Eco-physiological Adaptations that Favour Freshwater Cyanobacteria in a Changing Climate. *Water Res.* 46, 1394–1407. doi:10.1016/j.watres.2011.12.016

Chen, H., Guo, S., Xu, C.-y., and Singh, V. P. (2007). Historical Temporal Trends of Hydro-Climatic Variables and Runoff Response to Climate Variability and Their Relevance in Water Resource Management in the Hanjiang basin. *J. Hydrol.* 344, 171–184. doi:10.1016/j.jhydrol.2007.06.034

Cheng, B., Xia, R., Zhang, Y., Yang, Z., Hu, S., Guo, F., et al. (2019). Characterization and Causes Analysis for Algae Blooms in Large River System. *Sustain. Cities Soc.* 51, 101707. doi:10.1016/j.scs.2019.101707

Chung, S.-W., Lee, H., and Jung, Y. (2008). The Effect of Hydrodynamic Flow Regimes on the Algal Bloom in a Monomictic Reservoir. *Water Sci. Technol.* 58, 1291–1298. doi:10.2166/wst.2008.482

Chuo, M., Ma, J., Liu, D., and Yang, Z. (2019). Effects of the Impounding Process during the Flood Season on Algal Blooms in Xiangxi Bay in the Three Gorges Reservoir, China. *Ecol. Model.* 392, 236–249. doi:10.1016/j.ecolmodel.2018.11.017

Collos, Y. (1986). Time-lag Algal Growth Dynamics: Biological Constraints on Primary Production in Aquatic Environments. *Mar. Ecol. Prog. Ser.* 33, 193–206. doi:10.3354/meps033193

Fisher, W. (1996). Stream Ecology: Structure and Function of Running Waters. *Utaf* 125, 154–158. doi:10.1577/1548-8659-125.1.154

Ha, K., Jang, M.-H., and Joo, G.-J. (2002). Spatial and Temporal Dynamics of Phytoplankton Communities along a Regulated River System, the Nakdong River, Korea. *Hydrobiologia* 470, 235–245. doi:10.1023/a:1015610900467

Hallegraeff, G. M. (1993). A Review of Harmful Algal Blooms and Their Apparent Global Increase. *Phycologia* 32, 79–99. doi:10.2216/i0031-8884-32-2-79.1

Harris, G. P. (1983). Mixed Layer Physics and Phytoplankton Populations: Studies in Equilibrium and Non-equilibrium Ecology. *Prog. Phycological Res.* 2, 1–15.

Istvánovics, V., and Honti, M. (2012). Efficiency of Nutrient Management in Controlling Eutrophication of Running Waters in the Middle Danube Basin. *Hydrobiologia* 686, 55–71. doi:10.1007/s10750-012-0999-y

Jeong, K.-S., Kim, D.-K., and Joo, G.-J. (2007). Delayed Influence of Dam Storage and Discharge on the Determination of Seasonal Proliferations of Microcystis Aeruginosa and Stephanodiscus Hantzschii in a Regulated River System of the Lower Nakdong River (South Korea). *Water Res.* 41, 1269–1279. doi:10.1016/j.watres.2006.11.054

Ji, D., Wells, S. A., Yang, Z., Liu, D., Huang, Y., Ma, J., et al. (2017). Impacts of Water Level Rise on Algal Bloom Prevention in the Tributary of Three Gorges Reservoir, China. *Ecol. Eng.* 98, 70–81. doi:10.1016/j.ecoleng.2016.10.019

Jung, S. W., Kwon, O. Y., Lee, J. H., and Han, M.-S. (2009). Effects of Water Temperature and Silicate on the Winter Blooming DiatomStephanodiscus hantzschii(Bacillariophyceae) Growing in Eutrophic Conditions in the Lower Han River, South Korea. *J. Freshw. Ecol.* 24, 219–226. doi:10.1080/02705060.2009.9664286

Jung, S. W., Min Joo, H., Kim, Y.-O., Hwan Lee, J., and Han, M.-S. (2011). Effects of Temperature and Nutrient Depletion and Reintroduction on Growth ofStephanodiscus hantzschii(Bacillariophyceae): Implications for the Blooming Mechanism. *J. Freshw. Ecol.* 26, 115–121. doi:10.1080/02705060.2011.553927

Kim, D.-K., Jeong, K.-S., Whigham, P. A., and Joo, G.-J. (2007). Winter Diatom Blooms in a Regulated River in South Korea: Explanations Based on Evolutionary Computation. *Freshw. Biol* 52, 2021–2041. doi:10.1111/j.1365-2427.2007.01804.x

Kim, H. G., Hong, S., Jeong, K.-S., Kim, D.-K., and Joo, G.-J. (2019). Determination of Sensitive Variables Regardless of Hydrological Alteration in Artificial Neural Network Model of Chlorophyll a: Case Study of Nakdong River. *Ecol. Model.* 398, 67–76. doi:10.1016/j.ecolmodel.2019.02.003

Kim, M.-C., Jeong, K.-S., Kang, D.-K., Kim, D.-K., Shin, H.-S., and Joo, G.-J. (2009). Time Lags between Hydrological Variables and Phytoplankton Biomass Responses in a Regulated River (The Nakdong River). *J. Ecol. Environ.* 32, 221–227. doi:10.5141/jefb.2009.32.4.221

Lee, J. H. W., Huang, Y., Dickman, M., and Jayawardena, A. W. (2003). Neural Network Modelling of Coastal Algal Blooms. *Ecol. Model.* 159, 179–201. doi:10.1016/s0304-3800(02)00281-8

Lee, M., Kim, B., Kwon, Y., and Kim, J. (2009). Characteristics of the marine Environment and Algal Blooms in Gamak Bay. *Fish. Sci.* 75, 401–411. doi:10.1007/s12562-009-0056-6

Li, C. (2007). *Analysis and Research on Influencing Factors of Algae Bloom in Hanjiang River*. Kunming: Kunming University of Science and Technology.

Li, H.-M., Tang, H.-J., Shi, X.-Y., Zhang, C.-S., and Wang, X.-L. (2014). Increased Nutrient Loads from the Changjiang (Yangtze) River Have Led to Increased Harmful Algal Blooms. *Harmful Algae* 39, 92–101. doi:10.1016/j.hal.2014.07.002

Li, J., Yin, W., Jia, H., and Xin, X. (2020). Reserch Progress on Diatom Blooms in the Middle and Lower Hanjiang River: Review and Advances. *J. Hydroecology* 41, 136–144. doi:10.15928/j.1674-3075.2020.05.016

Li, M., Xu, K., Watanabe, M., and Chen, Z. (2007). Long-term Variations in Dissolved Silicate, Nitrogen, and Phosphorus Flux from the Yangtze River into the East China Sea and Impacts on Estuarine Ecosystem. *Estuarine, Coastal Shelf Sci.* 71, 3–12. doi:10.1016/j.ecss.2006.08.013

Li, S., Cheng, X., Xu, Z., Han, H., and Zhang, Q. (2009). Spatial and Temporal Patterns of the Water Quality in the Danjiangkou Reservoir, China. *Hydrological Sci. J.* 54, 124–134. doi:10.1623/hysj.54.1.124

Liu, D., Yang, Z., Ji, D., Ma, J., Cui, Y., and Song, L. (2016). A Review on the Mechanism and its Controlling Methods of the Algal Blooms in the Tributaries of Three Gorges Reservoir. *J. Hydraulic Eng.* 47, 443–454. doi:10.13243/j.cnki.slxb.20151304

Liu, X., Beusen, A. H. W., Van Beek, L. P. H., Mogollón, J. M., Ran, X., and Bouwman, A. F. (2018). Exploring Spatiotemporal Changes of the Yangtze River (Changjiang) Nitrogen and Phosphorus Sources, Retention and export to the East China Sea and Yellow Sea. *Water Res.* 142, 246–255. doi:10.1016/j.watres.2018.06.006

Liu, X. (2019). *Study on Time Lag Effect and Spatial-Temporal Distribution Model of Agricultural Drought — A Case Study of the Plain Area of South Hebei ProvinceSchool of Water Conservancy and Hydroelectric Power*. Handan City, China: Hebei University of Engineering.

Lucas, L. V., Thompson, J. K., and Brown, L. R. (2009). Why Are Diverse Relationships Observed between Phytoplankton Biomass and Transport Time? *Limnol. Oceanogr.* 54, 381–390. doi:10.4319/lo.2009.54.1.0381

Maavara, T., Parsons, C. T., Ridenour, C., Stojanovic, S., Dürr, H. H., Powley, H. R., et al. (2015). Global Phosphorus Retention by River Damming. *Proc. Natl. Acad. Sci. USA* 112, 15603–15608. doi:10.1073/pnas.1511797112

McKiver, W. J., and Neufeld, Z. (2009). Influence of Turbulent Advection on a Phytoplankton Ecosystem with Nonuniform Carrying Capacity. *Phys. Rev. E* 79, 061902. doi:10.1103/PhysRevE.79.061902

Mischke, U., Venohr, M., and Behrendt, H. (2011). Using Phytoplankton to Assess the Trophic Status of German Rivers. *Int. Rev. Hydrobiology* 96, 578–598. doi:10.1002/iroh.201111304

Mitrovic, S. M., Chessman, B. C., Davie, A., Avery, E. L., and Ryan, N. (2007). Development of Blooms of Cyclotella Meneghiniana and Nitzschia Spp. (Bacillariophyceae) in a Shallow River and Estimation of Effective Suppression Flows. *Hydrobiologia* 596, 173–185. doi:10.1007/s10750-007-9094-1

Oliver, A. A., Dahlgren, R. A., and Deas, M. L. (2014). The Upside-Down River: Reservoirs, Algal Blooms, and Tributaries Affect Temporal and Spatial Patterns in Nitrogen and Phosphorus in the Klamath River, USA. *J. Hydrol.* 519, 164–176. doi:10.1016/j.jhydrol.2014.06.025

Özbay, N., and Toker, S. (2021). Prediction Framework in a Distributed Lag Model with a Target Function: an Application to Global Warming Data. *Environ. Ecol. Stat.* 28, 87–134. doi:10.1007/s10651-020-00477-x

Qu, Y., Huang, Y., He, Z., and Wu, G. (2014). The Influence of the Backwater Support of the Yangtze River on the Water-Sediment Process from the Xinglong of the Hanjiang River to the Hanchuan River. *China Water Transport* 11, 62–64. doi:10.13646/j.cnki.42-1395/u.2014.11.027

Recknagel, F., Ostrovsky, I., Cao, H., Zohary, T., and Zhang, X. (2013). Ecological Relationships, Thresholds and Time-Lags Determining Phytoplankton Community Dynamics of Lake Kinneret, Israel Elucidated by Evolutionary Computation and Wavelets. *Ecol. Model.* 255, 70–86. doi:10.1016/j.ecolmodel.2013.02.006

Reynolds, C. S., and Descy, J.-P. (1996). The Production, Biomass and Structure of Phytoplankton in Large Rivers. *rs* 10, 161–187. doi:10.1127/lr/10/1996/161

Rose, J. M., and Caron, D. A. (2007). Does Low Temperature Constrain the Growth Rates of Heterotrophic Protists? Evidence and Implications for Algal Blooms in Cold Waters. *Limnol. Oceanogr.* 52, 886–895. doi:10.4319/lo.2007.52.2.0886

Rui, X., Zhi, C., and Yun, Z. (2012). Impact Assessment of Climate Change on Algal Blooms by a Parametric Modeling Study in Han River. *J. Resour. Ecol.* 3, 209–219. doi:10.5814/j.issn.1674-764x.2012.03.003

Wang, B. (2006). Cultural Eutrophication in the Changjiang (Yangtze River) Plume: History and Perspective. *Estuarine, Coastal Shelf Sci.* 69, 471–477. doi:10.1016/j.ecss.2006.05.010

Wang, W. (1974). Effect of Turbidity on Algal Growth. *Circular* 121, 1–12. doi:10.1149/1.2401768

Whitehead, P. G., Bussi, G., Bowes, M. J., Read, D. S., Hutchins, M. G., Elliott, J. A., et al. (2015). Dynamic Modelling of Multiple Phytoplankton Groups in Rivers with an Application to the Thames River System in the UK. *Environ. Model. Softw.* 74, 75–91. doi:10.1016/j.envsoft.2015.09.010

Xia, R., Wang, G., Zhang, Y., Yang, P., Yang, Z., Ding, S., et al. (2020). River Algal Blooms Are Well Predicted by Antecedent Environmental Conditions. *Water Res.* 185, 116221. doi:10.1016/j.watres.2020.116221

Xia, R., Zhang, Y., Critto, A., Wu, J., Fan, J., Zheng, Z., et al. (2016). The Potential Impacts of Climate Change Factors on Freshwater Eutrophication: Implications for Research and Countermeasures of Water Management in China. *Sustainability* 8, 229. doi:10.3390/su8030229

Xia, R., Zhang, Y., Wang, G., Zhang, Y., Dou, M., Hou, X., et al. (2019). Multi-factor Identification and Modelling Analyses for Managing Large River

Algal Blooms. *Environ. Pollut.* 254, 113056. doi:10.1016/j.envpol.2019.113056

Xie, M., Wang, X., Guan, G., and Hu, M. (2006). Analysis of Causes of "Water Bloom" in the Middle and Lower Reaches of Hanjiang River and its Countermeasures. *Yangtze River* 37 (8), 43–46. doi:10.16232/j.cnki.1001-4179.2006.08.017

Xie, P., Xia, J., Dou, M., and Zhang, W. (2004). Research into the Effects of the Middle Route of China's South-To-north Water Transfer Project on Water Bloom in the Middle-Down Stream of Hanjiang River and its Countermeasures Part I- an Analysis of the Key Factors Generating Water Bloom in Hanjiang River. *J. Nat. Resour.* 19, 418–423.

Xin, X., Zhang, H., Lei, P., Tang, W., Yin, W., Li, J., et al. (2020). Algal Blooms in the Middle and Lower Han River: Characteristics, Early Warning and Prevention. *Sci. Total Environ.* 706, 135293. doi:10.1016/j.scitotenv.2019.135293

Yang, J. R., Lv, H., Isabwe, A., Liu, L., Yu, X., Chen, H., et al. (2017). Disturbance-induced Phytoplankton Regime Shifts and Recovery of Cyanobacteria Dominance in Two Subtropical Reservoirs. *Water Res.* 120, 52–63. doi:10.1016/j.watres.2017.04.062

Yang, Q., Xie, P., Shen, H., Xu, J., Wang, P., and Zhang, B. (2012). A Novel flushing Strategy for Diatom Bloom Prevention in the Lower-Middle Hanjiang River. *Water Res.* 46, 2525–2534. doi:10.1016/j.watres.2012.01.051

Yang, Q., Xie, P., Xu, J., Shen, H., Zhang, M., Wang, S., et al. (2011). Research Advances of Diatom Blooms in Rivers. *Resour. Environ. Yangtze Basin* 20, 159–165.

Yin, D., Huang, W., Wu, X., and Song, L. (2012). Preliminary Study on Biological Characteristics of Spring Diatom Bloom in the Hanjiang River. *J. Yangtze River Scientific Res. Inst.* 29, 6–10.

Zeng, H., Song, L., Yu, Z., and Chen, H. (2006). Distribution of Phytoplankton in the Three-Gorge Reservoir during Rainy and Dry Seasons. *Sci. Total Environ.* 367, 999–1009. doi:10.1016/j.scitotenv.2006.03.001

Zhang, C., Wang, J., Zhu, D., Shi, X., and Wang, X. (2008). The Preliminary Analysis of Nutrients in Harmful Algal Blooms in the East China Sea in the spring and Summer of 2005. *Acta Oceanologica Sinica* 30, 153–159.

Zheng, L.-L., Song, L.-R., Wu, X.-H., and Zhuang, H.-R. (2009). Analysis of Morphology and 18s Rdna Gene from the Causative Specie Related Diatom Bloom in Hanjiang River. *Acta Hydr Sin* 33, 562–565. doi:10.3724/sp.j.1035.2009.00562

Zhou, J., Zhang, M., and Lu, P. (2013). The Effect of Dams on Phosphorus in the Middle and Lower Yangtze River. *Water Resour. Res.* 49, 3659–3669. doi:10.1002/wrcr.20283

Zhou, M., Zhu, M., and Zhang, J. (2001). Status of Harmful Algal Blooms and Related Research Activities in China. *Chin. Bull. Life Sci.* 13, 54–59.

Zhou, Z.-X., Yu, R.-C., and Zhou, M.-J. (2017). Resolving the Complex Relationship between Harmful Algal Blooms and Environmental Factors in the Coastal Waters Adjacent to the Changjiang River Estuary. *Harmful Algae* 62, 60–72. doi:10.1016/j.hal.2016.12.006

Conflict of Interest: The authors declare that the research was conducted in the absence of any commercial or financial relationships that could be construed as a potential conflict of interest.

Publisher's Note: All claims expressed in this article are solely those of the authors and do not necessarily represent those of their affiliated organizations, or those of the publisher, the editors, and the reviewers. Any product that may be evaluated in this article, or claim that may be made by its manufacturer, is not guaranteed or endorsed by the publisher.

frontiers in Earth Science

ORIGINAL RESEARCH
published: 09 February 2022
doi: 10.3389/feart.2021.827721

Resource Remobilization Efficiency Varies With Plant Growth Form but Not Between Fens and Bogs

Yu Cong[1,2], Zhongsheng Zhang[1,2], Bo Liu[1], Yingyi Chen[1], Xiao Li[1], Ming Jiang[1,2] and Mai-He Li[3,4]*

[1]Key Laboratory of Wetland Ecology and Environment, Northeast Institute of Geography and Agricultural Ecology, Chinese Academy of Sciences, Changchun, China, [2]Jilin Provincial Joint Key Laboratory of Changbai Mountain Wetland and Ecology, Changchun, China, [3]Swiss Federal Institute for Forest, Snow and Landscape Research WSL, Zürich, Switzerland, [4]Key Laboratory of Geographical Processes and Ecological Security in Changbai Mountains, Ministry of Education, School of Geographical Sciences, Northeast Normal University, Changchun, China

Resource resorption from senescing leaves is an important strategy for internal nutrient recycling in plants. However, our understanding of whether the responses of resource remobilization to mire types (fens vs. bogs) differ among various plant growth forms remains unclear. We thus assessed resource remobilization among various growth forms in fens and bogs in the Hani peatland in the Changbai Mountains, northeastern China. We analyzed and compared the concentrations of non-structural carbohydrates (NSCs), nitrogen (N), phosphorus (P), and potassium (K) in leaves and roots collected in August (mid-season) and September (end-season), and calculated the resource remobilization efficiency (RRE) of four species belonging to four growth forms grown in both fens and bogs. The deciduous dwarf trees (*Betula fruticosa*) and perennial grass (*Phragmites australis*) had relative higher leaf RRE than the moss (*Sphagnum magellanicum*). Although leaf nutrient RRE did not differ between fens and bogs, the deciduous dwarf trees had a higher leaf NSC RRE in bogs than in fens, and the moss NSC RRE was lower in bogs than in fens. Our results suggest that reallocation of mobile carbohydrates seems to be more sensitive to the growth condition than nutrients (N, P, and K) under nutrient-poor inhabits, which may be one of the reasons leading to nutrient limitation in peatlands.

Keywords: mires, non-structural carbohydrates, nitrogen, phosphorus, potassium, reallocation, storage, plant growth form

OPEN ACCESS

Edited by:
Guobin Fu,
CSIRO Land and Water, Australia

Reviewed by:
Feng Li,
Institute of Subtropical Agriculture (CAS), China
Xinhou Zhang,
Nanjing Normal University, China
Meng Wang,
Northeast Normal University, China

****Correspondence:***
Ming Jiang
jiangm@iga.ac.cn

Specialty section:
This article was submitted to Hydrosphere, a section of the journal Frontiers in Earth Science

Received: *02 December 2021*
Accepted: *24 December 2021*
Published: *09 February 2022*

Citation:
Cong Y, Zhang Z, Liu B, Chen Y, Li X, Jiang M and Li M-H (2022) Resource Remobilization Efficiency Varies With Plant Growth Form but Not Between Fens and Bogs. Front. Earth Sci. 9:827721. doi: 10.3389/feart.2021.827721

INTRODUCTION

Peatlands are usually classified into two categories: ombrogenous bogs and geogenous fens (Bridgham et al., 1996; Jonasson and Shaver, 1999). These peatlands types are characterized by high water tables, low nutrient availability, and dominant plant species (Aerts et al., 1999; Bridgham et al., 1996). The imbalance and shortage of nutrients can differ considerably between fens and bogs (Ohlson, 1995; Jonasson and Shaver, 1999), mainly due to the hydrological distinction (Waughman, 1980). Fens are fed by precipitation, mineral- and nutrient-rich surface water, and groundwater (Aerts & Chapin, 1999), whereas bogs lack groundwater input and receive nutrients mainly from precipitation (Charman, 2002), leading to different growth forms that occur in fens and bogs. Fens are often dominated by deciduous shrubs or dwarf shrubs and graminoids (mainly *Carex* and

Cladium species), while bogs are dominated by *Sphagnum* mosses and evergreen shrubs or dwarf shrubs and trees (Maimer et al., 1992; Bridgham et al., 1996). Previous studies have shown that plants in fens and bogs are often limited by nutrient availability (Charman, 2002; Wang et al., 2014; Li et al., 2019). This raises the question of how plants respond to low nutrient availability in fens and bogs.

Effective resource resorption from senescing leaves is an important strategy for internal nutrient recycling (Killingbeck, 1996), which reduces plants' dependence on external nutrient supply from the environment (Aerts and Chapin, 1999). It has been estimated that, in general, half of nitrogen (N) and phosphorus (P) contained in mature leaves would be withdrawn during senescence (Aerts, 1996). Vergutz et al. (2012) calculated that the mean nutrient resorption efficiency was over 60% for N and P and 70% for K of global terrestrial plants. The patterns of resource remobilization differ among various growth forms. A large-scale study found that differences of leaf nutrient-use efficiency in plant growth forms are more important than differences in mire type (fen vs. bog) (Aerts et al., 1999). Greater allocation to storage in deciduous than in evergreen species reflects the lower opportunity cost in deciduous species that experience a more pronounced asynchrony of supply and demand (Chapin et al., 1990). For example, storage of carbohydrates is particularly important for deciduous species that do not have green tissues in early season and relay on carbon storage for regrowth (Epron et al., 2012). Similarly, Aerts (1996) found that nitrogen resorption efficiency was significantly higher in deciduous species and graminoids than in evergreen species and forbs, while P resorption efficiency did not differ between these growth forms. Yuan and Chen (2009) had observed consistent differences between deciduous and evergreen species. However, Vergutz et al. (2012) reported that graminoid had much higher nutrient resorption efficiency, due to the smaller non-leaf pools, leading to a greater need for nutrient resorption compared to other growth forms. Moreover, several studies highlighted that roots or rhizome played a crucial role as resource storage tissues of deciduous species and herbaceous plants (Granéli et al., 1992; Millard et al., 2001; Cong et al., 2019). In contrast, evergreen species directly retained resources in over-wintering leaves rather than recycled back to roots (Wyka et al., 2016).

Various relationships between nutrient availability and nutrient resorption were found. Some species growing in nutrient-poor habitats have higher resource remobilization efficiency (RRE) than those in moderate habitats (Pensa and Sellin, 2003; Yuan et al., 2005). A large-scale study found that bog species had a higher P use efficiency than fen species (Aerts et al., 1999). High RRE may help plants to obtain a competitive advantage in the infertile habitats (Pugnaire and Chapin, 1993). However, some evidence showed no major differences in nutrient resorption between plants in infertile and fertile soils (Aerts, 1996; Yuan and Chen, 2009). Hence, response of RRE to nutrient availability remains controversial.

In this study, we investigated and compared resource remobilization among various growth forms in fens and bogs in the Hani peatland in the Changbai Mountains. We measured tissue concentrations of non-structural carbohydrates (NSCs), N, P, and K at the peak-growing season and at the end of growing season, and calculated and compared the RRE of species grown in both fens and bogs, to answer the following questions: (1) whether the RRE varies with growth forms and (2) whether the RRE differs between bogs and fens.

MATERIALS AND METHODS

Study Sites

The study was conducted at the Hani Peatland (42°13′N, 126°31′E) located in the west Changbai Mountain region in northeastern China. The area has a continental monsoon climate with a mean annual air temperature of 2.5–3.6°C (Bu et al., 2011). The annual precipitation ranges from 757 to 930 mm (Li et al., 2019). The peatland has a mean peat depth of 4 m; the deepest record was 9.6 m (Qiao, 1993). The peatland plants consist of dwarf trees (mainly *Betula fruticosa* Pall.), dwarf shrubs (mainly *Rhododendron tomentosum* Harmaja, and *Vaccinium uliginosum* L.), herbs [*Carex lasiocarpa* Ehrh., *Phragmites australis* (Clav.), *Eriophorum polystachion* L., and *Smilacina japonica* A. Gray], and peat mosses including *Sphagnum magellanicum* and *S. palustre* L. (Bu et al., 2017).

Field Sampling

To compare RRE patterns of plants growing in fens and bogs, four plant species that grow in both fens and bogs were selected. The four species included *B. fruticosa* Pall. (deciduous dwarf tree), *P. australis* (Clav.) (perennial grass), *C. lasiocarpa* Ehrh. (perennial grass), and *S. magellanicum* (moss). We selected five fens plots ($n = 5$) and four bogs plots ($n = 4$); within each plot, there were all the four species selected. We collected leaves and roots (<0.5 cm in diameter) from six to eight individuals for each plant species within each plot and pooled them for a mixed leaf sample and root sample for each plot. However, for *S. magellanicum*, we collected branch leaves only, because it does not have proper roots. For leaf samples, mature and healthy leaves were collected on August 6, 2020 (mid-season), while only freshly yellow/fallen leaves were selected on September 16 (end-season), to minimize growth-form differences in leaf phenology among plant species. Also, to diminish the effects of diurnal temperature range and sunlight differences, all samples were collected at noon, placed in a cool box with ice, and transported immediately to the laboratory (Cong et al., 2019). Tissue samples were heated in a microwave oven at 600 W for 40 s to minimize the physiological activities, and dried at 65°C to a constant weight (Li et al., 2008). All samples were ground to powder with a ball mill (MM400, Retsch, Germany), and stored after being sealed with silica gel at 4°C prior to analyses.

Analysis of NSC

Dried plant material (30 mg) was put into a 10-ml centrifuge tube and mixed with 5 ml of 80% ethanol. The mixture was incubated at 80°C in a water shaker (SHA-C, Jintan Jingda Instrument Manufacturing Co., Ltd., Jintan, China) for 30 min, cooled to ambient temperature, and then centrifuged at 4,000 rpm for

10 min. The precipitates were re-extracted twice with 80% ethanol to extract the soluble sugars (Li et al., 2018). The ethanol-insoluble pellets were used for starch extraction, and the combined supernatants were saved for soluble sugars analysis by the anthrone method (Dubois et al., 1956). Glucose was used as a standard. Starch was extracted from the ethanol-insoluble residue placed at an 80°C water bath to remove the ethanol by evaporation. The ethanol-insoluble residues were boiled in 2 ml of distilled water for 15 min. After cooling to room temperature, 2 ml of 9.2 M $HClO_4$ was added to hydrolyze the starch for 15 min and 4 ml of distilled water was added to the samples. The mixture was centrifuged at 4,000 rpm for 10 min. Thereafter, the solid residues were extracted once more with 2 ml of 4.6 M $HClO_4$. Soluble sugars and starch concentrations were both determined using a spectrophotometer (TU-1810, Beijing Purkinje General Instrument Co., Ltd., Beijing, China) at 620 nm (Wang et al., 2018). Starch concentration was calculated by the glucose concentration by a conversion factor of 0.9. The soluble sugars, starch, and NSC concentrations were expressed on a dry matter basis (% d.m.).

Analysis of Nitrogen, Phosphorus, and Potassium

Oven-dried plant samples (0.1 g) were digested in concentrated H_2SO_4 and H_2O_2 (Parkinson and Allen, 1975). Nitrogen (N) concentration was then determined with an automatic chemical analyzer (SmartChem 140, AMS-Alliance Instruments, Rome, Italy), using the indophenol blue colorimetric method. Phosphorus (P) was measured colorimetrically by the ammonium molybdate-ascorbic acid method (Murphy and Riley, 1962) on a spectrophotometer (TU-1810, Beijing Purkinje General Instrument Co., Ltd., Beijing, China). Potassium (K) concentration was determined on a flame photometer (FP6410, Shanghai Precise Scientific Instrument Co., Ltd., Shanghai, China).

METHODS FOR RESOURCE REMOBILIZATION EVALUATION

Remobilization efficiency (R) was determined by the resource concentrations at the mid-season and at the end of growing season. Therefore, remobilization efficiency (%) of each tissue was calculated according to **Eq. 1** (Killingbeck, 1996):

$$R\% = \frac{C_s - C_a}{C_a} \times 100\% = \left(\frac{C_s}{C_a} - 1\right) \times 100\% \quad (1)$$

where C_s and C_a represent the concentrations of NSC, N, P, or K of each tissue at the end-season (September) and at the mid-season (August), respectively. A negative R value ($C_s < C_a$) indicates resource transfer from that tissue, while a positive value ($C_s > C_a$) indicates resource accumulation in that tissue. A smaller negative R value suggests higher remobilization efficiency, whereas a larger positive R value suggests higher accumulation efficiency.

Data Analysis

We defined NSC as the sum of soluble sugars and starch within each sample (Li et al., 2001; Li et al., 2002; Zhu et al., 2012). Data of NSC, soluble sugars, starch, and nutrients (i.e., N, P, and K) were confirmed for normality by Kolmogorov–Smirnov tests before statistical analysis. The above-mentioned data were analyzed using three-way ANOVAs with mire types, species, and time as fixed factors. Within each sampling time, two-way ANOVAs, with mire types and species as factors, were repeatedly performed to detect differences in parameters studied. Three-way ANOVAs with main factors of mire types, species, and tissue types were performed to test the trends in the remobilization efficiency of NSC, N, P, and K. Overall differences between fens and bogs species were analyzed using independent t-test.

RESULTS

Plant NSCs and Nutrients in Bogs and Fens

Leaf concentrations of NSCs (i.e., soluble sugars and starch) and nutrients (i.e., N, P, and K) varied significantly with species and sampling time (**Table 1**), while only leaf soluble sugars and NSC_T were significantly affected by mire types (**Table 1**). Species interacted with sampling time to significantly influence leaf soluble sugars, NSC_T, and nutrients, whereas mire types interacted with species to affect leaf K and with sampling time to influence leaf sugars and NSC_T (**Table 1**). Within the August sampling date, leaf NSCs (except for leaf starch with a $p = 0.081$) and nutrients varied significantly with species (**Table 2**; **Figures 1A–C**, **Figures 2A–C**), while only leaf sugars, NSC_T and K significantly differed between fens and bogs (**Table 2**), showing higher levels in bogs than in fens for all the four species (**Figures 1A,C**, and **Figure 2C**). At the end-season in September, leaf NSCs and nutrients differed among species only but did not change with mire type (**Table 3**; **Figures 1A–C**, **Figures 2A–C**). Generally, *B. fruticosa* (S1) had the highest level of NSCs and *S. magellanicum* (S4) showed the lowest levels of leaf NSCs in August (**Figures 1A–C**), whereas *P. australis* (S2) had the highest leaf nutrient levels and *S. magellanicum* (S4) showed the lowest leaf nutrient levels in August (**Figures 2A–C**).

Root concentrations of NSCs and nutrients (except for root P with a $p = 0.762$) varied significantly with mire types and species (**Table 1**), whereas root soluble sugars, NSC_T, N, and P were significantly affected by sampling time (**Table 1**). Mire types interacted with sampling time to did not differ for all parameters, while species interacted with mire types to significantly influence root starch, N, and P and with sampling time to influence root sugars, NSC_T, N, and P (**Table 1**). Within the August sampling date, root NSCs and nutrients varied significantly with species (**Table 2**; **Figures 1D–F**, **Figures 2D–F**), while only root sugars, NSC_T, and N significantly differed between fens and bogs (**Table 2**), showing higher NSC_T and K in bogs than in fens for all the 3 species (**Figures 1D–F**, and **Figure 2F**), but lower N and K in bogs than in fens for *P. australis* (S2) (**Figures 2D,E**). At the end-season in September, root NSC_T (except for root starch with a $p = 0.804$) and nutrients differed among species, while only root starch, NSC_T, and N significantly differed between fens and

TABLE 1 | Effects of mire types, species, sampling time, and their interactions on concentrations of NSCs (i.e., sugars, starch, and NSC_T) and nutrients (i.e., N, P, and K) in plant leaves and roots, tested with three-way nested ANOVAs. *F* and *p* values are given.

Factors	Df	Soluble sugars		Starch		NSC_T		Nitrogen (N)		Phosphorus (P)		Potassium (K)	
		F	*p*	*F*	*p*	*F*	*p*	*F*	*p*	*F*	*p*	*F*	*p*
Leaves													
Mire types (M)	1	9.526	**0.003**	3.293	0.075	11.092	**0.002**	0.052	0.821	0.396	0.532	3.825	0.055
Species (S)	3	98.887	**<0.001**	7.13	**<0.001**	113.638	**<0.001**	129.768	**<0.001**	12.839	**<0.001**	72.329	**<0.001**
Time (T)	1	19.896	**<0.001**	8.132	**0.006**	30.214	**<0.001**	180.551	**<0.001**	194.279	**<0.001**	169.386	**<0.001**
M × S	3	1.146	0.338	1.327	0.275	0.414	0.743	0.201	0.895	0.993	0.403	2.884	**0.044**
M × T	1	9.536	**0.003**	<0.001	0.986	8.038	**0.006**	0.568	0.454	0.048	0.828	3.115	0.083
S × T	3	29.359	**<0.001**	0.037	0.991	28.384	**<0.001**	45.623	**<0.001**	37.713	**<0.001**	53.595	**<0.001**
M × S × T	3	2.192	0.099	0.964	0.416	2.516	0.067	1.224	0.309	0.659	0.581	3.039	**0.036**
Roots													
Mire types (M)	1	13.27	**0.001**	9.729	**0.003**	17.313	**<0.001**	11.917	**0.001**	0.093	0.762	6.731	**0.013**
Species (S)	3	14.864	**<0.001**	4.631	**0.015**	14.873	**<0.001**	221.578	**<0.001**	44.162	**<0.001**	63.949	**<0.001**
Time (T)	1	37.382	**<0.001**	0.306	0.583	31.384	**<0.001**	78.82	**<0.001**	30.189	**<0.001**	2.387	0.13
M × S	3	1.662	0.202	4.15	**0.023**	2.89	0.067	11.404	**<0.001**	3.766	**0.032**	3.009	0.06
M × T	1	2.507	0.121	1.43	0.238	1.114	0.297	0.605	0.441	0.257	0.615	0.019	0.892
S × T	3	7.325	**0.002**	2.023	0.145	7.968	**0.001**	104.713	**<0.001**	24.677	**<0.001**	1.372	0.265
M × S × T	3	2.428	0.1	1.941	0.156	0.978	0.384	1.045	0.361	2.472	0.097	1.498	0.235

Bold values highlight significant effects at $p < 0.05$.

TABLE 2 | Effects of mire types, species, and their interactions on concentrations of NSCs (i.e., sugars, starch, and NSC_T) and nutrients (i.e., N, P, and K) in plant leaves and roots in August, tested with two-way nested ANOVAs. *F* and *p* values are given.

Factors	Df	Soluble sugars		Starch		NSC_T		Nitrogen (N)		Phosphorus (P)		Potassium (K)	
		F	*p*	*F*	*p*	*F*	*p*	*F*	*p*	*F*	*p*	*F*	*p*
Leaves													
Mire types (M)	1	14.379	**0.001**	1.083	0.307	14.416	**0.001**	0.666	0.421	0.358	0.555	5.59	**0.025**
Species (S)	3	69.478	**<0.001**	2.493	0.081	76.86	**<0.001**	225.38	**<0.001**	44.569	**<0.001**	83.016	**<0.001**
M × S	3	1.625	0.206	1.205	0.326	1.259	0.307	1.531	0.228	1.123	0.357	4.349	**0.012**
Roots													
Mire types (M)	1	11.149	**0.003**	2.729	0.113	10.079	**0.005**	7.433	**0.013**	**0**	0.992	2.995	**0.098**
Species (S)	2	12.232	**<0.001**	9.387	**0.001**	12.57	**<0.001**	259.686	**<0.001**	32.711	**<0.001**	30.646	**<0.001**
M × S	2	2.029	0.156	6.477	**0.006**	1.611	0.223	7.835	**0.003**	4.78	**0.019**	0.85	0.442

Bold values highlight significant effects at $p < 0.05$.

bogs (**Table 3**; **Figures 1D–F**, **Figures 2D–F**). Species interacted with mire types to significantly influence root N and K (**Table 3**). Generally, *B. fruticosa* (S1) had the highest level of NSC_T in August (**Figures 1D–F**), whereas *P. australis* (S2) had the highest root nutrient levels and *B. fruticosa* (S1) showed the lowest root nutrient levels in August (**Figures 2D–F**).

Carbohydrate and Nutrients Remobilization

Mire types and mire types×species interaction only significantly affected the remobilization efficiency of NSC (**Table 4**). The NSC remobilization efficiency in *B. fruticosa* (S1) leaves was significantly higher in bogs than in fens (**Figure 3A**). In contrast, *S. magellanicum* (S4) leaves had lower NSC remobilization efficiency in bogs compared with fens (**Figure 3A**). Both species and tissue types, and their interaction had significant effects on NSC and nutrient remobilization efficiency (**Table 4**). At the end of the growing season, leaves resources in four species were reallocated and even for NSC accumulation in *C. lasiocarpa* (S3) and *S. magellanicum* (S4) (**Figures 3A–D**). However, roots accumulated NSC, but reallocated N, P, and K to other tissues, except for an N accumulation in *C. lasiocarpa* (S3) (**Figures 3E–H**). Generally, leaves resources remobilization efficiency were highest in *P. australis* (S2) and intermediate in *B. fruticosa* (S1) (**Figures 3A–D**). While *B. fruticosa* (S1) had the lowest root NSC remobilization efficiency and *P. australis* (S2) had the highest RRE (**Figure 3E**).

DISCUSSION

Growth Form-Dependent Reallocation of Mobile Carbohydrates and Nutrients

At the end of growing season, mobile carbohydrates translocated from senescing leaves (**Figure 3A**), whereas NSCs were stored in roots (**Figure 3E**). *P. australis* and *B. fruticosa* leaves reallocated NSC to roots (**Figures 3A,E**), leading to decreased leaf NSC concentrations (**Figure 1A**) but increased root concentrations (**Figure 1D**), which indicated that roots were the main NSC storage tissue in these two species. Our results supported the view

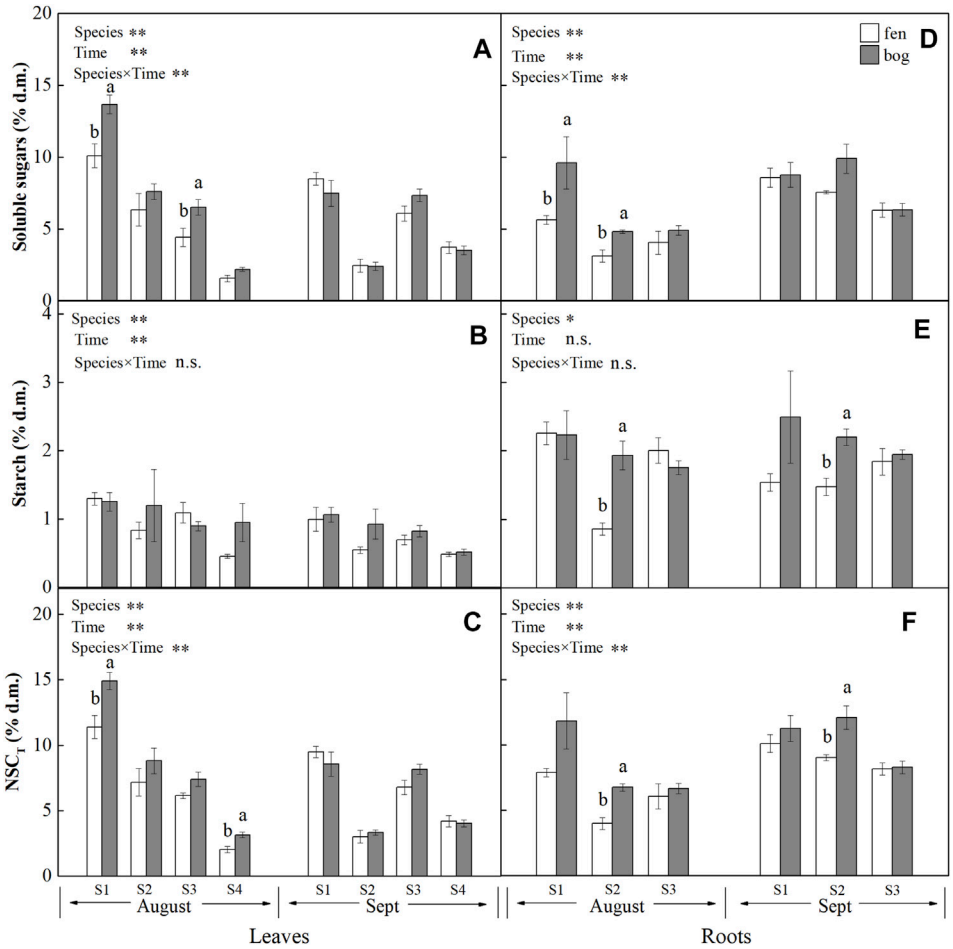

FIGURE 1 | Concentrations (mean ± SE; % of dry matter) of soluble sugars, starch, and NSC_T in leaves and roots of plants grown in fens (n = 5) and bogs (n = 4) in the mid-season and end-season. Different lowercase letters display significant differences between fens and bogs for each species within each time, tested with t-test (p < 0.05). S1–S4 represent *Betula fruticosa* Pall., *Phragmites australis* (Clav.), *Carex lasiocarpa* Ehrh., and *Sphagnum magellanicum*, respectively.

that leaf carbohydrates recycle from leaves to storage tissue at leaf abscission in perennial plants (Chapin et al., 1990; Cong et al., 2018), which is most likely associated with the storage of NSC to ensure winter survival (Tixier et al., 2020) and support new growth after dormancy (Yan et al., 2016). In contrast, *S. magellanicum* directly retain NSC in leaves rather than translocate carbon compounds to roots (**Figure 1A**). As *Sphagnum* mosses have no anatomically specialized internal conducting tissue, it has long been believed that mosses do not have nutrient remobilization processes (Aerts et al., 1999). However, as suggested previously by Rydin et al. (1989), mobile carbohydrates of *Sphagnum papillosum* were translocated from older parts to the capitulum. Our results confirmed internal redistribution of carbon compounds in *S. magellanicum*, and carbohydrates were stored in leaves due to no real roots for transport.

We found a growth-form-dependent NSC remobilization efficiency (**Table 4**). The result of the observed differences among species was that *P. australis* had the highest leaf NSC remobilization efficiency followed by the deciduous tree *B. fruticosa* (S2) (**Figure 3A**). *P. australis* also had the highest root remobilization efficiency followed by *C. lasiocarpa* (**Figure 3E**). The efficiency of NSC relocation from senescing leaves ranged from 55% to 60% in *P. australis* (**Figure 3A**), which is much higher than 28% reported by Gessner (2001) for the same species (Chapin et al., 1990; Gessner, 2001). Higher leaf NSC remobilization efficiency indicated that a major portion of carbohydrates was translocated to rhizome and roots, necessarily resulting in greater efficiency of *P. australis* roots. To resist environmental stress, such as deep water or late season frost, rhizome carbohydrates storage was much larger than needed to ensure establishment of spring shoots for *Phragmites* (Granéli et al., 1992). Intermediate leaf NSC remobilization efficiency of *B. fruticosa* should be associated with leaf traits; deciduous tree species produce new leaves at a low cost, rather than store carbohydrates with a high cost (Dickson, 1989), which might be due to the frequent alternation between new leaves and defoliation.

In spite of the different growth forms, nutrients (N, P, and K) were all remobilized from senescing leaves (**Figures 3B–D**),

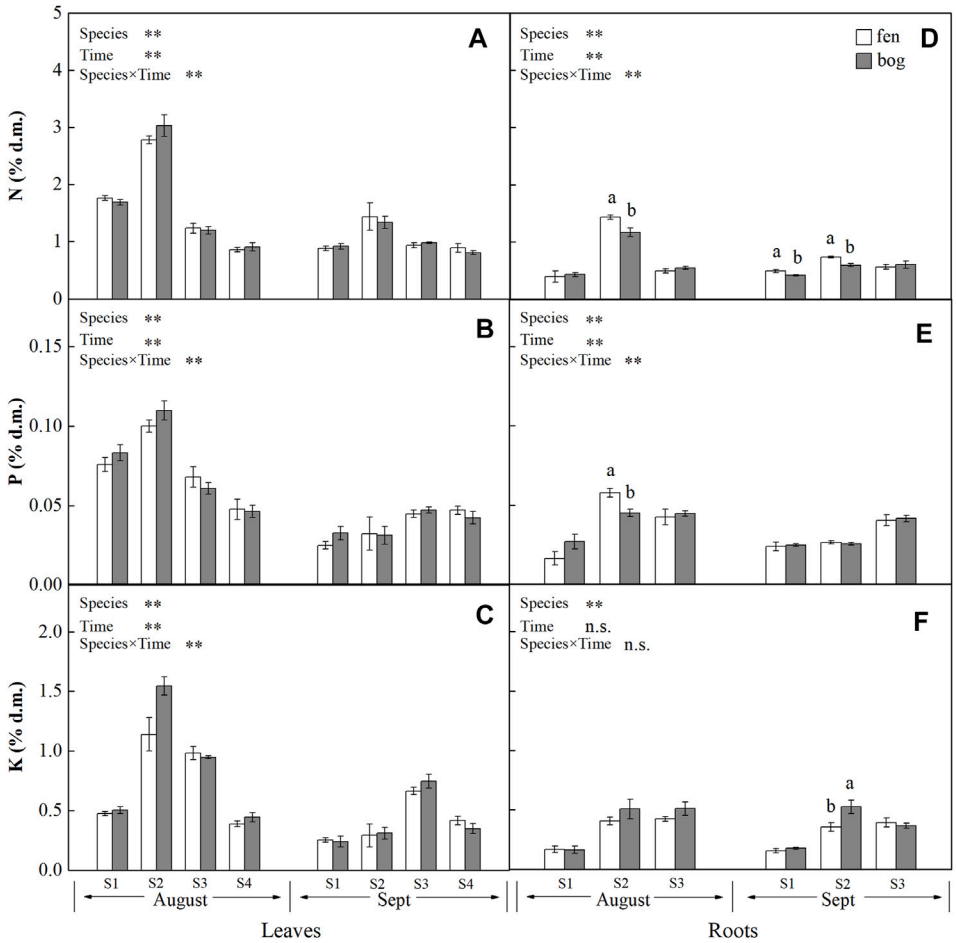

FIGURE 2 | Concentrations (mean ± SE; % of dry matter) of N, P, and K in leaves and roots of plants grown in fens ($n = 5$) and bogs ($n = 4$) in the mid-season and end-season. Different lowercase letters display significant differences between fens and bogs for each species within each time, tested with *t*-test ($p < 0.05$). S1–S4 represent *B. fruticosa*, *P. australis*, *C. lasiocarpa,* and *S. magellanicum*, respectively.

TABLE 3 | Effects of mire types, species, and their interactions on concentrations of NSCs (i.e., sugars, starch, and NSC_T) and nutrients (i.e., N, P, and K) in plant leaves and roots in September, tested with two-way nested ANOVAs. *F* and *p* values are given.

Factors	Df	Soluble sugars		Starch		NSC_T		Nitrogen (N)		Phosphorus (P)		Potassium (K)	
		F	*p*	*F*	*p*	*F*	*p*	*F*	*p*	*F*	*p*	*F*	*p*
Leaves													
Mire types (M)	1	0	0.999	3.586	0.069	0.18	0.675	0.108	0.745	0.085	0.773	0.024	0.878
Species (S)	3	53.596	**<0.001**	7.335	**0.001**	59.697	**<0.001**	9.849	**<0.001**	5.81	**0.003**	30.361	**<0.001**
M × S	3	1.755	0.179	0.939	0.435	1.863	0.159	0.25	0.861	0.526	0.668	0.707	0.556
Roots													
Mire types (M)	1	2.736	0.113	7.041	**0.015**	7.417	**0.013**	4.406	**0.048**	0.034	0.856	4	0.059
Species (S)	2	9.297	**0.001**	0.22	0.804	9.033	**0.001**	20.142	**<0.001**	33.57	**<0.001**	35.98	**<0.001**
M × S	2	2.071	0.151	1.287	0.297	2.606	0.098	3.851	**0.038**	0.131	0.878	4.567	**0.023**

Bold values highlight significant effects at $p < 0.05$.

supporting that nutrient remobilization is an important strategy employed by plants to conserve nutrients (Aerts, 1996; Chapin, 1980) and leaves play a primary role in nutrient remobilization (Eckstein et al., 1998). About half of N was recycled from senescing leaves in *P. australis* and deciduous trees (**Figure 1B**). These findings agreed with general perennials of Aerts (1996), who found that N resorption efficiency varied approximately 50% across different species or growth forms. However, N remobilization efficiency of *C. lasiocarpa* was 20% (**Figure 3B**), which is much lower than that value reported by

TABLE 4 | Effects of mire types, species, tissue types, and their interactions on resources remobilization between plant leaves and roots, tested with three-way nested ANOVAs. *F* and *p* values are given. R refers to remobilization efficiency.

Factors	Df	R NSC		R Nitrogen		R Phosphorus		R Potassium	
		F	*p*	*F*	*p*	*F*	*p*	*F*	*p*
Mire types (M)	1	22.321	<**0.001**	0.837	0.365	0.101	0.751	0.041	0.84
Species (S)	3	28.767	<**0.001**	36.539	<**0.001**	33.346	<**0.001**	8.184	<**0.001**
Tissue types (T)	1	92.608	<**0.001**	38.7	<**0.001**	51.364	<**0.001**	44.075	<**0.001**
M × S	3	4.357	**0.008**	0.541	0.657	0.624	0.603	0.567	0.639
M × T	1	1.853	0.18	0.138	0.712	0.235	0.63	0.454	0.504
S × T	2	29.653	<**0.001**	7.822	**0.001**	8.848	**0.001**	7.154	**0.002**
M × S × T	2	0.9	0.413	0.398	0.674	0.859	0.43	1.833	0.171

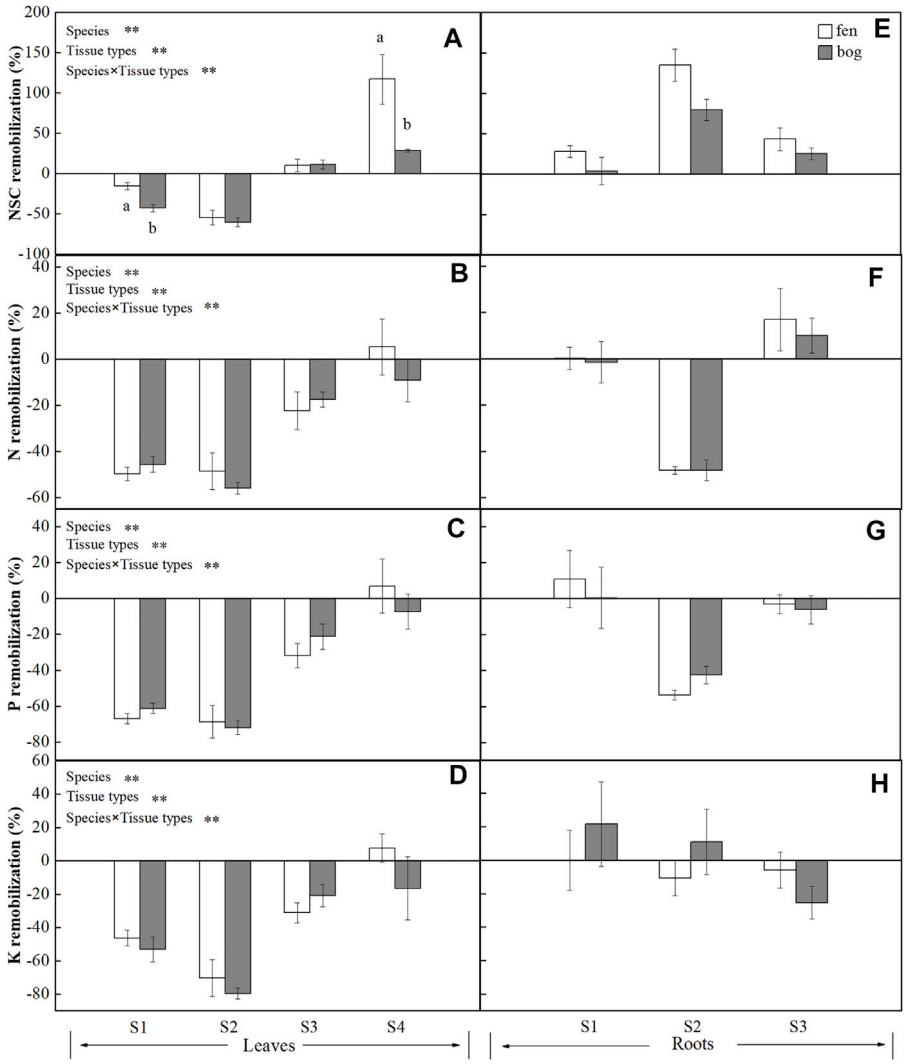

FIGURE 3 | Remobilization efficiency (mean ± SE; % of dry matter) of NSC, N, P, and K in leaves and roots of plants grown in fens (n = 5) and bogs (n = 4). Different lowercase letters display significant differences between fens and bogs for each species within each time, tested with t-test ($p < 0.05$). S1–S4 represent *B. fruticosa*, *P. australis*, *C. lasiocarpa,* and *S. magellanicum*, respectively.

Aerts (1996) for graminoids (mean 59%). Similarly, our results showed that P remobilization efficiency for *B. fruticose* and *P. australis* were comparable to the value (64.9%) reported by Vergutz et al. (2012) (**Figure 3C**). However, leaves had lower resorption efficiency for K (4–50%), except for *P. australis* (mean 75%) (Vergutz et al., 2012) (**Figure 3D**). In addition, N was only resorbed from leaves of *C. lasiocarpa* and stored in roots (**Figure 3F**), as nitrogen stored in specific tissue with an individual species due to leaf habit (Millard and Grelet, 2010). As we have already seen, however, there were significant differences in leaf nutrient efficiency between growth forms (**Table 4**). Leaf nutrient remobilization efficiency was much higher in deciduous tree and herbs compared with moss (**Figures 3B–D**). Thus, these would suggest that high nutrient remobilization from leaves prior to senescence is characteristic for most species (Aerts, 1996), whereas *Sphagnum* mosses have lower nutrient remobilization efficiency, probably due to their adaptation to nutrient-poor habitats. Previous studies indicated that moss species were highly tolerant to nutrient-poor inhabits (Aerts et al., 1999; Turetsky et al., 2012), even Li et al. (2019) demonstrated that long-term application of nitrogen did not increase but decreased the growth of *Sphagnum* mosses, implying the reasons of lower nutrient remobilization efficiency of *Sphagnum* mosses.

Effects of Fens and Bogs on Plant Resource Reallocation

We did not find differences in leaf nutrient remobilization efficiency between fens and bogs (**Table 4**; **Figures 3B–D**); this result may be caused by the similar habitat characteristics dominated by high water level for both fens and bogs. A large-scale analysis indicated that nutrient resorption did not differ between fens and bogs but varied with species or/and growth form (Aerts et al., 1999). Nevertheless, Bridgham et al. (1995) proposed that nutrient remobilization efficiency can be higher at low nutrient availability, representing an important adaptation to infertile habitats (Dissanayaka et al., 2017). For nutrient concentration in mature leaves, there were no differences in leaf nutrient concentrations between fens and bogs (**Table 2**; **Figures 2A–C**). This finding partly agreed with the conclusions of Aerts *et al.* (1999), who proposed that clear differences between fens and bogs species occurred in leaves' P concentrations, but not in leaves' N concentrations. However, there were no differences in nutrient remobilization of fine roots between fens and bogs (**Table 4**; **Figures 3F–H**). At the end of growing season, N concentrations of fine roots were significantly lower in *P. australis* and *B. fruticosa* in fens than in bogs (**Figure 2D**). No such pattern was found for P and K in fine roots (**Figures 2F,G**). These results suggested that N is the limiting mineral nutrient for *Phragmites* and deciduous tree, which also agreed with investigation on *Phragmites* in Sweden (Granéli et al., 1992).

We observed higher NSC remobilization efficiency and carbohydrates concentration of *B. fruticosa* leaves in bogs than in fens (**Table 1**, **4**; **Figures 1C**, **3A**). Thus, there are indications that translocation of non-structural carbon seems to be more important under nutrient-poor inhabits than translocation of nutrients (N, P, and K), suggesting that the species were limited more by carbon supply than by recycling of nutrients (Chapin et al., 1990). The availability of carbohydrates is strictly dependent on and linked to the growth of leaves and shoots, the allocation of carbohydrates being determined by resource availability, growth capacity, and maintenance requirement (Marchi et al., 2007). Many studies have demonstrated that the translocation of carbohydrates from leaves can be unloaded to storage tissues that reload to support new leaf and shoot growth in next spring (Marchi et al., 2005a; Marchi et al., 2005b; Cong et al., 2018; Cong et al., 2019). Larger NSC remobilization in bogs than in fens reflected that deciduous trees adapted to nutrient-poor inhabits may resorb more carbohydrates from the senescing leaves and have greater dependence on carbohydrate remobilization. Similarly, although tissue NSC remobilization efficiency did not differ for *Phragmites* between fens and bogs (**Figures 3A,E**), root starch and NSC concentrations of *Phragmites* were higher in bogs than in fens at the end-season (**Figures 1E,F**). The starch and NSC concentrations of roots increased in bogs, which may enhance the ability of *Phragmites* to adapt to winter environmental changes (i.e., low nutrient and cold temperature) (Sheen et al., 1999), because soluble carbon components participate in cell osmotic regulation and prevent intracellular ice formation by lowering the freezing point of the cytoplasm (Morin et al., 2007). Furthermore, Granéli *et al.* (1992) proposed that the rhizome of *Phragmites* stored excess carbohydrates. Since some carbohydrate stores may become inaccessible to the plant with time due to a winter rhizome mortality of approximately 30% (Granéli et al., 1992), carbohydrates remaining in dead cells cannot be retrieved (Ziegler, 1964). However, *Sphagnum* leaves had lower NSC remobilization efficiency in bogs, showing that *Sphagnum* mosses from nutrient-poor habitats have not adapted to oligotrophic environments by having a high NSC remobilization efficiency.

CONCLUSION

Our study clearly indicated that mobile carbohydrates and nutrients (N, P, and K) in four plant species (i.e., four growth forms) grown in both fens and bogs were reallocated from leaves to storage tissues at the end of the growing season. The NSCs and nutrient remobilization efficiency differ among different growth forms. Deciduous dwarf trees (*B. fruticosa*) and perennial grass (*P. australis*) had relative higher leaf resource remobilization efficiency, and moss (*S. magellanicum*) showed lower leaf nutrient remobilization efficiency. Differences in resource remobilization among plant growth forms seem to be related to different strategies in utilizing resources (Chapin et al., 1990). We also found that leaf nutrient remobilization efficiency did not differ between fens and bogs. Overall, our results suggest that reallocation of mobile carbohydrates seems to be more sensitive to the growth condition than nutrients (N, P, and K) under nutrient-poor inhabits, which may be one of the reasons leading to nutrient limitation in peatlands.

DATA AVAILABILITY STATEMENT

The raw data supporting the conclusion of this article will be made available by the authors, without undue reservation.

AUTHOR CONTRIBUTIONS

MJ and ZZ contributed to conception. M-HL, ZZ, and YuC designed the experiment. YuC, YiC, and XL performed the research. YuC analyzed the data and wrote the manuscript. M-HL commented and revised the manuscript.

FUNDING

MJ and YuC were supported by the National Natural Science Foundation of China (Grant No. U19A2042, 42001106). BL was funded by the Natural Science Foundation of Jilin Province, China (Grant No. 20200201195JC).

ACKNOWLEDGMENTS

We sincerely thank Xinhua Zhou and Haiyang Zhao for chemical analysis, and Huiyuan Sun for her assistance in the laboratory.

REFERENCES

Aerts, R., and Chapin, F. S. (1999). "The Mineral Nutrition of Wild Plants Revisited: A Re-evaluation of Processes and Patterns," in *Advances in Ecological Research*. Editors A. H. Fitter and D. G. Raffaelli (Academic Press), 1–67. doi:10.1016/s0065-2504(08)60016-1

Aerts, R. (1996). Nutrient Resorption from Senescing Leaves of Perennials: Are There General Patterns. *J. Ecol.* 84 (4), 597–608. doi:10.2307/2261481

Aerts, R., Verhoeven, J. T. A., and Whigham, D. F. (1999). Plant-mediated Controls on Nutrient Cycling in Temperate Fens and Bogs. *Ecology* 80 (7), 2170–2181. doi:10.1890/0012-9658(1999)080[2170:pmconc]2.0.co;2

Bridgham, S. D., Pastor, J., Janssens, J. A., Chapin, C., and Malterer, T. J. (1996). Multiple Limiting Gradients in Peatlands: A Call for a New Paradigm. *Wetlands* 16 (1), 45–65. doi:10.1007/bf03160645

Bridgham, S. D., Pastor, J., McClaugherty, C. A., and Richardson, C. J. (1995). Nutrient-Use Efficiency: A Litterfall Index, a Model, and a Test along a Nutrient-Availability Gradient in North Carolina Peatlands. *The Am. Naturalist* 145 (1), 1–21. doi:10.1086/285725

Bu, Z.-J., Rydin, H., and Chen, X. (2011). Direct and Interaction-Mediated Effects of Environmental Changes on Peatland Bryophytes. *Oecologia* 166 (2), 555–563. doi:10.1007/s00442-010-1880-1

Bu, Z. J., Sundberg, S., Feng, L., Li, H. K., Zhao, H. Y., and Li, H. C. (2017). The Methuselah of Plant Diaspores: Sphagnum Spores Can Survive in Nature for Centuries. *New Phytol.* 214 (4), 1398–1402. doi:10.1111/nph.14575

Chapin, F. S., Schulze, E., and Mooney, H. A. (1990). The Ecology and Economics of Storage in Plants. *Annu. Rev. Ecol. Syst.* 21, 423–447. doi:10.1146/annurev.es.21.110190.002231

Chapin, F. S. (1980). The Mineral Nutrition of Wild Plants. *Annu. Rev. Ecol. Syst.* 11 (1), 233–260. doi:10.1146/annurev.es.11.110180.001313

Charman, D. (2002). *Peatlands and Environmental Change*. New York: John Wiley & Sons.

Cong, Y., Li, M.-H., Liu, K., Dang, Y.-C., Han, H.-D., and He, H. S. (2019). Decreased Temperature with Increasing Elevation Decreases the End-Season Leaf-To-Wood Reallocation of Resources in Deciduous Betula Ermanii Cham. Trees. *Forests* 10 (2), 166. doi:10.3390/f10020166

Cong, Y., Wang, A., He, H., Yu, F., Tognetti, R., Cherubini, P., et al. (2018). Evergreen Quercus Aquifolioides Remobilizes More Soluble Carbon Components but Less N and P from Leaves to Shoots Than Deciduous Betula Ermanii at the End-Season. *iForest* 11 (4), 517–525. doi:10.3832/ifor2633-011

Dickson, R. E. (1989). Carbon and Nitrogen Allocation in Tree. *Ann. des Sci. Forestières* 46 (Suppl. ment), 347–350. doi:10.1051/forest:198905art0142

Dissanayaka, D. M. S. B., Maruyama, H., Nishida, S., Tawaraya, K., and Wasaki, J. (2017). Landrace of Japonica rice, Akamai Exhibits Enhanced Root Growth and Efficient Leaf Phosphorus Remobilization in Response to Limited Phosphorus Availability. *Plant and Soil* 414 (1/2), 327–338. doi:10.1007/s11104-016-3129-1

Dubois, M., Gilles, K. A., Hamilton, J. K., Rebers, P. A., and Smith, F. (1956). Colorimetric Method for Determination of Sugars and Related Substances. *Anal. Chem.* 28, 350–356. doi:10.1021/ac60111a017

Eckstein, R. L., Karlsson, P. S., and Weih, M. (1998). The Significance of Resorption of Leaf Resources for Shoot Growth in Evergreen and Deciduous Woody Plants from a Subarctic Environment. *Oikos* 81 (3), 567–575. doi:10.2307/3546777

Epron, D., Bahn, M., Derrien, D., Lattanzi, F. A., Pumpanen, J., Gessler, A., et al. (2012). Pulse-labelling Trees to Study Carbon Allocation Dynamics: A Review of Methods, Current Knowledge and Future Prospects. *Tree Physiol.* 32, 776–798. doi:10.1093/treephys/tps057

Gessner, M. O. (2001). Mass Loss, Fungal Colonisation and Nutrient Dynamics of Phragmites Australis Leaves during Senescence and Early Aerial Decay. *Aquat. Bot.* 69 (2), 325–339. doi:10.1016/s0304-3770(01)00146-2

Granéli, W., Weisner, S. E. B., and Sytsma, M. D. (1992). Rhizome Dynamics and Resource Storage in Phragmites Australis. *Wetlands Ecol. Manage.* 1 (4), 239–247.

Jonasson, S., and Shaver, G. R. (1999). Within-stand Nutrient Cycling in Arctic and Boreal Wetlands. *Ecology* 80 (7), 2139–2150. doi:10.1890/0012-9658(1999)080[2139:wsncia]2.0.co;2

Killingbeck, K. T. (1996). Nutrients in Senesced Leaves: Keys to the Search for Potential Resorption and Resorption Proficiency. *Ecology* 77 (6), 1716–1727. doi:10.2307/2265777

Li, M.-H., Jiang, Y., Wang, A., Li, X., Zhu, W., Yan, C.-F., et al. (2018). Active Summer Carbon Storage for winter Persistence in Trees at the Cold alpine Treeline. *Tree Physiol.* 38 (9), 1345–1355. doi:10.1093/treephys/tpy020

Li, M.-H., Xiao, W.-F., Shi, P., Wang, S.-G., Zhong, Y.-D., Liu, X.-L., et al. (2008). Nitrogen and Carbon Source-Sink Relationships in Trees at the Himalayan Treelines Compared with Lower Elevations. *Plant Cel Environ.* 31 (10), 1377–1387. doi:10.1111/j.1365-3040.2008.01848.x

Li, M., Hoch, G., and Körner, C. (2002). Source/sink Removal Affects mobile Carbohydrates in Pinus Cembra at the Swiss Treeline. *Trees* 16 (4-5), 331–337. doi:10.1007/s00468-002-0172-8

Li, M., Hoch, G., and Körner, C. (2001). Spatial Variability of mobile Carbohydrates within Pinus Cembra Trees at the alpine Treeline. *Phyton-Annales Rei Botanicae* 41, 203–213.

Li, T., Bu, Z., Liu, W., Zhang, M., Peng, C., Zhu, Q., et al. (2019). Weakening of the 'enzymatic Latch' Mechanism Following Long-Term Fertilization in a Minerotrophic Peatland. *Soil Biol. Biochem.* 136, 107528. doi:10.1016/j.soilbio.2019.107528

Maimer, N., Horton, D. G., and Vitt, D. H. (1992). Element Concentrations in Mosses and Surface Waters of Western Canadian Mires Relative to Precipitation Chemistry and Hydrology. *Ecography* 15 (1), 114–128. doi:10.1111/j.1600-0587.1992.tb00015.x

Marchi, S., Guidotti, D., Sebastiani, L., and Tognetti, R. (2007). Changes in Assimilation Capacity during Leaf Development in Broad-Leaved Prunus Persica and Sclerophyllous Olea Europaea. *J. Hortic. Sci. Biotechnol.* 82 (1), 69–78. doi:10.1080/14620316.2007.11512201

Marchi, S., Sebastiani, L., Gucci, R., and Tognetti, R. (2005a). Changes in Sink-Source Relationships during Shoot Development in Olive. *jashs* 130, 631–637. doi:10.21273/jashs.130.4.631

Marchi, S., Sebastiani, L., Gucci, R., and Tognetti, R. (2005b). Sink-source Transition in Peach Leaves during Shoot Development. *jashs* 130, 928–935. doi:10.21273/jashs.130.6.928

Millard, P., and Grelet, G.-A. (2010). Nitrogen Storage and Remobilization by Trees: Ecophysiological Relevance in a Changing World. *Tree Physiol.* 30, 1083–1095. doi:10.1093/treephys/tpq042

Millard, P., Hester, A., Wendler, R., and Baillie, G. (2001). Interspecific Defoliation Responses of Trees Depend on Sites of winter Nitrogen Storage. *Funct. Ecol.* 15 (4), 535–543. doi:10.1046/j.0269-8463.2001.00541.x

Morin, X., Ameglio, T., Ahas, R., Kurz-Besson, C., Lanta, V., Lebourgeois, F., et al. (2007). Variation in Cold Hardiness and Carbohydrate Concentration from Dormancy Induction to Bud Burst Among Provenances of Three European Oak Species. *Tree Physiol.* 27, 817–825. doi:10.1093/treephys/27.6.817

Murphy, J., and Riley, J. P. (1962). A Modified Single Solution Method for the Determination of Phosphate in Natural Waters. *Analytica Chim. Acta* 27, 31–36. doi:10.1016/s0003-2670(00)88444-5

Ohlson, M. (1995). Growth and Nutrient Characteristics in Bog and Fen Populations of Scots pine (Pinus Sylvestris). *Plant Soil* 172 (2), 235–245. doi:10.1007/bf00011326

Parkinson, J. A., and Allen, S. E. (1975). A Wet Oxidation Procedure Suitable for the Determination of Nitrogen and mineral Nutrients in Biological Material. *Commun. Soil Sci. Plant Anal.* 6 (1), 1–11. doi:10.1080/00103627509366539

Pensa, M., and Sellin, A. (2003). Soil Type Affects Nitrogen Conservation in Foliage of Small Pinus Sylvestris L. Trees. *Plant and Soil* 253 (2), 321–329. doi:10.1023/a:1024884516655

Pugnaire, F. I., and Chapin, F. S., III (1993). Controls over Nutrient Resorption from Leaves of Evergreen Mediterranean Species. *Ecology* 74 (1), 124–129. doi:10.2307/1939507

Qiao, S. (1993). A Preliminary Study on Hani Peat Mire in the West Part of the Changbai Mountain. *Scientia Geographica Sinica*.

Rydin, H., Clymo, R. S., and Fogg, G. E. (1989). Transport of Carbon and Phosphorus Compounds about *Sphagnum*. *Proc. R. Soc. Lond. B. Biol. Sci.* 237 (1286), 63–84.

Sheen, J., Zhou, L., and Jang, J.-C. (1999). Sugars as Signaling Molecules. *Curr. Opin. Plant Biol.* 2 (5), 410–418. doi:10.1016/s1369-5266(99)00014-x

Tixier, A., Guzmán-Delgado, P., Sperling, O., Amico Roxas, A., Laca, E., and Zwieniecki, M. A. (2020). Comparison of Phenological Traits, Growth Patterns, and Seasonal Dynamics of Non-structural Carbohydrate in Mediterranean Tree Crop Species. *Sci. Rep.* 10 (1), 347. doi:10.1038/s41598-019-57016-3

Turetsky, M. R., Bond-Lamberty, B., Euskirchen, E., Talbot, J., Frolking, S., McGuire, A. D., et al. (2012). The Resilience and Functional Role of moss in Boreal and Arctic Ecosystems. *New Phytol.* 196 (1), 49–67. doi:10.1111/j.1469-8137.2012.04254.x

Vergutz, L., Manzoni, S., Porporato, A., Novais, R. F., and Jackson, R. B. (2012). Global Resorption Efficiencies and Concentrations of Carbon and Nutrients in Leaves of Terrestrial Plants. *Ecol. Monogr.* 82 (2), 205–220. doi:10.1890/11-0416.1

Wang, A., Wang, X., Tognetti, R., Lei, J.-P., Pan, H.-L., Liu, X.-L., et al. (2018). Elevation Alters Carbon and Nutrient Concentrations and Stoichiometry in Quercus Aquifolioides in Southwestern China. *Sci. Total Environ.* 622-623, 1463–1475. doi:10.1016/j.scitotenv.2017.12.070

Wang, M., Murphy, M. T., and Moore, T. R. (2014). Nutrient Resorption of Two evergreen Shrubs in Response to Long-Term Fertilization in a Bog. *Oecologia* 174 (2), 365–377. doi:10.1007/s00442-013-2784-7

Waughman, G. J. (1980). Chemical Aspects of the Ecology of Some South German Peatlands. *J. Ecol.* 68 (3), 1025–1046. doi:10.2307/2259473

Wyka, T. P., Karolewski, P., Żytkowiak, R., Chmielarz, P., and Oleksyn, J. (2016). Whole-plant Allocation to Storage and Defense in Juveniles of Related evergreen and Deciduous Shrub Species. *Tree Physiol.* 36 (5), 536–547. doi:10.1093/treephys/tpv108

Yan, C. F., Gessler, A., Rigling, A., Dobbertin, M., Han, X. G., and Li, M. H. (2016). Effects of Mistletoe Removal on Growth, N and C Reserves, and Carbon and Oxygen Isotope Composition in Scots pine Hosts. *Tree Physiol.* 36, 562–575. doi:10.1093/treephys/tpw024

Yuan, Z.-Y., Li, L.-H., Han, X.-G., Huang, J.-H., Jiang, G.-M., Wan, S.-Q., et al. (2005). Nitrogen Resorption from Senescing Leaves in 28 Plant Species in a Semi-arid Region of Northern China. *J. Arid Environments* 63 (1), 191–202. doi:10.1016/j.jaridenv.2005.01.023

Yuan, Z. Y., and Chen, H. Y. H. (2009). Global-scale Patterns of Nutrient Resorption Associated with Latitude, Temperature and Precipitation. *Glob. Ecol. Biogeogr.* 18 (1), 11–18. doi:10.1111/j.1466-8238.2008.00425.x

Zhu, W.-Z., Cao, M., Wang, S.-G., Xiao, W.-F., and Li, M.-H. (2012). Seasonal Dynamics of Mobile Carbon Supply in Quercus Aquifolioides at the Upper Elevational Limit. *PloS one* 7, e34213. doi:10.1371/journal.pone.0034213

Ziegler, H. (1964). "Storage, Mobilization and Distribution of Reserve Material in Trees," in *Formation of Wood in Forest Trees*. Editor M. Zimmermann (New York: Academic Press), 303–320. doi:10.1016/b978-1-4832-2931-7.50022-7

Conflict of Interest: The authors declare that the research was conducted in the absence of any commercial or financial relationships that could be construed as a potential conflict of interest.

Publisher's Note: All claims expressed in this article are solely those of the authors and do not necessarily represent those of their affiliated organizations, or those of the publisher, the editors, and the reviewers. Any product that may be evaluated in this article, or claim that may be made by its manufacturer, is not guaranteed or endorsed by the publisher.

frontiers in Environmental Science

ORIGINAL RESEARCH
published: 31 March 2022
doi: 10.3389/fenvs.2022.833409

Characteristics of Phytoplankton Community Structure and Indication to Water Quality in the Lake in Agricultural Areas

*Yiqiang Huang[1,2†], Yucheng Shen[1†], Shouzhi Zhang[2], Yang Li[1,2], Zeyu Sun[1], Mingming Feng[1], Rui Li[1], Jin Zhang[1], Xue Tian[1] and Wenguang Zhang[2]**

[1]Jilin Provincial Joint Key Laboratory of Changbai Mountain Wetland and Ecology and CAS Key Laboratory of Wetland Ecology and Environment, Northeast Institute of Geography and Agroecology, Chinese Academy of Sciences, Changchun, China, [2]School of Geography and Marine Sciences, Yanbian University, Yanji, China

In recent years, lakes' water quality and quantity have been affected and damaged by agricultural activities. The sensitivity of phytoplankton to the hydrological environment can effectively indicate the health of the aquatic ecosystem and the change in water quality. Understanding the changes of phytoplankton communities in lakes contaminated by agriculture may contribute to determining the directions of protection of these water bodies and provide reference cases for wider research. It is found that there are 146 species, 63 genera, and 8 phyla of phytoplankton, including 57 species of Bacillariophyta, 46 species of Chlorophyta, 17 species of Cyanobacteria and Euglenophyta. The total abundance was changed successively with Bacillariophyta (75% in June), Cyanobacteria (50% in July–August), and Chlorophyta (75% in September–October). The total biomass decreased continuously over time. The biomass of Chlorophyta is highest in October (67.4%), and diatoms contribute the most biomass in other months (76.5%). The Redundancy analysis indicated that the main environmental factors affecting phytoplankton's dynamic change are total salt, water temperature, total phosphorus, and 5-day biochemical oxygen demand. The phytoplankton can be divided into 21 functional groups. The MP group has the highest frequency, mainly distributed in the frequently stirred and turbid shallow water. Representative functional groups indicate the high degree of eutrophication and nutrient-rich conditions and the good associated environment for phytoplankton and slow water flow rate. With the seasonal change of agricultural irrigation and drainage, the water quality of Xinmiao Lake began to deteriorate from medium pollution in July and reached serious pollution in October finally. Furthermore, this research discovered that the risk of cyanobacteria bloom is high in summer, primarily when thermal stratification occurs. This study provides necessary information for understanding and predicting the changes of the phytoplankton community caused by the increase of nutrients, human disturbance, and temperature conditions in eutrophic lakes in agricultural areas.

Keywords: phytoplankton, Xinmiao Lake, diversity index, functional group, Agricultural area, indicative function, Seasonal dynamics

OPEN ACCESS

Edited by:
Guobin Fu,
CSIRO Land and Water, Australia

Reviewed by:
Xin Leng,
Nanjing University, China
Elżbieta Zębek,
University of Warmia and Mazury in Olsztyn, Poland

****Correspondence:***
Wenguang Zhang
Zhangwenguang@iga.ac.cn

[†]These authors have contributed equally to this work

Specialty section:
This article was submitted to Freshwater Science, a section of the journal Frontiers in Environmental Science

Received: *11 December 2021*
Accepted: *04 March 2022*
Published: *31 March 2022*

Citation:
Huang Y, Shen Y, Zhang S, Li Y, Sun Z, Feng M, Li R, Zhang J, Tian X and Zhang W (2022) Characteristics of Phytoplankton Community Structure and Indication to Water Quality in the Lake in Agricultural Areas. Front. Environ. Sci. 10:833409. doi: 10.3389/fenvs.2022.833409

INTRODUCTION

Phytoplankton is regarded as one of the essential indicators of water environment because of its temporal and spatial distribution of community structure characteristics such as abundance, biomass and diversity (Kruk et al., 2010; Reynolds, 2012; Visser et al., 2016). Environmental conditions can also directly or indirectly affect the community structure of phytoplankton (Whitton, 2012). Therefore, monitoring phytoplankton community structure and diversity has become an essential water ecosystem health and water quality evaluation (Sabater et al., 2008; Nunes et al., 2018). It is feasible to predict and explain various models of phytoplankton through environmental factors. Previous studies have proved that the change characteristics of phytoplankton structure are closely related to hydrological conditions, and nitrate concentration (Negro et al., 2000), and also have a good coupling relationship with chemical oxygen demand (COD) and particulate organic matter (POM) (Lee and Kang, 2010). Similarly, it is common to use phytoplankton to indicate water quality. Reynolds first designed the phytoplankton classification system according to the classification method of plants and summarized 31 functional groups (Reynolds, 1980; Reynolds, 1984). Salmaso et al. proposed the division method of ecological functional group (MFG), and divided phytoplankton into 31 mfg groups (Salmaso and Padisák, 2007). Padisak et al. summarized 40 groups according to the sensitivity and tolerance of phytoplankton, which promoted the wide application of this method (Padisak et al., 2009). Phytoplankton pollution biological index can quantitatively analyze the state of water pollution (Chen et al., 2021). Furthermore, the phytoplankton diversity index (Spellerberg and peter, 2003), dominance index (Ignatiades, 2020), algae comprehensive index (Yang and Liu, 2020), and phytoplankton biological integrity index (Zhu et al., 2021)is commonly used to quantify the ecological status of lakes, rivers, and reservoirs in water pollution monitoring and evaluation. Therefore, understanding the relative impact of natural and artificial processes on hydrological and biochemical functions through phytoplankton diversity is essential for improving water resources management (Arab et al., 2019).

Due to the increase in agricultural production demand, the wetland ecosystem in the area faces environmental pressure, such as agricultural pollutants and water supply. The pollution from agriculture is more difficult to control than other point source pollution because of its dispersion diversity and regional (Wurtsbaugh et al., 2019). Under the current climate and human influence, agricultural reclamation increases the bioavailable P and N entering the wetland waters with increased rainfall intensity related to climate change (Glibert and Burford, 2017). High nutrient loads can promote the production of organic matter. Then the decomposition and release of regenerated ammonium in sediments provide a favorable environment for the growth of Cyanobacteria in summer (Newell et al., 2019). The consequent environmental risks (such as eutrophication and harmful water bloom outbreak) will further lead to the loss and degradation of wetlands (Mao et al., 2018). Due to the rapid economic development and population growth in recent years, many lakes in the world have been seriously eutrophized, such as the shallow agricultural lakes in the lower Mississippi River Basin (Henderson et al., 2021) in the United States (Henderson et al., 2021), Winnipeg Lake in Canada (Bunting et al., 2016), Greifensee in Switzerland (Niel et al., 2012) and 50 lakes in Western and northwest Ireland (Touzet, 2011), and the excessive investment of N and P in agricultural activities is one of the main reasons. Under these premises, it is imperative to strengthen wetland assessment, monitoring, and restoration through the comprehensive integration of human activities and climate change processes. Many scientists in China have paid more attention to the changes in phytoplankton structure in eutrophic lakes. However, most of these studies focus on the Yangtze River Basin in the subtropical region, such as Tai Lake (Paerl et al., 2011; Liu et al., 2021), Poyang Lake (Wu et al., 2013). Continental climate lakes in high latitudes, such as inland lakes in Northeast China, rarely study the coupling between phytoplankton and environmental factors. Under expanding agricultural production, lakes in these areas are prone to eutrophication. It is becoming more and more essential to study the changes of phytoplankton community structure to improve water quality assessment. The water environment of Xinmiao Lake has faced severe ecological and environmental problems such as agricultural non-point source pollution, salinization, and organic pollution (Dai and Tian, 2011), which provides a good research example. Because phytoplankton and environmental factors have high temporal and spatial heterogeneity, their relationship is usually complex and difficult to explain. For example, what factors in the lake (such as nutrition, light, temperature, etc.) regulate algae growth. Specifically, this work is devoted to clarify the correlation between phytoplankton and environmental factors in the lake adjacent to agriculture area and confirm the indicative function of the phytoplankton community on water quality.

MATERIAL AND METHOD

Research Area

Xinmiao Lake is a typical wetland ecosystem composed of lakes, swamps, swampy meadows, and other ecosystems, with shallow lakes as the core. It is located in 124°26′E–124°31′E, 45°8′30″N–45°13′30″N, belongs to a continental monsoon semi-arid climate with an area of 31 km^2, average water depth of 1.5 m, water storage about 6.5×10^7 m^3, and pH about 8.5 (Liu et al., 2020), which belongs to Chagan Lake National Nature Reserve in Jilin Province (**Figure 1A**). It is the front lake of Chagan Lake and plays an essential role in buffering and regulating about 2.3×10^2 km^2 irrigation backwater from the surrounding paddy fields (Yao et al., 2010; Guo, 2012). The soil in the lake basin is alkaline, and the total salt (TS) is mainly sodium carbonate and sodium bicarbonate, so the saline-alkali soda wetland is formed (Liu et al., 2020). Affected by suspended mineral and section particles, Xinmiao Lake has a high content of suspended sediments (Guo et al., 2020). Affected by

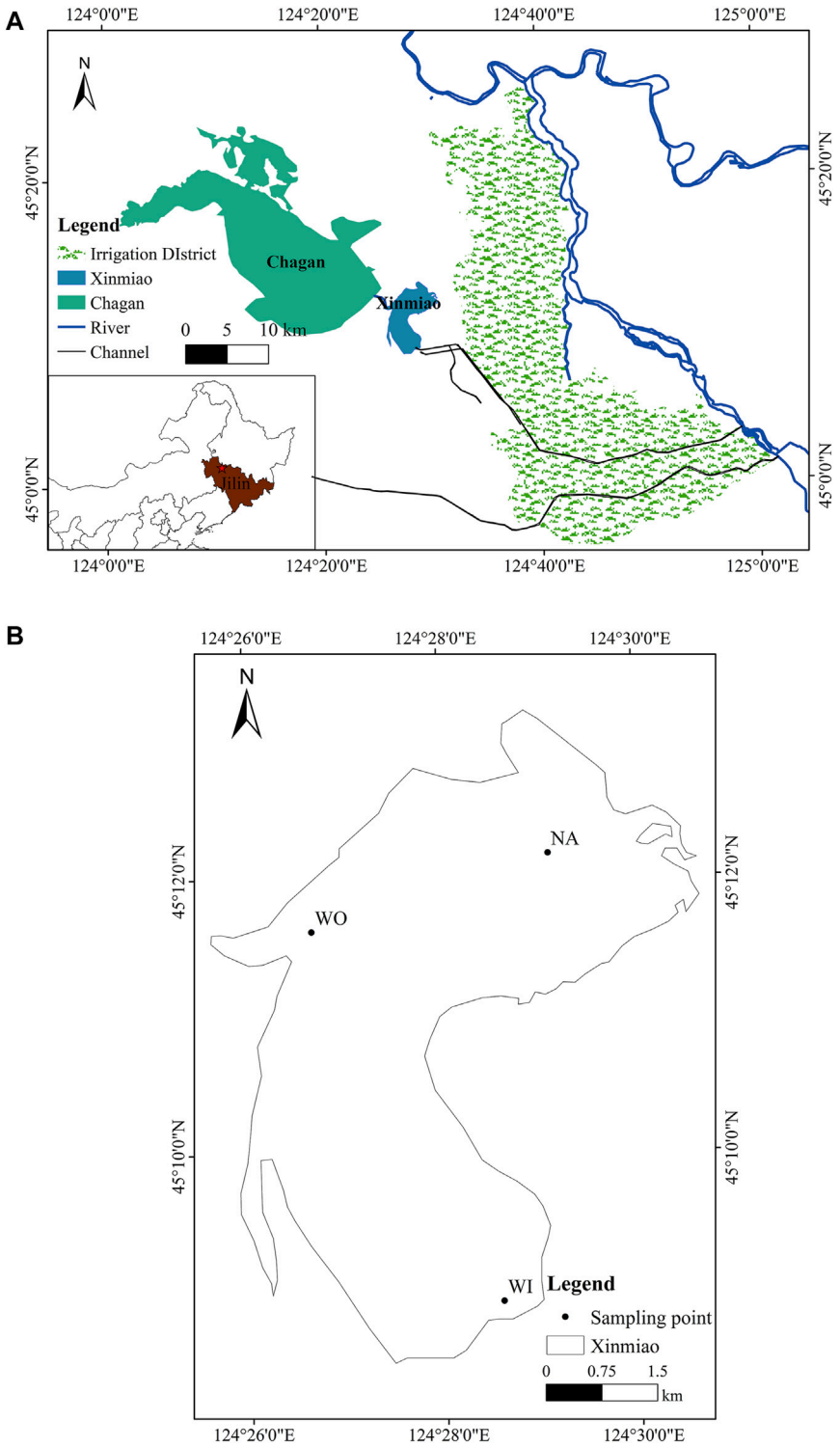

FIGURE 1 | Schematic diagram of sampling points. Panels show the geographical location of XinmiaoLake **(A)** and the specific layout of sampling points **(B)**.

water particles, the light conditions in water droplets are poor and the transparency is low (Li et al., 2016). The winter of Xinmiao lake is from October to May, and the light is the strongest in July and August (Zhang et al., 2016). With the expansion of the Qianguo agricultural area, the contents of TN, TP (total phosphorus), TS, and alkali entering the lake will significantly increase the risk of eutrophication and water bloom (Chen et al., 2015).

TABLE 1 | Environmental factors in Xinmiao Lake during the investigation period.

Environmental variables	Unit	Month				
		June	July	August	September	October
TS	mg·L^{-1}	219.17 ± 7.19	224.33 ± 5.44	252.11 ± 8.86	278.78 ± 17.15	363.33 ± 81.87
BOD_5	mg·L^{-1}	3.5 ± 0.63	6.78 ± 2.62	3.61 ± 2.12	2.51 ± 0.58	3.26 ± 0.49
CODCr	mg·L^{-1}	28.32 ± 1.38	16.62 ± 6.61	29.12 ± 9.54	15.56 ± 4.65	18.73 ± 3.25
TN	mg·L^{-1}	1.05 ± 0.23	0.97 ± 0.27	1.61 ± 0.45	0.77 ± 0.09	0.54 ± 0.14
TP	mg·L^{-1}	0.09 ± 0.04	0.1 ± 0.02	0.12 ± 0.08	0.1 ± 0.01	0.07 ± 0.06
N/P	—	12.98 ± 3.96	10.98 ± 4.69	19.1 ± 9.61	7.45 ± 1.31	20.382 ± 0.62
TK	mg·L^{-1}	4.07 ± 0.12	3.78 ± 0.64	3.4 ± 0.35	3.58 ± 0.21	3.14 ± 0.29
WT	°C	14.07 ± 0.21	27.28 ± 0.81	25.37 ± 0.82	20.9 ± 0.71	9.22 ± 0.42
pH	—	8.56 ± 0.24	8.59 ± 0.1	8.39 ± 0.03	8.52 ± 0.08	8.47 ± 0.13

Sample Collection

According to the natural morphological characteristics of Xinmiao Lake and the standard of sampling point setting (Tnno et al., 2021), sampling points are arranged at the inlet, outlet, and the northern area of Xinmiao Lake (abbreviated as WI, WO, NA) (**Figure 1B**). Both WI and NA grow reed and *Potamogeton crispus* L. There are almost no aquatic plants in WO. The water depth of the three sample points is the same, with an annual average of 1.5 m. The samples were taken once a month, from June to October 2020.

In terms of water environment parameter measurement, water temperature (WT) and pH are measured on-site by YSI portable multiparameter analyzer. After acid and low-temperature preservation, water samples were taken back to the analysis and testing centre of Northeast Institute of geography and Agroecology, Chinese Academy of Sciences. According to the methods for detection and analysis of water and wastewater (Fourth Edition), total nitrogen (TN), TP, total potassium (TK), TS, Dichromate Oxidizability (CODCr), and 5-day Biochemical Oxygen Demand (BOD_5) were measured.

When the water depth was less than 2 m, the water sample was taken at 0.5 m underwater. When the water depth was 2 ~ 5 m, another water sample was taken at 0.5 m from the bottom. Qualitative samples of phytoplankton were collected by plankton net 25 (aperture 64) μ m), after concentrating to 100ml, immobilizing them with 1–2 ml of Luger iodine solution. After standing for 48 h, they were concentrated to 30 ml for microscopic examination (Olympus CX21, 400×). Quantitative samples of phytoplankton were collected by a water collector. After precipitation for 48 h, it was concentrated to 50 ml with a siphon, and 4% formaldehyde solution was added for storage. Finally, 100 view fields were counted twice and the average value was taken. The abundance of phytoplankton was calculated by an optical microscope (Utermöhl, 1958). Meanwhile, the biomass of phytoplankton was estimated by biological volume (Hillebrand et al., 2010). The identification of phytoplankton species is based on "The Phytoplankton Manual" recommended by UNESCO (Sournia, 1978) and "Freshwater Algae in China-System, Classification and Ecology" (Hu and Wei, 2006).

Data Processing and Analysis

To determine the diversity of the phytoplankton community, the diversity indicators used in this study include phytoplankton dominance ($\boldsymbol{Y}$) (Mcnaughton, 1967), Shannon-Wiener index ($\boldsymbol{H'}$) (Shannon, 1950), Margalef richness index ($\boldsymbol{D_{Ma}}$) (Margalef, 1957), and Pielou evenness index ($\boldsymbol{J}$) (Li et al., 2018). The biodiversity index can evaluate the pollution status of water quality. High biodiversity index value means low water pollution (Wang et al., 2002). Phytoplankton dominance $\boldsymbol{Y} \geq 0.02$ is defined as the dominant species.

The abundance and biomass information of dominant phytoplankton species were analyzed by detrended correspondence analysis (DCA). The sorting axis gradient length (LGA) was 5.0 and 6.7, respectively, high than 4.0. It is suitable to use canonical correspondence analysis (CCA) based on linearity (Zhao et al., 2014). Environmental factors include WT, TN, TP, CODcr and BOD, and the Monte Carlo permutation test ($p < 0.05$) is conducted first. The phytoplankton species and codes used in CCA analysis are shown in **Table 2**.

RESULT

Water Environment

The water temperature first increases and then decreases with the season. The highest was 27.28 in July and the lowest was 9.22 in October (**Table 1**). From June to October, the contents of TS increased continuously from 219.17 mg L^{-1}–363.33 mg L^{-1}. BOD_5 was the highest in July (6.78 mg L^{-1}), and there was no significant difference in other periods, to vary between 2.51 mg L^{-1} and 3.61 mg L^{-1}. The seasonal fluctuation of CODCr is apparent. The peak occurred in June (28.32 mg L^{-1}) and August (29.12 mg L^{-1}), which means many were reducing substances in the water body, mainly organic pollutants. The contents of TN and TP increased at first and then decreased finally. They reached the highest in August (TN: 1.61 mg L^{-1} and TP: 0.12 mg L^{-1}), and the lowest in October (TN: 0.54 mg L^{-1} and TP: 0.07 mg L^{-1}). TK content decreased continuously from 4.07 mg L^{-1}–3.14 mg L^{-1}.

Seasonal Dynamics of Phytoplankton Composition

A total of 146 species (including varieties, modification, and undetermined species) belonging to 63 genera and 8 phyla of planktonic algae were identified. Bacillariophyta (57 species) and

TABLE 2 | List of dominant phytoplankton species in Xinmiao Lake.

Phyla	Dominant genera	Codon	Dominant degree				
			June	July	August	September	October
Chlorophyta	*Chlamydomonas globosa*	n1					0.247
	Scenedesmus quadricauda	n2	0.031			0.095	0.026
	Scenedesmus acuminatus	n3	0.026			0.093	
	Chlorella vulgaris	n4	0.022		0.031		
	Chlorella sp	n5					0.092
	Selenastrum minutum	n6		0.022		0.037	
	Planctonema sp	n7					0.089
	Ankistrodesmus angustus	n8		0.034		0.041	0.043
Bacillariophyta	*Nitzschia acicularis*	n9	0.038	0.143	0.052	0.066	
	Nitzschia palea	n10	0.056		0.024		
	Synedra amphicephala	n11	0.027				
	Synedra vaucheriae	n12	0.107				
	Melosira italica	n13		0.115	0.037		
	Melosira undulata	n14	0.063				
	Achnanthes minutissima	n15	0.188		0.050		
Cyanobacteria	*Merismopedia minima*	n16		0.311			
	Merismopedia tenuissima	n17			0.119		
	Anabaena cylindrica	n18			0.041		
	Chroococcus minor	n19				0.057	

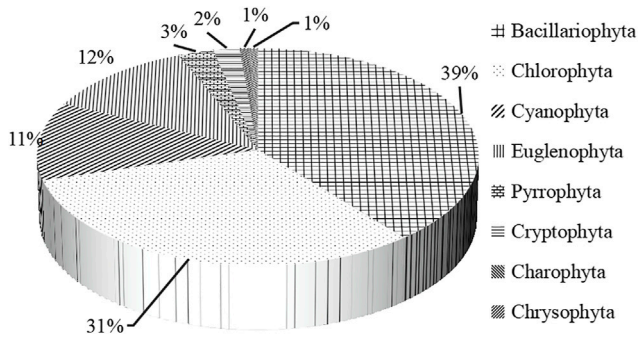

FIGURE 2 | Species composition of phytoplankton.

Chlorophyta (46 species) were the most abundant, accounting for 39.04 and 31.51% of the total species, respectively Cyanobacteria (**Figure 2**). Bacillariophyta has the largest number of species (**Figure 3A**), while Chlorophyta has the largest number of genera (**Figure 3B**).

The total phytoplankton abundance rose to the highest in August (1.94×10^7 ind./L) and decreased to a minimum in October (5.93×10^6 ind./L) (**Figure 4A**). The abundance was changed successively with Bacillariophyta (about 75% in June), Cyanobacteria (about 50% in July–August), and Chlorophyta (about 75% in September–October). Phytoplankton biomass continued to decline from 17.7 mg/L to 4.4 mg/L (**Figure 4B**). The total phytoplankton biomass from 17.7 mg/L continuously decreased to 4.4 mg/L (**Figure 4B**). Bacillariophyta accounts for the most, followed by Cyanobacteria and Chlorophyta, and other algae account for a relatively small proportion.

19 dominant phytoplankton species belonged to 13 genera and 3 phyla were identified during the research. Among them, there were 8 species of Chlorophyta, seven species of Bacillariophyta, and four species of Cyanobacteria (**Table 2**). Chlorophyta dominated in September and October. The dominant species of Bacillariophyta mostly appeared in June. Cyanobacteria took up the advantages part in July and August. The algae with the highest dominance were *Chlamydomonas globosa*, *Achnanthes minutissima*, *Merismopedia minima*, and reach 0.247, 0.188, 0.311, respectively. *Nitzschia acicularis* from diatom can serve as the dominant species for the longest time, lasting 4 months. *Scenedesmus quadricauda* and *Ankistodesmus angustus* follow Chlorophyta, lasting 3 months. Other species occur only once or twice.

The species-environment correlation coefficients of the first two axes of phytoplankton abundance and biomass ranking axis are high, which explain 41.06 and 41.95% of the cumulative percentage variation of species-environment relationship, respectively (**Table 3**), indicating that the species composition of phytoplankton in Xinmiao Lake is closely related to environmental factors. The environmental factors affecting the abundance of dominant species were mainly TS, WT and TP (**Figure 5A**), the main factors affecting the biomass of dominant species were TS, TP and BOD_5 (**Figure 5B**).

Spatial-Temporal Dynamics of Phytoplankton Diversity and Functional Groups

The biodiversity index reflects the low pollution of water quality in June and the highest pollution in October. NA has the lowest pollution, and WO is slightly higher than WI. (**Table 4**). In addition, the Shannon and Pielou indexes at WI did not fluctuate violently, with the mean values of 2.11 and 0.55, respectively, and the Margalef index reached the lowest of 0.47 in September. The Shannon indices and Pielou indices of NA were the highest in

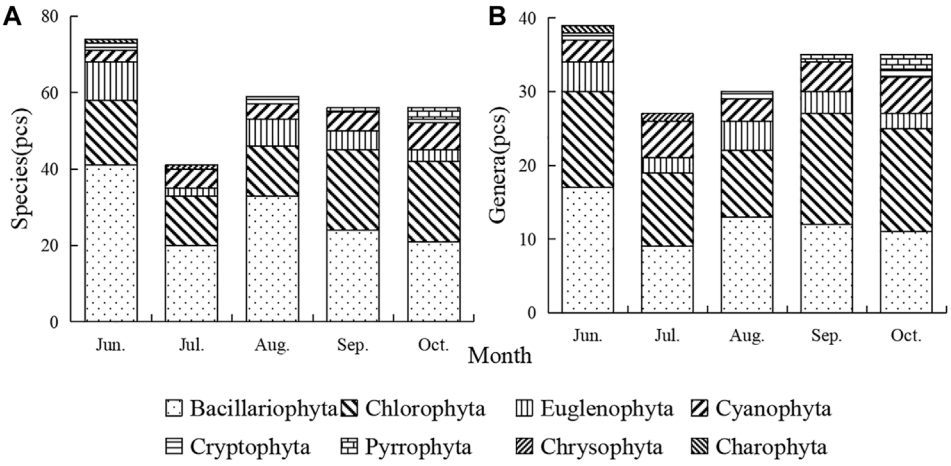

FIGURE 3 | Temporal variation of phytoplankton species **(A)** and genera **(B)**.

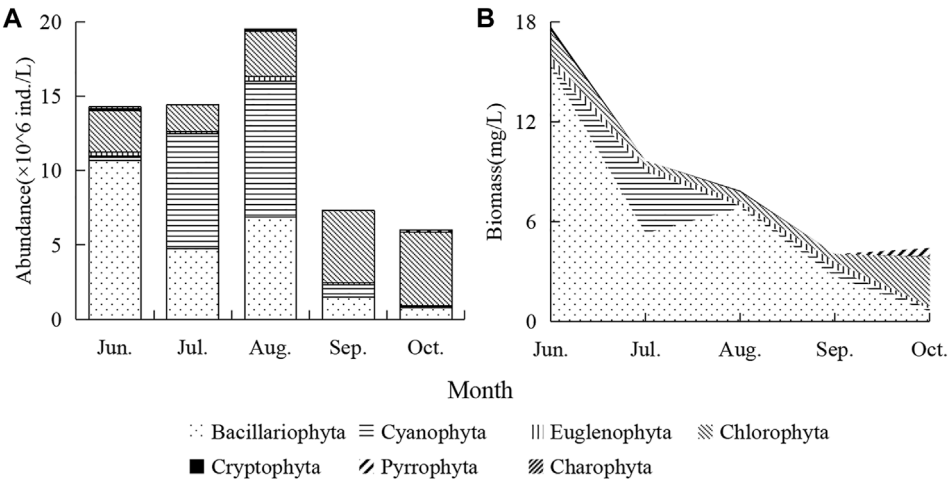

FIGURE 4 | Temporal changes of phytoplankton abundance **(A)** and biomass **(B)**.

TABLE 3 | Statistical information of CCA analysis of phytoplankton community.

Statistical information	Phytoplankton abundance		Phytoplankton biomass	
	Axis 1	Axis 2	Axis 1	Axis 2
Eigenvalues	0.7782	0.7013	0.828	0.7811
Explained variation (cumulative)	21.6	41.06	21.59	41.95
Pseudo-canonical correlation	0.9853	0.9466	0.933	0.9428
Explained fitted variation (cumulative)	27.66	52.59	37.34	72.57

June and July, reaching 3.22 and 0.67 respectively. The Margalef index fluctuated sharply, with a difference of 2.11 between the highest and lowest. However, the biodiversity trend of WO was bimodal. The Shannon and Pielou indexes were the highest in June, 2.62 and 0.63, respectively. The Margalef index peaked at 1.63 in August. The biodiversity evaluation showed that the pollution was the lowest in June and the heaviest in October and generally belonged to medium pollution.

The phytoplankton is divided into 21 groups (**Table 5**), and 12 groups with relative biomass greater than 10% are defined as representative functional groups (Reynolds et al., 2002; Padisák et al., 2009) (**Figure 6**). The species and frequency of the MP

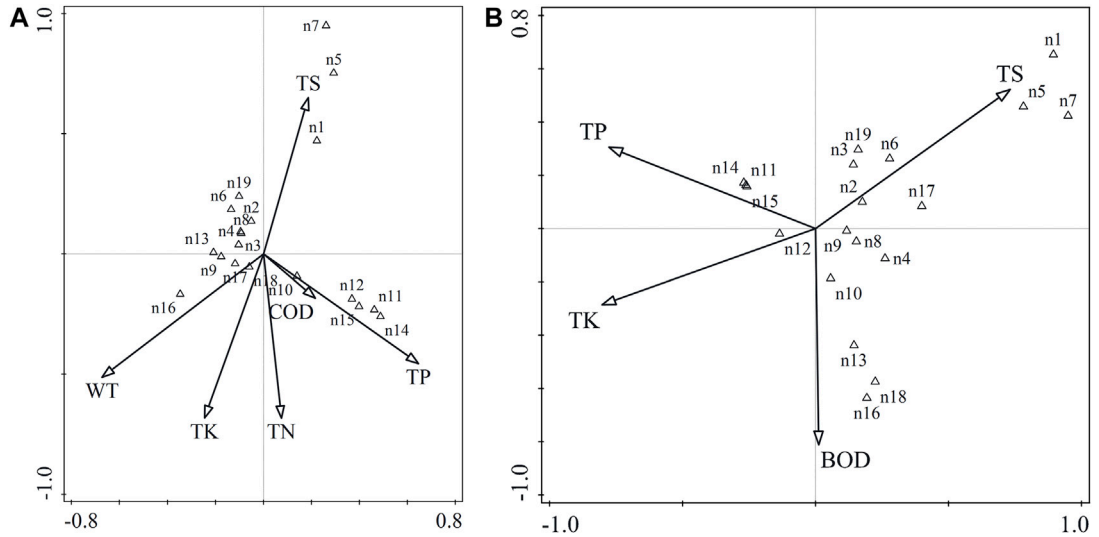

FIGURE 5 | Correlation plots of the redundancy analysis (CCA) on the relationship between the environment variables and dominant species of phytoplankton. Panels show CCA between the environment variables and abundance **(A)**, biomass **(B)**.In this figure, the black arrow represents the environment variable, and the arrow points to the direction in which the value of the environment variable increases most sharply. The angle between the arrows indicates the correlation between the various environment variables. The black triangle represents species, and the distance between symbols is similar to the relative abundance distribution of these species in the sample measured by chi-square distance. Adjacent points correspond to species that often occur at the same time. The species symbol can be projected vertically onto the line above the arrow of a specific environmental variable. These forecasts are made according to the predicted growth order of the best value of the prediction variables.

group in the whole year are the highest. At WI, the dominant relative abundances from June to October were MP (28.5%), D (34.8%), B (30.4%), J (42.1%), and X2 (41.5%). Furthermore, biomass transited from B, D, MP (about 30%) in summer to X2 (50.8%) in autumn. And the relative abundance advantage of Na changed from X1 (about 15% in summer) and MP (28.5% in Aug.) to X2 (52.7% in Oct.). Moreover, The group with the highest biomass contribution changed from TC and W2 (33.6%, and 42.1% in July) to X2 and W1 (58.7%, and 18.1% in September). The dominant groups change from Lo (64.6% in July) to J (48.4 %in September) was found in WO, and MP has contributed more than 16% of the biomass. Changes in functional group abundance and biomass are usually related, but mismatches are still found. For example, TC and W2 with less abundance contributed most of the biomass at NA, while the abundance of Lo and J with a high proportion at WO had little effect on the relative biomass.

DISCUSSION

Key Factors Affecting Phytoplankton Dynamics

In order to determine the seasonal pattern of water environment, it is necessary to take into account the seasonal changes of rainfall and water temperature and the impact of agricultural activities. Agricultural activities will affect the time and intensity of water supply, thus affecting the transparency, light and nutrition level of lakes (Miao et al., 2011; Michalak et al., 2013; Liu et al., 2021). There is sufficient research proving that water temperature significantly impacts the abundance of plankton (Ho et al., 2019). CCA showed that water temperature significantly affected phytoplankton abundance but could not clearly explain the change of biomass (**Figure 6**). Cyanobacteria and Chlorophyta are suitable for growing in warm water, while diatoms are mostly cold-water species (Zhang Y et al., 2019). This study supports that diatom reproduction rapidly and advanced in spring with low water temperature. The Cyanobacteria will take up the advantages part in July and August because the *Merismopedia minima*, *Merismopedia tenuissima*, and *Anabaena cylindrical* will be high in terms of thermal stability to their DNA, protein synthesis systems, and photosynthetic systems. Therefore, it can adapt to high temperatures, and the optimal temperature is 25–35 ˚C (Lurling et al., 2013). The average water temperature from July to August in Xinmiao Lake is 26.33˚C, suitable for the growth of Cyanobacteria. Although the abundance of Cyanobacteria was high in August, the biomass was low for the small cell size (Tian et al., 2016). The temperature changes not only directly affect the species composition of phytoplankton, but also affect the metabolism of heterotrophs (Taucher and Oschlies, 2011). Therefore, warming can control the community structure of phytoplankton from top to bottom by improving the grazing efficiency of consumption by herbivores (Winder and Sommer, 2012). The zooplankton in Xinmiao lake are mainly Rotifers and Sarcodina. These herbivores preferentially prey on small phytoplankton (Weithoff et al., 2000; Gomes et al., 2019; Sun et al., 2021). Therefore the balance change of Chlorophyta dominance from September to October may mainly be attributed to reduced competitive pressure from diatom and

TABLE 4 | Distribution of phytoplankton diversity index in Xinmiao Lake wetland.

Site	*H'*					D_{Ma}					*J*				
	June	July	August	September	October	June	July	August	September	October	June	July	August	September	October
WI	2.03	2.37	2.41	1.79	1.94	1.25	1.18	1.24	0.47	0.93	0.46	0.56	0.58	0.64	0.51
NA	3.22	2.14	2.03	2.58	1.86	3.16	0.60	1.33	1.48	1.05	0.57	0.67	0.46	0.56	0.47
WO	2.62	1.36	2.15	2.45	1.64	1.18	1.12	1.63	1.20	0.87	0.63	0.32	0.45	0.59	0.43
Average	2.63	1.95	2.20	2.27	1.82	1.86	0.97	1.40	1.05	0.95	0.56	0.52	0.50	0.60	0.47
Evaluation	β-M	α-M	β-M	β-M	α-M	α-M	S	α-M	α-M	S	L	L	M	L	M

L: Low pollution or cleaning; β-M: β-medium pollution; α-M: α-medium pollution; M: Medium pollution S: serious pollution.

Cyanobacteria and higher resistance to grazing losses (Goldyn and Kowalczewska-Madura, 2008; Nolan and Cardinale, 2019). This study's algae seasonal replacement model is similar to the Chagan Lake, the same type of lake (Li et al., 2014).

Depth reduces light availability by affecting the absorption and refraction of suspended solids and algae (Vadeboncoeur et al., 2008). High turbidity can limit light penetration into sediments, so limited light availability is usually controlled by water depth and transparency (Iachetti and Llames, 2015). The transparency of Xinmiao Lake is controlled by sediment resuspension under the influence of hydrodynamic forces. The water depth of this type of shallow turbid lake can determine light availability. In addition, the peak of algae biomass in spring is mainly due to the availability of nutrients and high light (Thamatrakoln, 2021). Meanwhile, the enormous growth of submerged plants shows that there is no photoinhibition at least before autumn. Light has no significant effect on the relative proportion of dominant species, but it can effectively change the total biomass of phytoplankton (Llames et al., 2009). The reduction of light energy input limits the net primary productivity. The loss of algae cannot be fully supplemented (Anneville et al., 2017), reducing algae biomass to an absolute minimum in winter.

In addition to the physical environment, such as water temperature and light, the steady-state phytoplankton assembly is also affected by nutrient levels and biological interactions (Rojo and Álvarez-Cobelas, 2003). TN and TP are the primary nutrients of agricultural non-point source pollution, which can affect the growth of phytoplankton in the process of lake evolution (Zhang et al., 2018). Due to the accumulation of a large number of phosphorus resources in sediment, the response of the lake ecosystem may be disturbed. The importance of N and P varies with N: P ratios in the lake, and the total biomass of phytoplankton will be strongly affected by the least supplied nutrients (Dolman et al., 2016). There is a significant positive correlation between phytoplankton and TP (**Figure 5**) and a complex relationship with TN. This shows that Xinmiao lake is a nitrogen-limited lake, which is also proved by nitrogen-fixing cyanobacteria in the phytoplankton community. Besides, *Melosiraitalica* of Bacillariophyta, *Merismopedia minima,* and *Anabaena cylindrica* of Cyanobacteria had a significant positive correlation with BOD_5. Rainwater and irrigation backwater injected into the lake will receive a large number of particles, nutrients, and organic matter, which constitutes a typical feature under the influence of agriculture (Taylor et al., 2019). There is a seasonal pattern of material import: it starts in mid-May and peaks in mid-August. This model shows that it will be more effective to implement best management practices in warm summer (Lizotte et al., 2014).

Indication of Phytoplankton Functional Groups and Diversity on Water Quality

The change of phytoplankton species richness is usually the result of species extinction or invasion. In contrast, the change of biodiversity and evenness is usually related to species dominance (Hillebrand et al., 2008). Phytoplankton biodiversity is affected by different developmental stages or habitat differences of the community

TABLE 5 | Main identification characteristics and representative species of Xinmiao Lake functional group during the survey period.

Codon	Representative Species (genus)	Tolerances	Sensitivities	Habitat
B	*Melosira italica* *Cyclotella stelligera*	Light deficiency	pH rise stratification	Vertically mixed, mesotrophic small-medium lakes
C	*Melosira ambigua* *Cyclotella meneghiniana*	Light, C deficiencies	Si exhaustion stratification	Mixed, eutrophic small-medium lakes
D	*Synedra* spp. *Nitzschia* spp.	Flushing	Nutrient depletion	Shallow, enriched turbid waters
F	*Oocystis borgei* *Sphaerocystis* sp	low nutrients high turbidity	CO2 deficiency	clear, deeply mixed meso-eutrophic lakes
H1	*Anabaena cylindrica* *Aphanizomenon gracile*	low carbon	mixing, poor light low phosphorus	eutrophic, low nitrogen stratified and shallow lakes
J	*Pediastrum* spp. *Scenedesmus* spp. *Coelastrum microporum*		settling into low light	shallow, mixed, highly enriched lakes
LM	*Ceratium hirundinella*	deficient C	mixing, poor stratification light	eutrophic to hypertrophic, small-to-medium lakes
Lo	*Peridinium* spp. *Chroococcus minor* *Merismopedia* spp.	Nutrient stratification	prolonged or deep mixing	mesotrophic to eutrophic, medium to large lakes
M	*Microcystis* spp.	high insolation	flushing, low total light	mixed layers of small eutrophic, low latitude lakes
MP	*Navicula* spp. *Cocconeis placentula* *Surirella* spp. *Oscillatoria* spp. *Nitzschia sigmoidea* *Achnanthes minutissima* *Gomphonema angustatum* *Ulothrix* spp.	Mixing and stirring		frequently stirred up, inorganically turbid shallow lakes
N	*Cosmarium* spp. *Staurastrum* spp.	Nutrient deficiency	stratification pH rise	mesotrophic epilimnia
P	*Fragilaria intermedia* *Closterium* spp. *Melosira* sp	Mild light and C deficiency	stratification Si depletion	eutrophic epilimnia
S1	*Limnothrix planctonica*	highly light deficient	fiushing	turbid mixed
TB	*Gomphonema* spp. *Melosira varians*	fiushing		highly lotic environments
TC	*Phormidium tenue*		flushing	eutrophic standing waters, or slow-flowing rivers with emergent macrophytes
W1	*Euglena* spp. *Phacus* spp.	high BOD	grazing	small organic ponds
W2	*Trachelomonas* spp. *Strombomonas angusta*		Low WT stirring	shallow mesotrophic lakes
X1	*Ankistrodesmus angustus* *Chlorella vulgaris* *Monoraphidium griffithii* *Schroederia nitzschioides*	stratfication	nutrient deficiency filter feeding	eutrophic shallow mixed layers
X2	*Chlamydomonas* spp.	stratification	mixing filter feeding	shallow, transparent mixed layers in meso-eutrophic lakes
X3	*Chlorella* sp	low base status	mixing grazing	shallow, clear, mixed oligotrophic layers
Y	*Cryptomonas* spp.	low light	phagocytosis	small, enriched static lakes

(Bandeira et al., 2013), so the water's biophysical and biochemical quality will directly affect the biodiversity of the lake waters. In this study, the WI sampling site is surrounded by farmland, the rapid changes of nutrient input and physical water state weaken the stability of the phytoplankton community structure, and WO is mainly disturbed by human activities in nearby scenic spots so that the phytoplankton biodiversity is low. On the contrary, the stable water environment of NA provides better development conditions for phytoplankton community. In the early stage of phytoplankton community construction, the frequent fluctuation of the environment interfered with the competition, so the population was mainly restricted by environmental factors (Barraquand et al., 2018). The increase of nutrient level and illumination time in June satisfied the growth of phytoplankton and increased the diversity. In

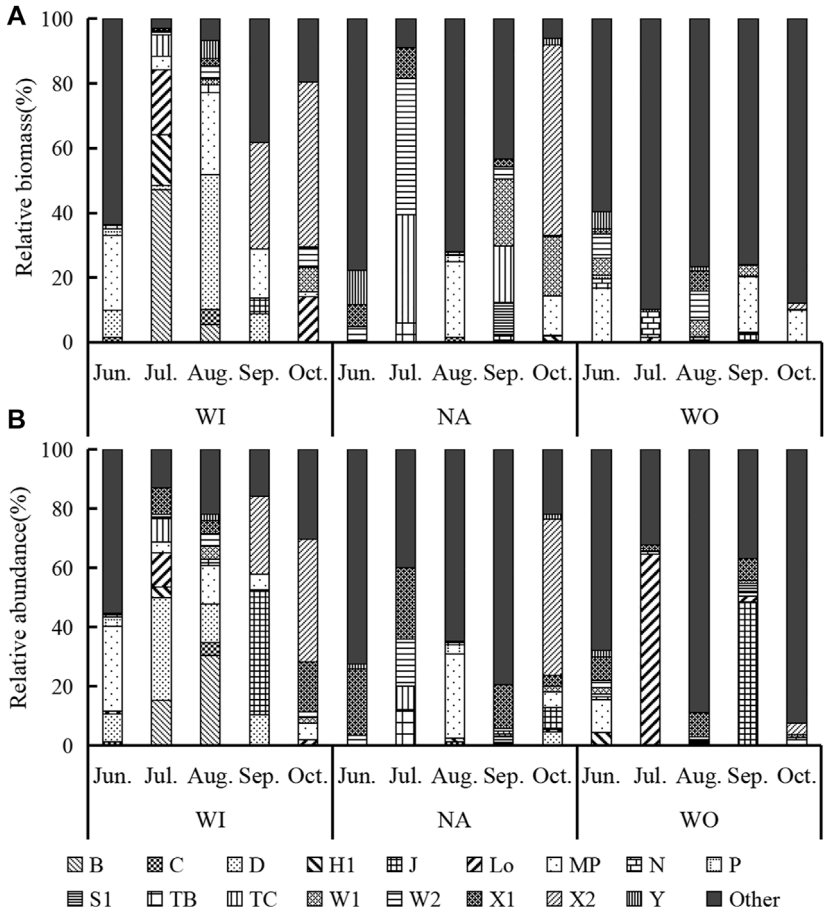

FIGURE 6 | Relative biomass **(A)** and relative abundance **(B)** of phytoplankton functional groups.

winter, the interference from agricultural activities almost disappeared, and the rainfall and backwater decreased, resulting in a slow flow rate. At this time, the ecological niche is separated due to competition, and competitors are inhibited by dominant species (such as Chlorophyta in this research), which reduces the diversity to the lowest level (Tilman et al., 1982). The results of the water quality evaluation based on the diversity index show that the water pollution degree of Xinmiao Lake is the lowest in June and the most serious in October. A large number of reeds grow in Xinmiao Lake (Zhang, 2015), its developed roots are more likely to produce an oxidizing environment in the water, to promote nitrification, accelerate the absorption of NO_3^-, NH_4^+, PO_4^{3-} plasma in water and sediments, consequently, purify nitrogen and phosphorus pollution in paddy field irrigation backwater (Li et al., 2021). However, the purification capacity of the lake is limited, especially in the peak season of agricultural irrigation, when a large amount of N and P enter the lake with irrigation backwater. The nutrition of lakes is further risen, which increases the risk of eutrophication.

The temporal and spatial changes of dominant phytoplankton species in water can be well described by using the functional group classification method, and it can also better evaluate the response of phytoplankton to environmental changes (Salmaso et al., 2015). During the survey period, the functional group MP dominated by Bacillariophyta occupied an absolute advantage. This is due to the low transparency of Xinmiao lake and the easily mixed water body. The decrease in water transparency shows lake eutrophication (Dodds, 2006). *Oscillatoria* spp. from the MP group is often found on the sludge surface with rich organic matter or in shallow water ponds, consistent with the environmental characteristics of swamps and wetlands of Xinmiao Lake. *Cocconeis placentula* is often attached to submerged plants (Jahn et al., 2009) and may rely more on the *Potamogeton crispus Linn.* in Xinmiao Lake. In July, the representative functional groups of WI are B, H1 and LO. Because WI is a small and medium-sized shallow water body, and between mesotrophic to eutrophic, which is suitable for the growth of *Melosiraitalica*, *Anabaena cylindrica* and *Merismopedia* spp. The appearance of cyanobacteria H1 shows that the lake has a trend of thermal stratification. The representative functional groups of NA are TC and W2, because the environment of NA is mesotrophic to eutrophic, shallow water with a slow flow, and there are a large number of reeds, which are suitable for the growth of *Phormidium tenue*, *Trachelomonas* spp. and *Strombomonas angusta*. The D-functional group appeared on WI in August, reflecting its rich nutrient content and turbid water body. In September and October, X2, dominated by *Chlamydomonas* spp, is the main functional group. It grows in shallow water

from mesotrophic to eutrophic, with less affected by stratification, and it is sensitive to water mixing and filtration (Raven et al., 2011), indicating that there is a low degree of stratification in the water body during this period. In addition, W1 (mainly includes *Euglena* spp. and *Phacus* spp.) at this time is dependent on the increase of BOD_5 (Gani et al., 2017) which is mainly due to decomposed submerged plant in early autumn (Lin et al., 2018). Overall, the representative functional groups of phytoplankton reflect Xinmiao Lake's high degree of eutrophication and nutrient content, slow water flow rate and low grazing pressure.

Risk Prediction of Cyanobacteria Bloom

Merismopedia sp. and *Anabaena* sp, which are dominant in summer, will produce water bloom under the condition of mass reproduction (Poot-Delgado et al., 2018). Nitrogen consumption is conducive to the reproduction of nitrogen-fixing algae *Anabaena* sp, and some species contain toxic substances (Chislock et al., 2014; Akagha et al., 2020). When the TP concentration exceeds 10 μg/L, the growth of Chlorophyta is primarily affected by physical factors, especially the stability of the water body (Steinberg and Hartmann, 2010). It has been proved that the increase of the stability of the water body, especially the surface water body, can better meet the hydrodynamic conditions for the occurrence of Cyanobacteria bloom (Zhang S et al., 2019). Moreover, the increased pH value may prolong this process in summer and prevent the diatom from recovering its dominance in autumn by inhibiting the growth rate and diatom silicon deposition (Zepernick et al., 2021). The growth rate of Cyanobacteria dominated by Microcystis will increase if the concentrations of TN and TP exceed 1.5 mg L^{-1} and 0.1 mg L^{-1}. Furthermore, if TN remains above 1.0 mg L^{-1} and TP remains above 0.08 mg L^{-1}, it is expected to increase the risk of water bloom (Xu et al., 2017). The average value of TN and TP in Xinmiao lake is about 0.99 mg/L and 0.10 mg/L, and the pH is often close to or greater than 8.5 in summer when the WT is higher than 25 °C (**Table 1**). Consequently, Xinmiao Lake has the hydrochemical environment for Cyanobacteria bloom in July and August in summer. The survey results also verify this hypothesis by the rapid increase of Cyanobacteria in July and August. Therefore, controlling the input of exogenous nitrogen and phosphorus is an important measure to reduce the risk of cyanobacteria bloom. Because the chemical environment in summer is suitable for the growth of cyanobacteria, it is imperative to accurately judge the physical environment of the water body, especially the stable state. Among the representative functional groups of phytoplankton, codon B dominated by *Melosira italica* and *Cyclotella stelligera* and codon C dominated by *Melosira ambigua* and *Cyclotella meneghiniana* are sensitive to water stratification (**Table 4**), which can be used to judge the stable state of water body and provide early warning for the outbreak of Cyanobacteria bloom.

CONCLUSION

By studying the relationship between phytoplankton and water quality in the wetland in agricultural areas, it is found that the backwater from farmland irrigation has dramatically changed the environment of phytoplankton growth by transporting nutrients, organic substances, and sediment to the lake. The reduction of interference in agricultural activities increases the competitive pressure among dominant species. When environmental factors change, it can still control the phytoplankton community structure to a great extent. Xinmiao Lake is a nitrogen-limited lake. Considering the functional groups and diversity of phytoplankton, the degree of eutrophication is deepening. Due to the increase in water temperature and nitrogen and phosphorus, the risk of cyanobacteria blooming from July to August is the highest. At this time, managers should control the input of phosphorus and pay close attention to the stable state of the water body. This study improves the understanding of the seasonal pattern of phytoplankton growth and its response to changes in environmental factors. In addition, it also provides available information for the control of Cyanobacteria bloom and the management of wetland ecosystem in agricultural areas.

DATA AVAILABILITY STATEMENT

The original contributions presented in the study are included in the article/Supplementary Material, further inquiries can be directed to the corresponding author.

AUTHOR CONTRIBUTIONS

YH designed the study under the direction and leadership of WZ, who conceived the original idea. Samples were collected and pretreated by YL, JZ, and RL. YH, MF, and ZS treated the samples together and identified the phytoplankton in them. SZ coordinates the sampling work and the experimental work in the identification process. XT and YS completed the data extraction and analysis. YH and YS completed the manuscript preparation in close consultation with WZ. All authors contributed to the article and approved the submitted version.

FUNDING

Class A strategic leading science and technology project of Chinese Academy of Sciences "scientific and technological innovation project of black land protection and utilization": comprehensive regulation of water quantity and quality of irrigation area wetland system based on the healthy water cycle (XDA28020502). Biodiversity Conservation and Sustainable Land Management in the SodaSaline-Alkaline Wetlands and Agro-Pastoral Landscapes in Western Jilin (GCP/CPR/048/GEF-JL).

ACKNOWLEDGMENTS

We want to thank the teachers and students of many Wetland Ecosystem Management Discipline groups who have contributed to sample collection and analysis. Specifically, thank you to

Xiangqin Jin, teacher of Changchun Fisheries Research Institute, Jilin Province, who plays a vital role in phytoplankton identification. We thank the management personnel of Xinmiao Lake for their indispensable role in sample collection. We would also like to thank the analysis and testing centre of Northeast Institute of geography and Agroecology, Chinese Academy of Sciences, for their professional and timely analytical services.

REFERENCES

Akagha, S. C., Nwankwo, D. I., and Yin, K. (2020). Dynamics of Nutrient and Phytoplankton in Epe Lagoon, Nigeria: Possible Causes and Consequences of Reoccurring Cyanobacterial Blooms. *Appl. Water Sci.* 10 (5), 1–16. doi:10.1007/s13201-020-01190-7

Anneville, O., Dur, G., Rimet, F., and Souissi, S. (2017). Plasticity in Phytoplankton Annual Periodicity: an Adaptation to Long-Term Environmental Changes. *Hydrobiologia* 824, 121–141. doi:10.1007/s10750-017-3412-z

Arab, S., Hamil, S., Rezzaz, M. A., Chaffai, A., and Arab, A. (2019). Seasonal Variation of Water Quality and Phytoplankton Dynamics and Diversity in the Surface Water of Boukourdane Lake, Algeria. *Arab J. Geosci.* 12 (2), 29. doi:10.1007/s12517-018-4164-4

Bandeira, B., Jamet, J.-L., Jamet, D., and Ginoux, J.-M. (2013). Mathematical Convergences of Biodiversity Indices. *Ecol. Indicators* 29, 522–528. doi:10.1016/j.ecolind.2013.01.028

Barraquand, F., Picoche, C., Maurer, D., Carassou, L., and Auby, I. (2018). Coastal Phytoplankton Community Dynamics and Coexistence Driven by Intragroup Density-Dependence, Light and Hydrodynamics. *Oikos* 127 (12), 1834–1852. doi:10.1111/oik.05361

Bunting, L., Leavitt, P. R., Simpson, G. L., Wissel, B., Laird, K. R., Cumming, B. F., et al. (2016). Increased Variability and Sudden Ecosystem State Change in Lake Winnipeg, Canada, Caused by 20th century Agriculture. *Limnol. Oceanogr.* 61 (6), 2090–2107. doi:10.1002/lno.10355

Chen, M., Zeng, G., Zhang, J., Xu, P., Chen, A., and Lu, L. (2015). Global Landscape of Total Organic Carbon, Nitrogen and Phosphorus in Lake Water. *Sci. Rep.* 5 (1), 15043. doi:10.1038/srep15043

Chen, X. J., Li, X., and Li, J. J. (2021). Indicator Species of Phytoplankton Pollution and Water Quality Evaluation in Wuliangsuhai. *Ecol. Sci.* 40 (03), 231–237. doi:10.14108/j.cnki.1008-8873.2021.03.027

Chislock, M. F., Sharp, K. L., and Wilson, A. E. (2014). Cylindrospermopsis Raciborskii Dominates under Very Low and High Nitrogen-To-Phosphorus Ratios. *Water Res.* 49, 207–214. doi:10.1016/j.watres.2013.11.022

Dai, X., and Tian, W. (2011). Analysis and Countermeasures on Water Pollution of lake Chagan. *J. Arid Land Resour. Environ.* 25 (8), 179–184. doi:10.1016/S1671-2927(11)60313-1

Dodds, W. K. (2006). Eutrophication and Trophic State in Rivers and Streams. *Limnol. Oceanogr.* 51, 671–680. doi:10.4319/lo.2006.51.1_part_2.0671

Dolman, A. M., Mischke, U., and Wiedner, C. (2016). Lake-type-specific Seasonal Patterns of Nutrient Limitation in German Lakes, with Target Nitrogen and Phosphorus Concentrations for Good Ecological Status. *Freshw. Biol.* 61 (4), 444–456. doi:10.1111/fwb.12718

Gani, M. A., Alfasane, M. A., and Khondker, M. (2017). Bloom Forming Phytoplankton and Their Comparative Limnology in Wastewater Lagoons of Bangladesh. *Bangladesh J. Bot.* 46 (1), 43–51. https://www.researchgate.net/publication/315492914.

Glibert, P., and Burford, M. (2017). Globally Changing Nutrient Loads and Harmful Algal Blooms: Recent Advances, New Paradigms, and Continuing Challenges. *Oceanog.* 30 (1), 58–69. doi:10.5670/oceanog.2017.110

Goldyn, R., and Kowalczewska-Madura, K. (2008). Interactions between Phytoplankton and Zooplankton in the Hypertrophic Swarzedzkie Lake in Western Poland. *J. Plankton Res.* 30 (1), 33–42. doi:10.1093/plankt/fbm086

Gomes, L. F., Pereira, H. R., Gomes, A. C. A. M., Vieira, M. C., MartinsRoitman, P. R. I., Roitman, I., et al. (2019). Zooplankton Functional-Approach Studies in continental Aquatic Environments: a Systematic Review. *Aquat. Ecol.* 53 (2), 191–203. doi:10.1007/s10452-019-09682-8

Guo, B. (2012). *Study on the Environmental Impact of Paddy Field Pesticides in Songyuan Irrigation Area on Chagan Lake*. Dissertation. Graduate School of Chinese Academy of Sciences.

Guo, W., Wang, Y., Shi, J., Zhao, X., and Xie, Y. (2020). Sediment Information on Natural and Anthropogenic-Induced Change of Connected Water Systems in Chagan Lake, North China. *Environ. Geochem. Health* 42 (3), 795–808. doi:10.1007/s10653-019-00280-z

Henderson, K. A., Murdock, J. N., and Lizotte, R. E. (2021). Water Depth Influences Algal Distribution and Productivity in Shallow Agricultural Lakes. *Ecohydrology* 14. doi:10.1002/eco.2319

Hillebrand, H., Bennett, D. M., and Cadotte, M. W. (2008). Consequences of Dominance: a Review of Evenness Effects on Local and Regional Ecosystem Processes. *Ecology* 89 (6), 1510–1520. doi:10.1890/07-1053.1

Hillebrand, H., DürselenPollingher, C.-D., Kirschtel, D., Pollingher, U., and Zohary, T. (1999). Biovolume Calculation for Pelagic and Benthic Microalgae. *J. Phycology* 35 (2), 403–424. doi:10.1046/j.1529-8817.1999.3520403.x

Ho, J. C., Michalak, A. M., and Pahlevan, N. (2019). Widespread Global Increase in Intense lake Phytoplankton Blooms since the 1980s. *Nature* 574 (7780), 667–670. doi:10.1038/s41586-019-1648-7

Hu, H. J., and Wei, Y. X. (2006). *Freshwater Algae in China – System, Classification and Ecology*. Beijing: Science Press, 334–339. Available at: http://ir.ihb.ac.cn/handle/342005/10582.

Iachetti, C. M., and Llames, M. E. (2015). Light Limitation Helps Stabilize the Phytoplankton Assemblage Steady-State in a Temperate and Highly Turbid, Hypertrophic Shallow lake (Laguna Chascomús, Argentina). *Hydrobiologia* 752 (1), 33–46. doi:10.1007/s10750-014-2045-8

Ignatiades, L. (2020). Taxonomic Diversity, Size-Functional Diversity, and Species Dominance Interrelations in Phytoplankton Communities: a Critical Analysis of Data Interpretation. *Mar. Biodivers.* 50 (4), 1–9. doi:10.1007/s12526-020-01086-4

Jahn, R., Kusber, W.-H., and Romero, O. E. (2009). Cocconeis Pediculus EHRENBERG and C. Placentula EHRENBERG Var. Placentula (Bacillariophyta): Typification and Taxonomy. *Fottea* 9 (2), 275–288. doi:10.5507/fot.2009.027

Kruk, C., Huszar, V. L. M., Peeters, E. T. H. M., Bonilla, S., Costa, L., Lürling, M., et al. (2010). A Morphological Classification Capturing Functional Variation in Phytoplankton. *Freshw. Biol.* 55 (3), 614–627. doi:10.1111/j.1365-2427.2009.02298.x

Lee, Y. S., and Kang, C.-K. (2010). Causes of COD Increases in Gwangyang Bay, South Korea. *J. Environ. Monit.* 12 (8), 1537–1546. doi:10.1039/c001733g

Li, Q.-W., Liang, J.-F., Zhang, X.-Y., Feng, J.-G., Song, M.-H., and Gao, J.-Q. (2021). Biochar Addition Affects Root Morphology and Nitrogen Uptake Capacity in Common Reed (Phragmites Australis). *Sci. Total Environ.* 766, 144381. doi:10.1016/j.scitotenv.2020.144381

Li Ranran, 李., Zhang Guangxin, 章., and Zhang Lei, 张. (2014). Multivariate Analysis of the Relations between Phytoplankton Assemblages and Environmental Factors in Chagan Lake Wetland. *Acta Eco Sin* 34 (10), 11. doi:10.5846/stxb201306091545

Li, S. J., Song, K. S., Zhao, Y., Mu, G. Y., Shao, T. T., and Ma, J. H. (2016). Absorption Characteristics of Particulates and CDOM in Waters of Chagan Lake and Xinlicheng Reservoir in Autumn. *Huan Jing Ke Xue* 37 (1), 112–122. doi:10.13227/j.hjkx.2016.01.016112-122

Li, Y., Dong, S., Liu, S., Su, X., Wang, X., Zhang, Y., et al. (2019). Relationships between Plant Diversity and Biomass Production of alpine Grasslands Are Dependent on the Spatial Scale and the Dimension of Biodiversity. *Ecol. Eng.* 127, 375–382. doi:10.1016/j.ecoleng.2018.12.015

Lin, L., Zhang, T. Y., and Dong, J. W. (2018). Analysis on Annual Variation Trend and Driving Mechanism of Dissolved Oxygen in Xinmiao Lake Water Body. *Jilin Water Conservancy* 36 (09), 5–8+11. doi:10.15920/j.cnki.22-1179/tv.2018.09.001

Liu, X., Chen, L., Zhang, G., Zhang, J., Wu, Y., and Ju, H. (2021). Spatiotemporal Dynamics of Succession and Growth Limitation of Phytoplankton for Nutrients and Light in a Large Shallow Lake. *Water Res.* 194 (7), 116910. doi:10.1016/j.watres.2021.116910

Liu, X., Zhang, G., Xu, Y. J., Wu, Y., Liu, Y., and Zhang, H. (2020). Assessment of Water Quality of Best Water Management Practices in lake Adjacent to the High-Latitude Agricultural Areas, China. *Environ. Sci. Pollut. Res.* 27 (3), 3338–3349. doi:10.1007/s11356-019-06858-5

Lizotte, R. E., Knight, S. S., Locke, M. A., and Bingner, R. L. (2014). Influence of Integrated Watershed-Scale Agricultural Conservation Practices on lake Water Quality. *J. Soil Water Conservation* 69 (2), 160–170. doi:10.2489/jswc.69.2.160

Llames, M. E., Lagomarsino, L., Diovisalvi, N., Fermani, P., Torremorell, A. M., Perez, G., et al. (2009). The Effects of Light Availability in Shallow, Turbid Waters: a Mesocosm Study. *J. Plankton Res.* 31 (12), 1517–1529. doi:10.1093/plankt/fbp086

Lürling, M., Eshetu, F., Faassen, E. J., Kosten, S., and Huszar, V. L. M. (2013). Comparison of Cyanobacterial and green Algal Growth Rates at Different Temperatures. *Freshw. Biol.* 58 (3), 552–559. doi:10.1111/j.1365-2427.2012.02866.x

Mao, D., Luo, L., Wang, Z., Wilson, M. C., Zeng, Y., Wu, B., et al. (2018). Conversions between Natural Wetlands and farmland in China: A Multiscale Geospatial Analysis. *Sci. Total Environ.* 634, 550–560. doi:10.1016/j.scitotenv.2018.04.009

Margalef, R. (1957). Information Theory in Ecology. *Gen. Syst.* 3, 36–71.

Mcnaughton, S. J. (1967). Relationships Among Functional Properties of Californian Grassland. *Nature* 216 (5111), 168–169. doi:10.1038/216168b0

Miao, Y., Stewart, B. A., and Zhang, F. (2011). Long-term Experiments for Sustainable Nutrient Management in China. A Review. *Agron. Sust. Developm.* 31 (2), 397–414. doi:10.1051/agro/2010034

Michalak, A. M., Anderson, E. J., Beletsky, D., Boland, S., Bosch, N. S., Bridgeman, T. B., et al. (2013). Record-setting Algal Bloom in Lake Erie Caused by Agricultural and Meteorological Trends Consistent with Expected Future Conditions. *Proc. Natl. Acad. Sci. U.S.A.* 110 (16), 6448–6452. doi:10.1073/pnas.1216006110

Negro, A. I., De Hoyos, C., and Vega, J. C. (2000). Phytoplankton Structure and Dynamics in Lake Sanabria and Valparaíso Reservoir (NW Spain). *Hydrobiologia* 424 (1-3), 25–37. doi:10.1007/978-94-017-3488-2_3

Newell, S. E., Davis, T. W., JohengenJohengen, T. H., Gossiaux, D., Burtner, A., Palladino, D., et al. (2019). Reduced Forms of Nitrogen Are a Driver of Non-nitrogen-fixing Harmful Cyanobacterial Blooms and Toxicity in Lake Erie. *Harmful Algae* 81 (JAN.), 86–93. doi:10.1016/j.hal.2018.11.003

Nolan, M. P., and Cardinale, B. J. (2019). Species Diversity of Resident green Algae Slows the Establishment and Proliferation of the Cyanobacterium Microcystis Aeruginosa. *Limnologica* 74, 23–27. doi:10.1016/j.limno.2018.09.002

Nunes, M., Adams, J. B., and Rishworth, G. M. (2018). Shifts in Phytoplankton Community Structure in Response to Hydrological Changes in the Shallow St Lucia Estuary. *Mar. Pollut. Bull.* 128 (MAR.), 275–286. doi:10.1016/j.marpolbul.2018.01.035

Odermatt, D., Pomati, F., Pitarch, J., Carpenter, J., Kawka, M., Schaepman, M., et al. (2012). MERIS Observations of Phytoplankton Blooms in a Stratified Eutrophic lake. *Remote Sensing Environ.* 126, 232–239. doi:10.1016/j.rse.2012.08.031

Padisák, J., Crossetti, L. O., and Naselli-Flores, L. (2009). Use and Misuse in the Application of the Phytoplankton Functional Classification: a Critical Review with Updates. *Hydrobiologia* 621 (1), 1–19. doi:10.1007/s10750-008-9645-0

Paerl, H. W., Xu, H., McCarthy, M. J., Zhu, G., Qin, B., Li, Y., et al. (2011). Controlling Harmful Cyanobacterial Blooms in a Hyper-Eutrophic lake (Lake Taihu, China): The Need for a Dual Nutrient (N & P) Management Strategy. *Water Res.* 45 (5), 1973–1983. doi:10.1016/j.watres.2010.09.018

Poot-Delgado, C. A., Okolodkov, Y. B., Aké-Castillo, J. A., and Rendón von Osten, J. (2018). Potentially Harmful Cyanobacteria in Oyster banks of Términos Lagoon, southeastern Gulf of Mexico. *Acta Biol. Colomb.* 23 (1), 51–58. doi:10.15446/abc.v23n1.65809

Raven, J. A., Giordano, M., Beardall, J., and Maberly, S. C. (2011). Algal and Aquatic Plant Carbon Concentrating Mechanisms in Relation to Environmental Change. *Photosynth Res.* 109 (1-3), 281–296. doi:10.1007/s11120-011-9632-6

Reynolds, C. S. (2012). Environmental Requirements and Habitat Preferences of Phytoplankton: Chance and Certainty in Species Selection. *Botanica Marina* 55 (1), 1–17. doi:10.1515/bot.2011.121

Reynolds, C. S., Huszar, V., Kruk, C., Naselli-Flores, L., and Melo, S. (2002). Towards a Functional Classification of the Freshwater Phytoplankton. *J. Plankton Res.* 24 (5), 417–428. doi:10.1093/plankt/24.5.417

Reynolds, C. S. (1980). Phytoplankton Assemblages and Their Periodicity in Stratifying lake Systems. *Ecography* 3, 141. doi:10.1111/j.1600-0587.1980.tb00721.x

Reynolds, C. S. (1984). Phytoplankton Periodicity: the Interactions of Form, Function and Environmental Variability. *Freshw. Biol* 14 (2), 111–142. doi:10.1111/j.1365-2427.1984.tb00027.x

Rojo, C., and Álvarez-Cobelas, M. (2003). Are There Steady-State Phytoplankton Assemblages in the Field? *Hydrobiologia* 502 (1-3), 3–12. doi:10.1023/B:HYDR.0000004266.79941.cc

Sabater, S., Artigas, J., Durán, C., Pardos, M., Romaní, A. M., Tornés, E., et al. (2008). Longitudinal Development of Chlorophyll and Phytoplankton Assemblages in a Regulated Large River (The Ebro River). *Sci. Total Environ.* 404 (1), 196–206. doi:10.1016/j.scitotenv.2008.06.013

Salmaso, N., Naselli-Flores, L., and Padisák, J. (2015). Functional Classifications and Their Application in Phytoplankton Ecology. *Freshw. Biol.* 60 (4), 603–619. doi:10.1111/fwb.12520

Salmaso, N., and Padisák, J. (2007). Morpho-Functional Groups and Phytoplankton Development in Two Deep Lakes (Lake Garda, Italy and Lake Stechlin, Germany). *Hydrobiologia* 578 (1), 97–112. doi:10.1007/s10750-006-0437-0

Shannon, C. E., Weaver, W., and Wiener, N. (1950). The Mathematical Theory of Communication. *Phys. Today* 3 (9), 31–32. doi:10.1063/1.3067010

Sournia, A. (1978). "Phytoplankton Manual," in *Monographs on Oceanographic Methodology*. Paris: UNESCO, 6, 337.

Spellerberg, I. F., and Peter, J. F. (2003). "A Tribute to Claude Shannon (1916–2001) and a Plea for More Rigorous Use of Species Richness, Species Diversity and the 'Shannon–Wiener' Index.". *Glob. Ecol. Biogeogr.* 12 (3), 177–179. doi:10.1046/j.1466-822x.2003.00015.x

Steinberg, C. E. W., and Hartmann., H. M. (1988). Planktonic Bloom-Forming Cyanobacteria and the Eutrophication of Lakes and Rivers. *Freshw. Biol* 20 (2), 279–287. doi:10.1111/j.1365-2427.1988.tb00452.x

Sun, T, Y., Liu, J., and Y Li, H. (2021). Biocommunity Structure of Chagan Lake. *J. Jilin Agric. Univ.* 43 (4), 8. doi:10.13327/j.jjlau.2019.5013

Taucher, J., and Oschlies, A. (2011). Can We Predict the Direction of marine Primary Production Change under Global Warming? *Geophys. Res. Lett.* 38, 1–6. doi:10.1029/2010gl045934

Taylor, J. M., Lizotte, R. E., and Testa, S. (2019). Breakdown Rates and Associated Nutrient Cycling Vary between Novel Crop-Derived and Natural Riparian Detritus in Aquatic Agroecosystems. *Hydrobiologia* 827 (1), 211–224. doi:10.1007/s10750-018-3766-x

Thamatrakoln, K. (2021). Diatom Ecophysiology: Crossing Signals on the Road to Recovery from Nutrient Deprivation. *Curr. Biol.* 31, R253–R254. doi:10.1016/j.cub.2021.01.016

Tian, W., Zhang, H., Zhao, L., Xu, X., and Huang, H. (2016). The Relationship between Phytoplankton Evenness and Copepod Abundance in Lake Nansihu, China. *Ijerph* 13 (9), 855. doi:10.3390/ijerph13090855

Tilman, D., Kilham, S. S., and Kilham, P. (1982). Phytoplankton Community Ecology: The Role of Limiting Nutrients. *Annu. Rev. Ecol. Syst.* 13 (1), 349–372. doi:10.1146/annurev.es.13.110182.002025

Tõnno, I., Talas, L., Freiberg, R., Kisand, A., Belle, S., Stivrins, N., et al. (2021). Environmental Drivers and Abrupt Changes of Phytoplankton Community in Temperate lake Lielais Svētiņu, Eastern Latvia, over the Last Post-Glacial Period from 14.5 Kyr. *Quat. Sci. Rev.* 263, 107006. doi:10.1016/j.quascirev.2021.107006

Touzet, N. (2011). Mesoscale Survey of Western and Northwestern Irish Lakes - Spatial and Aestival Patterns in Trophic Status and Phytoplankton Community Structure. *J. Environ. Manage.* 92 (10), 2844–2854. doi:10.1016/j.jenvman.2011.06.034

Utermöhl, H. (1958). Zur Vervollkommnung der quantitativen Phytoplankton-Methodik. *SIL Commun. 1953-1996* 9 (1), 1–38.

Vadeboncoeur, Y., Peterson, G., Vander Zanden, M. J., and Kalff, J. (2008). Benthic Algal Production across lake Size Gradients: Interactions Among

Morphometry, Nutrients, and Light. *Ecology* 89 (9), 2542–2552. doi:10.1890/07-1058.1

Visser, P. M., Verspagen, J. M. H., Sandrini, G., StalMatthijs, L. J., Matthijs, H. C. P., Davis, T. W., et al. (2016). How Rising CO2 and Global Warming May Stimulate Harmful Cyanobacterial Blooms. *Harmful Algae* 54 (apr), 145–159. doi:10.1016/j.hal.2015.12.006

Wang, M. C., Liu, X. Q., and Zhang, J. H. (2002). Assessment Methods and Classification Standards of lake Eutrophication. *China Environ. Monit.* 18 (5), 3. doi:10.3969/j.issn.1002-6002.2002.05.018

Weithoff, G., Lorke, A., and Walz, N. (2000). Effects of Water-Column Mixing on Bacteria, Phytoplankton, and Rotifers under Different Levels of Herbivory in a Shallow Eutrophic lake. *Oecologia* 125 (1), 91–100. doi:10.1007/pl00008896

Whitton, B. A. (2012). Changing Approaches to Monitoring during the Period of the 'Use of Algae for Monitoring Rivers' Symposia. *Hydrobiologia* 695 (1), 7–16. doi:10.1007/s10750-012-1121-1

Winder, M., and Sommer, U. (2012). Phytoplankton Response to a Changing Climate. *Hydrobiologia* 698 (1), 5–16. doi:10.1007/s10750-012-1149-2

Wu, Z., Cai, Y., Liu, X., XuXu, C. P., Chen, Y., and Zhang, L. (2013). Temporal and Spatial Variability of Phytoplankton in Lake Poyang: The Largest Freshwater lake in China. *J. Great Lakes Res.* 39, 476–483. doi:10.1016/j.jglr.2013.06.008

Wurtsbaugh, W. A., Paerl, H. W., and Dodds, W. K. (2019). Nutrients, Eutrophication and Harmful Algal Blooms along the Freshwater to marine Continuum. *WIREs Water* 6 (5), e1373. doi:10.1002/wat2.1373

Xu, H., Paerl, H. W., Zhu, G., Qin, B., Hall, N. S., and Zhu, M. (2017). Long-term Nutrient Trends and Harmful Cyanobacterial Bloom Potential in Hypertrophic Lake Taihu, China. *Hydrobiologia* 787 (1), 229–242. doi:10.1007/s10750-016-2967-4

Yang, L.-z., and Liu, M. (2020). A Double-Activity (Green Algae Toxicity and Bacterial Genotoxicity) 3D-QSAR Model Based on the Comprehensive Index Method and its Application in Fluoroquinolones' Modification. *Ijerph* 17 (3), 942. doi:10.3390/ijerph17030942

Yao, S. C., Xue, B., and Lv, X. G. (2010). Water Quality of Lakes Evolution in Songnen Plain. *Wetland Sci.* 8 (2), 169–175. doi:10.13248/j.cnki.wetlandsci.2010.02.007

Zepernick, B. N., Gann, E. R., Martin, R. M., Pound, H. L., Krausfeldt, L. E., Chaffin, J. D., et al. (2021). Elevated pH Conditions Associated with Microcystis Spp. Blooms Decrease Viability of the Cultured Diatom Fragilaria Crotonensis and Natural Diatoms in Lake Erie. *Front. Microbiol.* 12, 1–12. doi:10.3389/fmicb.2021.598736

Zhang, L., Zhang, G. X., and Li, R. R. (2016). Water Quality Analysis and Prediction Using Hybrid Time Series and Neural Network Models. *J. Agric. Sci. Tech.* 18 (4), 975–983. http://hdl.handle.net/123456789/3925.

Zhang, S., Xiao, Y., Li, Z., Wang, S., Guo, J., and Lu, L. (2019). Turbulence Exerts Nutrients Uptake and Assimilation of Bloom-Forming Dolichospermum through Modulating Morphological Traits: Field and Chemostat Culture Studies. *Sci. Total Environ.* 671, 329–338. doi:10.1016/j.scitotenv.2019.03.328

Zhang, T. Y. (2015). *Water Quality Migration and Transformation Law and Pollution Cause Analysis of Chagan Lake*. Dissertation. Jilin Architecture University.

Zhang, Y., Peng, C., Wang, J., Huang, S., Hu, Y., Zhang, J., et al. (2019). Temperature and Silicate Are Significant Driving Factors for the Seasonal Shift of Dominant Diatoms in a Drinking Water Reservoir. *J. Ocean. Limnol.* 37, 568–579. doi:10.1007/s00343-019-8040-1

Zhang, Y., Song, C., Ji, L., Liu, Y., Xiao, J., Cao, X., et al. (2018). Cause and Effect of N/P Ratio Decline with Eutrophication Aggravation in Shallow Lakes. *Sci. Total Environ.* 627, 1294–1302. doi:10.1016/j.scitotenv.2018.01.327

Zhao, Z., Jiang, Y., Xia, L., Mi, T., Yan, W., Gao, Y., et al. (2014). Application of Canonical Correspondence Analysis to Determine the Ecological Contribution of Phytoplankton to PCBs Bioaccumulation in Qinhuai River, Nanjing, China. *Environ. Sci. Pollut. Res.* 21 (4), 3091–3103. doi:10.1007/s11356-013-2265-x

Zhu, H., Hu, X.-D., Wu, P.-P., Chen, W.-M., Wu, S.-S., Li, Z.-Q., et al. (2021). Development and Testing of the Phytoplankton Biological Integrity index (P-IBI) in Dry and Wet Seasons for Lake Gehu. *Ecol. Indicators* 129, 107882. doi:10.1016/j.ecolind.2021.107882

Conflict of Interest: The authors declare that the research was conducted in the absence of any commercial or financial relationships that could be construed as a potential conflict of interest.

Publisher's Note: All claims expressed in this article are solely those of the authors and do not necessarily represent those of their affiliated organizations, or those of the publisher, the editors, and the reviewers. Any product that may be evaluated in this article, or claim that may be made by its manufacturer, is not guaranteed or endorsed by the publisher.

frontiers | Frontiers in Earth Science

ORIGINAL RESEARCH
published: 21 April 2022
doi: 10.3389/feart.2022.781204

Geographical Distribution and Driving Meteorological Forces of Facial Expressions of Visitors in Urban Wetland Parks in Eastern China

Hongyan Li[1,2], *Xuege Wang*[1,2], *Hongxu Wei*[3,4]*, *Tingting Xia*[3], *Mengnan Liu*[3] and *Shengshu Ai*[1,2]

[1]School of Water Conservancy and Environment Engineering, Changchun Institute of Technology, Changchun, China, [2]Jilin Provincial Key Laboratory of Municipal Wastewater Treatment, Changchun Institute of Technology, Changchun, China, [3]Key Laboratory of Wetland Ecology and Environment, Research Group of Urban Forest and Wetland, Northeast Institute of Geography and Agroecology, Chinese Academy of Sciences, Changchun, China, [4]University of Chinese Academy of Sciences, Beijing, China

Interacting with aquatic environments in blue spaces is believed to benefit mental well-being. Relevant understanding is limited to regional pilot studies using self-reported emotions on questionnaires. We assessed emotional response by rating facial expressions on a large geographical scale with the purpose of detecting a relationship to microclimates. A total of 920 facial photographs were collected from Sina Weibo from 20 wetland parks in 14 eastern cities of China during 2020. Daily average air temperature, rainfall, average relative humidity (RH), and wind velocity were also recorded from the days when photographs were posted online. We found that happy expressions were higher in wetlands of eastern cities than in northern and inland cities. Sad expressions varied statistically among wetland locations. Weather records differed between temperate and subtropical climatic zones and were highly varied among cities. Happy and sad scores were driven by the change in average air temperature. Combined multivariable regression and binomial correlation suggested that increasing air temperature would not evoke positive emotions unless higher than 11.5°C, and an air temperature range of 17.5–22.3°C will be optimum to induce the presentation of a smiling face. Air humidity generally imposed a negative effect on expressions of positive emotions. Further verification of our findings is suggested on a larger geographical scale using more powerful big-data to obtain more robust conclusions.

Keywords: blue space, aquatic environment, mental well-being, emotional perception, big-data, social network service

OPEN ACCESS

Edited by:
Guobin Fu,
CSIRO Land and Water, Australia

Reviewed by:
Ahmed Kenawy,
Mansoura University, Egypt
Iwao Uehara,
Tokyo University of Agriculture, Japan

***Correspondence:**
Hongxu Wei
weihongxu@iga.ac.cn

Specialty section:
This article was submitted to Hydrosphere, a section of the journal Frontiers in Earth Science

Received: *22 September 2021*
Accepted: *23 February 2022*
Published: *21 April 2022*

Citation:
Li H, Wang X, Wei H, Xia T, Liu M and Ai S (2022) Geographical Distribution and Driving Meteorological Forces of Facial Expressions of Visitors in Urban Wetland Parks in Eastern China. Front. Earth Sci. 10:781204. doi: 10.3389/feart.2022.781204

INTRODUCTION

Ongoing urbanization is associated with mental health risks (Ventimiglia and Seedat, 2019; He et al., 2020). Mental health has been listed as one of the greatest issues for citizens and can reduce physical and psychological well-being and cause chronic disease (American Psychological Association, 2021). Anxiety and stress arise from the perceived living environment, neighborhood safety, improper use of medicine, and living in a city (Chen and Chen, 2015; Adli and Schondorf, 2020). These conditions cannot be avoided by city dwellers. Therefore, citizens need a way to cope up with these issues without a significant cost.

Contact with nature can help by promoting attention restoration (Kaplan, 1995) and reducing stress and anxiety (Ulrich et al., 1991). In general, when people mention "nature," they mean "areas containing elements of living systems including plants and nonhuman animals across a range of scales and degrees of human management, from small urban parks to relatively pristine wilderness" (Bratman et al., 2015). Experiences in urban green space have been well documented to counter anxiety and stress (Guan et al., 2017; Van den Berg, 2017; An et al., 2019; Zhou et al., 2019). Evidence exists showing that contact with blue space (freshwater ecosystems such as sea, watershed, river, lake, and coast) can also elicit positive mental responses (White et al., 2016; White et al., 2017). As a type of coastal ecosystem, wetlands attract attention due to their role in stress reduction (Sandifer et al., 2015; Sutton-Grier and Sandifer, 2019).

Mental restoration by visiting wetlands can be recognized as a positive response explained by 'attention restoration theory (ART)' (Kaplan and Kaplan, 1989) and 'stress reduction theory (SRT)' (Ulrich et al., 1991). ART asserts that people can concentrate better following an experience with nature, even merely viewing a nature scene (Kaplan and Kaplan, 1989). SRT claims that exposure to nature can improve well-being by alleviating and reducing physiological and psychological stresses (Ulrich et al., 1991). According to these two theories, the perception of biodiversity in urban wetland parks can improve emotion and generate restoration (Fuller et al., 2007; Dallimer et al., 2012; Carrus et al., 2015). According to the 'blue gym' theory, positive emotions can also be associated with the distance to a waterbody in a wetland ecosystem (White et al., 2016). Interacting with water was considered to be the most crucial factor in making a blue space restorative (Volker and Kistemann, 2011). Environmental factors in an urban green space have been found to be major drivers of improved emotions and moods (Wei et al., 2020b; Liu et al., 2021b). Considering highly similar effects between green and blue spaces on mental health (Voelker and Kistemann, 2015), aquatic environments in wetland ecosystems may also be a key driver to improving mental well-being. Relative information is scarce, and relevant evidence is greatly needed.

Continuous urbanization has reduced the frequency of human contact with nature (Roberts and Foehr, 2008). Human beings have greatly impacted regional environments over the past 10,000 years (Torrey, 2004). Cities are the most populated areas in the world (United Nations, 2004). Urbanization alters regional environments through accelerated consumption of energy and natural products, contamination, and artificial management (Torrey, 2004). Regional environments are being altered due to the increasing population around coastal cities. The frequency of flood loss is being reduced in coastal cities due to decreased rainfall events (Brody et al., 2013). Thawing icebergs raise the sea level and stimulate seawater intrusion into the inland ecosystem (Guang-lan et al., 2002; Guo et al., 2016). As a result, regional climates change in response to modified water balance and biodiversity (Guo et al., 2016; Sarkar et al., 2019). It has been demonstrated that the change of regional climates in urban forest settings can induce the responses of psychological (Park et al., 2011; Wei et al., 2020b) and physiological well-being (An et al., 2019). Therein, local air temperature, relative humidity, and sunlight spectrum were all found to impose significant effects on perceived emotions. It will be beneficial to test these responses to the change of regional microclimates in blue spaces at a larger geographical scale.

Under the guidance of ART and SRT theories, the emotional dynamic was taken as a gauge to assess mental restoration and stress reduction (Zuckerman, 1977; Ulrich, 1979). Many studies evaluated the emotional changes of subjects through self-reported scores on questionnaires (Guan et al., 2017; Zhou et al., 2019). This methodology has been considered questionable due to errors from fatigue, subjective hiding of real thoughts (Kaplan and Kaplan, 1989), and lack of validation (Aerts et al., 2018). As an alternative, facial expressions have been taken into consideration to assess emotional changes more directly and accurately (Wei et al., 2019; Wei et al., 2020a). In studies on mental response to urban green space, facial expressions have been successfully used to evaluate perceived emotions at varied scales in a pilot study (Wei et al., 2021a; Wei et al., 2021b) to regional areas across provisional regions (Wei et al., 2019; Wei et al., 2020a; Liu et al., 2021b; Mao et al., 2022). Face-reading techniques have mainly been used to detect emotional responses to experiences in green spaces. Relevant studies testing mental well-being in wetland ecosystems have rarely been conducted. The assessment of facial expressions can efficiently monitor the emotional response to nature contact at a large scale. This methodology can also improve the detection of microclimates as driving forces.

In this study, a large-scale investigation across 14 cities and 20 urban wetland parks was conducted in typical blue spaces along the eastern coastal regions of China. Big-datasets of facial expressions of positive and negative emotions and climatic factors at the same location were recorded for spatial analysis and mechanism detection. Our objective was to map the spatial distribution of emotional expressions of people visiting urban wetland ecosystems and ascertain key meteorological factors that determined this effect. We also aimed to characterize the relationship between the regional climate and emotional perceptions in urban wetlands and depict the statistical curve of this relationship. Our data and results will facilitate future studies and supply a theoretical reference for sustainable planning of urban wetland parks.

MATERIALS AND METHODS

Selected Sites and Facial Photographs

This study was conducted on 20 urban wetland parks located in 14 cities along the eastern coast of mainland China. The spatial distribution of wetland parks is shown in **Figure 1**. Sina Weibo (can be recognized as Sina Micro-blog or China Twitter) was employed as the source of facial data from a social network service (SNS) platform (Wei et al., 2019; Wei et al., 2020a; Wei et al., 2020b; Liu et al., 2021b). Photographs were collected from daily records on Sina Weibo in 2020. Facial photographs were downloaded from Sina Weibo records where wetland parks were registered as check-in places. Matching facial

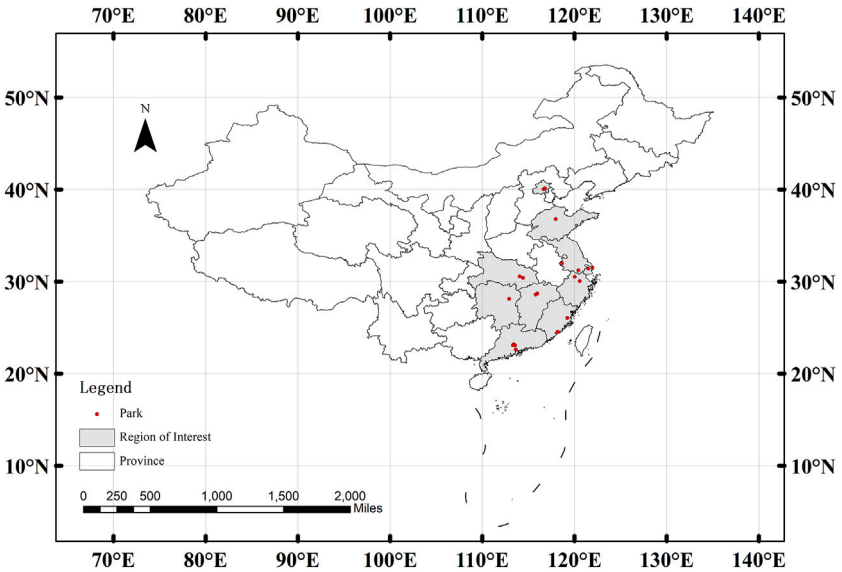

FIGURE 1 | Distribution of urban wetland parks along the eastern coast of mainland China. Red spots mark locations of wetland parks. Regions in light gray are provincial areas where objective wetlands are located.

photographs with check-in locations can enable further analysis between facial expression scores and climatic factors (Wei et al., 2020b; Liu et al., 2021b). These wetlands were chosen because there were more than 40 photographs found for each check-in place. Any parks where visitors were fewer than 40 were excluded from our dataset. The control of even distribution of replicated subjects among locations is needed because data about facial expressions were mostly abnormal and an even distribution will benefit running a regression model with expected confidence. Due to the COVID pandemic, no photograph records were found for some periods of 2020. We created data curation using a year-long dataset without specific monitoring for monthly records. A significant number of people were wearing masks during photographs, and all such photographs were excluded from our dataset. As a result, a total of 920 photographs were collected. Socioeconomic dimensions of host counties/districts for wetland parks in cities can be seen in **Supplementary Figure S1**.

Climatic Records

Climatic records were retrieved from the climatic data centre of national meteorological information of China (Climatic Data Centre, 2021). Daily records of rainfall, wind velocity, average air temperature, and average relative humidity (RH) were downloaded from historical records of meteorological stations located closest to the objective wetland park. Every record was assigned with the date as a daily mean value when each photograph was posted. A climatic record was derived from a city-wide average. Daily climatic data were collected from the day when an individual photo was downloaded from a specific wetland park. This enables regression analysis by closely matching facial data with climatic data on the same day. Mapping the distribution of climatic factors used an average of daily records when each photograph was posted to the micro-blog in Sina Weibo at the target location. Climatic records on sunshine duration, extreme air temperature, RH, etc. were not documented as independent variables to avoid significant variance inflations that could cause collinearity.

Treatment of Facial Photographs

As described before, photographs from people with facial masks were not usable. In addition, all photographs had to contain five facial organs, namely, the eyes, eyebrows, nose, mouth, and ears, for each subject. Selfies or photographs taken by others were kept, but photographs with more than one subject had to be cropped to leave only one face per image. Processed photographs were rotated to make the face perpendicular to the horizontal line to ensure the highest analyzing accuracy.

Facial Expression Analysis

Photographs were analyzed using FireFACE™ software version 1.0 to determine scores for happy and sad expressions (Wei et al., 2020a; Wei et al., 2021a; Liu et al., 2021b). This version of FireFACE can recognize three types of facial expressions, namely, neutral, happy, and sad (total frequency of 100%), but only happy and sad scores were used in this study. Happy and sad scores are percent frequencies that a face is about to present positive and negative emotions, respectively. The software was trained to recognize facial expressions using 30,000 photographs containing happy, sad, and neutral expressions (Wei et al., 2020a). The software was trained to recognize each emotion using about 10,000 photographs. Only one face was presented in each photograph for training, and all subjects were visitors to urban forest parks in mainland China. Training photographs were manually classified into three types of expressions, that is, happy, sad, and neutral for positive, negative, and indifferent

affects, respectively. Machine learning was carried out by training the computer to recognize affects by coding directions until matching accuracy reached 80%. During this process, the computer was trained by recognizing a facial photograph with typical characteristics of facial organs and all possible combinations of their muscles for each type of affect. The actual accuracy was validated to be as high as about 90% for happy and sad scores. In brief, a total of 20 photographs were randomly chosen from a pool with an objective affect that had been recognized by the machine. Experts were invited to evaluate the emotions in each photograph. Hence, their matching accuracies were averaged and used to compare with those in 20 most recently published studies in the domain of facial recognition and expression rating. Details concerning validation of scores for these two expressions can be found in the work of Guan et al. (2021).

Statistical Analysis

Both facial expression scores and climatic factors were averaged for every wetland park, and their spatial distributions were mapped using ArcGIS v10.2 software. The variations of happy and sad scores were mapped by pools of data in spring (May, April, and May), summer (June, July, and August), autumn (September, October, and November), and winter (December, January, and February) seasons. Scattered data and interquartile ranges (IQRs) were described in box–whisker plots for happy and sad scores. Statistics were finished using SAS software (SAS Institute, Cary, NC, United States). Data were log-transformed to enable statistical analysis, but results were transformed back to raw data when shown in tables and figures. Log-transformation was performed to enable statistics depending on the general linear (GLM) models for analyzing the hydrological response to climates (Engeland and Hisdal, 2009; Osuch et al., 2017). Analysis of variance (ANOVA) was used to detect differences across wetland parks. Stepwise regression was employed to analyze combined relationships between climatic factors and expressional scores using log-transformed data. Thereafter, a type-I analysis of likelihood ratio test was conducted on contributions of rainfall, wind velocity, average air temperature, and average RH to happy and sad scores. When significant contributions were detected, a zero-inflated negative binomial (ZINB) model was used to regress the four climatic factors to happy and sad scores (Wei et al., 2021a). The maximum likelihood parameters of climatic factors for each existing record were estimated, and a significant response to climatic dose was screened according to the Wald chi-square test at the 0.05 level. All maximum likelihood parameter (MLP) estimates on happy and sad scores were regressed by binomial models to detect the critical values of climates as driving forces that formed presentations of facial expressions. We employed the identical value of 0.5 as a standard to screen the availability of regressed results by binomial models (Tsakiri et al., 2018; Fu et al., 2021). This also reveals the upper or lower limits of estimated contributions to the critical climatic dose. The characteristics of binomial models were used to analyze the extent to which climatic factors drove the change of facial expressions. Pearson correlation was employed to detect the relationship between paired variables among parameters about topography (latitude and longitude), socioeconomic dimension (National Bureau of Statistics, 2020) (see **Supplementary Figure S1**), and meteorological records.

RESULTS

Spatial Distribution of Facial Expressions

Whisker–box plots for happy and sad scores are shown in **Figure 2**. Scattered data for happy scores (**Figure 2A**) were more homogeneous than those for sad scores (**Figure 2B**). The data of happy scores were mostly dispersed around the IQR between 95 and 5% with little dispersed diffusion (**Figure 2A**). However, sad scores showed a more heterogeneous dispersion pattern due to many over-medium data dispersed with big diffusions outside the 95% upper limit of IQR (**Figure 2B**). In addition, medium values of sad scores shared a closer IQR with a lower limit of 5% quartile across most cities.

Urban forest park visitors showed a heterogeneous pattern of happy scores' distribution in spring (**Figure 3A**). In summer, happy scores tended to be higher in the central part than those in northern and southern parts (**Figure 3B**). Although Dongguan, Fuzhou, and Guangzhou were close to the southern seaside, visitors did not show happy scores significantly higher than in other parks. In autumn and winter seasons, visitors showed a higher level of happy scores in the south than in the north (**Figures 3C,D**). The sad score was also distributed as a heterogeneous pattern among visitors in wetland parks (**Figure 3E**). Again, summer visitors showed higher levels of sad scores in the central part of the study area (**Figure 3F**). In autumn, sad scores tended to be higher in visitors of inland wetland parks than those at coastal parks (**Figure 3G**). Visitors mostly showed an even distribution pattern of sad scores in winter with regional levels lower than those in adjacent parks in Fuzhou and Huzhou (**Figure 3H**).

Spatial Distribution of Climatic Factors

The average air temperature showed extreme contrasting levels for adjacent places where visitors took photographs in wetland parks (**Figure 4A**). For example, the average air temperature in the Haishi Bridge Wetland Park was 23.61°C, which was higher than that in the Dongjiao Wetland Park (15.15°C) in Beijing (**Table 1**). In Shanghai, the average air temperature in the Dongtan Wetland Park (25.62°C) was higher than that in the Wusong-Fort Bay Park (18.28°C). Contrasting records of average air temperature were also observed between Nansha and Daguan wetland parks in Guangzhou. Extreme maximum and minimum daily climatic records are shown in **Supplementary Table S2**.

Rainfall was generally higher in wetlands located in southern cities than that in northern ones (**Figure 4B**). Rainfall in wetland parks in Beijing ranged from 0.06 to 0.07 mm, which was lower than that in the Jiulong Lake Wetland Park in Nanchang (8.62 mm) and Huayang Lake Wetland Park in Dongguan (10.97 mm) (**Table 1**). Contrasting records also existed for rainfall in regionally adjacent wetland parks (**Figure 4B**). For example, in Nanchang, rainfall in the

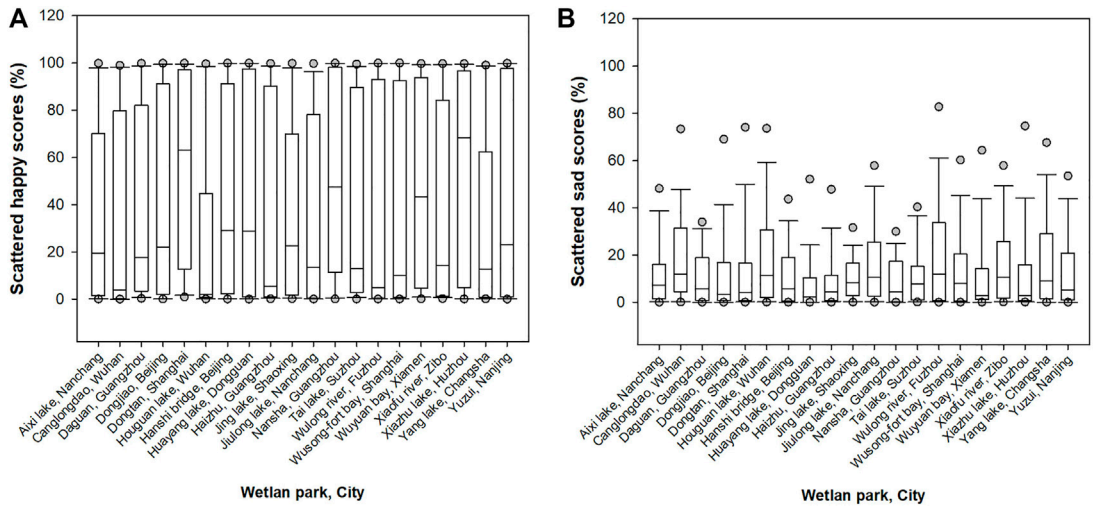

FIGURE 2 | Whisker–box plots for happy **(A)** and sad **(B)** scores of visitors in 20 urban wetland parks at the eastern cities of China. Whiskers label 95% (upper) and 5% (lower) quartiles to bars at the top and bottom, respectively; box ends at 75% (top) and 25% (bottom) quartiles; dash within the box labeles the median value of data in a city; and scattered dots in gray color label extreme records of raw data with the highest and lowest values at the top and bottom, respectively.

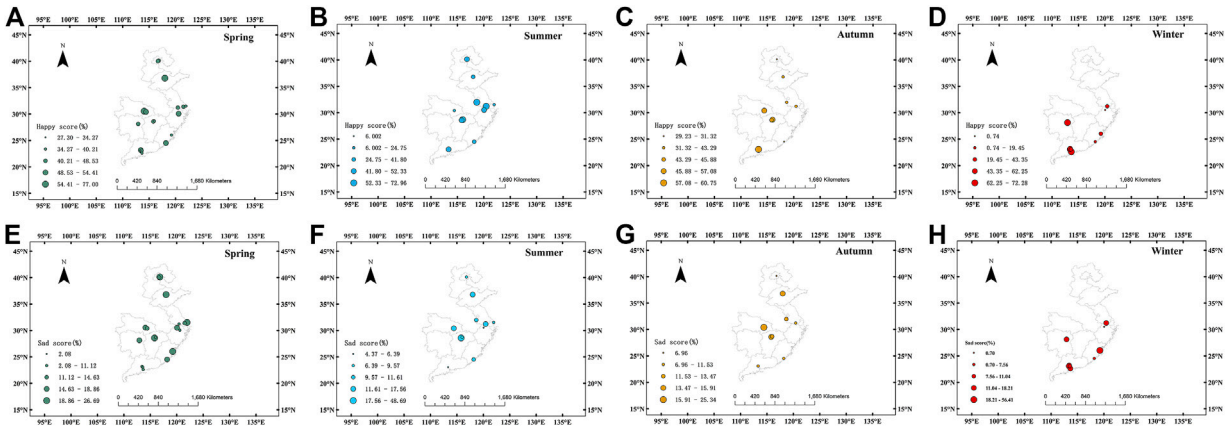

FIGURE 3 | Seasonal geographical distributions of happy **(A–D)** and sad **(E–H)** scores of visitors in urban wetland parks at cities of East China. The size of a spot and its adjacent value together remark the average of records when visitors posted their photographs to Sina Weibo at the aimed places.

Jiulong Lake Wetland Park was higher (8.62 mm) than that in the Aixi Lake Park (0.76 mm) (**Table 1**). In Dongguan, rainfall in Huayang Lake was higher than that in Daguan (0.76 mm) and Nansha (4.76 mm) wetland parks in Guangzhou.

The distribution of average RH in the study area showed a similar pattern with rainfall, which was higher in southern cities than in northern ones; contrasting records existed for adjacent wetland parks (**Figure 4C**). For example, the average RH in wetland parks in Beijing ranged between 32.55 and 52.07% which was generally lower than that in the Xiaofu Lake Wetland Park in Zibo (67.73%) and that in the Yuzui Wetland Park in Nanjing (66.08%) (**Table 1**). In Guangzhou, the average RH in the Nansha Wetland Park (81.50%) was higher than that in Haizhu (69.64%) and Daguan wetland parks (68.10%).

Wind velocity was higher in coastal cities than that in inland cities except for Beijing (**Figure 4D**). Wind velocity in wetland parks of Beijing city ranged from 2.0 to 2.5 m s^{-1}, which was higher than that in the Xiaofu River Wetland Park in Zibo (1.58 mg s^{-1}) (**Table 1**). Wind velocity in wetland parks in Wuhan ranged between 1.0 m s^{-1} and 1.5 m s^{-1}, which was lower than that in wetland parks in eastern coastal cities.

Stepwise Regression of Climatic Factors on Facial Scores

The average air temperature was the only climatic factor that generated a significant relationship with happy (F = 7.79; p = 0.0058) and sad scores (F = 3.90; p = 0.0499). The average air temperature had a positive relationship with happy scores, with a parameter estimate of 1.8079 ± 0.6477 (standard error) (type-II sum of squares [SS] = 36.51). In contrast, the average air

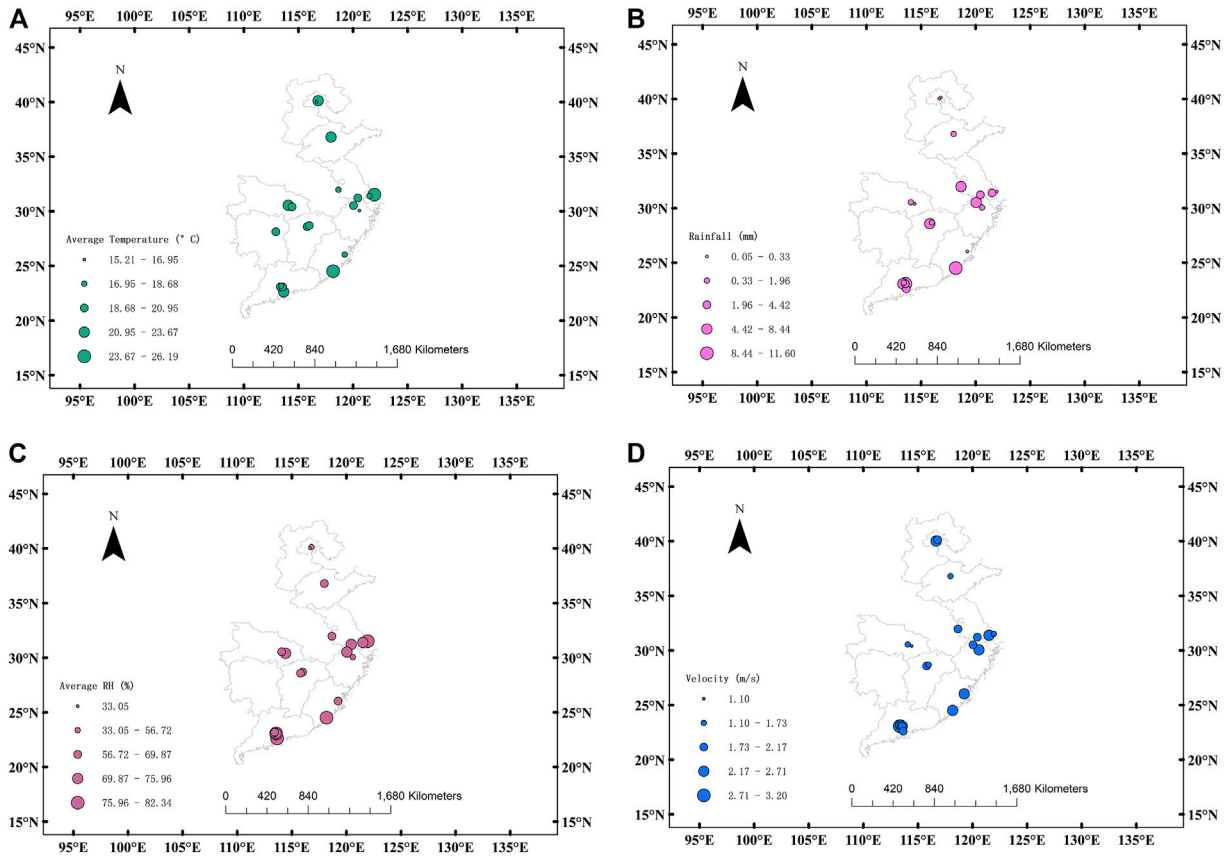

FIGURE 4 | Geographical distribution of annual average air temperature **(A)**, rainfall **(B)**, average relative humidity (RH) **(C)**, and wind velocity **(D)** in urban wetland parks. Spots in dark red, light blue, green, and pink mark annual average air temperature, rainfall, average RH, and wind velocity, respectively. The size of a spot and its adjacent value together remark the average of records when visitors posted their photographs to Sina Weibo at the aimed places.

temperature had a negative relationship with sad scores, with a parameter estimate of -1.3219 ± 0.6696 (type-II SS = 19.33). Therefore, the average air temperature had an overall higher direct contribution to happy scores than to sad scores.

Multivariable Regression Analysis of Climatic Factors on Facial Scores

The type-I analysis of likelihood ratio test by ZINB models indicated that all four types of climatic factors (average air temperature, rainfall, average RH, and wind velocity) had significant contributions to happy (**Supplementary Table S1**) and sad scores (**Supplementary Table S2**).

The average air temperature generated significantly negative contributions to happy scores in the range of 14–20°C (**Supplementary Table S3**). The estimates in the ZINB model fell in the range of -30 to -5. Rainfall only generated five significant contributions to happy scores. Generally, the estimates of rainfall contributions to happy scores increased with the increase in rainfall level from 0.5 to 33.7 mm; however, the contribution was estimated to be negative when rainfall was 23.9 mm (**Supplementary Table S3**). The average RH showed significant contributions to happy scores in the range of 14–67%. The estimate of RH contribution was generally indicated to decrease with the increase in RH level. When the average RH was 67%, contributions were estimated to be negative (**Supplementary Table S3**). Wind velocity showed a generally increasing trend of estimated contributions from 10 at 0.8 m s^{-1} to 22 at 3.4 m s^{-1} (**Supplementary Table S3**).

The average air temperature had fluctuant contributions to sad scores with estimates alternating between positive and negative levels in a range between 4.3 and 31°C (**Supplementary Table S4**). Rainfall had mostly positive contributions to sad scores at most levels, but the contributions were estimated to be negative at the levels of 0.7, 1.9, 8.4, and 11.0 mm (**Supplementary Table S4**). The average RH had a trend of decreasing contributions to sad scores from the levels of 26–58%. Thereafter, when RH increased higher than 58%, its contributions were mostly positive except for at the level of 66% (**Supplementary Table S4**). Wind velocity had fluctuant contributions of alternately positive and negative estimates to sad scores in a range between 0.2 m s^{-1}–5.0 m s^{-1} (**Supplementary Table S4**).

Model Description of Climatic Factors on Facial Scores

According to data in **Supplementary Table S3**, the relationship between levels of climatic factors (average air

TABLE 1 | Difference of climatic factor records for visitors taking photographs in different wetland parks from cities along the eastern coast of mainland China.

City	Wetland park	*n*	AveT (°C)			Rainfall (mm)			AveRH (%)			Wind velocity (m s^{-1})		
			Mean	SD	Difference	Mean	SD	Difference	Mean	SD	Difference	Mean	SD	Difference
Beijing (inland)	Dongjiao	43	15.15	2.02	g	0.06	0.38	bcd	32.55	12.49	k	2.59	0.90	bc
	Haishi Bridge	46	23.61	6.07	b	0.07	0.29	d	52.07	15.05	j	2.04	0.54	def
Changsha (inland)	Yang Lake	45	19.90	4.37	de	3.02	6.45	cd	73.12	15.08	bcde	2.20	0.93	def
Dongguan (coastal)	Huayang Lake	44	19.34	4.06	de	10.97	13.10	a	80.05	11.73	a	2.47	0.47	bc
Fuzhou (coastal)	Wulong River	48	18.68	4.30	def	0.33	0.49	d	67.06	10.27	efg	2.34	1.26	cde
Guangzhou (coastal)	Daguan	49	18.20	3.36	def	0.76	1.62	bcd	68.10	11.51	defg	2.52	1.27	bcd
	Haizhu	48	20.96	5.62	cd	8.31	24.38	ab	69.64	13.35	cdefg	3.25	0.99	a
	Nansha	41	23.10	5.24	b	4.23	11.58	cd	81.50	10.87	a	2.06	0.81	def
Huzhou (coastal)	Xiazhu Lake	47	20.85	5.55	cd	7.77	10.95	abcd	75.27	12.89	abcd	1.95	0.49	efg
Nanchang (inland)	Aixi Lake	48	19.74	4.54	de	0.76	2.09	bcd	64.82	13.56	gh	1.73	0.47	fgh
	Jiulong Lake	47	20.29	3.01	cd	8.62	27.87	a	62.02	17.88	hi	1.93	0.68	fg
Nanjing (coastal)	Yuzui	47	18.18	4.61	ef	7.24	24.45	abcd	66.08	13.87	fgh	1.86	0.47	fg
Shanghai (coastal)	Dongtan	46	25.62	3.41	a	0.25	1.26	e	82.03	10.69	a	1.64	0.47	gh
	Wusong-Fort Bay	45	18.28	5.41	ef	4.82	7.66	abc	72.16	13.86	bcdef	2.66	0.80	bc
Shaoxing (coastal)	Jing Lake	47	17.15	4.59	gf	1.74	6.54	abc	56.35	12.36	i	2.74	0.83	b
Suzhou (coastal)	Tai Lake	46	19.53	5.78	de	3.75	12.25	d	75.96	14.97	abc	1.84	0.86	fgh
Wuhan (inland)	Canglongdao	47	19.46	5.00	de	0.19	1.20	bcd	74.70	8.81	abcd	1.10	0.63	I
	Houguan Lake	41	22.73	3.71	b	0.96	2.94	abc	69.33	12.84	cdefg	1.58	0.59	h
Xiamen (coastal)	Wuyuan Bay	46	26.19	3.91	a	11.60	30.91	ab	78.08	7.75	ab	2.54	0.60	bc
Zibo (coastal)	Xiaofu River	49	22.43	3.21	bc	1.96	5.70	bcd	67.73	5.87	cdefg	1.58	0.66	h

AveT, average air temperature; rainfall, annual average precipitation; AveRH, average relative humidity; wind velocity, wind velocity per every 2 min; SD, standard deviation; n, number of observations; different letters along a vertical column indicate significant difference using log-transformed data according to the Duncan test at the 0.05 level.

temperature, rainfall, average RH, and wind velocity) and their estimated contributions on happy and sad scores can be described by binomial models (**Figure 5**).

The relationship between average air temperature and maximum likelihood parameter (MLP) estimates on happy scores can be described by U-shape binomial curves. MLP estimates on happy scores decreased with the increase in average air temperature up to 11.468°C, when MLP reached the lower limit of -25.988 (**Figure 5A**). The relationship between rainfall levels and MLP estimates on happy scores can also be described by a U-shape binomial curve where MLP estimates on happy scores decreased with the increase in rainfall up to 18.810 mm, when estimated MLP-happy scores reached the lower limit of 32.862 (**Figure 5B**). The relationship between average RH and MLP estimates on happy scores can be described by a negative binomial curve (**Figure 5C**). Theoretically, when the average RH became infinitesimal, the MLP estimate on happy scores was the lowest at a value of -44.394 (**Table 2**). In contrast, the relationship between wind velocity and MLP estimate on happy scores can be described by a positive binomial curve (**Figure 5D**). Theoretically, with the increase of wind velocity up to 6.538 m s^{-1}, MLP estimates increase to the upper limit of 17.091. Overall, the coefficient of determination, R^2, was higher than the identical value of 0.5 only for regressions against average air temperature and RH. Therefore, regressed results of MLP estimates on happy scores in response to changes of air temperature and RH were more reliable than regressions against rainfall and wind velocity changes.

The relationship between average air temperature and MLP estimates on sad scores can also be described by a reciprocal U-shape binomial curve (**Figure 6A**). With the increase of average air temperature to 22.270°C, MLP estimates reached the upper limit of 20.315 (**Table 2**). With the increase in rainfall, the MLP estimate on sad scores showed a small increasing trend (**Figure 6B**). Rainfall had an infinite closeness to the lowest level of 5.792 mm when MLP was estimated at the lower limit of 47.336 (**Table 2**). The relationship between average RH and MLP estimates on sad scores can be described by a U-shape binomial curve (**Figure 6C**). With the increase of the average to 53.285%, MLP estimates reached the lower limit of 13.340 (**Table 2**). The relationship between wind velocity and MLP estimates on sad scores was a barely increasing binomial curve (**Figure 6D**). Theoretically, with a wind velocity increase to 5.307 m s^{-1}, MLP estimates on sad scores had an infinite closeness to the upper limit of 17.537 (**Table 2**). However, because all R^2 values for regressions were lower than 0.5, none of the regressed MLP estimates on sad scores can be reliable.

Pearson Correlations

Latitude was detected to have a negative relationship with rainfall (R = -0.4720; p = 0.0356) and RH (R = -0.6355; p = 0.0026) (**Supplementary Figure S2**). In contrast, both population and gross domestic product (GDP) had positive relationships with wind velocity (R = 0.6439, p = 0.0022 and R = 0.6258, p = 0.0032, respectively).

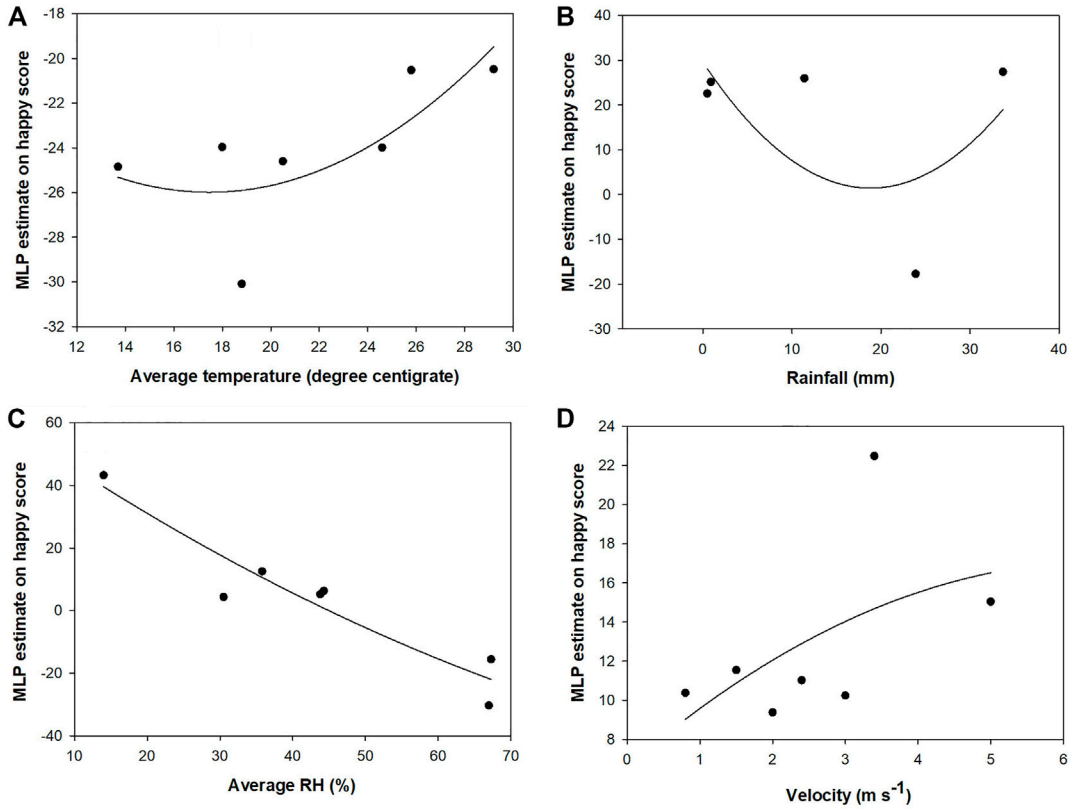

FIGURE 5 | Binomial regression of maximum likelihood parameter (MLP) estimates of climatic factors (average temperature, **(A)**; rainfall, **(B)**; average RH, **(C)**; wind velocity, **(D)**) on happy scores. Spots are significant MLP estimates of an existing microclimatic record indicated by a zero-inflated negative binomial model. Data are derived from **Supplementary Table S3**. Coefficients of regressed models can be found in **Table 2**.

TABLE 2 | Coefficients from binomial regressions of climatic factors on maximum likelihood parameter (MLP) estimates on happy and sad scores.

Facial expression	Climate	R^2	a	b	y0	Critical independent	Predicted dependent
Happy	AveT	0.5428	0.047	−1.653	−11.555	17.468	−25.988
	Rainfall	0.3563	0.079	−2.987	60.956	18.810	32.862
	AveRH	0.8921	0.006	−1.604	60.956	100.000	−44.394
	Wind velocity	0.2923	−0.245	3.204	6.620	6.538	17.091
Sad	AveT	0.1883	−0.414	18.426	−184.852	22.270	20.315
	Rainfall	0.0143	0.009	−0.108	47.645	5.729	47.336
	AveRH	0.0845	0.067	−7.098	202.439	53.285	13.340
	Wind velocity	0.0096	−0.573	6.083	1.393	5.307	17.537

*Data were calculated from sources of **Figures 4**, **5**; R^2, coefficient of determination; coefficients are adapted from the binomial function: $f(x) = ax^2 + bx + y0$.*

DISCUSSION

Spatial Variation of Emotional Expressions

In our study, happy scores of visitors in wetlands were mapped by a spatial distribution pattern in the range of longitudes between 20°N and 40°N. This pattern was formed by dual drivers of regional air temperature and RH as positive and negative forces, respectively. For example, the high level of happy scores found in the Xiaofu River Park at Zibo city was driven by the meanwhile records of high air temperature and low humidity. However, it was interesting to find that both happy and sad scores showed heterogeneous patterns in spring and winter, which were formed by alternatively high and low levels of scores in the same region although their meteorological conditions were not always different. We attribute these findings to four explanations. First, in natural spaces, emotional well-being can be perceived in response to not only regional weather conditions but also variations in locations (Wei et al., 2019), walking orientations (Wei et al., 2021b), time course (Wei et al., 2021a), and even biodiverse levels (Marselle et al., 2019; Methorst et al., 2021). Microclimates can drive changes in emotional expressions, but they are unlikely to be unique drivers.

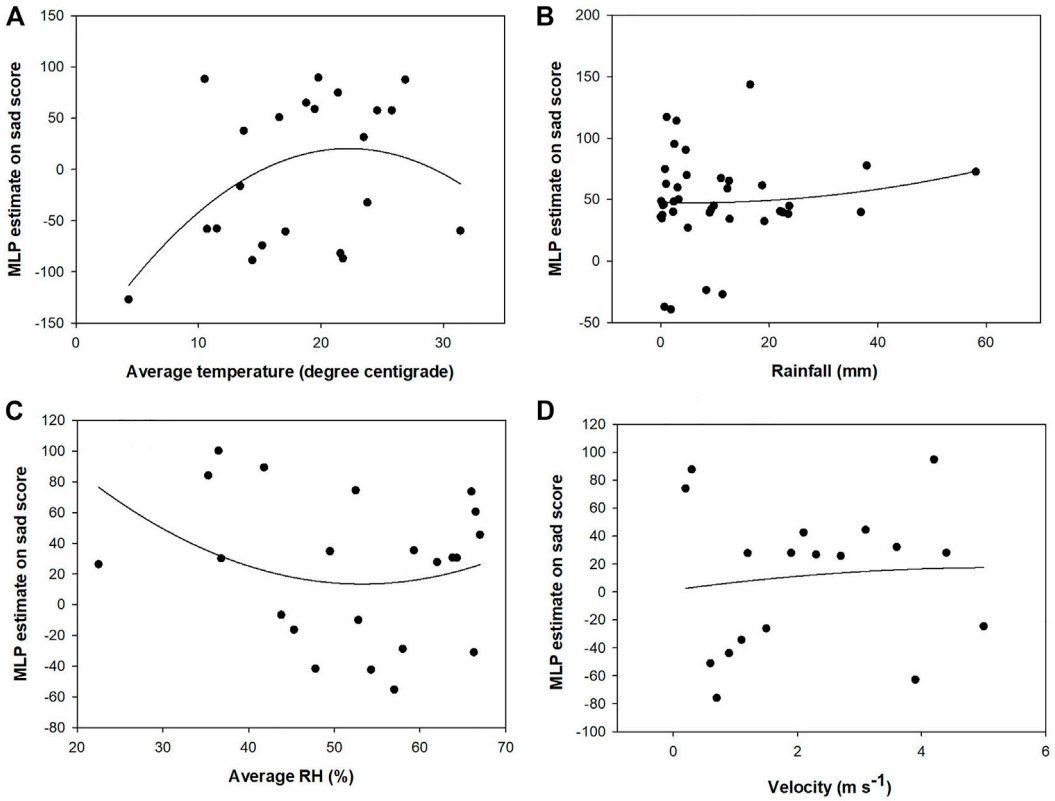

FIGURE 6 | Binomial regression of maximum likelihood parameter (MLP) estimates of climatic factors (average temperature, **(A)**; rainfall, **(B)**; average RH, **(C)**; wind velocity, **(D)**) on sad scores. Spots are significant MLP estimates of an existing microclimatic record indicated by a zero-inflated negative binomial model. Data are derived from **Supplementary Table S4**. Coefficients of regressed models can be found in **Table 2**.

Second, emotions can also be associated with socioeconomic factors, which, however, we did not detect in this study. In a study, facial expressions were obtained in university campuses across mainland China (Wei et al., 2020a). Therein, both happy and sad scores showed big spatial variations which were highly associated with municipal dimensions in host cities. Third, emotional responses in our study were perceived by combined experiences of landscape metrics of green plus green spaces rather than the single suite of patchy features in blue spaces. Studies have demonstrated that people can perceive different affects in face of varied landscape metrics in both green and blue spaces (Liu et al., 2021a; Zhang et al., 2021). Finally, because our data were obtained from an SNS platform of Sina Weibo, pieces of will by people to post their faces online had a nature of existing uncertainties, which belong to a type of human error to expose their affects (Kaplan and Kaplan, 1989). We admit our data regarding facial expressions had systematic errors during collection and screening. All of our data were randomly allocated, and all suffered possible errors at the same technical level. Therefore, our results concerning spatial distributions of emotional expressions are acceptable and are adequate for further analysis.

Spatial Distribution of Microclimates

Our climatic factors were not shaped by the long-term climatology of local microclimates. Instead, the distribution of our climatic factors was mapped according to daily records during the time photograph suppliers visited wetland parks in our study area. This is why none of our climatic records showed an expected distribution pattern, for example, along a north–south geographical gradient (Wang and Tang, 2003; Lu and Xiong, 2013; Li et al., 2015; Liu et al., 2016). Generally, the distribution of our climatic factors had two characteristics. First, regional climates greatly differed in different climatic zones, including climates in subtropical and tropical regions (Wei and He, 2021). For instance, the average RH of wetland parks in Beijing was lower than that in parks of Wuhan and Nanchang, but their wind velocity was higher. Second, climatic records may be extremely different for wetland parks in regional cities. This was usually found for air temperature and rainfall in wetland parks around Shanghai and Guangdong. This resulted from people taking photographs when they were visiting these wetland parks during specific weather. In subtropical regions, people were more likely to visit wetland parks in Shanghai in weather with higher air temperature and air humidity, but lower wind velocity occurred contrary to the weather when people visited the Jing Lake Wetland Park in Shaoxing. In tropical regions such as wetland parks in Guangzhou, people were prone to visit in weather with higher air temperature, but lower rainfall and air humidity occurred, in contrast to the Huayang Lake Wetland Park in Dongguan. To our knowledge, no available evidence accounts for these differences.

Our results can supply reference to further detect and explain why people like to visit these parks in different weathers.

Air Temperature Drives Presentation of a Smile

The average air temperature was the only climatic parameter that promoted positive emotions. Our results are supported by another set of data collected for urban forests across 12 cities in eastern China, which concurs with results found by Liu et al. (2021b). These results suggest a common phenomenon that air temperature can be the key driver among all climatic factors to determine positive expressions for visitors when both in urban green spaces (Guan et al., 2017; Van den Berg, 2017; An et al., 2019; Zhou et al., 2019) and when experiencing urban blue spaces (White et al., 2016; White et al., 2017). Hence, we conclude that those experiencing aquatic environments in wetland parks feel more comfortable when air temperature is warmer. In our study, critical values for average air temperature records fell in a range between 17.468 and 22.270°C, during which the influence of air temperature on negative expressions was the highest. Only when air temperature increased to be higher than this critical range up to approximately 30 °C, the negative effect of air temperature on positive expressions gradually reduced. Therefore, high air temperature favored the presentation of positive emotions by depressing the negative effects. The range of air temperature was also suggested to be comfortable for urban forest experiencers in a range of 12–22°C (Jeong et al., 2016), which was lower than the suggested air temperature range for comfort in wetland parks. However, our findings about the driving force from temperature were contradicted by those found in northern forest parks, where the beneficial effect of temperature on smile presentation tended to diminish when the annual temperature was higher than 6.05°C (Mao et al., 2022). Thus, people's perception toward temperature change should be differed by microclimatic conditions on contrasting landforms between the deep inland and the coast.

Potential Force of Climatic Drivers to Elicit a Smile

Rainfall did not have a direct relationship with facial expression. Standard deviation (SD) was much higher in parks with low rainfall (lower than 1.0 mm), which made these parks unlikely to receive precipitation. When rainfall was higher than 5.27 mm, the contribution to elicit negative expressions increased synchronously with continuously increasing rainfall levels. When rainfall increases to be over 18 mm, it has a large step effect on the presentation of happy scores. Hence, precipitation over 18 mm is likely to increase positive emotions. Although wind velocity had positive contributions to both expressional scores, the positive contributions were estimated to be higher for happy scores than sad scores when wind velocity increased up to 6.54 m s^{-1}. Wind velocity was indicated in wetland visitors subjected to counties/districts with greater population and higher GDP, which suggests that emotional perceptions of air flow were formed by feelings about the dense crowd and developed regions rather than the real awareness about winds. Due to low levels of coefficient of determination for regressed potential forces on happy and sad scores against rainfall and wind velocity, we cannot accept the likelihoods of facial expressions by the driving forces of these two parameters. Instead, regressions against air temperature and RH can be much more reliable. The increase of air temperature was found to lose its potential force on the presentation of smiles below 11.468°C. This was lower than the lower limit of optimum air temperature range of 17.468°C. Thereafter, the increase of air temperature over 11.468°C will evoke the response of growing force on happy scores, which also fell in the optimum range of 17.468 and 22.270°C. Air humidity between the levels of 14 and 67% generally had a negative contribution to happy scores, which suggests that, for most conditions in our park places, visitors would perceive negatively driving force if air RH increased.

Rainfall and RH had no relationship with socioeconomic dimensions. Instead, their spatial distributions were determined by the latitudinal gradient, which both decreased from the south to the north in our study area. As discussed before, the potential driving forces of rainfall and RH to activate presenting smiles resulted from natural responses to the latitudinal gradient among wetlands.

Limitations of This Study

Our study has several limitations. First, our dataset was limited by the sampling size due to the time of photograph collection. Our dataset comprises a total of 920 photographs from visitors of 20 urban wetland parks in 14 cities. This means that there were 40–50 photographs per park. Facial expression scores in our photographs were used as a bulked average for a park, but their relationships with microclimatic factors were regressed by daily records (n = 920). This dataset size is comparable with that used for regression in other geographical studies. For example, in the work of Sun et al. (2021), the regression of a logistical model was validated by a total of 22 factors and 1,522 landslides. Another instance is from the work of Shahani et al. (2021), where six parameters and 64 series framed a regression. Even so, the size of the dataset in our study is still limited by the time of our data collection. Since 2020 was the first year when the pandemic was felt globally, many people were wearing a mask and were unable to be chosen as our subject. Future studies can continue our design and methodology in the coming years when the public attitude toward COVID-19 is alleviated, increasing the number of people without facial masks in urban wetland parks.

Second, regression precision was limited by distinct dates of records. We run regression models by matching microclimatic records with facial expression scores for the same day. Technically, we were not able to fully determine that the date of photograph exposure was the same day when the photo was shot. This is unlikely to cause a strong technical error in our data variation. All photographs collected were derived from micro-blogs with specific check-in information concerning a specific location. According to common sense, a normal person will not likely take a photograph at a location and post it on a micro-twitter at the same place but at another time. We suggest further efforts in determining a way to make sure both the dates of micro-blog posting and photographing fully match one another.

Third, the use of posted photographs from SNS platforms potentially affects precision due to awareness of exposure. When facial expression scores were used as a gauge to evaluate emotional response to an experience in nature, two types of photographs were used. One is photographs of people who are not conscious of being photographed; therefore, all resulting facial scores will be natural to the nature experience (Wei et al., 2020b; Wei et al., 2021a; Wei et al., 2021b; Guan et al., 2021). This type of study usually needs a dataset of photographs collected from actual visitors to urban nature in cross-over designed studies (Guan et al., 2017; Stigsdotter et al., 2017; An et al., 2019; Zhou et al., 2019). The other type concerns posted photographs derived from SNS that the photograph subject is aware of (Wei et al., 2019; Wei et al., 2020a; Liu et al., 2021b). Photographs in our study belong to this type. Subjects were aware of the photographs that were being taken; hence, their facial expressions were not spontaneous. However, they were unaware their photographs would be used for an academic study. As a result, they do not change their expression due to any potential awareness of being involved in a study. This can especially happen for oriental people, who usually choose to hide the real and extreme expressions of feelings. Nevertheless, an upgraded methodology to obtain spontaneous facial expressions is needed.

Finally, meteorological records have a distinct characteristic of seasonal variation. We collected microclimatic records across a year-long span, and we should have analyzed the seasonal variation as one source of variance. However, because our timeframe for photograph collection was the first year of a global pandemic, many people in urban wetland parks were wearing facial masks and our data for seasonal variation were extremely scattered. Some seasons only had a few photographs that could be used, and some seasons even had none. Future work should be designed with a longer period for photograph collection, enabling a better likelihood of obtaining seasonal data.

CONCLUSION

No apparent gradient distribution was observed for happy and sad expressional scores from visitors to wetlands in the eastern cities at longitudes between 20°N and 40°N. Positive facial expression tended to be higher for wetland parks located in cities close to the eastern coasts of China but not for cities around the southern coasts. Weather records showed a general spatial difference between contrasting climatic zones or in regional cities. Both happy and sad scores were affected by the change in average air temperature. Combined multivariable regression and binomial correlation suggested that increasing air temperature would not evoke positive emotions unless higher than 11.5°C, and an air temperature range of 17.5–22.3°C will be optimum to induce the presentation of a smiling face. Air humidity generally imposed a negative effect on expressions of positive emotions. Our study introduces a new approach to evaluate ecosystem services for emotional perception by the experience of aquatic environments in wetland parks. Our results can be used as a reference for further studies on the emotional response to experiencing blue spaces.

DATA AVAILABILITY STATEMENT

Restrictions apply to the datasets: The datasets presented in this article are not readily available because data are derived from human subjects with a privacy protection restriction that has been declared in the Ethic Approval Statement. Requests to access the datasets should be directed to the corresponding author.

ETHICS STATEMENT

The studies involving human participants were reviewed and approved by the Ethics Committee of School of Water Conservancy and Environment Engineering, Changchun Institute of Technology. Written informed consent for participation was not required for this study in accordance with the national legislation and the institutional requirements.

AUTHOR CONTRIBUTIONS

HL is the first author, XW is the second author, HW is the third and corresponding author, TX is the fourth author, ML is the fifth author, and SA is the sixth author. Conceptualization: HL and HW; methodology: HL and HW; software: HW; validation: HW and SA; formal analysis: HL and HW; investigation: XW, TX and ML; resources: XW, TX and ML; data curation: TX and ML; writing–original draft preparation: HL; writing–review and editing: HW; visualization: HL and HW; supervision: HW and SA; project administration: HL, HW and SA; and funding acquisition: HL, HW and SA.

FUNDING

This study was financially supported by the National Key Research and Development Program of China (grant number: 2019YFC0409102), Scientific Research Project of Education Department of Jilin Province (grant number: JJKH20220638KJ), Project of Changchun Science and Technology Bureau (grant number: 21ZGM03), and the National Natural Science Foundation of China (grant numbers: 42001117, 41971122, and 41861017).

ACKNOWLEDGMENTS

The authors acknowledge the editor and reviewers for their contributions and assistances in promoting the manuscript to the current edition. Prof. Shengshu Ai from Changchun Institute of Technology is acknowledged for his assistance in article publication.

SUPPLEMENTARY MATERIAL

The Supplementary Material for this article can be found online at: https://www.frontiersin.org/articles/10.3389/feart.2022.781204/full#supplementary-material

Figure S1 | Socio-economic dimensions of population (A), gross domestic product (GDP) (B), administrative area (C), and the distance of objective park to downtown of host-city (D) in host-counties/districts for wetland parks as study sites. Data are derived from National Bureau of Statistics (2020).

Figure S2 | Correlations between paired variables among parameters about topography (longitude and latitude), socio-economy (population, GDP, administrative area [Aarea], and the distance of objective park to downtown of host-city [Distance]), and meteorological records (temperature [T], rainfall [rain], relative humidity [RH], and wind velocity [Wind]).

REFERENCES

Adli, M., and Schöndorf, J. (2020). Does the City Make Us Ill? the Effect of Urban Stress on Emotions, Behavior, and Mental Health. *Bundesgesundheitsblatt Gesundheitsforschung Gesundheitsschutz* 63 (8), 979–986. doi:10.1007/s00103-020-03185-w

Aerts, R., Honnay, O., and Van Nieuwenhuyse, A. (2018). Biodiversity and Human Health: Mechanisms and Evidence of the Positive Health Effects of Diversity in Nature and Green Spaces. *Br. Med. Bull.* 127 (1), 5–22. doi:10.1093/bmb/ldy021

American Psychological Association (2021). APA Dictionary of Psychology [Online]. Available: https://dictionary.apa.org/emotion.

An, B.-Y., Wang, D., Liu, X.-J., Guan, H.-M., Wei, H.-X., and Ren, Z.-B. (2019). The Effect of Environmental Factors in Urban Forests on Blood Pressure and Heart Rate in University Students. *J. For. Res.* 24 (1), 27–34. doi:10.1080/13416979.2018.1540144

Bratman, G. N., Daily, G. C., Levy, B. J., and Gross, J. J. (2015). The Benefits of Nature Experience: Improved Affect and Cognition. *Landscape Urban Plann.* 138, 41–50. doi:10.1016/j.landurbplan.2015.02.005

Brody, S., Kim, H., and Gunn, J. (2013). Examining the Impacts of Development Patterns on Flooding on the Gulf of Mexico Coast. *Urban Stud.* 50 (4), 789–806. doi:10.1177/0042098012448551

Carrus, G., Scopelliti, M., Lafortezza, R., Colangelo, G., Ferrini, F., Salbitano, F., et al. (2015). Go Greener, Feel Better? The Positive Effects of Biodiversity on the Well-Being of Individuals Visiting Urban and Peri-Urban Green Areas. *Landscape Urban Plann.* 134, 221–228. doi:10.1016/j.landurbplan.2014.10.022

Chen, J., and Chen, S. (2015). Mental Health Effects of Perceived Living Environment and Neighborhood Safety in Urbanizing China. *Habitat Int.* 46, 101–110. doi:10.1016/j.habitatint.2014.11.002

Climatic Data Centre (2021). Meteorological Data Centre of China Meteorological Administration [Online]. Available: http://data.cma.cn (Accessed September 13, 2021).

Dallimer, M., Irvine, K. N., Skinner, A. M. J., Davies, Z. G., Rouquette, J. R., Maltby, L. L., et al. (2012). Biodiversity and the Feel-Good Factor: Understanding Associations between Self-Reported Human Well-Being and Species Richness. *BioScience* 62 (1), 47–55. doi:10.1525/bio.2012.62.1.9

Engeland, K., and Hisdal, H. (2009). A Comparison of Low Flow Estimates in Ungauged Catchments Using Regional Regression and the HBV-Model. *Water Resour. Manage.* 23 (12), 2567–2586. doi:10.1007/s11269-008-9397-7

Fu, G., Chiew, F. H., Zheng, H., Robertson, D. E., Potter, N. J., Teng, J., et al. (2021). Statistical Analysis of Attributions of Climatic Characteristics to Nonstationary Rainfall-Streamflow Relationship. *J. Hydrol.* 603, 127017. doi:10.1016/j.jhydrol.2021.127017

Fuller, R. A., Irvine, K. N., Devine-Wright, P., Warren, P. H., and Gaston, K. J. (2007). Psychological Benefits of Greenspace Increase with Biodiversity. *Biol. Lett.* 3 (4), 390–394. doi:10.1098/rsbl.2007.0149

Guan, H., Wei, H., Hauer, R. J., and Liu, P. (2021). Facial Expressions of Asian People Exposed to Constructed Urban Forests: Accuracy Validation and Variation Assessment. *Plos One* 16 (6), e0253141. doi:10.1371/journal.pone.0253141

Guan, H., Wei, H., He, X., Ren, Z., and An, B. (2017). The Tree-Species-Specific Effect of Forest Bathing on Perceived Anxiety Alleviation of Young-Adults in Urban Forests. *Ann. For. Res.* 60 (2), 327–341. doi:10.15287/afr.2017.897

Guang-lan, M., You-song, H., Shao-qing, W., and Zhen-yan, W. (2002). Seawater Intrusion Types and Regional Divisions in the Southern Coast of Laizhou Bay. *Chin. J. Ocean. Limnol.* 20 (3), 277–284. doi:10.1007/BF02848859

Guo, P., Jin, H., Wei, H., Li, L., and Bao, Y. (2016). Fine Root Growth and Water Use Efficiency in Alfalfa (Medicago sativaL. Cv. Gongong No. 1) Planted Along a Salinity Gradient in Coastal Area of Dalian, Northeast China. *Soil Sci. Plant Nutr.* 62 (2), 164–172. doi:10.1080/00380768.2016.1149438

He, S., Song, D., and Jian, W.-Y. (2020). The Association Between Urbanization and Depression Among the Middle-Aged and Elderly: A Longitudinal Study in China. *Inquiry* 57, 004695802096547. doi:10.1177/0046958020965470

Jeong, M.-A., Park, S., and Song, G.-S. (2016). Comparison of Human thermal Responses Between the Urban Forest Area and the Central Building District in Seoul, Korea. *Urban For. Urban Green.* 15, 133–148. doi:10.1016/j.ufug.2015.12.005

Kaplan, R., and Kaplan, S. (1989). *The Epxerience of Nature: A Psychological Perspective*. New York, NY, USA: Cambridge University Press.

Kaplan, S. (1995). The Restorative Benefits of Nature: Toward an Integrative Framework. *J. Environ. Psychol.* 15 (3), 169–182. doi:10.1016/0272-4944(95)90001-2

Li, J., Liu, H., Su, Z., and Fan, X. (2015). Changes in Wind Activity from 1957 to 2011 and Their Possible Influence on Aeolian Desertification in Northern China. *J. Arid Land* 7 (6), 755–764. doi:10.1007/s40333-015-0050-z

Liu, P., Liu, M., Xia, T., Wang, Y., and Guo, P. (2021a). The Relationship Between Landscape Metrics and Facial Expressions in 18 Urban Forest Parks of Northern China. *Forests* 12 (12), 1619. doi:10.3390/f12121619

Liu, P., Liu, M., Xia, T., Wang, Y., and Wei, H. (2021b). Can Urban Forest Settings Evoke Positive Emotion? Evidence on Facial Expressions and Detection of Driving Factors. *Sustainability* 13 (16), 8687. doi:10.3390/su13168687

Liu, S., Yan, D., Wang, H., Li, C., Qin, T., Weng, B., et al. (2016). Evaluation of TRMM 3B42V7 at the Basin Scale Over Mainland China. *Adv. Water Sci.* 27 (5), 639–651. doi:10.14042/j.cnki.32.1309.2016.05.001

Lu, A., and Xiong, Y. (2013). Systematic Change in Air Humidity in China over Last 50 Years Under Global Climate Change. *Res. Soil Water Conservation* 20 (1), 141–143.

Mao, B., Liang, F., Li, Z., and Zheng, W. (2022). Microclimates Potentially Shape Spatial Distribution of Facial Expressions for Urban Forest Visitors: A Regional Study of 30 Parks in North China. *Sustainability* 14 (3), 1648. doi:10.3390/su14031648

Marselle, M. R., Martens, D., Dallimer, M., and Irvine, K. N. (2019). "Review of the Mental Health and Well-Being Benefits of Biodiversity," in *Biodiversity and Health in the Face of Climate Change*. Editors M. R. Marselle, J. Stadler, H. Korn, K. N. Irvine, and A. Bonn (Cham: Springer International Publishing), 175–211. doi:10.1007/978-3-030-02318-8_9

Methorst, J., Bonn, A., Marselle, M., Böhning-Gaese, K., and Rehdanz, K. (2021). Species Richness Is Positively Related to Mental Health - A Study for Germany. *Landscape Urban Plann.* 211, 104084. doi:10.1016/j.landurbplan.2021.104084

National Bureau of Statistics (2020). Statistical Yearbook of China: 2020 [Online]. Available: http://www.stats.gov.cn/ (Accessed February 9, 2022).

Osuch, M., Romanowicz, R., and Wong, W. K. (2017). Analysis of Low Flow Indices Under Varying Climatic Conditions in Poland. *Hydrol. Res.* 49 (2), 373–389. doi:10.2166/nh.2017.021

Park, B.-J., Furuya, K., Kasetani, T., Takayama, N., Kagawa, T., and Miyazaki, Y. (2011). Relationship Between Psychological Responses and Physical Environments in Forest Settings. *Landscape Urban Plann.* 102 (1), 24–32. doi:10.1016/j.landurbplan.2011.03.005

Roberts, D. F., and Foehr, U. G. (2008). Trends in media Use. *Future Child.* 18 (1), 11–37. doi:10.1353/foc.0.0000

Sandifer, P. A., Sutton-Grier, A. E., and Ward, B. P. (2015). Exploring Connections Among Nature, Biodiversity, Ecosystem Services, and Human Health and Well-Being: Opportunities to Enhance Health and Biodiversity Conservation. *Ecosystem Serv.* 12, 1–15. doi:10.1016/j.ecoser.2014.12.007

Sarkar, D., Bhattacherjee, M., and Chattopadhyay, D. (2019). Influence of Regional Environment in Guiding the Spatial Distribution of Marine Bivalves along the Indian Coast. *J. Mar. Biol. Ass.* 99 (1), 163–177. doi:10.1017/S0025315417001837

Shahani, N. M., Zheng, X., Liu, C., Hassan, F. U., and Li, P. (2021). Developing an XGBoost Regression Model for Predicting Young's Modulus of Intact Sedimentary Rocks for the Stability of Surface and Subsurface Structures. *Front. Earth Sci.* 9 (1010), 761990. doi:10.3389/feart.2021.761990

Stigsdotter, U. K., Corazon, S. S., Sidenius, U., Kristiansen, J., and Grahn, P. (2017). It Is Not All Bad for the Grey City - A Crossover Study on Physiological and Psychological Restoration in a Forest and an Urban Environment. *Health & Place* 46, 145–154. doi:10.1016/j.healthplace.2017.05.007

Sun, D., Wen, H., Xu, J., Zhang, Y., Wang, D., and Zhang, J. (2021). Improving Geospatial Agreement by Hybrid Optimization in Logistic Regression-Based Landslide Susceptibility Modelling. *Front. Earth Sci.* 9 (686), 713803. doi:10.3389/feart.2021.713803

Sutton-Grier, A. E., and Sandifer, P. A. (2019). Conservation of Wetlands and Other Coastal Ecosystems: A Commentary on Their Value to Protect Biodiversity, Reduce Disaster Impacts, and Promote Human Health and Well-Being. *Wetlands* 39 (6), 1295–1302. doi:10.1007/s13157-018-1039-0

Torrey, B. B. (2004). *Urbanization: An Environmental Force to Be Reckoned with*. Washington: PRB - Resource Library.

Tsakiri, K., Marsellos, A., and Kapetanakis, S. (2018). Artificial Neural Network and Multiple Linear Regression for Flood Prediction in Mohawk River, New York. *Water* 10 (9), 1158. doi:10.3390/w10091158

Ulrich, R. S., Simons, R. F., Losito, B. D., Fiorito, E., Miles, M. A., and Zelson, M. (1991). Stress Recovery During Exposure to Natural and Urban Environments. *J. Environ. Psychol.* 11 (3), 201–230. doi:10.1016/S0272-4944(05)80184-7

Ulrich, R. S. (1979). Visual Landscapes and Psychological Well-Being. *Landscape Res.* 4 (1), 17–23. doi:10.1080/01426397908705892

United Nations (2004). *World Urbanization Prospects: The 2003 Revision*. New York: UN: United Nations.

Van den Berg, A. E. (2017). From Green Space to Green Prescriptions: Challenges and Opportunities for Research and Practice. *Front. Psychol.* 8, 268. doi:10.3389/fpsyg.2017.00268

Ventimiglia, I., and Seedat, S. (2019). Current Evidence on Urbanicity and the Impact of Neighbourhoods on Anxiety and Stress-Related Disorders. *Curr. Opin. Psychiatry* 32 (3), 248–253. doi:10.1097/yco.0000000000000496

Völker, S., and Kistemann, T. (2015). Developing the Urban Blue: Comparative Health Responses to Blue and Green Urban Open Spaces in Germany. *Health Place* 35, 196–205. doi:10.1016/j.healthplace.2014.10.015

Völker, S., and Kistemann, T. (2011). The Impact of Blue Space on Human Health and Well-Being - Salutogenetic Health Effects of Inland Surface Waters: A Review. *Int. J. Hyg. Environ. Health* 214 (6), 449–460. doi:10.1016/j.ijheh.2011.05.001

Wang, H., and Tang, Y. (2003). Study on the Regional Characteristics of Air Temperature in East China. *Bull. Sci. Technol.* 19 (3), 247–251. doi:10.13774/j.cnki.kjtb.2003.03.018

Wei, H., Hauer, R. J., Chen, X., and He, X. (2019). Facial Expressions of Visitors in Forests Along the Urbanization Gradient: What Can We Learn from Selfies on Social Networking Services? *Forests* 10 (12), 1049. doi:10.3390/f10121049

Wei, H., Hauer, R. J., and Guo, S. (2021a). Daytime Dynamic of Spontaneous Expressions of Pedestrians in an Urban Forest Park. *Urban For. Urban Green.* 65, 127326. doi:10.1016/j.ufug.2021.127326

Wei, H., Hauer, R. J., and He, X. (2021b). A Forest Experience Does Not Always Evoke Positive Emotion: A Pilot Study on Unconscious Facial Expressions Using the Face Reading Technology. *For. Pol. Econ.* 123, 102365. doi:10.1016/j.forpol.2020.102365

Wei, H., Hauer, R. J., and Zhai, X. (2020a). The Relationship Between the Facial Expression of People in University Campus and Host-City Variables. *Appl. Sci.* 10 (4), 1474. doi:10.3390/app10041474

Wei, H., and He, X. (2021). Foliar C/N Stoichiometry in Urban Forest Trees on a Global Scale. *J. For. Res.* 32 (4), 1429–1443. doi:10.1007/s11676-020-01188-6

Wei, H., Ma, B., Hauer, R. J., Liu, C., Chen, X., and He, X. (2020b). Relationship Between Environmental Factors and Facial Expressions of Visitors During the Urban Forest Experience. *Urban For. Urban Green.* 53, 126699. doi:10.1016/j.ufug.2020.126699

White, M. P., Pahl, S., Wheeler, B. W., Fleming, L. E. F., and Depledge, M. H. (2016). The 'Blue Gym': What Can Blue Space Do for You and What Can You Do for Blue Space? *J. Mar. Biol. Ass.* 96 (1), 5–12. doi:10.1017/s0025315415002209

White, M. P., Weeks, A., Hooper, T., Bleakley, L., Cracknell, D., Lovell, R., et al. (2017). Marine Wildlife as an Important Component of Coastal Visits: The Role of Perceived Biodiversity and Species Behaviour. *Mar. Pol.* 78, 80–89. doi:10.1016/j.marpol.2017.01.005

Zhang, J., Yang, Z., Chen, Z., Guo, M., and Guo, P. (2021). Optimizing Urban Forest Landscape for Better Perceptions of Positive Emotions. *Forests* 12 (12), 1691. doi:10.3390/f12121691

Zhou, C., Yan, L., Yu, L., Wei, H., Guan, H., Shang, C., et al. (2019). Effect of Short-Term Forest Bathing in Urban Parks on Perceived Anxiety of Young-Adults: A Pilot Study in Guiyang, Southwest China. *Chin. Geogr. Sci.* 29 (1), 139–150. doi:10.1007/s11769-018-0987-x

Zuckerman, M. (1977). Development of a Situation-Specific Trait-State Test for the Prediction and Measurement of Affective Responses. *J. Consulting Clin. Psychol.* 45 (4), 513–523. doi:10.1037/0022-006X.45.4.513

Conflict of Interest: The authors declare that the research was conducted in the absence of any commercial or financial relationships that could be construed as a potential conflict of interest.

Publisher's Note: All claims expressed in this article are solely those of the authors and do not necessarily represent those of their affiliated organizations, or those of the publisher, the editors, and the reviewers. Any product that may be evaluated in this article, or claim that may be made by its manufacturer, is not guaranteed or endorsed by the publisher.

Advantages of publishing in Frontiers

OPEN ACCESS
Articles are free to read for greatest visibility and readership

FAST PUBLICATION
Around 90 days from submission to decision

HIGH QUALITY PEER-REVIEW
Rigorous, collaborative, and constructive peer-review

TRANSPARENT PEER-REVIEW
Editors and reviewers acknowledged by name on published articles

Frontiers
Avenue du Tribunal-Fédéral 34
1005 Lausanne | Switzerland

Visit us: www.frontiersin.org
Contact us: frontiersin.org/about/contact

REPRODUCIBILITY OF RESEARCH
Support open data and methods to enhance research reproducibility

DIGITAL PUBLISHING
Articles designed for optimal readership across devices

FOLLOW US
@frontiersin

IMPACT METRICS
Advanced article metrics track visibility across digital media

EXTENSIVE PROMOTION
Marketing and promotion of impactful research

LOOP RESEARCH NETWORK
Our network increases your article's readership